

2014

VEHICLE TECHNOLOGIES OFFICE



FY 2014 Annual Progress Report - Vehicle and Systems Simulation and Testing R&D

This document highlights work sponsored by agencies of the U.S. Government. Neither the U.S. Government nor any agency thereof, nor any of their employees, makes any warranty, express or implied, or assumes any legal liability or responsibility for the accuracy, completeness, or usefulness of any information, apparatus, product, or process disclosed, or represents that its use would not infringe privately owned rights. Reference herein to any specific commercial product, process, or service by trade name, trademark, manufacturer, or otherwise does not necessarily constitute or imply its endorsement, recommendation, or favoring by the U.S. Government or any agency thereof. The views and opinions of authors expressed herein do not necessarily state or reflect those of the U.S. Government or any agency thereof.

CONTENTS

| | | |
|-------------|--|-----------|
| I. | INTRODUCTION..... | 1 |
| | I.A. Approach and Organization of Activities..... | 6 |
| | I.B. Future Directions for VSST | 12 |
| II. | THE EV EVERYWHERE GRAND CHALLENGE | 13 |
| | II.A. Background | 13 |
| | II.B. Planned Activities | 16 |
| III. | INDUSTRY | 17 |
| | ADVANCED VEHICLE TESTING AND EVALUATION | 17 |
| | III.A. Advanced Vehicle Testing & Evaluation (AVTE)- DE-EE0005501 | 17 |
| | THERMAL LOAD REDUCTION | 23 |
| | III.B. Electric Phase Change Material Assisted Thermal Heating System (ePATHS)- DE-EE000644 | 23 |
| | III.C. Advanced Climate Control and Vehicle Preconditioning- DE-EE0006445 | 32 |
| | TRANSPORTATION ELECTRIFICATION | 36 |
| | III.D. Interstate Electrification Improvement Project- DE-EE0002613 | 36 |
| | WIRELESS POWER TRANSFER..... | 42 |
| | III.E. Wireless Charging for Electric Vehicles- FOA #667 | 42 |
| | III.F. High Efficiency, Low EMI and Positioning Tolerant Wireless Charging of EVs- DE-EE0005963 | 49 |
| | SUPERTRUCK | 53 |
| | III.G. Systems Level Technology Development and Integration for Efficient Class 8 Trucks -ARRA..... | 53 |
| | III.H. Technology and System Level Demonstration of Highly Efficient and Clean, Diesel Powered Class 8 Trucks- DE-EE0003403 | 56 |
| | III.I. Volvo Energy Efficient Vehicle - SuperTruck..... | 60 |
| | ZERO EMISSIONS CARGO TRANSPORT | 64 |
| | III.J. Hydrogen Fuel-Cell Electric Hybrid Truck Demonstration & Houston Zero Emission Delivery Vehicle Deployment (DE-EE0005978,DE-EE0005979) | 64 |
| | III.K. Zero Emission Heavy-Duty Drayage Truck Demonstration-EE00005691 | 69 |
| IV. | VEHICLE TEST AND EVALUATION..... | 73 |
| | LIGHT DUTY..... | 73 |
| | IV.A. EV Project, ChargePoint America, and West Coast Electric Highway Data Collection and Information Dissemination..... | 73 |
| | IV.B. Nissan Leaf DC Fast Charging Study and Electric Drive Advanced Battery Testbed | 84 |
| | IV.C. Level 1 Benchmark of Advanced Technology Vehicles..... | 89 |
| | IV.D. Level 2 Benchmark of Advanced Technology Vehicles: MY 2014 Honda Accord Plug-in Hybrid Electric Vehicle..... | 99 |
| | MEDIUM AND HEAVY DUTY | 105 |
| | IV.E. Fleet DNA Vocational Database Project..... | 105 |

| | | |
|-------------|---|------------|
| IV.F. | Fleet DNA Database Development and Support | 115 |
| IV.G. | Medium-Duty Electric Vehicle Data Collection and Performance Assessment | 119 |
| IV.H. | Commercial EV Battery Degradation Field Evaluation | 132 |
| IV.I. | Long-Haul Truck Thermal Load and Idle Reduction | 135 |
| IV.J. | Medium and Heavy-Duty Field Testing | 144 |
| V. | MODELING AND SIMULATION | 155 |
| | LIGHT DUTY | 155 |
| V.A. | Analyzing the Potential of Multiple Energy Storage Systems for a BEV 300..... | 155 |
| V.B. | Evaluation of the Fuel Economy Impact of Low Temperature Combustion (LTC) using Simulation and Engine in the Loop..... | 161 |
| V.C. | In-Vehicle Lower-Energy Energy Storage System (LEESS) Component Evaluation | 166 |
| V.D. | Advanced PHEV Gen-set Development and Demonstration..... | 172 |
| V.E. | APEEM Components Analysis and Evaluation | 176 |
| V.F. | ACEC Technology Analysis and Evaluation..... | 179 |
| V.G. | Prius PHEV Thermal Vehicle Model Validation | 185 |
| V.H. | Analysis for Improving Efficiency with Connected Vehicles..... | 194 |
| V.I. | Trip Prediction and Route-Based Control Using Digital Maps | 201 |
| V.J. | Impact of Advanced Vehicle Technologies on Engine Operation and Vehicle Energy Consumption Benefits | 206 |
| V.K. | Autonomie Maintenance and MBSE Enhancements..... | 214 |
| V.L. | Internal Combustion Engine Energy Retention (ICEER) | 221 |
| V.M. | Impact of VTO Technologies on Energy Consumption and Cost Using Large-Scale Simulation | 227 |
| V.N. | Advanced PHEV Powertrain Benefit Comparison | 233 |
| V.O. | Vehicle Thermal System Model Development in MATLAB/Simulink | 240 |
| V.P. | Advanced Transmission Impact on Fuel Displacement..... | 248 |
| | HEAVY DUTY | 256 |
| V.Q. | CoolCalc Rapid HVAC Load Estimation Tool..... | 256 |
| V.R. | Advanced Heavy Duty Engine Systems and Emissions Control Modeling and Analysis | 265 |
| VI. | CODES & STANDARDS | 271 |
| VI.A. | EV-Smart Grid Interoperability Center | 271 |
| VI.B. | Codes and Standards and Technical Team Activities | 278 |
| VI.C. | Model Reusability | 281 |
| VI.D. | SAE Standards Development Support | 287 |
| VI.E. | HEV, PHEV, EV Test Standard Development and Validation | 289 |
| VI.F. | Green Racing Technical Support | 293 |
| VII. | VEHICLE SYSTEMS EFFICIENCY IMPROVEMENTS | 299 |
| VII.A. | Cummins MD& HD Accessory Hybridization..... | 299 |
| VII.B. | Powertrain Controls Optimization for HD Hybrid Line Haul Trucks | 303 |

| | |
|--|-----|
| FAST AND WIRELESS CHARGING..... | 306 |
| VII.C. INL Wireless Power Transfer and EVSE Charger Testing | 306 |
| VII.D. Wireless Power Transfer (WPT) Systems Optimization | 312 |
| FRICITION AND WEAR | 319 |
| VII.E. DOE/DOD Parasitic Energy Loss Collaboration..... | 319 |
| VII.F. Development of High Power Density Driveline for Vehicle Efficiency Improvement..... | 325 |
| GRID INTEGRATION..... | 330 |
| VII.G. PEV Integration with Renewables | 330 |
| VII.H. PEV Smart Grid Requirements Study | 334 |
| VII.I. VT INTEGRATE | 336 |
| THERMAL CONTROL | 339 |
| VII.J. Thermal Control of Power Electronics of Electric Vehicles with Small Channel Coolant Boiling | 339 |
| VII.K. Aerodynamics and Underhood Thermal Analysis of Heavy / Medium Vehicles | 345 |
| VII.L. Development of Nanofluids for Cooling Power Electronics for Hybrid Electric Vehicles..... | 350 |
| VII.M. Experimental Investigation of Coolant Boiling in a Half-Heated Circular Tube – CRADA with PACCAR | 358 |
| VII.N. Thermal Control through Air-Side Evaporative Heat Removal | 370 |
| DRAG REDUCTION | 377 |
| VII.O. DOE's Effort to Improve Heavy Vehicle Fuel Efficiency through Improved Aerodynamics..... | 377 |

LIST OF FIGURES

| | |
|--|----|
| Figure I-1 : VSST outcome objectives and mission | 1 |
| Figure I-2 : VSST primary processes, project objectives, and outcome objectives | 2 |
| Figure I-3: VSST activities integration – Arrows represent information flow between activity focus areas that enhances effectiveness of individual activities. | 6 |
| Figure I-4: VSST activities providing estimates of national benefits and impacts of advanced technologies..... | 7 |
| Figure III-1: AVTE 2013 Volkswagen Jetta TDI in Total Transit color scheme | 21 |
| Figure III-2: Heavy-Duty trucks in platoon formation (courtesy of Peloton Technology, Inc.)..... | 21 |
| Figure III-3: ePATHS System Design | 25 |
| Figure III-4: CapHX and Configurations..... | 25 |
| Figure III-5: Quarter-Width PCM Heat Exchanger | 27 |
| Figure III-6: Enclosed Quarter-Width PCM Heat Exchanger | 27 |
| Figure III-7:10% Scale VIP..... | 28 |
| Figure III-8: Delphi Thermal HVAC Developmental Controller..... | 28 |
| Figure III-9: PCM Charging Control Algorithm Design | 29 |
| Figure III-10: Heat Transfer (Predicted vs. Test) | 29 |
| Figure III-11: Charging Time and Temperature Profiles | 29 |
| Figure III-12: Heat Flux during Charging and Energy Storage in PCM HX..... | 29 |
| Figure III-13: Freezing of PCM in VIP | 30 |
| Figure III-14: Fin Pitch Study for PCM Heat Exchanger | 30 |
| Figure III-15: Latent Heat and Melting Temperature for Sample AAW12DA | 30 |
| Figure III-16: 2015MY Kia Soul EV | 33 |
| Figure III-17: Power consumption during 5°C warm-up test..... | 33 |

| | |
|--|----|
| Figure III-18: Initial System Model to Empirical Data Correlation | 34 |
| Figure III-19: Kia Soul Cabin Model with Occupants | 34 |
| Figure III-20: CFD Interior Temp. Predictions 15 Minutes into 28°C Cool-Down Test | 35 |
| Figure III-21: 28°C Cool-Down (CFD Predictions vs. Test Values) | 35 |
| Figure III-22: Shorepower stations serving long haul trucks at Duke's Travel Plaza on I-20 in Canton, Texas Objectives..... | 36 |
| Figure III-23: Map of Shorepower truck stop electrification facilities. A full list of sites can be found at www.shorepowerconnect.com. | 37 |
| Figure III-24: Some host site staff are proud of their system and take personal interest in telling drivers about Shorepower. One is Nelson Whitaker at Dukes Travel Plaza in Canton TX. | 38 |
| Figure III-25: There is a distinct seasonal pattern of use, and a roughly 1:1 ratio of KWH used to hours used..... | 39 |
| Figure III-26: Truck drivers have reported seeing the pedestals often, but not knowing what they were for. Large stickers were added to clarify their purpose. | 39 |
| Figure III-27: Owner-operator Dave Magistrale contacted Shorepower and offered to speak with drivers about plugging in. He answers questions and relays feedback. Dave also cleans around the pedestals and reports technical issues to company technicians..... | 40 |
| Figure III-28: The new map depicts the cumulative hours plugged-in per site, instead of cumulative power consumption | 41 |
| Figure III-29: Analytical expression of vector potential for coupler design..... | 44 |
| Figure III-30: ORNL designed new primary (top) and secondary (bottom) coil design and dimensions..... | 44 |
| Figure III-31: ORNL designed new primary coil winding meeting design requirements | 45 |
| Figure III-32: Coil performance characteristics: coupling factor variation at different airgaps | 45 |
| Figure III-33: Coil performance characteristics: AC resistance variation at different operating frequencies | 45 |
| Figure III-34: Grid side unit operational block diagram with Evatran control module and the DSP | 45 |
| Figure III-35: Operational block diagram for the wireless-J1772 integration | 46 |
| Figure III-36: Operational block diagram for the direct battery connection of vehicle side WPT equipment | 46 |
| Figure III-37: Cascaded power conversion stages efficiency results | 46 |
| Figure III-38: GCEDV wireless coil placement..... | 51 |
| Figure III-39: Second-generation asymmetric coil set..... | 51 |
| Figure III-40: DC-DC System efficiency measurements over x-axis misalignment in centimeters | 51 |
| Figure III-41: DC-DC System efficiency measurements over y-axis misalignment in centimeters | 52 |
| Figure III-42: SuperTruck Project Schedule | 54 |
| Figure III-43: A-Sample Test Results..... | 54 |
| Figure III-44: SuperTruck Aerodynamic Drag Validation | 54 |
| Figure III-45: SuperTruck Demo 2 | 57 |
| Figure III-46: SuperTruck final results and original roadmap | 58 |
| Figure III-47: Initial diesel technology roadmap for a 55% BTE engine..... | 58 |
| Figure III-48: Volvo Supertruck Project Schedule FY 2011-2016 | 60 |
| Figure III-49: Typical "tank-to-wheel" energy analysis for long-haul trucks (black) and technology matching (white)..... | 61 |
| Figure III-50: Ultra-lightweight frame assembly | 62 |
| Figure III-51: Engine "right-sizing" approach..... | 62 |
| Figure III-52: Balqon Prototype MX-30 | 70 |
| Figure III-53: Balqon BEV System | 70 |
| Figure III-54: TransPower Prototype ElecTruck..... | 70 |
| Figure III-55: TransPower BEV System | 70 |
| Figure III-56: US Hybrid BEV System | 71 |
| Figure III-57: Vision Industries Prototype Tyrano..... | 71 |
| Figure III-58: Vision Fuel Cell Hybrid Electric Drive System..... | 71 |
| Figure III-59: TransPower EDD-1 | 72 |
| Figure III-60: TransPower EDD-2 | 72 |
| Figure III-61: International Prostar | 72 |

| | |
|--|----|
| Figure IV-1: Overview of INL's data and information transfer process for the EV Project and ChargePoint Project, as well as all data collection activities..... | 75 |
| Figure IV-2: Major processing steps for handling wireless vehicle and charging infrastructure data | 75 |
| Figure IV-3: EV Project Nissan Leaf battery SOC at the start of charging events | 76 |
| Figure IV-4: EV Project Chevrolet Volt battery SOC at the start of charging events | 76 |
| Figure IV-5: Median eVMT and VMT per vehicle month over time | 76 |
| Figure IV-6: Average distance driven between charging and average charging energy per charge for each vehicle, with EV% denoted by color..... | 77 |
| Figure IV-7: Percent of Nissan Leaf charging events performed by location, power level, and time of day..... | 77 |
| Figure IV-8: Percent of Chevrolet Volt charging events performed by location, power level, and time of day | 78 |
| Figure IV-9: EV Project Nissan Leaf charging frequency by location (drawn to scale)..... | 78 |
| Figure IV-10: EV Project Chevrolet Volt charging frequency by location (drawn to scale) | 79 |
| Figure IV-11: Level 2 EVSE sites categorized by their primary venue | 80 |
| Figure IV-12: The distribution of average charging events per week per site. Each site's average number of charging events is displayed using a white circle | 80 |
| Figure IV-13: The number of DCFC sites per primary venue | 80 |
| Figure IV-14: The distribution of average charging events per week per site. The white circles represent each site's average number of charging events per week..... | 81 |
| Figure IV-15: Usage of Blink and AeroVironment DCFC along major highways in Washington and Oregon | 81 |
| Figure IV-16: Nissan Leaf DC Fast Charging in Phoenix, Arizona | 85 |
| Figure IV-17: Two 2012 Nissan Leaf battery packs testing in a thermal chamber at INL | 85 |
| Figure IV-18: Rendering of Toshiba lithium titanate battery pack..... | 86 |
| Figure IV-19: Locations of the drive motor, generator, and motor controllers are shown from a top view of the EDAB..... | 86 |
| Figure IV-20: Remaining capacity for each vehicle pair, as a percent of as-new capacity, after 50 thousand miles of on-road operation in Phoenix Arizona | 87 |
| Figure IV-21: Nissan Leaf battery capacity shown for each vehicle pair, AC Level 2 and DC Fast Charged, from laboratory, test-track, and on-road analyses..... | 87 |
| Figure IV-22: Capacity and discharge resistance from reference performance tests through the testing of the EnerDel battery pack..... | 87 |
| Figure IV-23: Advanced Vehicle Testing Activity process..... | 90 |
| Figure IV-24: Illustration of testing at 95°F with sun emulation (left) and at 20°F cold ambient temperature (right) | 90 |
| Figure IV-25: Data dissemination and project partners..... | 90 |
| Figure IV-26: Map of Downloadable Dynamometer Database content..... | 91 |
| Figure IV-27: 2013 Ford Cmax Hybrid energy use at varying climate control settings | 92 |
| Figure IV-28: Ford Cmax Hybrid engine operation at steady state speeds | 92 |
| Figure IV-29: 2013 Cmax Energi engine operation at 20°F, with and without driver heat demand..... | 93 |
| Figure IV-30: Regenerative power of the Cmax Energi and Hybrid..... | 93 |
| Figure IV-31: Cmax Hybrid and Energi charge sustaining fuel economy | 93 |
| Figure IV-32: 2012 Mitsubishi I-MiEV energy consumption | 94 |
| Figure IV-33: 2012 Mitsubishi I-MiEV energy use by major component..... | 94 |
| Figure IV-34: Effect of ambient temperature on 2013 Nissan Leaf range..... | 95 |
| Figure IV-35: Temperature effect on UDDS cold start energy consumption | 95 |
| Figure IV-36: Temperature effect on UDDS hot start energy consumption | 96 |
| Figure IV-37: 2014 Dodge Ram HFE idle stop system benefits for varying drive cycles..... | 96 |
| Figure IV-38: CNG storage tank installed in the 2014 Dodge Ram 1500 HFE | 96 |
| Figure IV-39: 2013 Ford Fusion Energi engine operation on hill 2 of a UDDS hot start | 97 |
| Figure IV-40: 2013 Ford Focus electric energy consumption | 98 |
| Figure IV-41: HV battery parameters during charging at 95°F ambient temperature | 98 |
| Figure IV-42: Honda Accord PHEV on the APRF Dynamometer | 99 |

| | |
|--|-----|
| Figure IV-43: High-voltage and 12 V electrical instrumentation..... | 100 |
| Figure IV-44: High temperature coolant loop (engine/cabin) instrumentation | 100 |
| Figure IV-45: Low-temperature (PCU) coolant loop instrumentation | 100 |
| Figure IV-46: Exhaust system instrumentation | 100 |
| Figure IV-47: Example exhaust system sampling ports..... | 101 |
| Figure IV-48: Cabin and vent temperature instrumentation | 101 |
| Figure IV-49: Inverter 3-phase voltage tap locations | 101 |
| Figure IV-50: Inverter and break-out box following 3-phase voltage tap installation | 101 |
| Figure IV-51: Tested charge-sustaining fuel economy versus EPA database..... | 102 |
| Figure IV-52: UDDS charge sustaining engine speed trace (both cold and hot start operation shown)..... | 102 |
| Figure IV-53: US06 charge sustaining engine speed trace | 102 |
| Figure IV-54: Estimated charge-sustaining EV envelope | 102 |
| Figure IV-55: Charge-sustaining operating mode usage over UDDS, Hwy, US06..... | 102 |
| Figure IV-56: Fuel consumption versus energy consumption for charge-depleting operation over the UDDS and US06 | 103 |
| Figure IV-57: Hwy cycle integrated current and R _{cda} example..... | 103 |
| Figure IV-58: Estimated charge depleting EV envelope | 103 |
| Figure IV-59: Comparison of charge-depleting and charge-sustaining EV operational envelopes | 104 |
| Figure IV-60: Map of data locations for Fleet DNA through FY 2014 | 106 |
| Figure IV-61: Summary of Fleet DNA vocational data | 106 |
| Figure IV-62: Example Fleet DNA vehicle subcategory interface..... | 107 |
| Figure IV-63: Sample data summary of Fleet DNA database sorted by vocation | 107 |
| Figure IV-64: Sample performance analysis of entire Fleet DNA database | 107 |
| Figure IV-65: Server configuration and security layout for fleet DNA network..... | 108 |
| Figure IV-66: Simplified Fleet DNA structure | 108 |
| Figure IV-67: Example of Fleet DNA data layers..... | 108 |
| Figure IV-68: Example of analyses via interconnected data layers | 108 |
| Figure IV-69: Illustration of Fleet DNA database structure | 109 |
| Figure IV-70: Two-folder data storage structure | 110 |
| Figure IV-71: Sample data quality visualization | 110 |
| Figure IV-72: Example road network analysis | 111 |
| Figure IV-73: Example of vehicle utilization breakdown | 111 |
| Figure IV-74: Fleet DNA DC extraction tool – parameters..... | 116 |
| Figure IV-75: Fleet DNA DC selection criteria | 116 |
| Figure IV-76: Fleet DNA DC selection criteria and search results..... | 117 |
| Figure IV-77: Data flow from vehicle to final reporting | 120 |
| Figure IV-78: Data processing and analysis | 121 |
| Figure IV-79: Smith Newton delivery vehicle (PIX# 22851)..... | 121 |
| Figure IV-80: Smith EV Data Received through the FTP Site | 122 |
| Figure IV-81: Home locations of Smith vehicles: Gen1 (Orange), Gen2 (Green)..... | 122 |
| Figure IV-82: Distribution of Smith data by state | 122 |
| Figure IV-83: Time of day when Smith vehicles are driving..... | 123 |
| Figure IV-84: Time of day when plugging in (charging begins)..... | 123 |
| Figure IV-85: Time of day when Smith vehicles are charging..... | 123 |
| Figure IV-86: Distribution of daily driving distance and estimated range..... | 123 |
| Figure IV-87: Smith energy consumption per mile and per year and cumulative | 123 |
| Figure IV-88: Effect of driving aggressiveness on mpge | 124 |
| Figure IV-89: Smith diesel equivalent fuel economy by quarter..... | 124 |
| Figure IV-90: Smith Newton kinetic intensity vs. average driving speed | 124 |

| | |
|--|-----|
| Figure IV-91: Navistar eStar, battery electric delivery vehicle (PIX# 18624) | 124 |
| Figure IV-92: Navistar vehicle data received through the FTP site..... | 125 |
| Figure IV-93: Home locations and hours of data transmitted per vehicle | 125 |
| Figure IV-94: Distribution of data by state..... | 125 |
| Figure IV-95: Time of day when driving | 126 |
| Figure IV-96: Time of day when charging | 126 |
| Figure IV-97: Daily driving distance | 126 |
| Figure IV-98: Effect of driving aggressiveness on fuel economy | 126 |
| Figure IV-99: Daily driving compared with standard cycles | 126 |
| Figure IV-100: Quarterly energy consumption | 126 |
| Figure IV-101: Map showing energy consumption by site and PADD regions | 127 |
| Figure IV-102: Seasonal and weekly utilization | 127 |
| Figure IV-103: Odyne parallel hybrid architecture; compliments of www.odyne.com/ | 128 |
| Figure IV-104: Vocational vehicles with the Odyne plug-in hybrid EV system; compliments of www.odyne.com/ | 128 |
| Figure IV-105: Frito-Lay delivery vehicle operation | 129 |
| Figure IV-106: Typical truck stop booking start and stop times along with average power | 129 |
| Figure IV-107: Second-generation Smith vehicle battery use..... | 130 |
| Figure IV-108: Sample cumulative report. | 131 |
| Figure IV-109 Intended data collection—collecting several points over a period of years will help to validate life models | 133 |
| Figure IV-110: Load test conducted at Casa Grande, AZ (NREL PIX 29613)..... | 134 |
| Figure IV-111: Example of sample drive cycle data from the ARRA Smith data collection project (top) used to generate models fit to a root-mean-square error of less than 6% open circuit voltage (bottom); voltages of four EVs skewed to protect intellectual property..... | 134 |
| Figure IV-112: NREL's vehicle testing and integration facility | 137 |
| Figure IV-113. (A) Cab and (B) sleeper thermocouple locations. Dimensions: A = 12", B = 6", C = 18". Blue: TMC standard [5]; red: NREL added | 138 |
| Figure IV-114. Cumulative totals of long-haul truck paint colors for the incremental addition of truck stop data | 139 |
| Figure IV-115. Daily A/C energy calibration data for test and control bucks | 139 |
| Figure IV-116. Average interior air temperature for solar soak calibration check day | 139 |
| Figure IV-117. Effect of vehicle rotation on average interior air temperature—single-day temperatures with three-day average beta | 140 |
| Figure IV-118. Experimental and model results for maximum possible reduction in rise over ambient temperature of a north-facing truck compared to a south-facing truck | 140 |
| Figure IV-119. Effect of glazing film on average interior air temperature | 140 |
| Figure IV-120. Percent improvement in daily A/C energy for the complete-cab solution for varying A/C loads and weather conditions | 141 |
| Figure IV-121: Fuel economy comparison of diesels and EVs | 147 |
| Figure IV-122: Subset of data from Chateau Energy management system | 147 |
| Figure IV-123: Time of day when vehicles are charging during the diesel comparison period (April-May 2014)..... | 147 |
| Figure IV-124: Fleet depot utility bill monthly peak demand | 148 |
| Figure IV-125: Charge management schemes developed by NREL could save FLNA in peak demand charges | 148 |
| Figure IV-126: Truck platooning air flow | 148 |
| Figure IV-127: Trucks in platoon formation during testing. NREL #31237 | 148 |
| Figure IV-128: Platoon team percent fuel savings | 150 |
| Figure IV-129: Platoon team fuel economy..... | 150 |
| Figure IV-130: Parker IVT hydraulic hybrid schematic..... | 151 |
| Figure IV-131: Laboratory fuel economy chart. Error bars are 95% confidence interval | 152 |
| Figure IV-132: NO _x emissions chart. Error bars are 95% confidence interval | 153 |
| Figure V-1: Variation in battery cost with discharge power and usable energy for the Li-S single-battery option | 156 |

| | |
|--|-----|
| Figure V-2: Variation in battery cost with discharge power and usable energy for the LMOG battery pack..... | 157 |
| Figure V-3: Battery requirements and cost for the single-battery and two-battery options..... | 157 |
| Figure V-4: Vehicle manufacturing and battery pack costs..... | 158 |
| Figure V-5: Battery power required for the single-battery option..... | 158 |
| Figure V-6: Battery power comparison during performance..... | 158 |
| Figure V-7: All-electric range simulated for various drive cycles..... | 159 |
| Figure V-8: Electric consumption simulated for various drive cycles..... | 159 |
| Figure V-9: LCOE simulated for various drive cycles..... | 159 |
| Figure V-10: Battery current from the energy battery can be controlled to a varying extent by using the power battery..... | 159 |
| Figure V-11: Brake-specific fuel consumption and engine-out NOx for LTC compared to gasoline SI and diesel engines..... | 161 |
| Figure V-12: Design of experiment..... | 162 |
| Figure V-13: Specifications of the conventional and BISG powertrains..... | 162 |
| Figure V-14: Engine-in-the-loop setup with the 1.9-L TDI engine used for the LTC tests..... | 162 |
| Figure V-15: Improvement in fuel consumption with updated fuel rate at low and medium loads at 2500 RPM..... | 163 |
| Figure V-16: Engine downspeeding via updated shift parameters during a section of the UDDS cycle..... | 163 |
| Figure V-17: Reduction in engine fuel consumption due to downspeeding..... | 163 |
| Figure V-18: Increase in NOx due to downspeeding..... | 164 |
| Figure V-19: Photo of the Fusion Hybrid's HVTB. <i>Image by John Ireland, NREL</i> | 167 |
| Figure V-20: Schematic of connections among replacement components and the vehicle..... | 167 |
| Figure V-21: JSR LIC modules in an environmental chamber during bench testing, with the production 2012 Fusion Hybrid NiMH modules in the background. <i>Image by John Ireland, NREL</i> | 168 |
| Figure V-22: Fully integrated conversion system mounted in the trunk of the Fusion Hybrid test platform. <i>Image by Jon Cosgrove, NREL</i> | 168 |
| Figure V-23: Closed-road acceleration performance testing. <i>Image by Petr Sindler, NREL</i> | 168 |
| Figure V-24: Acceleration distance for NiMH, eight-module LIC, and six-module LIC configurations while performing 0–60, 40–60, and 60–80 accelerations..... | 168 |
| Figure V-25: ESS energy profile and fuel use for 24°C UDDS tests of production NiMH and low-energy LIC configurations..... | 169 |
| Figure V-26: Fuel consumption and engine on/off cycling during hot (35°C) SC03 testing with air-conditioning..... | 169 |
| Figure V-27: ESS energy profile and fuel use for 24°C UDDS tests of production NiMH and low-energy LIC configurations..... | 169 |
| Figure V-28: Summary of fuel consumption and energy window results for multiple test cycles and vehicle configurations..... | 170 |
| Figure V-29: Pack level 2-second and 0.5-second resistance for the (“high-energy”) eight-module LIC and the seven-module EDLC configurations..... | 170 |
| Figure V-30: Installed Maxwell EDLC seven-module configuration. <i>Image by Jon Cosgrove, NREL</i> | 170 |
| Figure V-31: Trade-off between APU costs and ESS size depending on range and ESS cost..... | 172 |
| Figure V-32: Conventional diesel engine truck model validation..... | 173 |
| Figure V-33: Baseline fuel economy study..... | 173 |
| Figure V-34: Delivery truck gradeability study..... | 173 |
| Figure V-35: Genset fuel economy results for various electric machine technologies combined with an Ethanol Direct Injected engine..... | 174 |
| Figure V-36: Genset fuel economy results for various engine technologies combined with an induction machine..... | 174 |
| Figure V-37: Conventional powertrain transit bus model validation..... | 174 |
| Figure V-38: Hybrid powertrain transit bus model validation..... | 174 |
| Figure V-39: Hybrid powertrain and conventional powertrain fuel economy comparison..... | 174 |
| Figure V-40: Genset fuel economy results for various electric machine technologies combined with an ethanol direct injected engine..... | 175 |
| Figure V-41: Genset fuel economy results for various engine technologies combined with an induction machine..... | 175 |
| Figure V-42: Rendering of VSI lab with the component testcell in the foreground and the powertrain test cell in the background..... | 176 |
| Figure V-43: Dynamic behavior characterization of electric machine using hardware-in-the-loop test configuration..... | 177 |

| | |
|--|-----|
| Figure V-44: Component test cell bedplate and dyno..... | 177 |
| Figure V-45: Battery emulator behavior: example of voltage control when emulating a 700V nominal voltage ESS coupled to a heavy duty truck hybrid powertrain | 177 |
| Figure V-46: Electric machine mounting bracket and bearing assembly..... | 178 |
| Figure V-47: Electric machine installed in testcell..... | 178 |
| Figure V-48: dSPACE Hardware-in-the-loop real time computer used in powertrain testcell..... | 178 |
| Figure V-49: Example of steady-state engine maps for the GM 1.9L engine with the RCCI-enabled zone highlighted. The green marks in both the upper and lower figures indicate operating conditions for which RCCI measurements have been made | 181 |
| Figure V-50: Comparison of the simulated fuel economy with measurements for the 2010 Ford Fusion power-split hybrid operating over the hot UDDS drive cycle..... | 182 |
| Figure V-51: Fuel economies in the simulated vehicles powered by different combustion engine technologies over various city and highway drive cycles | 182 |
| Figure V-52: Hybrid vehicle engine speed vs. load operating points depicted on the steady-state engine maps for PFI, lean GDI, CDC/RCCI and CDC-only over a UDDS cycle. Each blue cross represents the engine state at 1s intervals. The red circle with internal green color in RCCI represents cold-start CDC operation..... | 183 |
| Figure V-53: Simulated exhaust temperatures of the PFI, lean GDI, CDC/RCCI and CDC-only engines in the simulated vehicles under the cold-start FTP cycle | 183 |
| Figure V-54: Modeling results of the potential tradeoff between the LNT regen fuel penalty and NOx tailpipe emissions from hybrid and non-hybrid vehicles powered by either CDC only or CDC/RCCI engines over a FTP cycle with 20C cold start. The solid markers are CDC/RCCI and the unsolid markers are CDC..... | 183 |
| Figure V-55: The configuration of the Toyota Prius PHEV is the same as that of the Prius HEV | 186 |
| Figure V-56: Toyota Prius PHEV loaded on a dynamometer in the APRF | 186 |
| Figure V-57: Importing process in Autonomie (all test data are imported into Autonomie, and signals required for the analysis are calculated in the importing process) | 186 |
| Figure V-58: Analysis process (Autonomie provides functions to analyze the control behaviors from the imported test data) | 187 |
| Figure V-59: Running simulation model in Autonomie (the simulation results are validated with the test data obtained from the APRF) | 187 |
| Figure V-60: Engine efficiency change according to engine coolant temperature..... | 187 |
| Figure V-61: Engine fuel consumption rate according to the engine coolant temperature | 188 |
| Figure V-62: Battery Round-Trip Efficiencies..... | 188 |
| Figure V-63: Internal resistance of the battery according to the SOC and battery pack temperature | 188 |
| Figure V-64: Wheel loss according to tire temperature (the torque loss significantly increases as tire temperature decreases)..... | 188 |
| Figure V-65: Variation of input energy at the wheel (all test results were obtained from the UDDS cycle, and the output energy at the wheel did not show any difference, whereas the input energy was significantly different according to the ambient temperature)..... | 189 |
| Figure V-66: Wheel speed and demand torque when the engine is turned on (points on the high power demand line are obtained when the vehicle is under CD mode) | 189 |
| Figure V-67: The engine is forced to be turned on if it needs to provide waste heat to the passenger compartment (dots represent the moments when the engine is turned on)..... | 190 |
| Figure V-68: Output power of the battery for SOC balancing (the points were obtained only when the engine is turned on) | 190 |
| Figure V-69: Battery output power according to SOC (the recuperating power is constrained by the SOC) | 190 |
| Figure V-70: Engine operating target (red points are the engine operating points when the engine is hot enough, and the blue points are the points when the engine is not hot enough) | 191 |
| Figure V-71: Engine speed constraint by engine coolant temperature | 191 |
| Figure V-72: Control flows for the Prius PHEV (the mode decision for CD or CS mode is added in the engine on/off control compared with the control of the HEV [12]) | 191 |
| Figure V-73: Vehicle Configuration of 2010 Toyota Prius in Autonomie..... | 191 |
| Figure V-74: Comparison between the test and the simulation on the UDDS cycle under cold ambient conditions: (a) engine coolant temperature; (b) engine speed and engine torque | 192 |
| Figure V-75: Comparison between the test and the simulation on the UDDS cycle under cold ambient conditions: (a) fuel consumption; (b) battery SOC | 192 |

| | |
|---|-----|
| Figure V-76: Fuel consumption versus average speed for various driving cycles [28] | 197 |
| Figure V-77: Fuel consumption metamodel corresponding to the FTP driving cycle | 197 |
| Figure V-78: Two vehicles with V2V communication while approaching the intersection at the same time | 198 |
| Figure V-79: The blue vehicle reduces speed through the decentralized control to avoid full stop at the intersection | 198 |
| Figure V-80: Both vehicles pass the intersection avoiding stop-and-go driving | 198 |
| Figure V-81: Conceptual view of speed prediction and route-based control in the context of a vehicle..... | 202 |
| Figure V-82: Distribution of speed and acceleration of the processed Chicago database | 202 |
| Figure V-83: Screenshot of SVTrip | 203 |
| Figure V-84: Bi-directional Markov Chain | 203 |
| Figure V-85: Probability density function of fuel consumption for HEV and conventional vehicle (using kernel density estimation)..... | 204 |
| Figure V-86: Probability Density of Powertrain-Specific Variables: Number of Gear Shifts for the Conventional Car (left) and Number of Engine Starts for the HEV (right)..... | 204 |
| Figure V-87: Fuel savings as a function of EQF for all 10 trips..... | 204 |
| Figure V-88: Naturally aspirated engine maps with incremental engine and friction improvements | 207 |
| Figure V-89: Turbocharged engine maps | 207 |
| Figure V-90: Design of experiment | 207 |
| Figure V-91: Golf gear ratios (actual versus algorithm design)..... | 208 |
| Figure V-92: Mazda gear ratios (actual versus algorithm design) | 208 |
| Figure V-93: Engine operation with a 6-speed automatic transmission..... | 208 |
| Figure V-94: Engine operation with an 8-speed automatic transmission..... | 208 |
| Figure V-95: Engine operation with an 8-speed DCT | 209 |
| Figure V-96: Engine operation with a 6-speed automatic, without lightweighting..... | 209 |
| Figure V-97: Engine operation for the 1-L turbo engine, with a 6-speed automatic transmission | 209 |
| Figure V-98: Engine operation for the conventional and BISG powertrain, HWFET cycle | 209 |
| Figure V-99: Impact of engine technology on fuel consumption | 210 |
| Figure V-100: Impact of engine technology on performance | 210 |
| Figure V-101: Impact of friction reduction on vehicle fuel consumption | 210 |
| Figure V-102: Impact of transmission technology on vehicle fuel consumption | 210 |
| Figure V-103: Impact of turbocharging on vehicle fuel consumption | 211 |
| Figure V-104: Impact of Turbocharging on Performance..... | 211 |
| Figure V-105: Impact of mild hybridization (BISG) on fuel consumption | 211 |
| Figure V-106: Decrease in fuel consumption compensates for increased technology cost | 211 |
| Figure V-107: Shift map and parameters selected for optimization for each engine transmission pair..... | 211 |
| Figure V-108: Fuel consumption as a function of the parametric sweep of shift parameters and the trajectory of the optimization algorithm | 212 |
| Figure V-109: Comparison of fuel consumption benefits (l/100km) with and without the use of shift parameter optimization | 212 |
| Figure V-110: BatPaC model integration | 215 |
| Figure V-111: HHV configurations | 215 |
| Figure V-112: Development of series-parallel PHEV 2-motor configuration | 215 |
| Figure V-113: New shifting calibrations | 215 |
| Figure V-114: Thermal model development..... | 216 |
| Figure V-115: CVT transmission model development | 216 |
| Figure V-116: DCT transmission model development | 216 |
| Figure V-117: Gearbox, final drive, and wheel models connected via physical ports..... | 216 |
| Figure V-118: Double clicking on the vehicle will open it directly in Autonomie | 216 |
| Figure V-119: Work in Simulink | 217 |
| Figure V-120: HTML report of simulation results | 217 |

| | |
|--|-----|
| Figure V-121: Graphical configuration editor | 217 |
| Figure V-122: Conventional vehicle architecture built in the configuration builder | 218 |
| Figure V-123: Setting up CosiMate options | 218 |
| Figure V-124: FMU integration using the Modelon toolbox | 218 |
| Figure V-125: Autonomie MPI distributes simulations across cores | 219 |
| Figure V-126: Generic Optimization Editors | 219 |
| Figure V-127: Example time series data of engine fueling rate (250-second section of UDDS); measured test data from chassis dynamometer (solid black) overlaid with the model estimate (dashed magenta) | 222 |
| Figure V-128: Best-fit engine efficiency map as function of output mechanical power and engine oil temperature (considering operation over 16 test cycles) | 222 |
| Figure V-129: Example time series data of engine oil temperature (measured at dipstick). Measured test data from chassis dynamometer (solid black) overlaid with the model estimate (dashed magenta) | 223 |
| Figure V-130: Example time series data of engine coolant temperature (measured at heater core inlet). Measured test data from chassis dynamometer (solid black) overlaid with the model estimate (dashed magenta) | 223 |
| Figure V-131: Map of average ambient temperatures for the contiguous United States (hot climates in red, cold in blue) as sourced from NREL's database of typical meteorological years | 224 |
| Figure V-132: Time series examples of thermal simulations predicting engine oil and coolant temperatures. Real-world drive cycle data overlaid with TMY climate data. Results are shown at two horizontal zoom windows: 1—one week (top) and 2—one hour (bottom) | 224 |
| Figure V-133: Distance-weighted fleet average MPG by week of year for three U.S. climates | 225 |
| Figure V-134: Distribution of simulated vehicle history MPG by week of year (approximately 50% of data is bounded between 23 and 28 MPG) | 225 |
| Figure V-135: Relative fuel consumption model contributions shown for various combinations of drive cycle datasets and year-long TMY climate data. Results are compared with the simulated EPA 5-cycle test procedure | 226 |
| Figure V-136: Running Large-Scale Simulations Using Autonomie | 228 |
| Figure V-137: Analyzing Large-Scale Simulations Data | 228 |
| Figure V-138: The Number of Required Runs Accumulates Quickly | 228 |
| Figure V-139: Example Autonomie parameters to add to the database | 229 |
| Figure V-140: Database structure | 230 |
| Figure V-141: Quickly filter data | 230 |
| Figure V-142: View simulation parameters | 230 |
| Figure V-143: Scenario analysis with data recalculation | 230 |
| Figure V-144: Export data to Excel | 230 |
| Figure V-145: Available plots for battery analysis in the database GUI | 230 |
| Figure V-146: Standard plots for the battery generated through the plotter tool | 231 |
| Figure V-147: Battery energy requirements decrease with time (for all vehicle classes) | 231 |
| Figure V-148: Battery peak power requirements decrease significantly with time | 231 |
| Figure V-149: Fuel consumption trends for PHEV 10 and 20 for UDDS and HWFET | 231 |
| Figure V-150: Trends in the ratio of fuel-specific energy to battery-specific energy | 232 |
| Figure V-151: Specific energy ratio of the powertrain at the wheel | 232 |
| Figure V-152: PHEV models | 233 |
| Figure V-153: Vehicle configuration, AER, and risk levels considered | 234 |
| Figure V-154: Configuration of series-parallel system and vehicle model in Autonomie | 234 |
| Figure V-155: Fuel-to-wheel efficiency in parallel mode, series mode, and difference of efficiency | 235 |
| Figure V-156: Detailed component performances when shifting from series to parallel mode | 235 |
| Figure V-157: Simulation results on the UDDS | 235 |
| Figure V-158: Transmission loss modeling | 236 |
| Figure V-159: Vehicle curb weight | 237 |
| Figure V-160: Vehicle component power | 237 |
| Figure V-161: Vehicle manufacturing cost | 237 |

| | |
|---|-----|
| Figure V-162: Charge-sustaining fuel consumption – combined | 238 |
| Figure V-163: Fuel and electricity consumption results on U.S. standards | 238 |
| Figure V-164: Incremental manufacturing cost as a function of fuel consumption for all powertrains | 238 |
| Figure V-165: Fuel and electricity consumption results on certified cycles | 238 |
| Figure V-166: Available A/C system simulation versions | 241 |
| Figure V-167: Fluid network example—green marker: loops; red marker: nodes; blue marker: branches | 242 |
| Figure V-168: Coolant flow rate calculation flow chart | 242 |
| Figure V-169: Distributed-Parameter model example for two-pass liquid coolant heat exchanger | 243 |
| Figure V-170: Schematic of NREL’s CFL EDV Thermal Management System | 243 |
| Figure V-171: CFL active heating mode | 244 |
| Figure V-172: CFL active cooling mode | 244 |
| Figure V-173: Top-level view of the Simulink model of the CFL system | 244 |
| Figure V-174: Selected coolant loops for modeling purposes | 244 |
| Figure V-175: Activated loops for active heating mode | 244 |
| Figure V-176: Activated loops for active cooling mode | 244 |
| Figure V-177: Calibration results for the chiller model | 245 |
| Figure V-178: Heat transfer calibration for the radiator | 245 |
| Figure V-179: Simulink lookup function (with labels) for obtaining the effectiveness of the radiator | 245 |
| Figure V-180: Radiator Mapped Component model | 245 |
| Figure V-181: System refrigerant mass flow rates | 246 |
| Figure V-182: Capacities of chiller and condenser | 246 |
| Figure V-183: Capacities of liquid-coolant-based heat exchangers | 246 |
| Figure V-184: Coolant temperatures just upstream of heat exchangers | 246 |
| Figure V-185: Study process for developing advanced transmission models and shifting algorithm | 249 |
| Figure V-186: Schematic of DCT powertrain for HEVs | 249 |
| Figure V-187: DCT controller development for HEVs | 250 |
| Figure V-188: Detailed component performance for the DCT | 250 |
| Figure V-189: The vehicle systems in Autonomie | 250 |
| Figure V-190: Wheel torque vs. vehicle speed in Autonomie | 251 |
| Figure V-191: (Upper panel) SOC vs. time and (lower panel) engine power vs. wheel power in Autonomie | 251 |
| Figure V-192: Simulation and test results for the 2013 VW Jetta conventional vehicle with 6-speed DCT on the UDDS cycle | 251 |
| Figure V-193: Simulation and test results for the 2013 VW Jetta HEV with 7-speed DCT on the (a) UDDS cycle and (b) SC03 cycle | 252 |
| Figure V-194: Hydraulic pump loss and mechanical loss for metal V-belt CVT [2] | 252 |
| Figure V-195: F_{PFs} ratio map | 253 |
| Figure V-196: Block diagram of model-based ratio control | 253 |
| Figure V-197: Optimal operation line from test data | 254 |
| Figure V-198: Simulation and testing results for the 2013 Nissan Altima conventional vehicle on the UDDS cycle | 254 |
| Figure V-199: Simulation and testing results for the 2013 Honda Civic HEV on the UDDS cycle | 254 |
| Figure V-200: CoolCalc process tool | 258 |
| Figure V-201: CoolCalc post-processing tool | 258 |
| Figure V-202: (Left) CoolCalc and (right) VTCab graphical user interfaces | 258 |
| Figure V-203: CoolCalc geometry of the generic long-haul truck model | 259 |
| Figure V-204: Thermal HVAC loads of the generic truck cab model compared to three validated CoolCalc models | 260 |
| Figure V-205: Effect of normalized cooling degree-days with respect to truck cab orientation angle | 260 |
| Figure V-206: Relative impact of individual technologies for both cooling and heating thermal loads | 261 |
| Figure V-207: National contour plots of normalized daily cooling thermal load for both baseline and complete-cab solution CoolCalc analysis results | 262 |

| | |
|--|-----|
| Figure V-208. Battery charge and discharge states for electric A/C systems | 262 |
| Figure V-209. Effect of paint color national results on electric A/C battery size requirements | 262 |
| Figure V-210. Fuel use estimation modeling process | 263 |
| Figure V-211: Auxiliary-load comparison between conventional and hybrid trucks; ME and EE represent mechanical and electrical energy consumption, respectively | 267 |
| Figure V-212: Comparison of the simulated accessory load for the Class 8 conventional and parallel-hybrid trucks UDDS truck cycle; the simulated truck weight is 25,000 kg | 267 |
| Figure V-213: Comparison of simulated fuel economy for the conventional and hybrid buses over five different city drive cycles; Series_LH and Series_HH refer to the same two series-hybrid cases described above | 268 |
| Figure V-214: Comparison of simulated engine-out and tailpipe emissions change for CO, HC, and NOx from parallel- and series-hybrid buses; Series_LH and Series_HH refer to the same two series-hybrid cases described above | 268 |
| Figure V-215: Comparison of fuel economy among the conventional and hybrid trucks over the freeway-dominated heavy-duty driving cycle | 269 |
| Figure V-216: Energy loss distribution for the 25ton conventional and hybrid trucks operating over the freeway-dominated heavy-duty driving cycle; the energy losses are shown relative to the conventional truck's overall energy use | 269 |
| Figure V-217: Comparison of fuel economy of the conventional and parallel hybrid trucks with the targeted aerodynamic drag and rolling resistance reductions over the freeway-dominated heavy duty driving cycle | 269 |
| Figure V-218: Predicted fuel economy and emissions impact of the combined technology target goals identified by the 21CTP over a freeway-dominated heavy-duty truck cycle | 270 |
| Figure VI-1: Argonne AC interoperability test matrix | 272 |
| Figure VI-2: Argonne IOC task schedule | 273 |
| Figure VI-3: Reference vehicle – BMW i3 with range extender | 273 |
| Figure VI-4: Argonne's AC Interop Test Fixture (Version 2) | 274 |
| Figure VI-5: Argonne's PEV Compliance Tool | 274 |
| Figure VI-6: Argonne's SpEC communication controller module | 275 |
| Figure VI-7: Laboratories and capabilities of the Argonne EV-Smart Grid Interoperability Center | 276 |
| Figure VI-8: Relationship between the four major projects for enabling and facilitating model reusability | 283 |
| Figure VI-9: Top-level ground vehicle system model organization | 283 |
| Figure VI-10: Vehicle subsystem model organization | 283 |
| Figure VI-11: Power subsystem model organization | 284 |
| Figure VI-12: Chassis subsystem model organization | 284 |
| Figure VI-13: Trailer subsystem model organization (for a single trailer) | 284 |
| Figure VI-14: Trailer subsystem model organization (for a tandem trailer) | 284 |
| Figure VI-15: Trailer subsystem model organization (for the i-th trailer of a train of trailers) | 284 |
| Figure VI-16: Body-frame subsystem model organization | 284 |
| Figure VI-17: Trailer I body-frame subsystem model organization | 284 |
| Figure VI-18: Example of a subsystem summary and interface definition for the propulsion power subsystem | 284 |
| Figure VI-19: Example of a Single Subsystem Connectivity Diagram for the Propulsion Power Subsystem | 285 |
| Figure VI-20: Total Connectivity Diagram for the Power Subsystem | 285 |
| Figure VI-21: Total Connectivity Diagram for the Chassis Subsystem | 285 |
| Figure VI-22: Total Connectivity Diagram for the Trailer Subsystem | 285 |
| Figure VI-23: Chassis Dynamometer Approach to Measure System Power Using Axle Torque Sensors | 290 |
| Figure VI-24: Axle Hub Dynamometer Approach to Measure System Power | 290 |
| Figure VI-25: Results of Road Test Showing Power Gap | 290 |
| Figure VI-26: Initial Chassis Dynamometer Testing of Volt System Power Test | 291 |
| Figure VI-27: Initial Chassis Dynamometer Testing of Volt System Power Test | 291 |
| Figure VI-28: MY2010 Prius System Power Tests at Fixed Dynamometer Speeds | 291 |
| Figure VI-29: Formula 1 introduced new powertrains in 2014 emphasizing efficiency, energy recovery, and significantly more hybridization (photo: espn.f1.com) | 293 |

| | |
|---|-----|
| Figure VI-30: An Audi R18 e-tron quattro diesel HEV took first and second place in the 2014 24 Hours of Le Mans in (photo: Audi Sport) | 295 |
| Figure VI-31: DeltaWing Coupe continues its development in 2014 (photo: deltawingracing.com) | 295 |
| Figure VI-32: Green Challenge Awards were given in all ten TUSC races in 2014 (photo: press.porsche.com) | 296 |
| Figure VI-33: Mazda Skyactiv-Diesel production-based race engine competed in all ten TUDOR United Sportscar Championship races using 100% renewable synthetic diesel fuel (photo by mazdamotorsports.com) | 296 |
| Figure VI-34: Fans and professional racing drivers alike try their hand at the GRS; Tommy Milner of Corvette Racing puts the simulated E85/Hybrid Corvette to the test | 296 |
| Figure VII-1: HD transit bus and MD P&D Autonomie vehicle models | 300 |
| Figure VII-2: HD class 8 line haul sleeper cab based on a chassis tested Kenworth T700..... | 300 |
| Figure VII-3: Vehicle speed trace, total accessory power consumption, and total engine drag torque from the accessories | 301 |
| Figure VII-4: Air conditioning system traces; power, torque, and cabin temperature | 301 |
| Figure VII-5: Engine cooling fan system traces; power and torque | 301 |
| Figure VII-6: Air compressor and brake system traces; power, torque, and tank pressure | 301 |
| Figure VII-7: Power steering system traces; power and torque | 301 |
| Figure VII-8: Manhattan Bus Cycle | 302 |
| Figure VII-9: HTUF6 cycle with key on and off events..... | 302 |
| Figure VII-10: Project focus areas | 304 |
| Figure VII-11 ORNL HTDC "real world" drive cycle from Nashville, TN, to Knoxville, TN | 305 |
| Figure VII-12 Cummins ISX-450 installed in the ORNL VSI laboratory | 305 |
| Figure VII-13 ORNL transient engine model and associated aftertreatment models | 305 |
| Figure VII-14 Model framework for the dual energy stoarge system model | 305 |
| Figure VII-15: GE smart grid enabled EVSE..... | 308 |
| Figure VII-16: Energy measurement testing from the GE smart grid enabled EVSE | 308 |
| Figure VII-17: Several of the thirteen EVSEs for interoperability testing with production plug-in vehicles | 309 |
| Figure VII-18: Vehicle-level testing of the pre-production Evatran wireless charger operation on a Chevy Volt..... | 310 |
| Figure VII-19: Open-air testing of the pre-production Evatran wireless charger using the proposed SAE J2954 mock floor-pan design..... | 310 |
| Figure VII-20: Debris items evaluated in support of SAE J2954 test procedure development | 310 |
| Figure VII-21: Vehicle-level testing of conducting and wireless charging systems in INL's Electric Vehicle Charging Infrastructure Test Facility..... | 310 |
| Figure VII-22: Roads identified as options for in-motion WPT (black lines) within defined CSAs (yellow lines)..... | 314 |
| Figure VII-23: analysis of overlapping FC1 and FC2 travel within each CSA..... | 315 |
| Figure VII-24: Simulated HEV fuel consumption over the GPS driving profiles..... | 315 |
| Figure VII-25: Fuel consumption reductions by WPT rollout for five HEV models..... | 316 |
| Figure VII-26: Net present lifetime cost and fuel savings of in-motion WPT scenario relative to baseline conventional and HEV truck scenarios | 317 |
| Figure VII-27: Map showing Δ FMEP between an SAE20 WT (90% reduction in asperity friction) and an SAE 40WT oil (with baseline asperity friction) as function of speed and load (BFR = boundary friction reduction) | 321 |
| Figure VII-28: Comparison of FMEP simulation data (red circles) to linear-regression fit (mesh)..... | 321 |
| Figure VII-29: FCSF for an SAE40WT oil (with a 90% BFR) relative to an SAE 40WT oil with baseline asperity friction | 322 |
| Figure VII-30: Lorentzian fit to fuel consumption rate | 322 |
| Figure VII-31: Predicted change in fuel consumption for a HDDE vehicle as function of viscosity and change in asperity friction..... | 323 |
| Figure VII-32. Friction vs. time for 1-hour ball-on-flat tests at different temperatures..... | 323 |
| Figure VII-33: Asperity friction as a function of temperature for four lubricants | 323 |
| Figure VII-34: Typical weight distribution of different systems in automotive vehicle | 326 |
| Figure VII-35: Typical automotive transmission gearbox | 326 |
| Figure VII-36: Average scuffing load for different coatings in three lubricants | 327 |
| Figure VII-37: SEM micrographs showing coating wear through prior to scuffing failure in coated surfaces | 327 |

| | |
|--|-----|
| Figure VII-38: SEM micrograph of scuffed substrate surface showing shear instability indicated by serration | 327 |
| Figure VII-39: SEM micrographs showing micro-spalling wear mechanism of coatings | 328 |
| Figure VII-40: Schematic and picture of fatigue test configuration with PCS three-ring-and-roller contact | 328 |
| Figure VII-41: (a) Optical micrograph of case crushing failure mode under severe contact conditions and (b) SEM micrograph of a typical contact fatigue failure on a gear tooth | 328 |
| Figure VII-42: Forecasted typical trends in aggregate net load profile in California ISO with high penetration of solar generation (www.caiso.com/Documents/FlexibleResourcesHelpRenewables_FastFacts.pdf) | 330 |
| Figure VII-43: Under high-penetration scenarios, solar production dynamics can lead to net demand peak event; data are one representative day on the NREL South Table Mountain Campus | 331 |
| Figure VII-44: Scenarios demonstrating the management of PEV charging in aggregate aligned with solar production..... | 331 |
| Figure VII-45: Residential charging load profile from EV project through Q2 2013; highlights evening starts and TOU impacts | 331 |
| Figure VII-46: Public charging load profile from EV project through Q2 2013; highlights morning and mid-day loads that could be shifted to align with solar production (www.theevproject.com/cms-assets/documents/127233-901153.q2-2013-rpt.pdf)..... | 332 |
| Figure VII-47: One year of aggregate EVSE power demand (kW) for 36 EVSEs installed in the NREL parking garage (03/05/2013-03/04/2014) | 332 |
| Figure VII-48: Commercial building attributes analysis suggests market opportunity for 1 million–2.5 million vehicles with 6 kW bi-directional power interface to generate peak demand reduction value | 332 |
| Figure VII-49: Implementation of 20 kW bi-directional vehicle power management system for building and renewables integration | 332 |
| Figure VII-50: Multi-lab collaboration meeting to design the PEV smart grid requirements study (photo credit: Ted Bohn) | 335 |
| Figure VII-51: Systems diagram depicting the interaction of PEV loads with buildings and renewables | 337 |
| Figure VII-52: INTEGRATE networking strategy to address grid needs using systems and devices from multiple levels and technologies | 337 |
| Figure VII-53: Concept of subcooled flow boiling system | 340 |
| Figure VII-54: Vehicle power electronics package | 340 |
| Figure VII-55: Side view of vehicle power electronics package | 340 |
| Figure VII-56: Fin structure | 341 |
| Figure VII-57: Mesh structure (all units in meters) | 341 |
| Figure VII-58: TIM Thermal Conductivity Effects | 341 |
| Figure VII-59: Junction Temperatures | 342 |
| Figure VII-60: Coolant Flow Velocity Effects | 342 |
| Figure VII-61: Fluid Inlet Temperature Effects | 342 |
| Figure VII-62: Heat Flux Effects | 343 |
| Figure VII-63: Junction temperatures for high heat flux applications | 343 |
| Figure VII-64: Conventional heavy-duty vehicle, a) cabin, b) cabin+flatbed, c) base case, and d) base case+side skirts | 347 |
| Figure VII-65: Cab-over engine heavy-duty vehicle; a) cabin, b) cabin+flatbed, c) base case, and d) base case+side skirts | 347 |
| Figure VII-66: Aerodynamic drag performance of conventional design over cab-over engine design for Yaw 0, 6 and 12° | 347 |
| Figure VII-67: Conventional heavy-duty vehicle performance with curvy-edges at trailer rear end [Yaw 0°] | 347 |
| Figure VII-68: Conventional heavy-duty vehicle velocity profile at trailer wheels [Yaw 0°] (a) without wheel covers and (b) With wheel covers | 348 |
| Figure VII-69: Cabin-trailer gap analysis of cab-over engine design at Yaw 0° | 348 |
| Figure VII-70: Temperature and velocity profiles of CAC (i,iii) Conventional (ii,iv) Cab-over engine | 348 |
| Figure VII-71: Temperature and velocity profiles of radiator (i,iii) Conventional (ii,iv) Cab-over engine | 348 |
| Figure VII-72: Schematics of the project approach | 351 |
| Figure VII-73: Results of the heat transfer analysis | 352 |
| Figure VII-74: SEM images of three graphite morphologies before and after the surface modification | 352 |
| Figure VII-75: Effects of the GnP surface treatment | 353 |
| Figure VII-76: Effects of surface treatment of thermophysical properties of nanofluids | 353 |
| Figure VII-77: Effects of nanoparticle morphology of thermo-physical properties of nanofluids | 354 |

| | |
|--|-----|
| Figure VII-78: Calculated ratio of heat transfer coefficients for 5 wt% B-grade f-GnP in EG/H ₂ O with laminar and turbulent flow regimes | 354 |
| Figure VII-79: Effects of base fluid and ball-milling for the 5 wt.% B-grade f-GnP nanofluids | 355 |
| Figure VII-80: Experimental heat transfer coefficient results | 355 |
| Figure VII-81: Experimental heat transfer coefficient results | 356 |
| Figure VII-82: Schematic of heat transfer facility | 359 |
| Figure VII-83: Test section heating wire arrangement | 359 |
| Figure VII-84: Overview of heat transfer facility | 360 |
| Figure VII-85: Heat loss calibration | 360 |
| Figure VII-86: Experimental versus calculated turbulent heat transfer coefficients for (a) water, (b) 40/60 EG/W, and (c) 50/50 EG/W..... | 361 |
| Figure VII-87: Experimental versus calculated laminar heat transfer coefficient for (a) 40/60 EG/W and (b) 50/50 EG/W..... | 362 |
| Figure VII-88: Water turbulent flow boiling curves at 75°C–90°C and (a) 0.125 m/s, (b) 0.25 m/s, (c) 0.5 m/s, (d) 1 m/s, and (e) 1.5 m/s | 363 |
| Figure VII-89: Turbulent flow boiling curves for 40/60 EG/W mixture at 80°C–95°C and (a) 0.25 m/s, (b) 0.5 m/s, (c) 1 m/s, and (d) 1.5 m/s | 364 |
| Figure VII-90: Turbulent flow boiling curves for 50/50 EG/W mixture at 82°C–97°C and (a) 0.25 m/s, (b) 0.5 m/s, (c) 1 m/s, and (d) 1.5 m/s | 365 |
| Figure VII-91: Laminar flow boiling curves for (a) 40/60 EG/W and (b) 50/50 EG/W mixtures | 366 |
| Figure VII-92: Boiling heat transfer coefficients for (a) water and (b) EG/W mixtures | 366 |
| Figure VII-93: Correlation of boiling number term for (a) water and (b) EG/W mixtures..... | 367 |
| Figure VII-94: Experimental versus predicted heat transfer coefficient for (a) water and (b) EG/W mixtures | 367 |
| Figure VII-95: Correlation of boiling number term for all data | 368 |
| Figure VII-96: Experimental versus predicted heat transfer coefficient for all data | 368 |
| Figure VII-97: Experimental and predicted wall temperatures for 50/50 EG/W at (a) 82°C and (b) 97°C | 368 |
| Figure VII-98: Pressurizing system | 369 |
| Figure VII-99: Hybrid Radiator System | 371 |
| Figure VII-100: Top View of a Section of the Hybrid Radiator | 371 |
| Figure VII-101: Radiator Heat Transfer..... | 371 |
| Figure VII-102: Effect of Radiator Size | 372 |
| Figure VII-103: Droplet Movement..... | 372 |
| Figure VII-104: Droplet evaporation | 372 |
| Figure VII-105: Air flow effect..... | 373 |
| Figure VII-106: Droplet Evaporation with Air Flow Effect..... | 373 |
| Figure VII-107: Experimental test system overview..... | 374 |
| Figure VII-108: Experimental test strip assembly | 374 |
| Figure VII-109: Heating Wire and Thermocouples..... | 375 |
| Figure VII-110: Droplet dispersing head assembly | 375 |
| Figure VII-111: a) Clay exterior of the GSF1 tractor; b) tractor and trailer reshaping during a wind tunnel test..... | 378 |
| Figure VII-112: GSF1 model (1/8th scale) in the NASA Ames 7×10 wind tunnel | 378 |
| Figure VII-113: GSF1 tractor-trailer design..... | 378 |
| Figure VII-114: Body-axis drag coefficient as a function of vehicle yaw angle (-18° to 18°) for the GSF1 configuration shown in Figure VII-113..... | 379 |
| Figure VII-115: Body-axis surface force (pressure and shear stress) obtained from CFD simulations of the GSF1 configuration shown in Figure VII-113 | 379 |
| Figure VII-116: Body-axis drag coefficient as a function of vehicle yaw angle (-30° to 0°) for the configuration shown in Figure VII-113..... | 379 |
| Figure VII-117: a) Baseline tanker-trailer; b) gap fairing | 379 |
| Figure VII-118: Percent reduction in the wind-averaged drag coefficient as a function of tractor-tanker gap size (Figure VII-117) | 380 |

| | |
|---|-----|
| Figure VII-119: Tanker-trailer with a fully extended gap fairing and a) tanker skirts and b) a tanker “drape” | 380 |
| Figure VII-120: PIV setup in the NASA Ames 7×10 wind tunnel | 380 |
| Figure VII-121: PIV measurement planes | 380 |
| Figure VII-122: Velocity streamlines in the wake of Pro-Star tractor and straight-frame trailer at 0° yaw: a, c) baseline configuration and b,d) 48” (full-scale) trailer boattail and trailer skirts configuration | 381 |

LIST OF TABLES

| | |
|---|-----|
| Table II-1: VSST EV Everywhere Achievements for FY 2014 | 14 |
| Table III-1 FY 2014 AVTE Vehicle Mileage | 19 |
| Table III-2: Project Test Conditions | 33 |
| Table III-3: Weighted Range Improvement Targets | 34 |
| Table III-4: Electrical parameters of the coils | 45 |
| Table III-5: Coil system z-dimension breakdown | 51 |
| Table IV-1: 2013 Ford Cmax Hybrid Powertrain Specifications | 91 |
| Table IV-2: 2013 Ford Cmax Energi Powertrain Specifications | 92 |
| Table IV-3: 2012 Mitsubishi I-MiEV Specifications | 94 |
| Table IV-4: 2013 Nissan Leaf Specifications | 95 |
| Table IV-5: 2014 Dodge Ram 1500 HFE Specifications | 96 |
| Table IV-6: Fuel Economy and Emissions Comparison for CNG and Gasoline Operation | 97 |
| Table IV-7: 2013 Ford Fusion Energi Specifications | 97 |
| Table IV-8: 2013 Ford Focus Electric Specifications | 97 |
| Table IV-9: Estimated charge depleting range (Rcda per SAE J1711) | 103 |
| Table IV-10: Highlighted charge depleting usage parameters over the UDDS, Hwy, and US06 cycle | 103 |
| Table IV-11: Fleet DNA Files by Vocation and Vehicle No | 117 |
| Table IV-12: Smith Newton Vehicle Specifications | 121 |
| Table IV-13: Navistar eStar Vehicle Specifications | 124 |
| Table IV-14: Smith EV Subjects of Battery Degradation Testing | 133 |
| Table IV-15: Technology Configurations for Baseline and Complete-Cab Package Experimental Evaluations | 140 |
| Table IV-16: Percent Improvement in Daily A/C Load for Varying Curtain Configurations Combined With Ultra-White Paint and Advanced Insulation Package | 141 |
| Table IV-17: Federal Way Vehicles Monitored in Second Logger Deployment | 146 |
| Table IV-18: Platooning Test Matrix | 149 |
| Table IV-19: Percent Fuel Saved (Gravimetric) of Platooned Tractors | 149 |
| Table IV-20: Hybrid Propulsion-Related Systems | 151 |
| Table V-1: Overall vehicle specifications for BEV with one energy storage system (1-ESS BEV) | 156 |
| Table V-2: Cost of manufacturing and owning a BEV 300 with one battery that provides both energy and power | 157 |
| Table V-3: Cost comparison of battery systems and vehicles | 157 |
| Table V-4: Overall vehicle specifications for 2-ESS BEV | 158 |
| Table V-5: Vehicle specifications | 162 |
| Table V-6: Fuel consumption and emissions with diesel fuel for the GM 1.9-L TDI engine, from engine-in-the-loop data | 163 |
| Table V-7: Impact of downspeeding on fuel consumption and emissions (mean values) | 164 |
| Table V-8: Engine resizing for the conventional and the BISG powertrain to match the IVM-60 mph performance for the three engines | 164 |
| Table V-9: Fuel economy benefits of LTC compared to PFI and SIDI (simulation study results) for BISG powertrain with earlier-generation bsfc map | 164 |
| Table V-10: Fuel economy benefits of LTC compared to PFI and SIDI (simulation study results) for conventional powertrain with updated bsfc map | 164 |
| Table V-11: Comparative Results for Fuel Consumption and Final SOC between Test Data and Simulation Results on the HWFET Cycle | 192 |

| | |
|--|-----|
| Table V-12: Performance of Original Algorithm and Improved One with Bi-Directional Markov Chains | 203 |
| Table V-13: Vehicle Specifications | 207 |
| Table V-14: Transmission and Final Drive Ratios..... | 208 |
| Table V-15: Matrix of test conditions run at APRF (16 tests in total) | 221 |
| Table V-16: Cumulative fuel error between measured test data and the model estimate (positive error indicates model overestimation)..... | 222 |
| Table V-17: Root-mean-square error for engine oil temperature between measured test data and the model estimate | 223 |
| Table V-18: Root mean square error for engine coolant temperature between measured test data and the model estimate | 223 |
| Table V-19: Engine Peak Efficiencies for Gasoline | 236 |
| Table V-20: Electric Machine Assumptions | 236 |
| Table V-21: Battery Energy Density and Cost for High Energy Applications..... | 236 |
| Table V-22: Glider Weight, Aerodynamic, and Tire Assumptions..... | 236 |
| Table V-23: Vehicle specifications | 250 |
| Table V-24: Shifting Algorithm Model Validation for 2013 VW Jetta Conventional Vehicle and HEV | 252 |
| Table V-25: Vehicle specifications | 253 |
| Table V-26: Shifting Algorithm Model Validation for 2013 Nissan Altima Conventional Vehicle and 2013 Honda Civic HEV | 254 |
| Table V-27: Percent improvement for technology combinations for cooling and heating daily loads at the 95th percentile | 261 |
| Table VII-1: Modelled vehicle vs chassis roll data (HD class 8 line haul sleeper cabin) | 301 |
| Table VII-2: Accessory entitlements for the Manhattan Cycle (HD class 8 transit bus)..... | 302 |
| Table VII-3: Accessory entitlements for the HTUF6 Cycle (MD class 6 P&D vehicle)..... | 302 |
| Table VII-4: Accessory entitlements for the Cummins Proprietary Cycle (HD class 8 line haul sleeper cabin)..... | 302 |
| Table VII-5: GE smart grid enabled EVSE efficiency testing | 308 |
| Table VII-6: EVSE standby power (watts)..... | 308 |
| Table VII-7: EVSE Participants | 309 |
| Table VII-8: Vehicle Participants..... | 309 |
| Table VII-9: Standardized debris test items | 310 |
| Table VII-10: Class 8 Truck Power Level Characterization Over Sections of the 5-Day Driving Sample with Positive Grade..... | 316 |
| Table VII-11: Class 8 Truck Fuel Economy Results | 317 |
| Table VII-12: Assumptions for Class 8 Truck Cost vs. Benefit Analysis, With In-Motion WPT on Interstate Highway Road Segments Having Grades of 1.5% or Greater | 317 |
| Table VII-13: Linear regression coefficients of FMEP for a HDDE | 321 |
| Table VII-14: Engine Conditions | 322 |
| Table VII-15: Calculated fuel savings for NEDC in different classes of gasoline and diesel automotive vehicles..... | 326 |
| Table VII-16: EV Smart Grid Lab Roles and Responsibilities | 335 |
| Table VII-17: Materials and Dimensions of Each Layer..... | 340 |
| Table VII-18: Comparison of Convection and Subcooled Boiling | 344 |
| Table VII-19: Heavy-duty vehicle wind-tunnel operating conditions for aerodynamic drag simulations | 346 |
| Table VII-20: Heavy-duty vehicle wind-tunnel operating conditions for underhood simulations..... | 346 |
| Table VII-21: Conventional vehicle normalized aerodynamic drag..... | 347 |
| Table VII-22: Cab-over engine vehicle normalized aerodynamic drag | 347 |
| Table VII-23: Cabin-trailer gap sensitivity analysis of Cab-over engine at three yaw angles (normalized aerodynamic drag profiles) | 348 |
| Table VII-24: Conventional and cab-over engine thermal performance data of CAC, radiator, and fan | 349 |

I. INTRODUCTION

On behalf of the Vehicle Technologies Office (VTO) of the U.S. Department of Energy (DOE) we are pleased to submit the Annual Progress Report for Fiscal Year (FY) 2014 for the Vehicle and Systems Simulation and Testing (VSST) program activities.

Mission and Objectives

VSST is concerned with advancing light-, medium-, and heavy-duty (HD) vehicle systems to support DOE goals of reducing petroleum consumption, and reducing greenhouse gas (GHG) emissions in the U.S. transportation sector. To help reach those goals, VTO conducts research and development (R&D) programs implementing strategies to help maximize the number of electric vehicle miles driven, and increase the energy efficiency of transportation vehicles.

VSST's R&D mission is to accelerate the market introduction and penetration of advanced vehicles and systems that have a significant impact on petroleum displacement, GHG reduction, and vehicle electrification goals.

Figure I-1 below outlines the outcome objectives that VSST uses to fulfill its mission.

Figure I-2 lists the primary processes and examples of tangible R&D project objectives that contribute to one or more VSST outcome objectives.

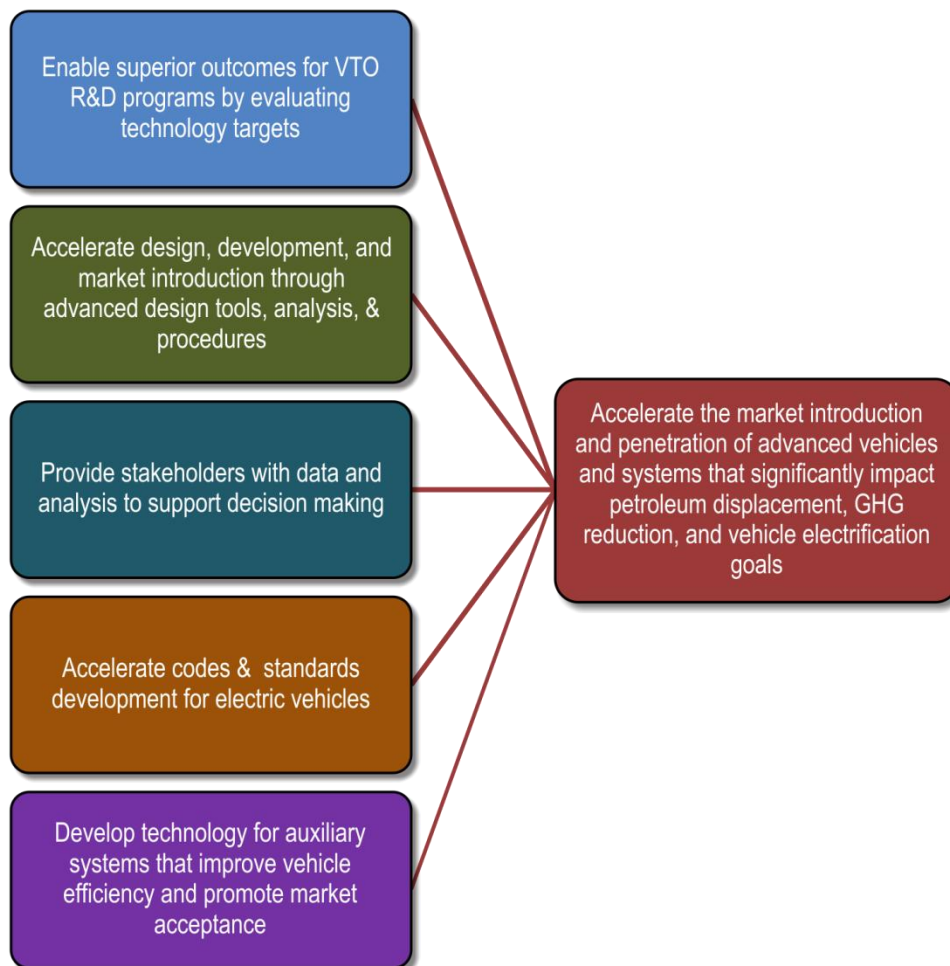


Figure I-1 : VSST outcome objectives and mission

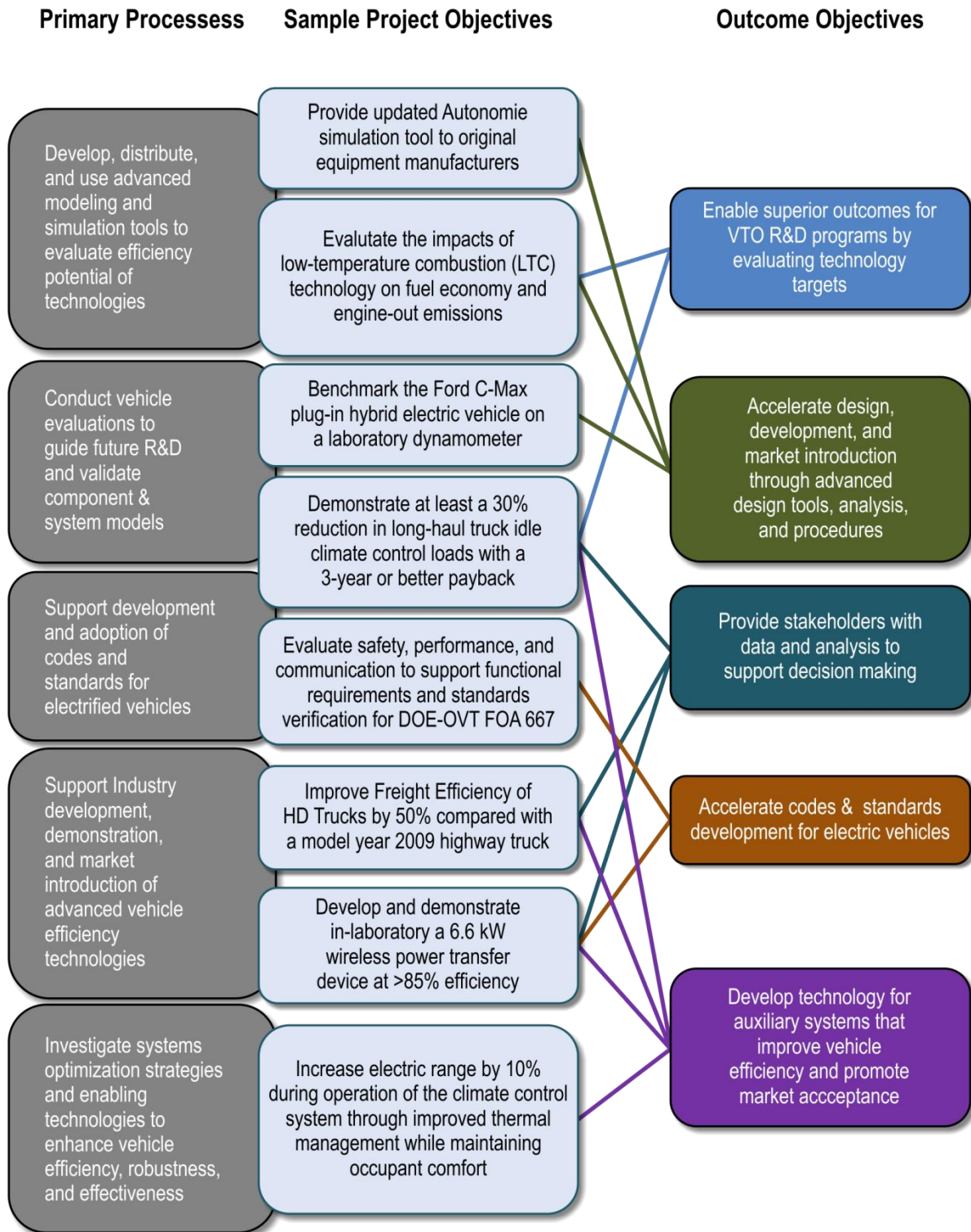


Figure I-2 : VSST primary processes, project objectives, and outcome objectives

Major Accomplishments for FY 2014

- Developed and applied engineering procedures to address vehicle operations that have an adverse impact on the energy efficiency of light-duty electric vehicles:
 - NREL collaborated with Argonne National Laboratory (ANL) to quantify impacts of cold starts on fuel economy. The project created a detailed engine fuel use model from high-resolution thermal test data, and then incorporated this model in a large-scale simulation of real-world speed/acceleration traces, grade profiles, and ambient temperatures. The results suggest that engine thermal effects plus enrichment could account for 8% of real-world fuel consumption, and that cold-start mitigation techniques may yield greater real-world fuel savings than would be reflected in standard test cycles. Because of the prevalence of internal combustion engine (ICE) vehicles, even a modest fuel savings of 1% applied across the fleet would have an impact equivalent to taking 2.5 million vehicles off the road (see V.L.).
- Evaluated the contributions of advanced component technologies to vehicle system performance:
 - Evaluated low-energy energy storage systems (LEESS) for potential to increase hybrid electric vehicle (HEV) market penetration. The cooperative research and development activity (CRADA) with Ford exercised a test platform to evaluate LEESS devices that were provided by system suppliers (see V.C.).
 - Evaluated the impacts of low-temperature combustion (LTC) technology on fuel economy and engine-out emissions by using simulation. Completed a simulation study comparing the fuel economy benefits of LTC to those of port fuel injection (PFI) and spark ignition direct injection (SIDI) (see V.B.).
 - Benchmarked eight advanced-technology production vehicles ranging from conventional to plug-in hybrids (see IV.C and IV.D.).
- Developed technologies and designs that address objectives:
 - Combined fluid loop (CFL) systems show potential to increase electric drive vehicle (EDV) driving range by 9%. The National Renewable Energy Laboratory (NREL) completed bench testing of a CFL system developed to reduce vehicle thermal management energy consumption and increase EDV range. Using a concept developed at NREL and components provided by industry partners Delphi and Halla Visteon Climate Control, NREL built a prototype system to meet the thermal demands of all EDV systems without separate cooling loops. This CFL system was tested in an environmental chamber at temperatures from 10°F to 109°F. In cold conditions, the waste heat recovered from the power electronics and electric motor increased driving range by ~2%. Realizing the benefits of heat pump operation, when the CFL system was weighted for summer/winter ambient temperature during real-world vehicle use, range increased by 9%. This technology is being developed and demonstrated by a Delphi/NREL partnership under a VTO funding opportunity announcement (FOA) project awarded in FY 2014 (see V.O.).
 - Experimental heat transfer measurements for water/ethylene glycol coolants have been completed in the subcooled nucleated boiling regime. Models to predict the heat transfer behavior have been developed that correlate well with the experiments. These models and experiments have implications in cooling applications from heavy-duty (HD) engines to power electronics in which subcooled nucleated boiling as a heat transfer mechanism can be deployed with significantly enhanced performance as compared to baseline convective heat transfer (see VII.M. and VII.J.).
 - HD truck petroleum consumption is decreased via reduced aerodynamic drag (see VII.O.).
 - Improved technologies can increase the convenience of recharging electric vehicles. Wireless power transfer (WPT) projects led by Hyundai North America and Oak Ridge Nation Laboratory (ORNL) developed laboratory prototypes of high-power chargers for light-duty (LD) vehicles (see III.F. and III.E.).
 - Vehicle-to-building (V2B) load balancing scenarios were analyzed to determine the number of V2B-capable vehicles required to significantly reduce a building's local peak demand charges. The analysis revealed that application of V2B technologies to 20% of commercial buildings could require as many as 1 million–2.5 million vehicles, each capable of delivering 6 kW. Break-even projections for the technology required to implement these systems and diminish monthly loads by 5% demonstrated the greatest potential with installation of low-cost elements in small commercial buildings of 25,000 square feet or less. Conclusions suggest that even with low-power (6 kW–10 kW) systems, value creation is possible (see VII.G.).

- The CoolCab project enabled reduction in long-haul truck idle loads to help move toward electric heating, ventilation and air conditioning (HVAC). Based on CoolCalc modeling results, NREL configured and tested a long-haul truck rest period idle climate control load reduction package with ultra-white paint, advanced insulation, and advanced curtains. NREL measured more than a 35.7% reduction in daily electric air conditioning load, exceeding the project target. Climate control load reduction has the potential to help reduce the 667 million gallons used annually for long-haul truck rest period idling in the United States (see IV.I).
- Platooned trucks were tested to demonstrate 6.4% fuel savings. NREL partnered with Intertek to test the impact of semi-autonomous Peloton technology platooning equipment on the fuel efficiency and emissions performance of Class 8 line-haul trucks. Using SAE Type II track testing, NREL evaluated two platooned vehicles outfitted with vehicle-to-vehicle communications, as well as radar-based active braking systems and controls, across a range of speed profiles and distances between the lead and following truck. Tests showed a combined “team” fuel savings of both trucks ranging from 3.7% to 6.4%. Study results were published in an SAE paper titled “Effect of Platooning on Fuel Consumption of Class 8 Vehicles Over a Range of Speeds, Following Distances, and Mass,” presented at the 2014 SAE Commercial Vehicle Engineering Conference (see III.A. and IV.J.).
- Provided stakeholders with data and analysis:
 - Research results from one project were used to support off-cycle GHG credits (EPA 2017–2025). The U.S. Environmental Protection Agency (EPA) significantly leveraged NREL/DOE vehicle ancillary load reduction research to support the off-cycle GHG credits under the 2017–2025 CAFE/GHG regulation. Along with using NREL air conditioning (A/C) fuel use calculations, EPA used NREL research results to determine credits for solar reflective glass, climate control seats, solar reflective paint, and cabin ventilation. These credits provide motivation for automobile manufacturers to incorporate energy efficient technologies (see IV.I. for load reduction activities).
 - Vehicle accessory load analysis and characterization was conducted on several vehicle models as part of the advanced vehicle testing activity (AVTA) on-road vehicle evaluation. This effort responds to a request from Chrysler, Ford, and General Motors in regard to off-cycle fuel economy credits. The analysis details the accessory load of conventional vehicles (non-electric) and how it is affected by various driving and ambient conditions (see IV.A. and III.A.).
 - An electric vehicle miles traveled (eVMT) analysis was conducted on 158,000,000 miles of on-road data from 21,600 plug-in hybrid electric vehicles and battery electric vehicles in collaboration with Honda, Ford, Toyota, and General Motors. The results showed the three all-electric vehicles ranged in annual eVMT from 9,550 miles to 9,700 miles, and the PHEVs’ annual eVMT ranged from 2,500 miles to 9,100 miles. Per the request of the automotive manufacturers, the results were presented twice to the California Air Resources Board in regards to zero-emissions vehicle credit on the Advanced Clean Cars Program Mid-Term Review (see IV.A.).
 - One electric vehicle project’s goal (titled the EV Project) was to develop a real-world laboratory of plug-in electric vehicle charging infrastructure that can be used to understand how, where, and when electric vehicle supply equipment (EVSE) and DC fast chargers are used in order to support the design of future EVSE deployments, thus reducing the costs and risks of future deployments. With the last set of EV Project data collected in September 2014, more than 60 additional lessons learned white papers have been identified for analysis. To date, 650 white papers, technical and quarterly reports, and presentations have been produced for governments, universities, air quality management districts, automotive and EVSE manufacturers, utility companies, and miscellaneous requesting organizations (see IV.A.).
 - NREL has compiled an extensive database and developed online reporting based on medium-duty and HD all-electric vehicle demonstration projects originally funded through the American Recovery and Reinvestment Act of 2009. NREL collected 25 channels of 1-Hz propulsion system operation, use, and performance data from 560 medium-duty electric commercial fleet vehicles and 50 Shorepower Technologies electrified truck stops across the United States. The project collected, compiled, and analyzed data from 459 Smith electric vehicles and 101 Navistar electric delivery vehicles operated by participating fleets including Frito-Lay, Staples, FedEx,

Duane Reade, PG&E, and Coke. The project has amassed data on a collective 150,972 vehicle days and 3.75 million miles of operation (see IV.G.).

- Fostered superior outcomes from VTO component research programs by providing system-level requirements:
 - A modeling and simulation study was performed in collaboration with USDrive's ACEC (Advanced Combustion and Emission Control) Tech Team and leveraged advanced engine models from IAV. One of the main outcomes was a recommendation to the ACEC to revisit their current targets to better represent where future engines will operate. Additionally, energy consumption was quantified for 17 engine technologies for multiple transmissions (e.g., automatic, dual-clutch transmission, and continuously variable transmission) and powertrain configurations (e.g., conventional, start–stop, and hybrid electric vehicle) (see V.J.).
 - Pacific Northwest National Laboratory (PNNL) evaluated the economics of using plug-in electric vehicle and V2G charging as a grid resource, and tested foundational capabilities needed to develop a realistic plug-in electric vehicle/grid integration value proposition (see VI.D.).
- Accelerated the development of codes & standards for electric vehicles:
 - The SAE J2953 electric vehicle interoperability standard, interoperability requirements, and verification test procedures developed by ANL were issued as recommended standard practices via the SAE consensus-based process with industry and other stakeholders (see VI.A.).
 - The AC InterOP Test Fixture (Version 2) was used to verify compliance with the SAE J2953 standard. The first test fixture was transferred to a DOE project to test production electric vehicles and electric vehicle supply equipment (EVSE) (see VI.A.).
 - The plug-in electric vehicle compliance test tool, smart Level 2 AC EVSE, is based on Argonne's SpEC module. The tool tests for compliance with the SAE J1772 charge coupler standard (see VI.A.).
 - One project investigated industrial applications of the SpEC module, communication controllers for a DC fast charging power system (to emulate a vehicle and/or EVSE), and combined AC/DC charging (see VI.A.). Commercialization of the SpEC module was recognized with a Federal Lab Consortium (FLC) Award for Technology Transfer (see VI.A.).
- Provided tools that accelerate development of advanced vehicles by U.S. OEMs and enable assessments on the impact of advanced component technologies on system performance. The assessments are used to guide component R&D:
 - The Autonomie simulation environment was enhanced and maintained to support the U.S. Department of Energy (DOE), the user community, and hardware-in-the-loop/rapid control prototyping (HIL/RCP) projects. All major U.S. vehicle OEMs hold licenses for Autonomie (see V.K.).
 - One activity developed comprehensive thermal models and controllers for vehicle components such as the engine, battery, and cabin system of the Toyota Prius plug-in electric vehicle (see V.G.). Models and controllers developed are compatible with Autonomie.
 - The CoolCalc modeling tool was developed to help quantify the impact of advanced load reduction technologies for HD trucks (see V.Q). Developed an A/C component model that improves the robustness and accuracy of the fully detailed A/C system model (see VII.O.).
 - ANL developed an analytical model to quickly predict the improvement in fuel economy that can be expected with the use of advanced low-friction, low-viscosity lubricants. The rapid prediction model enables one to quickly estimate the impact of advanced lubrication technologies on fuel economy gains without performing costly, complex simulations of losses (see VII.E.).

I.A. Approach and Organization of Activities

VSST groups its projects into focus area activity categories that implement its primary processes (see Figure I-2). In FY 2014, these focus areas were Modeling and Simulation (M&S), Vehicle Technology Evaluations (VTE), Codes and Standards (C&S), Industry Projects, and Vehicle Systems Efficiency Improvements (VSEI).

Projects within each focus area typically produce outputs in one or more of the following forms: data, analysis, reports, tools, specifications, and procedures. The outputs from one project are often used as the inputs for one or more projects in other focus areas. The integration of computer modeling and simulation, laboratory and field vehicle evaluations, and codes and standards development and validation for vehicle classes from LD to HD is critical to the success of the VSST program. Information exchange between focus area activities enhances the effectiveness of each activity (illustrated in Figure I-3).



Figure I-3: VSST activities integration – Arrows represent information flow between activity focus areas that enhances effectiveness of individual activities.

An example of beneficial data exchange is the increased accuracy of predictive simulation models for advanced technology vehicles made possible by empirical test data that characterize a vehicle's real-world performance. (In the example case, vehicle technology evaluation activities feed information to the M&S activity). Another example is that the credibility and scope of laboratory and field technology evaluation studies benefit from real-world performance data collected from thousands of advanced technology vehicles from the vehicle electrification demonstration projects.

VSST provides an overarching vehicle systems perspective in support of the technology R&D activities of DOE's VTO and Hydrogen Fuel Cells Technologies Program (HFCTP). VSST uses analytical and empirical tools to model and simulate potential vehicle systems, validate component performance in a systems context, verify and benchmark emerging technologies, and validate computer models. HIL testing allows components to be controlled in an emulated vehicle environment. Laboratory testing then provides measurement of progress toward VTO technical goals and eventual validation of DOE-sponsored technologies at the Advanced Powertrain Research Facility (APRF) for light- and medium-duty vehicles and at NREL's Renewable Fuels and Lubricants (ReFUEL) facility for HD vehicles. For this program to be successful, extensive collaboration with the technology development activities within the VTO and HFCTP is required for both analysis and testing. Analytical results of this sub-program are used to estimate national benefits and/or impacts of DOE-sponsored technology development (illustrated in Figure I-4).

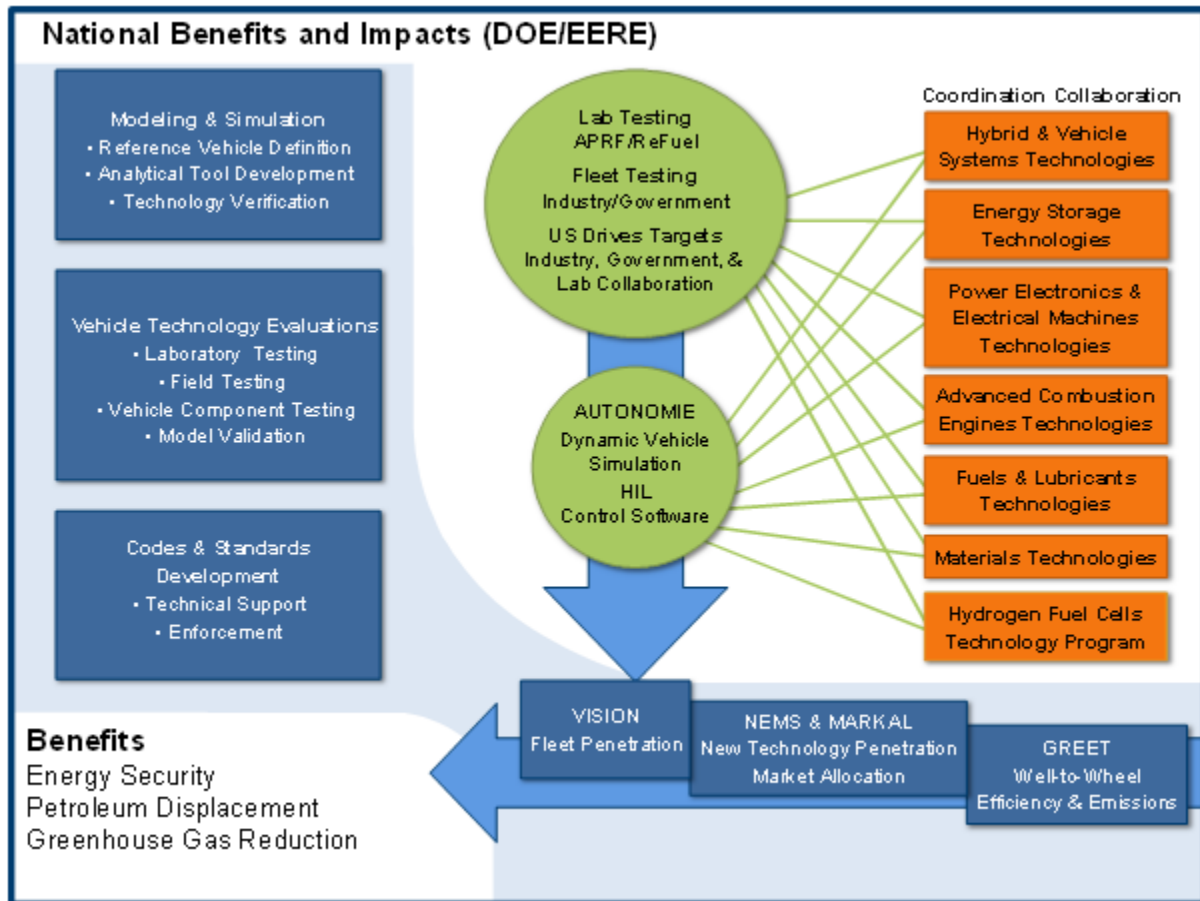


Figure I-4: VSST activities providing estimates of national benefits and impacts of advanced technologies.

VSST R&D activities are performed by the national laboratories and industry. National laboratory R&D activities are organized into the four focus areas. A brief description of each focus area and its major accomplishments for FY 2014 are outlined below.

1. Modeling and Simulation

DOE has developed and maintains software tools that support VTO research. VISION, NEMS, MARKAL, and GREET are used to forecast national-level energy, environmental, and economic parameters, including oil use, market impacts, and GHG contributions of new technologies. These forecasts are based on VTO vehicle-level simulations that predict fuel economy and emissions using VSST's Autonomie modeling tool. Autonomie's simulation capabilities allow for accelerated development and introduction of advanced technologies through computer modeling rather than through expensive and time-consuming hardware building. Modeling and laboratory and field testing are closely coordinated to enhance and validate models as well as ensure that laboratory and field test procedures and protocols comprehend the needs of new technologies that may eventually be commercialized.

Autonomie is a MATLAB-based software environment and framework for automotive control system design, simulation, and analysis. This platform enables dynamic analysis of vehicle performance and efficiency to support detailed design, hardware development, and validation. Autonomie was developed under a CRADA with General Motors and included substantial input from other OEMs, and replaces its predecessor, the Powertrain Systems Analysis Toolkit (PSAT). One of the primary benefits of Autonomie is its plug-and-play foundation, which allows integration of models of various degrees of fidelity and abstraction from multiple engineering software environments. This single powerful tool can be used throughout all the phases of model-based design of the vehicle development process (VDP).

HIL simulation provides a novel and cost-effective approach to isolate and evaluate advanced automotive component and subsystem technologies while maintaining the rest of the system as a control. HIL allows actual hardware components to be tested in the laboratory at a full vehicle level without the extensive cost and lead time of building a complete prototype vehicle. This approach integrates modeling and simulation with hardware in the laboratory to develop and evaluate propulsion subsystems in a full vehicle-level context. The propulsion system hardware components—batteries, inverters, electric motors, and controllers—are further validated in simulated vehicle environments to ensure that they meet the vehicle performance targets established by the government–industry technical teams.

High-energy traction battery technology is important to the successful development of plug-in electric vehicles. To support the evaluation of advanced prototype energy storage systems, in FY 2014 Idaho National Laboratory (INL), with assistance from ORNL, continued to develop and implement the electric drive advanced battery (EDAB) test platform. This testbed allows advanced battery packs to be evaluated in real-world operating conditions in an on-road vehicle that emulates a variety of electric drive powertrain architectures.

2. Vehicle Technology Evaluations

This section describes the activities related to laboratory validation and fleet testing of advanced propulsion subsystem technologies and advanced vehicles. In laboratory benchmarking, the objective is to test production vehicle and component technology to ensure that VTO-developed technologies represent significant advances over technologies that have been developed by industry. Technology validation involves the testing of DOE-developed components or subsystems to evaluate the technology in the proper systems context. Validation helps to guide future VTO research and facilitates the setting of performance targets.

The facilities that perform laboratory and field testing include the APRF, INL's transportation testing facilities, NREL's ReFUEL and thermal test facilities, and ORNL's Vehicle Systems Integration (VSI) laboratory.

The APRF is equipped with dynamometers (for testing integrated components such as engines, electric motors, and powertrains), and a thermal chamber (for testing battery electric vehicles, hybrid electric vehicles, and plug-in hybrids in temperatures from as low as 20°F to as high as 95°F).

INL's transportation testing facilities encompass the Advanced Vehicle Test and Evaluation Activity (AVTE) facility for LD vehicles, the Heavy Duty Transportation Test Facility, and the Energy Storage Technologies Laboratory. AVTE's capability to securely collect, analyze, and disseminate data from multiple field tests located throughout the United States is critical to VSST laboratory and field activities.

NREL's ReFUEL facility is equipped with dynamometers for testing medium-duty vehicles and components. NREL's thermal test facilities have capabilities for LD vehicle cabin thermal studies and outdoor HD vehicle cabin studies. NREL also has facilities for testing subsystems (such as energy storage systems and EVSE) and functions as the VSST data collection and evaluation hub for medium-duty and HD vehicle fleet tests.

ORNL's facilities for integrated testing include advanced engine technologies (e.g., advanced combustion modes, fuels, thermal energy recovery, and emissions after-treatment), advanced power electronics and electric machines (e.g., motor drives, components, power electronics devices, and advanced converter topologies), and vehicle testing and evaluation (e.g., chassis and component dynamometers, integrated powertrain stands, test track evaluations, and field operational testing).

The AVTE, working with industry partners, conducts field and fleet testing to accurately measure real-world performance of advanced technology vehicles via a testing regime based on test procedures developed with input from industry and other stakeholders. The performance and capabilities of advanced technologies are benchmarked to support the development of industry and DOE technology targets. The testing results provide data for validating component, subsystem, and vehicle simulation models and hardware-in-the-loop testing. Fleet managers and the public use the test results for advanced technology vehicle acquisition decisions. INL conducts LD testing activities. In FY 2014, INL continued its partnership with an industry group led by Intertek. Accelerated reliability testing provides reliable benchmark data of the fuel economy, operations and maintenance requirements, general vehicle performance, engine and component (such as energy storage system) life, and life cycle costs. These tests are described below.

Baseline Performance Testing

The objective of baseline performance testing is to provide a highly accurate snapshot of a vehicle's performance in a controlled testing environment. The testing is designed to be repeatable. Hence it is conducted on closed tracks and dynamometers, providing comparative testing results that allow "apples-to-apples" comparisons within respective vehicle technology classes. The APRF at ANL is used for the dynamometer testing of the vehicles.

Fleet Testing

Fleet testing provides a real-world balance to highly controlled baseline performance testing. Some fleet managers prefer fleet testing results to the more controlled baseline performance or the accelerated reliability testing.

During fleet testing, a vehicle or group of vehicles is operated in normal fleet (field) applications. Operating parameters such as fuel use, operations and maintenance, costs/expenses, and all vehicle problems are documented. Fleet testing usually lasts one to three years and, depending on the vehicle and energy storage technology, between 5,000 and 12,000 miles are accumulated on each vehicle.

For some vehicle technologies, fleet testing may be the only viable test method. Neighborhood electric vehicles are a good example. Their manufacturer-recommended charging practices often require up to 10 hours per charge cycle, while they operate at low speeds (<26 mph). This makes it impractical to perform accelerated reliability testing on such vehicles.

Accelerated Reliability Testing

The objective of accelerated reliability testing is to quickly accumulate several years or an entire vehicle-life's worth of mileage on each test vehicle. The tests are generally conducted on public roads and highways, and testing usually lasts for up to 36 months per vehicle. The miles to be accumulated and time required depend heavily on the vehicle technology being tested. For instance, the accelerated reliability testing goal for plug-in hybrid electric vehicles and battery electric vehicles is to accumulate 12,000 miles per vehicle in one year, while the testing goal for hybrid electric vehicles is to accumulate 160,000 miles per vehicle within three years. This is several times greater than most hybrids will be driven in three years, but it is required to provide meaningful vehicle-life data within a useful time frame. Generally, two vehicles of each model are tested to ensure accuracy. Ideally, a larger sample size would be tested, but funding tradeoffs necessitate testing only two of each model.

Depending on the vehicle technology, a vehicle report is completed for each vehicle model for both fleet and accelerated reliability testing. However, because of the significant volume of data collected for hybrid electric vehicles, the test results are published in the form of summary fleet testing fact sheets (including accelerated reliability testing) and maintenance sheets.

3. Codes and Standards Development

A comprehensive and consistent set of codes and standards addressing grid-connected vehicles and infrastructure is essential for the successful market introduction of electric drive vehicles. The VTO is active in driving the development of these standards through committee involvement and technical support by the national laboratories. The VTO also supports activities of the U.S. DRIVE's Grid Interaction Tech Team (GITT), a government/industry partnership aimed at ensuring a smooth transition for vehicle electrification by closing technology gaps that exist in connecting vehicles to the electric grid. In FY 2014, GITT worked with PNNL and ANL to participate in SAE and National Institute of Standards and Technology (NIST) standards development for connectivity and communication for grid-connected vehicles.

The consumer markets for electric vehicles transcend national boundaries. ANL was employed in international cooperative initiatives to adopt international electric drive vehicle standards and promote market penetration of grid-connected vehicles. Many new technologies require adaptations and more careful attention to specific procedures. ANL supported development of interoperability validation procedures and operated the SmartGrid Joint Interoperability Center as the U.S. base for international cooperative work between the European Union and U.S. energy R&D laboratories.

4. Vehicle Systems Efficiency Improvements

This focus area involves R&D on a variety of mechanisms to improve the energy efficiency of LD, medium-duty, and HD vehicles. Projects involve reducing the aerodynamic drag of vehicles, thermal management approaches to increase the engine thermal efficiency and reduce parasitic energy losses, the development of advanced technologies to improve the fuel efficiency of critical engine and driveline components by characterizing the fundamental friction and wear mechanisms, and fast and wireless charging technology development.

Aerodynamic Drag Reduction

The primary goal of this focus area is improving the freight efficiency of vehicles. Aerodynamic drag reduction, thermal management, and friction and wear are the main focuses of this area. Reduction of aerodynamic drag in Class 8 tractor-trailers can result in a significant improvement on fuel economy while satisfying regulatory and industry operational constraints. An important part of this effort is to expand and coordinate industry collaborations with DOE and establish buy-in through CRADAs and to accelerate the introduction of proven aerodynamic drag reduction devices into new vehicle offerings.

The primary approach in drag reduction is through the control of the vehicle's flow field. This can be achieved with geometry modifications, integration, and flow conditioning. During 2014, the goal of the research was to develop and design the next generation of aerodynamically integrated tractor-trailers.

Thermal Management

Thermal management of vehicle engines and support systems is a technology area that addresses reduction in energy usage through improvements in engine thermal efficiency and reductions in parasitic energy uses and losses. Fuel consumption is directly related to the thermal efficiency of engines and support systems. New methods to reduce heat-related losses are investigated and developed under this program.

FY 2014 thermal management R&D focused on exploring:

- The possibilities of repositioning the Class 8 tractor radiator and modifying the frontal area of the tractor to reduce aerodynamic drag
- The possibilities of using evaporative cooling under extreme conditions of temperature and engine load
- The assessment of use of nanofluids to cool power electronics.

Friction and Wear

Parasitic engine and driveline energy losses arising from boundary friction and viscous losses consume 10% to 15% of fuel used in transportation, and thus engines and driveline components are being redesigned to incorporate low-friction technologies to increase fuel efficiency of passenger and HD vehicles. Research to improve the fuel efficiency and reliability of critical engine and driveline components included:

- Experimentally investigating fundamental friction and wear mechanisms
- Modeling and validating the impact of friction on components and overall vehicle efficiency
- Developing advanced low-friction technologies (materials, coatings, engineered surfaces, and advanced lubricants)
- Developing requirements of a high-power density driveline system that can be applied across many of the vehicle types regardless of the powertrain or fuel type.

Fast and Wireless Charging

Electrification of the transportation sector will be enabled by charging technologies that minimize costs in terms of time and money while maximizing energy throughput, battery life, safety, and convenience.

Industry Awards

Industry projects for FY 2014 include the categories of transportation electrification, SuperTruck, wireless charging, zero-emissions cargo transport (ZECT), and energy load reduction and management. In FY 2014, the following new projects were added to the VSST portfolio:

- Design and Implementation of a Thermal Load Reduction System in a Hyundai PHEV to Improve Range
- Unitary Thermal Energy Management for Propulsion Range Augmentation (UTEMPRA)
- Multi-Speed Gearbox for Commercial Delivery Medium-Duty Plug-In Electric Drive Vehicles

- Integrated Boosting and Hybridization for Extreme Fuel Economy and Downsizing
- Friction and Wear Reduction.

The new technology development and demonstration projects listed above were awarded through DOE's competitive solicitation process and involve resource matching by DOE and industry.

This report describes major projects conducted by the national laboratories and industry partners in support of these areas in FY 2014. The reports describe the approaches, accomplishments and future directions for the projects. For further information on an individual project, please contact the DOE project leader.

I.B. Future Directions for VSST

Near-term solutions for reducing the nation's dependence on imported oil, such as plug-in hybrid electric vehicles, will require the development, integration, and control of vehicle components, subsystems, and support systems. These solutions will require exploration of high-capacity energy storage and propulsion system combinations to get the most out of hybrid propulsion. Analysis and testing procedures at the national laboratories will be enhanced to study these advanced powertrains with simulation tools, component/subsystem integration, and hardware-in-the-loop testing. DOE-sponsored hardware developments will be validated at the vehicle level, using a combination of testing and simulation procedures.

In FY 2015, the VSST will continue activities in the area of vehicle M&S and laboratory and field testing, including further baseline performance testing of conversion and OEM electric drive vehicles. Field and laboratory testing will continue to be integrated with M&S activities, including validation of simulation models for advanced vehicles tested in the APRF. Fleet evaluation of plug-in vehicles will continue, with continued emphasis on evaluation fleets of OEM production vehicles.

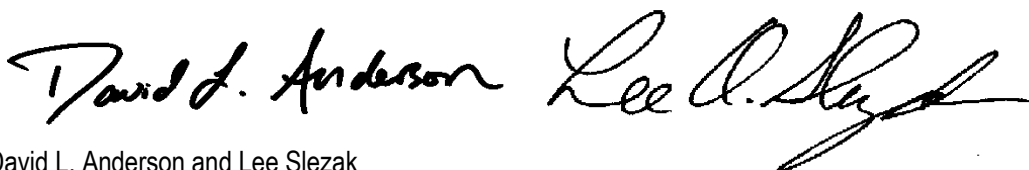
In addition to the hybrid electric vehicle and plug-in hybrid electric vehicle activities, a full range of simulation and evaluation activities will be conducted on battery electric vehicles as they are brought to market by OEMs. Because electric vehicles are dependent on a robust charging infrastructure for their operation and ultimate consumer acceptance, VSST will greatly increase efforts to address issues related to electric vehicle codes and standards, charging infrastructure, and vehicle/grid integration.

VSST will pursue the objective of using less energy for cabin climate control of LD and HD vehicles. This work will contribute to progress on reaching the DOE *EV Everywhere* Grand Challenge Blueprint's Efficient Climate Control Technologies Objective and the VSST 2015 target objective to increase freight efficiency of HD vehicles by 50% through system-level innovations.

VSST will also be continuing the collection and analysis of data from the American Recovery and Reinvestment Act of 2009 Transportation Electrification Demonstration projects. These eight demonstrations have placed several thousand electric drive vehicles and recharging stations in service, and VSST will direct the collection and analysis of data from these units. In addition to performance, reliability, and petroleum displacement results, VSST will use the data to determine the impact of concentrations of electric drive vehicles on the electricity grid, as well as the changes in operators' driving and recharging patterns as they become more comfortable with this new technology.

Vehicle systems efficiency improvement work in the areas of aerodynamics, thermal management, grid integration, zero emission cargo transport, and friction and wear will continue. The focus of these activities will revolve around cooperative projects with industry partners with the goal of bringing developed technologies to market quickly. New efforts will be supported to conduct evaluations of methods to improve thermal heat transfer efficiencies and reduce parasitic loads with coordination from industry partners. Additionally, activities to develop solutions for wireless power transfer and fast charging of electric drive vehicles, while evaluating the market barriers and technology impacts for deploying this infrastructure, will continue to ramp up within the VSEI area.

Inquiries regarding the VSST activities may be directed to the undersigned.



David L. Anderson and Lee Slezak
Technology Managers
Vehicle and Systems Simulation and Testing Program
Vehicle Technologies Office

II. THE EV EVERYWHERE GRAND CHALLENGE

II.A. Background

In March 2012, President Obama announced the *EV Everywhere* Grand Challenge: to produce plug-in electric vehicles (PEVs) as affordable and convenient for the American family as gasoline-powered vehicles by 2022. Realizing the promise of PEVs is one of the grand challenges of this era. Today, our transportation system is dependent on internal combustion engines and oil. In fact, 93% of our transportation fuel is derived from petroleum, and much of this is imported. PEVs can decouple personal mobility from oil, cut pollution, and help build a 21st century American automotive industry that will lead the world.

America is the world's leading market for electric vehicles and is producing some of the most advanced PEVs available today. Consumer excitement and interest in PEVs continues to grow—in 2014, PEV sales in the United States increased by 23%, with more than 118, 773 cars sold.

PEVs have won critical acclaim with awards such as the 2011 World Car of the Year (Nissan Leaf), 2013 Motor Trend Car of the Year (Tesla Model S), and 2012 Green Car Vision Award Winner (Ford C-MAX Energi). To maintain this leadership, strong growth in the U.S. PEV sector will need to continue.

The Department of Energy (DOE) developed an *EV Everywhere* “Blueprint” document that provides an outline for technical and deployment goals for PEVs over the next five years: energy.gov/eere/vehicles/downloads/ev-everywhere-grand-challenge-blueprint. DOE will pursue these targets in cooperation with a host of public and private partners. The technical targets for the DOE PEV program fall into four areas: battery R&D, electric drive system R&D, vehicle lightweighting, and advanced climate control technologies. Some specific goals include:

- Cutting battery costs from their current \$500/kWh to \$125/kWh.
- Reducing the cost of electric drive systems from \$30/kW to \$8/kW.
- Eliminating almost 30% of vehicle weight through lightweighting.

These numbers represent difficult-to-reach “stretch goals” established in consultation with stakeholders across the industry—including the *EV Everywhere* workshops held during the summer and fall of 2012. When these goals are met, the levelized cost of an all-electric vehicle with a 280-mile range will be comparable to that of an internal combustion engine (ICE) vehicle of similar size. Even before these ambitious goals are met, the levelized cost of most plug-in hybrid electric vehicles—and of all-electric vehicles with shorter ranges (such as 100 miles)—will be comparable to the levelized cost of ICE vehicles of similar size. Meeting these targets will help to reduce the purchase price for PEVs.

The *EV Everywhere* Blueprint document also describes the deployment programs related to charging infrastructure and consumer education. Efforts to promote home, workplace, and public charging can also help speed PEV deployment.

EV Everywhere Technical Targets

DOE defined *EV Everywhere* technology targets using an analytical framework that evaluated the performance of component technologies as well as vehicle cost and performance. The Department synthesized data about future vehicle potential using expert projections of component technology to create virtual vehicles of the future via computer modeling and simulation. The range of vehicle costs and efficiencies made possible a comparison of the degree to which the portfolio of these technologies must progress, in both performance and cost terms, to yield PEVs that are cost-competitive, as measured by the initial vehicle purchase price and the fuel expenditure accrued over a five-year ownership period. Ultimately, an analysis of this balance yielded technical targets at the technology progress frontier: *EV Everywhere* targets are consistent with what experts see as very aggressive but still possible within the *EV Everywhere* timeframe. The complete set of *EV Everywhere* technical targets are presented in the Blueprint document.

VSST achieved sub-objectives for achieving the goals of (a) extending vehicle range by reducing and managing auxiliary loads, (b) integrating electric vehicles into the electrical grid, and (c) accelerating market penetration of electric vehicles by supporting codes and standards development. Table II-1 below provides an executive summary of the accomplishments and the R&D project reports that contain the details.

Table II-1: VSST EV Everywhere Achievements for FY 2014

| Goals & Objectives | Accomplishment | Benefit | Where to find the Details of R&D Activities |
|--|---|--|---|
| Extend Range by Reducing and Managing Auxiliary Loads | Developed new heating, ventilating and air conditioning (HVAC) component models compatible with Autonomie. | The models reduce industry costs to evaluate candidate strategies for improving electric vehicle range. Validated HVAC component models enable virtual system design experiments to determine impact of candidate technologies. | M&S, Lustbader, Vehicle Thermal System Model Development in MATLAB/Simulink, NREL |
| Extend Range by Reducing and Managing Auxiliary Loads | Ran a broad range of tests for general energy consumption, performance assessment, component evaluation, and technology benchmarking across a range of ambient temperatures and HVAC conditions. | Test data and analysis provide researchers with the information needed to focus development of technology solutions that minimize the impact of hot and cold temperatures on electric vehicle range. | VTE, Level 2 Benchmark of Advanced Technology Vehicles: model year 2014 Honda Accord Plug-in Hybrid Electric Vehicle, ANL |
| Foster Integration of Electric Vehicles into Electrical Grid | Published real-world EVSE data collection products usage informing decision makers about consumer demand patterns. During FY 2014, numerous studies were completed using data from the EV Project and Charge Point projects to better understand PEV and charging infrastructure usage. | This effort increases market efficiency for adoption of EVSE technologies. The empirical information fills the knowledge gaps that hinder accurate prediction of demand for EVSE equipment and public infrastructure. Accurate predictions are critical for infrastructure planning and business model assessments. | VTE, EV Project, ChargePoint America, and West Coast Electric Highway Data Collection and Dissemination, INL |
| Foster Integration of Electric Vehicles into Electrical Grid | Analyzed workplace charging patterns and demand charging in commercial buildings. Collected and analyzed electric vehicle charging station usage data for 18 months from the NREL parking garage. The data confirm initial expectations of workplace charging patterns and energy demands (typically 2–4 hours and ~5–8 kWh per vehicle). | The analysis identifies opportunities to reduce demand charges and maximize renewable energy power sources; helps improve the economic viability of PEVs and minimize environmental impacts of transportation vehicles. | VSEI, PEV Integration with Renewables, NREL |
| Foster Integration of Electric Vehicles into Electrical Grid | Benchmarked lifecycle characteristics of a PEV production vehicle with DC fast charging capability. Reached 60,000 test miles on each of four Nissan Leafs while recording and storing vehicle system data continuously. Conducted battery capacity and power capability testing at 40, 50, and 60 thousand miles for the four Nissan Leafs being operated on-road. | Benchmarking informs vehicle designers of the consequences of different charging strategies on the performance of specific on-board energy storage technologies. Benchmarking the impacts (if any) that DC fast charging has on battery life in Nissan Leaf battery electric vehicles compared to Level 2 charging of the same vehicle model helps inform consumers and technology developers. Benchmarking informs OEMs of the real-world performance of specific vehicles by testing a variety of advanced energy storage systems that are at or near commercialization. The testing is performed while the vehicle is | VTE, Nissan Leaf DC Fast Charging Study and Electric Drive Advanced Battery Testbed, INL |

| Goals & Objectives | Accomplishment | Benefit | Where to find the Details of R&D Activities |
|--|---|--|--|
| | | <p>on road, during real-world operation. The tests quantify the energy storage system capabilities and limitations by measuring the performance fade over the life of the system.</p> | |
| <p>Eliminate Barriers to Electric Vehicle Market Penetration by Supporting Codes and Standards Development</p> | <p>SAE J2953 EV interoperability standard; interoperability requirements and verification test procedures developed by ANL were issued as recommended standard practices via the SAE consensus-based process with industry and other stakeholders. ANL also developed an AC InterOP Test Fixture (Version 2) to verify compliance with the SAE J2953 standard; the first test fixture was transferred to a DOE project to test production electric vehicles and EVSE.</p> | <p>Accelerates market penetration of PEVs by providing an SAE standard that formalizes interoperability requirements between PEVs and charging devices (EVSE). ANL's AC InterOP Test Fixture provides the hardware and software to test whether PEVs and EVSE devices conform to the SAE J2953 standard. This test fixture is being used by the VTO's AVTE project to test interoperability of several production PEVs and EVSE devices.</p> | <p>Codes and Standards, Bohn, EV-Smart Grid Interoperability Center, ANL</p> |

II.B. Planned Activities

Using less energy to achieve comfortable climate control in PEVs will allow for a smaller, less expensive battery and thus will contribute to lowering the cost of PEVs (assuming travel distance is held constant). Currently, these climate control loads on a PEV can double vehicle energy consumption, effectively halving vehicle range. *EV Everywhere* will focus on the following specific research areas:

- **Energy Load Reduction and Energy Management** strategies can minimize energy consumption by reducing the thermal loads that the systems must address. Advanced windows and glazing, surface paints, advanced insulation, thermal mass reduction, and ventilation and seating technologies can better control heat transfer between the passenger cabin and the environment, minimizing the thermal loads that the HVAC systems must address to ensure passenger comfort.
- **Advanced HVAC Equipment**, such as advanced heat pumps or novel heating/cooling subsystems, can reduce the auxiliary loads. Innovative heating and cooling concepts to achieve passenger comfort, such as infrared and thermoelectric devices and phase change materials, can also reduce energy requirements.
- **Cabin Pre-Conditioning** while the vehicle is connected to the grid can reduce the amount of energy needed from the battery upon initial vehicle operation to either decrease (hot conditions) or raise (cold conditions) the temperature in the cabin. Another approach to cabin pre-conditioning is to utilize waste heat generated within the battery and/or charging circuit during charging.

In support of the *EV Everywhere* Grand Challenge, DOE released a FOA in March 2014, soliciting proposals in the areas of energy storage, electric drive systems, lightweight materials, and auxiliary load reductions. DOE announced the selection of awards from FOA 991 in September 2014. These projects were initiated in September 2014 and will be described in more detail in next year's annual report.

In the area of advanced climate control to reduce auxiliary load energy consumption, two projects representing a DOE investment of \$5 million were awarded to Delphi and NREL. Reducing the impact of heating and cooling on PEVs can significantly increase all-electric driving range. The objective of the Delphi UTEMPRA project is to design and develop a complete thermal management system for cooling heating and waste heat harvesting to reduce auxiliary loads in grid-connected electric drive vehicles. The compact refrigerant system will chill or heat coolant, which can be pumped anywhere in the vehicle to provide heating or cooling to the passenger compartment, vehicle batteries, and other thermal components. The objective of the NREL-led project is to increase grid-connected electric drive vehicle range 20% during operation of the climate control system by designing and developing technology to reduce thermal loads. This includes developing solar reflective glass, solar reflective/absorbing films, improved insulation, cabin prevention, solar reflective paint, small localized positive temperature coefficient (PTC) spot heaters for defogging sidelights, and an electrically heated windshield (as well as interactions and synergies) to reduce thermal loads. These two new climate control R&D projects are focused on developing innovative heating and cooling technologies that reduce battery demands and improve range by 20%–30%.

III. INDUSTRY

ADVANCED VEHICLE TESTING AND EVALUATION

III.A. Advanced Vehicle Testing & Evaluation (AVTE)- DE-EE0005501

Principal Investigator: Richard Jacobson

Intertek Testing Services NA, Inc.
430 S. 2nd Avenue
Phoenix, AZ 85003
Phone: (480) 525-5871
E-mail: richard.jacobson@intertek.com

DOE Program Manager: Lee Slezak

Phone: (208) 586-2335
E-mail: Lee.slezak@ee.doe.gov

- University of Nebraska–Lincoln Agricultural Vehicle Technology report completed.

Future Achievements

- Continue acquisition and testing of planned vehicles for testing based on their advanced technology and market availability.
- Complete interoperability testing of vehicles and Level 2 EVSE units scheduled through FY 2015.
- Implement a Storage-Assisted Recharging (StAR) unit at a current testing fleet location.



III.A.1. Abstract

Objectives

- Test and evaluate advanced vehicle technologies that reduce the consumption of petroleum.
- Produce lifecycle cost data for vehicles that are utilizing these advanced technologies.
- Provide fleet operations data to the Idaho National Laboratory database in order to disseminate the results of vehicle and infrastructure testing & analysis.
- Provide benchmark data for advanced technology vehicles and their associated fueling infrastructure.

Major Accomplishments

- Acquired 34 advanced technology vehicles during FY 2014 for a total of 70 vehicles under test during the year.
- Completed baseline testing information on 29 vehicles consisting of 8 vehicle models.
- A total of 54 vehicle component durability tests were completed on 47 different vehicles in FY 2014.
- Updated advanced vehicle component testing intervals for all vehicles.
- Collaboration between Intertek and DOE national laboratories in baseline vehicle and interim component report creation.
- Implemented an additional testing fleet location with 12 AVTE vehicles.
- Interoperability between original equipment manufacturers (OEMs) and electric vehicle supply equipment (EVSE) started with the Intertek Plymouth, Michigan location.
- Completed testing of semi-autonomous driving with heavy-duty vehicles in a platoon.

III.A.2. Technical Discussion

Background

The objective of the AVTE project is to conduct laboratory and field evaluations of advanced technology vehicles and their associated fueling infrastructures, and the development of new test procedures and/or modifications of existing test procedures necessary to accomplish these performance evaluations. The scope of the work included baseline performance, accelerated reliability, and fleet testing of state-of-the-art light-, medium-, and heavy-duty advanced technology vehicles and the required vehicle-to-infrastructure interface required for fueling/charging the vehicles.

Introduction

The AVTE project focuses on testing and evaluating commercially-available, early production, and pre-production light-, medium-, and heavy-duty advanced technology vehicles using internal combustion engines burning advanced fuels (such as hydrogen and compressed natural gas (CNG) fuels); electric (EV), extended range electric (EREV), hybrid electric (HEV), Plug-in Hybrid Electric (PHEV), or fuel cell (FCV) powertrains; advanced energy storage technologies (such as batteries, ultra-capacitors, and hydrogen storage tanks); advanced drive trains; as well as the necessary infrastructure required to fuel and/or charge (EV, PHEV) advanced technology vehicles, including the interaction between infrastructure, vehicles, and the electric grid. The onboard engines may include, but are not limited to, fuel cells, advanced internal combustion engines (ICE), and other energy-enabling engines and motors. The evaluation data

collected through the AVTE project is used to validate the results of research, modeling, and simulation activities using laboratory and field tests.

Approach

The AVTE project is managed into separate tasks to accomplish testing of advanced technology vehicles and their respective infrastructure. The tasks are as follows:

Project Management

This task includes the activities necessary to provide management of AVTE activities, including budget and schedule control, fleet coordination, procurement, status reporting, presentations of activity results and status to DOE and industry, preparation of the project management plan, and quarterly updates of the project management plan. Work under this task also includes management of test results reports and/or data sheets for each task.

Vehicle Specification and Test Procedure Development

Specifications for vehicles, components and infrastructure are prepared to define specific design and performance requirements. Test procedures are developed that will evaluate requirements stated in the specification.

New testing procedures incorporate industry standard test procedures as applicable. Vehicle tests typically include on-track testing of performance and operating characteristics as well as DOE Laboratory chassis dynamometer testing. Special tests for components and infrastructure are developed along with test facilities uniquely to validate specification requirements.

Existing procedures for Accelerated and Fleet Testing are revised, as necessary, to include the unique aspects of each class of the anticipated subject vehicles and to keep them current with new industry standards and requirements. Procedures incorporate mission-based requirements (i.e., simulating actual fleet operating practices). Data collection techniques are developed to measure and record the data necessary to provide the information required for each class of vehicle.

Baseline Performance Testing

Baseline Test procedures include, but are not limited, to testing of acceleration, speed at distance, grade ability and durability, braking distance, time to recharge and charging efficiency (for grid-connected vehicles), energy storage capacity, and fuel efficiency on various dynamometer test cycles and in various operating modes. Additional Baseline Test procedures are developed, as required, for vehicles with unique operational characteristics.

Baseline vehicle performance testing is performed at a limited access test track. Chassis dynamometer testing is conducted at Argonne National Laboratory. Dynamometer testing of vehicle technologies with unique operational characteristics (transit, agricultural, military, etc.) will be provided as required. As part of baseline testing, beginning-of-test battery testing is performed on all vehicles with battery energy storage. Vehicles will be purchased, leased, or rented unless provided by the DOE or manufacturers. All vehicles will

be insured, operated, and maintained in accordance with manufacturer's recommendations.

Accelerated Vehicle Testing

During Accelerated Testing, at least one vehicle is tested under supervised and semi-controlled conditions in order to evaluate one or more characteristics of the vehicle's performance or operational characteristics, and to obtain data in an accelerated time frame, evaluating vehicle reliability, maintenance requirements, long-term performance, energy efficiency, and lifecycle costs. The assumption with Accelerated testing is that the vehicle is unlikely or too expensive to operate in a long-term fleet application due to technical and manufacturing robustness.

The accelerated testing duration is based on the objectives of the testing for the particular subject vehicle. Testing typically achieves about 6,000 miles on a subject vehicle, but may reach higher mileage as documented in the project management plan. Vehicles are purchased, leased, or rented unless provided by another program. All vehicles are insured, operated and maintained in accordance with manufacturer's recommendations. Fueling infrastructure is provided, as required, to conduct testing and evaluation.

Fleet Testing

Fleet testing includes high-mileage testing four production vehicles of the same make and model in an operating fleet to determine vehicle reliability, maintenance requirements, long-term performance, lifecycle costs, and user acceptance. Vehicles are driven on-road at an assumed average of 6,500 miles/month, accumulating up to 195,000 miles as defined in the project management plan. Vehicles are purchased, leased, or rented unless provided another organization. All vehicles are insured and maintained in accordance with manufacturers recommendations. Fueling infrastructure is provided, as required, to conduct testing and evaluation.

Data collection systems necessary to collect operating data as required per test procedures are installed on all fleet vehicles. Repair and maintenance costs are collected manually. The fleet operator maintains logs of fuel dispensed (including electricity on plug-in vehicles) and mileage. Operating data, repair and maintenance costs are maintained current on a monthly basis. Quality checks and trend analysis are performed to ensure that the data are accurate and that the vehicles are performing properly.

Interim Component Testing

This task includes testing of vehicle components during accelerated or fleet testing. Interim component durability (ICD) tests for traction-battery equipped vehicles are capacity and performance related between baseline and end-of-testing. Other advanced vehicle technology component testing specifications and procedures will be developed as other technologies and components are tested. Raw data from the testing is provided to the AVTA at the Idaho National Laboratory for analysis and verification.

End-of-Test Vehicle and Component Testing

This task consists of vehicle and component testing at the completion of fleet or accelerated testing including, but not limited to, vehicle performance, mechanical components, batteries, and other energy storage devices. Tests are performed as required by the project management plan and are conducted in accordance with procedures developed under Test Procedure Development. Raw data from the testing is provided to the AVTA at the Idaho National Laboratory for analysis and verification.

Infrastructure Test and Evaluation

This task consists of testing vehicle and infrastructure interface, operations, and reliability. For grid-connected electric-drive vehicles, the testing will include charger efficiency, vehicle to grid communication, and bi-directional power flow (if applicable). The evaluation will collect data on the installation, operation, energy, and maintenance costs of the infrastructure and track user feedback related to the overall interface and operations of the infrastructure. Deliverables include test result data sheets and a report on the cost, safety, operations, maintenance, and reliability of the infrastructure.

Additional Procedure Development, Testing or Test Support

This task consists of various additional procedure developments, testing, and test support activities that may be determined necessary by the DOE or Intertek. The activities will be detailed in the project management plan, and the work will be reviewed and approved by the DOE.

Results

Vehicle Testing

Mileage accumulation during the fiscal year is summarized in Table III-1.

Table III-1 FY 2014 AVTE Vehicle Mileage

| # | YEAR | MAKE | MODEL | VEHICLE # | MILEAGE | COMMENTS |
|----|------|------------|----------------------|-----------|------------------|--------------------------------|
| 1 | 2011 | Honda | CR-Z | 2982 | 17,228 | AVTA - Completed Jan 2014 |
| 2 | 2011 | Honda | CR-Z | 4466 | 5,913 | AVTA - Completed Dec 2013 |
| 3 | 2011 | Chevy | Volt | 0815 | 29,888 | Carryover AVTA vehicle |
| 4 | 2011 | Chevy | Volt | 0914 | 32,843 | Carryover AVTA vehicle |
| 5 | 2011 | Nissan | Leaf (3.3kW Charger) | 0356 | 4,039 | AVTA - Sold September 2014 |
| 6 | 2011 | Nissan | Leaf (3.3kW Charger) | 0178 | 6,886 | Carryover AVTA vehicle |
| 7 | 2013 | Chevy | Malibu ECO | 6605 | 44,060 | Acquired in FY 2013 |
| 8 | 2013 | Chevy | Malibu ECO | 3800 | 50,625 | Acquired in FY 2013 |
| 9 | 2013 | Chevy | Malibu ECO | 6791 | 48,646 | Acquired in FY 2013 |
| 10 | 2013 | Chevy | Malibu ECO | 7249 | 38,845 | Acquired in FY 2013 |
| 11 | 2012 | Honda | Civic CNG | 0612 | 29,379 | Acquired in FY 2013 |
| 12 | 2012 | Honda | Civic CNG | 0672 | 29,874 | Acquired in FY 2013 |
| 13 | 2012 | Honda | Civic CNG | 2486 | 27,408 | Acquired in FY 2013 |
| 14 | 2012 | Honda | Civic CNG | 2590 | 39,090 | Acquired in FY 2013 |
| 15 | 2013 | Chevy | Volt | 3929 | 45,966 | Acquired in FY 2013 |
| 16 | 2013 | Chevy | Volt | 1078 | 32,158 | Acquired in FY 2013 |
| 17 | 2013 | Chevy | Volt | 3491 | 47,782 | Acquired in FY 2013 |
| 18 | 2013 | Chevy | Volt | 4313 | 34,187 | Acquired in FY 2013 |
| 19 | 2013 | VW | TDI Jetta | 6371 | 21,046 | Acquired in FY 2013 |
| 20 | 2013 | VW | TDI Jetta | 6221 | 22,244 | Acquired in FY 2013 |
| 21 | 2013 | VW | TDI Jetta | 5286 | 25,161 | Acquired in FY 2013 |
| 22 | 2013 | VW | TDI Jetta | 6578 | 19,613 | Acquired in FY 2013 |
| 23 | 2013 | Honda | Civic Hybrid | 0594 | 51,958 | Acquired in FY 2013 |
| 24 | 2013 | Honda | Civic Hybrid | 0244 | 48,843 | Acquired in FY 2013 |
| 25 | 2013 | Honda | Civic Hybrid | 1260 | 54,313 | Acquired in FY 2013 |
| 26 | 2013 | Honda | Civic Hybrid | 1356 | 69,642 | Acquired in FY 2013 |
| 27 | 2013 | Toyota | Prius Plug-In | 6237 | 59,131 | Acquired in FY 2013 |
| 28 | 2013 | Toyota | Prius Plug-In | 8660 | 40,495 | Acquired in FY 2013 |
| 29 | 2013 | Toyota | Prius Plug-In | 8661 | 51,084 | Acquired in FY 2013 |
| 30 | 2013 | Toyota | Prius Plug-In | 8663 | 56,228 | Acquired in FY 2013 |
| 31 | 2013 | VW | Jetta Hybrid | 9918 | 29,704 | Acquired in FY 2013 |
| 32 | 2014 | VW | Jetta Hybrid | 0875 | 7,109 | Acquired in December 2013 |
| 33 | 2014 | VW | Jetta Hybrid | 2708 | 26,154 | Acquired in December 2013 |
| 34 | 2014 | VW | Jetta Hybrid | 7542 | 6,941 | Acquired in December 2013 |
| 35 | 2012 | Mitsubishi | i-MiEV | 3178 | 6,095 | Acquired in FY 2013 |
| 36 | 2012 | Mitsubishi | i-MiEV | 4550 | 9,283 | Acquired in FY 2013 |
| 37 | 2013 | Nissan | Leaf (6.6kW Charger) | 5045 | 9,725 | Acquired in FY 2013 |
| 38 | 2013 | Nissan | Leaf (6.6kW Charger) | 0646 | 7,652 | Acquired in December 2013 |
| 39 | 2013 | Nissan | Leaf (6.6kW Charger) | 7885 | 9,594 | Acquired in December 2013 |
| 40 | 2013 | Nissan | Leaf (6.6kW Charger) | 9270 | 11,224 | Acquired in December 2013 |
| 41 | 2013 | Ford | C-Max Hybrid | 8698 | 50,088 | Acquired in FY 2013 |
| 42 | 2013 | Ford | C-Max Hybrid | 2158 | 49,116 | Acquired in December 2013 |
| 43 | 2013 | Ford | C-Max Hybrid | 5138 | 55,949 | Acquired in December 2013 |
| 44 | 2013 | Ford | C-Max Hybrid | 5139 | 50,118 | Acquired in December 2013 |
| 45 | 2013 | Ford | C-Max Energi | 0852 | 39,380 | Acquired in FY 2013 |
| 46 | 2013 | Ford | C-Max Energi | 3813 | 30,139 | Acquired in December 2013 |
| 47 | 2013 | Ford | C-Max Energi | 3817 | 29,797 | Acquired in December 2013 |
| 48 | 2013 | Ford | C-Max Energi | 3818 | 34,732 | Acquired in December 2013 |
| 49 | 2013 | Ford | Focus EV | 8207 | 5,265 | Acquired in December 2013 |
| 50 | 2013 | Ford | Focus EV | 1700 | 6,016 | Acquired in December 2013 |
| 51 | 2013 | Ford | Focus EV | 2578 | 6,356 | Acquired in December 2013 |
| 52 | 2013 | Ford | Focus EV | 4791 | 5,238 | Acquired in December 2013 |
| 53 | 2013 | Ford | Fusion Energi | 3776 | 6,938 | Acquired in December 2013 |
| 54 | 2013 | Ford | Fusion Energi | 1518 | 40,011 | Acquired in December 2013 |
| 55 | 2013 | Ford | Fusion Energi | 3875 | 41,235 | Acquired in December 2013 |
| 56 | 2013 | Ford | Fusion Energi | 7094 | 26,325 | Acquired in December 2013 |
| 57 | 2014 | Smart | ED | 5544 | 3,969 | Acquired in March 2014 |
| 58 | 2014 | Smart | ED | 2457 | 2,516 | Acquired in April 2014 |
| 59 | 2014 | Smart | ED | 2764 | 2,239 | Acquired in April 2014 |
| 60 | 2014 | Smart | ED | 7525 | 2,096 | Acquired in April 2014 |
| 61 | 2013 | RAM | 1500 w/Idle/Stop | 1319 | 4,543 | On test at ANL |
| 62 | 2014 | Chevy | Cruze Diesel | 6917 | 3,692 | Acquired in July 2014 |
| 63 | 2014 | Chevy | Cruze Diesel | 1014 | 3,057 | Acquired in August 2014 |
| 64 | 2014 | Chevy | Cruze Diesel | 4736 | 3,729 | Acquired in August 2014 |
| 65 | 2014 | Chevy | Cruze Diesel | 8875 | 3,357 | Acquired in August 2014 |
| 66 | 2014 | Mazda | Mazda3 i-ELOOP | 9972 | 4,067 | Acquired in July 2014 |
| 67 | 2014 | Mazda | Mazda3 i-ELOOP | 0179 | 75 | Acquired in August 2014 |
| 68 | 2014 | Mazda | Mazda3 i-ELOOP | 1135 | 866 | Acquired in August 2014 |
| 69 | 2014 | Mazda | Mazda3 i-ELOOP | 7631 | 456 | Acquired in August 2014 |
| 70 | 2014 | BMW | i3 w/ Range Extender | 3436 | 0 | Acquired in September 2014 |
| | | | | | 1,696,280 | = FY 2014 Mileage Total |

Seven vehicles were transferred from the AVTA contract (DE-FC26-05NT42486) to AVTE on March 22, 2013, to continue mileage accumulation and component testing. One vehicle, a 2011 Hyundai Sonata Hybrid 3539, was completed with its mileage accumulation during FY 2013. Two Honda CR-Z Hybrids completed their mileage accumulation during FY 2014. Final component testing reports for all of these vehicles were published during FY 2014 on the Advanced Vehicle Testing Activity (AVTA) website at: avt.inel.gov. A 2011 Nissan Leaf 0356 was continuing with mileage accumulation, but the indicated high voltage battery capacity of the vehicle was below the Nissan manufacturer warranty specifications. The high-voltage battery was replaced in the vehicle and the vehicle was sold and credit issued for its salvage value. The remaining vehicles, consisting of two 2011 Chevrolet Volts and one 2011 Nissan Leaf, continue to accumulate mileage and perform component testing.

Prior to FY 2014, there were 29 vehicles that had been acquired during FY 2013 and were underway with mileage accumulation and advanced component testing at the beginning of FY 2014. These vehicles, along with the 6 remaining vehicles from AVTA, continued mileage accumulation and advanced component testing through the bankruptcy and eventual sale of ETEC to Intertek.

New vehicles were acquired starting in late December 2013. These vehicles have been vetted with the DOE during annual reviews and project management plan updates. . These vehicles include the remaining 3 of 4 2013 Volkswagen Jetta Hybrids, 3 of 4 2013 Nissan Leafs, 3 of 4 2013 Ford C-Max Hybrids and 3 of 4 2013 Ford C-Max Energi (PHEV). In addition, all 4 2013 Ford Focus Electric (BEV) and all 4 2013 Ford Fusion Energi (PHEV) were acquired during Q1 of FY 2014. These vehicles were able to complete instrumentation and baseline testing in a short time frame due to matching the initial vehicle already in the fleet or sharing similarities in the communication to the data logger to vehicles already instrumented in the fleet.

Additional vehicles were acquired in Q3 of FY 2014. They include the 2014 Smart Electric Drive, which offers a comparison to the microhybrid Smarts that were under test in the AVTA project. The 2014 Chevrolet Cruze Turbo Diesel is the first diesel available in a domestic passenger vehicle and offers a comparison to the Volkswagen Jetta TDIs already in the AVTE fleet. The 2014 Mazda Mazda3 with i-ELOOP is one of the first vehicles in production equipped with an ultracapacitor as an energy storage system. Its component testing will begin in FY 2015. The BMW i3 with Range Extender is a BEV with a 1.9 gallon fuel tank for the range extending two cylinder engine. While this vehicle is classified as a PHEV by the EPA, for component testing, the high voltage battery will be tested at mileage intervals for the BEVs starting in FY 2015.

A RAM 1500 with stop-start capability was added to the fleet to obtain baseline information at Argonne National Laboratory on the chassis dynamometer prior to the vehicle being updated to be CNG-capable. The vehicle completed its baseline with the CNG conversion at the end of FY 2014.

An additional 34 advanced technology vehicles were acquired for testing during FY 2014 for a total of 70. Of the

vehicles acquired and under test in FY 2014, 29 vehicles completed baseline testing consisting of 8 different models.

A total of 54 vehicle component durability tests were completed on 47 different vehicles in FY 2014.

Vehicle Testing Intervals

After discussion at the DOE annual review in February 2014, it was determined that all fleet vehicles will be tested based upon mileage intervals, except for PHEVs which will continue on time-based intervals. All BEVs will target testing at close to their initial mileage at acquisition with an initial ICD test at approximately 4,000 miles after the standard break-in period. Baseline vehicle performance testing for all vehicles remains at 4,000 miles.

The update to the initial ICD test for BEVs is to capture any loss of performance from the energy storage system prior to the 4,000 mile break-in period.

PHEVs will remain on a time interval for component testing with the expectation that each vehicle will be charged overnight and initially operate in charge depletion mode each day during normal fleet mileage accumulation. The PHEV would then operate in charge-sustaining mode for the remainder of the day's operation before recharging the energy storage system overnight.

Collaboration between Intertek and the DOE National Laboratories

The deliverables for the AVTE project consist of vehicle baseline reports, interim component reports, and end-of life component reports. The initial vehicle baseline report compiles data from literature review, track testing at a proving ground, vehicle inspection, and dynamometer testing. The dynamometer testing process has been further refined during fuel economy testing to provide information on the cycle results at multiple ambients for inclusion into the baseline report. The multiple ambients provide background on the function of the propulsion systems and their fuel economy, which is not evident in the EPA fuel economy of the vehicle.

The energy storage system component testing process has been improved by Idaho National Laboratory. Baseline and ICD reports have been automated to have a similar look from report to report and graphs and tables auto-populate in an INL format based on data provided electronically by Intertek from component durability testing. As each component test is completed, the report is updated on the same location on the AVTA website.

Additional Testing Fleet

Prior to the start of FY 2014, an agreement was established with Total Transit, Inc., which is a local taxi service to Phoenix, Arizona. Total Transit is a green company and was the first in the Phoenix area to switch a majority of their fleet to Toyota Prius Hybrids. Their most experienced drivers would be selected to drive AVTE vehicles. During 2014, Total Transit began conversion of four 2013 Volkswagen Jetta TDIs to taxis. An additional four 2013 and 2014 Volkswagen Jetta Hybrids and four 2013 Chevrolet Malibus were also added to their fleet for a total of 12 vehicles under test. The vehicles were chosen due to their capability to perform as a taxi and there is no EVSE required overnight. The vehicles were

painted to match their fleet and will be returned to stock at the end of life.



Figure III-1: AVTE 2013 Volkswagen Jetta TDI in Total Transit color scheme

EZ Messenger, a courier and legal document delivery service, has the remainder of the AVTE fleet vehicles in multiple fleet locations, including Phoenix, Tucson, Dallas, Houston, and Oklahoma City.

Both fleets report their mileage and fuel consumed at the end of the month for integration into a report by Intertek that is electronically sent to INL for incorporation on the vehicle fuel economy and maintenance fact sheets.

SAE J2953 Interoperability between vehicles and EVSE

The SAE J2953 Interoperability testing between OEM vehicles and EVSE manufacturers began in the second quarter of FY 2014 and is ongoing into FY 2015. The testing consists of 11 OEMs (who are providing 14 vehicles) and 11 EVSE manufacturers (who provided 13 units) participating in the activity. Testing continues on schedule at Intertek's Plymouth, Michigan laboratory with project management from Phoenix. The Intertek Plymouth Laboratory was selected due to their proximity to OEMs, their ongoing participation in the SAE J2953 committee, and their experience with EVSE testing.

Ten vehicles have completed the round-robin testing with all EVSE units. The interim test results have been disseminated to SAE for four vehicles. Interoperability testing is scheduled for completion in the first quarter of FY 2015 followed by a final report in the second quarter of FY 2015.

Semi-autonomous driving with heavy-duty vehicles in a platoon

Testing began at the end of the second quarter of FY2014 to evaluate the fuel consumption of two Class 8 tractor-trailer combinations that platooned together, compared to their individual fuel consumption. The project was managed by the National Renewable Energy Laboratory (NREL), while the testing was organized by Intertek. SAE Type II J1321 fuel consumption track tests were performed to document fuel consumption of two platooned vehicles and a separate control vehicle at varying steady-state speeds, following distances, and gross vehicle weights (GVWs). The steady-state speeds ranged from 55 mph to 70 mph, while the following distances ranged from a 20-ft to 75-ft, and the GVWs were 65K lbs and 80K lbs. Effects of vehicle speed, following distance, and GVW on fuel consumption were observed and analyzed. The platooning demonstration system used in this study consisted of radar systems, Dedicated short-range communication (DSRC) vehicle-to-vehicle (V2V) communications, vehicle braking and torque control interface, cameras and driver

displays. In all cases, both the lead and following truck benefited from the platooning, with the best combined result being for 55 mph, 30-ft following distance, and 65k GVW.



Figure III-2: Heavy-Duty trucks in platoon formation (courtesy of Peloton Technology, Inc.)

University of Nebraska-Lincoln Agricultural Vehicle Technology Report

The Nebraska Tractor Testing Laboratory (NTTL) was tasked to identify equipment, both current and planned, with significant potential to impact petroleum displacement. A report was completed in the third quarter of FY 2014 and posted to the AVTA website with an emphasis on tractor petroleum reduction targeting tractor engines and equipment, powertrain efficiencies, remote power and tire improvements, implement / Power Take-Off operation with secondary fuels, alternative fuels and distribution for farm use, biofuels, Hydrogen and CNG, and tillage and operations efficiency.

Conclusions

The AVTE project provides real-world testing of production vehicles, their energy storage systems, and their associated infrastructure. The amount of available production vehicles and their energy storage systems have improved in FY 2014, and multiple vehicles have been able to be implemented in fleets to accumulate mileage over a period of three years. Data and reports from testing are available to the DOE national laboratories for further study and dissemination to the public.

III.A.3. Products

Publications

1. Lammert, M., A. Duran, J. Diez, K. Burton, K. et al., *Effect Of Platooning on Fuel Consumption of Class 8 Vehicles Over a Range of Speeds, Following Distances, and Mass*, NREL/CP-5400-62348, National Renewable Energy Laboratory, September 2014.
2. Gray, T., M. Shirk, J. Wishart. *2011 Honda CR-Z 2982 – Hybrid Electric Vehicle Battery Test Results*, Idaho National Laboratory, INL/EXT-14-32475, September 2014.
3. Gray, T., M. Shirk, J. Wishart. *2011 Honda CR-Z 4466 – Hybrid Electric Vehicle Battery Test Results*, Idaho National Laboratory, INL/EXT-14-32474, September 2014.
4. Gray, T., M. Shirk, J. Wishart. *2011 Hyundai Sonata 3539 – Hybrid Electric Vehicle Battery Test Results*, Idaho National Laboratory, INL/EXT-14-32109, September 2014.
5. Baseline Performance Testing, Series of Reports, Idaho National Laboratory, Intertek Testing Services NA, 2014. The reports can be found on the AVTA website at:
avt.inel.gov/hev.shtml for HEVs,
avt.inel.gov/phev.shtml for PHEVs and EREVs,
avt.inel.gov/ice.shtml for advanced ICE, and
avt.inel.gov/fsev.shtml for BEVs.

Patents

This is a test program that is not intended to develop patents. The intent is to provide independent testing and feedback to the DOE regarding petroleum-reducing technologies available in production vehicles and their associated infrastructure.

Tools and Data

The data generated by this testing are used to populate publications found on the DOE Laboratory and AVTA websites in the form of testing fact sheets and reports.

THERMAL LOAD REDUCTION

III.B. Electric Phase Change Material Assisted Thermal Heating System (ePATHS)- DE-EE000644

Mingyu Wang

Delphi Automotive Systems, LLC
350 Upper Mountain Road
Lockport, NY 14051
Phone: (716) 431-2493
E-mail: mingyu.wang@delphi.com

David Anderson

Phone: (202) 287-5688 (David Anderson)
E-mail: David.Anderson@ee.doe.gov

III.B.1. Abstract

Objectives

- During charging of an EV's battery, it is proposed to simultaneously charge a thermal energy storage (TES) system that can store sufficient thermal energy to heat the electric vehicle (EV) cabin for an extended period of time. Depending on the sizing of the system, the TES can provide up to 100% of the thermal energy necessary to heat the cabin during typical commuter driving. Using the TES system for heating can increase the electric drive range more than 20% in cold ambient conditions.
- For this project, the goal is to design and develop a prototype TES system through analysis and testing that can be quickly commercialized. The project scope includes the development of an advanced phase change material (PCM) along with the component and system architecture for integration into a grid-connected electric drive vehicle (GCEDV) environment to provide heating comfort. The system performance will be demonstrated at both a bench and vehicle level.
- In operation, the TES system will incorporate a high temperature PCM that will be housed in a standalone container and will seamlessly integrate with the existing charge control architecture. Energy from the electric grid will provide the charging energy used to heat the TES system while the EV is charged at home or at an EV charge station. The TES will be heated via an electrical resistance heater during the plug-in charging cycle. An intelligent TES charge control algorithm will also be implemented.
- The basis of the TES is a PCM storage unit. Innovative to this storage unit is that it incorporates a PCM that has up to 50% more latent heat during phase change when compared to PCMs on the market today. Further, the

storage unit will be insulated to minimize parasitic energy loss while the vehicle is not operating.

Major Accomplishments

- The vehicle and sub-system specification is complete. This is one of the key milestones for the first budget period. This document defines the system objectives, performance requirements, system architecture and full system content. In addition, it contains the targets for packaging the system in the vehicle and describes the components that make up the system
- The system control architecture has been defined and the specification for control software and hardware will be complete by the end of BP-1. More specifically, the specification defines both the hardware and software that will be developed to control the ePATHS system when integrated into the Ford Focus BEV.
- Component specifications were initiated for the PCM Heat Exchanger, PCM, insulation, pumps, valves and hoses. Included in these specifications are the product construction, performance and validation requirements for advanced development products. Once the requirements of these specifications are met, the ePATHS system may be marketed to vehicle OEMs for potential commercialization. These specifications will be complete by the end of BP-1.
- A major focus of the project is the development of a PCM that increases the latent heat capacity by 50% compared to those currently in the marketplace. Toward that end, after investigating 6 families and 40 individual PCM samples, a PCM approaching 90% of the project targets has been synthesized by Entropy Solutions. Currently, steps are being investigated to enable the new PCMs to have stability when exposed to thermal cycling. A 5.5 kg sample of the most advanced PCM developed to date is to be supplied to Delphi in the 4th quarter of 2014 for testing in one of the quarter-width prototype PCM heat exchangers. The testing will help to calibrate the ORNL PCM heat exchanger model and the Delphi team to understand the impact of various design parameters.
- A PCM heat exchanger (HX) design simulation model has been completed by ORNL. The model uses a finite volume approach and builds into a complete heat exchanger assembly capable of storing the heating energy required. Additionally, the PCM HX design model will be integrated in a full system model for system and component design optimization.
- A concept quarter-width PCM HX design was completed and two sample parts were built. Following the HX build, it

was encased in a sealed aluminum chamber to create a PCM containment volume. The PCM HX was subsequently filled with a low enthalpy, commercial PCM that has a phase change temperature of approximately 100°C. The assembly is being instrumented for testing in the 4th quarter of 2014.

Future Achievements

- Complete PCM development to meet project objectives.
- PCM HX design, fabrication, and tests.
 - Complete PCM HX specification and CAD design.
 - Fabricate full size PCM HX to prepare for prototype bench testing.
 - Integrate PCM HX into a system on the bench.
 - Carry out bench test at Delphi and validation test at ORNL.
 - Improve PCM HX component simulation MATLAB model and ePATHS system simulation MATLAB model.
- Vehicle Build and Test.
 - Complete packaging study with Ford Focus Electric and baseline range evaluation.
 - Vehicle garage build with final system components.
 - Vehicle performance and range tests in Climatic Tunnel and on road.



III.B.2. Technical Discussion

Background

Climate control poses a severe challenge for battery electric vehicles (BEVs), plug-in hybrid electric vehicles (PHEVs), extended range electric vehicles (EREVs), and even hybrid electric vehicles (HEVs). Cabin heating, depending on the size of the vehicle and the environmental conditions, typically requires 3.2 to 6.5 kW of battery power at the ambient of -10°C to meet transient and steady state comfort requirements. For the larger sized electric vehicles of various genres (xEV), the required battery power may be even greater. The battery power used to generate the heating, either through a heat pump or direct resistive heating, leads to dramatic decrease in the driving range of xEVs. It is estimated that the range of a BEV can be reduced by 20%–40%, depending on the drive cycle. It is essential, therefore, to develop a reliable, cost-competitive, and more energy efficient occupant heating system that can help reduce the battery load and increase the vehicle electrical driving range while still ensuring occupant comfort.

Introduction

The term “phase change material” (PCM) is used to describe materials that use phase changes (e.g., melting) to absorb or release relatively large amount of latent heat at essentially constant temperature. The most commonly used

PCM is water/ice. Because ice takes in a large quantity of heat when it melts, ice is very effective when used in a cooler to keep food or beverages at temperatures near water’s freezing point of 0°C. In general, when the temperature becomes warmer than the freeze point, PCMs liquefy and absorb and store heat. Conversely, when the temperature drops, the material will solidify and give off heat to warm a medium for productive use.

The Delphi team is working with its project partner Entropy Solutions, a leading PCM material supplier in the industry, to custom-develop an advanced PCM material with a latent heat value equal to or greater than 350 J/g with phase transition occurring near 100°C, and integrate the PCM material into an innovative, self-contained system to provide charging and discharging of heat to support BEV climatic heating for passenger comfort. The ePATHS project aims to develop a light-weight, compact, and scalable TES system to meet a wide range of grid connected vehicles’ heating needs. Delphi is working with its OEM partner, Ford Motor Company, to integrate the ePATHS system into Ford Focus Electric to demonstrate its capability and commercial viability. The development of the ePATHS system is also be supported by the analysis and testing capabilities from Oak Ridge National Laboratory (ORNL) to achieve optimization in performance, packaging, weight and other key metrics.

Approach

System Architecture Development

The ePATHS system is designed to store heat using power from the electric grid and release heat to warm up vehicle cabin during driving (as shown in Figure III-3) in low temperature ambient conditions. The objective is to facilitate range extension for BEV vehicles. The PCM HX is the core of the ePATHS system. It contains the PCM heat storage medium and an internal heat exchanger that allows heat to be added to or removed from the PCM material by passing a high-temperature ethylene–glycol–water (EGW) coolant stream (approximately 120°C), or a low-temperature (less than 100°C) coolant stream. A pump is used to provide the pressure head required to circulate the coolant stream.

During heat storage operation while the vehicle is parked in the garage and attached to the power grid, a coolant heater (of the types PTC, glow plug, or surface heater) is used to generate the high temperature coolant stream. During this time, the cabin heater is bypassed by the heater bypass valve (HBV) to reduce heat loss. The high temperature coolant stream circulates through the PCM HX to release the heat to the PCM material for thermal storage.

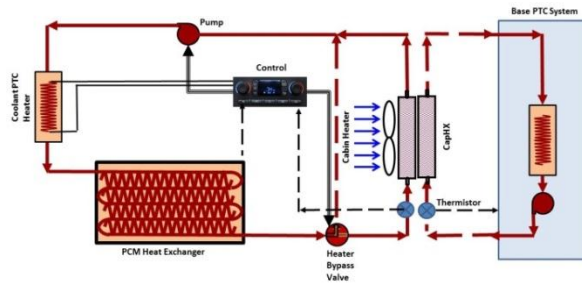


Figure III-3: ePATHS System Design

In production mode during a trip, the coolant valve is controlled to include the cabin heater in the coolant flow path. A coolant stream near 100°C is sent through the cabin heater to exchange heat with the outside air (OSA) or recirculated air (RA). Warm air up to 65°C is generated by the cabin heater and is circulated by a HVAC blower into the cabin to provide passenger comfort. As a result of passing through the cabin heater, the coolant stream's temperature is reduced and it is pumped back to the PCM HX via the coolant PTC heater for reheating. By design, the PCM material releases its sensible and latent heat to warm up the coolant temperature back to 100°C. Depending on the ambient condition and cabin thermal load, the PTC heater may be powered to supply additional heating capacity by using the electrical battery power.

The system of Figure III-3, takes advantage of a double layered, internally configurable heat exchanger that was first demonstrated in a DOE ARPA-e project and known as the CapHX. Figure III-4 shows an isometric view of the heat exchanger at the top and the configurations at the bottom. Two coolant inlets and two outlets are available on the CapHX. One inlet-outlet pair may be used for a hot stream connection and another pair may be used for a cold stream connection. At least three main configurations are obtainable by actuating the internal valves. Either the cold or hot streams may be routed to go through both the front and rear slabs of the two layer heat exchanger to achieve pure cooling or heating modes of operation. Additionally, the CapHX may be configured for the front slab to run with the colder stream and rear slab to run with a hotter coolant stream. This capability is perfectly suited to enable a PCM based heating system and provide deep level of heat energy extraction from the PCM HX.

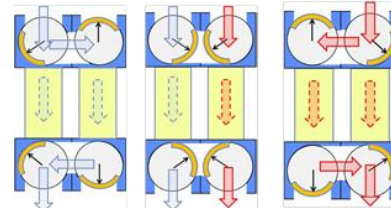
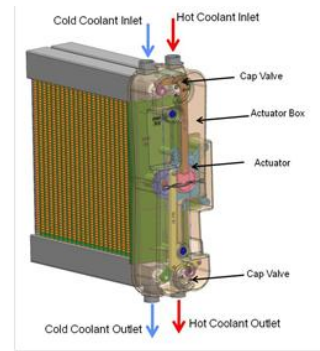


Figure III-4: CapHX and Configurations

In the system design of Figure III-3, when PCM HX is used to provide all the heating to the cabin, the CapHX is configured in the pure heating mode, in which the hot coolant stream from the PCM HX is fed into both the front and the rear slabs of the CapHX. The full heat exchanger capacity of the CapHX is utilized to provide transient cabin heating. When the coolant temperature from the PCM HX drops below certain temperature level, it becomes insufficient to provide comfort to the cabin on its own. In all previous variations of system design, energy extraction from the PCM HX will be terminated. Cabin heating responsibility is transitioned to the vehicle battery driven PTC heater. The residual energy in the PCM HX is left unused. With the CapHX, however, it is possible to continue to extract heat from the PCM HX until the PCM temperature drops near the inlet air temperature, such as 0°C in a -10°C environment. The warmed air from the front slab of the CapHX can be further heated up by the second slab using the heat from the vehicle PTC heater. A seamless transition of heating can be achieved.

The "control" unit in the ePATHS system coordinates the charging and discharging operations by controlling the coolant circulation pump, the bypass Valves, and the PTC Heater, etc. The sensory inputs to the Control unit come directly from connected sensors and indirectly from the vehicle controlled area network (CAN) bus. The PCM HX is installed with temperature sensors (thermocouples or thermistors) to allow calculation of the PCM state of charge (pSOC). The vehicle ignition state, the electrical battery state of charge (bSOC), and the heating system settings commanded by the driver, are communicated to the Control unit via the CAN bus.

While connected to the grid, electrical battery charging takes precedence over ePATHS' system charging. As the electric battery gains full charge, such as greater than 75% (or if excess power is available that can be used for the ePATHS system charging), thermal charging of the PCM may start. Total charging current is monitored for fire safety. The charging of PCM in the PCM HX will continue until it is fully charged. Thereafter, a trickle charge may be applied to maintain the charging status.

Predictive charging control is possible when a standard daily routine is established by the controller, either through manual input or through smart learning algorithm. For example, charging may be scheduled to start three hours ahead of vehicle departure for the morning trip to work. The benefit of predictive charging includes reduced heat loss overnight from the PCM HX and increased energy efficiency to the charging system. However, obtaining a full charge before leaving the garage is desirable to ensure that maximum range extension will be achieved with the ePATHS system.

Predictive charging also makes it possible to “charge based on need” by using historical and/or predicted climatic data and location information to determine the amount of charging needed for a particular date. For deep winter temperatures, full charge is required. For early fall or late spring, partial charge may suffice for a day’s need.

Meanwhile, during predictive charging control, cabin pre-conditioning can be incorporated by allowing a specified portion of the coolant stream to go through the cabin heater, such that both the PCM HX charging and the pre-conditioning are completed before departure. The HBV may be proportionally positioned to regulate coolant flow into the cabin heater. Given the fixed capacity of ePATHS PTC heater, charging time of the ePATHS system may be prolonged due to the diversion of coolant stream for cabin pre-conditioning. Heating of the cabin will be performed in a manner that it will not extract stored energy from the PCM. The PTC heater will provide all of the thermal power needed to pre-heat the cabin.

The rate of discharge of the PCM HX is controllable by means of the coolant flow rate. Slower coolant flow rate provides reduced PCM discharging rate due to reduced heat transfer coefficient (and a direct limit of the thermal capacity of the fluid, $\dot{m} c_p \Delta T$) on the coolant side of the PCM HX, thus prolonging the availability of heat from the PCM material. The reduced discharging rate may be used to extend the duration within which a minimum level of comfort can be maintained. Conversely, a higher coolant flow rate through the PCM HX allows a quicker discharge of the PCM material. Depending on the bSOC near the end of the day, it may be beneficial to allow the PTC heater to turn on at defined power level to supplement PCM-based heating.

Phase Change Material Development

Entropy’s patented fat and oil based PCMs were developed under three years of research sponsored by the USDA. These PCMs are made from a green technology, in that bio-based products—namely soybean oil—are converted into PCMs. They are non-toxic and provide a new value-added non-food product for American farmers. They are capable of thousands of melting and freezing cycles without performance degradation. There is no concern for oxidation or concern that these fat and oil products will become rancid because they are fully hydrogenated. Fully hydrogenated fats can be stable for decades as they do not have chemical sites for oxidation to occur.

Entropy Solutions follows an established process to develop and evaluate PCM for the ePATHS project. Six families of PCMs are under investigation. The development process starts with synthesizing a chemical compound through chemical reactions that produce sufficient PCM for

characterization of the melting temperature and the latent heat of solidification. Once synthesized, the sample is purified as required for characterization. The characterization of the compound is then done using differential scanning calorimetry (DSC) machine measuring the melt temperature and the latent heat. If the resulting sample shows melt temperature and latent heat approaching the project target values, the sample is then cycled thermally to establish the temperature stability of the PCM.

To date, many candidate compounds have been assessed within each family. Although multiple candidates have shown the thermal properties of melting temperature and latent heat near the project target values, they did not pass thermal stability testing under normal exposure to air.

Data has shown that these families of PCM deteriorate chemically when exposed to moisture or air. Thermal properties can degrade to unacceptable levels when compared to the target values. However, it has been shown that by isolating the PCM from exposure to air and moisture, the PCM thermal properties remain stable over extended number of thermal cycles. It is possible, though not preferred, to use nitrogen to provide isolation during transportation and during the PCM heat exchanger manufacturing process.

Modeling for PCM Heat Exchanger and ePATHS System

A detailed heat transfer model for the PCM HX was developed to facilitate the optimization of HX design. The model calculates the heat transfer from the PCM to a 50–50 mix EGW coolant fluid. The inlet temperature and mass flow rate of the EGW are inputs to the model.

A preliminary ePATHS system model was developed and implemented in MATLAB Simulink. It calculates the heat transfer and fluid flow conditions that are present in the ePATHS system as the PCM HX is charged and discharged. With the model, the PCM heat storage system’s performance can be more realistically evaluated and its design better optimized.

For the PCM heat exchanger model to run sufficiently fast to allow ePATHS system simulation, an innovative map-based approach for the PCM heat exchanger was taken to reduce computational effort. The theoretically high accuracy discretized PCM heat exchanger model was run in advance in batch to build a database of heat transfer results. Analysis was then performed to develop a map for the functional dependence of the heat transfer on (1) the fraction of PCM liquid contained in each cell, (2) the temperature difference between the coolant and the PCM and (3) the local wall heat transfer coefficient. It was discovered that a single heat transfer coefficient, which depends only on the fraction of PCM liquid present locally in each cell of the heat exchanger, could be used to characterize the heat flow to the coolant from the PCM, and the local temperature difference between the PCM freezing temperature (which remains constant) and the coolant is the appropriate temperature difference controlling this heat transfer.

The heat transfer correlation for the PCM HX corresponds to the period when freezing of the PCM takes place in each cell. Generally, this represents the majority of the heat transfer from the PCM. However, sensible heat remains in the solidified PCM and single phase conduction to the coolant

stream takes place even after freezing is complete. For simplicity, a basic two-node analysis was employed to calculate the transient conduction from the solid PCM to complete the parametric PCM heat exchanger model. The heat transfer calculation using this simplified methodology was implemented into the ePATHS system model. Initial validation tests indicate high potential. Full validation is still to be completed.

PCM Heat Exchanger Development

Quarter-Width PCM Heat Exchanger

The PCM thermal storage HX is a key component of the ePATHS system. A full-size PCM HX has been designed that will meet heat capacity requirements of the project. As a development step, a quarter-width heat exchanger was designed in Unigraphics using solid modeling. In Figure III-5, the completed CAD model of the quarter-width PCM heat exchanger is shown. The design includes 2 PCM filling ports, 12 internal PCM temperature measurement thermocouples, coolant tubes, PCM fins, tanks, coolant inlet and outlet couplers, and a pressure measurement tap. The HX has a two pass design for the coolant side. As the coolant flows through the PCM HX, it will either melt or freeze the PCM material depending on the operating mode of charging or discharging.

The HX was constructed with aluminum components in Delphi's Lockport Technical Center (LTC) model shop. The manifolds were formed with a Delphi made punch. The HX core was made with production PCM centers and coolant tubes. Two assembled cores were then brazed in a high-temperature furnace. After braze, the inlet and outlet tanks were welded to the core to finish the build.

After passing a pressurized leak test (prior to welding the enclosure to house the PCM), the unit was installed on a radiator test stand and dissipated for heat transfer performance as an air to coolant heat exchanger. The air to coolant heat dissipation test was used as braze quality check.

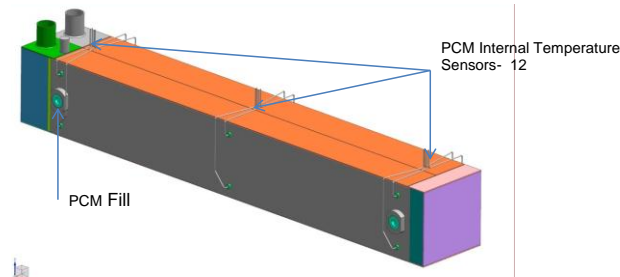


Figure III-5: Quarter-Width PCM Heat Exchanger



Figure III-6: Enclosed Quarter-Width PCM Heat Exchanger

The quarter-width heat exchanger (Figure III-6) was then filled with 5 kg of PCM material. That put the total mass of the quarter-width PCM HX at 8.3kg and the total volume at 8.2 liters. Based on the quarter-width HX data, the mass of the full size PCM HX is projected to be 33.3 kg (vs. the target of 33.4 kg). HX insulation will add another 1~2 kg. The full sized PCM HX volume is predicted to be 32.9 liters without insulation, 35.0 liters with insulation versus the stated target of 31.0 liters. This would indicate further work will be needed to minimize the volume to achieve the project target. Options for reducing the volume include utilizing the CapHX heat exchanger technology to extract more heat from the PCM and the use of partial recirculation of cabin air to reduce the heating load.

PCM Heat Exchanger Insulation

The present project requires an insulation system that is allowed to lose only 10% of the PCM stored energy over an 8 hour period. Vacuum insulated panels (VIPs) are assessed as the primary candidate technology to meet the heat loss requirement.

The scope of the insulation development was broken down into three phases. Phase 1 was to design, build, and test a 10% scale model of the full PCM heat exchanger. The 10% scale PCM HX was wrapped with 2 mm of aerogel insulation and enclosed in the VIP chamber. This phase has been completed.

Phase 2 will use the selected VIP and aerogel to surround the quarter-width heat exchanger. Effectiveness of the insulation system will be evaluated before embarking on the final phase, where the full size PCM heat exchanger will be evaluated to assess whether the target of less than 10% energy loss over 8 hours can be achieved.



Figure III-7: 10% Scale VIP

The technical challenges to implement VIP insulation along with an underlayment of aerogel are significant. VIP barriers are generally designed for “cold” applications. From previous research performed by VIP suppliers, it was determined that at 120°C the performance will decrease about 3% in 24 hours for a 12.7 mm thick panel. For a 25.4 mm thick panel the decrease will be about 1.5% in 24 hrs. The conclusion is that barrier development will be necessary to meet desired performance requirement.

The Delphi team has been actively working with VIP insulation system suppliers to develop the best performing VIP insulation system. Figure III-5 shows a VIP insulation jacket for the 10% scale HX from supplier A. The performance tests of this system indicate a loss in the 20% range over a period of 8 hours. Other concepts from suppliers B and C are being investigated.

System Controls Development

The Delphi Thermal HVAC development controller Figure III-8) is the main stream candidate for the ePATHS system controls operations. It is an automotive grade controller meeting validation requirements for automotive applications. The controller is equipped with a 7 inch color touch screen interface for displaying and inputting system data and control values. It support various communication protocols and can communicate with the vehicle CAN bus through a bridging module. A laptop PC can be used directly to communicate with the controller for calibration and data logging. Sufficient input and out channels, both digital and analog, should allow the ePATHS system to be controlled effectively.



Figure III-8: Delphi Thermal HVAC Developmental Controller

Communication Development

SAINT II is the targeted bridge module to the vehicle CAN bus. Delphi Thermal Electronics Integration Group will provide software to bridge communication between the vehicle CAN bus and the Delphi ePATHS Controller.

Human Machine Interface

Human-machine interface (HMI, aka control panel) will be used to provide occupant interaction with the PCM heating system. Touch screen will be used to interface with ePATHS controller. Touch screen graphics will be developed to enable control. During vehicle operation, key PCM system parameters (pSOC, coolant temp, flow rate, etc.) will be displayed. During charging while parked at work or home garage, control functions will be provided to allow occupant override of the charging process.

Charging Hardware and Software Development

Because of scarcity of high-voltage charging (240 V) at home garages, the present project will assume workplace charging with a dedicated charging station operating at 240 V. When the vehicle is at home, 120 V trickle charge will be enabled when excess current is available above and beyond electric battery charging. Delphi ePATHS Controller will supervise current draw from PCM heater to prevent overloading the electrical circuit.

The PCM charging will share the same power cord from charging station to Ford Focus Electric. AC power of 120 V/240 V will be tapped from within Ford Focus Electric with an internal connector. The PCM charging heater current draw will be controlled via a voltage controller (targeting Watlow DIN-A-MITE C) to prevent overloading of the electric circuit.

Figure III-9 represents the initial charging algorithm design. Key considerations include intelligent charging to reduce energy cost, compatibility with electric battery charging, quick charging at day's end to be ready for short errand trips, etc.

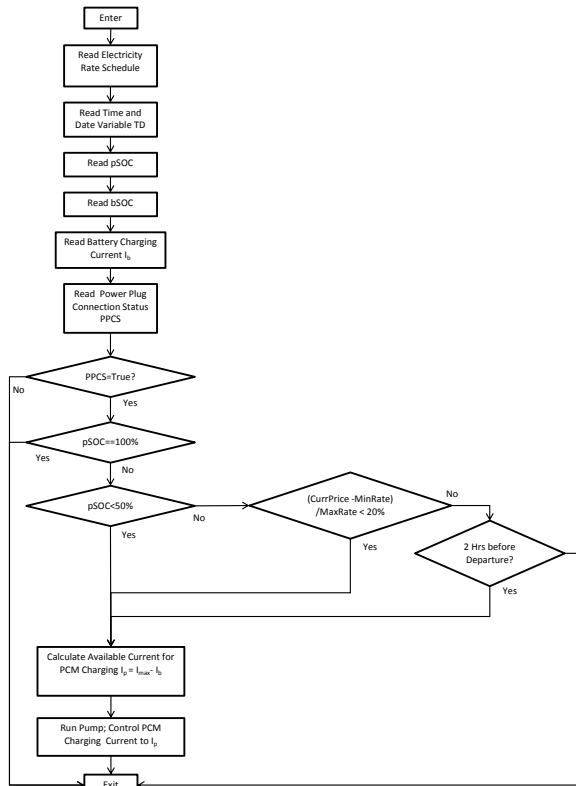


Figure III-9: PCM Charging Control Algorithm Design

Results

PCM Heat Exchanger and Insulation System

The quarter-width PCM HX unit was installed on the radiator test stand and dissipation tests for heat transfer performance (from coolant to air) were run. The test data were compared to the performance data predicted by Delphi's heat exchanger analysis software. Very good agreement with the prediction was achieved. Discrepancies are generally within 8% of predicted values, as shown in Figure III-10. Additional tests were run on the radiator dissipator to confirm that the temperature variations across the core face area were acceptable. A maximum temperature spread of 2.2°C was seen from the top of the core to the bottom of the core. On the coolant side, good coolant distribution was achieved, which will allow the PCM material to melt and freeze uniformly across the entire core.

Subsequent to the air-coolant test as a preliminary quality check, the quarter-width PCM HX was tested with a PCM having latent heat of 175 J/g and a melting temperature of 101°C. Even though this PCM has significant lower latent heat than the target PCM to be developed for the present project, the charging and discharging should still be indicative of the HX's ability to transfer heat. Figure III-11 shows the PCM temperature profiles at various locations within the HX. It can be seen that the quarter-width PCM HX was charged after about 8 minutes with a 120°C coolant flow at 0.75 gallons/minute flow rate.

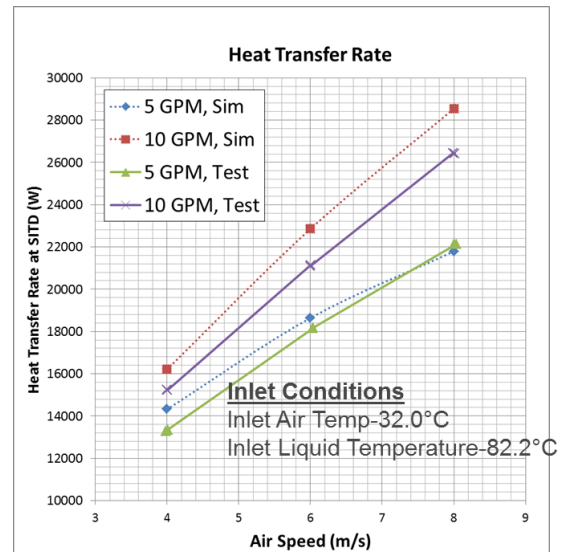


Figure III-10: Heat Transfer (Predicted vs. Test)

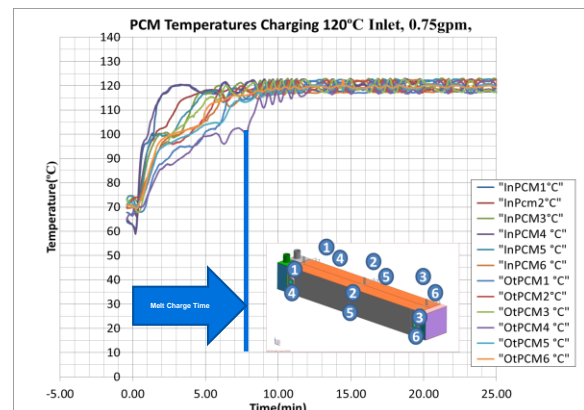


Figure III-11: Charging Time and Temperature Profiles

The heat transfer rate during charging is shown in Figure III-10. A maximum rate of 9 kW was achieved in the beginning of charging and the rate gradually decreased to zero as the PCM material became fully charged. Figure III-12 also shows the total energy stored in the quarter-width PCM HX. At the end of charging, the total energy was 0.64 kWh.

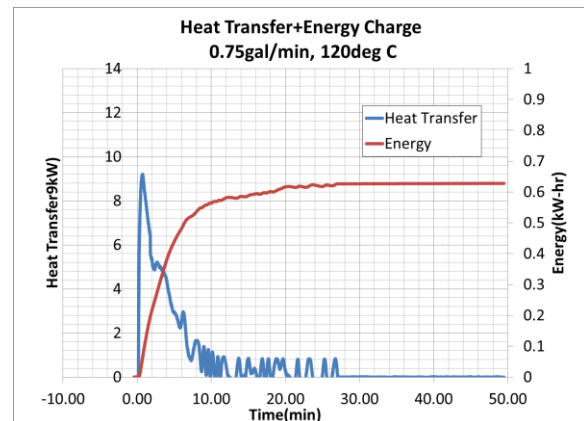


Figure III-12: Heat Flux during Charging and Energy Storage in PCM HX

For insulation system development, the 10% scale PCM HX was filled with 345 g of PCM with 101°C melting temperature and 175 J/g latent heat. The 10% scale PCM HX with aerogel was heated to 120°C to charge the PCM, then removed from the heating chamber and immediately placed into the prototype VIP insulation jacket. The VIP and HX were then put into a second chamber at -10°C to measure the amount of thermal energy loss. Figure III-13 presents the temperature profile at various points of the insulated 10% scale PCM HX. The tests indicate that the prototyped VIP technology's loss rate is over 20% of the stored energy over a period of 8 hours.

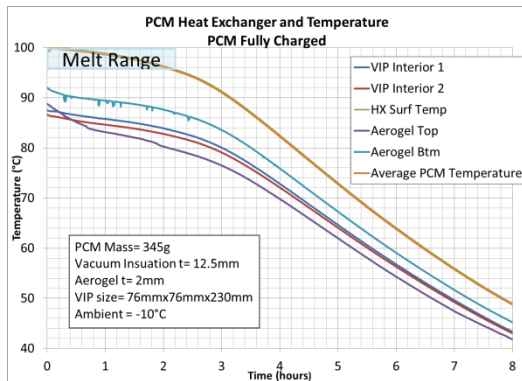


Figure III-13: Freezing of PCM in VIP

PCM Heat Exchanger Parametric Study

PCM HX parametric analysis was performed by ORNL using the higher accuracy discretized PCM HX model to evaluate the impact of various HX design and operational variations. Figure III-14 shows the results from the parametric evaluation of the fin pitch on PCM HX performance. The baseline design uses a pitch of 2 mm. The results indicate that the overall heat transfer efficiency is not strongly improved with increases to the density of fins, and it may be possible to achieve the design goals with somewhat reduced fin density and the associated mass.

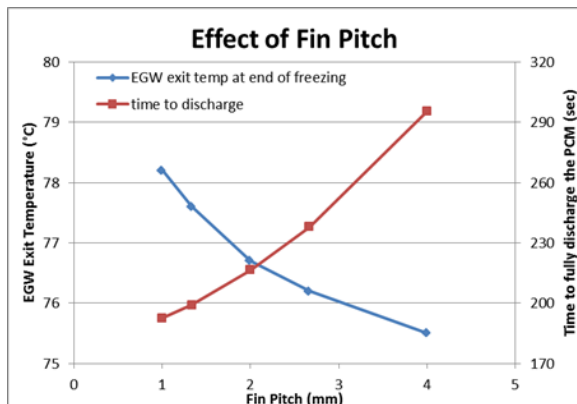


Figure III-14: Fin Pitch Study for PCM Heat Exchanger

The effect of change of EGW flow rate was also evaluated, and the simulation results indicate that higher flow rate can have a rather large effect on the exit temperature from the PCM HX. Since the analysis was run using a constant fluid inlet temperature of 70°C, the impact is most likely exaggerated relative to how the HX would operate in the

ePATHS system. At higher flow rate conditions, for the same cabin heating load, the temperature drop of the returning fluid should decrease, resulting in a higher inlet temperature. However, this effect is not easily assessed in the PCM HX model by itself but will be visible in the results of the system simulation model.

Phase Change Material Development

Six families of chemical compounds have been investigated for latent heat, melting temperature, and chemical stability:

- Family A Analysis – Samples AADA5 and AADA9 produced adequate melting points. However, the remaining members of this family produced melting points below the targeted range (90°C–100°C). Additionally, the latent heats produced by this family are much lower than the targeted value.
- Family B Analysis – As a group, Family B produced much higher latent heats relative to Family A but produced substantially lower melting points. Additionally, while this family produces relatively high latent heats (223–255 J/g), the latent heats are still 100 J/g lower than the targeted value.
- Family C Analysis – This family produced melting points in the desired range; however, the recorded latent heats are much lower than the targeted value.
- Family D Analysis – The synthesis of Family D has been completed but purification and characterization are ongoing. Latent heats will be measured upon the completion of the purification and characterization steps.
- Family E Analysis – Latent heats have been measured for both members of Family E. AAWB1 satisfies the required melting point and latent heat requirements. Relative to AAWB1, AAWB2 has a sharper melting point and refreezes easily; however, the latent heat is drastically lower than that of AAWB1. These results are encouraging; therefore additional members of this family will be identified and synthesized.

While several chemical compounds exhibited 350 J/g latent heat, they were disqualified by thermal stability or low melt point. However, Compound AAW12DA demonstrated high latent heat and thermal stability over a thousand thermal cycles when isolation is applied (Figure III-15). The melt temperature is at 70°C, which is lower than the desired phase change temperature.

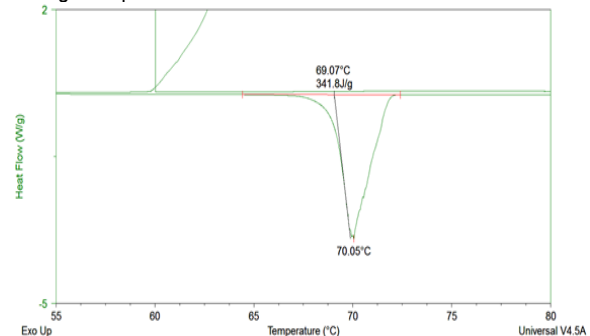


Figure III-15: Latent Heat and Melting Temperature for Sample AAW12DA

Members of Family B demonstrated high latent heat and the potential for high melting temperature. Significant effort is now being applied to explore members of Family B. Specifically, the development of Family B is now focused on the synthesis of higher molecular weight molecules, which should afford higher melting points and latent heats.

Conclusions

As part of the *EV Everywhere* initiative, the U.S. Department of Energy’s Office of Energy Efficiency and Renewable Energy (EERE) is funding Delphi Automotive Systems and sub-recipients to develop a thermal storage system that will eliminate the need to use the on-board electric battery energy for heating the cabin during typical cold weather worker commutes in the United States for grid-connected vehicles. The ultimate goal is the extension of BEVs’ driving range.

The Delphi team and its partners, Ford, ORNL, and Entropy Solutions, have executed the ePATHS development project according to the tasks laid out in the statement of work and by the committed timing. Substantial progress has been made toward the development objectives of the project and the team is confident that the BP-1 milestones will be met. The BP-1 milestones include completion of both the system and component technical specifications and the engineering designs for the developmental level components such that they can be released for developmental part build. Both of these tasks are on track to finish by the end of BP-1.

III.B.3. Products

Publications

1. Sutterlin, W. R. “Developing PCMs that Exhibit Latent Heat Values Above 350 J/g Using Renewable and Non-Toxic Resources,” 2014 Advancements in Thermal Management Conference, Denver, CO, August 6, 2014.

Patents

1. N/A

Tools and Data

1. LaClair, T. and Z. Gao, PCM Heat Exchanger Simulation Model, ORNL, 2014.
2. LaClair, T. and Z. Gao, ePATHS System Simulation Model, ORNL, 2014.

III.C. Advanced Climate Control and Vehicle Preconditioning- DE-EE0006445

John Meyer, Principal Investigator

Halla Visteon Climate Control
One Village Center Drive
Van Buren Twp., MI 48111
Phone: (734) 710-5420
E-mail: jmeyer8@hvccglobal.com

David Anderson, DOE Program Manager

Phone: (202) 287-5688
E-mail: David.Anderson@ee.doe.gov

III.C.1. Abstract

Objectives

- Increase the range of light duty electric drive vehicles through climate system load-reducing technologies.
- Maintain occupant comfort.
- Validate energy efficient technologies through the use of computer-aided engineering (CAE) models.
- Develop a commercial pathway toward utilizing the load-reducing technologies in light-duty electric vehicles.
- Integrate and validate technologies in a vehicle.

Major Accomplishments (FY 2014)

- Vehicle selection completed.
- Test conditions defined.
- Range improvement targets set.
 - Baseline vehicle testing complete.
- Computer-aided engineering (CAE) models.
 - Creation of 1-D system model including detailed componentry.
 - Creation of 3-D cabin model with and without mannequin information.
 - Validation and refinement of model prediction accuracy through use of system bench data and vehicle data.

Future Achievements

- Phase 1: Architecture Determination.
- Phase 2: Component Design, Fabrication, and Validation.
- Phase 3: Vehicle Integration, Validation, and Demonstration.



III.C.2. Technical Discussion

Background

The transportation sector is an industry segment that must contribute to reducing petroleum dependence in the United States, as well as greenhouse gas emissions. One area with a high potential to decrease oil consumption and emissions is the electric drive vehicle. However, a barrier to its widespread acceptance is consumer “driving range anxiety.” Can an electric vehicle take me the distance I need to go? Increasing the range of electric vehicles is a key factor in achieving its mass market adoption. Since the climate system is the largest auxiliary load on electric drive vehicles, it is a prime candidate for onboard load reduction, which in turn increases vehicle range, thus positively impacting consumer acceptance of electric vehicles. This is especially true in intense hot and cold climates where range is significantly diminished by the climate system load.

Introduction

This project is exploring a technical approach to reducing the power required to operate the climate control system on a grid connected electric drive vehicle while still maintaining occupant comfort. It focuses on three main technology areas for climate system load reduction in an electric drive vehicle: thermal energy storage with preconditioning, refrigerant system performance, and zonal cabin comfort.

Providing occupant thermal comfort can consume upwards of 40% of the energy stored in GCEDV batteries, and thus improving the way comfort is achieved will result in extending the range of these vehicles. Achievements in electric vehicle climate load reduction have the opportunity to improve the current electric vehicle market, as well as open the market to climate zones previously unable to utilize these vehicles.

Approach

A three phase approach is taken to define, design, and demonstrate climate power reduction technologies. This method ensures positive progress and results of shorter term objectives, which are vital to overall project success, before moving between phases. During Phase 1, the major project metrics are defined. These metrics will be used throughout the project to guide and measure the success of the technologies introduced. In addition, the computer aided engineering (CAE) models are built and correlated to data from baseline vehicle and system level testing. These validated models are then used to support trade studies that assess various technology

alternatives. This phase ends with a decision on the most favorable technologies to be applied to the baseline vehicle architecture to improve range. In Phase 2, the componentry necessary for each of the three technology areas are designed, fabricated, and verified through bench testing. Finally in Phase 3, the vehicle is integrated with the new technology and the vehicle level impacts confirmed. The project is currently in Phase 1.

Results

Vehicle Selection

The 2015 model year Kia Soul electric drive vehicle, shown in Figure III-16, with a positive temperature coefficient (PTC) heater and heat pump was selected as the vehicle to be used for evaluation and demonstration of the project technologies. This vehicle choice challenges the project to expand technologies beyond the most current production electric vehicle designs.



Figure III-16: 2015MY Kia Soul EV

Defined Test Conditions

Identifying test conditions that are representative of electric vehicle driving patterns required a look into U.S. population densities, regional weather data, real world driving patterns, electric vehicle characteristics, and clothing considerations. These factors were considered to adequately cover conditions occupants of electric drive vehicles experience in today’s market, as well as those that could be experienced in an expanded future market. From the analysis, six environmental test conditions were derived to assess the climate control system performance that represents conditions seen in the United States. These conditions include the extremes of weather experienced in cities like Phoenix Arizona and Fairbanks Alaska, along with milder conditions experienced in California, and warm areas like the gulf southeast and upper east. A matrix showing the 6 test conditions is shown in Table III-2

Table III-2: Project Test Conditions

| Test | Temp | Solar Load (W/m ²) | Humidity | Number of Occupants |
|--------|--------------|--------------------------------|----------|---------------------|
| Cold 3 | -18°C (0°F) | N/A | N/A | 2 |
| Cold 2 | -5°C (23°F) | N/A | N/A | 4 |
| Cold 1 | 5°C (41°F) | N/A | N/A | 1 |
| Hot 1 | 28°C (82°F) | 750 | 70% | 1 |
| Hot 2 | 32°C (90°F) | 850 | 70% | 2 |
| Hot 3 | 43°C (109°F) | 1000 | 40% | 1 |

Range Improvement Target

From vehicle and system knowledge, and confirmed by baseline vehicle testing, it is understood that the steady-state power consumption of the HVAC system to provide thermal comfort is small compared to the power needed to move the vehicle. However, during initial cool-down (hot weather) or warm-up (cold weather) the HVAC system can use more than 50% of the power required to move the vehicle. This is illustrated in Figure III-17, obtained from the baseline wind tunnel testing data. For this reason, employing thermal storage with preconditioning offers the biggest benefit in improving the vehicle range.

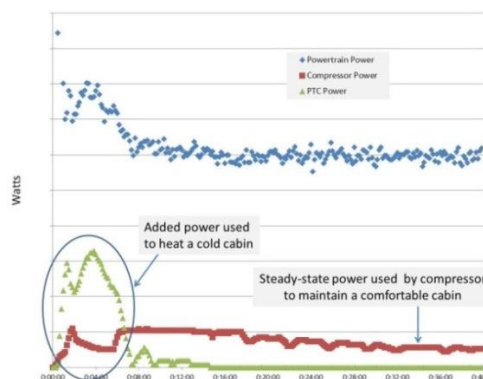


Figure III-17: Power consumption during 5°C warm-up test

Component power consumption was measured during baseline vehicle wind tunnel testing. Using that data, along with initial assumptions for improvement opportunities, the calculation of estimated power reduction and therefore improved vehicle range was possible. The resulting improvement calculations for each of the 6 test conditions were made assuming a constant drive length of 40 minutes for each leg of a trip. The resulting improvement values are shown in Table III-3. For each test condition two calculations were made. For the “Depart” value it was assumed that the vehicle was plugged in prior to the trip, so thermal storage with precondition could be used. For the “Return” calculation it was assumed that no plug is available, so no thermal storage with preconditioning was used. A composite percentage of all assumed improvement technologies was then generated for two scenarios: (1) the vehicle is preconditioned before departure, but not preconditioned before the return, and (2) both legs of the trip employed preconditioning.

Table III-3: Weighted Range Improvement Targets

| Values in table assume all trips are 40 minutes | | | | | | | |
|---|--------------------------------------|---|----------------|--------------------|---------------------------|---------|------|
| Test Conditions | Technologies evaluated independently | | | | All technologies combined | | |
| | Improved Refrigerant System (%) | Thermal Storage w/ Pre-conditioning (%) | -3Amp BYAC (%) | +3C Evaporator (%) | (1) (%) | (2) (%) | |
| Cold 3 (-18C) | Depart | 0.8 | 8.8 | 0.4 | 0.0 | 5.5 | 9.9 |
| | Return | 0.8 | 0.0 | 0.4 | 0.0 | | |
| Cold 2 (-5C) | Depart | 1.8 | 11.3 | 0.6 | 0.0 | 8.1 | 13.9 |
| | Return | 1.8 | 0.0 | 0.5 | 0.0 | | |
| Cold 1 (5C) | Depart | 1.5 | 11.4 | 0.6 | 0.0 | 7.7 | 13.3 |
| | Return | 1.5 | 0.0 | 0.6 | 0.0 | | |
| Hot 1 (28C) | Depart | 1.9 | 3.7 | 0.7 | 3.6 | 7.9 | 9.5 |
| | Return | 1.9 | 0.0 | 0.7 | 3.6 | | |
| Hot 2 (32C) | Depart | 2.8 | 6.8 | 0.6 | 5.3 | 12.7 | 15.0 |
| | Return | 2.8 | 0.0 | 0.6 | 5.3 | | |
| Hot 3 (43C) | Depart | 4.7 | 13.9 | 0.6 | 8.7 | 20.6 | 27.2 |
| | Return | 4.7 | 0.0 | 0.6 | 8.7 | | |

[1] Assumes all 40 minute trips. Thermal storage before depart only.

[2] Assumes all 40 minute trips. Thermal storage before every trip.

The improvement assumptions in Table III-3 show roughly a 7%–8% improvement can be expected for an occupant making an 80-minute round trip at -5°C or 28°C ambient temperature with preconditioning before their departure. The range improvements are further enhanced on trips of shorter duration or when preconditioning can be utilized on the return leg of the trip. In addition, substantial vehicle benefits from the energy-saving technologies occur when operated in extreme hot or cold temperature conditions, such as -18°C or 43°C. Advances in the vehicle range in extreme environmental conditions improve the opportunities for drivers to select an EV in their specific geographic location which broadens the potential EV market. All improvement estimates are a strong function of ambient temperature and drive cycle.

Computer-Aided Engineering (CAE) Models

The system model was created using detailed component information from the baseline climate system. The model is based on the 1-Dimensional Dymola simulation tool. Once the model was constructed and solved, the first model-to-test data correlation, shown in Figure III-18, was completed. This figure shows predicted refrigerant temperatures were generally within 2°C–3°C of the experimental values. The predicted air discharge temperature was off by only 0.1°C. This initial comparison data shows very positive results. Once all test point assessments are complete some additional tuning will undoubtedly be required. This will result in the accuracy increasing for some points and decreasing for others until a best fit is achieved.

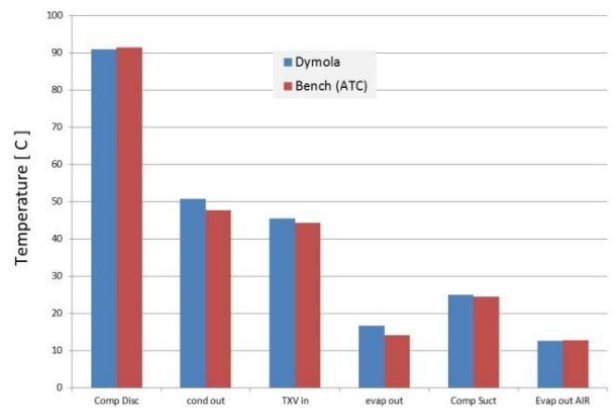


Figure III-18: Initial System Model to Empirical Data Correlation

The cabin model, a full 3-dimensional computational fluid dynamics (CFD) model, is complete in structure. It is modeled as just the vehicle cabin, as well as the vehicle cabin with occupants. Its initial comparisons to wind tunnel test data were favorable. The Kia Soul cabin model, with mannequins, is shown in Figure III-19.

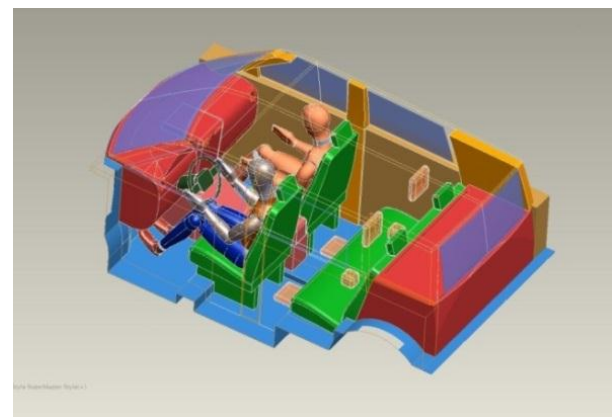


Figure III-19: Kia Soul Cabin Model with Occupants

The model predictions for the 28°C cool down test are shown in Figure III-20.

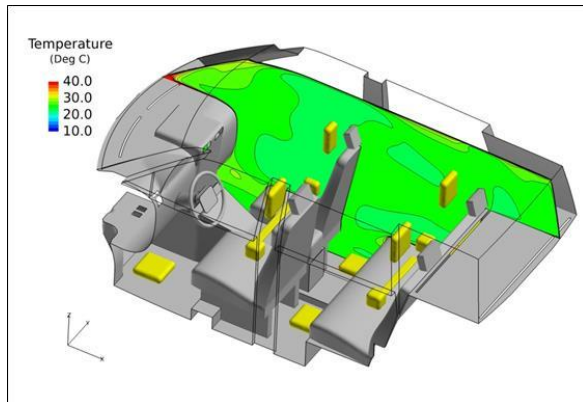


Figure III-20: CFD Interior Temp. Predictions 15 Minutes into 28°C Cool-Down Test

This represents predicted interior temperatures 15 minutes into the drive cycle. Figure III-21 shows the predicted model values and the measured values for the average interior temperature for the duration of the drive cycle.

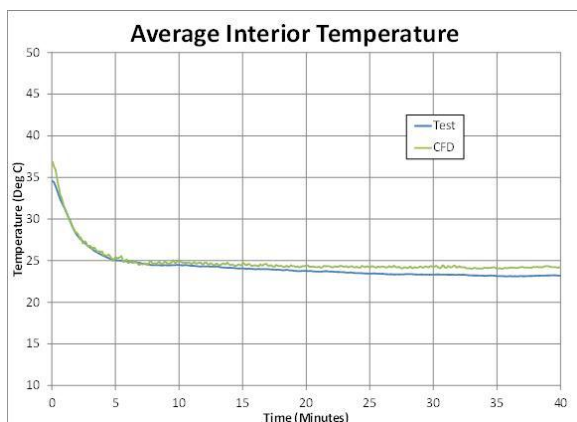


Figure III-21: 28°C Cool-Down (CFD Predictions vs. Test Values)

The majority of data are within our objective delta of $\pm 3^{\circ}\text{C}$. The model correlations are considered acceptable to move forward. Any additional fine tuning of the CFD model will be assessed during the technology trade studies.

The 1-D system model will be used to calculate discharge air temperatures and associated power consumption. The 3-D cabin model will be used to predict the interior temperatures and airflow distribution during a given drive cycle. This information will then be used in a comfort model, where air and surface temperatures can be used to predict passenger comfort. This model is being created and verified using subjective wind tunnel data.

Once model validation is complete, these modeling tools can be used to evaluate an improvement's impact on discharge air temperature and system power consumption, the interior temperature of the vehicle, and ultimately occupant thermal comfort. These tools will be used during the trade-off analysis to assess various technology opportunities.

Conclusions

- Choosing the 2015MY Kia Soul EV with PTC and heat pump promotes technology advancements beyond current state-of-the-art production climate systems.
- Testing metrics and improvement targets have been identified to measure and define project success.
- Vehicle and system level testing has provided direction in prioritizing technology area focus.
- Computer prediction tools have been utilized to generate models with sufficient accuracy to aid in evaluating technology benefits.

3.6.1 Products

Publications

1. Meyer, J. and J. Schneider. "Advanced Climate Systems for EV Extended Range." 2014 DOE Merit Review Conference, Washington DC, June 19, 2014.
2. Shim, H. R., T. Vespa, S. H. Kang, and J. Meyer. "Production Heat Pump System for a Battery Electric Vehicle." 2014 SAE Thermal Management Systems Symposium, Denver, CO, September 23, 2014.

Acknowledgements

1. Special thanks to our partners: Hyundai America Technical Center, Inc. and the National Renewable Energy Laboratory.

Tools and Data

1. Dymola published by Dassault Systems – HVAC modeling.
2. HVCC Simulation-Based Design – Occupant Comfort – multiple modeling tools.
3. CoolSim published by NREL – HVAC modeling.
4. RadTherm published by ThermoAnalytics – occupant comfort modeling tool.
5. Simulink published by MathWorks – thermal storage modeling.

TRANSPORTATION ELECTRIFICATION

III.D. Interstate Electrification Improvement Project- DE-EE0002613

Principal Investigator: Jeff Kim

Shurepower LLC, dba Shorepower Technologies
5210 NE Elam Young Parkway, Unit 160
Hillsboro, OR 97214
Phone: (503) 892-7345
E-mail: jkim@shorepower.com

DOE Program Manager: David Anderson

Phone: (202) 287-5688
E-mail: david.anderson@ee.doe.gov

III.D.1. Abstract

This project was originally named the Interstate Electrification Improvement Project, but is publically known as the Shorepower Truckstop Electrification Project (STEP). Truck idling is a common practice that consumes significant fuel and increases economic and environmental costs. Idle reduction is seen as essential to reduce petroleum imports and harmful air emissions, and increase economic benefits for truck transportation industries. When parked, trucks are idled to provide cab power for air conditioning, heat, or appliances; keep the engine warm in cold temperatures; or operate a transport refrigeration unit (TRU) or “reefer.” This proof-of-concept project tests whether (1) supplying alternative clean energy to trucks in the parking lot will reduce the idling practice; and (2) a clean energy service provider will be economically viable to sustain the service. Fifty Shorepower electric power installations have been installed at truck stops along major interstates in thirty states. Data on power usage, duration, use patterns, and motivation are being monitored and analyzed. Clear seasonal variations stand out, but user demographics, behavior, and idling choices are complex. New approaches to increasing idle reduction are being implemented.



Figure III-22: Shorepower stations serving long haul trucks at Duke's Travel Plaza on I-20 in Canton, Texas

Objectives

Reduce use of diesel fuel:

- Improve air quality.
- Support cost savings in the trucking industry.
- Reduce national dependence on imported oil.

Increase power utilization at truckstops:

- Launch effective marketing strategies to drivers and fleets to promote power use.
- Good relationships with host sites (truck stops and travel centers).
- Ongoing hardware and software improvement.
- System stability and maintenance.

Acquire and monitor data on the system and users:

- Provide NREL with data for determining driver behavior and fleet behavior.
- Monitor information impacting truck idling, to include time and duration of use, power drawn, and on-board equipment, location, and truck stop amenities.
- Analyze data to improve operations and maintenance, and marketing.

Result in an economically viable alternative energy service provider (Shorepower Technologies).

Achieve revenue levels sufficient for investing in additional power installations at other truck stops.

Major Accomplishments

(Note: this section lists accomplishments based on work performed by Shorepower as the prime recipient.)

Novation

- Shorepower became the grantee for this project, DE-EE0002613, on June 20, 2014.

Technical accomplishments

- Software and firmware improvements were made that increased system uptime and reduced customer wait times.
- Web and database improvements were made that provided more security and back-up for transactions; and faster service for customers.
- Uptime was improved from a low of 86% per week to 95% per week.
- Two chronically offline sites were brought back online.

Education and Outreach

- A new marketing campaign launched education and outreach efforts with Host Sites; and implemented an updated “success kit” (a checklist of retailing items designed to spur utilization).
- Three account managers were added to serve the needs of all host sites.
- An “Onsite Expert” program was implemented at some sites to identify and reward a truck stop staff person who agreed to be Shorepower’s main contact, and to support maintenance, replenish marketing materials, train other staff about Shorepower, and encourage drivers to plug-in.
- Added the Comdata fleet fuel card as an option for payment. Most major fleets use Comdata.

Adaptor kits

- Eighty-eight adaptor kits were distributed to drivers--half of these by the Owner-Operator Independent Driver Association (OOIDA).

Professional recognition

- Shorepower was at the OOIDA 2014 Mid America Trucking Show in Louisville, KY, with five equipment vendors, and had a demo pedestal on display. An OOIDA table distributed almost 40 kits.
- In November 2013, Securing America’s Future Energy (SAFE) awarded Shorepower Technologies its Advanced Technology Award for their leadership in driving fundamental improvements to America’s energy security.

Future Goals

- Increase system-wide uptime to 98%.
- Improve updates to software, firmware, and hardware.
- Increase promotions and retail staff training at host sites.
- Support the analysis activities of NREL.
- Increase utilization:
 - Increase power utilization up to a steady 10,000 hours per week system wide.
 - Continual software/firmware updates to ensure 95% system reliability targets.
 - Expand the participation of independent owner/operators and fleets.
 - Complete final report.
- Install Shorepower systems at additional truck stops and travel plazas after the close of the project.



III.D.2. Technical Discussion

Background

Idle Reduction Study

Using data collected beginning January 1, 2013, through December 31, 2014, a truck stop electrification (TSE) study will identify conditions that discourage idling and promote the

use of on-board anti-idling equipment and Shorepower. It will examine individual driver behavior and driver behavior of fleet employees. The study will characterize the extent that transportation logistical situations impact truck idling (e.g., hours of service). Study data include time and duration of use; power drawn; indices of driver behavior and preferences; and it will correlate data with equipment, location, ambient temperature, truck stop, amenities, etc.

Truck Stop Electrification System

The system consists of 50 geographically distributed truck stop installations of Shorepower pedestals, located in the parking lot, that vend electric power. A diverse set of truck stops were selected for the project to compare performance of different types of facilities. These facilities include: large corporate chains, independently owned truck stops, smaller sites, larger facilities and a host of other variable amenities. This study was designed to discover which amenities attract Shorepower users, so diversity was the goal of site selection.

The installations include: heavy-duty protection infrastructure (wheel-stops and bollards) to prevent pedestal damage from trucks backing into a parking spots; power panel and a computer, which is installed in a kiosk either outdoors near the pedestals or inside the truck stop’s convenience store. The power vending system depends on custom software and wireless communication between pedestals and kiosk, and between kiosk and a cloud-based server. The service is easy to use with a heavy-duty 12 gauge (or larger) power cord. Available is standard 110 volt and 220 volt AC service; some sites also offer 480 volt service for powering electric standby capable TRUs.



Figure III-23: Map of Shorepower truck stop electrification facilities. A full list of sites can be found at www.shorepowerconnect.com.

HVAC carts

In addition to the power pedestals, Shorepower manufactured roll around carts (HVAC carts) that carry heating/air conditioning units. These plug into the Shorepower pedestals, and a vent hose from the unit is inserted through the cab window to provide direct heating and cooling. These carts were made available to most sites, to be used by trucks that are not already equipped with an electric HVAC system.

Introduction

Novation

The project was novated to Shorepower Technologies on June 20, 2014. Upon novation, Shorepower intensified the operations and maintenance efforts throughout the country to ensure reliability and uptime of all facilities.

Approach

Operations and Maintenance

This section covers only the last Quarter of FY 2014, after which the project was novated to Shorepower Technologies. Presently, operations are emphasizing: repairs, routine maintenance, responsiveness to urgent maintenance, system improvements, and cost reduction.

- Shorepower began using more robust communication chips to improve reliability and robustness of the system. Surge protection was also added at many locations to help endure power surges and lightning strikes during storms. These measures will continue to be implemented, particularly in locations with frequent electrical storms and/or poor grounding.
- Operations and maintenance visits to each site increased in frequency from an average of one visit per 6 months to at least once per quarter. An attempt is made to visit 3 to 6 sites in a particular region on each trip to streamline operations and costs.
- Shorepower hired additional staff and enlisted existing onsite personnel to assist with maintenance issues and increase responsiveness.

Network and Information System

Ongoing investment in upgrades to software, firmware, and hardware are being made to continually improve system reliability and user experience. These have been implemented in FY 2014 and will continue into the following year.

Firmware

- To avoid potential customer issues, intermittent communications redundancy and detection has been installed at the firmware level. As a result, writes/rewrites have significantly dropped, which promotes longevity of the non-volatile memory.
- Discovery protocol now allows detection of all devices within a local pedestal network, which results in faster determination on abnormalities.

Web Infrastructure

- Improved server reliability is now being utilized for all backend transactions for all sites, which promotes stability throughout the Shorepower network and decreases downtime incidents.

Database

- The improved Relational Database Server is resulting in higher uptime and better execution of our main database.
- Indexes were created to allow for faster performance for end-users.



Figure III-24: Some host site staff are proud of their system and take personal interest in telling drivers about Shorepower. One is Nelson Whitaker at Dukes Travel Plaza in Canton TX.

Education and Outreach, Marketing

Marketing has been aimed at increasing utilization to increase data available for the study analysis.

- Year-end goal: triple current levels of use.
- In the short time frame before grant completion, support increased use at sites.
- Focus outreach on owner operators instead of fleets because feedback indicates that large fleets need more locations to serve all their trucks.
- Focus on host-sites with potential for high utilization.

Renewed Efforts

- Retaining existing users, some who may have lost confidence due to sporadically offline conditions.
- Recruiting new users, of which the majority are independent owner-operators.
- Developing good working relationships with host sites.
- Changing driver behavior to choose not to idle; to choose to rely on an electric power source for cab power, battery charging, and engine block heating.
- Creating and solidifying partnerships with equipment manufacturers that produce shore power capable systems.
- Working with trade groups, air quality groups, and other stakeholders to communicate idle-reduction goals.
- Focusing on utilization during the next quarter to ensure financial stability by the conclusion of the grant.

Results

Data Collection and Analysis

Over the past year, an average of 600 hours was used at the STEP sites each week. Following are weekly averages and annual totals for all sites reporting sales:

- 34 users.
- 8 repeat users.
- 29,980 hours total connect time.
- 24,934 KWH power used.

Other results in FY 2014:

- CO₂ not emitted: 336 tons.
- Diesel displaced: 29,980 gallons.

Like the previous year, utilization fell in spring when mild temperatures reduced the need for heating or cooling. Utilization increased slightly in late summer for air conditioning loads, but the power demand for air conditioning is not generally as high as heating for the cab interior and engine block in severely cold temperatures. Shorepower may not be ideal for AC at this point in time unless the truck has a roof top or back wall electric HVAC unit, or a standalone unit. Shorepower cannot operate the factory installed air conditioner that comes with the tractor, because it operates with a belt driven pulley while the main engine is running (idling).

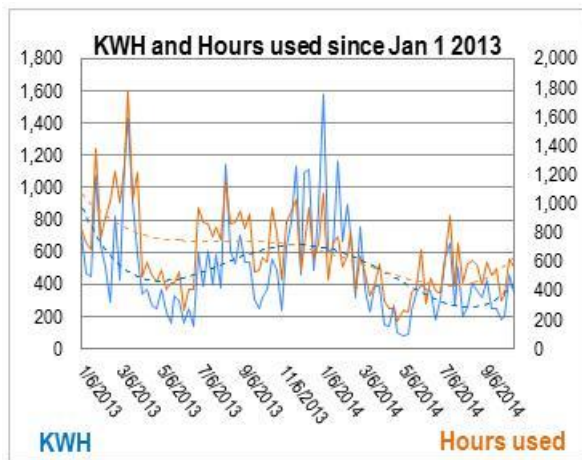


Figure III-25: There is a distinct seasonal pattern of use, and a roughly 1:1 ratio of KWH used to hours used

As the weather starts to cool, utilization is beginning to increase towards the end of Q4, and like last year, it is expected to peak in Winter due to the need for cab heat and engine block heating.

Rebate Program

The rebate program ended prior to novation. Therefore Shorepower did not partake in and activities directly related to rebates.

HVAC Carts

As originally planned, each host site received up to two HVAC carts.

Marketing and Retailing

Since July 2014, marketing staff began addressing the retailing needs of all host sites. Each site was provided a large supply of brochures, FAQ sheets for placement at the fuel desk, brochure holders and other retailing units, and outdoor directional signs.



Figure III-26: Truck drivers have reported seeing the pedestals often, but not knowing what they were for. Large stickers were added to clarify their purpose.

Incentives

As a promotion since August 2013, all first time users who register for a new account have been eligible to receive their first 10 hours of power free. This appears to have been working. In FY 2014, there were 273 new users, or an average of 6 first time users per week.

Operations and Maintenance

Shorepower is rebuilding capacity to maintain continuous uptime at all sites. Technicians are traveling around the country to maintain, repair, and upgrade components. Although infrequent, if there has been damage from trucks, contractors are being dispatched.

An additional technician was hired to address maintenance and repair at host sites in the Northeast. When possible, suitable contractors near site locations are being identified, and trained on technical aspects of the system, and dispatched for service calls as needed. When using outside contractors at a site, these contractors can communicate by phone with Shorepower technicians as they work on repairs or routine maintenance.

Network and Information System

The Shorepower network operating system is maturing but each geographical location presents unique challenges, for example: excessive heat in the kiosk location which impacts computer reliability (usually when the kiosk is installed in direct sunlight); ants getting into pedestals and damaging the circuit boards; and problems with the reliability of the local ISP, particularly in remote locations.

Conclusions

Outlook

Operational maintenance and outreach activities have been increasing, which should show benefits in subsequent reporting periods. Seasonal temperature variability plays a large role in utilization. As the winter season approaches, utilization is expected to increase. Site dynamics, management, size, and amenities also greatly affect utilization at each site.

There are three primary factors that affect utilization at each site:

1. Location: A strategic location on a corridor, at a natural stopping point in a day's drive of 600-700 miles.
2. Amenities: A clean well-managed site with attractive amenities (restaurant, hotel, showers, laundry, comfortable driver's lounge, free wifi).
3. Site staff commitment or "ownership" of the Shorepower installation: the company or a staff person (e.g., general manager or maintenance person) takes a personal interest in the amenity. They actively market it to their customers based on a belief in its benefits.

Data

Data collection continued through 2014. A total of nearly 30,000 hours were used throughout the year, representing a diesel fuel savings of approximately \$120,000 to owner operators and fleets. Utilization during Q4 2014 is lower than Q4 2013. This may reflect the general reduction in activity during the novation process and several months prior while CSS was winding down their operations. Also, there may be a time lag in the renewed efforts after novation. Additionally, free promotional hours were reduced from a maximum of 99 hours to 10 hours, for each new user. However, the free promo is still working. A total of 273 new users took advantage of the new user promo in FY 2014, which equates to an average of 6 users per week.



Figure III-27: Owner-operator Dave Magistrale contacted Shorepower and offered to speak with drivers about plugging in. He answers questions and relays feedback. Dave also cleans around the pedestals and reports technical issues to company technicians.

Education and Outreach

An intensive marketing campaign has been underway for most of Q4, thus far resulting in increased visibility; closer relationships with host sites; positive feedback; requests for signage, retail materials, and training materials; and requests for lessons on how to troubleshoot their site's system if needed. Account managers have elicited praise and constructive feedback from both drivers and host sites.

Direct communication with drivers can be improved. Education and outreach is most effective face-to-face, but is time intensive and costly. Future outreach efforts are planned to address this by recruiting truck drivers (who routinely use Shorepower) to be ambassadors to communicate the benefits trucker-to-trucker.

Tools and Data

Data from the STEP Project is being analyzed by the National Renewable Energy Lab (NREL), which has been producing quarterly updates on the results. Recently, Shorepower requested that NREL update their map to substitute KWH-used data with to hours-used data.

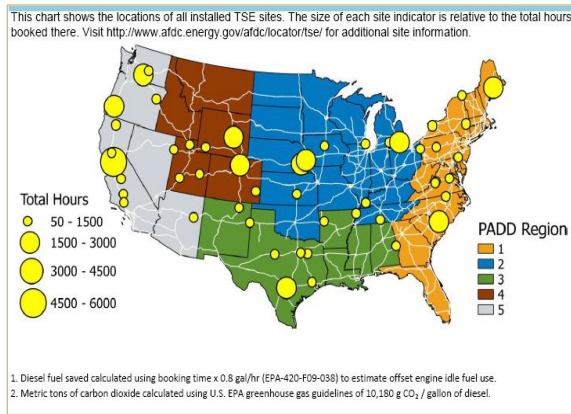


Figure III-28: The new map depicts the cumulative hours plugged-in per site, instead of cumulative power consumption

Since the goal of this project is to reduce truck idling, power use per site is not as valuable as hours used per site. Measuring hours used eliminates multiple other variables affecting power consumption also. It better indicates driver behavior, provides clues on how to influence driver behavior, and reveals revenue potential.

Publications

Fleet Equipment

“Implementing idling-reduction solutions to save money, meet regulations”

By Jason Morgan, Aug 27, 2014

Land Line Magazine

“Shorepower gains full control of Electrification Project”

OOIDA, July 17, 2014

Carbon War Room

“Confidence Report: Idle Reduction Solutions”

North American Council for Freight Efficiency, June 25, 2014

Fleet Maintenance

“How one fleet leverages technology and best practices to reduce operating expenses”

David A. Kolman, March 13, 2014

CBS Pittsburgh, KDKA Channel 2 (video)

“ ‘Idle Threat’ To Debut At Three Rivers Film Festival”

George Pakenham and Rachel Filippini of CBS stop by to talk about “Idle Threat.”

Nightly Business Report (video)

NBR Staff, October 16, 2013

Patents

1. No patents have been filed with this project.

WIRELESS POWER TRANSFER

III.E. Wireless Charging for Electric Vehicles- FOA #667

Principal Investigator: Omer C. Onar

Project Manager: P.T Jones

Oak Ridge National Laboratory
Power Electronics and Electric Machinery Group
National Transportation Research Center
2360 Cherahala Boulevard Knoxville, TN 37932
Phone: (865) 946-1351; Fax: (865) 946-1262
E-mail: onaroc@ornl.gov

DOE Program Managers: Lee Slezak, David Anderson

Phone: (202) 586-2335
E-mails: Lee.Slezak@ee.doe.gov,
David.Anderson@ee.doe.gov

III.E.1. Abstract

Wireless power transfer (WPT) is a paradigm shift in electric-vehicle (EV) charging that offers the consumer an autonomous, safe, and convenient option to conductive charging and its attendant need for cables. WPT can be fully autonomous due to the vehicle and grid side radio communication systems, and is non-contacting; therefore issues with leakage currents, ground faults, and touch potentials do not exist. It also eliminates the need for touching the heavy, bulky, dirty cables and plugs. It eliminates the fear of forgetting to plug-in and running out of charge the following day and eliminates the tripping hazards in public parking lots and in highly populated areas such as malls, recreational areas, etc. Furthermore, the high-frequency magnetic fields employed in power transfer across a large air gap are focused and shielded, so that fringe fields (i.e., magnetic leakage fields) attenuate rapidly over a transition region to levels well below limits set by international standards for the public zone (which starts at the perimeter of the vehicle and includes the passenger cabin). The convenience of WPT cannot be overstated. Oak Ridge National Laboratory (ORNL) approach to WPT charging places strong emphasis on radio communications in the power regulation feedback channel augmented with software control algorithms. The over-arching goal for WPT is minimization of vehicle on-board complexity by keeping the secondary side content confined to coil tuning, rectification, filtering, and interfacing to the regenerative energy-storage system (RESS). This report summarizes program work performed during the second phase of the project.

Objectives

- Coordinate multi-party team for the cost optimization and fabrication of the WPT grid side unit (GSU) and WPT coils and getting prepared for the end of phase #2

demonstrations. ORNL is the leading and coordinates the following responsibilities with the partners:

- Evatran is the commercialization partner and under ORNL guidance works on cost and component optimization and fabrication of GSUs and also the primary and secondary coils. Evatran is also working on vehicle integrations in coordination with ORNL and other partners.
- Clemson University ICAR Center is the demonstration site for Phase #2 deliverables and Phase #3 field evaluation for the project. They are also supporting the radio communications developments and radio integrations to the vehicles and the WPT equipment on the vehicles.
- Toyota Motor Corporation is the vehicle OEM partner providing the vehicles and support on the vehicle integrations.
- Overall program goal is to integrate ORNL developed WPT power electronics and coils into demonstration vehicles and validate in an independent testing laboratory and to provide a facility for continued field testing of this technology which will assist in standards development.
- There are five main objectives of the Phase #2 of the project:
 - Complete building the coils and GSUs for the Phase #2 demonstrations and Phase #3 field test.
 - Complete vehicle integrations for the Toyota Prius Plug-in, Scion IQ, Toyota RAV4, and the Chevy Volt.
 - Build a single GSU / single coil setup and associated integrated vehicle hardware for evaluation.
 - Build a single GSU / dual coil setup.
 - Validate full wireless operation including vehicle integration and system regulation at program efficiencies and power level.

Major Accomplishments

- Coordinated hardware and software updates, technology developments, as well as project strategies with partners.
- During the end of the Phase #1 demonstrations, team achieved:
 - Achieved >10 kW power transfer to the secondary side battery with direct DC power supply connection to the inverter input at 89.71% dc-to-dc efficiency at 160 mm airgap.
 - For the above mentioned test, at 0.8 meter away from the center of the primary coil, the E-field was measured 3.52 V/m and B-field was measured 0.58 μ T. Both values are well below the international guideline limit values specified by the International

- Commission on Non-Ionizing Radiation Protection (ICNIRP).
- Achieved >6.6 kW power transfer to the secondary side battery including the active front-end rectifier with power factor correction at 85.11% end-to-end efficiency at 160 mm airgap.
 - Designed new WPT transmit and receive coils with higher efficiency and higher misalignment tolerance. The new design of coils can handle >20 kW power transfer levels. Evatran fabricated the ORNL designed primary and secondary coils, and matched the system characteristics with their units.
 - During June and July of 2014 the ORNL-Evatran team worked performed at ORNL to refine the first system built by Evatran. The team improved the end-to-end system efficiency to >88% at ~6.6 kW power transfer to the load side at 160 mm airgap.
 - ORNL and Evatran worked together and came up with cost reduction recommendations which resulted in \$8,000–\$9,000 cost savings per grid side unit including materials and labor.
 - ORNL designed and built a switch box system that will serve as a power routing interface between the grid side unit and two primary coils in order to energize them depending on different vehicles parking on the coils and time sequencing the coils if two vehicles parked on two coils.
 - Evatran began integration of coils and vehicle side electronics to the Toyota Prius Plug-in in collaboration with ORNL.
 - Controls and communications architectures for both the “direct battery connection” or through the “on-board charger” options have been developed during Phase #2.
 - Site preparation is on-going at the Clemson University International Center for Automotive Research (ICAR) facilities.

Future Achievements

- Evatran to duplicate multiple WPT coils systems of latest ORNL design.
- Evatran to build 4 GSUs for field deployment and a possible single second generation prototype.
- Evatran to complete vehicle integrations.
- ORNL/Evatran team to complete control system refinements and testing.
- Complete the full integration, field tests, code debugging, updates and modifications if needed.



III.E.2. Technical Discussion

Background

Wireless charging of electric vehicles has the potential to eclipse conductive chargers because of its flexibility and convenience to the customer. Use of private and secure radio communications, especially vehicle to infrastructure (V2I), and standardization means that any vehicle would be able to charge at any location. The wireless charging process can be totally transparent to the customer, which would increase the use of opportunity charging with the appropriate infrastructure. The goals and accomplishments of this project during this year cover several advancements and refinements in areas including coils, control systems, vehicle integrations, and the site preparations for Phase #2 demonstrations. Through this project, ORNL and partners developed a deep understanding of WPT, real vehicle implementations, control system design and communications for closed loop regulation of power transfer, and the design improvements for higher performance and cost effectiveness.

Introduction

During Phase #2 of the FOA #667 project, the team improved the overall operation of the active front-end rectifier with power factor correction, high-frequency power inverter, high-frequency isolation transformer, and the efficiency of the primary and secondary electromagnetic induction resonance coupling coils. The team designed and built a new pair of coils for improved efficiency, came up with cost reduction opportunities for the grid side unit, and currently working on vehicle integrations, control system modifications, and the site preparations for the Phase #2. These developments are detailed in next section.

Approach

The approach followed for achieving the goals of the Phase #2 is summarized in following subsections.

Cost Reduction Opportunities for the Grid Side Development Unit

ORNL team came up with several cost saving opportunities for the GSUs. These include:

1. Eliminated the need for zero cross detection board by controlling the PFC with already existing AC input voltage and current sensors. This eliminated the cost of the parts and materials of the zero cross detection circuitry as well as the time and labor to fabricate the board.
2. Differential line drivers and differential line receivers of the PFC gate drivers eliminated with some layout architectural modifications. Cost of the parts and labor eliminated on these electronic boards.
3. Tamura L03S400D15 current sensors at the H-bridge transformer output and H-bridge DC-link input were eliminated since these sensors were not used for controls (monitoring only).

4. Isolated sensor I/O boards have been removed as well since they were used only for the prototype level monitoring and not for the controls.
5. Two LV25P sensors boards at the H-bridge output and HV AC input and one LEM LV25P/600 H-bridge DC link input voltage sensor have been removed for similar reasons.
6. Isolated voltage and current monitoring connector has been removed for similar reasons.
7. CAN and RS232 connectors at the outside of the GSU enclosure have been removed.
8. Isolated gate signal monitoring connections have been removed.

All of these cost reduction opportunities were discussed with Evatran and they were all agreed upon. These cost saving recommendations resulted in \$8,000–\$9,000 of cost savings.

New Electromagnetic Induction Resonance Coupling Coil Design and Fabrication

Electromagnetic design of WPT coupling coils provides the most fundamental investigation into their performance. At ORNL, the WPT team developed couplers based on the magnetic vector potential at a field point due to current flowing in an ideal primary coil conductor. The potential at this field point is defined to lie at the location of the secondary coil. For a coil pair of radius *a*, assuming infinitesimal conductor radius, and having a coil to coil spacing, *z*, then the radius vector from the primary coil origin to the field point becomes $r = \sqrt{(a^2 + z^2)}$. The corresponding vector potential, A_{ϕ} , for the case of N_1 primary turns and I_1 Amps yield a primary excitation of $N_1 I_1$ amp-turns. This primary excitation is depicted as I_{d1} in Figure III-29 where $a_1 = a_2 = a$ for convenience.

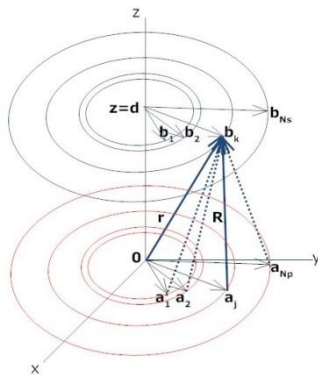


Figure III-29: Analytical expression of vector potential for coupler design

- The process given below was used for coil designs:
- Vector potential at each secondary coil turn is computed as the result of applied current in each of the primary coil turns.
 - Flux linking the secondary coil is then the line integral of the vector potential at each turn, which is then summed for total flux linkage.
 - Summed flux linkage is then averaged.
 - Inductance is the ratio of flux linkage to the current.

The sizing diagram and dimensions of the primary and secondary coil is provided in Figure III-30.

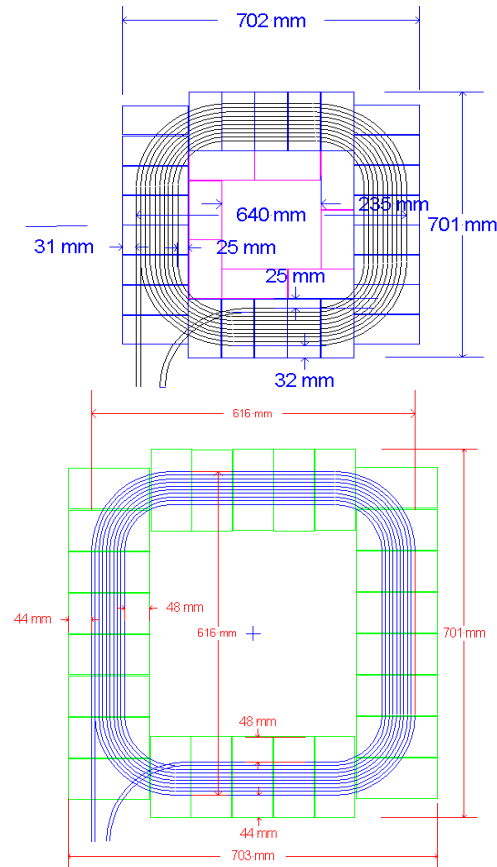


Figure III-30: ORNL designed new primary (top) and secondary (bottom) coil design and dimensions

The picture of the new primary coil winding is presented in Figure III-31.



Figure III-31: ORNL designed new primary coil winding meeting design requirements

Primarily, the new coils are designed to result in a higher coupling factor at $z=150$ mm airgap as compared to the coils developed and built during Phase #1. The analysis resulted in coupling $k(z)\sim 0.3$ at 150 mm airgap whereas the Phase #1 coils had a coupling factor of $k(z)\sim 0.2$ at the same airgap. The higher coupling factor for the same coil separation distance results in reduced magnetizing current to the mutual inductance branch in the equivalent circuit; therefore, it reduces the reactive power needed from the inverter to magnetize the coils. This also reduces the primary coil losses as the reactive power oscillates from inverter DC link capacitors to the primary coil winding. The coupling factor variation of the new pair of coils as a function of the airgap is obtained as given in Figure III-32 through a set of experimental results.

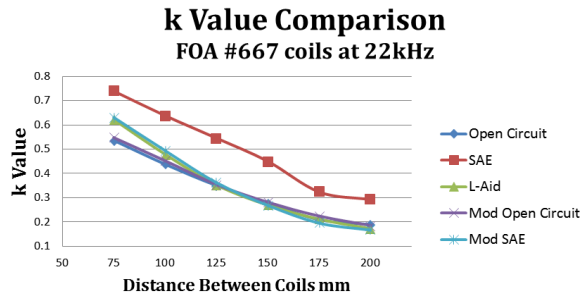


Figure III-32: Coil performance characteristics: coupling factor variation at different airgaps

In addition to the coupling factor, the winding AC resistance is also important since AC resistance of the Litz wire determines the Joule or copper losses. The iron losses of the coils are about 100 W/meter at $f_s=25$ kHz according to the MnZn ferrite material characteristics. The AC coil resistance as a function of the operating frequency is represented in Figure III-33.

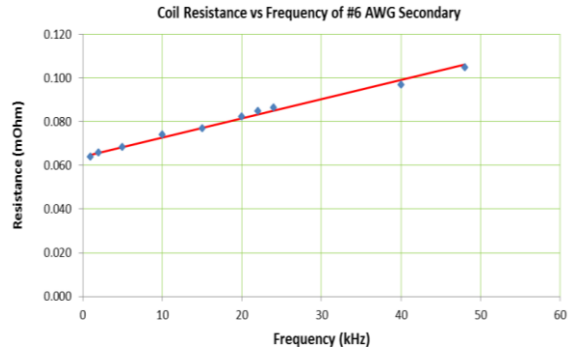


Figure III-33: Coil performance characteristics: AC resistance variation at different operating frequencies

The electrical parameters of the primary and secondary coils are provided in Table III-4.

Table III-4: Electrical parameters of the coils

| Inductance [μ H] | AC resistance [Ω] (@ 22kHz) | DC resistance (Ω) |
|-----------------------|--------------------------------------|----------------------------|
| $L_1=115.79$ | $R_{AC1}=0.1227$ | $R_{DC1}=0.0121$ |
| $L_2=132.6$ | $R_{AC2}=0.1508$ | $R_{DC2}=0.0299$ |

WPT Integrated Vehicle and GSU Operations with Controls and Communications

Evatran and ORNL are currently working together for the WPT integrated vehicle and GSU operations. These operations are summarized below:

Grid Side Unit Operation

The function of the primary system is to take the AC power from a 208/240V AC supply and generate high frequency current to the primary coil for electromagnetic field generation. During this operation, the PFC gets the AC voltage from the grid, rectifies it while boosting and provides a regulated voltage to the inverter input. Inverter uses the input voltage provided by PFC and generates high frequency AC voltage to the primary coil. Evatran controller handles the alignment of the secondary coil to the primary coil and communicates to the vehicle side through the radios and commands to the slave digital signal processor (DSP) unit. The operation and normal or emergency shut down commands, reference secondary power or voltage commands are all communicated to the DSP through the Evatran control module. This operation is illustrated in Figure III-34.

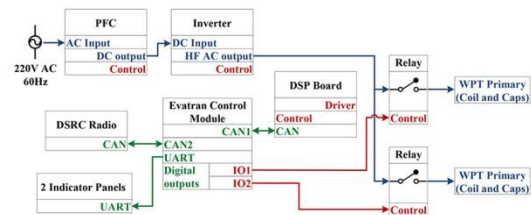


Figure III-34: Grid side unit operational block diagram with Evatran control module and the DSP

For the Prius Plug-in electric vehicle, the team needs to utilize the vehicle on-board charger (OBC). Based on the OBC restrictions, a secondary inverter will be connected at the output of the vehicle side rectifier in order to generate AC voltage again for the OBC. The selected inverter has a wide input range and its output voltage is regulated. In this mode of operation for the Prius, the control system utilizes a voltage regulation feedback control loop. The reference DC link voltage at the vehicle side is communicated to the DSP controller and the DSP controller regulates the PFC output voltage at the grid side to accommodate this need. The block diagram of this operation is featured in Figure III-35.

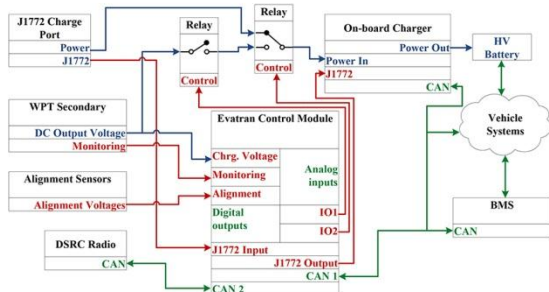


Figure III-35: Operational block diagram for the wireless-J1772 integration

For the direct battery connection, which is featured for the add-on battery system of the modified Toyota Rav4 EV vehicle, a reference current is applied to the battery in current regulation mode while monitoring the battery maximum voltage limit. This mode of operation is illustrated in Figure III-36.

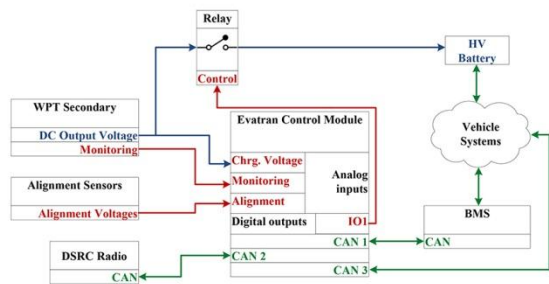


Figure III-36: Operational block diagram for the direct battery connection of vehicle side WPT equipment

Results

This subsection presents the efficiency improvement of the new WPT coupler coils. At $z=160$ mm airgap, while transferring 6.63 kW to the vehicle battery terminal, the PFC efficiency was 95.57%, inverter efficiency was 97.61%, isolation transformer efficiency was 98.56%, coil-to-coil efficiency was 97.51%, and vehicle side rectifier efficiency was 99.25%. Accordingly, the end-to-end efficiency was recorded 88.99%. The cascaded efficiency block diagram is shown in Figure III-37.

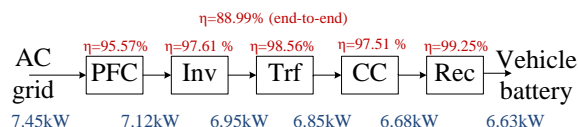


Figure III-37: Cascaded power conversion stages efficiency results

Conclusions

This report summarizes significant progress, deep insights, and promotion of international standards for wireless charging technology at ORNL and advocated by the U.S. Department of Energy. The team has demonstrated cost savings for the WPT power electronics equipment and also improved coil-to-coil efficiency and the overall end-to-end efficiency. Vehicle integrations for the phase #2 demonstrations are in process at Evatran with a planned demonstration in Q1 of FY2015.

Technology innovations also occurred during execution of this program during this year. Specifically, a vehicle side integration plan has been designed and utilized. Along with the communication systems, team built the closed loop feedback control system for the grid side regulation of vehicle battery power and vehicle side DC link voltage.

ORNL has also worked closely with our program partners, especially for commercialization and shared with them specifics of the WPT system design, schematics, BOM, and test data.

III.E.3. Products

Publications

1. O. C. Onar, M. Chinthavali, S. Campbell, C. P. White, L. Seiber, L. Tang, C. Coomer, P. Chambon, J. M. Miller, and P. T. Jones, "Oak Ridge National Laboratory's Research Activities on Wireless Power Transfer Systems," *IEEE Transportation Electrification Initiative (TEI) e-Newsletter*, July 2014.
2. J. M. Miller, O. C. Onar, and M. Chinthavali, "Primary side power flow control of wireless power transfer for electric vehicle charging," accepted for publication, *IEEE Journal of Emerging and Selected Topics in Power Electronics – Special Issue on Wireless Power Transfer*, March 2014.
3. J. M. Miller, O. C. Onar, C. White, S. Campbell, C. Coomer, L. Seiber, R. Sepe, and A. Steyerl, "Demonstrating dynamic wireless charging of an electric vehicle: The benefit of electrochemical capacitor smoothing," *IEEE Power Electronics Magazine*, vol. 1, no. 1., pp. 12-24, March 2014.
4. L. Tang, M. Chinthavali, O. Onar, S. Campbell, and J. Miller, "SiC MOSFET based single phase active boost rectifier with power factor correction for wireless power transfer applications," in *Proc., IEEE Applied Power Electronics Conference and Exposition (APEC)*, March 2014, Fort Worth, TX.

5. O. Onar, M. Chinthavali, S. Campbell, P. Ning, C. White, and J. Miller, "A SiC MOSFET based inverter for wireless power transfer applications," in *Proc., IEEE Applied Power Electronics Conference and Exposition (APEC)*, March 2014, Fort Worth, TX.
6. O. C. Onar, S. Campbell, P. Ning, J. M. Miller, and Z. Liang, "Fabrication and evaluation of a high performance SiC inverter for wireless power transfer applications," in *Proc., IEEE Workshop on Wide Bandgap Power Devices and Applications (WIPDA)*, pp. 125-130, October 2013, Columbus, OH.
7. P. Ning, J. M. Miller, O. C. Onar, and C. P. White, "A compact charging system for electric vehicles," in *Proc., IEEE Energy Conversion Congress and Exposition (ECCE)*, pp. 3629-3634, September 2013, Denver, CO.
8. M. S. Chinthavali, O. C. Onar, J. M. Miller, and L. Tang, "Single-phase active boost rectifier with power factor correction for wireless power transfer applications," in *Proc., IEEE Energy Conversion Congress and Exposition (ECCE)*, pp. 3258-3265, September 2013, Denver, CO.
9. O. C. Onar, "Electric Dreams: Sustainable Mobility without Plugging-in," *Coil Winding, Insulation, Electrical Manufacturing Conference and Expo*, September 2014, Chicago, IL.
10. Pavol Bauer (panel session chair), O. C. Onar (ORNL, panelist and panel organizer), Kevin Bai (Kettering University, panelist), Roger Burns (OLEV Technologies, panelist), and Konrad Woronowicz (Bombardier, panelist), *IEEE Transportation Electrification Conference and Expo (ITEC) Panel Session on Wireless Power Transfer Systems for PEV Charging Applications*, June 2014, Dearborn, MI.
11. O. C. Onar, Madhu Chinthavali, J. M. Miller, and P. T. Jones, "ORNL Developments in Stationary and Dynamic Wireless Charging," *IEEE Applied Power Electronics Conference and Exposition, Industry Session on Key Vehicle Power Electronics*, March 2014, Fort Worth, TX.
12. Matt Roush (WWJ's Tech Report, CBS, moderator), O. C. Onar (ORNL, panelist), T. Bohn (ANL, panelist), S. Stanton (ANSYS, panelist), J. Muhs (WiTricity, panelist), J. Curry (Qualcomm Inc., panelist), *Wireless Power Transfer Workshop, organized by IEEE, ANSYS, University of Michigan, and DOE GATE Center for Electric Drive Transportation*, March 2014, Dearborn, MI.
13. O. C. Onar, "ORNL WPT Developments," *USCAR Electrical and Electronics Technology Team Meeting*, March 2014, Southfield, MI.
14. O. C. Onar, "ORNL Wireless Power Transfer Technology," *Friends of the ORNL (FORNL) Meeting*, February 2014, Oak Ridge, TN.
15. O. C. Onar, "ORNL WPT Developments," *International Forum on Eco-Friendly Vehicle and System Forum (IFEV), Distinguished Speaker at the Plenary Session*, October 2013, Daejeon, Korea.
16. O. C. Onar, J. M. Miller, and P. T. Jones, "ORNL Developments in Stationary and Dynamic Wireless Charging," *IEEE Energy Conversion Congress & Exposition (ECCE) Special Session on: Advances in Wireless Power for Electric Vehicles*, September 2013, Denver, CO.
17. Omer C. Onar, Guest Editorial, *IEEE Journal of Selected and Emerging Topics in Power Electronics – Special Issue on Wireless Power Transfer Systems*.
18. Omer C. Onar, Guest Editorial, *IEEE Transactions on Power Electronics – Special Issue on Wireless Power Transfer Systems*.

Patents / Invention Disclosures

1. J. M. Miller, "Above resonance frequency operation for wireless power transfer," US 2013/0270919 A1, October 2013.
2. C. P. White, P. H. Chambon, P. T. Jones, J. M. Miller, O. C. Onar, L. Tang, "Overvoltage protection system for wireless power transfer systems," S-124,787, 201303196, October 2013.
3. C. P. White, S. L. Campbell, P. H. Chambon, M. S. Chinthavali, C. Coomer, P. T. Jones, J. M. Miller, O. C. Onar, L. E. Seiber, L. Tang, "Automotive wireless charging control system – Vehicle side," S-124,907, 201403293, March 2014.
4. O. C. Onar and M. S. Chinthavali, "120V plug adapter for wireless or wired charging of EVs," S-124,900, 201403287, March 2014.
5. O. C. Onar and M. S. Chinthavali, "A cost effective in-motion wireless charging system for electric vehicles," S-124,899, 201403286, March 2014.

Tools and Data

ORNL and partners used a variety of tools for building, testing, and analysis of the hardware and software components of the project. The testing equipment includes:

1. Yokogawa DL 2Gs/s 500MHz digital oscilloscope
2. Tektronix DPO 7104 digital phasor oscilloscope
3. LEM IST Ultrastab current transducer
4. Yokogawa 700924 100MHz differential probes
5. Tektronix TCPA400 AC/DC current probe amplifier
6. Tektronix TCP404XL gun type current probe
7. Yokogawa PZ400 power analyzer
8. Yokogawa WT1800 precision power analyzer
9. Yokogawa WT3000 power analyzer
10. LEM IT 200-S Ultrastab current sensors
11. Chroma DC programmable electronic load bank model 63210 14.5kW
12. Magna Power MT Series DC power supplies at various ratings (1000V/160A, 2500V/40A, 1000V/100A)
13. Lambda DC power supplies at various ratings (450V/200A, 300V/200A, 45V/2000A, 600V/600A)
14. Chroma AC power supply, 400V/40A

The software capabilities used for this project include:

15. Texas Instruments Code Composer Studio v3.3
16. Microsoft Windows Software Development Kit 7.1.NET Framework 4.0
17. Microsoft Visual C++ 2010 Professional SP1
18. MathWorks family of products for modeling, simulation, rapid prototyping, and control system code development
 - a. MATLAB & Simulink
 - b. Real Time Windows Target
 - c. Embedded Coder
 - d. MATLAB Coder
 - e. Simulink Coder
 - f. Control System Toolbox
 - g. Signal Processing Toolbox
 - h. Stateflow
 - i. SimElectronics
 - j. SimPowerSystems
 - k. DSP System Toolbox
 - l. Simulink Real-Time

III.F. High Efficiency, Low EMI and Positioning Tolerant Wireless Charging of EVs- DE-EE0005963

Principal Investigator: Allan Lewis

Hyundai America Technical Center Inc
6800 Geddes Road
Superior Township, MI 48198
Phone: (734) 337-3170
E-mail: alewis@hatci.com

DOE Program Manager: John Jason Conley

Phone: (304) 285-2023
E-mail: John.Conley@netl.doe.gov

III.F.1. Abstract

Objectives

- The objective of this project is to develop, implement, and demonstrate a wireless power transfer system that is capable of the following metrics.
- Total system efficiencies of more than 85%.
- Power transfer at over 6.6 kW.
- Maximum lateral positioning tolerance that can be achieved while meeting regulatory emission guidelines.

Major Accomplishments

- Developed custom in-house AC/DC front end with power factor correction capabilities that can provide >19.2kW of power to the system.
- Created WiFi 802.11d server/client software set to allow charger to receive wireless communications.
- Developed smaller charger and receiver coil set to prepare for vehicle integration.
- Completed coil misalignment test structure and control system.
- Developed surrogate vehicle packaging study to prepare for mounting fixture design.

Future Achievements

- The work in Phase II will also include a commercial viability analysis to show initial production costs for the system and potential petroleum reduction due to system deployment.
- The system will be further developed and integrated into a vehicle while meeting safety standards. A commercial viability analysis of the system and cost benefits for components both on-board and off-board the vehicle will be performed.
- In Phase III, the real-world test results of operation of the system on a fleet of five light-duty electric vehicles will be

demonstrated and all required safety and electromagnetic field (EMF) emission test results and real world performance results obtained and provided.



III.F.2. Technical Discussion

Background

Timeline

- Start date – October 2012
- End date – September 2015

Partner

- Mojo Mobility

Technical Barriers

- Conductive charging stations introduce limitations regarding access, range, and usability.
 - ADA access
 - Cord length and inconsistent vehicle port placement
 - Overall usability
- Wireless charging systems are prone to EMI, position intolerance, and low efficiency.

Introduction

The purpose of this project is to address the following technical barriers

- Reduce the dependence on conductive charging stations which will allow more convenience to the user, increased access and usability in support of ADA, and provide a charge with potentially no action required by the driver.
- Develop a wireless charging system that meets industry guidelines, while operating with position tolerance, large vertical distance, and efficiency of more than 85%.

Approach

The project team has formed a team to review and monitor regulatory requirements and standards. The team has joined, and interfaces regularly with the following Society of Automotive Engineers (SAE) task forces.

- SAE J2954 Wireless Charging Task Force and the following subgroups:
 - Alignment & Communication
 - Safety, Performance, Robustness Testing & Validation
 - Magnetic Field Interoperability

- Verification Testing
- Bus Charging
- Frequency Determination & EMC/EMF Definition
- SAE J2836/6 Wireless Charging Specific Use Cases
- SAE J2847/6 Wireless Charging Specific Messages
- SAE J2931/6 Wireless Charging Specific Protocols

The project team has completed the electrical and magnetic system modeling tasks required to develop component-level specifications:

- Electrical system from AC outlet to DC into high-voltage battery.
- Electromagnetic models of receiver and transmitter coils and magnetics.
- Combining the coil and magnetics modeling with the electrical model.
- Optimize total system.

The prototyping strategy for our high power wireless charging system is to develop discrete functional sub-systems with the following functions that will become further integrated into a packaged system:

- AC/DC front end:
 - High efficiency (93%–94%)
 - 240VAC single phase input
 - 500V DC output
- High-frequency resonant converter sub-system (charger system):
 - Custom electrical circuit PC board with microprocessor control
 - Closed loop power control loop
 - Rectification, filtering and resonating circuitry
 - Current and voltage measurement
 - Wireless communication control loop
- Electro-magnetic power transfer sub-system:
 - Custom designed charger system coil and magnetics
 - Custom designed vehicle system coil and magnetics
- High frequency rectifier sub-system(vehicle system):
 - Custom electrical circuit PC board with microprocessor control
 - Rectification of resonant power from coils
 - Filtering
 - Current and voltage measurements
 - Wireless communication control loop.

The hardware and software systems are being designed to account for real world conditions that will allow for the complete usage life cycle.

- Power level flexibility.
- Interface with vehicle onboard battery and charge system.
- Charger and receiver coil alignment systems.
- Receiver Identification, Error or Fault handling, End of Charge, etc.

The design team has made efficiency considerations in every area of the system. These considerations include:

- Material, geometry, component selection.
- Feedback control.

Based on the project schedule demands, there is little allowance for trial and error in the hardware design process; therefore a specific concentration has been made in the area of electromagnetic interference mitigation.

- Charger and receiver coil and magnetics design.
- Board layout.
- Secondary system placement and packaging.

The project team has identified the surrogate Grid Connected Electric Drive Vehicle's (GCEDV) make and model thus allowing for more informed mechanical considerations.

- Thermal issues, size, weight, integration into vehicle.

Based on our goal of wireless charging system tolerance enhancement, a considerable amount of time and effort has been spent defining and developing the coil and magnetics design and geometry that will allow our significant improvement over existing industry metrics.

As with any comprehensive engineering development project, our design efforts are evaluated against predefined verification tests that measure the system capabilities in the following disciplines:

- Power transfer rates.
- Efficiency.
- Position tolerance.
- Electromagnetic emission.

In summary, our approach is a systematic design and development of a grid-connected electric drive vehicle (GCEDV) wireless charging system that meets the expectations of low EMI, high position tolerance, and operates with high efficiency.

The goal upon completion of Phase III of our development project is the introduction of system that meets the needs of electric vehicle drivers that allows for series manufacturing and commercialization of the technology with the following considerations:

- Cost of materials throughout the design process.
- Emphasis on simplicity and user convenience.

Current SAE guideline direction relating to coil placement indicates that the charging coil will be located 1.5–3.0 m from the center front of a parking space. This will allow automakers with on-vehicle packaging flexibility. The development team has determined that the secondary coil will be located immediately below the engine compartment of the Kia Soul EV surrogate vehicle (Figure III-38).

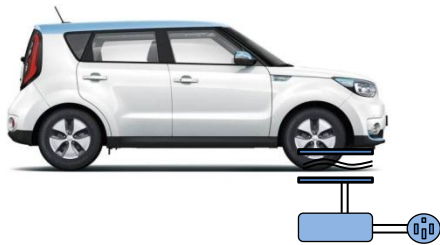


Figure III-38: GCEDV wireless coil placement

Based on the objectives of the project, our system will provide inherent position tolerance to the driver. This area of EV charging is quickly emerging, and therefore our team is ensuring that all alignment and communication strategies are in line with the SAE J2954 works in progress.

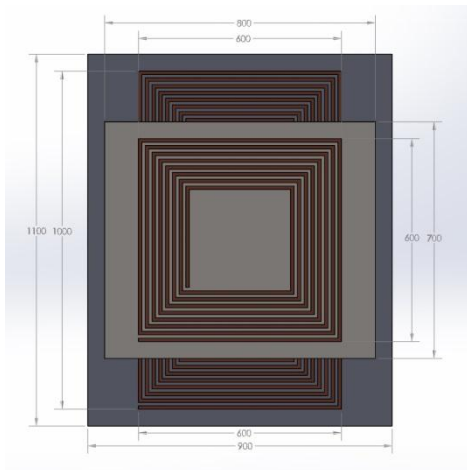


Figure III-39: Second-generation asymmetric coil set

Table III-5: Coil system z-dimension breakdown

| Layer (From top to Bottom) | Thickness |
|----------------------------|-----------|
| Shielding | 2 mm |
| Ferrite | 2 mm |
| RX Coil | 10 mm |
| TX Coil | 10 mm |
| Ferrite | 2 mm |

Table III-5 shows the development team’s current achievement in making the coil set components as thin as possible to assist in weight and space savings.

Results

Our current wireless charging system equipped with the second-generation asymmetric coil set (Figure III-39) features charger and receiver coils that are significantly smaller than what was presented during our Phase 1 developments. Significant effort was put towards creating a coil set that was suitable for vehicle integration while maintaining a large misalignment tolerance.

Figure III-40 shows the efficiency performance (y-axis of graph) of the new coil set while being moved across the x-axis of the charging coil (length of the vehicle).

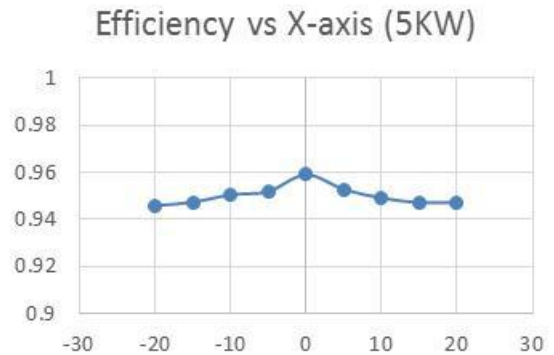


Figure III-40: DC-DC System efficiency measurements over x-axis misalignment in centimeters

Figure III-41 shows the efficiency performance (y-axis of graph) of the new coil set while being moved across the y-axis of the charging coil (width of the vehicle).

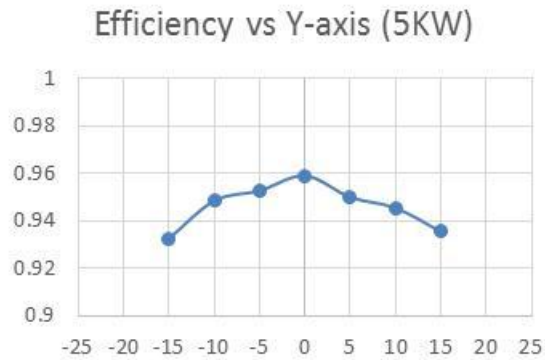


Figure III-41: DC-DC System efficiency measurements over y-axis misalignment in centimeters

Conclusions

The benefits provided by wirelessly charging GCEDV are motivating innovation in the area to address technical challenges. The early design work by HATCI and Mojo Mobility is leading towards the ability to present new state of the art performance capabilities in the areas of:

- Low spurious unwanted emissions into the environment
- High power transfer efficiencies
- Large coil to coil misalignment allowance and large vertical gap separation.

The cooperation of HATCI and Mojo Mobility provides an opportunity to develop a next generation GCEDV wireless charging system that can be quickly integrated into production ready vehicles for vehicle level testing that will provide proof of concept systems for evaluation for commercial potential.

Commercial Viability Study performed in FY 2014 will provide and understanding of the following considerations:

- Commercial viability and cost benefits
- Comparison with SAE 1772 compliant conductive charging system
- Expected market penetration
- Potential petroleum reduction.

III.F.3. Products

Publications

1. None

Patents

1. None

Tools and Data

1. NH Research Model 4760-12 Programmable DC electronic load, up to 24 kW
2. Magna Power model TSA800-30 High power AC/DC programmable power supply (up to 24 kW) with over current and over voltage protection
3. High current measurement probes
4. High voltage measurement probes
5. Yokogawa Model WT3000 Precision Power Analyzer
6. Rohde & Schwarz – ZNB Vector Network Analyzer
7. Agilent Model CXA signal Analyzer
8. Tektronics Digital oscilloscope model MSO2024
9. Rigol DG1022U Arbitrary Waveform Generator
10. FLIR Thermal Imaging Camera
11. Electromagnetic simulation software
12. Firmware integrated development environment development software
13. Laboratory laptops and multimeters

SUPERTRUCK

III.G. Systems Level Technology Development and Integration for Efficient Class 8 Trucks -ARRA

Principal Investigator: Derek Rotz

Daimler Trucks North America
4747 N. Channel Avenue
Portland, OR 97217
Phone: (503) 745-6303
E-mail: Derek.Rotz@Daimler.com

DOE Program Manager: Roland Gravel

Phone: (301) 938-3347
E-mail: Roland.Gravel@ee.doe.gov

- Buildup and Test of Final Demonstrator Vehicle
 - Initiated build of final demonstrator vehicle, incorporating A-Sample vehicle technologies and additional technologies.

Future Achievements

- Completion of Fuel Economy Testing with Final Demonstrator Vehicle
 - Two highway routes
 - City route
 - Summer and winter mode parked tests.



III.G.1. Abstract

Objectives

Overall Objectives

- Demonstration of a 50% total increase in vehicle freight efficiency measured in ton-miles per gallon (at least 20% improvement through the development of a heavy-duty diesel engine).
- Development of a heavy-duty diesel engine capable of achieving 50% brake thermal efficiency on a dynamometer under a load representative of road load.
- Identify key pathways through modeling and analysis to achieving a 55% brake thermal efficient heavy-duty diesel engine.

FY 2014 Objectives

- Experimental demonstration of technology building blocks that achieve 50% vehicle freight efficiency improvement on a vehicle level.
- Experimental demonstration of 50% engine brake thermal efficiency in a test cell.

Major Accomplishments

- Buildup and Test of A-Sample Vehicle
 - Integration of waste heat recovery, eHVAC, AccuSteer and cooling including controls optimization and tuning
 - Successful fuel economy test on two highway routes in Oregon and Texas, reaching 52% and 61% fuel economy improvement respectively.

III.G.2. Technical Discussion

Background

SuperTruck is a five-year research and development program with a focus on improving diesel engine and vehicle efficiencies. The objective is to develop and demonstrate a Class 8, long-haul tractor-trailer which achieves a 50% vehicle freight efficiency improvement (measured in ton-miles per gallon) over a best-in-class 2009 baseline vehicle. The engine for the SuperTruck program will deliver 50% brake thermal efficiency.

Introduction

Daimler's SuperTruck program is currently on track to meet the project deliverables by the scheduled Q1 2015 target date. In FY 2014, phase 4 targets of reaching 50% vehicle freight efficiency on a vehicle level were met. This was achieved with the buildup of and testing of the "A-Sample" SuperTruck, the first vehicle-level integration of multiple complex systems onto a single truck.

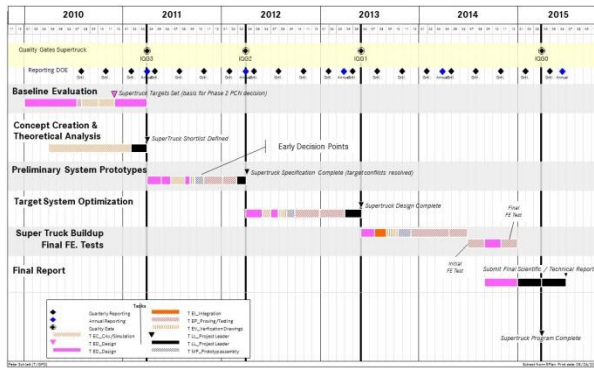


Figure III-42: SuperTruck Project Schedule

Approach

Systems-Level Testing

Phase 3 activities during the previous reporting period encompassed the detailed design, installation and testing of technologies on a system level by conducting on-highway fuel economy tests. In this phase the program target of experimentally demonstrating 50% vehicle freight efficiency was successfully reached, through individual system tests. Further tests encompassed measurement of improvement of external aerodynamic systems, powertrain components and hybrid.

In the current phase (Phase 4), the build of the A-Sample vehicle was completed and a single fuel economy test of several systems on vehicle was conducted. Furthermore the build of the final demonstrator vehicle was initiated. This section discusses these two major milestones.

A-Sample Build and Test

The A-sample build represents the first attempt at integrating several technologies simultaneous on a single vehicle. The purpose of which was two fold: first to identify and resolve vehicle integration issues from thermodynamic and high voltage interfaces across systems, as well as to integrated the electronics architecture onto one vehicle.

Thermodynamic systems encompass meeting cooling requirements of conventional truck systems (e.g. engine, charged intake air and a/c refrigerant) as well as the Waste Heat Recovery and Hybrid components. The design incorporated remote mounting of heat exchangers, ducts/vents and auxiliary fans and pumps. The cooling system needed to package under an aerodynamic hood, while keeping underhood temperatures in check.

High voltage interfaces were also integrated and functionally checked including safety requirements, electrical faults detection and response. Systems to be integrated include the hybrid eMotor and battery, electric a/c compressor, waste heat recovery electrical generator and trailer solar panels, all operating at 360 Volts.

The powertrain was also in scope of the A-Sample build, including the target engine displacement & rating, direct-drive automated manual transmission (AMT) and taller rear axle ratio. Lastly the auxiliary systems for SuperTruck were also

including a redesign of the power steering and air compressor, controlled by clutch.

Once these systems were functionally integrated, including optimization and tuning of relevant controls systems, the A-Sample vehicle was tested against the 2009 baseline Cascadia tractor, using the TMC Type IV test method for competitive benchmarking. Testing was conducted on two highway routes; Interstate 5 in Oregon and Interstate 35 in Texas. The test results measured a 52% fuel economy improvement on the Oregon route and a 61% improvement on the Texas route. The combined A-Sample tractor/trailer weighed in at 1500 lbs less than the baseline, further improving freight efficiency.

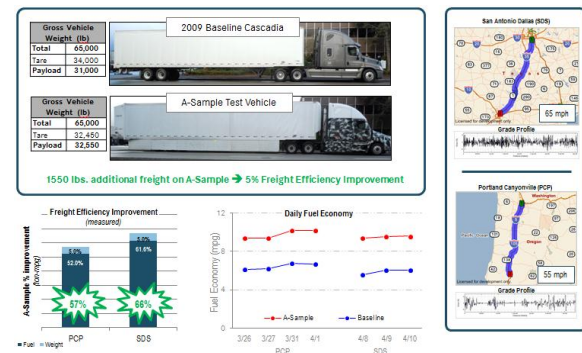


Figure III-43: A-Sample Test Results

Final Demonstrator Build

Another main activity in the current phase entailed the build up of a final demonstrator. The purpose is to incorporate all SuperTruck technologies onto a single vehicle to conduct the complete final demonstration test. These technologies include everything from the A-sample vehicle, plus several more. These include a 50% BTE engine and waste heat recovery system, full tractor and trailer aerodynamics, lightweight truck exterior and frame, a 6x2 axle configuration with active oil management among others.

Aerodynamic development has also concluded on the final demonstrator, with a final validation of the full SuperTruck tractor trailer combination compared to the baseline 2009 tractor trailer. A composite aerodynamic drag reduction of 54% was achieved over the baseline; 39% coming from trailer aerodynamic improvements and 15% coming from the tractor.

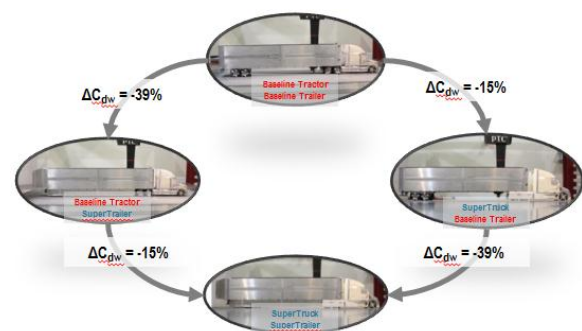


Figure III-44: SuperTruck Aerodynamic Drag Validation

The final demonstrator is currently almost built and will accumulate miles before conducting a fuel economy test on all highway, city and parked cycles. The freight efficiency improvement is expected to exceed that of A-sample.

Results

The fuel economy testing of the A-sample truck provided a unique opportunity to study how several systems interact with each other on as single vehicle. The main question posed was whether or not the efficiency improvements of systems are additive or not.

During data analysis after testing, observations were made, in which diminishing returns occurred when combining multiple systems on a single vehicle. These include the behavior of waste heat recovery together with 'eCoast', a feature that shifts the transmission into neutral during ONm torque operating condition to decouple engine friction torque from the driveline. This decoupling resulted in a heat load reduction, causing the waste heat system to lose power and in some instances switch off.

Also the waste heat recovery system as designed and installed in vehicle experienced a measurable loss in exhaust temperature from the SCR outlet to the WHR boiler. This is caused by exposure of the system to high velocity air that removes heat by convection; under wet conditions, exposure to moisture leads to further heat loss. This consequently reduced the amount and quality of heat into the boiler and hence energy recovery.

Predictive Technologies—the use of 3D Maps and GPS to control vehicle speed—competed against the hybrid system for the same inefficiency, i.e., energy lost due to braking. In the instance of hybrid, braking energy is recuperated, stored in the battery and subsequently used for propulsion at a later time. The hybrid system benefit is essentially 'capped' by the proportion of braking occurring on a drive cycle. In the case of highway driving, brake energy is low. Predictive technologies aim to reduce braking energy by more intelligently controlling vehicle speed across terrain. Consequently the use of both technologies results in diminishing net returns.

Despite these challenges and setbacks, the fuel economy testing of the A-Sample vehicle confirmed that the A-Sample truck exceeded the 50% program targets on the highway routes one year before program end. This not only proved that integration of several systems onto one vehicle is possible, the test also provided valuable insights regarding the system benefits as they interact with other systems and how they behave on vehicle.

Conclusions

The analysis in phase 1 provided a technology path that when implemented and tested will demonstrate the overall 50% freight efficiency target and 50% engine brake thermal efficiency. Phase 2 built upon these results through the design, implementation and on-vehicle testing of systems which met the interim program target.

In Phases 3 and 4, the 50% vehicle freight efficiency targets were met on a systems level and an A-sample vehicle was built to provide out vehicle interfaces and perform vehicle level test of multiple integrated system.

The last phase of SuperTruck entails completing the build of final demonstrator vehicle and conducting the fuel economy testing on all highway, city and parked cycles to demonstrate 50% vehicle freight efficiency.

III.G.3. Products

Publications

1. Singh, Sandeep: "Super Truck Program: Engine Project Review Recovery Act –Class 8 Truck Freight Efficiency Improvement Project", Project ID:ACE058, DoE Annual Merit Review, June 20, 2014.
2. Rotz, Derek: "Super Truck Program: Vehicle Project Review Recovery Act –Class 8 Truck Freight Efficiency Improvement Project", Project ID ARRAVT080, DoE Annual Merit Review, June 19, 2014.

III.H. Technology and System Level Demonstration of Highly Efficient and Clean, Diesel Powered Class 8 Trucks- DE-EE0003403

Principal Investigator: David Koeberlein

Cummins Inc.
P.O. Box 3005
Columbus, IN 47201-3005
Phone: (812) 377-5285
Email: david.e.koeberlein@cummins.com

DOE Program Manager: Ralph Nine

Phone: (304) 285-2017
E-mail: ralph.nine@netl.doe.gov

III.H.1. Abstract

Objectives

- Objective 1: Engine system demonstration of 50% or greater brake thermal efficiency in a test cell at an operating condition indicative of a vehicle traveling on a level road at 65 mph.
- Objective 2:
 - a. Tractor-trailer vehicle demonstration of 50% or greater freight efficiency improvement (freight-ton-miles per gallon) over a defined drive cycle utilizing the engine developed in Objective 1.
 - b. Tractor-trailer vehicle demonstration of 68% or greater freight efficiency improvement (freight-ton-miles per gallon) over a defined 24 hour duty cycle (above drive cycle + extended idle) representative of real world, line haul applications.
- Objective 3: Technology scoping and demonstration of a 55% brake thermal efficiency engine system. Engine tests, component technologies, and model/analysis will be developed to a sufficient level to validate 55% brake thermal efficiency.

Major Accomplishments

- Demonstrated an 86% freight efficiency improvement with the SuperTruck Demo 2 vehicle on a 24-hour cycle, which includes overnight hoteling and operating the Texas highway drive cycle route.
- Demo 2 demonstrated a 76% freight efficiency improvement on the Texas highway drive cycle.
- Demonstrated a Li-Ion battery pack APU capabilities to support full sleeper cab hotel loads.
- Validated an advanced transmission efficiency model
- Completed an Alternate Fuel Compression Ignition (AFCI), i.e. dual fuel multi-cylinder engine build and initial testing with cylinder-to-cylinder and cycle-to-cycle control system.
- Completed an initial conventional diesel engine technologies roadmap to 55% thermal efficiency
- Completed selective analytical validation tests in a conventional diesel single cylinder engine (SCE) of revised injector and piston configurations.
- Completed multi-cylinder engine (MCE) tests to validate analysis of both conventional diesel and AFCI technologies.

Future Achievements

- Analysis and targeted testing of technologies for achievement of a 55% thermal efficient engine.
- Develop the technology roadmap for a 55% thermal efficient engine with supporting analysis and test results.



III.H.2. Technical Discussion

Background

Cummins Inc. is engaged in developing and demonstrating advanced diesel engine technologies to significantly improve the engine thermal efficiency while meeting US EPA 2010 emissions. Peterbilt Motors is engaged in the design and manufacturing of heavy-duty Class 8 trucks.

Together, Cummins and Peterbilt provide a comprehensive approach to achievement of a 68% or greater increase in vehicle freight efficiency over a 24-hour operating cycle. The integrated vehicle demonstration includes a highly efficient and clean diesel engine with 50% or greater brake thermal efficiency including advanced waste heat recovery, aerodynamic Peterbilt tractor-trailer combination, reduced rolling resistance tire technology, advanced transmission, and a lithium ion battery APU for idle management. In order to maximize fuel efficiency, each aspect associated with the energy consumption of a Class 8 tractor/trailer vehicle will be addressed through the development and integration of advanced technologies.

In addition, Cummins will scope and demonstrate evolutionary and innovative technologies for a 55% BTE engine system.

Introduction

Cummins Inc. is engaged in developing and demonstrating advanced diesel engine technologies to significantly improve the engine thermal efficiency while meeting US EPA 2010 emissions. Peterbilt Motors is engaged in the design and manufacturing of heavy-duty Class 8 trucks.

Together, Cummins and Peterbilt provide a comprehensive approach to achievement of a 68% or greater increase in vehicle freight efficiency over a 24-hour operating cycle. The integrated vehicle demonstration includes a highly efficient and clean diesel engine with 50% or greater brake thermal efficiency including advanced waste heat recovery, aerodynamic Peterbilt tractor-trailer combination, reduced rolling resistance tire technology, advanced transmission, and a lithium ion battery APU for idle management. In order to maximize fuel efficiency, each aspect associated with the energy consumption of a Class 8 tractor/trailer vehicle will be addressed through the development and integration of advanced technologies.

In addition, Cummins will scope and demonstrate evolutionary and innovative technologies for a 55% BTE engine system.

Approach

Cummins and Peterbilt's approach to these program objectives emphasizes an analysis led design process in nearly all aspects of the research. Emphasis is placed on modeling and simulation results to lead to attractive feasible solutions. Vehicle simulation modeling is used to evaluate freight efficiency improvement technologies. Technologies are evaluated individually along with combination effects resulting in our path to target measure of program status and for setting program direction.

Data, experience, and information gained throughout the research exercise will be applied wherever possible to the final commercial products. We continue to follow this cost-effective, analysis-led approach both in research agreements with the U.S. Department of Energy as well as in our commercial product development. We believe this common approach to research effectively shares risks and results.

Results



Figure III-45: SuperTruck Demo 2

The SuperTruck Demo 2 vehicle demonstrated an 86% freight efficiency improvement on a 24-hour cycle, which included both overnight hoteling and operating the Texas highway drive cycle route. On this test cycle, the Demo 2 fuel economy gains were 75%, and calculated greenhouse gas emission reduction of 43%. The test weight of both vehicles was 65,000 lb. The result is the average of three runs, where the 95% confidence was calculated at 4.5% and standard deviation of 2%. Freight efficiency runs include effects of the Cummins fuel quantity manager algorithm. All comparisons were made with the MY 2009 baseline Peterbilt 386 operating with the same test protocol on the same day, with the same weather conditions.

The 24-hour cycle the test protocol included both the Demo 2 truck and baseline trucks being hotel loaded to a prescribed load bank current draw profile. The baseline truck's engine idled during this period, while the Demo 2 vehicle drew power from its Li-Ion battery APU. At the start of the drive cycle test, fuel flow measurement commenced upon startup of the Demo 2 engine. Both vehicles retrieved their respective trailers and proceeded on the 500 mile round trip route to/from Memphis, TX from Peterbilt's Denton facility. This completed Objective 2b of the SuperTruck deliverables.

The SuperTruck Demo 2 vehicle also demonstrated a 76% freight efficiency improvement on our drive cycle run on U.S. Route 287 between Fort Worth and Vernon, Texas (see Figure III-46). On this test cycle, the Demo 2 fuel economy gains were 66%. The tractor-trailer had a combined gross weight of 65,000 lbs. The result is the average of three runs, where the 95% confidence was calculated at 6% and standard deviation of 8%. The cruise control system had some operational issues on the last run which increased test variation. All comparisons were made with the MY 2009 baseline Peterbilt 386 operating with the same test protocol on the same day, with the same weather. This repeated with improvements those accomplishments documented in the previous annual report. This completed Objective 2a of the SuperTruck.

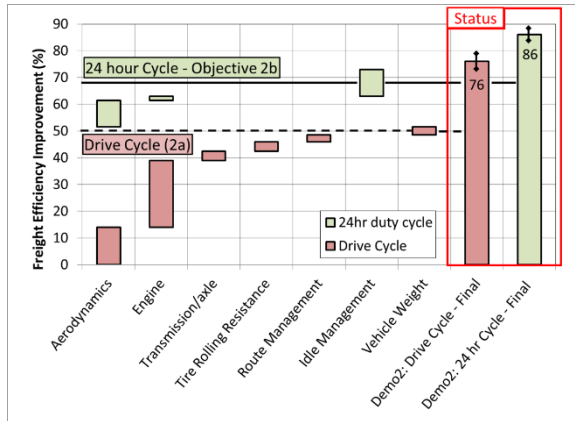


Figure III-46: SuperTruck final results and original roadmap

An AFCI multi-cylinder engine demonstrated a 49.4% BTE at a 10bar BMEP load. The alternate fuel substitution rate was 97%. The engine control system with in-cylinder pressure sensing adjusted each cylinder’s operating parameters on a cylinder-to-cylinder and cycle-to-cycle basis for maximum efficiency. This combustion system technology enables higher efficiency with low emissions. Research continues to increase the load capacity of this engine. The initial cost analysis of this dual fuel engine design appears attractive, if the engine requirements do not demand full engine operability and capability on each fuel independently, i.e. bi-fuel.

Combustion bowl analysis was completed to identify bowl shape commensurate with a new injector specification. The analysis optimization work of bowl volume, shape factors and diameter resulted in a predicted 0.5% BTE improvement from that demonstrated on the SuperTruck 50% BTE engine.

A single cylinder engine (SCE) test of a new injector specification that seeks to minimize combustion duration for maximum efficiency has shown a closed cycle efficiency improvement of 1.3%. This SCE validation testing confirms earlier combustion analysis work and will be followed with validation in multi-cylinder engine testing. The validation testing on this second injector iteration directionally points to a critical 55% technology roadmap element(see Figure III-47).

Reduction of in-cylinder heat loss increases closed cycle efficiency. Analysis of in-cylinder heat loss in conventional diesel engine showed that the piston rejects 50% of the in-cylinder heat losses, followed by the cylinder head at 30% and the cylinder liner at 20%. Since the piston is the largest component to in-cylinder heat losses, analysis of various piston materials and coatings and their influence to close cycle efficiency has been studied. Current analysis of multiple piston design variants relative to the baseline piston show a potential brake efficiency gain of 0.8%, through a combination of closed cycle efficiency gains and increased exhaust energy.

An advanced design of a WHR turbine expander has been rig tested with a 1.8 hp improvement over the turbine expander used on the SuperTruck Demo 2. This turbine expander improvement, in addition to a plumbing “pre-heat” circuit of the low-pressure loop system, is expected to increase engine cycle efficiency by 0.7% BTE.

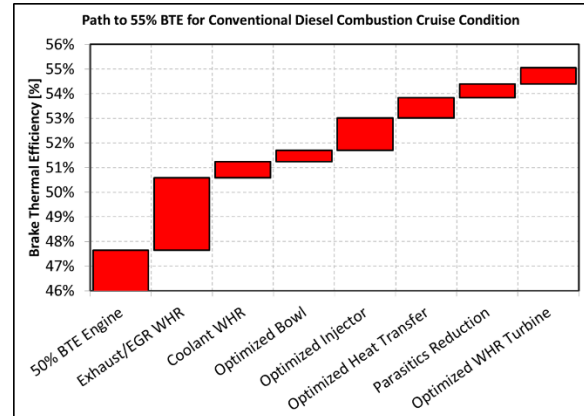


Figure III-47: Initial diesel technology roadmap for a 55% BTE engine

Conclusions

The SuperTruck Engine and Vehicle System Level Demonstration of Highly Efficient and Clean, Diesel Powered Class 8 Truck program has successfully completed the third year of the four-year program. The following achievements have come from the third year:

- Demonstrated Class 8 truck freight efficiency improvements of 86% on a 24-hour cycle and drive cycle improvements of 76%.
- Demonstrated a Li-Ion battery pack APU with capabilities for all anticipated hoteling loads.
- Validated an advanced transmission efficiency model.
- Completed an AFCI, i.e., dual-fuel multi-cylinder engine build and initial testing with cylinder-to-cylinder and cycle-to-cycle control system.
- Completed an initial conventional diesel engine technologies roadmap to 55% thermal efficiency.
- Completed selective analytical validation tests in a conventional diesel single cylinder engine (SCE) of revised injector and piston configurations.
- Completed multi-cylinder engine (MCE) tests to validate analysis of both conventional diesel and AFCI technologies.

III.H.3. Products

Publications

Journal Paper Submissions:

Gurneesh Jatana, Sameer Naik, Robert Lucht, and Gregory M. Shaver, High-speed diode laser measurements of temperature and water vapor concentration in the intake manifold of a diesel engine, *International Journal of Engine Research*, vol. 15 no. 7 773–78, October 2014.

Akash Garg, Mark Magee, Chuan Ding, Leighton Roberts, and Gregory M. Shaver, Exhaust Thermal Management Using Cylinder Throttling via Intake Valve Closing Timing Modulation, *Journal of Automobile Engineering*, revised version submitted October 2014.

Leighton Roberts, Mark Magee, Akash Garg, Gregory M. Shaver, Eric Holloway, Edward Koeberlein, Raymond Shute, David Koeberlein, James McCarthy Jr., and Douglas Nielsen, Modeling the Impact of Early Exhaust Valve Opening on Exhaust Aftertreatment Thermal Management and Efficiency for Compression Ignition Engines, submitted for review to the *International Journal of Engine Research*, online October 6, 2014.

Gurneesh S Jatana, Sameer V Naik, Gregory M Shaver, and Robert P Lucht, Simultaneous high-speed gas property measurements in the turbocharger inlet, the EGR cooler exit, and the intake manifold of a multi-cylinder diesel engine using diode-laser-absorption-spectroscopy. Submitted for review to *Applied Optics*, August 25, 2014.

Patents

1. N/A

Tools and Data

1. N/A

III.I. Volvo Energy Efficient Vehicle - SuperTruck

Principal Investigator: Pascal Amar

Volvo Technology of America
 7825 National Service Road
 Greensboro, NC 27409
 Phone: (336) 291-5842
 E-mail: pascal.amar@volvo.com

DOE Program Manager: Roland Gravel

Phone: APR_Box Address
 E-mail: Roland.Gravel@ee.doe.gov

- Implement all technologies selected onto the demonstrator engine and validate brake thermal efficiency in test cell.
- Commercialize trailer aerodynamic devices developed during this fiscal year.



III.I.2. Technical Discussion

Background

SuperTruck is a five-year research and demonstration program with the objective to identify technologies that could significantly reduce fuel use by Class 8 long-haul trucks. The program focuses equally on diesel engine efficiency and vehicle efficiency.

Introduction

Volvo's SuperTruck project is divided into two main phases, as shown below: the first phase utilized a mule vehicle to evaluate concepts and technologies during FY 2013; the second phase will deliver the SuperTruck demonstrator comprising the technologies selected to achieve the program objectives.

The Volvo SuperTruck project team has completed all activities planned for FY 2014 according to the original schedule. An overview of the main achievements is presented in this report.

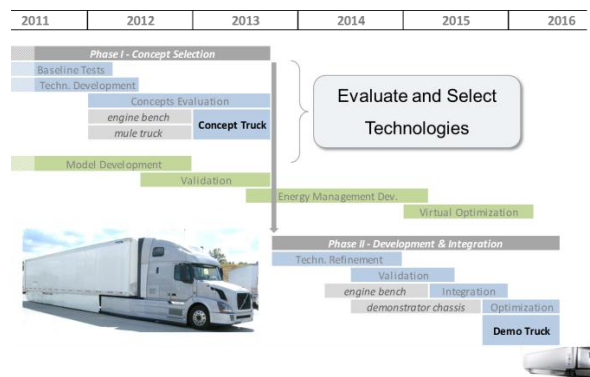


Figure III-48: Volvo Supertruck Project Schedule FY 2011-2016

III.I.1. Abstract

Objectives

- Demonstrate 50% increase in freight efficiency (ton-miles/gallon) compared with a best-in-class MY 2009 highway truck.
- Demonstrate 50% brake thermal efficiency.
- FY 2014 objectives:
 - Evaluate technologies on mule vehicle.
 - Complete technology selection.
 - Start development and integration of technologies into demonstrator vehicle.

Major Accomplishments

- Completed on-road and chassis dynamometer testing of the mule vehicle and demonstrated 43% Freight Efficiency improvement.
- Completed vehicle testing of a 48% brake thermal efficiency (BTE) powertrain system, which confirmed the performance behavior exhibited in the engine test cell.
- Completed on-road testing of the mule vehicle in the optimized aerodynamic configuration and demonstrated 13% fuel economy improvement at 0 yaw wind condition, which confirms the 30% aerodynamic drag reduction.
- Completed virtual build of the demonstrator, and initiated detailed design iterations on schedule to support prototype parts fabrication.
- Initiated performance evaluation and technology screening of the demonstrator powertrain ahead of schedule.
- Began assembly of the demonstrator early in FY 2014, on schedule for completion planned in early FY 2015.

Future Achievements

- Complete the build of the demonstrator vehicle and initiate validation testing.

Approach

Complete Vehicle Simulations

The SuperTruck project aims at developing multiple technologies to achieve significant freight efficiency and thermal efficiency improvements. These new technologies can

interact with each other; therefore the Volvo team uses its complete vehicle simulation capabilities to support the concept development and technology selection. This tool provides a quantitative insight into potential trade-offs and supports the development of a completely integrated vehicle.

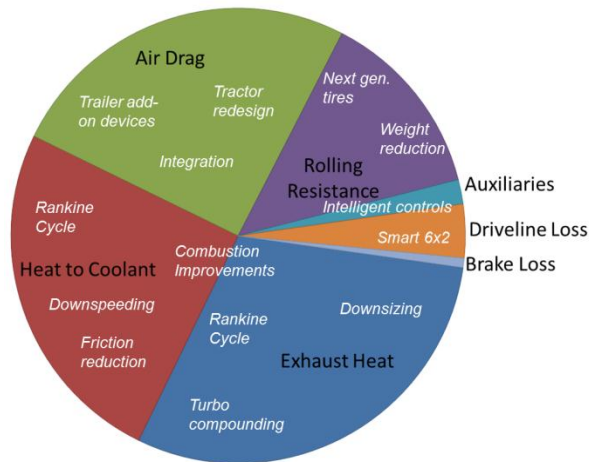


Figure III-49: Typical "tank-to-wheel" energy analysis for long-haul trucks (black) and technology matching (white)

The simulation platform was used to analyze the energy usage of the baseline truck, as illustrated in Figure III-49, and helped set engineering targets for the technologies (shown in white text) addressing each of the areas.

Complete Vehicle Aerodynamics

Since aerodynamic drag is the primary contributor to fuel use of a highway vehicle, the target was set to reduce it by 40% using an integrated design approach between tractor and trailer. The team uses a combination of complete vehicle computational fluid dynamics (CFD) simulations and wind tunnel scale testing to design and optimize geometries. Track and on-road testing are used to verify aerodynamic performance and fuel savings.

In addition to the design and optimization activities Ridge/Freight Wing is dedicated to making the trailer add-on devices more practical from an operational perspective. One particular focus is to find methods enabling the tail fairing to fold and provide convenient access to cargo.

Advanced Materials and Structures

The team is evaluating new structure concepts and materials in order to reduce the weight of the vehicle. Even though long haul trucks are typically not limited in weight carrying capacity, it is important to offset the curb weight increase brought by new technologies in order to maintain the payload capacity of the vehicle. One key challenge is to identify advanced materials which could become cost effective for the highway truck operating environment.

A study of new chassis concepts was started in late FY 2012 with the goal to reduce the weight of the frame rails and mounting brackets by 40% compared with the baseline vehicle. This resulted in a design freeze and build of a prototype lightweight frame in FY 2013, which was the starting point for the assembly of the demonstrator truck this fiscal year.

Parasitic Losses

Efficient LED lights are used for both interior and exterior lighting in order to reduce energy usage, which adds up to over 120 Gal of diesel fuel saved per vehicle per year. The trailers' exterior lights use Grote's LightForm lightweight and low profile technology.

The Volvo team plans on implementing advanced driver assistance solutions and intelligent vehicle controls to reduce driver impact on the efficiency of the complete vehicle. Telematics will also be investigated as a mean to improve transport efficiency.

Idle Reduction

In order to maximize overall system efficiency, the team is working to increase the insulation of the cab and improve the efficiency of the heating and cooling systems. This allows for downsized climate unit components and auxiliary power unit system.

Results

Complete Vehicle Aerodynamics

The design and optimization activities performed during the concept selection (Phase I) culminated in the road testing of the mule vehicle, which confirmed the simulated predictions of 30% drag reduction. The fuel economy improvements observed during these tests range from 13%–15%. Phase I provided the team with a deeper understanding of interactions between tractor and trailer, which set the design direction for the final demonstrator.

Aerodynamic iterations of the demonstrator have been the focus this year to address conflicting requirements between drag reduction and cooling capacity, manufacturability, etc. The final design is still on target to deliver 40% overall drag reduction compared with the MY 2009 baseline truck.

Ridge/freight wing focused its efforts on preparing for the commercialization of the aerodynamic trailer devices that have been developed in the project. Fuel economy testing was conducted in accordance with EPA protocols and several packages were tested with estimated fuel savings in excess of 9% at 65 mph. Plans are now in place to develop manufacturing capability in anticipation of the market launch of the products.

Extensive operational and durability tests were also completed this year, including field testing of several prototype units with six leading national fleets. Feedback from operational testing has been very positive and has provided valuable input that was incorporated in the product design. Because aerodynamic add-on devices must be designed to last the life of the trailer and mileage accumulation is limited in fleet trailers, accelerated endurance tests were performed to simulate 300,000 miles of operation with positive results and no major problems seen.

Advanced Materials and Structures

The prototype ultra-lightweight frame assembly designed last year was built and delivered on schedule in the first quarter of this year, see Figure III-50. It was a remarkable achievement to deliver such a complex assembly, fully engineered and virtually tested in less than 18 months from the definition of the concept.

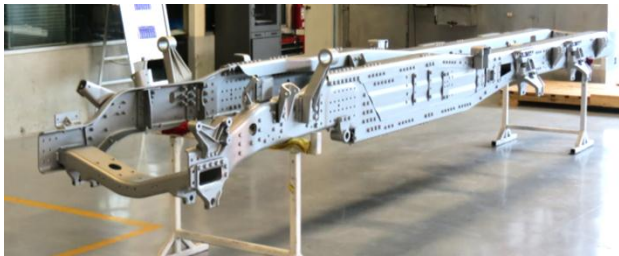


Figure III-50: Ultra-lightweight frame assembly

The weight savings achieved exceeded the target of 40% compared with the equivalent steel frame ladder. The subsequent assembly of axles and chassis mounted components uncovered no issues with the design. Work is therefore underway to build a second vehicle for track evaluation and data collection, with a plan to perform further analysis on the chassis assembly. These next steps will help evolve this promising concept closer to a mature customer solution.

Powertrain Integration

The knowledge gained from testing conducted on the mule truck in Phase I has been fed into the engineering requirements for the demonstrator powertrain in order to fully optimize the system for the targeted usage of the vehicle.

In order to maximize engine thermal efficiency on-road, the team decided to 'downsize' the engine for the demonstrator to 11-litre displacement. This allows the smaller engine to operate at a higher, more efficient load point despite the reduced power demand resulting from overall vehicle improvements as illustrated in Figure III-51.

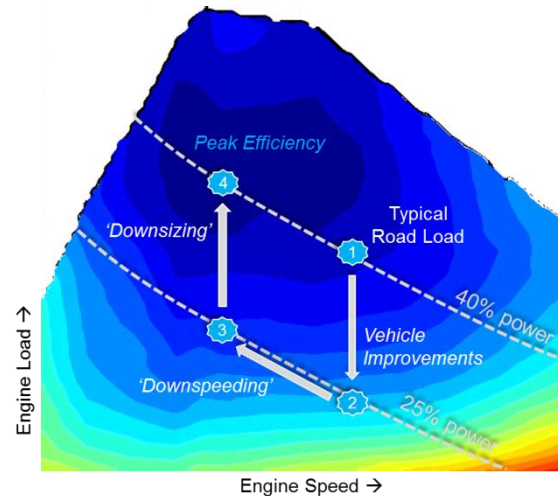


Figure III-51: Engine "right-sizing" approach

The second generation waste heat recovery (WHR) system components are in house, and system build is progressing on schedule with anticipated system start-up next year.

Cost, weight, and reliability of the WHR system remains a major hurdle, and this along with efficiency improvement is the focus of the second generation development for the demonstrator powertrain.

Idle Reduction

The air conditioning concept selected last year has been fully engineered and tested and is ready to be installed in the demonstrator for validation. It consists of a two-zone electrified A/C circuit powered by energy dense batteries, and can be connected to an external power supply (Shore Power). The system is sized to provide approximately 12 hours of operation on a full charge.

A new design concept for the integration of a solar panel in the roof of the tractor was initiated. The goal is to use solar energy to power a fan which extracts hot air from the cab in order to reduce cooling requirements. This helps reduce total energy consumption and allows for a downsized air conditioning system. The concept is fully designed and most prototype parts are ready to be installed on the demonstrator.

Parasitic Loss Reduction

The development of an intelligent energy management control strategy for the demonstrator ramped up during this fiscal year. The concept has been designed and refined in our simulation platform using the 24-hour duty cycle created previously. One key feature of this system is the ability to reduce fuel use by utilizing recovered kinetic energy to charge the hotel load batteries. The concept is being converted to a software package for integration into the demonstrator by the end of the fiscal year.

Conclusions

During this fiscal year the focus shifted from concept selection (Phase I) to integration of the validated technologies into the demonstrator (Phase II). Final testing of the mule vehicle from Phase I showed 43% freight efficiency improvements, which confirmed that the Volvo SuperTruck team is on track to meet or exceed the program goals in Phase II. The build of the demonstrator started early this year and has progressed on schedule, along with the further development of the advanced 50% BTE powertrain system.

The next fiscal year will see the initial validation tests of the demonstration vehicle.

3.2.1 Products

Publications

1. N/A

Patents

To date, the project team has generated eight subject inventions, and five patent applications have been filed. We look forward to sharing the details of these applications once they become publicly available.

Tools and Data

1. N/A

ZERO EMISSIONS CARGO TRANSPORT

III.J. Hydrogen Fuel-Cell Electric Hybrid Truck Demonstration & Houston Zero Emission Delivery Vehicle Deployment (DE-EE0005978, DE-EE0005979)

Principal Investigator: Nicholas Williams

Houston-Galveston Area Council
 3555 Timmons Lane, Suite 120, Houston, TX 77027
 Phone: (713) 993-4567
 E-mail: Nicholas.Williams@h-gac.com

DOE Program Manager: Lee Slezak

E-mail: Lee.Slezak@ee.doe.gov

NETL Program Manager: Charles Alsup

Phone: (304) 265-5432
 E-mail: Charles.Alsup@netl.doe.gov

III.J.1. Abstract

Objectives

EE0005978

- Accelerate the introduction and penetration of electric transportation technologies (ETT) into the cargo transport sector.
- Demonstration of at least three Class 8 zero-emission port drayage trucks:
 - Vehicles will be selected through a Call for Projects process.
 - Vehicles will meet or exceed all applicable federal and state emission requirements and safety standards.
- Operate vehicles under real world conditions at or near the Port of Houston to measure and demonstrate operational cost-effectiveness and commercial viability.

EE0005979

- Accelerate the introduction and penetration of electric transportation technologies (ETT) into the cargo transport sector.
- Deploy thirty (30) all-electric trucks.
- Vehicles included in the project will be selected through a Call for Projects process.
 - Vehicles will be operated by selected fleet operators including large national fleets and progressive regional fleets with delivery operations.
- Testing and data collection for vehicles in real-world conditions to measure and demonstrate operational cost-effectiveness and commercial viability.

Major Accomplishments

EE0005978

- Development and release of a Call for Projects to solicit new project partners after originally proposed partners were unable to move forward with project as originally anticipated.

EE0005979

- Development and release of a Call for Projects to solicit new project partners after originally proposed partners were unable to move forward with project as originally anticipated.

Future Achievements

EE0005978

- Full deployment and demonstration of at least three Class 8 zero-emission port drayage trucks.
- Release of technical report on cost-effectiveness of Class 8 zero-emission trucks in regional fleet(s).

EE0005979

- Full deployment of 30 zero-emission all electric delivery vehicles.
- Reduce emission of 4,180 tons of criteria pollutants over the two year project deployment phase.
- Reduce emissions of greenhouse gases by 75 MMTCE over the two year project deployment phase.
- Reduce over 250,000 gallons of diesel fuel over the year project deployment phase.
- Release of technical report on cost-effectiveness and emission reductions related to vehicle deployment.



III.J.2. Technical Discussion

Background

EE0005978

The Houston-Galveston Area Council (H-GAC) will partner with a regional fleet and zero-emission Class 8 truck OEM for a Zero-Emission Class 8 Drayage Truck Demonstration Project. The primary objective of the project is to accelerate the introduction and penetration of electric transportation technologies into the cargo transportation sector. The project will deploy vehicles, establish required fueling infrastructure, and demonstrate that vehicles will meet or exceed all emissions requirements.

To meet this objective, the grant will support development and demonstration of at least three Class 8 zero-emission trucks in the Houston-Galveston-Brazoria NAAQS 8-hour ozone nonattainment area. These vehicles will be selected through a Call for Projects process. The project will demonstrate vehicle operations, collect data, and report on project results for a period of two years after deployment.

Long term benefits of the program may include improved air quality in highly traveled areas in the Houston region and particularly near the active port facilities. Additionally fleets may realize savings on fuel expenditures and can work towards meeting sustainability and corporate social responsibility goals.

EE0005979

The Houston-Galveston Area Council (H-GAC), Center for Transportation & the Environment (CTE), have partnered to establish the Houston Zero Emission Delivery Vehicle Demonstration Project. The primary objective of the project is to demonstrate the effectiveness of all-electric delivery vehicles to perform at the same level of operation as similarly sized diesel delivery vehicles, while reducing vehicle emissions and petroleum consumption.

To meet this objective, this project will support the deployment of 30 all-electric delivery trucks in the Houston-Galveston-Brazoria NAAQS 8-hour ozone nonattainment area.

Vehicles selected through a Call for Projects process will be demonstrated by selected national, regional, and/or local fleets. All vehicle deployment and operation of the vehicles will occur within the Houston-Galveston region. In addition to the deployment of delivery vehicles and charging infrastructure, the project will demonstrate vehicle operations, collect data, and report on project results for a period of two years after deployment.

Introduction

EE0005978

This project supports ongoing efforts to reduce criteria pollutant emissions, greenhouse gas emissions, and fossil fuel use among drayage truck vehicles within the Houston region. As the project team works to create a demonstration of zero-emission Class 8 drayage trucks, the vehicles will be monitored and fleet operators will be surveyed in order to measure and demonstrate operational cost-effectiveness and commercial viability of the trucks.

EE0005979

The primary objective of this project is to deploy thirty zero-emission all electric trucks and demonstrate the effectiveness of the all-electric delivery vehicles to at the same level of operation as similarly sized diesel delivery vehicles while reducing vehicle emission and petroleum consumption.

The vehicles deployed will be selected through a Call for Projects process and will be deployed on delivery routes in the Houston- Galveston area. Large national fleets and progressive regional fleets that operate diesel and gasoline delivery vehicles in the region and will be the initial targets for fleet deployment and testing. Integration of all-electric vehicles into their fleets will result in both emission and noise reductions over diesel and gasoline counterparts. The fleets will also reduce their reliance on petroleum-based fuels and realize significant cost savings.

Approach

EE0005978

Vehicle eligible to respond to the Call for Projects include zero-emission heavy-duty Class 8 drayage trucks. The vehicles must be cargo-carrying on-road trucks with an expected gross vehicle weight rating of at least 80,000 lbs. Project vehicles must be designed and used for the sole purpose of moving and/or delivering cargo, freight, goods. The vehicles must be on-road and used under real-world drayage freight movement activities. Drayage operations include operation on or through port or intermodal rail yard property for the purpose of loading, unloading or transporting cargo, such as containerized, bulk or break-bulk goods.

Project vehicles must be zero emission and use an electric motor for all of the motive power of the vehicles, including battery electric, fuel cell, and hydrogen hybrid electric fuel cell vehicles. Ineligible vehicles include light duty vehicles, shuttle buses, transit buses, and hybrid electric vehicles. The vehicles must meet or exceed all applicable federal or state emission requirements and safety standards.

Testing

Qualitative evaluations and quantitative documentation for the tested parameters will be collected during the program using a combination of an on-board data collection system and input obtained by surveying drivers and maintenance personnel. These findings will be included in the monthly, quarterly and final reports.

Testing Variables

- Vehicle Operations:
 - Daily Mileage
 - Operating Time
 - Payloads
 - Speed
 - State of Charge
 - Auxiliary Loading
 - Maintenance Costs
- Charging Operations:
 - Daily Charge Times
 - State of Charge
 - Energy Consumption
 - Utility Costs
 - Maintenance Costs

Demonstration Period

The project will include a two-year demonstration of zero-emission Class 8 vehicles under real world conditions.

Infrastructure Requirements

Recharging/refueling infrastructure needed for this project will be located to allow the proper charging of the trucks utilizing the facility.

Commercialization

The experience and data collected from this project will help validate hydrogen and/or electric as a feasible alternative fuel options. Confirming durability and driver acceptance are also key results expected from this demonstration that would advance commercialization of zero-emission Class 8 vehicles.

EE0005979

CTE will work with fleets and OEMs selected through the Call for Projects to plan, select, and model routes on which the vehicles will be deployed. The project team will also install and test the charging stations in preparation for vehicle deployment. Once the vehicles are delivered, the project team will conduct a series of test to validate vehicle performance against the model. Once deployed in delivery service, the team will collect operational data and submit reports for two years.

As of the date of this progress report, one fleet/OEM team has successfully responded to the Call for Projects: UPS and AMP Electric Vehicles. The following information pertains to this project. It is intended that at least one fleet/OEM team will be added to the project.

System Description

AMP is developing a new chassis for this project and for the commercial market. The W88 chassis is designed to meet the needs of a wide range of customers. At the same time, it is a universal chassis from an operations perspective.

The vehicle is 100% electric powered by a 120 kWh battery pack giving it a useful range of 80 miles in a typical 120–150 stops per 8-hour package delivery shift. The range of the AMP/Workhorse truck will be more than adequate to cover the 50 to 65 mile per day routes in Houston. The vehicle has no transmission—it is a direct drive to the differential making it very efficient. The electric motive drive is a 2200 NM regenerative drive capable of powering a 23,000 pound vehicle from a dead stop up a 23% incline.

Top speed of the vehicle is limited to 65 mph. Typical differential ratios are 4.78 to 1 and 5.1 to 1 for the direct drive. The vehicle has a supervisory controller that interfaces with the Battery Management System, the Body Control Module, and the Brake Module, and the charging system to control the vehicle. There is an onboard level two J1772 charger, either 7 kW or 18 kW, depending on the customer preference. The vehicle can also be fitted with inductive charging.

Testing

The recipient fleet, in partnership with CTE and the OEM, will report vehicle and charger specifications and will collect operational and maintenance data for vehicles. Data collected may include powertrain and battery operational data. Additionally, data from non-electric fleet vehicles may be required for comparative analysis. All information collected shall be provided to CTE. CTE will analyze the data and summarize for submittal to DOE.

Testing Variables

- Vehicle Operations:
 - Daily Mileage
 - Operating Time
 - Payloads
 - Speed
 - State of Charge
 - Auxiliary Loading
 - Maintenance Logs
- Charging Operations:
 - Daily Charge Times
 - State of Charge
 - Energy Consumption
 - Utility Costs
 - Maintenance Logs
- Data collected will be used to calculate a number of analytical factors, including, but not limited to:
 - Fuel Efficiency (i.e., \$/mile, kWh/mile, etc.)
 - Cargo Ton-Miles/Vehicle
 - Cargo Ton-Miles/Fleet

- Reduction in Petroleum Consumption
- Reduction of Green House Gas Emissions (Million Metric Tons of Carbon Equivalent (MMTCE)/year)
- Reduction of Criteria Pollutant and Toxic Emissions
- Expected Life Cycle Benefit Analysis

Demonstration Period

The project will include a two-year demonstration of each all-electric truck under real world conditions.

Data Collection Strategy

New vehicles are tested by the OEM for durability and are equipped with data collection and monitoring systems to track variables from the battery management, drive system, cooling systems, etc. Coast-down testing is used to determine projected energy usage per mile; use case testing is accomplished to verify that vehicle energy usage is consistent with projected usage. Limits of charge and discharge are set as to ensure that the main battery will operate to its projected life without overstressing it.

Real time data is sent to a server for storage and analysis and parameters are modified as necessary to insure the vehicle performs to its design parameters.

Vehicles prototypes are tested on steep hills and anticipated normal driving conditions locally to get baseline data before TRC testing. Data is collected to determine energy usage per mile under various driving conditions and compared to predicted models to determine battery life, range, acceleration etc. Major vehicle maintenance for production vehicles can be performed at Workhorse dealers across the country.

Infrastructure Requirements

Each vehicle comes with a water-cooled J1772 level 2 charger on-board. The charger is typically 12kWh, 220 Vac. Vehicles may be optionally equipped with 25KW induction charging.

Commercialization

It is believed that the vehicles used in this project will result in a positive business case on a total cost of ownership basis for UPS and other selected fleets. This is due to the lower cost of electricity and lower maintenance costs as compared to fuel and maintenance of diesel medium- and heavy-duty vehicles.

Results

EE0005978

The project team is currently in the process of selecting a fleet and OEM through a Call for Projects. To date, no performance data has been collected.

Expected results:

H-GAC anticipates the following actions to occur as a result of this project:

1. Increased adoption of zero-emission Class 8 technology for drayage fleets

2. Increased adoption of technology for regional port operators as a result of outreach and exposure to the project
3. Increased adoption of technology through other outreach and education efforts to ports in other areas, through DOE meetings, participation in DOE Clean Cities/Clean Fleets partnership programs.

EE0005979

The project team is currently in the process of selecting fleet participants and preparing for the manufacture and delivery of vehicles. To date, no performance data has been collected.

Expected results:

H-GAC anticipates the following actions to occur as a result of this project:

1. Reduction of petroleum use in the demonstration period during and after the project activities
2. Reduction of greenhouse gases, criteria pollutants, and toxic emissions
3. Demonstration and evaluation of market viability
4. Opportunity to increase adoption of the demonstration technologies
5. Expansion of U.S. manufacture and production of electric vehicles and U.S. suppliers of batteries and equipment for electric vehicles.

Conclusions

EE0005978

This project will produce on-road experience and gather data which will serve to accelerate the introduction and penetration of electric transportation technologies. Specifically, at least three zero-emission Class 8 trucks will be deployed into the drayage cargo transportation sector. Current delays in project initiation will require an aggressive timeline for manufacture of advanced vehicle technologies and the establishment of adequate fueling and/or charging infrastructure in early 2015.

EE0005979

This project will produce on-road experience and gather data which will serve to accelerate the introduction and penetration of electric transportation technologies. Specifically, 30 zero emission all-electric trucks will be deployed across the Houston region. The project has experienced delays due to financial challenges faced by the originally intended OEM and in identifying appropriate routes in the Houston area as a result of typically longer travel routes. Continued outreach and education have identified routes and vehicles for deployment of vehicles in early 2014.

III.J.3. Products

Publications

EE0005978

None to Date

EE0005979

None to Date

Patents

EE0005978

None to Date

EE0005979

None to Date

Tools and Data

EE0005978

None to Date

EE0005979

None to Date

III.K. Zero Emission Heavy-Duty Drayage Truck Demonstration-EE00005691

Principal Investigator: Matt Miyasato

South Coast Air Quality Management District
21865 Copley Drive
Diamond Bar, CA 91765
Phone: (909) 396-3249
E-mail: mmiyasato@aqmd.gov

Project Manager: Brian Choe

Phone: (909) 396-2617
E-mail: bchoe@aqmd.gov

DOE Program Manager: Lee Slezak

Phone: (202) 586-2335
E-mail: lee.slezak@ee.doe.gov

- Analyze the field test data to evaluate the performance and O&M costs of demonstration vehicles.



III.K.2. Technical Discussion

Introduction

On-road heavy-duty diesel trucks are one of the largest sources of diesel particulate matter and NOx emissions in the South Coast Air Basin. The impact on air quality and public health is more pronounced in the surrounding communities along the goods movement corridors near the Ports of Los Angeles and Long Beach, and next to major freeways in Southern California. As a measure to reduce the impact and to meet future Federal ambient air quality standards, South Coast Air Quality Management District has been working with other regional stakeholders, including the Ports of Los Angeles and Long Beach, to promote and support the development and deployment of advanced zero emission cargo transport technologies.

Approach

This project will develop 13 zero emission heavy-duty drayage trucks for demonstration based on four different architectures, consisting of three types of battery electric drivetrains from Balqon, TransPower, and U.S. Hybrid and one fuel cell hybrid electric drive system by Vision Industries. The trucks will be deployed in revenue drayage service for a two-year demonstration with Total Transportation Services, Inc (TTSI) and other partnering fleets at the Ports of Los Angeles and Long Beach to evaluate technical feasibility and market viability of the technologies in cargo transport operations.

Balqon

Three Class 8 BEV drayage trucks will be developed by Balqon based on their prototype, MX-30 (Figure III-52). The drivetrain will consist of a 240 kW induction motor with an automatic transmission powered by a 380 kWh lithium iron phosphate battery pack. Balqon will also provide a 500 kWh energy storage system that can be used to fast charge vehicles during mid-day for extended operations while avoiding high demand charges.

III.K.1. Abstract

Objectives

- The objective of this project is to demonstrate and evaluate technical feasibility and market viability of zero emission truck technologies in drayage service to promote and accelerate deployment of zero emission cargo transport technologies in the South Coast Air Basin.
- This project will fund development of 13 zero emission drayage trucks based on four different architectures, consisting of three battery electric drivetrains and one fuel cell hybrid electric drive system for a two-year demonstration in revenue drayage service between the Ports of Los Angeles and Long Beach and nearby rail yards and warehouses.

Major Accomplishments

- Completed initial system and components design for all four technologies.
- Incorporated design upgrades through validation and optimization processes.
- Completed a data collection template for BEV trucks.
- Two BEV trucks completed and road tested, to be deployed in drayage service by November 2014.

Future Achievements

- Complete the rest of 13 demonstration vehicles.
- Complete validation of demonstration vehicles including chassis dynamometer testing.
- Deploy vehicles in revenue drayage service with partnering fleets for field demonstration.



Figure III-52: Balqon Prototype MX-30

Figure III-53 shows an overview of the Balqon BEV system with major components identified including:

- 240 kW induction motor coupled to an Allison six speed automatic transmission.
- Liquid cooled traction controller with 450–700 VDC input and 460 VAC 3-phase output.
- 380 kWh lithium iron phosphate battery pack, air cooled
- 40 kW liquid cooled auxiliary controller.
- Approximately 100 miles of range in normal drayage operation.
- Recharge in 3-4 hours with a 160 kW charger.



Figure III-53: Balqon BEV System

TransPower

- Four Class 8 BEV drayage trucks will be developed for demonstration by TransPower building on their prototype, ElecTruck (Figure III-54). The motive power will be provided by an innovative dual motor system with two 150 kW Fiskar motors, leveraging mass produced components for cost savings and proven reliability. The trucks will be equipped an automated manual transmission with proprietary software for high vehicle performance and improved efficiency. Also, TransPower will use unique Inverter-Charger Units (ICUs) that combine the functions of both vehicle inverter and battery charger in the demonstration vehicles to reduce the size and cost of power electronics.



Figure III-54: TransPower Prototype ElecTruck

Figure III-55 shows an illustration of the TransPower BEV system which is comprised of:

- 300 kW dual motor assembly with two 150 kW Fiskar motors coupled to a 10-speed Eaton AMT.
- Power control and conversion system with two ICUs, each rated at 150 kW for motor control and 70 kW for charging.
- 269 kWh lithium iron phosphate battery pack, air cooled.
- 70 to 100 miles of range in normal drayage operations.
- Recharge in 4 hours with a 70 kW ICU.

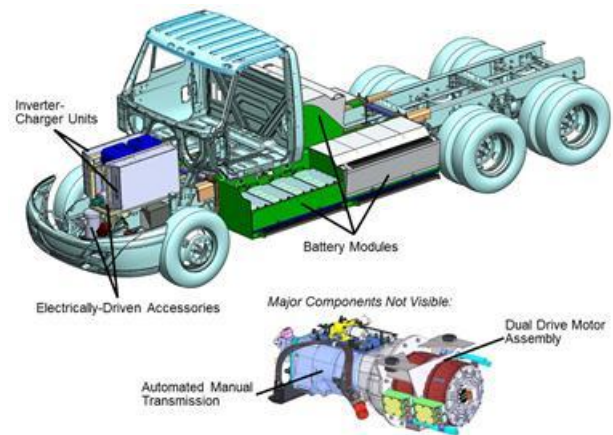


Figure III-55: TransPower BEV System

US Hybrid

US Hybrid will develop two Class 8 BEV trucks in this project. Each truck will be powered by a dual motor combination coupled with an automated manual transmission to provide higher continuous torque and power rating without compromising efficiency. 300 kWh lithium-ion battery pack will provide an estimated operating range of 100 miles in normal drayage operations.

Figure III-56 shows an illustration of US Hybrid BEV system which comprises:

- 320 kW powertrain with a dual motor combination and automated manual transmission.
- 320 kW MCU with 6.6 kW on-board charger.

- Lithium-ion battery pack with 300 kWh in total capacity, air cooled.
- Approximately 100 miles of range in normal drayage operations.
- Recharge time of three hours with a 120 kW charger.

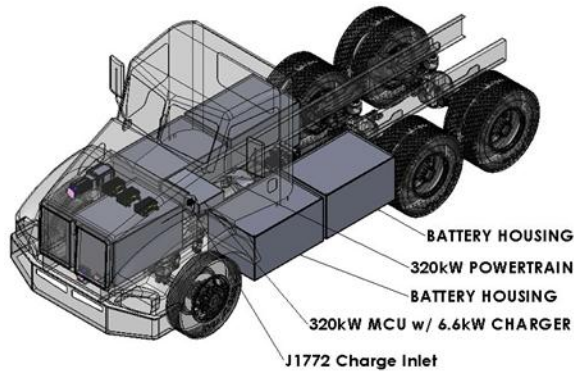


Figure III-56: US Hybrid BEV System

Vision Industries

Vision will use a fuel cell hybrid electric drive system to build four Class 8 drayage trucks. Sharing the same drivetrain architecture from their prototype Tyrano (Figure III-57), each truck will be powered by a Siemens 320 kW ELFA motor with direct control system and a 130 kWh lithium iron phosphate battery pack. For an extended range, two 16.5 kW Hydrogenics PEM fuel cells will be used to provide up to 200 miles in normal drayage operations. The truck will also feature an on-board Level 2 charging system to fully charge the battery in less than 8 hours.



Figure III-57: Vision Industries Prototype Tyrano

Figure III-58 shows an illustration of Vision Industries fuel cell hybrid electric drive system which consists of:

- Siemens 320 kW ELFA drivetrain with two 165 kW inverters.
- Lithium iron phosphate battery pack with 130 kWh in total capacity, air cooled.
- Two Hydrogenics 16.5 kW PEM fuel cells.
- On-board hydrogen storage tanks with 21 kg in total capacity.

- 200 miles of range in normal drayage operations.
- Recharge/Refuel Time – 8 hours with Level 2 charger/10-15 minutes for hydrogen refueling.

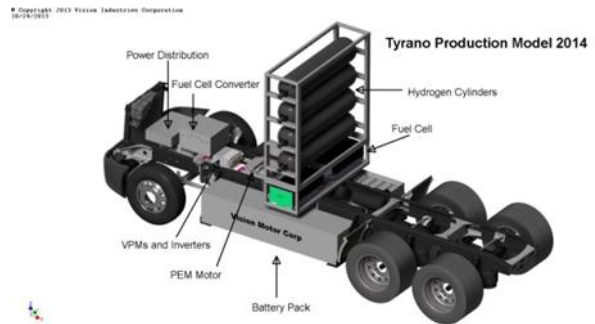


Figure III-58: Vision Fuel Cell Hybrid Electric Drive System

Finally, NREL will analyze data collected by on-board data collection devices for vehicle performance and efficiency in this project. NREL will also analyze operations and maintenance data to assess the vehicle and infrastructure operating costs.

Results

In FY 2014, the project has made steady progress in the development of demonstration vehicles although it was slower than initially projected. TransPower made the most progress having completed two demonstration vehicles with the remaining two to be completed by December 2014. The other manufacturers are in different stages of vehicle development as discussed below:

Balqon

Balqon completed system and component designs with the following upgrades for improved safety and efficiency:

- Integrated all logic and controls into single NEMA rated enclosure to protect from environment and improve reliability.
- Improved logic and power control design to reduce electromagnetic interference.
- Weather-proofed battery boxes and interconnectors.
- Consolidated BMS system for improved maintenance.

Balqon is also working on a dual mode transmission control system to change gear shift points when pulling an empty container for improved energy efficiency.

The new drive system will be first tested on a mule truck for validation and further refinements before it is installed in demonstration vehicles. Balqon expects to begin vehicle integrations by early Q2 FY 2015.

TransPower

The first demonstration vehicle, EDD-1 in Figure III-59 was completed in April 2014 and has undergone extensive on-road testing with approximately 2,500 accumulated miles, including a round trip of nearly 200 miles to University of California, Riverside in May. During the trip, the truck averaged 51.7 mph with 1.5 kWh/mile vehicle efficiency. The

top speed was 64 mph and the range was extrapolated to be more than 125 miles unloaded. EDD-2 (Figure III-60) was also completed recently and is currently undergoing on-road testing on a 10-mile test loop covering 800 feet of elevation. The completion of EDD-2 was delayed to incorporate several design changes which include:

- Larger and more robust battery enclosures requiring fewer wiring and connectors with savings in assembly costs and labor.
- Rearrangement of battery modules to improve accessibility for inspection and service.
- Advanced BMS with greater processing capability and high-current active charge shuffling to improve system efficiency, operating range and battery life.

TransPower plans to deploy EDD-1 in drayage service by November once the charging infrastructure at the TTSI facility is completed. EDD-2 will be also deployed shortly after it is tested on a chassis dynamometer at UCR in mid November.



Figure III-59: TransPower EDD-1



Figure III-60: TransPower EDD-2

US Hybrid

In FY 2014, US Hybrid completed high level engineering design including specifications and requirements for major systems as highlighted below:

- A dual permanent magnet motor combination was selected to provide higher continuous torque and power rating.

- After review of gear ratios, torque capability, weight, control scheme and availability, Eaton AMT was selected for its higher overdrive ratio and torque capability.
- Enerdel battery configuration was selected with detailed design of each battery enclosure in progress.

US Hybrid also selected International Prostar (Figure III-61) as their platform which is widely used as drayage and regional trucks. Vehicle integration work is set to start in mid November.



Figure III-61: International Prostar

Vision Industries

With the first draft of system design completed, Vision's engineering team had been conducting system validations including conceptual mounting and stress testing. However, Vision filed for the Chapter 11 bankruptcy protection in September suspending their operations at least temporarily. Vision intends to continue with the project once they reemerge from the reorganization process with a healthier balance sheet.

III.K.3. Products

Publications

1. N/A

Patents

1. N/A

Tools and Data

1. N/A

IV. VEHICLE TEST AND EVALUATION

LIGHT DUTY

IV.A. EV Project, ChargePoint America, and West Coast Electric Highway Data Collection and Information Dissemination

Principal Investigator: James Francfort

Idaho National Laboratory
P.O. Box 1625
Idaho Falls, ID 83415-2209
(208) 526-6787
James.francfort@inl.gov

DOE Program Manager: Lee Slezak

(208) 586-2335
Lee.slezak@ee.doe.gov

IV.A.1. Abstract

Objectives

- Study the behavior of plug-in electric vehicle (PEV) owners and how they use the PEV charging stations that are part of three large PEV charging infrastructure deployment projects.
- Report lessons learned to inform PEV and charging infrastructure deployment and purchase decisions by federal and state agencies, fleet managers, other EV Everywhere stakeholders, and the general public.
- Provide information based on real-world usage data to researchers and industry to reduce the uncertainties about PEV acceptance and use, including driver preferences for residential, workplace, and public charging at various power levels and prices.
- Blend data streams from multiple sources, namely the Blink Network, OnStar, Nissan, Daimler, ChargePoint, and AeroVironment, into usable formats to allow analysis across numerous makes/models of vehicles and charging equipment in regions across the United States.
- Continue to provide analysis results to other DOE programs and national laboratories, as well as the several U.S. DRIVE technical teams, of which Idaho National Laboratory (INL) staff are members.

Major Accomplishments

- PEV charging behavior data were collected from 12,419 Level 2 (electric vehicle supply equipment (EVSEs) and DC fast chargers (DCFC) from the Blink Network as part of the EV Project. As Fiscal Year (FY) 2014 ended, 5.7 million charge events occurred and 45,837 MWh of electricity were used.

- PEV use data were collected from 8,228 Nissan Leafs, Chevy Volts, and Smart EVs in the EV Project. PEV data collection for The EV Project concluded at the end of Calendar Year (CY) 2013, by which time 124 million test miles of PEV use were documented.
- Continued data collection from 4,647 ChargePoint AC Level 2 (240 V) charge ports that were deployed in the ChargePoint America project. At the end of CY 2013 (the conclusion of project data collection), data had been collected from 1.8 million charge events that used 13,399 MWh of electricity.
- Data were collected from AeroVironment charging stations installed in Oregon and Washington State as part of the West Coast Electric Highway. Usage data spanned CY 2012–CY 2013 and included 27,373 charge events from 101 charging units that consumed 230 MWh of electricity.
- As a result of these data collection activities, much information has been disseminated by INL on the real-world usage of PEVs and charging infrastructure, including trends in charging station use over time as fees for use were implemented, electric vehicle miles traveled, public charging station usage at different types of locations, and PEV driver preference for charging at home, workplace, and public charging stations.
- Lessons learned about workplace charging behavior have been published for DOE to provide guidance for participants of DOE's Workplace Charging Challenge, which encourages greater workplace charging options.

Future Achievements

- INL will continue to report on performance and use of the vehicles and charging infrastructure based on observations made using data from the EV Project, ChargePoint America, and the West Coast Electric Highway.
- Reports and presentations of results of studies in the following areas will be published:
 - Use of charging infrastructure along the I-5 travel corridor. Results will be provided to U.S. Department of Transportation and the departments of transportation for Washington State and Oregon.
 - Battery electric vehicle (BEV) driving range and the efficacy of public infrastructure in enabling long-distance trips
 - Characterization of public charging station usage at different venues, such as venues or retail stores, to

- determine the value of different types of charging equipment at these locations
- Installation cost for charging equipment of different power levels at residential and commercial locations.



IV.A.2. Technical Discussion

Background

DOE's Advanced Vehicle Testing Activity (AVTA) is part of DOE's Vehicle Technologies Office, which is within DOE's Office of Energy Efficiency and Renewable Energy. AVTA is the only DOE activity tasked by DOE to conduct field evaluations of vehicle technologies and fueling infrastructure that use advanced technology systems and subsystems in light-duty vehicles to reduce petroleum consumption.

INL activities conducting AVTA have resulted in INL developing data collection systems from vehicles and charging infrastructure that use wireless data collection and transmission methodologies. INL has accumulated this experience over 20 years of PEV, hybrid electric vehicle, and internal combustion engine vehicle testing, including laboratory, track, and field testing. Approximately 18 million miles of vehicle testing data had been accumulated by the late 2000's when DOE decided on a series of deployment and demonstration projects that included The EV Project and ChargePoint America. Given the anticipated large amount of data to be generated from vehicles and charging infrastructure, DOE tasked INL with collecting, managing, and analyzing data generated by the light-duty PEVs and charging infrastructure in the projects and disseminating the information synthesized from the data to a broad range of stakeholders.

Introduction

The DOE-funded data collection activities described in this section of this report include The EV Project, ChargePoint America, and AeroVironment's operation of PEV charging stations in the West Coast Electric Highway project.

The EV Project was the largest plug-in electric vehicle infrastructure demonstration project in the world, equally funded by the United States Department of Energy (DOE) through the American Recovery and Reinvestment Act and private sector partners. The EV Project deployed over 12,000 AC Level 2 charging stations for residential and public use, as well as over 100 dual-port DCFCs. Approximately 8,300 Nissan LEAF, Chevrolet Volts, and Smart ForTwo Electric Drive vehicles were enrolled in the project.

The EV Project was conducted in the following metropolitan areas:

- Phoenix and Tucson, Arizona areas
- San Diego, San Francisco, and Los Angeles, California areas
- Atlanta, Georgia area
- Chicago, Illinois area

- Southern New Jersey
- Portland, Eugene, Salem, and Corvallis, Oregon areas
- Philadelphia, Pennsylvania area
- Chattanooga, Nashville, Knoxville, and Memphis, Tennessee areas
- Dallas, Fort Worth, and Houston, Texas areas
- Washington, D.C. area
- Washington State.

Project participants gave written consent for The EV Project researchers at INL to collect and analyze data from their vehicles and/or charging units. The data collection phase of The EV Project ran from January 1, 2011, through December 31, 2013. INL is responsible for analyzing the data and publishing summary reports, technical papers, and lessons learned on vehicle and charging unit use.

ChargePoint America was led by ChargePoint, with American Recovery and Reinvestment Act funding support from DOE. The project deployed 4,700 residential and commercial charging stations in nine U.S. regions. The data collection phase of ChargePoint America ran from May 1, 2011, through December 31, 2013. INL is responsible for analyzing the data collected and publishing results.

ChargePoint America was conducted in the following regions:

- Boston, Massachusetts
- Washington, DC
- Multiple areas in central Florida
- Los Angeles, California
- Multiple areas in southern Michigan
- New York City, New York
- San Francisco and Sacramento, California
- San Antonio and Austin, Texas
- Bellevue, Washington.

The West Coast Electric Highway is a network of electric vehicle AC Level 2 and DCFC located every 25 to 50 miles along Interstate 5 and other major roadways in the Pacific Northwest (i.e., Washington, Oregon, and California). It contains a large electric vehicle charging network with thousands of AC Level 2 stations and dozens of DCFCs. Many of the charging stations installed along Interstate 5 and other major highways were from AeroVironment. AeroVironment provided data about, and collected from, these charging stations located in Washington and Oregon, to INL for analysis.

The overall purpose of these PEV infrastructure demonstrations was to create areas of dense infrastructure, study the infrastructure deployment process, how PEV drivers use the industry, and also to understand the impact of charging infrastructure usage on the electric grid.

Approach

Ensuring the security of the data collected was critical for protecting the proprietary interests of industry partners and the privacy of individual participants. To accomplish this, INL applied its highest non-classified level of security protocols to data handling and storage processes. Figure IV-1 is a schematic showing the data transfer process between industry partners and INL and the multiple layers of protection in INL’s data management system.

Non-disclosure agreements were also put in place between INL and industry partners. For the EV Project, data collection agreements and non-disclosure agreements were signed with Nissan (Leafs), ECOtality North America (infrastructure), OnStar (for Chevrolet Volt data), and Daimler (Smart EVs). The importance of successfully negotiating the non-disclosure agreements cannot be understated. In the case of OnStar, this was their first ever partnership where they shared raw vehicle data with an outside party. Similarly with Nissan, ECOtality, and Daimler, a project of this type was revolutionary in that raw data from very competitive entities would allow a third party (INL) to have all the raw data and the ability to produce reports that accurately benchmarked how over 11,000 general public partners were operating their vehicles and the charging infrastructure. The EV Project also necessitated signing agreements with the 11,000 individual owners of the vehicles and the public charging infrastructure.

For the ChargePoint America and West Coast Electric Highway Projects, non-disclosure agreements negotiated with ChargePoint and AeroVironment enabled INL to receive raw data that documented charging infrastructure use. Given the lack of vehicle data, there were not as many concerns with personal identification issues.

INL has highly automated the data collection, processing, and reporting system used to collect most data from vehicles and charging infrastructure. The history of automated data collection at INL goes back to the use of databases for tracking electric vehicle performance and use in the mid 1990s. These systems have been refined as technology options (such as cellular communications and much lower cost data loggers) have progressed. Today, a multi-step process (Figure IV-1) is used to transmit vehicle and charger data from the vehicle, through the INL firewalls, and into the INL protected enclave.

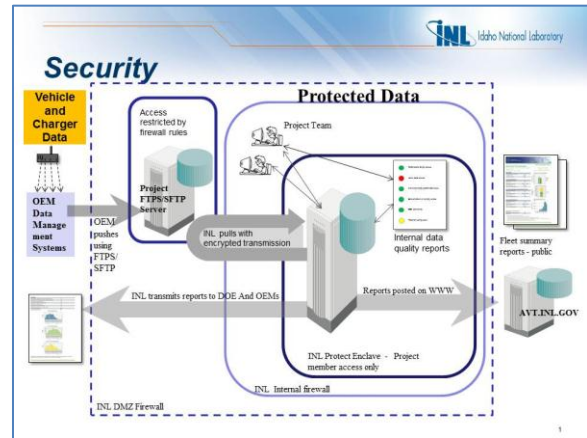


Figure IV-1: Overview of INL’s data and information transfer process for the EV Project and ChargePoint Project, as well as all data collection activities

From there, additional processing steps are used within INL (Figure IV-2) to develop summary reports and various partner-requested custom reports.

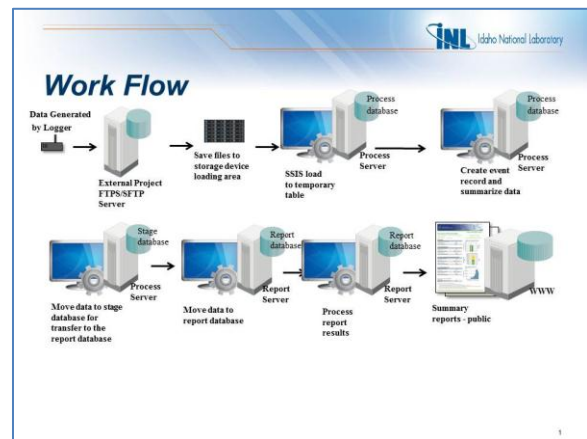


Figure IV-2: Major processing steps for handling wireless vehicle and charging infrastructure data

INL reviews the reports with its industry partners before publishing them online to the general public and/or disseminating to other organizations.

Results

In the EV Project, the total reported project mileage was 124 million miles contributed by 8,228 Leafs, Volts, and Smart EVs. Figure IV-3 shows the distribution of these vehicles by EV Project regions. By the end of FY 2014, more than 12,000 public and residential AC Level 2 EVSE and DCFC had reported 5.7 million charging events. Figure IV-4 shows the distribution of these vehicles by EV Project regions.

By the end of the ChargePoint America project, 4,647 ChargePoint AC Level 2 (240 V) charge ports were deployed in the ChargePoint America project. At the end of CY 2013 (the conclusion of project data collection), data had been collected from 1.8 million charge events that used 13,399 MWh of electricity.

Usage data from AeroVironment AC Level 2 and DCFC along the West Coast Electric Highway spanned CY 2012 – CY 2013. The data included 27,373 charge events from 101 charging units that consumed 230 MWh of electricity.

INL produced Q3 2014 and Q4 2013 (Q3 means third quarter of 2014) reports to document the use of the EVSE and PEVs in the final two calendar quarters of the data collection periods for The EV Project and ChargePoint America. These were the final quarterly reports to be produced for these two projects. Focus then shifted to deep-dive analysis of the data. Numerous studies were completed in FY 2014 using data from these three projects to better understand PEV and charging infrastructure usage. This section summarizes the findings of some of those studies.

Electric Vehicle Miles Traveled

One of the most frequently asked questions was how far PEVs have been driven using only electricity. This was answered by studying Nissan Leaf and Chevrolet Volt driving patterns between October 1, 2012, and December 31, 2013. During this period, Nissan Leaf drivers in The EV Project averaged 808.1 electric vehicle miles traveled per month. Chevrolet Volt drivers in The EV Project Volt averaged 759.3 electric vehicle miles traveled per month and 1,019.8 total vehicle miles traveled per month. This is significant because the estimated electric range of the Leaf is approximately double that of the Volt. However, Leaf drivers in the EV Project averaged only 6% more actual electric miles per month than Volt drivers.

The reason for this near-parity is that the Leaf is a BEV, which is powered by electricity alone. When its battery is fully depleted, it cannot be driven. The Volt, on the other hand, is a plug-in hybrid electric vehicle capable of being powered exclusively by electricity or by an internal combustion engine after the battery pack is depleted below a minimum threshold. The Volt has a smaller capacity battery and, therefore, shorter electric vehicle (EV) mode range than the Leaf, but Volt drivers do not need to worry about being stranded if their battery is completely drained. As a result, Volt drivers commonly drove their vehicles in EV mode to the point where the battery was fully depleted, whereas Leaf drivers tended to limit their driving to prevent the battery from being drained below a certain point.

This behavior is evident in Figure IV-3 and Figure IV-4, which show the distribution of battery state of charge (SOC) for Volts and Leafs in The EV Project during Q4 2013 when the vehicles began charging. Leaf drivers recharged their batteries at widely varying battery SOC, and rarely let the SOC drop below 20%. Volt drivers allowed their batteries to be fully or nearly fully depleted (i.e., below 10% SOC) prior to about one quarter of their charges.

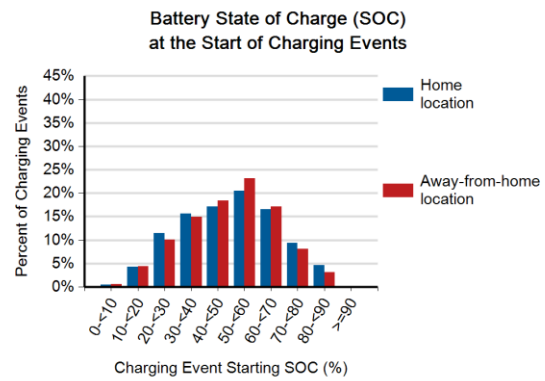


Figure IV-3: EV Project Nissan Leaf battery SOC at the start of charging events

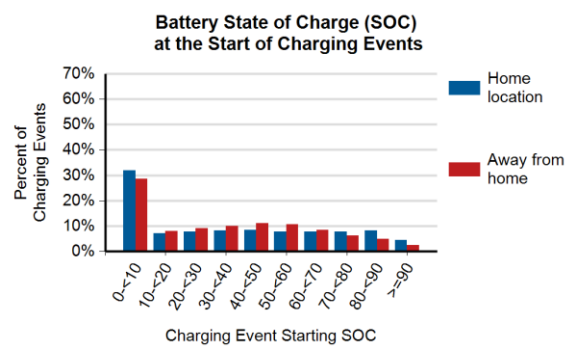


Figure IV-4: EV Project Chevrolet Volt battery SOC at the start of charging events

Electric vehicle miles traveled (eVMT) for Leafs and Volts was also examined on a month-by-month basis to determine if there was any change over time. Figure IV-5 shows how the median eVMT for the groups of Leaf and Volt drivers changes. It also included the total vehicle miles traveled (VMT) for the Volt, which sums the distance driven in EV mode and in extended-range mode.

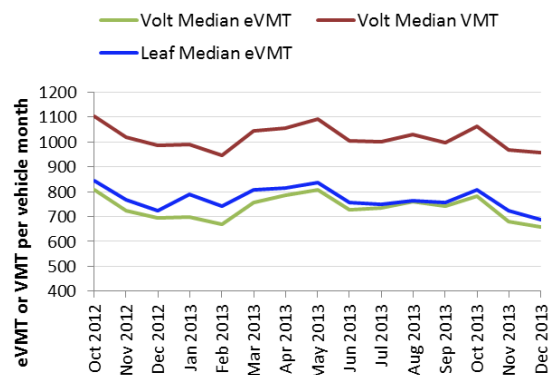


Figure IV-5: Median eVMT and VMT per vehicle month over time

The Leaf’s median eVMT (blue line) is slightly higher than the Volt’s median eVMT (green line) throughout the 15-month study period; however, the medians are nearly equal in August 2013. The eVMT medians rise and fall fairly proportionally, with only a few exceptions. The 25th and 75th percentile values for the distributions each month (not shown) rise and fall with the medians, indicating that the shapes of the distributions are relatively constant month after month. This proportional shifting of the distributions over time suggests that seasonal effects influence both Leaf and Volt drivers in the same way.

The ratio of the Volt’s median eVMT to its median VMT (red line) is the percentage of distance traveled in EV mode each month. Visual inspection of Figure IV-5 shows this value remained relatively consistent. There was seasonal variation, however; the months of April through October saw 74% to 77% of distance in EV mode, whereas vehicles averaged 70% to 74% miles in EV mode in November through March.

Fraction of Chevrolet Volt Driving in EV Mode

Another study examined the fraction of distance that EV Project Volts drove in EV mode and found it to be 73%, overall. Volt drivers accomplished this by charging their vehicles any number of ways: by long infrequent charging sessions, by short frequent charging sessions, or any combination of frequency and duration. Charging frequency is best described in terms of how far a vehicle has driven between. Figure V-6 shows the average distance each vehicle traveled between consecutive charging events and the average energy consumed per charging event. Each vehicle’s EV% is represented by the color of each data point.

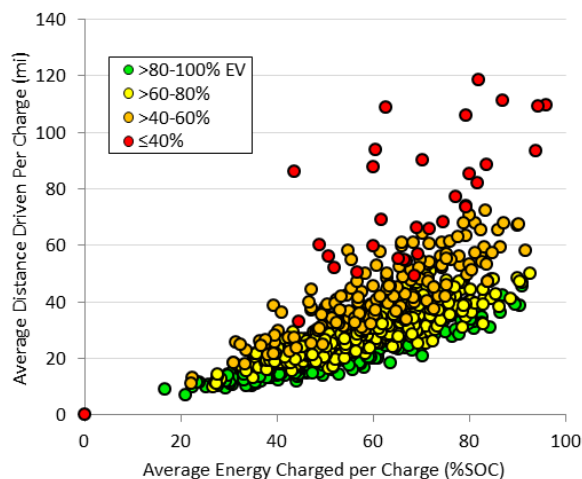


Figure IV-6: Average distance driven between charging and average charging energy per charge for each vehicle, with EV% denoted by color

The majority of vehicles in Figure V-6 were driven relatively short distances between charging events. In fact, 75% of drivers averaged less than 35 miles between charges. However, not all vehicles consumed the same amount of energy per charge. Many vehicles were consistently charged enough per charging event, relative to miles driven prior to charging and driving conditions, to maintain high EV%. These

vehicles are represented by green data points. Other vehicles were charged at the same mileage interval, but averaged less energy per charging event. This variation in charging energy consumed from vehicle to vehicle results in varying EV% for the same distance driven. This is also a reason why some vehicles achieved an EV% of far less than 100%, even though they were consistently driven less than the expected EV range of the vehicle prior to recharging. In general, however, drivers of vehicles with high EV% typically took fewer trips of shorter length between charging events. They also charged more frequently for shorter durations.

Preferences for Charging Location, Power Level, and Time of Day

Nissan Leaf

The EV Project provided an opportunity to determine driver preference for different types of charging equipment, as well as charging location and time of day. From a sample of 4,038 Nissan Leaf drivers who performed 867,293 charges at AC Level 1, AC Level 2, and DCFC units over a 15-month period, it was determined that Leaf drivers relied on home charging for the bulk of their charging. Of all charging events, 84% were performed at drivers’ home locations. Over 80% of those home charges were performed overnight and about 20% of home charges were performed between trips during the day. The remaining 16% of charging events were performed away from home. The vast majority of these were daytime Level 1 or Level 2 charges. The overall split of the 867,293 charges by location, power level, and time of day is shown in Figure IV-7.

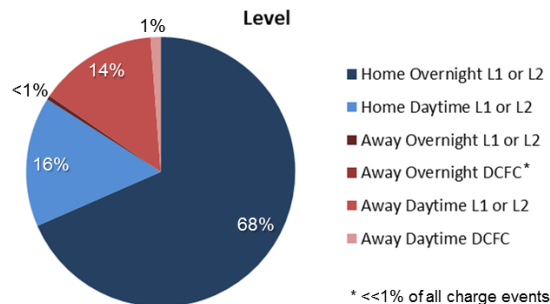


Figure IV-7: Percent of Nissan Leaf charging events performed by location, power level, and time of day

DCFC charging events represented only 1% of all charging events. Ignoring charges by vehicles that never charged away from home, DCFC were used for 6% of all away-from-home charging events. Even though overall use of DCFC was low, some drivers may have relied on occasional or even frequent fast charging to extend their driving range or otherwise charge their batteries sufficient to meet their needs for driving range.

Not all Leaf drivers used away-from-home charging infrastructure equally. In fact, three quarters of the away-from-home charging was performed by 20% of the vehicles. A significant portion of vehicles (i.e., 13%) were never charged away from home.

Half of the away-from-home charging was performed by a group of Leafs who averaged 1.5 charging events per day driven. Drivers of these vehicles supplemented near-daily home charging with frequent away-from-home charging. This allowed these vehicles to average 43 miles per day driven, a 72% increase over vehicles that were never charged away from home.

Although all vehicles in the EV Project had access to home charging, some Leafs rarely charged at home. Instead, they relied on frequent away-from-home charging during the day. This demonstrates the viability of publicly accessible and/or workplace charging infrastructure for drivers of electric vehicles without access to home charging.

Chevrolet Volt

Chevrolet Volt drivers showed similar charging preferences. A sample of 1,867 Chevrolet Volt drivers participating in the EV Project performed 87% of their charging events at home and 13% away from home over a 15-month study period. Figure IV-8 shows the percent of charging performed at home and away-from-home locations, and also categorizes charging by power level and location.

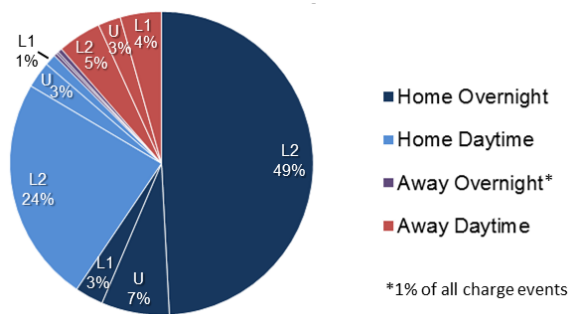


Figure IV-8: Percent of Chevrolet Volt charging events performed by location, power level, and time of day

Although the majority (i.e., 59%) of all charging events were performed at home overnight, 28% of all events were performed at home during the day. Only 12% of charging events were performed away from home during the day. The fact that 70% of daytime charging was performed at home is significant, because typically daytime “opportunity” charging has been thought of as away-from-home charging.

All vehicles in this study had access to AC Level 2 (240-V) charging at home; therefore, it is not surprising that nearly all home charging was conducted using Level 2 charging equipment. Away-from-home charging was split evenly between Level 2 charging units and AC Level 1 (120-V) charging units or standard 120-volt outlets.

Like Leaf drivers, not all Volt drivers used away-from-home charging infrastructure equally. In fact, three quarters of the away-from-home charging was performed by 20% of the vehicles. A small portion of vehicles (i.e., 5%) were never charged away from home.

Volt drivers who performed 30 to 60% of their charging events away from home tended to supplement daily home charging with regular away-from-home charging. All together, these drivers averaged 2.0 charges per day. Frequent charging allowed them to average 40.3 miles driven in electric vehicle (EV) mode per day, which is a 60% increase in daily EV miles over the group of vehicles that never charged away from home.

Volt drivers who charged away from home for more than 60% of their charging events tended to supplement frequent away-from-home charging with home charging. Their away-from-home charging frequency was the same as the home charging frequency of the group of drivers that never charged away from home.

Across all of the away-from-home charging frequency groups, groups averaged 74 to 80% of their distance driven in EV mode. Overall average charging frequency increased as average daily distance driven increased, suggesting that drivers changed their charging behavior in order to extend EV mode operation. This is consistent with finding of other studies discussed above.

Workplace Charging

Away-from-home charging locations include workplace charging. The fact that vehicles spend a lot of time parked at their owners’ places of work has led to a wide-spread belief that work sites make ideal places to install PEV charging equipment. The EV Project and ChargePoint America provided opportunities to examine how much PEV drivers used workplace charging and how workplace charging could be managed to accommodate as many vehicles as possible (or desired).

Nissan Leaf

A study of 707 Nissan Leafs from The EV Project, whose drivers had the opportunity to charge at work, was conducted. These drivers were found to have performed 65% of their charging events at home, 32% at work, and 3% at other locations over the period between January 1, 2012, and December 31, 2013. The proportion of charging energy consumed by location during this time period was similar. Figure IV-9 shows the overall proportion of charging, in terms of number of charging events, performed by drivers in this study at home, work, and other locations.

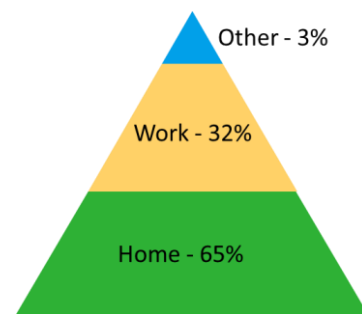


Figure IV-9: EV Project Nissan Leaf charging frequency by location (drawn to scale)

During this study period, this group charged their vehicles away from home more than twice as much as the overall group of Nissan Leaf drivers enrolled in The EV Project. This study's drivers of Nissan Leafs with workplace charging performed 91% of their away-from-home charging events at work and 9% at non-workplace away-from-home locations.

On days when this study's drivers of Nissan Leafs went to work, they performed 98% of their charging events either at home or work and only 2% at other locations. On days when this study's drivers of Nissan Leafs did not go to work, they performed 92% of their charging events at home and 8% at other locations.

Chevrolet Volt

EV Project Chevrolet Volt drivers with known access to workplace charging favored home and workplace charging even more the Nissan Leaf drivers. A group of 96 Chevrolet Volts from The EV Project, whose drivers had the opportunity to charge at work, performed 57% of their charging events at home, 39% at work, and 4% at other locations over the period between January 1, 2013, and December 31, 2013. The proportion of charging energy consumed by location was similar. Figure IV-10 shows the overall proportion of charging, in terms of number of charging events, performed by Volt drivers in this study at home, work, and other locations.

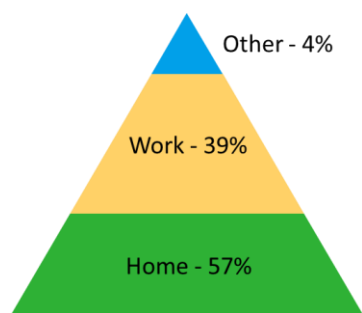


Figure IV-10: EV Project Chevrolet Volt charging frequency by location (drawn to scale)

During this study period, this group charged their vehicles away from home more than 2.5 times as much as the overall group of Chevrolet Volt drivers enrolled in The EV Project. This study's drivers of Chevrolet Volts with workplace charging performed 92% of their away-from-home charging events at work and 8% at non-workplace away-from-home locations.

On days when this study's drivers of Chevrolet Volts went to work, they performed 98% of their charging events either at home or work and only 2% at other locations. On days when this study's drivers of Chevrolet Volts did not go to work, they performed 89% of their charging events at home and 11% at other locations.

Work Site Case Study: Facebook

In addition to examining vehicle data to understand charging behavior, data were examined from charging equipment at work sites to understand how it was used. To this end, usage of numerous workplace charging stations from May to August 2013 at Facebook's office campus in Menlo Park, CA was studied. The charging stations at this facility included alternating current (AC) Level 1- and AC Level 2-

capable units and a direct current (DC) fast charger. The AC Level 2 charging units were the most heavily utilized, accounting for 83% of the charging events, with 11% of the charging events being performed using the DC fast charger. Drivers opted for AC Level 1 charging only 6% of the time.

The AC Level 2 charging units were used heavily during the work day, averaging 8.7 hours connected per cord per work day. Drivers tended to stay connected to Level 2 cords for around 4 hours or for around 9 hours – either half a work day or an entire work day. Most of the time, vehicles fully charged their batteries in less than 5 hours.

AC Level 1 outlets were used infrequently and typically remained connected to vehicles for 8 or more hours per charging event. Because of the slower charge rate, many charging events required 5 to 10 hours to fully charge the vehicles' batteries. However, a significant number of charging events required only 2 to 3 hours to reach full charge because the vehicles being charged had small battery packs.

Drivers overwhelmingly preferred using hard-wired AC Level 2 charge cords over retrieving and plugging in their own AC Level 1 charge cord. Data were collected from 10 charging units at this work site that were capable of both AC Level 1 and AC Level 2 charging. When drivers arrived at these units and both Level 1 and Level 2 options were available, they chose to use the Level 2 cord 98% of the time. With only a few exceptions, the Level 1 outlet was only used if the Level 2 cord was already connected to another vehicle.

Facebook followed a few simple guidelines to encourage employees to self-manage electric vehicle supply equipment (EVSE) usage. First, charging units were installed to allow access from multiple parking spaces. Drivers were encouraged to plug in neighboring vehicles after their vehicle completed charging. Second, employees were provided with an online message board – in this case, a Facebook page – allowing them to coordinate charging station usage. Data from the EVSE suggest that drivers leveraged these resources to minimize the time EVSE were not in use. Thirty-seven percent of the time when one charging event ended and the next began at the same AC Level 2 EVSE during the same work day, less than 30 seconds elapsed between the two charging events. Sixty percent of the time, less than 3 minutes elapsed between consecutive charging events.

The DC fast charger was typically used between 2 and 6 times per work day for 24 minutes or less per charging event. Eleven percent of the time when a DC fast charge event ended and another event began on the same work day, a vehicle had been connected to the second DC fast charger cord prior to the end of the first vehicle's charging event.

Public Charging Station Usage at Different Venues

Many stakeholders are considering supporting the emerging electric vehicle market by installing or funding EVSE. They have asked where the best locations are to install public charging stations and how the EVSE will be used in those locations. Data collected by INL can provide insight regarding real-world usage of EVSE at various locations. To begin addressing these factors, an analysis of EVSE usage by venue was conducted to provide a basic comparison of how public charging units are used in different locations. EVSE usage at different venues was quantified to identify whether

EVSE at some venues were consistently used more than EVSE at other venues.

Blink, ChargePoint, and AeroVironment's publicly accessible charging sites containing EVSE that reported usage data to INL were given a primary venue classification. This venue classification is a coarse classification that gives a broad definition of the site location and provides a general perspective on the reason a plug-in electric vehicle driver would be utilizing that location. Figure IV-11 categorizes the 774 public AC Level 2 sites in this study into primary venues.

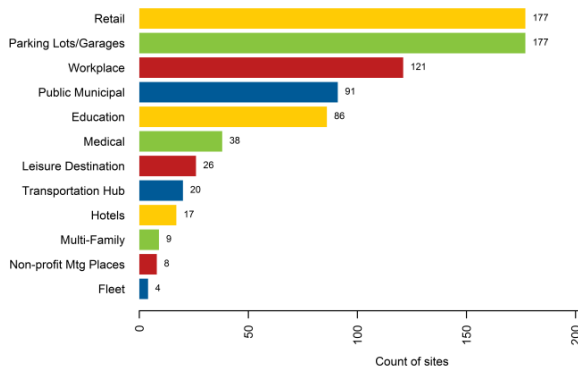


Figure IV-11: Level 2 EVSE sites categorized by their primary venue

Over 89% of the sites were contained within six venue types, including retail, parking lots/garages, workplace, public municipal, education, and medical. The retail and parking lots/garages venues contained over 45% of all Level 2 sites.

The average number of charging events performed per week at each site was calculated as a measure of site usage frequency over the study period (excluding the first 4 weeks of operation). Figure IV-12 shows the distribution of the average number of charging events per week per site for each venue category.

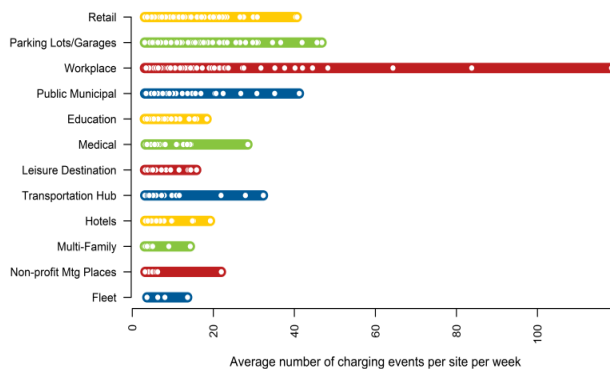


Figure IV-12: The distribution of average charging events per week per site. Each site's average number of charging events is displayed using a white circle

The white circles in Figure IV-12 represent each site's average charging frequency. The range is shown by the colored bar. For example, the site with the greatest number of average charging events per week at retail venues averaged 40 average events per week. Alternatively, the site with the lowest number had three average charging events per week. This means the range in the retail venue was 3 to 40 average charging events per week.

All charging events performed using any EVSE installed at a charging site were included in the calculation of average charging frequency for a site. For example, the top seven workplace sites averaged over 40 charging events per week or over six events per day. These sites all have at least four Level 2 EVSE. On many days, multiple EVSE at each site were used on the same day. It would have been difficult to achieve such high usage frequency at these Level 2 sites if they only contained one EVSE.

For each venue type, the distribution of site average charging frequency was skewed to the left, meaning that most sites did not experience much usage. The median average number of charging events ranged from four to seven events per week. This means that more than 50% of all charging sites averaged less than seven events per week. Also, 75 to 100% of the sites for each venue type had usage frequency that fell between three and 14 charging events per week. Because there was so little difference in median usage frequency from venue type to venue type and the bulk of the sites all fell within the same range, it is not possible to say that charging sites of a certain venue type were consistently used more than sites at other venue types.

DCFC data in this study were collected from AeroVironment and Blink units. There were 102 DCFC sites containing more than three average charging events per week. Similar to Level 2 EVSE, there were not an equal number of DCFC sites within each venue category. Figure IV-13 shows the distribution of DCFC sites with respect to venue. The retail venue contains 62% of all deployed DCFC.

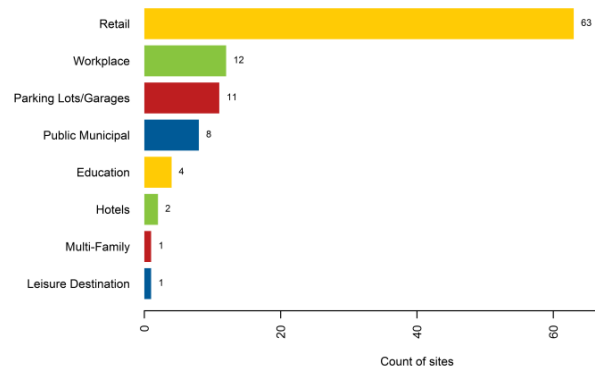


Figure IV-13: The number of DCFC sites per primary venue

Figure IV-14 shows the average number of charging events per week per site for DCFC sites by venue. The site with the most usage is at a workplace venue. However, the ranges of charging frequency between sites for venue types having more than two sites are similar.

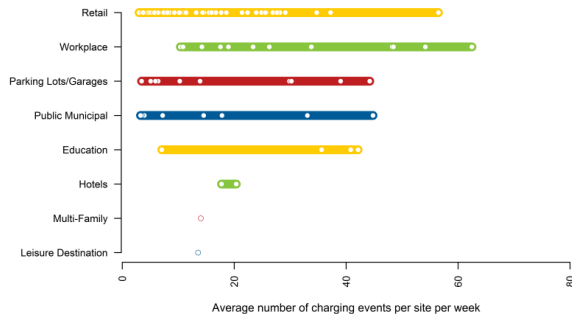


Figure IV-14: The distribution of average charging events per week per site. The white circles represent each site’s average number of charging events per week

DCFC utilization ranged from three charging events to just over 60 per week. Workplace DCFC saw the greatest number of charging events per week. Median values for Figure IV-15 range from 9 to 38 events per week. This is a much larger spread than was seen for Level 2 EVSE sites. Workplace and education venues had the highest median charging frequency at 25 and 38 events per site per week, respectively. However, there is still considerable overlap between the range of average charging frequency at these sites and sites within other venue types.

DCFC Usage in Washington and Oregon

Blink and AeroVironment DCFC data were also used to determine which charging sites along major highways in Washington and Oregon were most frequently used. Figure IV-15 depicts the distribution of usage of these stations by location. This figure represents AeroVironment DCFC sites as circles and Blink DCFC sites as squares. The color of the circles and squares represents the usage frequency of the DCFC at that site.

All but one of the top nine most frequently used DCFC sites are in the greater Seattle metro area. Other locations along the I-5 corridor and intersecting arterial highways have some usage, but it is much more limited. The four most highly used DCFC units were at the following locations, in order of use from highest to lowest:

1. Grocery store in close proximity to an exit ramp to I-5 south of Tacoma.
2. Retail Outlet in close proximity to an exit ramp to I-5 north of Everett.
3. Gas Station in close proximity to an exit ramp to I-5 south of Olympia.
4. Grocery store in the Seattle suburbs.

Based on initial analysis of EV Project Nissan Leaf and Chevrolet Volt driving data, it is believed that the top three most highly used DCFCs are frequently used by vehicles traveling between cities or towns within the Seattle metro area, rather than to other outer-lying locations. Additional analysis will be performed in FY 2015 to confirm these initial findings.

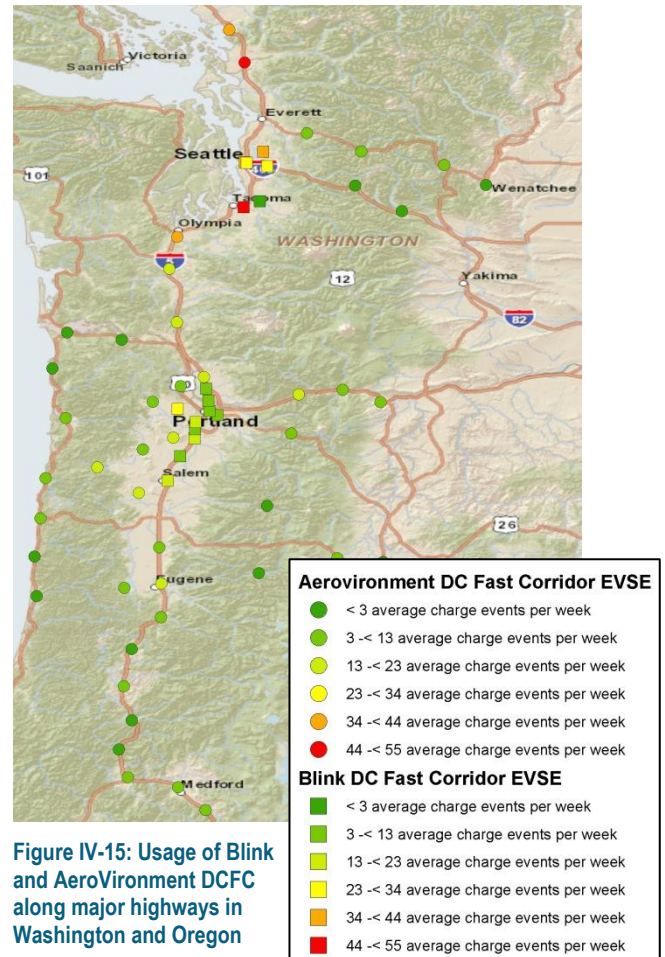


Figure IV-15: Usage of Blink and AeroVironment DCFC along major highways in Washington and Oregon

Conclusions

Taking multiple data streams from competitive vehicle and charger providers that had never before shared raw data and blending those data streams into useable research products has been a significant accomplishment. There continue to be legal and personally identifiable information constraints on handling the raw data, but a wealth of information for DOE and other cooperative research purposes now exists.

During FY 2014, INL completed publication of quarterly reports for The EV Project and ChargePoint America and transitioned focus to answering specific questions about how PEVs and charging infrastructure has been used. INL produced numerous reports on the real-world usage of PEVs and charging infrastructure, including trends in charging station use over time as fees for use were implemented, electric vehicle miles traveled, public charging station usage at different types of locations, and PEV driver preference for charging at home, workplace, and public charging stations. Some lessons learned about workplace charging behavior was also published. These reports were provided to DOE as guidance for participants of DOE’s Workplace Charging Challenge, which encourages greater workplace charging options. Results were also provided to numerous organizations in government, industry, and academia. These

include auto and EVSE manufacturers, electric utilities, universities, and other research organizations.

In FY 2015, INL will continue to report on performance and use of the vehicles and charging infrastructure based on observations made in data from the EV Project, ChargePoint America, and the West Coast Electric Highway.

IV.A.3. Products

Publications

1. *Observations from The EV Project in Q3 2013*, INL/EXT-13-30965, Idaho National Laboratory, Idaho Falls, ID, December 2013.
2. *Overview Report Project to date through September 2013*, INL/MIS-12-21898, Idaho National Laboratory, Idaho Falls, ID, October 2013.
3. *Nissan Leaf Vehicle Summary Report. July – September 2013*, INL/MIS-11-21904, Idaho National Laboratory, Idaho Falls, ID, October 2013.
4. *Chevrolet Volt Vehicle Summary Report. July – September 2013*, INL/MIS-11-24041, Idaho National Laboratory, Idaho Falls, ID, October 2013.
5. *Electric Vehicle Charging Infrastructure Summary Report: July – September 2013*, INL/MIS-10-19479, Idaho National Laboratory, Idaho Falls, ID, October 2013.
6. *Blink Charging Units Reporting Data in The EV Project through September 2013* [map], INL/MIS-12-26073, Idaho National Laboratory, Idaho Falls, ID, December 2013.
7. *Nissan Leafs and Chevrolet Volts Reporting Data in The EV Project through September 2013* [map], INL/MIS-12-26073, Idaho National Laboratory, Idaho Falls, ID, December 2013.
8. *Observations from The EV Project in Q4 2013*, INL/EXT-14-31462, Idaho National Laboratory, Idaho Falls, ID, February 2013.
9. *Overview Report Project to date through December 2013*, INL/MIS-12-21898, Idaho National Laboratory, Idaho Falls, ID, February 2014.
10. *Nissan Leaf Vehicle Summary Report. October – December 2013*, INL/MIS-11-21904, Idaho National Laboratory, Idaho Falls, ID, February 2014.
11. *Chevrolet Volt Vehicle Summary Report. October – December 2013*, INL/MIS-11-24041, Idaho National Laboratory, Idaho Falls, ID, February 2014.
12. *Electric Vehicle Charging Infrastructure Summary Report: October – December 2013*, INL/MIS-10-19479, Idaho National Laboratory, Idaho Falls, ID, February 2014.
13. *Blink Charging Units Reporting Data in The EV Project through December 2013* [map], INL/MIS-12-26073, Idaho National Laboratory, Idaho Falls, ID, March 2013.
14. *Nissan Leafs and Chevrolet Volts Reporting Data in The EV Project through December 2013* [map], INL/MIS-12-26073, Idaho National Laboratory, Idaho Falls, ID, March 2013.
15. *ChargePoint America Vehicle Charging Infrastructure Summary Report through September 2013*, INL/MIS-11-24311, Idaho National Laboratory, Idaho Falls, ID, November 2013.
16. *ChargePoint America Vehicle Charging Infrastructure Summary Report through December 2013*, INL/MIS-11-24311, Idaho National Laboratory, Idaho Falls, ID, April 2014.
17. *ChargePoint America Charging Units By Type through December 2013* [map], INL/MIS-12-26073, Idaho National Laboratory, Idaho Falls, ID, April 2014.
18. *EV Charging Infrastructure Usage in Large-scale Charging Infrastructure Demonstrations: Public Charging Station Case Studies for ARB*, California Air Resources Board Plug-In Electric Vehicle Infrastructure Information Gathering Meeting, Sacramento, CA, July 15, 2014.
19. *Electric Vehicle Charging Infrastructure Usage Observed in Large-scale Charging Infrastructure Demonstrations – ARB*, California Air Resources Board Plug-In Electric Vehicle Infrastructure Information Gathering Meeting, Sacramento, CA, May 27, 2014.
20. *Electric Vehicle Charging Infrastructure Usage Observed in Large-scale Charging Infrastructure Demonstrations*, National Research Council Seventh Meeting of the Committee on Overcoming Barriers to Electric Vehicle Deployment, Irvine, CA, February 25, 2014.
21. *PEV Infrastructure Deployment Costs and Drivers' Charging Preferences in the EV Project*, SAE 2014 Hybrid and Electric Vehicle Technologies Symposium, La Jolla, CA, February 11, 2014.
22. *Trends Observed in Plug-in Electric Vehicle Infrastructure Demonstrations*, SAE 2014 Government/Industry Meeting, Washington, D.C., January 23, 2014.
23. Smart, J., Bradley, T., and Salisbury, S., *Actual Versus Estimated Utility Factor of a Large Set of Privately Owned Chevrolet Volts*, SAE Int. Journal of Alternative Powertrains, 3(1):2014, doi:10.4271/2014-01-1803.
24. *What Kind of Charging Infrastructure Did Nissan Leaf Drivers in The EV Project Use and When Did They Use It?* INL/EXT-14-33005, Idaho National Laboratory, Idaho Falls, ID, September 2014.
25. *Analyzing Public Charging Venues: Where are Publicly Accessible Charging Stations Located and How Have They Been Used?* INL/MIS-14-33019, Idaho National Laboratory, Idaho Falls, ID, September 2014.
26. *Categorizing EVSE Venues: Describing Publicly Accessible Charging Station Locations*, INL/MIS-14-33021, Idaho National Laboratory, Idaho Falls, ID, September 2014.
27. *Workplace Charging Case Study: Charging Station Utilization at a Work Site with AC Level 1, AC Level 2 and DC Fast Charging Units*, INL/EXT-14-32340, Idaho National Laboratory, Idaho Falls, ID, June 2014.
28. *How many electric miles do Nissan Leafs and Chevrolet Volts in The EV Project travel?* INL/EXT-14-32135, Idaho National Laboratory, Idaho Falls, ID, May 2014.

29. Where do Chevrolet Volt drivers in The EV Project charge when they have the opportunity to charge at work? INL/EXT-14-31487, Idaho National Laboratory, Idaho Falls, ID, March 2014.
30. Where do Nissan Leaf drivers in The EV Project charge when they have the opportunity to charge at work? INL/EXT-14-31486, Idaho National Laboratory, Idaho Falls, ID, March 2014.

Patents

This is a test program that is not designed to develop patents. The intent is to provide independent testing and feedback to DOE and industry on DOE and other funded technologies and technology improvements.

Tools and Data

Because of the proprietary and private nature of the data collected from the PEV charging infrastructure demonstrations described, the data were not available for direct dissemination to other parties. Instead, the data were used to populate publications in the form of testing fact sheets, reports, and industry-referred papers. In FY 2014, INL also prepared a multitude of special reports to fulfill requests for information from a variety of organizations in government, industry, and academia.

IV.B. Nissan Leaf DC Fast Charging Study and Electric Drive Advanced Battery Testbed

Principal Investigator: James Francfort

Idaho National Laboratory
P.O. Box 1625, Idaho Falls, ID 83415-2209
Phone: (208) 526-6787
E-mail: James.francfort@inl.gov

DOE Program Manager: Lee Slezak

Phone: (208) 586-2335
E-mail: Lee.slezak@ee.doe.gov

IV.B.1. Abstract

Objectives

- Provide the U.S. Department of Energy (DOE) with independent and unbiased benchmarked testing results that evaluate battery technologies in which DOE and industry have invested.
- Benchmark the impacts (if any) that DC fast charging (DCFC) has on battery life in Nissan Leaf battery electric vehicles compared to Level 2 charging of the same vehicle model.
- Test a variety of advanced energy storage systems (ESS) that are at or near commercialization in on road, real-world operation; quantify the ESS capabilities and limitations; and performance fade over the life of the ESS.
- Continue to provide testing results to other DOE programs and national laboratories, as well as several U.S. Drive technical teams of which Idaho National Laboratory (INL) staff are members.

Major Accomplishments

- Reached 60,000 test miles on each of four Nissan Leafs while recording and storing vehicle system data continuously.
- Conducted battery capacity and power capability testing at 40, 50, and 60 thousand miles for the four Nissan Leafs being operated on-road.
- Conducted closed track testing of four Nissan Leafs at 50 thousand miles, including range tests at several constant speeds, and acceleration testing.
- Two model-year 2012 Nissan Leaf battery packs began laboratory-based cycling and testing at INL's battery test center using a dedicated thermal chamber and power processing machines. Four reference performance tests were completed at intervals through cycling equivalent to more than 10,000 miles of driving.
- The EnerDel lithium-ion battery in the Electric Drive Advanced Battery Testbed (EDAB) completed testing after

reaching 75% of its rated capacity and discharging over 45,000 amp-hours.

- A Toshiba lithium-titanate battery pack was built and installed in the EDAB.
- The EDAB control system was configured to operate as a plug-in hybrid electric vehicle with similar characteristics to the Chevrolet Volt. The calibration was validated on a chassis dynamometer.

Future Achievements

- The four Nissan Leafs will each continue on-road testing to 70,000 miles.
- The two Nissan Leaf battery packs being laboratory cycled packs will continue to 50,000 miles of equivalent cycling and testing.
- The Toshiba battery will run in the EDAB until 77% of original capacity is reached.



IV.B.2. Technical Discussion

Background

DOE's Advanced Vehicle Testing (AVTA) is part of DOE's Vehicle Technologies Office, which is within DOE's Office of Energy Efficiency and Renewable Energy. AVTA is the only DOE activity tasked by DOE to conduct field evaluations of vehicle technologies and fueling infrastructure that use advanced technology systems and subsystems in light-duty vehicles to reduce petroleum consumption, and exhaust emissions.

Most of these advanced technologies include the use of electric drive propulsion systems and ESS. However, other vehicle technologies that employ advanced designs, control systems, or other technologies with production potential and significant petroleum reduction potential are also considered viable candidates for testing by AVTA.

The ESS is generally considered the Achilles heel of electric drive vehicles for several reasons, including cost, life uncertainties under real-world environmental and charging conditions, and the large mass and volume of today's battery technologies. This is especially true for battery electric vehicles and plug-in hybrid electric vehicles. Hybrid electric vehicles, often utilizing nickel metal hydride chemistry batteries, and having smaller energy capacities and tighter state-of-charge windows, have proven to generally have excellent cycle and calendar life. Therefore, the core interest for both DCFC testing and battery mule-type testing is developing and using testing methods that best predict cycle and calendar life uncertainties for plug-in electric vehicles.

The AVTA light-duty vehicle activities are conducted by INL for DOE. INL has responsibility for AVTA technical execution, direction, management, and reporting. INL maintains advanced and secure data collection, analysis, archival, and test reporting capabilities.

The current AVTA staff has 20+ years of experience testing grid-connected, plug-in electric vehicles, including plug-in vehicle charging infrastructure. This experience includes significant use of DCFC systems with various battery chemistries since the mid-1990s. AVTA is currently collecting performance and use data from more than 16,000 Level 2 EVSE and DCFC, as well as from approximately 8,000 plug-in hybrid vehicles.

Introduction

INL and Intertek Testing Services NA have collaborated to purchase, operate, and conduct battery tests at 10,000-mile intervals to determine battery capacity fade for groups of vehicles exclusively utilizing two charging methods: DCFC and AC Level 2.

INL and Intertek have collaborated with the Oak Ridge National Laboratory to develop an on-road testbed for testing advanced ESSs for the EDAB Project. The project objective is to be able to test a variety of advanced ESSs that are at or near commercialization in on-road, real-world operation and to quantify the ESS capabilities, limitations, and performance fade over the life of the ESS. This system has a flexible architecture, capable of charge and discharge signatures of most light duty plug-in electric vehicles.

Approach

Nissan Leaf DC Fast Charging Study

INL purchased four new 2012 Nissan Leaf battery electric vehicles that were instrumented with data loggers and operated over a fixed on-road test cycle. Each vehicle is operated over the test route and charged twice daily. Two vehicles are charged exclusively by AC Level 2 EVSE, while two are exclusively DCFC with a Hasetec 50 kW charger. The vehicles were each performance tested on a closed test track when new and after 50,000 miles of operation. The traction battery packs were removed and laboratory tested when the vehicles were new and at 10,000-mile intervals. Battery tests include constant-current discharge capacity, electric vehicle power characterization, and low peak power tests. The on-road operations and 10,000-mile battery testing is currently scheduled to continue until 70,000 miles. At the conclusion of on-road cycling, the final battery tests will be performed. All of the raw test data and raw data collected from the onboard data loggers are stored and used for analysis and reporting. It should be noted that a small set of dedicated drivers are being used; they rotate driving duties in a method designed to give equal miles to all operating vehicles under the same set of conditions.



Figure IV-16: Nissan Leaf DC Fast Charging in Phoenix, Arizona

Two additional 2012 Nissan Leaf vehicles were purchased, with their battery packs being removed and shipped to INL for laboratory testing in environmental test chambers (Figure IV-17). This testing will serve as a controlled condition set of data to compare against on-road testing, and will demonstrate whether laboratory-based DOE battery testing procedures can predict DCFC impacts that occur in on-road environments. The results will provide guidance for procedure development.



Figure IV-17: Two 2012 Nissan Leaf battery packs testing in a thermal chamber at INL

Electric Drive Advanced Battery Testbed

Performance and utilization of the ESS being tested in the battery mule are measured by the following metrics:

- Discharge rate
- Capacity
- Charge rate
- Durability
- Reliability
- Lifetime
- Temperature

The performance is measured under both controlled and real-world conditions and the project results will inform the research community and automotive original equipment manufacturers about the state-of-the-art of ESSs for plug-in hybrid electric vehicles and battery electric vehicles. The data and findings from this project have also been made available to support U.S. DOE modeling and energy storage development efforts.

The first ESS selected for testing was the EnerDel Type I Electric Vehicle lithium-ion chemistry with a mixed-oxide cathode and amorphous hard carbon anode. The pack has 384 cells (96 in series, four strings in parallel) and each cell has a maximum voltage (at 100% SOC) of 4.1 V and a rated capacity of 17.5 Ah (at a C/3 rate). The pack has a maximum

voltage of 393.6 V, a nominal voltage of 345 V, and a rated capacity and energy of 70 Ah and 23 kWh, respectively. The ESS is a sealed unit, meaning there is no thermal management system and cooling can be done only by passive radiation or forced air on the enclosure. The ESS uses controller area network communications. This EnerDel ESS is designed for a small electric vehicle and was operated as a Nissan Leaf battery pack in the EDAB. Testing has been completed for this pack.

The second and currently on-test ESS was constructed from Toshiba SCiB lithium titanate cells (Figure IV-18). The pack is configured from 24 cells (two cells in parallel, twelve in series) making pack rated at 13.2 kWh and 40 Ah. The pack is cooled by chilled air, and was designed and constructed by AVL California. The pack is claimed to support high charge and discharge rates, have superb thermal performance, and long cycle life.



Figure IV-18: Rendering of Toshiba lithium titanate battery pack

The base test platform is a Colorado pickup truck; it was converted into a series plug-in hybrid electric vehicle by mating a UQM 145-kW motor/generator to the stock 5.3-L, V8 engine to form an auxiliary power unit; removing the stock driveshaft; introducing a second UQM 145-kW motor/generator as the drive motor; and inserting a custom-built driveshaft assembly. The power electronics, including the motor controllers, DC/DC converters, onboard charger, and ESS cooling fans were located in the bed of the truck, along with the ESS. The motor/generator configuration is shown in Figure IV-19. The components in the figure, from left to right, are the motor controllers of the drive motor and generator, the drive motor, and the generator on the right.

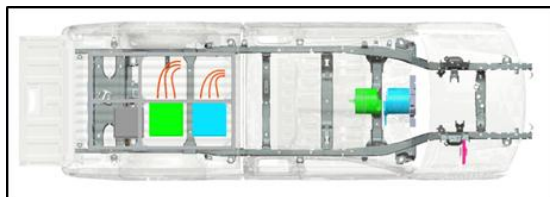


Figure IV-19: Locations of the drive motor, generator, and motor controllers are shown from a top view of the EDAB

The hybrid controller is overlaid on top of the base vehicle controls, and it manages the driver requests and translates these into control of the various vehicle subsystems and components. Acceleration and braking requests are also sent via controller area network to the high-level system controller. The high-level system controller contains the physical

characteristic algorithms that determine the demand on the ESS, based on the algorithms and on the information provided by the battery management system on the battery SOC, temperature, maximum available charge, and discharge current. Once the ESS demand is determined, the value is sent back to the hybrid controller and the amount of drive power or mechanical braking that must be made up by the auxiliary power unit and friction brakes, respectively, is determined.

Battery testing is normally conducted in a laboratory with maintained environments and repeatable test cycles. While repeatability is excellent for comparing battery to battery results, there are shortcomings to this method, including the usual practice of only testing modules, not packs. This type of testing does not allow for the variability that on road testing introduces, including the following:

- On-road pack size testing introduces a larger number of cells, allowing for the greater probability of failures.
- On-road pack size testing also introduces greater variability in internal pack heat and possible negative impacts.
- On-road testing introduces vibration that can impact pack integrity.
- On-road testing may introduce irregular charge/discharge cycles, which are present in real-world operations.

Results

Nissan Leaf DC Fast Charging Study

The DC fast charged Leafs did experience capacity fade at a higher rate than their AC level 2 charged counterparts, however the difference is minimal compared to the overall loss in capacity. The environmental conditions and usage cycling of the AC level 2 control vehicles lost capacity by 25% to 27%. The amount of capacity loss varies slightly for the three analyses performed: lab, track, and on-road. The DC fast charged vehicles lost capacity of 27% to 33%. This is shown in Figure IV-20. The lab testing saw the DCFC packs losing 2.6% more capacity than the ACL2 packs, while on-road operation indicated 5% more capacity loss and constant speed track testing showed 6.4% more capacity loss. All of these numbers are with respect to capacity measured during baseline tests, or in the first 10,000 miles for the on-road method.

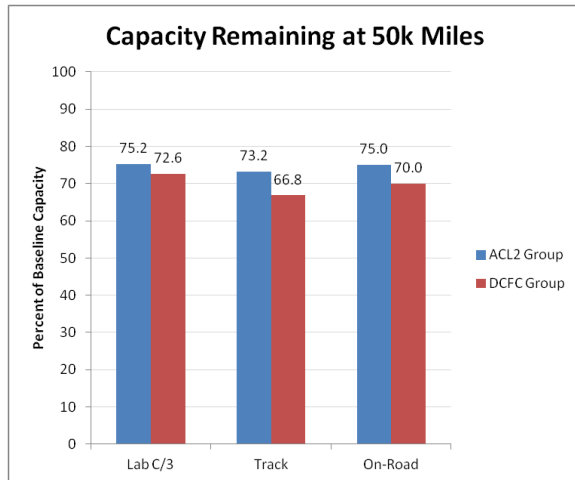


Figure IV-20: Remaining capacity for each vehicle pair, as a percent of as-new capacity, after 50 thousand miles of on-road operation in Phoenix Arizona

The additional capacity loss of the fast charged cars is relatively small in comparison to the overall capacity loss, as illustrated in Figure IV-20. Temperature of each pack was measured throughout the life of the project, and the difference in pack temperature was small compared to the seasonal temperature variation. However, the DC fast charged packs did spend more time at slightly higher temperatures. For all of the vehicle batteries, the rate of fade between tests, indicated by the steepness of the lines in Figure IV-20, varies. While not directly proportional, the fade was slower during periods of cooler temperatures, and faster when ambient conditions were hot. Throughout the project, no pack ever exceeded 55°C in the hot conditions of Phoenix, Arizona.

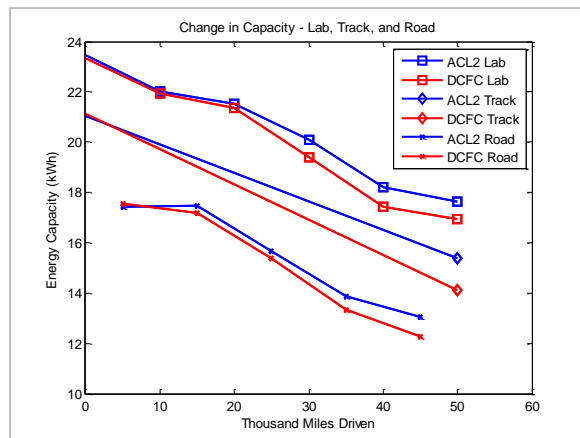


Figure IV-21: Nissan Leaf battery capacity shown for each vehicle pair, AC Level 2 and DC Fast Charged, from laboratory, test-track, and on-road analyses

Electric Drive Advanced Battery Testbed

The EnerDel battery, which had been in testing from March 2012, was completed in December 2013. As of the final test (i.e., September 2013), a total of 27,880 miles were driven. The breakdown of route type is 54% city, 46% highway driving. The total Amp-hour throughput has been 47,767. The vehicle is controlled to operate using both the EnerDel traction battery and the original gasoline engine as required for safety

and drivability purposes. Controlling the electric power for the battery in this method allows for battery testing in any cycle or mode desired. For the EnerDel battery, the average energy consumption has been 232 DC Wh per mile. This compares favorably with the DC fast charge study Nissan Leaf data which, using a similar route, average 230 Wh/mi. This indicates that the control strategy employed to emulate a Nissan Leaf was very accurate in its reflection of Leaf operation. Figure IV-21 shows the capacity fade and resistance growth for the battery for each test performed throughout the testing of the EnerDel pack.

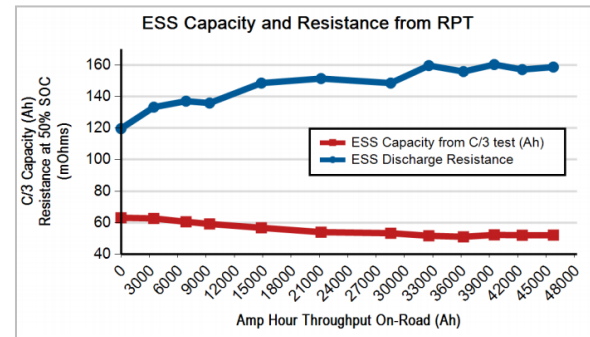


Figure IV-22: Capacity and discharge resistance from reference performance tests through the testing of the EnerDel battery pack

The Toshiba pack has recently begun testing and no reference performance tests were yet completed to report.

Conclusions

The DCFC study with the four Nissan Leafs is demonstrating greater battery capacity loss in the two vehicles being DCFC when compared to the capacity losses demonstrated by the two Nissan Leafs being charged at Level 2. The four vehicles are being operated in the Phoenix, Arizona area; therefore, there are some high ambient temperatures that are impacting all vehicles, which may be compounding heat production within the batteries of the DCFC vehicles. Additional testing at 60 and 70 thousand miles will provide more data points and more seasonal variation to study these effects.

The capacity reduction results for the EnerDel lithium-ion battery being tested in the battery mule have been well documented, with the result that testing ended at 78% of capacity remaining. It should be noted that at the initial baseline test, the battery was only able to produce 90% of the rated capacity.

IV.B.3. Products

Publications

1. *DC Fast Charge Effects on Battery Life and Performance Study – 40,000 Mile Update*, INL/MIS-13-29877, Idaho National Laboratory, 2014.
2. *Electric Drive and Advanced Battery and Components Testbed (EDAB): March 5, 2012 – December 31, 2013*, INL/MIS-12-25146, Idaho National Laboratory, January 2014.

Patents

This is a test program that is not designed to develop patents. The intent is to provide independent testing and feedback to DOE and industry on DOE and other funded technologies and technology improvements.

Tools and Data

The data generated by this testing are used to populate publications in the form of testing fact sheets, reports, and industry-referred papers. The data is also shared among labs to support modeling and procedure development efforts.

IV.C. Level 1 Benchmark of Advanced Technology Vehicles

Principal Investigator: Kevin Stutenberg

Argonne National Laboratory
9700 South Cass Ave, Argonne, IL, 60439
Phone: (630) 252-6788
E-mail: kstutenberg@anl.gov

DOE Program Manager: Lee Slezak

Phone: (202) 586-2335
E-mail: Lee.Slezak@ee.doe.gov

Future Achievements

- Continued evaluation of advanced technology vehicles and components in support of the Department of Energy's mission.



IV.C.2. Technical Discussion

IV.C.1. Abstract

Objectives

- Provide independent evaluation of advanced automotive technology via benchmarking of hybrids, plug-in hybrids, battery electric vehicles, and alternative fuel vehicles as part of the U.S. Department of Energy's (DOE's) mission of laboratory and field evaluations.
- Establish the baseline for state-of-the-art automotive technology in powertrain systems and components through acquisition of test data and corresponding analysis.
- Disseminate vehicle and component testing data to partners of the DOE, such as other national laboratories, the U.S. Council for Automotive Research (USCAR), OEMs, suppliers and universities.
- Provide data to support both codes and standards development and powertrain simulation model development and validation.

Major Accomplishments

- Completed thorough benchmarking of eight advanced technology vehicles. Vehicles evaluated were of multiple classes and fuel use types. These included:
 - 2013 Ford Cmax Hybrid (HEV)
 - 2013 Ford Cmax Energi (PHEV)
 - 2012 Mitsubishi I-MiEV (BEV)
 - 2013 Nissan Leaf (BEV)
 - 2013 Ford Fusion Energi (PHEV)
 - 2013 Ford Focus (BEV)
 - 2013 Dodge Ram 1500 HFE (Conv)
 - 2013 Dodge Ram 1500 HFE (Alt Fuel-CNG)
- Restructured data management process to hasten the availability of testing data to DOE partners and public.
- Enhanced capabilities for noninvasive capture of data from standard network communication of test vehicles, to benefit insight gained from both laboratory and fleet vehicle evaluation.

Background

Since its inception, the Advanced Powertrain Research Facility (APRF) at Argonne National Laboratory has been testing advanced-technology vehicles to benchmark the latest automotive technologies and components for the U.S. Department of Energy (DOE). The staff has tested a large number of vehicles of different types, such as hybrid electric vehicles (HEVs), plug-in hybrid electric vehicles (PHEVs), battery electric vehicles (BEVs), and conventional vehicles, including those operating on alternative fuels.

Introduction

Over the last decade, the researchers have developed a fundamental expertise in the testing of the next generation of energy-efficient vehicles. Throughout this time, methods of vehicle instrumentation and evaluation have continuously been refined. Two levels of testing exist today. The first level (Level-1) involves comprehensive but non-invasive instrumentation of a vehicle, leaving the vehicle unmarked after the testing. The second level (Level 2) involves comprehensive invasive instrumentation of a vehicle and its powertrain components, which leaves the vehicle with irreversible alterations.

This report summarizes the Level-1 benchmark activities of FY 2014. The first section describes the test approach for the DOE's Advanced Vehicle Testing Activity (AVTA) followed by a second section where each of the fiscal year's vehicles' test results and accompanying analysis are presented.

Approach

Vehicle Acquisition

The Level 1 benchmark program leverages the DOE's AVTA activities. Through this program, Idaho National Laboratory, in collaboration with Intertek Testing Services, procures new advanced-technology vehicles to evaluate through accelerated fleet testing. As part of the evaluation, these vehicles are benchmarked at Argonne National Laboratory's APRF. Figure IV-23 illustrates the process.



Figure IV-23: Advanced Vehicle Testing Activity process

Further information on the AVTA is available at avt.inel.gov/.

Test vehicles are often acquired for evaluation in addition to those supplied within the AVTA program. No matter the method or purpose for testing, level 1 test vehicles require non-invasive instrumentation, and are returned to service following the evaluation.

General Test Instrumentation and Approach

The testing presented in this report is focused on the comprehensive non-invasive Level-1 type of testing. Typically, Argonne receives these vehicles on loan; therefore, the vehicles need to leave the test facility in the “as-received” condition. This requirement limits instrumentation to sensors that can be easily equipped and removed without leaving any permanent damage.

Despite this limitation, Argonne strives to achieve the maximum level of instrumentation to facilitate relevant data collection. If the vehicle has an internal combustion engine, instrumentation is applied to monitor the engine speed, fuel flow (at least from modal emissions or a fuel flow meter if possible) and engine oil temperature (achieved through dipstick instrumentation). For electrified vehicles, a power analyzer is used to record the voltage and main current from the stored-energy system. If the vehicle requires charging, the electric power from the charging source is recorded. Furthermore, any sensors that can be fitted without permanent damage to the vehicle, such as temperature sensors, are typically included in locations of interest (a battery pack vent, for example). These additional sensors vary from vehicle to vehicle. A final part of the level-1 benchmark is the recording of messages from the vehicle’s information buses, the content of which varies widely from vehicle to vehicle. This is completed by determining and recording either transmitted diagnostic or broadcast network messages.

Depending on the vehicle powertrain and its unique interest, further sensors may be added to the minimum instrumentation described above - so long as they are non-invasive.

Advanced Powertrain Research Facility

In order to evaluate vehicles in a variety of real-world conditions, the 4WD chassis dynamometer of the APRF is EPA 5-cycle capable. The test cell includes a thermal chamber and an air-handling unit with a large refrigeration system that enables vehicle testing at the EPA “Cold CO Test” ambient temperature of 20°F (-7°C). The other standard test temperatures are 72°F (25°C) and 95°F (35°C). Additionally, testing occurs as desired at temperatures of 0°F (-17°C), and 40°F (4.5°C). All temperatures can be evaluated with or

without solar emulation lamps providing up to 850 W/m² of radiant sun energy. The test cell is shown in Figure IV-24.



Figure IV-24: Illustration of testing at 95°F with sun emulation (left) and at 20°F cold ambient temperature (right)

Purpose of Benchmarking

A major goal of the benchmarking activity is to enable petroleum displacement through data dissemination and technology assessment. The data generated from the vehicle testing and analyses are shared through several mechanisms, such as raw data, processed data, presentations and reports.

The data directly serve the development of codes and standards as well as the development and validation of simulation models. These activities in turn impact the modification of test plans and instrumentation for current and future test vehicles. Partners in the testing are U.S. manufactures and suppliers, through the U.S. Council for Automotive Research. Many of the research activities of the DOE rely on the benchmark laboratory and fleet testing results to make progress towards their own goals. Figure IV-25 details some of these DOE research activities and partners.

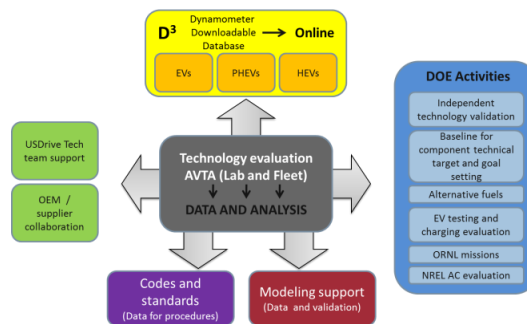


Figure IV-25: Data dissemination and project partners

An additional avenue for data distribution is Argonne’s Downloadable Dynamometer Database (D3), which is a public website at www.transportation.anl.gov/D3. The D3 website provides access to a subset of data and reports.

Downloadable Dynamometer Database (D3)

D3 is an independently held public library of highly detailed accurate vehicle test data, of critical utility in the research community. This web-based portal to Argonne vehicle test data is designed to provide access to

dynamometer data that are normally too expensive for most research institutions to generate. Shared data is intended to enhance the understanding of system-level interactions of advanced vehicle technologies for researchers, students, and professionals engaged in energy-efficient vehicle research, development, or education. Figure IV-26 shows the structure and content of the database.



Figure IV-26: Map of Downloadable Dynamometer Database content

The data and analysis from each vehicle tested under this program are posted to D3. A significant effort was spent this year on automating the standard analysis process, streamlining the data processing, and reducing the time from vehicle testing to data availability. The reader is encouraged to visit the D3 website to get significantly more information and analysis for each vehicle presented in this report.

This document will provide a quick summary of powertrain operation and one or two points of interest for each vehicle that was tested on the dynamometer for the AVTA in FY 2014. Each year the AVTA partners select a set of vehicles that best represents the latest fuel-saving technologies available in the market. This year, the selected vehicles were as follows:

- 2013 Ford Cmax Hybrid (HEV)
- 2013 Ford Cmax Energi (PHEV)
- 2012 Mitsubishi I-MiEV (BEV)
- 2013 Nissan Leaf (BEV)
- 2014 Dodge Ram 1500 HFE (Gasoline)
- 2014 Dodge Ram 1500 HFE (CNG conv.)
- 2013 Ford Fusion Energi (PHEV)
- 2013 Ford Focus (BEV)

Results

2013 Ford Cmax Hybrid

Vehicle description

The Ford Cmax Hybrid was released in the US in the summer/fall of 2012 as a 2013 MY vehicle. The US model was offered both as a charge-sustaining hybrid, the Cmax Hybrid, and a blended plug-in hybrid, the Cmax Energi. During FY2014, both versions of the Cmax were evaluated. Table IV-1 includes the specifications of the Cmax Hybrid.

Table IV-1: 2013 Ford Cmax Hybrid Powertrain Specifications

| | |
|--|--|
| Architecture | Power-split hybrid electric vehicle |
| Engine* | 2.0L DOHC I4, Atkinson Cycle Engine- 141hp, 129 lb-ft torque Total System- 188 hp |
| Transmission | HF35 eCVT Hybrid Powersplit |
| Motor * | Permanent Magnet AC Synchronous 88kW@6000 rpm / 240Nm |
| Battery * | Lithium Ion, 1.4 kWh capacity 35kW Peak Power |
| EPA Label Fuel Economy (mpg)^ | CS mode: 42 city / 37 hwy /40 combined |
| * Manufacturer's data ^ www.fueleconomy.gov | |

Vehicle instrumentation

Thorough, noninvasive instrumentation for this level 1 test vehicle focused on capturing data from current and voltage measurements, fuel flow, several analog thermocouples, and decoded messages from the vehicle's communication network.

Current measurements were captured at the high-voltage (HV) battery terminals, downstream of the DC/DC converter on the HV bus, the low voltage side of the DC/DC converter, and the 12V battery. A high voltage tap was installed at the high voltage battery junction box.

Other parameters of interest for vehicle operation were captured from the vehicle communication network. These included: pedal position (accelerator and brake), engine and motor speeds, brake system pressure (allowing for an understanding of blending of regenerative braking), and coolant system temperatures. Thermocouples were installed at standard level 1 test locations including: engine oil (by replacing the oil dipstick), radiator outlet, under hood (atop the engine), cabin vent, and ambient cabin. Additionally a fuel scale for fuel flow measurements was plumbed in series with the engine fuel rail, and an emissions bench was utilized for measurement of CO, CO₂, NO_x, THC, and CH₄ through the majority of testing.

Points of interest

Energy Impact of Climate Control Settings

The APRF has conducted extensive research into the effects of climate control systems since the completion of a test cell upgrade in 2011 which allowed for test temperatures below 72°F. The APRF test cell was further sealed and insulated in FY 2014, allowing for test temperatures down to 0°F, in addition to the 20°F test cell temperature which was the minimum prior to the modification.

The Ford Cmax Hybrid test vehicle was utilized to perform an evaluation of the impact of the driver selected automatic climate control temperature setting on the energy use of the vehicle. The set point temperature within the vehicle was varied from the standard testing set point of 72°F, to the set points of A/C Off, 78°F, 75°F, 68°F, 62°F, and A/C Max. With these setpoints, the vehicle was driven on a custom driving cycle combining the first 505 seconds of an Urban Dynamometer Driving Schedule (UDDS), as well as a set of steady state speeds tests while at a test cell temperature of 95°F with 850 W/m² of solar emulation. A strict 10 min soak under solar loading occurred prior to each test. The results of the energy consumption through the first phase of this testing can be seen in in Figure IV-27 below.

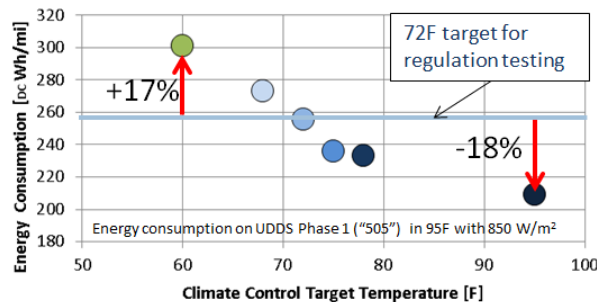


Figure IV-27: 2013 Ford Cmax Hybrid energy use at varying climate control settings

Through this testing, it was found that the energy consumption during the initial 505s, which would include initial cabin cooling, could vary by up to 35% depending on the HVAC setting. Further analysis was completed, but will not be included in this brief report.

Engine operational characteristics

Several custom test cycles are conducted within standard AVTA level 1 evaluation including stabilizing the vehicle at several steady state speeds (0% grade) in order to develop an understanding of the vehicle energy use and systems operation. Figure IV-28 demonstrates the engine operation and battery SOC of the Ford Cmax Hybrid during evaluation of the vehicle energy use at these steady state speeds.

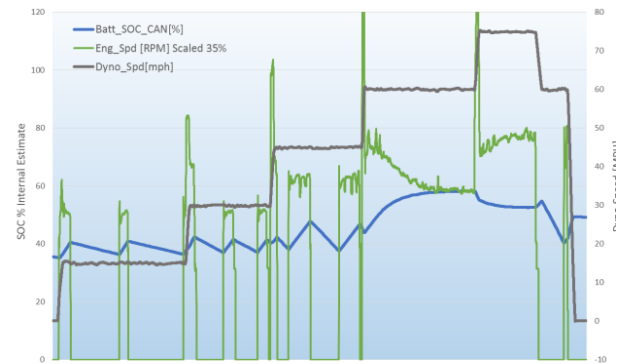


Figure IV-28: Ford Cmax Hybrid engine operation at steady state speeds

At the test speeds of 15, 30 and 45 mph shown, the vehicle will cycle the engine state in order to maintain a desired range of State of Charge (SOC). At the test speeds of 60 and 75 mph, the engine remains active, charging and maintaining the battery at a desired SOC, rather cycling between combined and EV-only operation.

2013 Ford Cmax Energi

Vehicle description

The Ford Cmax Energi utilizes a common powertrain with the Cmax Hybrid, while increasing battery power and capacity in order to allow for fully electric vehicle operation. As the vehicle platform is consistent with the Cmax Hybrid, the Cmax Energi provides an interesting test point for comparison. The specifications of the 2013 Ford Cmax Energi evaluated through this AVTA effort can be found in Table IV-2 below.

Table IV-2: 2013 Ford Cmax Energi Powertrain Specifications

| | |
|--|---|
| Architecture | Power-split plug-in hybrid electric vehicle |
| Engine* | 2.0L DOHC I4, Atkinson Cycle Engine- 141hp, 129 lb-ft torque Total System- 188 hp |
| Transmission | HF35 eCVT Hybrid Powersplit |
| Motor * | Permanent Magnet AC Synchronous 88kW@6000 rpm / 240Nm |
| Battery * | Lithium Ion 7.6 kWh 35kW Peak Power in Charge Sustaining 68kW Peak Power in Charge Depleting |
| EPA Label Fuel Economy (mpg)^ | 95 city / 81 hwy / 88 combined 19 miles EPA estimated EV Range |
| * Manufacturer's data ^ www.fueleconomy.gov | |

Vehicle instrumentation

Vehicle instrumentation of the Cmax Energi consisted of all signals captured from the Cmax Hybrid, with some specific additions to PHEV vehicle operation. These included: current measurements captured at the HV battery, the low voltage side of the DC/DC converter, the inlet to the positive temperature coefficient (PTC) coolant heater, the 12V battery, and the building AC power supply to the electric vehicle support equipment (EVSE). A tap was also installed in the high voltage junction block to measure the high voltage bus voltage. Analog, thermocouple, and controller area network (CAN) signals were all similar to that of the Cmax Hybrid. In addition, a fuel scale and the APRF emissions bench were used for measurement of fuel and CO, CO₂, NO_x, THC, and CH₄ emissions through the majority of testing.

Point of interest

Climate Control Effects at Cold Temperatures

Tests were conducted on the Cmax Energi at 20°F in Charge-Depleting operation with and without the automatic climate control system active. Figure IV-29 displays the fuel power and engine speed of the vehicle during the first 505 seconds of a UDDS cycle.

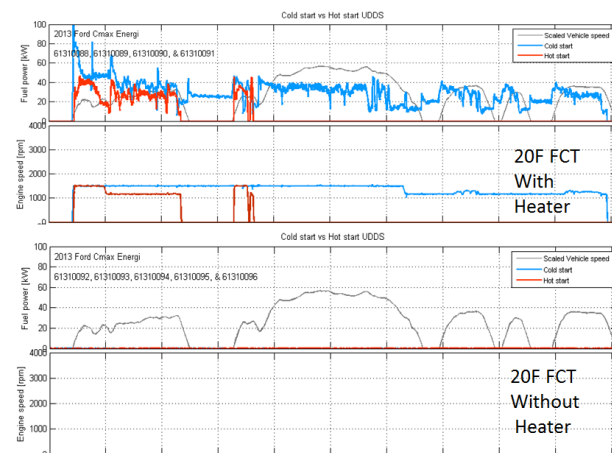


Figure IV-29: 2013 Cmax Energi engine operation at 20°F, with and without driver heat demand

Blue lines indicate the engine speed and fueling rate during the UDDS cold start test, while the red lines indicate the engine speed and fueling rate during a subsequent UDDS hot start test conducted following a 10 minute soak. As can be seen from this test data, the Cmax Energi HV battery provides a discharge current limit during these conditions sufficient to enable the vehicle to operate electric only. Engine-on operation only occurs due to the additional energy requirements of the climate control system when active.

Cmax Hybrid vs Cmax Energi regenerative braking operation

Though the energy storage systems are considerably different between the two vehicles, the regenerative braking strategy was found to be consistent between them. This includes the maximum battery power during regenerative braking (found to be 30kw) as well as the strategy for “ramping out” regenerative braking torque at lower speeds.

Figure IV-30 displays the regenerative braking power of the Cmax Hybrid as compared to the Cmax Energi.

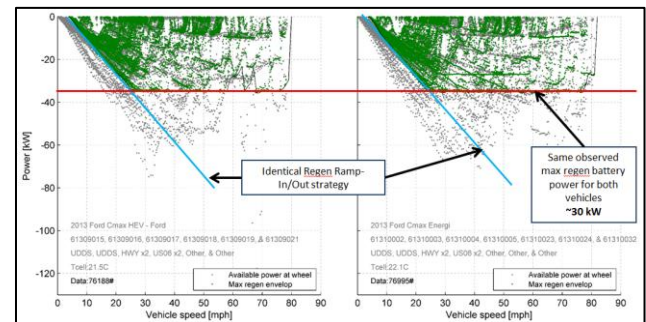


Figure IV-30: Regenerative power of the Cmax Energi and Hybrid

Cmax Hybrid vs Cmax Energi Charge Sustaining Fuel Economy

The overall vehicle charge-sustaining fuel economy of the Cmax Hybrid as compared to that of the Cmax Energi can be seen in Figure IV-31. As would be expected, the added weight of the drivetrain has a negative impact on the vehicles fuel economy in charge-sustaining operation.

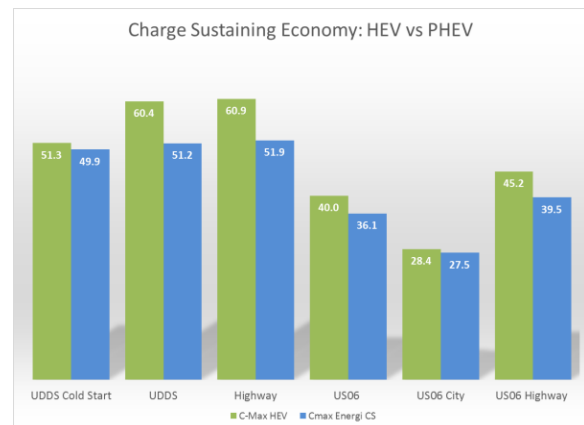


Figure IV-31: Cmax Hybrid and Energi charge sustaining fuel economy

2012 Mitsubishi I-MiEV

Vehicle description

The Mitsubishi I-MiEV is a five-door battery electric vehicle, released in the US for the 2012 MY. As a subcompact all electric car with a curb weight of 2579 lbs., the I-MiEV is an extremely compact electric vehicle. It incorporates air cooling system for the sealed lithium Ion battery mounted to the base of the car, and an electric PTC heater to supply heat to the cabin when desired. General specifications of the vehicle can be found in Table IV-3

Table IV-3: 2012 Mitsubishi I-MiEV Specifications

| | |
|--|---|
| Architecture | Subcompact All Electric Vehicle |
| Transmission* | RWD, Single Speed Reduction Gear, Final Drive Ratio- 7.065:1 |
| Motor * | 49 kW Permanent Magnet Synchronous AC Electric Motor |
| Battery * | Lithium Ion 330V, 88 cell, 16kWh |
| EPA Label Fuel Economy (mpg)^ | 126 city / 99 hwy / 112 combined 62 miles EPA estimated EV Range |
| * Manufacturer's data ^ www.fueleconomy.gov | |

Vehicle instrumentation

Instrumentation of the vehicle at the APRF included multiple electrical bus measurement locations, capturing current: into the HV inverter, into the DC/DC converter, out of the DC/DC converter, into the air conditioning (A/C) compressor, into the PTC heater, and 12V system current to the 12V battery. Voltage was captured for both the HV bus (through the inverter cover), and the 12V system.

In addition to the standard analog instrumentation, a large list of CAN messages were decoded on the vehicle, capturing energy use and operation of multiple major components such as: the electric machine (speed and torque), high voltage battery (SOC, current, voltage, temperature), HVAC system (PTC and A/C compressor energy consumption), PTC Heater temps, and control pedal positions (accelerator and brake).

Following instrumentation, testing was then performed at the standard AVTA test temperatures of 20°F, 72°F, and 95°F with 850 W/m² of solar emulation. UDDS, HWY, US06, and SC03 tests were performed using the J1634 shortcut methodology. Supplemental tests were also performed to measure passing maneuver time at varying grade levels, and steady state energy consumption at steady state speeds in increments of 10 mph from 10-80 mph as well as at varying grades.

Point of interest

Variation of energy use with temperature.

Consistent with the current generation of electric vehicles, the Mitsubishi I-MiEV exhibits a large increase in overall energy use at cold temperatures due to the operation of the PTC providing heat to the passenger compartment. The difference in the increase in energy consumption is heavily dependent on the drive cycle. This is due to the proportion of climate control energy use as compared to that required to complete the desired drive cycle. As driver aggressiveness increases, energy consumption required to drive the vehicle increases, while the energy required for HVAC operation remains consistent. This effect, and the results of testing, can be seen in Figure IV-32.

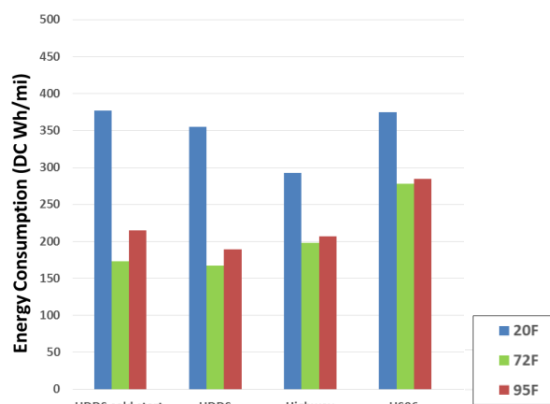


Figure IV-32: 2012 Mitsubishi I-MiEV energy consumption

On the UDDS cold start and UDDS hot start cycles, energy consumption increased by 118%, and 112% respectively, while the highway cycle found an increase of 48%.

Also of note is the effect of the 95°F test condition on energy consumption. Energy requirements by the AC compressor at this temperature drive higher energy consumption at lower vehicle speeds. Again, as vehicle speeds increase, energy consumption required to drive the Motor/Inverter becomes proportionally larger than that required to drive the HVAC system. In addition, drag forces seen on the dynamometer (tire loss, frictional losses) are reduced as the ambient temperature increases. These two mechanisms combined cause the energy consumption requirements for the US06 highway cycle at 95°F to be 12% lower than those found at 72°F. As a decrease in energy consumption when A/C operation is occurring is not common with conventional vehicles, this is worth noting.

As current measurements were captured for major components throughout the high voltage bus, an analysis of the energy loss to each section of components can be completed for a subset of testing, as seen in Figure IV-33, for the UDDS cold start and UDDS hot start.

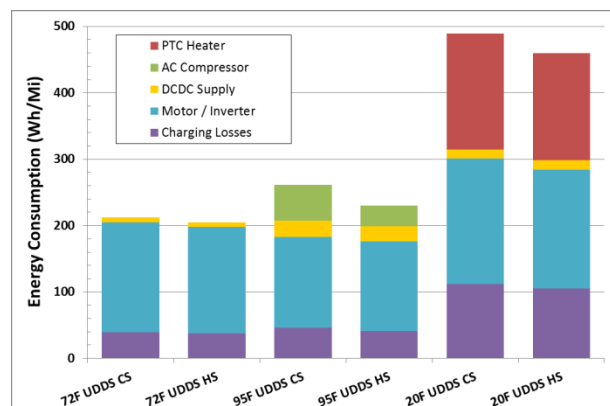


Figure IV-33: 2012 Mitsubishi I-MiEV energy use by major component

Charging losses were determined for the complete SAE J1634 multi cycle test (MCT), and then attributed equally to all test cycles during that MCT. This was completed by determining the AC energy supplied to the EVSE during a full charge occurring immediately post-testing, and determining efficiency from the ratio this AC charge to DC energy used throughout the MCT. Due to this, charging losses can be attributed to internal HV battery heating, variations in charging efficiency due to temperature, or variations in vehicle operation while at the test temperature.

2013 Nissan Leaf

Vehicle description

The 2013 Nissan Leaf underwent multiple updates from the previous year resulting in increased range and efficiency. As stated by the manufacturer, these included improvements to vehicle aerodynamics (effecting the target coefficients used in dynamometer testing), availability of a heat pump for improved operation at cold temperatures, and repackaging of the vehicles electric drive components for improved efficiency. High voltage battery capacity, and electric drive specifications remained consistent with the previous model year. Table IV-4 lists the specifications of the 2013 Nissan Leaf.

Table IV-4: 2013 Nissan Leaf Specifications

| | |
|---|---|
| Architecture | Midsize All Electric Vehicle |
| Transmission* | Single Speed Reduction Gear, Final Drive Ratio- 7.9377:1 |
| Motor * | 80 kW DC Permanent Magnet 250 Nm torque Synchronous AC Electric Motor |
| Battery * | Lithium Ion 23kWh |
| EPA Label Fuel Economy (mpg)[^] | 110 city / 99 hwy / 105 combined 76 miles EPA estimated EV Range |
| * | Manufacturer's data |
| [^] | www.fueleconomy.gov |

Vehicle instrumentation

Of key interest during testing of the Leaf was the effect of the climate control system on vehicle energy use. As such, a considerable amount of effort was spent on the instrumentation of this climate control system. This included capturing the control voltage of analog sensors, and desired temperature and pressure measurements from the vehicles CAN communication. During testing temperatures, speeds, and control positions from throughout the HVAC system were logged.

Electric current flow was measured at critical points on the vehicle as well including: the Power Distribution Module (PDM), DC/DC (low voltage), A/C compressor, 12 V battery, and electric vehicle support equipment (EVSE) supply. A high voltage tap was installed within the PDM, at the wiring terminals from the HV battery.

Point of interest

Extended Temperature Testing

The testing plan for the Leaf was enhanced in order to determine how and when blending occurred between the heat pump and PTC heater at low temperatures. A combination of J1634 multi-cycle tests and full charge tests were conducted at test temperatures of 0°F, 20°F, 20°F with solar emulation, 40°F, 72°F, and 95°F with solar emulation.

During testing the vehicle was operated with the HVAC system set to 72°F for all tests, with the exception of 72°F ambient test temperature where it was set to off. Overall range was then calculated for the varying test cycles as recommended by J1634. The effect on overall vehicle range at these test temperatures can be seen in Figure IV-34.

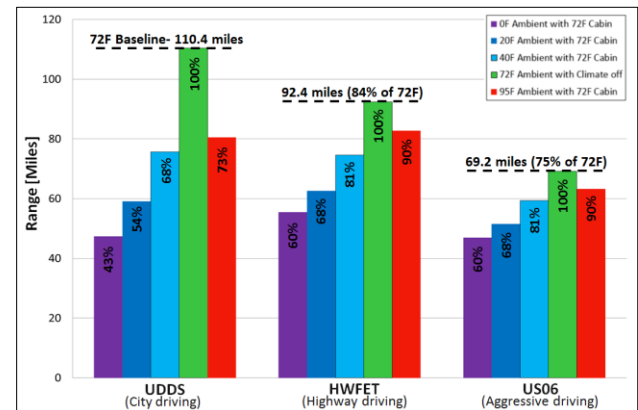


Figure IV-34: Effect of ambient temperature on 2013 Nissan Leaf range

Energy consumption of the PTC heater and the heat pump system were captured at test temperatures of 0°F, 20°F, 40°F, and the variations in the use of the heat pump during the UDDS cold start can be seen in Figure IV-35 and Figure IV-36. Of note is the blending of the PTC heater and the heat pump as temperatures decrease. Heat pump operation increases as demand is increased at 20°F. At the 0°F test temperature, the PTC heater is solely used due temperature limits of components in the heat pump system.

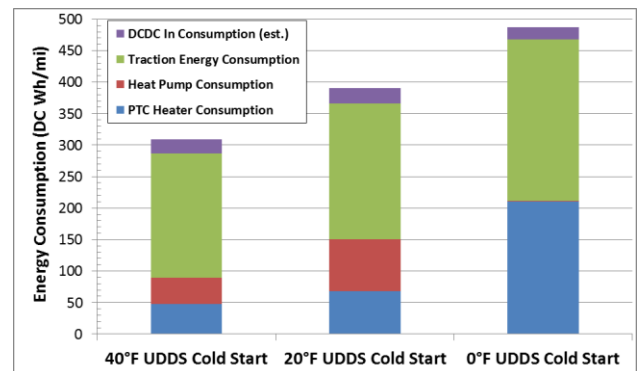


Figure IV-35: Temperature effect on UDDS cold start energy consumption

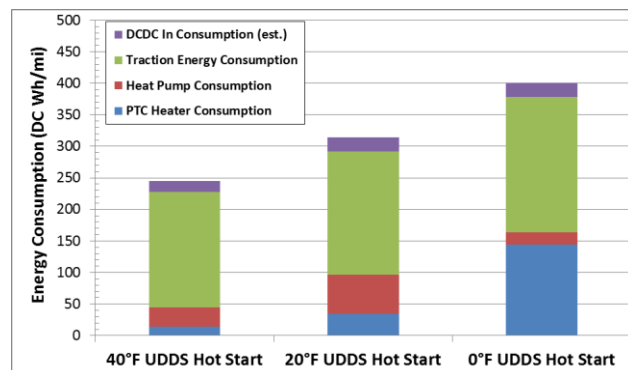


Figure IV-36: Temperature effect on UDDS hot start energy consumption

2013 Dodge Ram 1500 HFE

Vehicle description

The 2013 Dodge Ram HFE ties multiple fuel saving technologies into a light duty pickup truck platform. These include implementation of a start stop system, an 8 speed transmission, and active grille shutters, among others. The test vehicle was evaluated twice. The first evaluation was completed with the vehicle in stock form, following the 4000 mile break in period. Following this initial evaluation, an aftermarket CNG conversion was completed.

Table IV-5: 2014 Dodge Ram 1500 HFE Specifications

| | |
|--------------------------------------|---|
| Architecture | Standard pickup truck – 2WD |
| Engine* | 3.6-Liter V6 24-Valve VVT Engine with Stop-Start 305 HP @6350 RPM , 364.7 Nm |
| Transmission* | 8 speed Torqueflite auto 845RE |
| EPA Label Fuel Economy (mpg)^ | 18 city / 25 hwy / 21 combined |
| * | Manufacturer’s data |
| ^ | www.fueleconomy.gov |

Vehicle instrumentation

Test vehicle instrumentation focused on determining the impacts on efficiency of the stop start system, development of an understanding of the use of the 8 speed transmission across varying drive cycles, and determination of the energy and emissions impact of the use of CNG as a fuel.

Liquid fuel flow measurements were made with a positive displacement fuel scale, while gaseous fuel flow measurement was completed with two Coriolis fuel meters integrated into the gaseous fuel system of the APRF test cell. A database of broadcast CAN messages was developed, with parameters such as: engine and transmission component speeds, engine torque, pedal position, engaged transmission gear, pedal positions, as well as several others. The APRF emissions bench was used for measurement of CO, CO2, NOx, THC, and CH4 through the majority of testing.

Note that two different sets of dynamometer target coefficients were used during testing and were established through AVTA track testing for the vehicle in the stock state, as well as following the CNG retrofit (tank enclosure fitted, etc.).

Point of interest

Start Stop Operation

An array of drive cycles were completed with the start stop system enabled and disabled in order to determine the impact on energy use. This was conducted similar in scope to the idle stop study conducted at the APRF in FY2011, a summary of which can be found on D3 in the idle stop vehicle section. Test cycles were selected to capture a variation of cycle idle time and cycle energy requirement. A comparison of the fuel economy, as well as the percentage improvement in terms of fuel consumption, can be found in Figure IV-37.

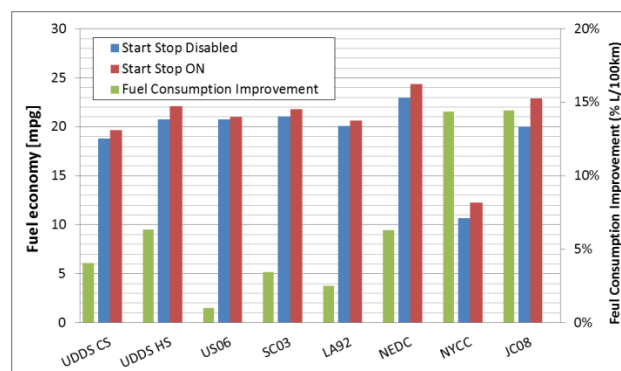


Figure IV-37: 2014 Dodge Ram HFE idle stop system benefits for varying drive cycles

Of note is the effectiveness of the start stop system at reducing fuel consumption during low speed cycles with high amounts of idle time, indicative by the New York City Cycle (NYCC). This cycle, as well as the Japanese JC08 cycle, found fuel consumption improvements of 14.4%.

CNG Conversion

The CNG conversion of the Dodge Ram incorporated a bed mounted 3600psi CNG tank and distribution system, plumbed to a port fuel injection system incorporated under the stock vehicle intake manifold. The CNG storage system located in the truck bed can be seen with a cover panel removed, in Figure IV-38.



Figure IV-38: CNG storage tank installed in the 2014 Dodge Ram 1500 HFE

An overview of the effects on vehicle fuel economy, and emissions can be found in Table IV-6.

Table IV-6: Fuel Economy and Emissions Comparison for CNG and Gasoline Operation

| | | HWY | | UDDS Hot Start, SS Off | |
|---------------------------|-------------------|-------------|-------------|------------------------|-------------|
| | | CNG | Gasoline | CNG | Gasoline |
| Fuel Economy (GGE) | | 28.4 | 31.9 | 19.0 | 20.5 |
| Emissions Bench | Bag THC [g/mi] | 0.005 | 0.003 | 0.017 | 0.005 |
| | Bag CH4 [g/mi] | 0.014 | 0.006 | 0.052 | 0.009 |
| | Bag NMHC [g/mi] | 0.000 | 0.001 | 0.000 | 0.002 |
| | Bag NOx [g/mi] | 0.006 | 0.004 | 0.086 | 0.013 |
| | Bag CO mid [g/mi] | 0.114 | 0.181 | 0.210 | 0.437 |
| | Bag CO2 [mg/mi] | 0.224 | 0.280 | 0.341 | 0.441 |

2013 Ford Fusion Energi

Vehicle description

The Ford Fusion Energi utilizes the same powertrain, and battery system as the Cmax Energi. The specifications of this system can be seen in Table IV-7 below.

Table IV-7: 2013 Ford Fusion Energi Specifications

| | |
|--------------------------------------|---|
| Architecture | Power-split plug-in hybrid electric vehicle |
| Engine* | 2.0L DOHC I4, Atkinson Cycle Engine - 141hp, 129 lb-ft torque Total System - 188 hp |
| Transmission* | HF35 eCVT Hybrid Powersplit |
| Motor * | Permanent Magnet AC synchronous 88kW@6000 rpm / 240Nm |
| Battery * | Lithium Ion, 7.6 kWh 35kW Peak Power in Charge Sustaining 68kW Peak Power in Charge Depleting |
| EPA Label Fuel Economy (mpg)^ | 95 city / 81 hwy / 88 combined 19 miles EPA estimated EV Range |
| * | Manufacturer's data |
| ^ | www.fueleconomy.gov |

Vehicle instrumentation

Vehicle instrumentation of the Fusion Energi was identical to that of the Cmax Energi. This included level 1 standard temperatures, high voltage bus and 12V current and voltage measurement, fuel scale and emissions measurements, and a logging of specific broadcast CAN messages.

Additionally, a new methodology and toolset for logging of requested diagnostic messages was employed on the Fusion Energi. These diagnostic messages included parameter useful for developing a better understanding of HV battery and powertrain (both during operation and charging).

Point of interest

Mapping of Blended Operation of the Power Split Transmission

The enhanced diagnostics messages captured during testing were used to determine the blending of engine, generator, and motor powertrain torque during the standard test cycles. An example of these signals can be seen in Figure IV-39.

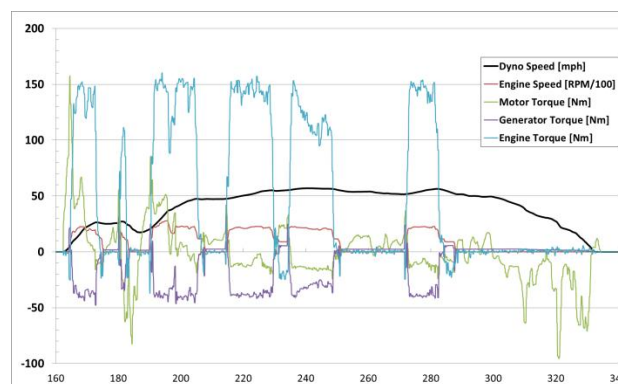


Figure IV-39: 2013 Ford Fusion Energi engine operation on hill 2 of a UDDS hot start

2013 Ford Focus Electric

Vehicle description

The 2013 Ford Focus Electric is a compact electric vehicle constructed on the Ford Focus platform. This vehicle was also evaluated extensively as a level 2 APRF test vehicle, and the results were used for verification of vehicle operation and testing error. The vehicle specifications for the Ford Focus Electric can be found in Table IV-8 below.

Table IV-8: 2013 Ford Focus Electric Specifications

| | |
|--------------------------------------|---|
| Architecture | Compact All Electric Vehicle |
| Transmission* | Single Speed Reduction Gear, Final Drive Ratio- 7.82:1 |
| Motor * | 107 kW Permanent Magnet 250 Nm torque Synchronous AC Electric Motor |
| Battery * | Lithium Ion 23kWh |
| EPA Label Fuel Economy (mpg)^ | 110 city / 99 hwy / 105 combined 76 miles EPA estimated EV Range |
| * | Manufacturer's data |
| ^ | www.fueleconomy.gov |

Vehicle instrumentation

Instrumentation of the vehicle included multiple electrical measurement locations. Current was measured: into the HV Battery at the service disconnect, into the DC/DC converter, out of the DC/DC converter, and the overall 12 V current into the negative terminal of the 12 V battery. Voltage was captured for both the HV bus (through the inverter cover), and the 12 V system.

In addition to the standard analog instrumentation, a large list of CAN messages were logged on the vehicle, developed from the Level 2 2012 Ford Focus Electric. Additionally, a considerable amount of diagnostic messages were received on the vehicle, capturing information from HV battery, power electronics, and HVAC system operation.

Following instrumentation, testing was then performed at the standard AVTA test temperatures of 20°F, 72°F, and 95°F with 850 W/m² of solar emulation. Standard UDDS, HWY, US06, and SC03 tests were performed using the J1634 shortcut methodology.

Point of interest

Energy use throughout varying drive cycles

Energy use for standard test cycles completed can be seen in Figure IV-40.

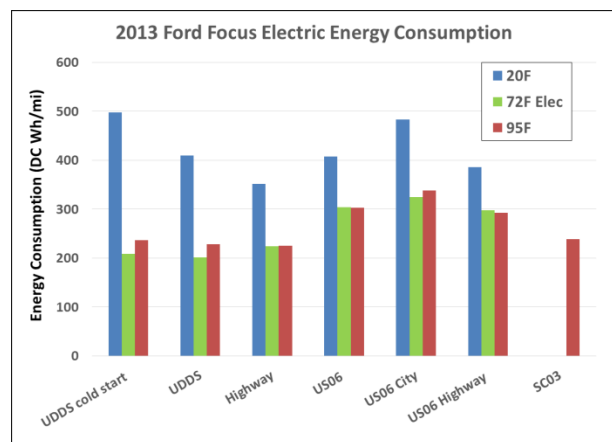


Figure IV-40: 2013 Ford Focus electric energy consumption

Vehicle Charging at High Ambient Temperatures

High voltage battery parameters (current, voltage, temperatures) were logged during the battery recharging that followed each full-charge tests. The Ford Focus BEV features a HV battery cooling system, which may be active during charging at Level 2 power (≥ 6.6 kW). Logging of charging signals allowed for a determination of the variation in energy required if cooling was active. An example of the variations in battery temperature and charge current can be seen in the charge log in Figure IV-41.

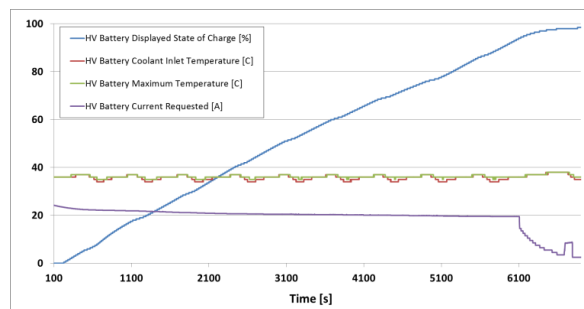


Figure IV-41: HV battery parameters during charging at 95°F ambient temperature

Conclusions

During the Fiscal Year 2014, the APRF continued to enhance the benchmark research of advanced-technology vehicles. Considerable advancements were made in the areas of data collection, testing summaries, and data distribution.

The data and analyses generated from this testing continue to be used to generate reports and presentations, and is distributed both as raw data through the APRF online website and directly to DOE collaborators. Additionally, the work performed within this project supports both codes and standards and model development through test data validation.

This report provides a high-level, brief overview of Argonne National Laboratory’s basic vehicle benchmark activity, as a reference summary of the numerous vehicles studied in FY 2014. For more detailed analyses, the reader is encouraged to view the vehicle testing reports and utilize the raw data on the APRF website at www.transportation.anl.gov/D3/.

IV.C.3. Products

Tools and Data

1. The basic vehicle test data are uploaded to APRF’s Downloadable Dynamometer Database and are available for public download at www.transportation.anl.gov/D3/.
2. A more thorough listing of test data and vehicle signals is available for DOE and partnering organizations upon request.
3. Additionally, some of the dynamometer test results are integrated into the AVTA website maintained by Idaho National Laboratory at avt.inel.gov.

IV.D. Level 2 Benchmark of Advanced Technology Vehicles: MY 2014 Honda Accord Plug-in Hybrid Electric Vehicle

Principal Investigator: Eric Rask

Argonne National Laboratory
 9700 S. Cass Avenue
 Argonne, IL 60349
 Phone: (630) 252-3110
 E-mail: erask@anl.gov

DOE Program Manager: Lee Slezak

Phone: (202) 586-2335
 E-mail: Lee.Slezak@ee.doe.gov

IV.D.1. Abstract

Objectives

This project aims to perform thorough vehicle instrumentation, testing, and analysis on the MY2014 Honda Accord Plug-in Hybrid Electric Vehicle (PHEV). Data collected will be used for a wide range of tasks including technology benchmarking and evaluation, simulation validation, advanced vehicle component evaluation, and vehicle testing procedure development and validation.

Major Accomplishments

- Leveraged previous high-level data collection and insight from other PHEV and BEV testing.
- Performed significant instrumentation development and installation.
- Recorded Controller Area Network (CAN) signals through testing as a means of measuring parameters that would otherwise be too difficult, too expensive, or impossible to obtain.
- Ran a broad range of tests for general energy consumption, performance assessment, component evaluation, and technology benchmarking across a range of ambient temperatures and HVAC conditions.
- Analyzed efficiency and vehicle behavior during charge events.

Future Achievements

- Continued data collection leveraging installed vehicle instrumentation. Areas of particular interest include improved electric machine and inverter testing/mapping and vehicle efficiency sensitivity testing when exposed to more extreme ambient conditions.



IV.D.2. Technical Discussion

Background

This work revolves around in-depth instrumentation, testing, and analysis of new and emerging vehicle technologies. Vehicles are selected for evaluation on the basis of technical merit for technology assessment and data collection. Vehicles are tested primarily on a chassis dynamometer using state-of-the-art instrumentation and data analysis equipment. Testing and instrumentation plans are specifically developed for each vehicle to reflect the specific technical merits and unique features of each.

Introduction

The vehicle selected for this year’s in-depth testing and analysis is the MY 2014 Honda Accord PHEV. The vehicle represents one of the most recent PHEVs to arrive on the market and possesses several unique features making it a highly relevant research vehicle. Most interesting, the Accord PHEV uses a unique powertrain configuration that utilizes three main operating modes. During lower speed/power operation, the vehicle runs in engine-off (EV) mode as would be expected for a “strong” hybrid. At higher power levels but moderate speeds, or at generally high power levels across the entire speed range, the vehicle runs as a series hybrid. Lastly, at moderate speeds and power levels, the vehicle operates using a direct coupling (single speed) of the engine to drive the wheels, while allowing for some electric torque smoothing in a parallel type hybrid architecture arrangement. Figure IV-42 shows the Accord on the dynamometer in Argonne National Laboratory’s Advanced Powertrain Research Facility (APRF).



Figure IV-42: Honda Accord PHEV on the APRF Dynamometer

Although only a few highlighted instrumentation examples are shown in the following discussion, the in-depth Accord PHEV research vehicle was fitted with numerous sensors to better understand overall vehicle operation as well as component usage and efficiency. Moreover, a wide range of vehicle data was also collected from various communications busses including CAN and the vehicle's diagnostic network.

On any hybrid electric or plug-in hybrid electric vehicle, the electrical system is always of particular interest. As with other recent in-depth vehicles, the electrical instrumentation was fairly exhaustive in terms of collecting information regarding the high-voltage DC loads from the traction battery and high-voltage HVAC equipment, as well as 12 V accessory loads related to vehicle hotel loads and devices such as fans and pumps. Additionally, recording AC energy from the wall into the EVSE during recharge allows for a wealth of information related to vehicle charging loads and behavior during off-line charging. Figure IV-43 below illustrates the major electrical nodes collected during this testing.

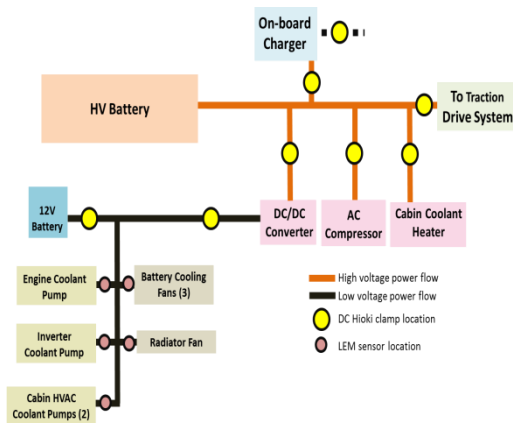


Figure IV-43: High-voltage and 12 V electrical instrumentation

The flow of engine coolant is also of interest for this vehicle. Engine coolant not only is used to cool the engine and related components, but also is used to heat the cabin. During EV operation a secondary high-voltage heater is used to provide cabin heating. Figure IV-44 shows the instrumentation related to the “high-temperature” loop which includes: the engine block and head, related components such as the EGR cooler and throttle body, the radiator, and cabin heater core loop. Within these coolant circuits, efforts have been made to assess inlet and outlet temperature, as well as total flow, to aid in the assessment of general operating conditions. Moreover, this information can be used to estimate losses associated with component cooling since the temperature change and flow across a particular component can often be used to estimate some proportion of overall thermal losses. On the cabin heatercore side, inlet and outlet temperatures have been included for both the high-voltage coolant heater (typically used during select CD operation) and cabin heater core. To better understand total vehicle energy consumption as well as cooling system operation, the Accord’s electric coolant pumps have been instrumented with current sensors.

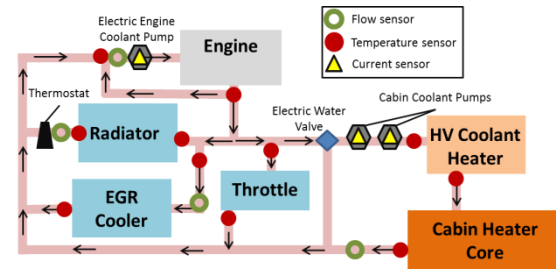


Figure IV-44: High temperature coolant loop (engine/cabin) instrumentation

While less complex, the “low temperature” cooling loop has been instrumented as well. This loop is used to cool the inverter and motor controller (often referred to as the Power Converter Unit or PCU), as can be seen below in Figure IV-45. As with the high-temperature loop, this coolant loop has been instrumented to observe inlet/outlet temperature, total coolant flow, and electric pump current.

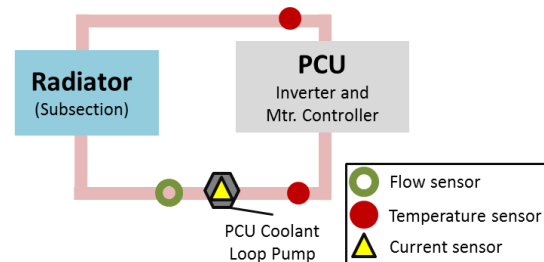


Figure IV-45: Low-temperature (PCU) coolant loop instrumentation

In common with several other recent hybrid vehicles, the Accord uses cooled EGR to assist in operating the engine efficiently across a wide usage envelope. Instrumentation was added to the exhaust system to better understand the Accord’s use of cooled EGR as well as the general behavior of the catalysts. More specifically, in addition to EGR cooler inlet and outlet temperature, plus post-EGR valve exhaust temperature sensors, pressure transducers were also installed to estimate EGR system usage and effectiveness. The exhaust instrumentation layout is summarized below in Figure IV-46.

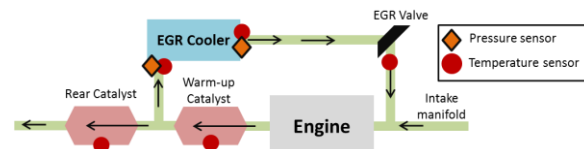


Figure IV-46: Exhaust system instrumentation

Catalyst brick temperature for each catalyst was taken in order to better understand the vehicle’s emissions behavior relative to fueled operation and catalyst state. This type of information is of particular interest for a PHEV since engine-off behavior may be much more prevalent during both CS and CD operation due to increased electric-only operating capability. To further understand the emissions implications of the Accord’s operating strategy, measurement ports have been installed along the exhaust system to facilitate emissions measurements before, between, and after the catalysts. The installed ports, shown in Figure IV-47, allow for the “fast” measurement of criteria emissions without the lag normally associated with an emissions bench.

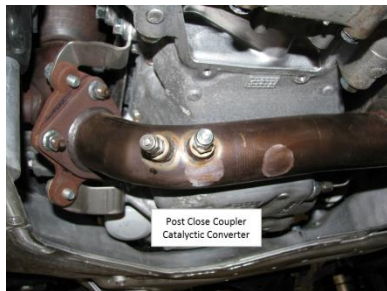


Figure IV-47: Example exhaust system sampling ports

To aid on-going DOE research related to vehicle HVAC usage and electrical loads, cabin and vent temperatures have been instrumented to understand heating, cooling, and dehumidification needs across a range of ambient temperatures and conditions. Figure IV-48 summarizes the majority of in-cabin temperature signals collected for this vehicle.



Figure IV-48: Cabin and vent temperature instrumentation

In response to a variety of research requests related to inverter and motor operation, and in collaboration with Oakridge National Laboratory’s on-going inverter and electric machine research, instrumentation to collect 3-phase voltage, current, and power was included for both electric machines contained in the Accord’s transmission. This instrumentation allows for even greater understanding of vehicle operation and energy flows and has been a useful and exciting addition to the APRF’s vehicle benchmarking activities. Figure IV-49 shows the inverter voltage tap locations with the inverter cover removed. Figure IV-50 shows the inverter with the cover replaced and with the voltage taps leading to a new break-out box, facilitating safe observation of the voltage waveforms between the inverter and electric machines.

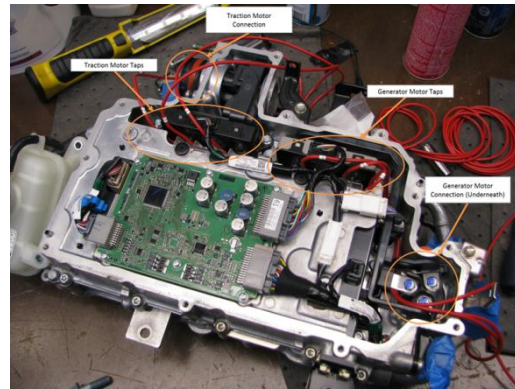


Figure IV-49: Inverter 3-phase voltage tap locations



Figure IV-50: Inverter and break-out box following 3-phase voltage tap installation

Approach

As discussed in the Background section, the Accord was outfitted with a significant number of sensors to provide a range of information from temperatures to mechanical and electrical power flows. A specific test plan was developed to evaluate the particularly interesting facets of this PHEV and its related components. Testing was done using a vehicle chassis dynamometer and sophisticated instrumentation under laboratory conditions to aid in repeatability, accuracy, and sensitivity.

Results

The following paragraphs discuss some of the noteworthy findings related to the testing of this vehicle. These discussion items represent a small fraction of the information and insight gained during testing and analysis of this vehicle.

Charge Sustaining Operation:

The Accord PHEV was run through a wide variety of drive-cycles in charge-sustaining mode, but often the most useful starting point is simply the standard US regulatory cycles, which serve as a common reference point across the vehicles tested at the APRF. Figure IV-51 shows the ANL tested charge-sustaining fuel economy versus the EPA database entry provided for this vehicle. As is typically the case, the APRF UDDS and Hwy numbers are very close to the EPA’s estimates suggesting the tested vehicle behavior and consumption is in-line with expectations. Interestingly, the Accord has a slightly higher Hwy fuel economy as compared to its UDDS fuel economy, which is in contrast to other “strong” hybrids such as the Toyota Prius and Ford Fusion Hybrid. As discussed earlier, this difference in relative cycle fuel economy is likely in part due to the Accord’s unique powertrain configuration which provides for a relatively low loss directly coupled engine-drive mode. While out of the scope of this summary discussion, the benefits and issues related to this type of transmission architecture are of great research interest and were a major goal of the in-depth testing and analysis.

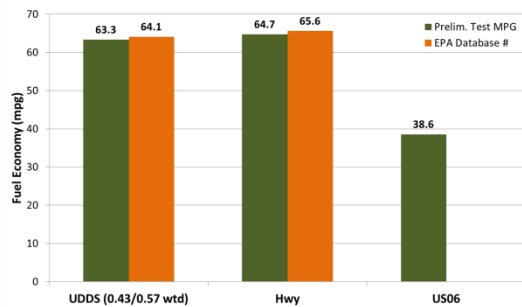


Figure IV-51: Tested charge-sustaining fuel economy versus EPA database

Although a lengthy discussion regarding the operating behavior of the Accord is out of the scope of this document, Figure IV-52 and Figure IV-53 show the Accord’s engine operation over the UDDS and US06, respectively. It should be noted that the UDDS figure contains both “cold” and “warm” operation. As would be expected for this vehicle, the Accord shows a significant amount of engine-off operation for the UDDS cycle and less-so for the more aggressive and higher speed US06. Although somewhat limited, the Accord does show a relatively high amount of engine-off operation even on the US06 cycle as compared to some other recently tested hybrid vehicles.

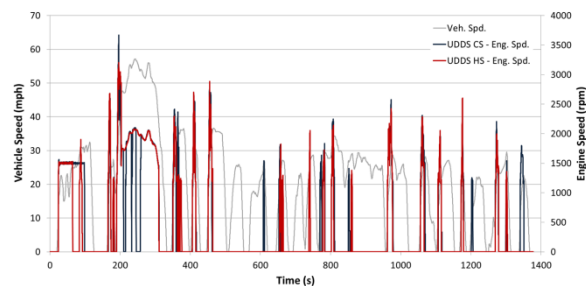


Figure IV-52: UDDS charge sustaining engine speed trace (both cold and hot start operation shown)

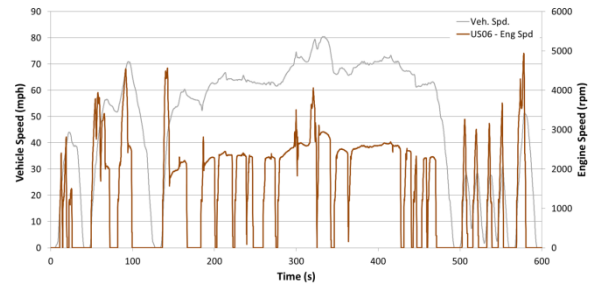


Figure IV-53: US06 charge sustaining engine speed trace

To better summarize the vehicle’s operation, Figure IV-54 shows the vehicle’s charge-sustaining engine-off operation during the UDDS, Hwy, and US06 cycles overlaid on a scatter plot of all operating points over the same three cycles.

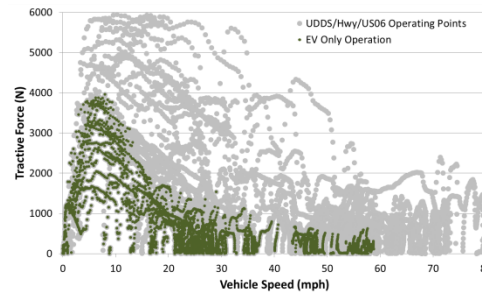


Figure IV-54: Estimated charge-sustaining EV envelope

In addition to engine-off operation, it is also informative to observe when the vehicle uses a particular operating mode. As mentioned in the introduction, the Accord offers three operating modes: EV, series, and parallel. Figure IV-55 shows the operating mode observed during charge sustaining operation for the same UDDS/Hwy/US06 set of drive cycles.

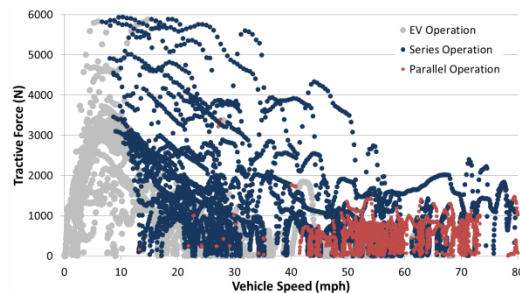


Figure IV-55: Charge-sustaining operating mode usage over UDDS, Hwy, US06

Charge Depleting Operation:

As with the previous charge-sustaining section, the Accord was run across a wide range of drive cycles in charge-depleting mode. Depending on the operating point, the Accord will run either electrically or supplement the battery power with the engine power during charge depleting operation. Since two sources of energy are used (fuel and off-board battery energy) a discussion of PHEV fuel economy is often complicated using a single metric. With this difficulty in mind, PHEV energy consumption is often shown as a 2-d plot including both battery energy consumption and fuel consumption. Figure IV-56 shows this plot for a full depleting set of UDDS and US06 cycles including the transition and first

sustaining cycle. The Accord drives electrically (fuel consumption = 0) for two UDDS cycles and shows a transition cycle before finally running in an approximately charge-sustaining fashion. Interestingly, a slight increase in “cold” energy consumption can be observed for the first cycle in that the energy consumption is slightly higher than the following cycle of approximately 150 W-hr/mi. In contrast, the more aggressive US06 cycle shows elevated fuel consumption and slightly decreased battery energy consumption. This is due to the US06 cycle having operating points outside of the Accord’s EV operating envelope and thus having fueled engine operation. Although battery energy is still being consumed during engine-on depletion, the overall battery energy level used is lower due to the presence of the engine power. Again, the full scope of this discussion is outside this quick summary document, but the figures and discussion are provided in hopes of giving some appreciation for the vehicle’s basic operation.

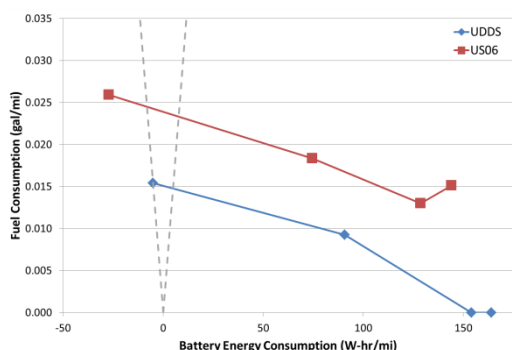


Figure IV-56: Fuel consumption versus energy consumption for charge-depleting operation over the UDDS and US06

Table IV-9 shows the calculated Actual Charge Depleting Range (Rcda per SAE J1711) for the UDDS, Hwy, and US06 cycles. Broadly speaking Rcda provides the mileage value associated with a particular drive cycle at the point at which charge depleting behavior deviates from the previous cycle and is approximately at the level of normal charge-sustaining behavior (a transition cycle which is not counted in Rcda).

Table IV-9: Estimated charge depleting range (Rcda per SAE J1711)

| | Rcda (mi) |
|------|-----------|
| UDDS | 19.7 |
| Hwy | 15.9 |
| US06 | 21.2 |

To better illustrate the concept of Rcda, Figure IV-57 shows the actual integrated current, linear cycle estimated per cycle integrated current, and the Rcda calculated for this cycle. As can be seen in the figure, the Accord actually depletes well past the level of normal charge-sustaining operation and then recovers near the end of the second highway cycle. This recovery is not considered part of the depleting range in the Rcda calculations and thus is excluded, leaving the highway Rcda to appear quite a bit shorter compared to the UDDS value. In addition to this information being useful from an overall vehicle energy consumption standpoint, this behavior is also used to validate test

procedures related to plug-in hybrid vehicle testing, namely SAE J1711.

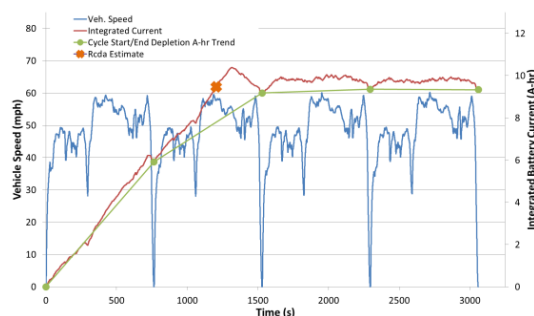


Figure IV-57: Hwy cycle integrated current and Rcda example

Table IV-10 below highlights some relevant high-level usage information for the Accord’s depleting operation over the UDDS, Hwy, and US06 cycles. This information excludes transition operation and thus reports the usage from the start of the first cycle to the point at which Rcda is achieved. Both the UDDS and Hwy cycles see a significant portion of operation in EV mode as might be expected for a PHEV, whereas the US06 shows roughly 54% EV (engine off) operation. A peak positive (tractive) battery power of roughly 66kW is observed during US06 operation, whereas the Hwy and UDDS cycles show lower battery power as well as lower required tractive power. As was discussed in previous years, peak regenerative braking power (negative) is appreciably lower than the maximum amount of power provided during US06 braking events, yet is very similar to the maximum achieved seen on the UDDS cycle. For more information related to this issue, the reader shall refer to the discussion in the previous year’s annual report.

Table IV-10: Highlighted charge depleting usage parameters over the UDDS, Hwy, and US06 cycle

| | UDDS | Hwy | US06 |
|-----------------------|-------|-------|-------|
| Eng Off % | 98% | 100% | 54% |
| Max Batt. Power (kW) | 59.9 | 53.7 | 66.6 |
| Min Batt. Power (kW) | -39.5 | -47.3 | -52.6 |
| Max Tract. Power (kW) | 49.2 | 45.1 | 90.3 |
| Min Tract. Power (kW) | -40.3 | -56.0 | -97.8 |

In a similar manner to the figure in the charge-sustaining section, Figure IV-58 overlays the Accord’s EV operating points with the total usage over several drive cycles to illustrate the larger EV operating envelope utilized during charge-depleting operation.

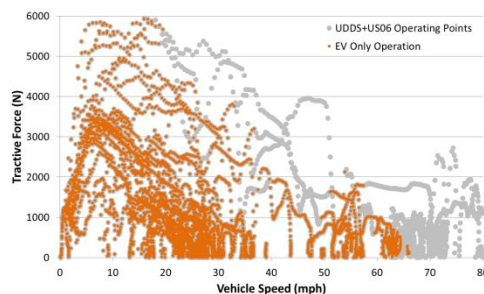


Figure IV-58: Estimated charge depleting EV envelope

To better contrast the differences between charge-depleting and charge-sustaining operation for the Accord, Figure IV-59 highlights both the charge-depleting and charge-sustaining envelopes for comparison. As would be expected, the charge-depleting envelope utilizes much more EV operation, particularly at lower speeds and elevated torques as well as exhibiting a slightly higher observed maximum speed of EV operation (~65 mph vs ~60 mph). Again, a full discussion of the differences in vehicle operation is outside the scope of this document, but these figures do aid in developing a better understanding of the main difference between sustaining and depleting operation: more engine-off usage.

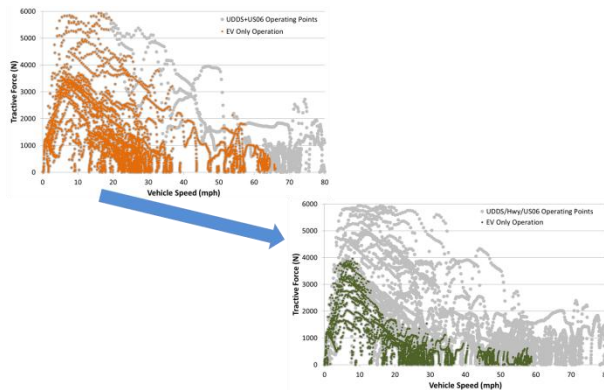


Figure IV-59: Comparison of charge-depleting and charge-sustaining EV operational envelopes

This data and analysis is only a brief snapshot of the work that has gone into the testing and analysis of the Honda Accord PHEV. Moreover, it is expected that this data will be used in many upcoming research projects by Argonne researchers as well as many other interested parties.

Conclusions

As with previous years, a significant amount of time and effort was spent on the instrumentation, testing, and analysis of the MY 2014 Honda Accord PHEV. Specific instrumentation was developed to evaluate the most noteworthy aspects of the vehicle. Additionally, testing was tailored to highlight both PHEV and HEV testing issues in order to assess the unique features of this vehicle. The results and analysis contained in this report represent a small but important subset of the entire project. Research regarding these, as well as additional hybrid vehicles should continue, given the ever-changing dynamics of the advanced vehicle marketplace. For more in-depth work regarding this and many additional advanced vehicles, the reader is pointed toward the *Argonne Downloadable Dynamometer Database*: www.transportation.anl.gov/D3/

IV.D.3. Products

Publications

1. Bucher, J., Bradley, T., Lohse-Busch, H., and Rask, E., "Analyzing the Energy Consumption Variation during Chassis Dynamometer Testing of Conventional, Hybrid Electric, and Battery Electric Vehicles," *SAE Int. J. Alt. Power.* 3(1):36-43, 2014, doi:10.4271/2014-01-1805.
2. Anderson, J., Rask, E., Lohse-Busch, H., and Miers, S., "A Comparison of Cold-Start Behavior and its Impact on Fuel Economy for Advanced Technology Vehicles," *SAE Int. J. Fuels Lubr.* 7(2):427-435, 2014, doi:10.4271/2014-01-1375.
3. Kim, N., Rask, E., and Rousseau, A., "Control Analysis under Different Driving Conditions for Peugeot 3008 Hybrid 4," *SAE Int. J. Alt. Power.* 3(1):44-55, 2014, doi:10.4271/2014-01-1818.
4. Lee, D., Rousseau, A., and Rask, E., "Development and Validation of the Ford Focus Battery Electric Vehicle Model," SAE Technical Paper 2014-01-1809, 2014, doi:10.4271/2014-01-1809.

MEDIUM AND HEAVY DUTY

IV.E. Fleet DNA Vocational Database Project

Principal Investigator: Kenneth Kelly

National Renewable Energy Laboratory
15013 Denver West Parkway, MS 1633
Golden, CO 80401
Phone: (303) 275-4465
E-mail: Kenneth.kelly@nrel.gov

DOE Program Manager: David Anderson

Phone: (202) 287-5688
E-mail: David.Anderson@ee.doe.gov

DOE Program Manager: Lee Slezak

Phone: (202) 586-2335
E-mail: Lee.Slezak@ee.doe.gov

- The second phase of the Fleet DNA project website was developed and released to the public (www.nrel.gov/fleetdna).
- Updated vocation/vehicle-type data reports were developed and posted for public viewing via the Fleet DNA website for each of the eight vehicle vocations within Fleet DNA.
- Existing DOE tools and analyses such as FASTSim were integrated into Fleet DNA to provide enhanced functionality.
- Processing routines were expanded to include data collected from the vehicle onboard diagnostics (OBD) in addition to the standard latitude, longitude, time stamp, and speed.
- Fleet DNA data storage was adapted to a NoSQL format from a traditional SQL-based database to improve the efficiency of data processing and enhance the data handling versatility of the database.
- “Data-Driven Decision-Making Tools—City of Indianapolis Case Study” was presented at the Green Truck Summit 2014, demonstrating the benefit of drive-cycle analysis and comparison to other fleets when examining investments in new technology.
- “Transportation Database Development Using Floating Car Data” was presented at the Intelligent Transportation Society of America World Congress 2014. It discussed the novel approach to data management and application developed for the Fleet DNA project.
- Fleet DNA capabilities were leveraged to support numerous partners, including the California Air Resource Board, South Coast Air Quality Management District, and the U.S. Environmental Protection Agency (EPA).

IV.E.1. Abstract

Objectives

The objective of Fleet DNA is to accelerate the evolution of advanced vehicle development and support the strategic deployment of market-ready technologies that reduce costs, fuel consumption, and emissions. The Fleet DNA clearinghouse of commercial fleet transportation data helps vehicle manufacturers and developers optimize vehicle designs; helps fleet managers match appropriate advanced vehicle technologies to their fleets; and provides in-use data for standard drive-cycle development, research and development, tech targets, and rule making. Specific objectives of the Fleet DNA project include:

- Capture and quantify drive-cycle and technology variation for the multitude of medium- and heavy-duty vocations.
- Provide a common data storage warehouse for medium- and heavy-duty vehicle fleet data across U.S. Department of Energy (DOE) activities and laboratories.
- Integrate existing DOE tools, models, and analyses to provide data-driven decision-making capabilities.

Major Accomplishments

- National Renewable Energy Laboratory (NREL) researchers expanded the overall size of the Fleet DNA database. Fleet DNA currently contains more than 8 TB of data collected from approximately 550 vehicles, amounting to more than 8,000 days, 480,000 miles traveled, and more than 560 million driving data points. In addition, there are several billion fueling, emissions, and powertrain data points.

Future Achievements

Data Collection and Reporting

- Expand reports to include fueling, powertrain, and emissions data collected from the controller area network bus.
- Expand the size and breadth of the Fleet DNA database through additional partner recruitment and data collection.
- Integrate Fleet DNA results into the Alternative Fuels Data Center.

Modeling and Simulation

- Develop and validate on-road, dynamic mass estimation method validation.
- Integrate additional modeling software such as Autonomie with the Fleet DNA database for large-scale detailed modeling activities (FY 2015).

- Integrate non-DOE tools, such as the EPA MOVES model for emissions analyses.
- Evaluate “what if” scenarios—select drive cycles and vehicle type and evaluate potential for fuel and cost savings over a range of technologies and fuels.

High-Performance Computing

- Utilize NREL’s high-performance computing (HPC) center to conduct large-scale analysis of multivariate problems within the Fleet DNA framework.

Applying Fleet DNA

- Continue to support government, industry, and fleets in developing and adopting energy-efficient heavy- and medium-duty vehicles through access to duty-cycle data and analysis.



IV.E.2. Technical Discussion

Background

The Fleet DNA clearinghouse of commercial fleet transportation data helps vehicle manufacturers and developers optimize vehicle designs while assisting fleet managers with the selection of advanced technologies for their fleets, all with the goal of reducing petroleum consumption and improving energy efficiency. This online database and tool—available at www.nrel.gov/fleetdna—provides both static and interactive data summaries and visualizations representative of the real-world “genetics” for medium- and heavy-duty commercial fleet vehicles. The data for each visualization/report have been drawn from multiple fleets operating a variety of vocations for each vehicle type, across multiple locations within the United States. This extensive breadth of data is necessary to capture the wide range of vehicle operation resulting from different geographies and fleet applications demonstrated by medium- and heavy-duty vehicles. In addition to providing public access to commercial fleet data summaries and visualizations, Fleet DNA also serves as a portal for users to explore related DOE programs and projects such as NREL’s fleet testing activities and reports, the DOE Office of Energy Efficiency and Renewable Energy’s Alternative Fuels Data Center, and the Clean Cities National Clean Fleet Partnership program. Designed by DOE’s NREL in partnership with Oak Ridge National Laboratory, this online database and the accompanying reports help vehicle manufacturers and fleets understand the broad operational range of many of today’s commercial vehicle vocations.

Introduction

This report presents an overview of the major accomplishments of the Fleet DNA project in FY 2014, followed by a detailed discussion of technical accomplishments, including current and future data collection and reporting plans, database development, and new tools and capabilities. In addition to a discussion of technical developments, the report also presents applications of Fleet DNA in supporting both internal and external DOE programs and projects. These applications demonstrate and validate the benefits of Fleet DNA to DOE as well as to public and private partners. Finally, the report discusses future plans for the project, including project priorities, an exploration of remaining project hurdles, and the presentation of a preliminary list of objectives for FY 2015.

Data Collection Status

Data Collected through FY 2014

Building on FY 2013 efforts, at the conclusion of FY 2014 Fleet DNA contains more than 8 TB of data. This includes data from multiple geographic layers housed in the database, coupled with operating data collected from more than 550 vehicles. In total, the operating data accounts for more than 8,000 days of real-world operation and more than 480,000 miles traveled, and it is represented in the database by more than 560 million data points. With the inclusion of additional data channels such as fueling, emissions, and powertrain information, the database contains multiple billions of data points overall. Additionally, at the conclusion of FY 2014, data collected as part of the Fleet DNA data project had expanded to include an additional 22 unique geographic locations, 3 unique vehicle vocations, and 6 vehicle types. Figure IV-60 and Figure IV-61 for more detailed information regarding the specific data stored in the Fleet DNA database.



Figure IV-60: Map of data locations for Fleet DNA through FY 2014

| | Vehicles | Vehicle Days | Distance | Deployments |
|-----------------|----------|--------------|----------|-------------|
| Delivery Vans | 135 | 1,835 | 93,506 | 42 |
| Delivery Trucks | 21 | 237 | 12,246 | 4 |
| School Buses | 212 | 368 | 22,223 | 4 |
| Bucket Trucks | 20 | 216 | 5,858 | 2 |
| Service Vans | 14 | 143 | 3,310 | 2 |
| Class 8 trucks | 185 | 1,368 | 149,854 | 16 |
| Transit Buses | 20 | 378 | 48,738 | 6 |
| Refuse Trucks | 13 | 142 | 5,140 | 1 |

Figure IV-61: Summary of Fleet DNA vocational data

Fleet DNA FY 2015-Plus Data Reporting Plans

Moving forward into FY 2015 and beyond, the primary focus of Fleet DNA data reporting work will be centered on expanding the Fleet DNA “Phase 2” website to include additional data sets, tools, and user interfaces for data download and graphing. The Fleet DNA project will aim to include downloadable drive-cycle data in addition to daily summary results and data reports, along with standard chassis test cycles and dynamometer test results.

In addition, it is the aim of the Fleet DNA project to perform downstream analyses such as parameter sweeps and fuel economy investigations using the data stored in Fleet DNA and making the results available to the public, for example, by performing a powertrain evaluation to compare the benefits of hybridization throughout the range of collected delivery van drive cycles and evaluating the range of benefits observed from the technology based on the drive cycle.

Approach

Data Reporting

Fleet DNA FY 2014 Updated Phase 1 Reporting

In FY 2013, NREL Fleet DNA researchers developed a series of 34-page unique vocation/vehicle-type data reports that were released to the public via a static website: www.nrel.gov/fleetdna. As part of the initial reporting of Fleet DNA data, these static reports were developed with users’ needs in mind and highlight the most common metrics and graphics typically reported. With the completed integration of road grade and road type data layers into Fleet DNA in late FY 2013, 13 additional report visuals were developed and added into existing reports, which were reposted in early FY 2014. The new data products included in the report explore areas of interest such as the amount of time spent at different grade levels and acceleration rates by grade and speed.

Fleet DNA FY 2014 Phase 2 Reporting

In FY 2014, the Fleet DNA project team focused on developing new capabilities for a second phase of web-based reporting, known internally as Phase 2. Phase 2 is housed on the Fleet DNA website (www.nrel.gov/fleetdna) and has been integrated into an updated website and user interface. This new system includes the capability to provide custom query-driven data reporting and graphic generation while supporting data download requests for composite data products from the Fleet DNA database via the Fleet DNA website. To keep data products simple and high-value for the project target audience, an initial dozen interactive graphics were developed for each of the eight categories of vehicle types currently in the Fleet DNA database along with composite graphics for the total composite data set. Plans are in place in FY 2015 and beyond to gather feedback from Fleet DNA users and expand the list of graphics available while also developing a custom graphing and data download interface. An example of the current Phase 2 data interface is shown in Figure IV-62.

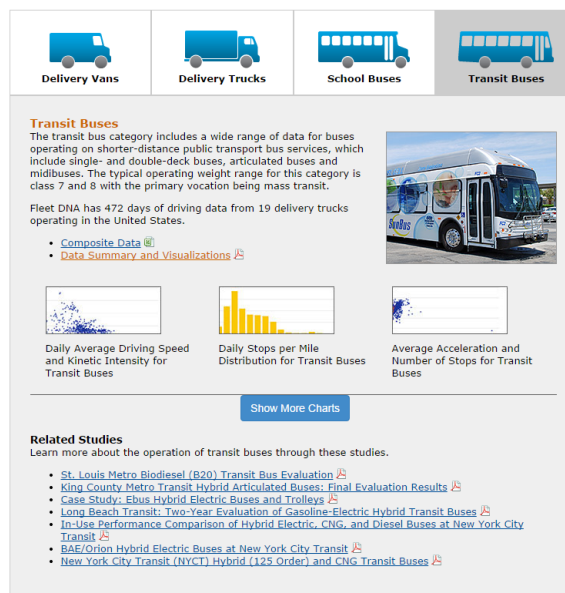


Figure IV-62: Example Fleet DNA vehicle subcategory interface

A sample data summary downloaded from the updated Fleet DNA website illustrating the relationship between average driving speed and kinetic intensity of a vehicle is shown in Figure IV-63. An illustration of a sample performance analysis by vehicle speed is shown in Figure IV-64.

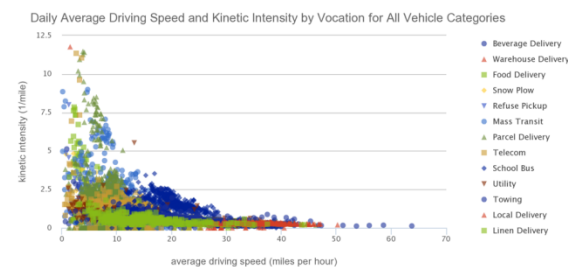


Figure IV-63: Sample data summary of Fleet DNA database sorted by vocation

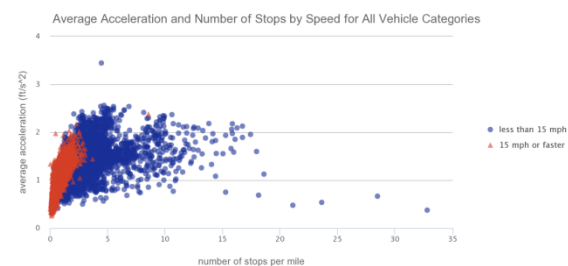


Figure IV-64: Sample performance analysis of entire Fleet DNA database

In addition, the interactive data sets developed in FY 2014 have been posted on the Phase 2 Fleet DNA website developed in FY 2014 and are currently being integrated into the Alternative Fuels Data Center website for additional project visibility and user base. It is the goal of the continued development of Fleet DNA to make available data and tools necessary for users to interact with medium- and heavy-duty data and explore potential avenues for improved vehicle

design, understand operating behavior, and examine fuel consumption reduction options, along with being able to appropriately match vehicle technologies based on usage.

Technical Developments

Fleet DNA Database Overview

Fleet DNA is organized within a broad system configuration to support both internal and external (public) data access operations. It maintains multiple levels of security to ensure protection of sensitive data while facilitating data access for both internal and public users. Although at first glance these dual mandates may appear conflicting, they are accomplished by providing internal users full access to underlying data through a series of secure virtual desktops. Using the same virtual desktops in place for internal users, public access is restricted to a “cleansed” data area, supporting public distribution.

The cleansed data area provides users access to information about existing data sets as described above and allows users to query and create information from the data set. Raw data, individual vehicle data, and source data are not disclosed; this provides anonymity to existing data. Internal users (e.g., NREL and Oak Ridge National Laboratory) have access to raw data, and individual users have access to their own data, once uploaded, and they can compare it to information from other sets as needed.

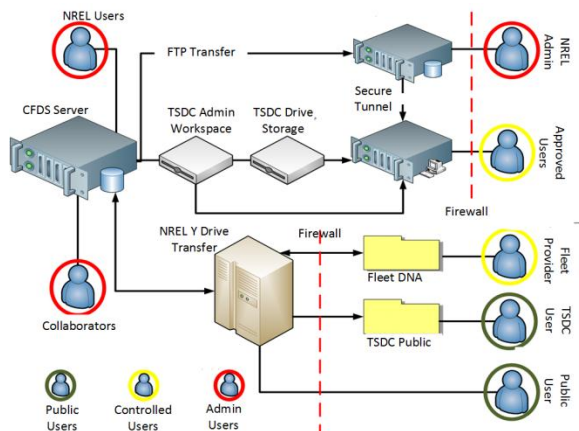


Figure IV-65: Server configuration and security layout for fleet DNA network

When examining current Fleet DNA data security measures, it is important to understand the unique challenges associated with data from a fleet provider’s perspective. When analyzing data via Fleet DNA, a fleet provider is interested in characterizing its fleet and vehicle operation and comparing its operation to other fleets in similar applications. However, at the same time, it is in the fleet provider’s interest not to share operational information that may be considered proprietary with either the public or competitors. To ensure that unwanted data release does not occur, extensive security is in place to protect partner data while allowing for comparison. Fleet DNA protects data provider information through a combination of a unique user ID and a password that is used to query the database and return only data and results specific to a single user.

Fleet DNA can be thought of as a combination of three major components. The primary component that drives Fleet DNA is the data supplied by users and partners (as shown by the yellow box in Figure IV-66), which are uploaded to the database via data loading modules (green box), then stored in the greater Fleet DNA analysis server (red box).

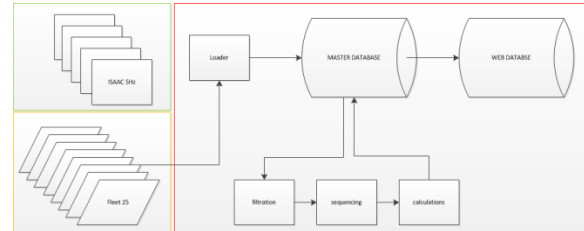


Figure IV-66: Simplified Fleet DNA structure

Data loaders are designed for each unique data format supplied by participants in the Fleet DNA project and are used to ensure uniform data storage and analysis within the Fleet DNA database.

After Fleet DNA data have been uploaded using the data loaders, they can be combined with additional data layers found in the database (Figure IV-67) to perform extended analyses, such as exploring road utilization and grade effects on drive-cycle power requirements (Figure IV-68).

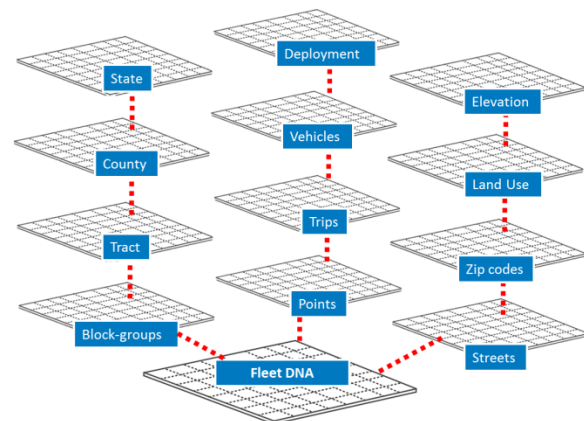


Figure IV-67: Example of Fleet DNA data layers

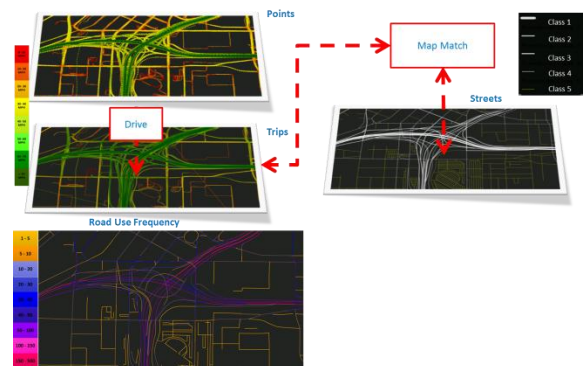


Figure IV-68: Example of analyses via interconnected data layers

FY 2014 Database Developments

Overview of Database Technical Accomplishments

The FY 2014 Fleet DNA database technical accomplishments fall into one of four categories: data processing, data structure, quality control, and analysis.

Data processing improvements build upon the processing routines developed in FY 2013 and attempt to improve the accuracy of the data warehoused, the speed at which reports can be generated, the number of data channels archived, and the versatility of the workflow across multiple computing environments. These accomplishments along with alterations to the data structure have allowed the Fleet DNA project team to increase the amount of data reported on while simultaneously increasing the speed, accuracy, and versatility of the software supporting Fleet DNA.

Changes to the data structure focus on taking the processing routines that normalize the data into a standard package and using time-based indexes to quickly access a small amount of data from an extremely large archive for reporting and analysis. The results data structure implemented in FY 2013 remains constant, but the way the data are packaged within the Fleet DNA archive was completely overhauled.

Quality control improvements attempt to track the inputs and outputs of the processing routine as vehicle data pass through. The metrics logged during the routine feed directly to a set of pre-rendered visuals, allowing the Fleet DNA team to visualize the data during processing to ensure the most accurate aggregates possible. The metrics further allow the Fleet DNA team to optimize processing routines by examining how the processing steps are performing and the time taken to complete them.

Analysis improvements expanded on the existing map-matching routine from FY 2013 to further divide vehicle data in interesting ways to assess vehicle operation using network-based analysis approaches. The networks analysis methods developed in FY 2014 will feed directly into optimization tools and future work in which increased context of how a vehicle is operating will be necessary to provide useful insight to public users and data providers without sacrificing data provider anonymity.

In summary, the technical accomplishments completed in FY 2014 have provided a full overhaul of the back-end data warehouse and processing routines while maintaining the final reporting developed in FY 2013. In addition to improving the archive, the Fleet DNA team created the infrastructure necessary to expand the level of detail we can present publicly through the addition of analysis methods.

Data Processing

The data processing routine developed in FY 2013 included speed filtration, sequencing, grade processing, map matching, and reporting. This multistep routine was developed for the purposes of normalizing variable source data to then feed to reporting. In FY 2014, the Fleet DNA team further divided up the routine into a workflow that allows for a quality check to be implemented prior to reporting, as shown in Figure IV-69.

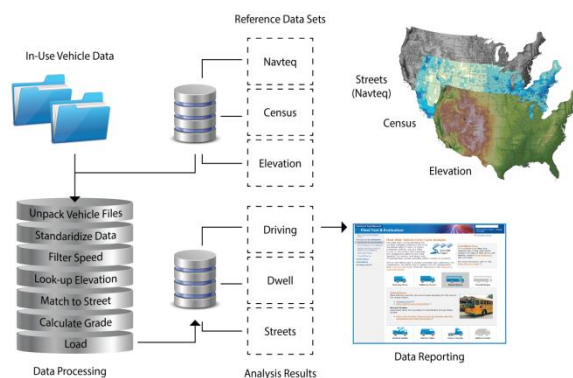


Figure IV-69: Illustration of Fleet DNA database structure

After a vehicle is registered using the data management system, the processing routine extracts data from the file and converts them to a standard data structure in memory before writing data to a file in the new Fleet DNA format. This is commonly referred to as extract transform load (ETL).

An ETL routine is required to compensate for differences and weaknesses in the raw data sets collected from multiple sources. The ETL routine implemented in FY 2014 focuses on four channels of data recorded at intervals ranging from five records per second (5 Hz) to one record per second (1 Hz).

- Coordinates (latitude/longitude).
- Time stamp.
- Speed.

These data channels are referred to as floating car data (FCD) and provide the dimensions necessary to link driving data to additional data sets to then perform analysis on vehicle operations. The FCD provide the dimensions used to sort, index, link, and analyze data, making it the focus of the ETL routine.

Although FCD include the information necessary to perform detailed operations analysis, additional data channels are logged from the vehicle's OBD system to allow analysis of the vehicle's systems. These additional channels include anywhere from 10 to 250 variables indicating how or under what state components within the vehicle are operating. Because of the variability in data returned by different OBD systems, the additional channels are interpreted, but no standardized processing routines are applied to ensure data quality. For now, the channel interpretation consists of a conversion of the channel to the appropriate data type.

All of the processing as well as the data structure outlined in the next section was designed to operate on any computer system in which a standard set of open-source software is available. This means that the processing routine can be transferred or distributed across many environments without costly software purchases. The ability to transition processing and analysis to any system was proven in FY 2014 through the incorporation of the Peregrine HPC cluster housed at the Energy Systems Integration Facility on NREL's campus. This capability will prove valuable as the size of the data archives grows and the type of analyses performed increases in complexity.

Data Structure

The addition of data channels logged from a vehicle’s OBD system into NREL’s data archives requires alterations to the existing data storage to enable NREL to incorporate the additional channels while not sacrificing efficiency.

Traditional databases store data as tables with a fixed structure. To find data within a table, the whole table is read off a disk and then divided into a subset of smaller pieces for analysis. When dealing with billions of records, the approach will scale well as long as the number of columns within a table is minimized. When the number of columns in a table increases, the speed at which data can be accessed decreases exponentially. The loss of efficiency is the result of the increase in the amount of data needed to be sorted through within a table. Further, all tables in a database require the data being archived to have a fixed structure so that every time records are inserted, the same columns are always available.

To ensure that the normalized Fleet DNA data archive can handle the variability in the number of columns archived while not sacrificing efficiency, a NoSQL data storage approach was implemented. NoSQL is a combination of tools and methods for web-scale data storage. The approach is more robust, because it does not rely on a rigid data table structure and focuses on organizing data in a way in which only what is needed is ever read off a disc. This data structure is detailed in Figure IV-70.

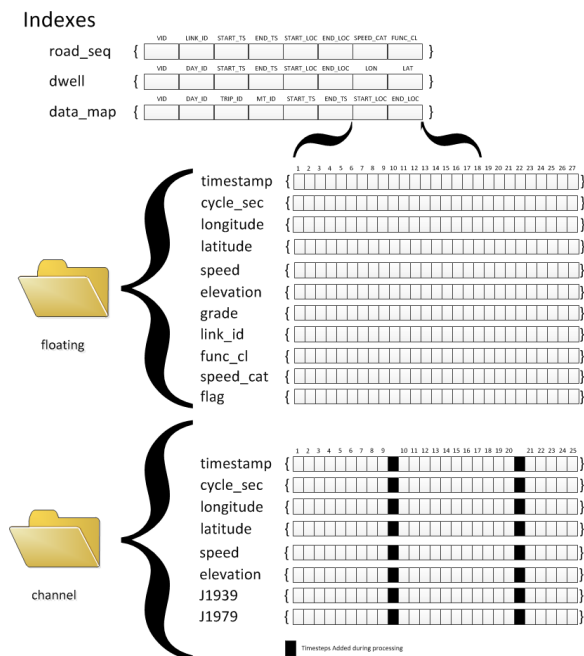


Figure IV-70: Two-folder data storage structure

Quality Control

To ensure that the data provided to the public are accurate and to assess the efficiency of the processing routines, a set of quality-control steps were implemented in FY 2014. The quality control steps track the data as they move through the processing routine to identify what has taken place at the end of each step and how long it took. Not only

are the variables tracked, but the data are plotted in a pre-rendered set of visuals to allow the NREL Fleet DNA project team to quickly verify that the data being written to file have no significant errors.

Several quality assurance visualizations were implemented, including a map, a timeline of operation, heat plots of second-by-second data, and daily road use metrics by speed. The visuals further ensure that the data being fed to the reporting are accurate by using visual assessments and by incorporating several metrics from the config.txt into a paragraph describing operations for the vehicle. An example of the data quality visualizations is shown in Figure IV-71.

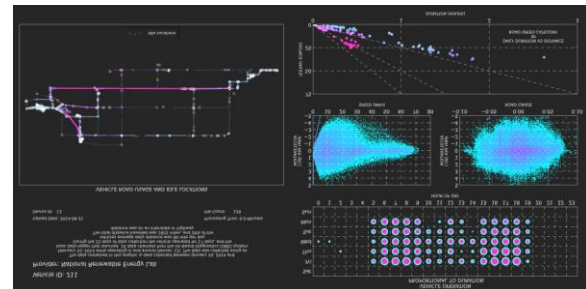


Figure IV-71: Sample data quality visualization

Analysis

In FY 2014, NREL developed tools to evaluate how vehicles operate relative to more general networks feeding into vocation-based analyses. This is important for vocations like transit buses that operate relative to bus stops along routes or delivery vehicles that operate in a stem-and-leaf pattern, because it provides opportunity for greater depth of analysis and better understanding of vehicle operation relative to geography.

To be able to look at a vocation using a network that defines its operation, a set of standard routines were developed to build network indices for point-based networks, polygon-based networks, and line-based networks.

A good example of this was an analysis implemented on the NREL campus shuttle buses. In the analysis, the time when the vehicle was keyed on was recorded, with the vehicle operating time accounted for using an index grouping data by the vehicle’s operating location. In this case, the public transit pick-up locations that the shuttle serves are the relative polygons to which the vehicle is being tracked. The set of polygons represents the bounds of the locations visited, and the time of entry and exit for the time the vehicle spent within the polygon is recorded. Any time the vehicle is not within one of the polygons, the record within the index is recorded as “in transit.” The indexes are ordered by start time, and the identifiers of the previous location and the next location visited are appended to each record. This indicates where a vehicle is going to or coming from, as well as where the vehicle currently is. See Figure IV-72 for an example of the NREL shuttle bus analysis.

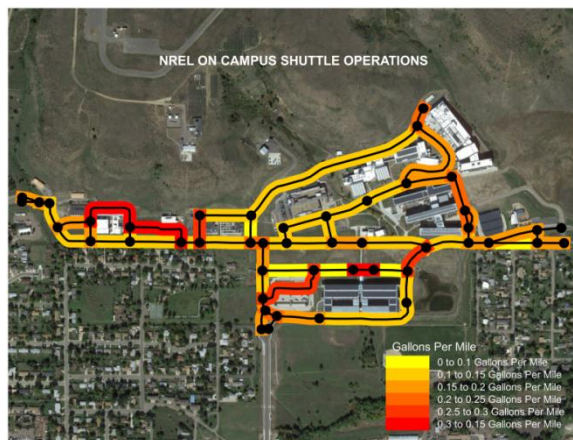


Figure IV-72: Example road network analysis

By organizing the data in this way, it is possible to isolate segments of operation and then implement the standard set of Fleet DNA calculations on the sequence. In the shuttle bus case, we can isolate all the data recorded by the shuttles when they are going from their storage depot to the NREL campus and analyze these drive cycles across the entire shuttle bus fleet. See Figure IV-73 for a visualization of this type of analysis.

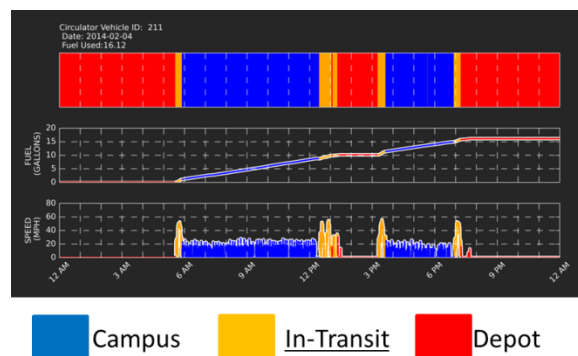


Figure IV-73: Example of vehicle utilization breakdown

Vehicle Mass Estimation

Understanding vehicle mass is a fundamental requirement when trying to characterize vehicle operation, fuel consumption, and the potential for the use of alternative fuels and advanced technologies. Unlike light-duty vehicles, medium- and heavy-duty vehicle mass for many of the commercial vocations and vehicle types stored in Fleet DNA changes throughout the day and duty cycle. Given that a significant amount of vehicle energy, and therefore fuel, is consumed by moving vehicle mass, it is necessary to develop a method to estimate the weight of vehicles during their duty cycle as a means of better understanding fuel consumption as well as to provide enhanced inputs for vehicle modeling software.

Ongoing efforts were made in FY 2014 to develop a method to estimate vehicle mass based on data collected from GPS and controller area network loggers. Using known vehicle specifications such as bulk drag coefficient (drag coefficient multiplied by vehicle frontal area), rolling resistance coefficient, and powertrain/auxiliary losses, a method

employing a univariate recursive least squares approach was developed and tested using vehicle coast-down test data. Initial test results show that the accuracy of the mass estimation was within 5%. Additional experimental validation of the method is planned for early FY 2015. An experimental test plan is currently in development to test vehicles during a variety of drive cycles while loaded with multiple known cargo loads. These data will be used to refine the existing mass estimation model. A publication associated with this experiment and method is planned for FY 2015.

Vehicle Parameter Estimation

In addition to developing a method to determine vehicle mass from on-road data, initial efforts were made in FY 2014 to develop a multivariate recursive least squares method to identify unknown vehicle parameters such as bulk drag coefficient and rolling resistance based on drive-cycle and fueling information as a means of validating existing model assumptions and also as a means of providing baseline values for new vehicle model development. If successful, the parameters identified using this method would be used to generate vehicle models based on real-world on-road vehicle data much quicker and at less expense than using current methods. The initial approach developed in FY 2014 has shown promise in limited testing using coast-down testing captured from delivery vans; however, additional testing in FY 2015 will be necessary to fully evaluate the viability of this approach. Should the approach continue to show promise, it is proposed that additional resources be made available to further tune and validate this approach.

Integrating Existing Tools

In addition to improving the existing Fleet DNA database through additional data collection, reporting, and database development, another significant area of effort in FY 2014 was to integrate existing DOE modeling tools with the database to better leverage the data stored in the database for downstream applications and applied research. One of the first tools integrated with Fleet DNA in FY 2014 was NREL’s Drive-Cycle Rapid Investigation, Visualization, and Evaluation Analysis (DRIVE) tool, a drive-cycle characterization and generation tool. By integrating DRIVE into Fleet DNA, researchers are now able to identify standard chassis dynamometer test cycles representative of data selected in the database as well as generate representative drive cycles based on Fleet DNA data. This is advantageous for both computational simulation and laboratory-based experimental work. This approach was used in the Indianapolis analysis presented at the Green Truck Summit in early 2014 and will be a key feature of the EPA project work being performed by NREL in FY 2015. See “Applying Fleet DNA” for more information.

In addition to integrating DRIVE with Fleet DNA, significant effort was made in FY 2014 to integrate NREL’s Future Automotive Systems Technology Simulator (FASTSim) vehicle modeling software with the database. Having FASTSim coupled to the Fleet DNA database allows researchers to perform large-scale simulations, explore parametric sweep studies, and examine the effects of different control strategies using real-world drive-cycle data. FASTSim was chosen as the initial vehicle modeling platform to

integrate with Fleet DNA because of its speed and limited complexity when compared to other DOE modeling tools such as Autonomie. Efforts will be made in FY 2015 to examine the opportunity to integrate Autonomie with Fleet DNA, along with other tools external to DOE such as EPA's Greenhouse Gas Emissions Model (GEM) and MOtor Vehicle Emission Simulator (MOVES) models, which would provide emissions modeling capabilities.

In addition to direct integration with existing DOE tools, efforts were also made in FY 2014 to strengthen existing relationships with DOE's Clean Cities Program, and in particular the National Clean Fleet Partnership and Alternative Fuels Data Center projects. The Alternative Fuels Data Center is home to numerous tools developed through Clean Cities, and Fleet DNA has made the effort to provide users with access to these tools through links on the Fleet DNA website. Ongoing development of Phase 2 and Phase 3 of the Fleet DNA website will further enhance user access.

HPC Demonstration

In FY 2014, preliminary work was done to explore the potential for Fleet DNA to operate in a HPC environment. Because one of the goals of the Fleet DNA project is to develop a database that would serve as a foundation for large-scale vehicle simulation and component optimization studies, a copy of the Fleet DNA database was uploaded to NREL's Peregrine supercomputer in which a large-scale FASTSim modeling exercise was performed on the distributed computing network. The results of this experiment demonstrated that given the unique NoSQL structure of the database, and the parallel nature of vehicle simulation studies, it will be possible in the future to leverage both Fleet DNA and NREL's HPC capabilities to support additional projects such as large-scale parameter sweep studies for fuel economy optimization and component-sizing exercises to optimize vehicle configuration and to perform powertrain assessments through the application of real-world drive-cycle-based simulation to evaluate current and future hybrid and electric gearing and energy storage control strategies.

Results

Applying Fleet DNA

EPA—Development of Medium-Duty/Heavy-Duty Phase II Greenhouse Gas Regulations

The Fleet DNA database of medium- and heavy-duty vocational duty cycles and analysis capabilities has played a fundamental role in NREL's support of the EPA through assistance in development of the Phase II medium- and heavy-duty greenhouse gas regulations. In particular, NREL was tasked with evaluating the effectiveness of the existing chassis certification test cycles employed by the EPA as well as developing new cycles based on the Fleet DNA database of in-use vehicle data. In addition, given Fleet DNA's unique ability to append road grade to drive cycles, NREL was tasked with generating a representative road grade profile that would also be included in future test procedures. To accomplish these tasks, DRIVE is being leveraged along with the data contained within Fleet DNA to generate representative drive

cycles that include road grade information. This project officially kicked off at the close of FY 2014, and an update on the status will be provided in the FY 2015 milestone report.

DOE Clean Cities Program—City of Indianapolis Refuse Truck Fleet

In addition to leveraging Fleet DNA to support other government agencies such as the EPA, NREL was also able to successfully leverage the information and analysis capabilities of this project in ongoing support of the DOE's Clean Cities Program and, more specifically, the National Clean Fleet Partnership program. Fleets such as Waste Management and PG&E were instrumented in an effort to collect additional data for the Fleet DNA project, and in exchange Fleet DNA analyses were performed on the fleet data, providing additional insight into fleet behavior and potential technology options for improved vehicle efficiency.

California Air Resources Board—Hybrid Voucher Incentive Program

Medium- and heavy-duty commercial fleet vehicles are good candidates for the deployment of low-emission and fuel-efficient advanced technologies, specifically hybrid technology. These vehicles are good candidates because of their large population, high vehicle miles traveled and fuel consumption, operation in urban areas, central fueling and maintenance facilities, and consistent operation and routes.

Many commercial fleets in California are utilizing the California Hybrid Truck and Bus Voucher Incentive Project (HVIP) to deploy vehicles. This is a program funded by the California Air Resources Board; according to the HVIP website, it is "a program to help speed the early market introduction of clean, low-carbon hybrid trucks. HVIP accomplishes this by addressing the biggest barrier for fleet purchase of medium- and heavy-duty hybrids: the high incremental cost of these vehicles in the early market years when production volumes are still low. HVIP provides a meaningful 'kick-start' to the low-emission hybrid truck and bus industry; it could help deploy up to 1,200 vehicles, potentially growing the nation's early market hybrid truck volumes by 50 percent."

In addition to the HVIP vehicles planned or already funded, many other eligible vocations and/or applications in California are ready for hybrid deployment but have not yet applied for or received funding from HVIP.

Previous efforts to intelligently deploy or place vehicles into fleets, including testing and analysis conducted by NREL and the DOE, have illustrated the relationship between duty cycle, fuel economy, and emissions. This initial work has shown that knowledge of real-world vocational drive cycles and vehicle operation is key to selecting the right technology for the given application. Gathering these data is critical to understanding the performance of various technologies under different operating conditions. Without this fundamental data, chassis dynamometer-derived emissions and fuel economy results may not be representative of real-world performance, and vehicle and/or deployment models cannot be optimized for real-world vocational conditions. Fleet DNA captures and characterizes data from various vocations for further vehicle design and strategic deployment.

This project utilized the existing Fleet DNA framework and data set to perform a California-specific study to evaluate the California Air Resource Board's HVIP program benefits to original equipment manufacturers producing hybrid vehicles and the various fleets that are purchasing vehicles in California based on information characterizing the effectiveness of the technology in real-world conditions. Specifically, the objectives of this project were to:

- Obtain the necessary data for HVIP-eligible vehicles (and their diesel equivalent) on relevant vehicle usages/vocations in California.
- Provide testing and analysis showing the performance of technology on the measured usage/vocation.
- Provide a framework, data set, and methodology to estimate fuel consumption and emissions of current and future deployments of HVIP vehicles or other advanced technology vehicles in California.

South Coast Air Management District—Fleet DNA Analysis

NREL and DOE have been conducting research, development, and demonstration projects to facilitate the deployment of advanced vehicle technologies and alternative fuels into the marketplace to reduce petroleum use and enhance the reduction of mobile source emissions in California and the United States. NREL and the South Coast Air Quality Management District have begun to collaborate on a joint project to collect and analyze data on medium- and heavy-duty vehicles in the South Coast district to analyze the usage characteristics and develop an approach that will enable the South Coast Air Quality Management District to better understand vocational differences and associated vehicle performance.

With highway transportation responsible for more than half of the petroleum demand in the United States, medium- and heavy-duty vehicles consume a significant portion of on-road fuels annually. Original equipment manufacturers, commercial fleets, and research organizations have identified a lack of medium- and heavy-duty vehicle use data as a barrier to intelligent design and deployment. This usage data helps identify average and extreme use patterns for various types of vehicle vocations. The data could also help identify similar use patterns across dissimilar vocations, which could lead to more optimized and efficient designs that are appropriate to multiple uses. The goal of this project is to acquire and analyze this type of data, responding directly to the critical need to provide analysis and decision support to enable the intelligent deployment of advanced vehicle technology within key vocations.

Conclusions

As of the end of FY 2014, the Fleet DNA project continued to progress and build on the initial framework developed in FY 2012 and FY 2013. An initial static reporting website was developed that housed eight unique vocation reports in FY 2012, and additional data layers such as road grade and road type were incorporated into the database in FY 2013, providing the opportunity for additional analyses. As a result of the additional data layers, more than 80 new metrics were developed and incorporated into the reporting process in FY 2014, providing researchers and industry members with additional insight into the effects of road grade on drive cycles. In FY 2014, the Fleet DNA database and website were updated to Phase 2, which includes interactive data sets and graphics and better integrates into the Alternative Fuels Data Center to provide users additional insight and access to information such as current laws and incentives and the medium- and heavy-duty vehicle reference database, which includes lists of currently available vehicles for purchase.

The Fleet DNA project plans to continue to grow and develop additional capabilities and reports in FY 2015. Moving forward, Fleet DNA will continue to recruit additional data partners and complete vocational sets, which can then be reported to the public. NREL would also like to expand its vocational sets and add new vocations/vehicle types to its report lists, such as shuttle buses and special use vehicles (cement mixers, fuel trucks, emergency vehicles, etc.).

In addition to expanding Fleet DNA data and capabilities, in FY 2015 the project will focus on expanding outward-facing components of Fleet DNA, such as the website. In addition to building upon the updated interactive reporting website developed in FY 2014, in FY 2015 the Fleet DNA project plans to develop and deploy an enhanced interactive data portal that will provide users the ability to download additional information from the database as well as expand the analyses and information available. Improving visibility and increasing interaction with users will also serve as a source for continued feedback, which will be used to drive future project developments. Toward that end, significant efforts will be made in FY 2015 to continue to promote the Fleet DNA project through ongoing publications and presentations at industry conferences and events such as the Green Truck Summit, SAE world and commercial vehicle congress, and Intelligent Transportation Society of America.

Finally, Fleet DNA development in FY 2015 and beyond will be driven toward building bridges for integration with existing and planned analytic tools and interfaces, such as the Alternative Fuels Data Center, Autonomie, and EPA's GEM and MOVES tools, to provide even greater value-added opportunities and offer users the ability to select, model, and generate custom representations of data drawn from the database.

IV.E.3. Products

Publications

1. “Contributing Data to the Fleet DNA Project Document.” NREL/BR-5400-62771. Golden, CO: National Renewable Energy Laboratory, 2011, www.nrel.gov/docs/fy14osti/62771.pdf.
2. “Data Driven Decision Making Tools – City of Indianapolis Case Study.” Presented at the Green Truck Summit 2014.
3. “Transportation Database Development Using Floating Car Data.” Presented at the Intelligent Transportation Society of America World Congress, September 2014.

Tools and Data

1. “Fleet DNA: Vehicle Drive Cycle Analysis.” National Renewable Energy Laboratory, 2014, www.nrel.gov/vehiclesandfuels/fleettest/research_fleet_dna.html.

IV.F. Fleet DNA Database Development and Support

Principal Investigator: Oscar Franzese, Ph.D.

Oak Ridge National Laboratory
2360 Cherahala Blvd.
Knoxville, TN 37932
Phone: (865) 946-1304
E-mail: franzeseo@ornl.gov

DOE Program Manager :Lee Slezak

Phone: (202) 586-2335
E-mail: Lee.Slezak@ee.doe.gov

749 MTDC 2 files) were uploaded and distributed to NREL. (Year 1).

- Submission to NREL of revised Fleet DNA files with four additional channels where requested by NREL –i.e.; 1) actual engine percent torque, 2) actual gear ratio, 3) percent load, and 4) current gear. (Year 2).
- Development and deployment of a methodology to organize and catalogue the duty cycles contained in the Fleet DNA database. These files were processed and indexed so they could be searched using user defined criteria. (Year 2).

IV.F.1. Abstract

Objectives

- To merge the existing ORNL Heavy Truck Duty Cycle (HTDC) and Medium Truck Duty Cycle (MTDC) databases into the Fleet DNA data repository at NREL by:
 - Identifying and standardizing in conjunction with NREL, high priority 1Hz drive cycle data channels (such as speed, elevation, and other necessary data) recognizing DOE and other partner preferences.
 - Filtering and correcting, where feasible and without degradation of the information, the data collected by ORNL for inclusion into the database.
 - Porting the extracted information into the format required by the Fleet DNA project.
 - (Accomplished in Year 1)
- To provide summary statistics of each the five vocations included in the HTDC and MTDC databases (Year 2).
- To provide additional indexing and cataloguing of the information contained in the HTDC and MTDC databases for quick searching and retrieval of specific duty cycles (Year 2).

Major Accomplishments

- Development of a methodology and procedures to correct short segments of the data collected in the HTDC and MTDC projects that contain errors due to short losses of GPS signals, sensor issues, databus issues, and data-collection equipment issues. (Year 1).
- Development of visualization software to quickly display DC characteristics of the files that ORNL include in the Fleet DNA database. This tool was used to visually inspect the files and allowed identifying any errors that were not corrected by the ORNL data-correction methodology. (Year 1).
- Submission to NREL of the ORNL Fleet DNA files. A total of 3,241 files (1,562 HTDC files, 930 MTDC 1 files, and

Future Achievements

- N/A (Project ended).



IV.F.2. Technical Discussion

Background

Fleets DNA was funded in FY 2012 through NREL by the Vehicle Systems Simulation and Testing (VSST) project within DOE's Vehicle Technologies program. The project was designed to provide a common location for storage and basic analysis of medium and heavy-duty drive cycles. Work performed within NREL, ORNL, other labs and DOE as well as other state and federal agencies has generated data but a common portal and processing routine does not currently exist to store, access, and apply all of this data. As VSST's primary medium and heavy duty data collection laboratories, NREL and ORNL have agreed to collaborate and bring together data analysis techniques and previously collected data, while coordinating future data collection activities. This and future efforts will provide industry (OEM's and fleets), other DOE programs and other federal agencies with valuable drive cycle information to be used to intelligently deploy and design advanced technology vehicles.

Introduction

Previous projects sponsored by DOE and performed by ORNL have generated a highly detailed dataset of real-world information for five vocations including long-haul operations, regional delivery, public transit (buses), electrical utility vehicles, and tow and recovery vehicles. These databases include 60 or more channels of information collected at 5Hz or five readings every second.

During the first year of this project, ORNL worked with NREL to derive from the data collected in the HTDC and MTDC efforts, a database of duty cycle information that was in accordance to the guidelines of the NREL Fleet DNA project.

The data was parsed and selected channels extracted and filtered using different techniques and methodologies developed exclusively for this project, and included in the Fleet DNA database.

In the second year of the project, ORNL developed methodologies and algorithms to build searching tools that would allow to extract from the ORNL Fleet DNA DB duty cycles with user’s selected criteria such as percentage of stop time compared to total DC time; DCs with total distance traveled that falls within a user-defined range; DCs with average speed that is within a user-defined range; and other criteria.

Approach

The work accomplished in the first year of this project generated the Fleet DNA database. The database, which covers five vocations (i.e.; long-haul operations, regional delivery, public transit (buses), electrical utility vehicles, and tow and recovery vehicles), includes a time channel; three vehicle information channels: vehicle speed, vehicle engine speed, and fuel rate; three spatial location channels: latitude, longitude, and altitude; and where available, three channels with the vehicle mass information: steer-axle weight, driver-axle weight, and trailer axle weight. The Fleet DNA database includes information derived from 3,241 files (each file corresponding to a 24-hr period) that were extracted from the ORNL HATD and MTDC databases (1,562 HTDC files, 930 MTDC 1 files, and 749 MTDC 2 files) and were resampled (from 5Hz to 1Hz) and formatted according to NREL specifications.

The extensive information included in the Fleet DNA database makes it difficult to manually search for specific duty cycles that have certain characteristics of interest for researchers and/or industry. To alleviate this problem, during the second phase of this project ORNL first developed a methodology to catalogue and characterize the information contained in the Fleet DNA database. Software was written to identify duty cycles (i.e., segments of data between engine power-on/power-off events) and then to characterize those duty cycles according to given parameters. For example, the data collected in each duty-cycle was used to generate probability distributions of vehicle speed (other parameters, such as vehicle weight or vocation type –i.e., only long-haul operations were included– were not processed since the project was put on hold four month after start).

These probability distributions were used later on to quickly characterize each DC in terms of average speeds, percentage of stops, distance traveled, etc. A second application was developed by ORNL to combine and integrate information from different duty cycles so a given user’s selected criterion (or criteria) could be used to identify and extract from the Fleet DNA duty cycles that comply with these criteria.

The duty cycle selection and extraction processes works as follows. The user is presented with a dialog box shown in Figure IV-74 below and he/she selects the vehicle number (there are 18 vehicles included in the Fleet DNA database),

the type of criteria (only speed in this version of the software), and enters any resampling frequency if needed.

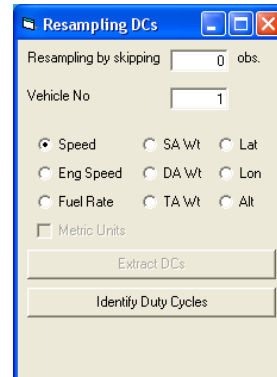


Figure IV-74: Fleet DNA DC extraction tool – parameters

After pressing the “Identify Duty Cycles” button (see Figure IV-74), the utility presents the user with the dialog box shown in Figure IV-75. The user then specifies ranges for criteria of interests such as lower and upper bounds of the percentage of stops that a duty cycle in the database has to have to be selected, the lower and upper bounds of distance covered in the DC, and the number of DCs needed.

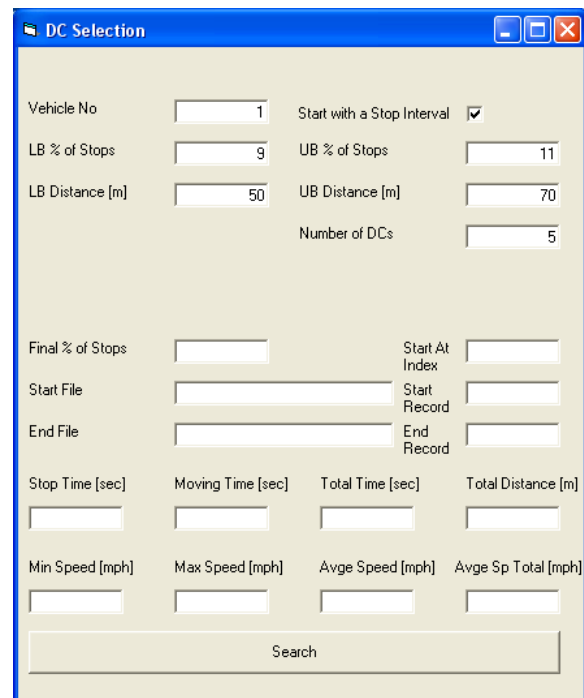


Figure IV-75: Fleet DNA DC selection criteria

As an illustration, Figure IV-76 below shows that the user is interested in extracting 5 DCs which should have a percentage of stop time compared to total time that is between 9% and 11% and each DC should cover a distance that is between 50 and 70 miles. When the user presses the "Search" button, the utility uses the catalogue and other functions developed by ORNL to identify 5 DCs from the Fleet DNA for vehicle 1 that have the characteristics specified by the user. Once the results are obtained, the application presents on the screen information about the first DC found. In this particular example, the DC corresponds to the Fleet DNA file SD1_20061114_HTDC_1. This DC starts at record 47,395 and ends at record 52,679, has 10.48% of stops, a duration of 5,285 seconds, covering a total distance of 67.7 miles, with an average (moving) speed of 51.6 mph.

Only the first DC found is shown on the screen (if nothing is shown, it is an indication that the Fleet DNA database does not contain any DCs with the user's specified criteria for the selected vehicle). Information regarding all the DCs selected (5 in this case) is added to a comma-separated values (csv) file that contains the information shown in Table IV-11 below. The table shows that all of the 5 identified DCs comply with the criteria selected by the user (i.e., all of them have percentage of stops between 9% and 11% and traveled distance between 50 and 70 miles). The table presents the user with additional information that could be used to refine the DC selection. Perhaps the user is interested only on DCs that have an average speed that is larger than 45 mph, in which case only the first DC in the table would qualify. Or perhaps the user is interested only on DCs that have maximum speeds below 70 mph in which case only DCs 2 and 4 would qualify.

Results

The implementation of the cataloguing and search methodologies developed during the second phase of the project resulted in the development of an application that allows users to identify and extract from the extensive Fleet DNA database DCs that comply with user's-defined criteria in a quick and efficient manner.

Figure IV-76: Fleet DNA DC selection criteria and search results

Table IV-11: Fleet DNA Files by Vocation and Vehicle No.

| Final % Stops | Start File Name | Start Rec. # | End File Name | End Rec. # | Time | | | Total Distance [m] | Speed | | | |
|---------------|---------------------|--------------|---------------------|------------|----------|------------|-----------|--------------------|-----------|-----------|-------------------|---------------------|
| | | | | | Stop [s] | Moving [s] | Total [s] | | Min [mph] | Max [mph] | Avg. MOVING [mph] | Avg. TOTAL DC [mph] |
| 10.48% | SD1_20061114_HTDC_1 | 47,395 | SD1_20061114_HTDC_1 | 52,679 | 554 | 4,731 | 5,285 | 67.7 | 1.19 | 74.23 | 51.55 | 46.15 |
| 9.13% | SD1_20061116_HTDC_1 | 78,994 | SD1_20061117_HTDC_1 | 4,714 | 590 | 5,870 | 6,460 | 66.1 | 1.15 | 67.29 | 40.51 | 36.81 |
| 10.15% | SD1_20061127_HTDC_1 | 39,088 | SD1_20061127_HTDC_1 | 44,053 | 504 | 4,463 | 4,967 | 50.3 | 0.00 | 72.47 | 40.55 | 36.43 |
| 9.08% | SD1_20061201_HTDC_1 | 24,855 | SD1_20061201_HTDC_1 | 30,284 | 493 | 4,937 | 5,430 | 58.0 | 1.20 | 68.47 | 42.32 | 38.48 |
| 10.68% | SD1_20061215_HTDC_1 | 18,049 | SD1_20061215_HTDC_1 | 24,918 | 734 | 6,138 | 6,872 | 61.2 | 0.00 | 73.05 | 35.91 | 32.08 |

Conclusions

During the first phase of the project, data collected as part of the Heavy Truck Duty Cycle (HTDC) and Medium Truck Duty Cycle 1 and 2 projects was organized, resampled at one-second resolution (from the original 5 Hz), and cleansed. The Fleet DNA files (version 1) contain ten main channels: time (elapsed time since midnight, each file corresponds to a date), latitude, longitude, altitude, vehicle speed, engine speed, fuel consumption, and steer, drive, and trailer axle weight information (where available). In the first phase of this project, errors that were due to equipment problem (mostly loss of GPS signal) were corrected without changing the information of the main channels. For cases in which these corrections were not possible because they would have changed the raw data for key channels (e.g., files for which vehicle speed information was missing at the start of a trip when the data collection equipment was turned on as the vehicle engine was turned on), the file was not included in the Fleet DNA database.

In the second phase of the project the focus was on the addition of other channels that were originally collected but were not included in the phase-one files (e.g., engine torque, cruise control engagement, etc.). The information contained in the files included in the Fleet DNA database was catalogued and characterized by certain parameters of interests (only speed since the project was put on hold at month 4 after start). For example, even within a given vocation (there are 5 vocations included in the Fleet DNA database) there may be many different types of duty cycles (different lengths, different shapes, etc.). Those duty cycles were catalogued according to a given set of parameters and using predefined ranges for these parameters, the corresponding duty cycles were indexed to allow users to quickly find duty cycles with specific characteristics of interest.

The indexing and cataloging of the extensive Fleet DNA database will allow industry users and researchers to better identify real world duty cycles with certain characteristics of interest that could serve as the basis for testing new engine and vehicle technologies.

IV.F.3. Products

Publications

1. N/A

Patents

1. N/A

Tools and Data

1. A database of real-world information for five vocations and 18 vehicles containing 10 channels of information and in the Fleet DNA format required by NREL (a total of 3,241 files corresponding to 3,241 days of data collection, one file per day).
2. A set of tools to extract, cleanse, resample, and format the information from the HTDC and MTDC databases to the Fleet DNA database.
3. A Fleet DNA Visualization Tool to quickly and visually examine the information and identify any errors that escaped the numerical cleansing procedures applied to the raw data.
4. A Duty Cycle search and selection application based on user-defined criteria.

IV.G. Medium-Duty Electric Vehicle Data Collection and Performance Assessment

Principal Investigator: Kenneth Kelly

National Renewable Energy Laboratory
15013 Denver West Parkway, MS 1633
Golden, CO 80401
Phone: (303) 275-4465
E-mail: Kenneth.Kelly@nrel.gov

DOE Program Managers: David Anderson

Phone: (202) 287-5688
E-mail: David.Anderson@ee.doe.gov

DOE Program Manager: Lee Slezak

Phone: (202) 586-2335
E-mail: Lee.Slezak@ee.doe.gov

IV.G.1. Abstract

Objectives

The objective of this project is to securely collect, store, and analyze vehicle data transmitted from medium-duty plug-in electric vehicles (EVs) and equipment being deployed/developed as a part of U.S. Department of Energy (DOE)-funded activities (under the American Recovery and Reinvestment Act [ARRA] Transportation Electrification Awards). The project includes extensive data collection from Smith Newton and Navistar eStar EVs, Cascade Sierra Solutions (CSS) truck stop electrification, and Odyne Plug-in hybrid electric vehicle (HEV) utility trucks. Objectives for FY 2014 included:

- Obtain vehicle and component performance parameters each second from each EV participating in the ARRA data collection, to be logged and stored at NREL.
- Obtain truck stop electrification usage records that provide a timestamp and energy consumption information each time a plug-in site is used.
- Report data and progress of the data collection efforts as well as analyzed vehicle/equipment performance data to the DOE and the general public.
- Provide for the secure storage of data with routine backups.
- Refine and optimize processing routines to handle an increasing volume of data as more vehicles come online.
- Process results to protect proprietary and private information and post on an NREL website quarterly for public review.

Major Accomplishments

Data collection and reporting activities for medium-duty EVs in FY 2014 included the addition of second generation Smith vehicles along with continued data collection from the first generation vehicles. The Navistar data collection came to a close at the end of June 2014, and data collection from truck stop electrification sites has resumed after a change in management. A few ARRA deployment projects are highlighted below:

- Smith Electric Vehicles: Data transmission, analysis, and reporting of performance from the Smith Newton EVs to NREL continue:
 - First Generation Vehicles: FY 2014 included four new quarterly reports and a cumulative report covering data collected from November 2011 through June 2014 was posted on the website. Data from a total of 259 first-generation vehicles were recorded through June 2014. This represented 96,461 vehicle-days of operation covering more than 2.4 million miles over 32 months.
 - Second Generation Vehicles: NREL began receiving data from second-generation Smith vehicles in FY 2014. Reports included a CY13 annual report that summarized the 2013 operation, three quarterly reports, and a cumulative report covering data collected from January 2013 through June 2014 was posted. Data from a total of 200 second-generation vehicles were recorded through June 2014. This represented 37,064 vehicle-days of operation covering nearly one million miles over 18 months.
- Navistar: Although the production of the Navistar eStar has stopped, there were still over 100 vehicles transmitting data back to NREL through June 2014, which marks the end of the data collection period for these vehicles. FY 2014 included three additional quarterly reports and a cumulative report covering August 2012 through June 2014. Data from a total of 101 vehicles were recorded, which represented 17,447 vehicle-days of operation covering 353,733 miles over 23 months.
- Cascade Sierra Solutions: A cumulative report covering January 2013 through June 2014 has been posted and includes monthly usage statistics over this period. As of June 2014, all 50 sites were active and have recorded 3,847 plug-in events using 41,029 kWh of electricity.
- Reports: Detailed cumulative and quarterly reports for these projects can be found on the NREL website: www.nrel.gov/vehiclesandfuels/fleetest/

Future Achievements

- Analysis will continue on all ongoing projects. Efforts for FY 2015 will focus on improved integration with data sets from other projects and expanding the number of metrics that are being considered.
- Additional data will be received in early 2015 on plug-in hybrid electric bucket trucks from Odyne. Similar data collection, screening, and analysis efforts will be completed in FY 2015 for this data set, and reports will be posted for public consumption.



IV.G.2. Technical Discussion

Background

ARRA deployment and demonstration projects are helping to commercialize technologies for HEVs, plug-in hybrid EVs, all-electric vehicles, and electric charging infrastructure.

This effort, which is funded by the DOE's Vehicle Technologies Office within the Vehicle & Systems Simulation and Testing Activities, will utilize data collected from the medium- and heavy-duty ARRA EV demonstration projects. Data from EVs from Smith Electric Vehicles (Smith) and Navistar will be collected, compiled, and analyzed. Data from ARRA-funded CSS truck stop electrification sites have also been included. CSS entered receivership earlier this year, but site utilization data are still being provided through Shorepower Technologies. Also, data from plug-in hybrid electric utility trucks will be supplied by Odyne starting in FY 2015.

Introduction

NREL will compile the data received from each original equipment manufacturer (OEM) through the NREL Commercial Fleet Data Center (CFDC). This includes more than 25 parameters, which are recorded each second from each vehicle and transmitted to NREL on a regular basis. Compiled data products will be used to better understand the behavior and operating characteristics of electric-drive vehicles being operated in the field. This is in direct support of the Vehicle Technology Office's goals of developing and deploying plug-in EVs.

Information gathered on vehicle drive cycle characteristics along with data collected on specific components, such as electric motors, power electronics, auxiliary loads, and battery performance, can be used to support other DOE-sponsored research and development activities.

NREL will prepare and deliver detailed non-proprietary reports of vehicle performance to the DOE. This information, which will be processed to obscure any proprietary or private information, will also be made available on the NREL website for public review.

Approach

Overall Approach

On-board diagnostic data are collected, typically from the controller area network (CAN) bus, along with global positioning system and any additional sensors. The data are transmitted wirelessly back over the cellular network and eventually on to the OEM. The data are then uploaded by the OEM to the NREL secure FTP site, usually as a text file. Once the data have arrived at NREL, a number of automated processes handle downloading, filtering, sorting, and processing the data. The raw and processed data are stored in the CFDC PostgreSQL central database, and summary reports are generated for the DOE and general public. This process is outlined in the schematic shown in Figure IV-77.

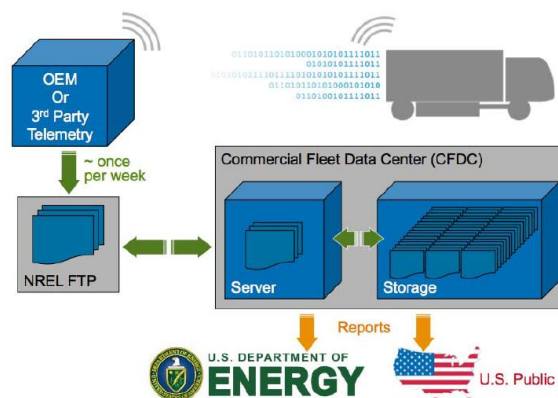


Figure IV-77: Data flow from vehicle to final reporting

The procedure for taking a more detailed look at the data processing, which takes place at the CFDC, can be broken down into a number of steps. The two primary software packages used for calculations and analysis are MATLAB and Python. Raw data can be loaded directly from individual files or read from the CFDC PostgreSQL central database. All data received by the secure FTP site are stored; however, if data are found to be erroneous or corrupt during the filtering process, they are flagged and are not included in the subsequent processing steps. Time and date are adjusted for geographic location, and then binned into “driving days” that capture one full day of driving and any subsequent charging, even if the charge cycle goes past midnight. Specific analysis is then carried out on individual aspects, including drive cycle, powertrain, power electronics, batteries, and any individual components of interest. These routines include code and calculations specifically designed for these projects, as well as incorporating more universal calculations from NREL's Fleet Analysis Toolkit, which allows the performance of these vehicles and vehicle components to be compared across a large number of current and past projects within the secure data center. This information can be combined with demographic data to better understand localized trends and markets. Final data products are then posted to the NREL website for public access. This process is outlined in the schematic shown in Figure IV-78.

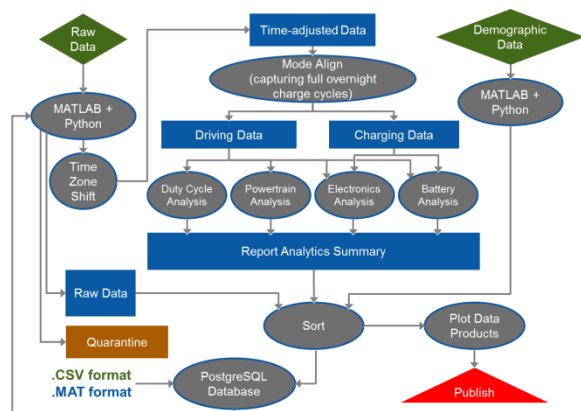


Figure IV-78: Data processing and analysis

Results: Smith Electric Vehicles Data Collection, Analysis, and Reporting

The main focus for the Smith Newton deployment project in FY 2014 was to acquire and incorporate data from second-generation vehicles (Smith Gen 2) into the normal processing routine. This required refining the processing scripts to handle a new file format and adjustments for increasing the speed of calculations as vehicle usage and raw data volume increased. Also refinements to the overall PostgreSQL database management have drastically decreased the amount of time required for large data uploads. For example, parallel sessions of Python code now allow calculations to be run on multiple vehicles simultaneously, reducing the processing time. For more information on data processing, filtering, and storage please refer to the FY 2014 Fleet DNA Milestone Report (NREL/MP-5400-62850).

The main data storage structure for the Smith EV data is a PostgreSQL database. This is not only neater and cleaner from an organizational standpoint, when compared with the raw files, but also adds functionality in which the database allows multiple users to interact with the data while simultaneously processing results. The database also integrates seamlessly with the new Python scripting and calculations, allowing raw data to be extracted from the database, calculations made, and results saved back to the database all in one step. In parallel with the database, a file system of binary (not human-readable) concatenated MATLAB files are maintained, one file per unique vehicle identifier. These files allow the full second-by-second history of a vehicle to be loaded quickly for unique one-off calculations that are not part of the standard calculations made as data are loaded into the database. Mirrored copies of the raw data and binary copies are stored on the NREL High Performance Computing Data Center’s mass storage system, which is linked to NREL’s flagship supercomputer, Peregrine. Although Peregrine is not currently used for any of the routine quarterly reporting, it has the potential to leverage the Smith in-use performance data to tune large-scale EV and battery simulation models for vehicles and components in similar applications.

A Smith Newton delivery vehicle is shown in Figure IV-79.



Figure IV-79: Smith Newton delivery vehicle (PIX# 22851)

Currently, all the Smith Newton full electric-drive vehicles participating in this demonstration project have 80-kWh battery packs, with the exception of a handful of utility trucks that have 120-kWh packs, but which are not in regular service at this time. Battery packs for these vehicles were supplied by Valence and A123. The vehicle is advertised as having a number of battery pack size options ranging from 40 kWh to 120 kWh and comes in a number of chassis configurations feeding a number of vocations including box truck, step van, refrigerated, aerial lift, utility, flat bed, shuttle bus, and military transport. The vehicles participating in this demonstration project are primarily delivery, distribution, and utility maintenance vehicles. Participating fleets include Frito-Lay, Staples, FedEx, Duane Reade, PG&E, and Coke. The second-generation vehicles benefit from an improved battery chemistry and battery management system and a redesigned driveline. Some vehicle specifications are listed in Table IV-12.

Table IV-12: Smith Newton Vehicle Specifications

| | |
|-----------------------------|------------------|
| Gross Vehicle Weight Rating | 16.5k–27k lbs. |
| Drag Coefficient | ~0.5 |
| Charging Standards | J1772 or 3-phase |
| Onboard Charger Power | 5–6 kW |
| Battery Capacity | 80–120 kWh |
| Inverter Efficiency | 94% |
| Peak Motor Power | 134 kW |
| Motor Efficiency | 90% |

NREL has been receiving data from Smith as part of this demonstration project since November 2011 for first-generation vehicles and since September 2013 for second-generation vehicles. The latest cumulative report posted to the web captures all data that have passed through the filtering and analysis steps described above through the end of June 2014. Some statistics from these cumulative reports are summarized below. Figure IV-80 shows the number of files and quantity of data received to date.

| Smith Newton Electric Vehicles | Gen 1 | Gen 2 |
|--------------------------------|-------------------|------------------|
| Reporting period | 11/1/11 – 6/30/14 | 1/1/13 – 6/30/14 |
| Number of vehicles | 259 | 200 |
| Number of vehicle days driven | 96,461 Days | 37,064 Days |
| Number of operating cities | 81 | 40 |

| Trip Data | Gen 1 | Gen 2 |
|---|---------------------------|--------------------|
| Overall Diesel Equivalent Fuel Economy ¹ | 24.8 mpge | 28.1 mpge |
| Overall AC Energy ² | 1,851.0 Wh/mi | 1,784.2 Wh/mi |
| Overall DC Electrical Energy Charged | 1,627.1 Wh/mi | 1,649.8 Wh/mi |
| Overall DC Electrical Energy Discharged | 1,516.9 Wh/mi | 1,336.3 Wh/mi |
| Driving DC Electrical Energy Consumption ³ | 1,410.7 Wh/mi | 1,275.9 Wh/mi |
| Total Number of Charges | 179,463 | 68,446 |
| Total Charge Energy Delivered | 4,508,000 kWh | 1,712,524 kWh |
| Total Distance Traveled | 2,441,756 miles | 963,201 miles |
| City Highway Distance ⁴ | 1,581,149 860,607 miles | 87 403,015 miles |
| City Highway Distance ⁴ | 64.8 35.2 % | 58.2 41.8 % |

| Route Information | Gen 1 | Gen 2 |
|--|--------------|--------------|
| Average Distance Traveled per Day | 25.2 miles | 25.9 miles |
| Median Daily Driving Aggressiveness ⁵ | 1.7 [0–10] | 1.5 [0–10] |
| Average Number of Stops per Day per Mile | 48.0 2.4 | 49.5 3.0 |
| Average Brake (Regen) Events | 9.1 per mile | 8.7 per mile |
| Average Maximum Acceleration | 0.33 g | 0.26 g |
| Average Daily Maximum Driving Speed | 50.8 mph | 47.4 mph |
| Average Daily Driving Speed | 21.3 mph | 21.9 mph |

1. Miles per gallon diesel equivalent (mpge) is calculated based on a 128,450 Btu/gallon energy density provided by U.S. Department of Energy's Alternative Fuels Data Center. Using this information, diesel fuel mpge equates to 37.6 kWh.
2. Assumed charger efficiency of 90%.
3. Total in-motion energy consumption averaged per mile. These figures cover multiple vehicle configurations, in multiple cities, with multiple environments, topologies, and load profiles. These numbers are averages of a diverse fleet of vehicles and cannot be used to predict the efficiency of any particular Smith vehicle.
4. City and highway distance classifications are distinguished by a 35-mph trip speed limit. Trips classified as "highway" achieved a maximum driving speed in excess of 35 mph, while trips classified as "city" do not.
5. Daily driving aggressiveness is kinetic intensity scaled by a factor of two. Kinetic intensity is a characteristic of the duty cycle that measures hybrid advantage. For more information on kinetic intensity, please refer to O'Keefe, M.; Simpson, A.; Kelly, K.; Pedersen, D., (2007). "Duty Cycle Characterization and Evaluation Towards Heavy Hybrid Vehicle Applications." SAE Technical Paper 2007-01-0302, doi:10.4271/2007-01-0302.

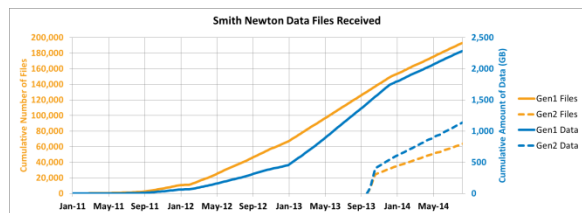


Figure IV-80: Smith EV Data Received through the FTP Site

Figure IV-81 shows the home locations of Smith vehicles currently reporting data back to NREL on a regular basis. Figure IV-82 gives a breakdown of the total data received by state.

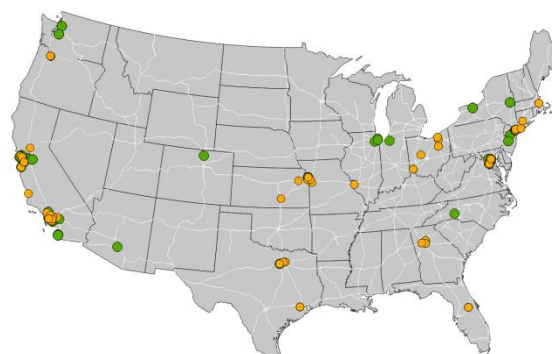
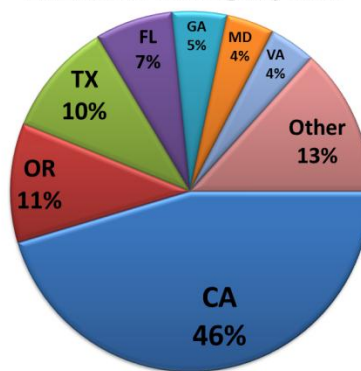


Figure IV-81: Home locations of Smith vehicles: Gen1 (Orange), Gen2 (Green)

Smith Gen 1 Mileage by State



Smith Gen 2 Mileage by State

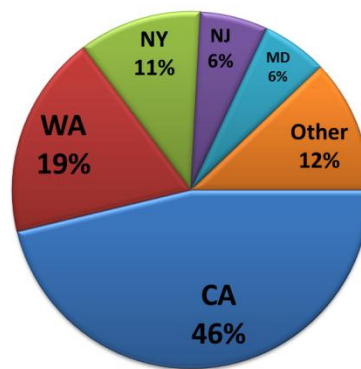


Figure IV-82: Distribution of Smith data by state

The following graphs summarize the operational characteristics of these vehicles. Figure IV-83 shows that the second-generation Smith EVs follow a typical pattern for daily commercial use with the vehicles starting operation in the early morning and returning in the evening. Figure IV-84 indicates most vehicles are connecting the charger in the late afternoon to early evening with the largest spike around 4 p.m.–5 p.m. Figure IV-85 shows charging continues well into the night with some vehicles still charging as fleet activity starts the next morning.

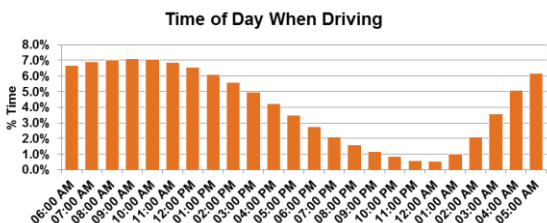


Figure IV-83: Time of day when Smith vehicles are driving

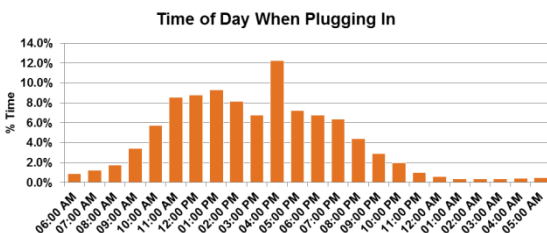


Figure IV-84: Time of day when plugging in (charging begins)

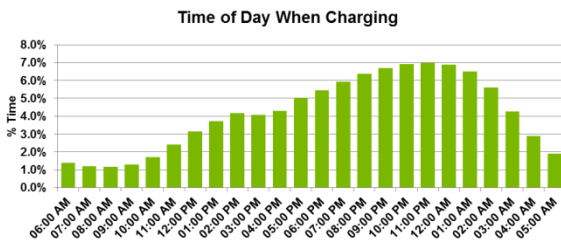


Figure IV-85: Time of day when Smith vehicles are charging

Figure IV-86 shows the distribution of daily driving distance and estimated range. Figure IV-87 shows the distribution of daily energy consumption per mile, which varies significantly depending on how the vehicle is being operated. This is also highlighted in Figure IV-88, which quantifies the impact of driving aggressiveness on energy consumption. Quarterly average fuel consumption is shown in Figure IV-89 along with annual cumulative totals from Figure IV-87.

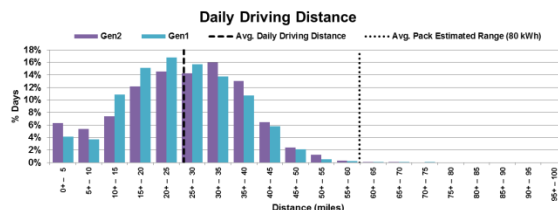


Figure IV-86: Distribution of daily driving distance and estimated range

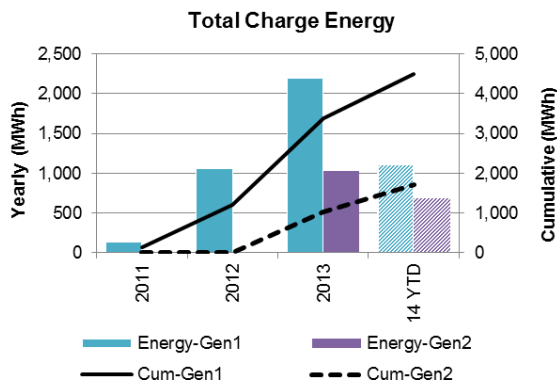
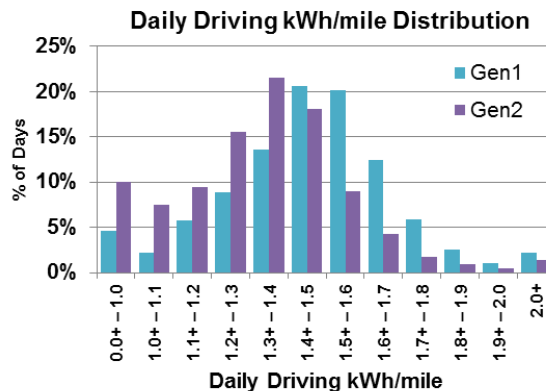


Figure IV-87: Smith energy consumption per mile and per year and cumulative

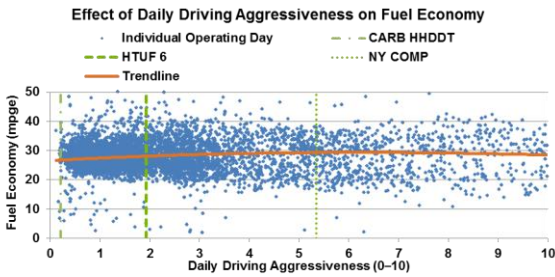


Figure IV-88: Effect of driving aggressiveness on mpge

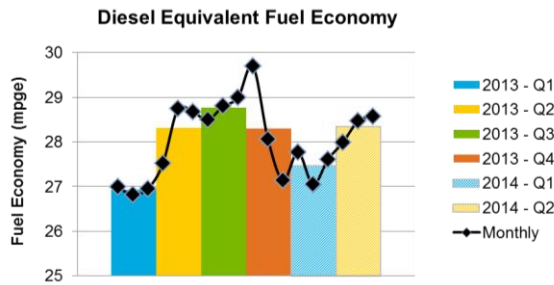


Figure IV-89: Smith diesel equivalent fuel economy by quarter

Figure IV-90 shows daily driving kinetic intensity and average driving speed compared with some standard chassis dynamometer test cycles for the Smith Newton vehicles.

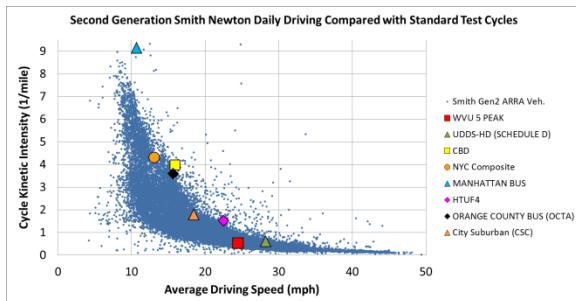


Figure IV-90: Smith Newton kinetic intensity vs. average driving speed

The latest reports and more detailed results, including data through June 2014, can be found at: www.nrel.gov/vehiclesandfuels/fleettest/research_electric.html

Results: Navistar Data Collection, Analysis, and Reporting

All of the Navistar eStar vehicles that reported data back to NREL are first-generation vehicles with 80-kWh battery packs. We do not expect any more vehicles to come online as production has been discontinued. Vehicles that have already been deployed continued transmitting data through the end of June 2014. The Navistar eStar is shown in Figure IV-91, and some vehicle specifications are presented in Table IV-13.



Figure IV-91: Navistar eStar, battery electric delivery vehicle (PIX# 18624)

Table IV-13: Navistar eStar Vehicle Specifications

| | |
|-----------------------------|-----------------|
| Gross Vehicle Weight Rating | 12,122 lbs. |
| Payload (Max) | 5,100 lbs. |
| Curb Weight | 7,022 lbs. |
| Charging Standard | J1772 |
| Battery Capacity | 80 kWh |
| Motor Power | 70 kW |
| Top Speed | 50 mph |
| Advertised Range | Up to 100 miles |

During FY 2014, NREL saw continued steady transmission of data from the Navistar eStar vehicles funded by ARRA up through the final upload of data at the end of June. Figure IV-92 shows the data received over the course of the project, which spans approximately two years. Files received before July 2012 have been omitted for data quality and consistency.

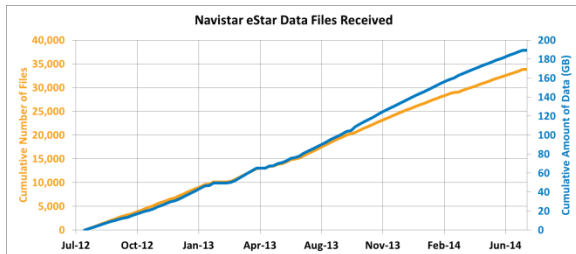


Figure IV-92: Navistar vehicle data received through the FTP site

The ARRA-funded Navistar eStar vehicles were deployed to a number of different fleets across the United States. The map in Figure IV-93 shows the home charging location of each vehicle, and Figure IV-94 shows the corresponding mileage accumulation by state.



Figure IV-93: Home locations and hours of data transmitted per vehicle

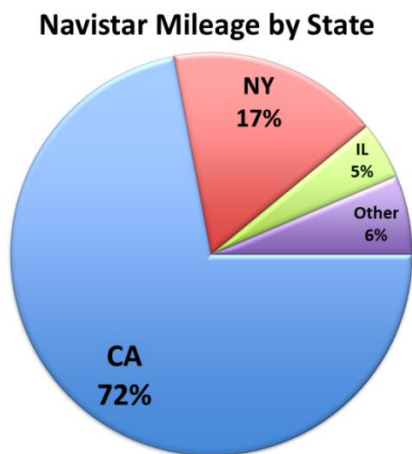


Figure IV-94: Distribution of data by state

The latest cumulative report posted to the web captures all data that have passed through the filtering and analysis steps in the timeframe above, through the end of June 2014. Below are some summary statistics from this report:

Navistar eStar Vehicles

| | |
|-------------------------------|------------------|
| Reporting period | 7/1/12 – 6/30/14 |
| Number of vehicles | 101 |
| Number of vehicle days driven | 17,447 Days |
| Number of operating cities | 35 |

Trip Data

| | |
|---|------------------------|
| Overall Diesel Equivalent Fuel Economy ¹ | 46.2 mpge |
| Overall AC Electrical Energy Charged ² | 892.2 Wh/mi |
| Overall DC Electrical Energy Charged | 843.2 Wh/mi |
| Overall DC Electrical Energy Discharged | 813.3 Wh/mi |
| Driving DC Electrical Energy Consumption ³ | 737.3 Wh/mi |
| Total Number of Charge Events | 16,152 |
| Total Charge Energy Delivered | 298,260.1 kWh |
| Total Distance Traveled | 353,733.3 miles |
| City Highway Distance ⁴ | 269,806 83,927 miles |
| City Highway Distance ⁴ | 76.3 23.7 % |

Route Information

| | |
|--|---------------|
| Average Distance Traveled per Day | 20.3 miles |
| Median Daily Driving Aggressiveness ⁵ | 4.3 [0–10] |
| Average Number of Stops per Day per Mile | 123.7 6.1 |
| Average Brake (Regen) Events | 16.3 per mile |
| Average Maximum Acceleration | 0.39 g |
| Average Daily Maximum Driving Speed | 50.4 mph |
| Average Daily Driving Speed | 14.2 mph |

Plug-In Charging

| | |
|---------------------------------------|------------------------|
| Average Fleet Charging Frequency | 5384.0 charges / month |
| Average Fleet Charge Energy per Month | 99,420.0 kWh/month |
| Average Vehicle Charging Frequency | 0.93 per day driven |
| Average Vehicle Charge Energy per Day | 17.1 kWh/day driven |
| Average Energy Delivered per Charge | 18.5 kWh |
| Average Duration of Charge Event | 3.5 hours |
| Average Distance between Charges | 21.9 miles |

1. Miles per gallon diesel equivalent (mpge) is calculated assuming U.S. Environmental Protection Agency standard energy density of 37.6 kWh per gallon of diesel.
2. Not all vehicles are reporting AC charge information.
3. Total in-motion energy consumption averaged per mile.
4. City and highway distance classifications are distinguished by a 35-mph trip speed limit. Trips classified as "highway" achieved a maximum driving speed in excess of 35 mph, while trips classified as "city" do not.
5. Daily driving aggressiveness is kinetic intensity scaled by a factor of two. Kinetic intensity measures hybrid advantage. For more information on kinetic intensity, please refer to O'Keefe, M.; Simpson, A.; Kelly, K.; Pedersen, D. (2007). "Duty Cycle Characterization and Evaluation Towards Heavy Hybrid Vehicle Applications," SAE Technical Paper 2007-01-0302, doi:10.4271/2007-01-0302).

Figure IV-95 and Figure IV-96 show what time of day the vehicles are being driven and charged, which follow a typical “daytime” operation pattern with the vehicle being operated roughly between 6 a.m. and 7 p.m. Figure IV-97 shows the distribution of daily driving distance. The average pack estimated range shown in Figure IV-98 estimates the range of the vehicle based on the 80-kWh pack and the 0.813-kWh/mile average energy consumption.



Figure IV-95: Time of day when driving

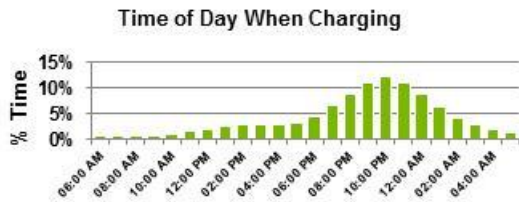


Figure IV-96: Time of day when charging

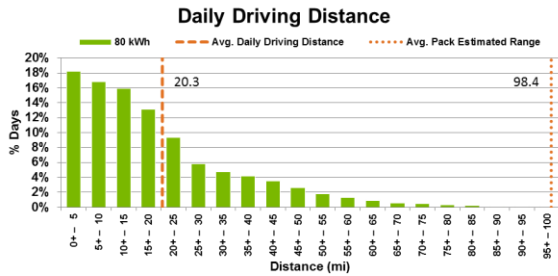


Figure IV-97: Daily driving distance

Figure IV-98 shows the effect driving aggressiveness has on energy consumption. It shows that as driving aggressiveness increases, the energy consumed per mile increases and the calculated mile per gallon equivalent (mpge) decreases.

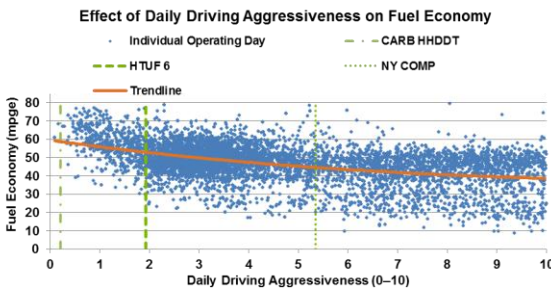


Figure IV-98: Effect of driving aggressiveness on fuel economy

In Figure IV-99, each Navistar eStar point represents one vehicle-day of driving. Kinetic intensity and average driving speed for each day can be compared with standard chassis dynamometer tests. To provide a reference for driving style, typical medium-duty drive cycles are plotted along with the daily data points. The Central Business District (CBD), Orange County Bus, and NY City Composite Cycles appear to be good matches for a typical day of driving for this vehicle on average across all applications. The NY Bus and West Virginia University 5 Peak cycles bound either end with >96% of the drive cycle kinetic intensities falling between these points.

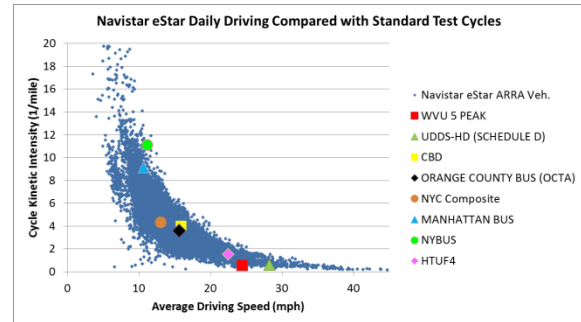


Figure IV-99: Daily driving compared with standard cycles

Figure IV-100 shows the fleet average diesel equivalent fuel economy and energy consumption by quarter. The overlaid monthly fuel economy numbers show the typical trend of higher energy consumption during the winter months due to higher viscous losses from the cold temperatures and energy required to run the resistive heater.

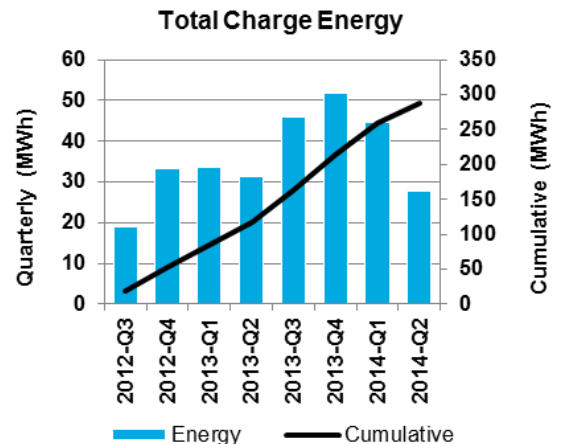
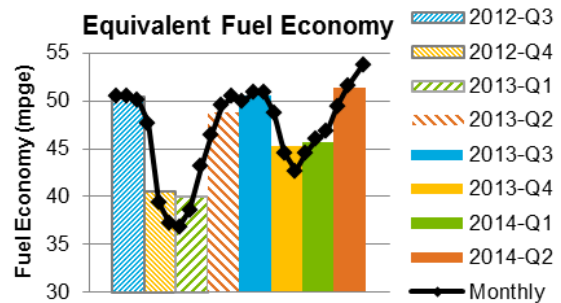


Figure IV-100: Quarterly energy consumption

The latest reports and more detailed results can be found at: www.nrel.gov/vehiclesandfuels/fleetttest/research_electric.html

Results: Cascade Sierra Solutions Data Collection, Analysis, and Reporting

In mid- FY 2013, CSS began sending truck stop electrification usage statistics to NREL. In early FY 2014, CSS entered receivership, but utilization data continue to be supplied by Shorepower Technologies. Each funded site has several pedestals, and each pedestal has four connection points where vehicles equipped with electrified equipment can be plugged in. The data set from CSS includes a summary of each transaction, which contains location, date, person/business contact information, hours booked, total energy used, and a reference ID that can be linked to truck equipment if available. This reference ID is the only link between energy consumption and the equipment on the truck. The latest cumulative report shows usage statistics through the end of June 2014. Some summary statistics from this report are shown below:

Utilization Summary

| | |
|---|--------|
| Idle-reduction rebate approvals: | 4,370 |
| Completed equipment installations: | 4,353 |
| Number of TSE sites with >90% uptime: | 50 |
| Number of plug-in events: | 3,847 |
| Total hours booked: | 53,979 |
| Total kWh used: | 41,029 |
| Average kWh/event: | 10.7 |
| Estimated gallons of diesel fuel saved ¹ : | 43,183 |
| Metric tons of CO2 avoided ² : | 440 |

- Diesel fuel saved calculated using booking time x 0.8 gal/hr (EPA-420-F09-038) to estimate offset engine idle fuel use.
- Metric tons of carbon dioxide calculated using U.S. EPA greenhouse gas guidelines of 10,180 g CO₂ / gallon of diesel.

The map in Figure IV-101 shows the total energy consumption by location and by Petroleum Administration for Defense District (PADD) over the current reporting period.

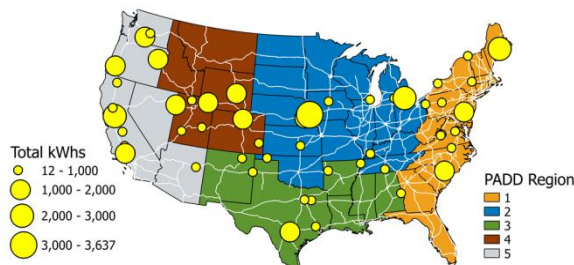


Figure IV-101: Map showing energy consumption by site and PADD regions

Figure IV-102 shows weekly and seasonal trends of site utilization. From an energy standpoint, Tuesday shows the lowest use, whereas Friday and Saturday see the highest use. This is typical for truck stop use where drivers may spend a considerable period of time at one stop over the weekends, waiting for a business to open the following Monday. On a seasonal scale, usage appears to be highest during the winter months; however, these trends are complicated by the fact that some individuals received free credits in 2013, and some of the utilization drop-off in mid-2014 could also be due to issues revolving around the receivership. More data are needed to establish a sound trend in usage patterns.

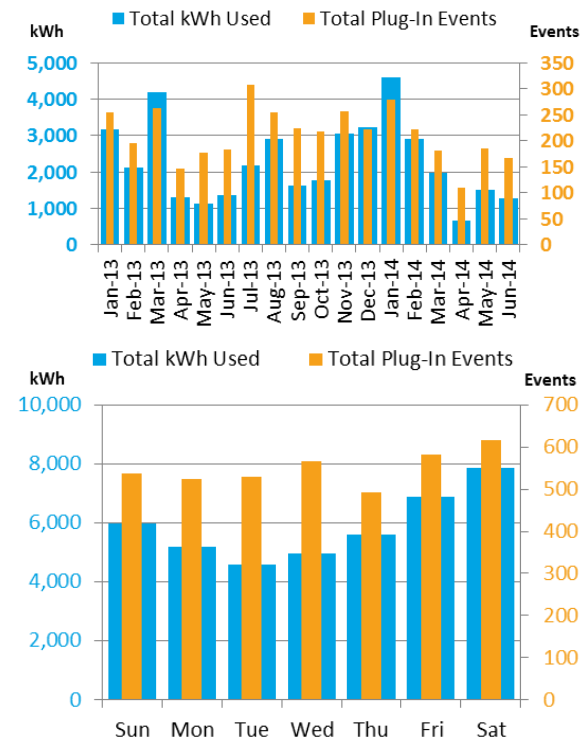


Figure IV-102: Seasonal and weekly utilization

The latest reports and more detailed results can be found at www.nrel.gov/vehiclesandfuels/fleetttest/

Odyne Plug-In Hybrid Electric Utility Trucks Background

Introduction

Odyne Systems has developed a plug-in hybrid electric power take-off (PTO)-based system for use with medium- and heavy-duty vehicles. Its system interfaces with Allison 2000, 3000, and 4000 series transmissions and targets vocational vehicles in the utility and maintenance sector. As part of the medium- and heavy-duty demonstration projects under the ARRA, Odyne plans to deploy over 120 vehicles into real-world service that will be reporting data back to NREL for further analysis. A schematic of the system is shown in Figure IV-103.

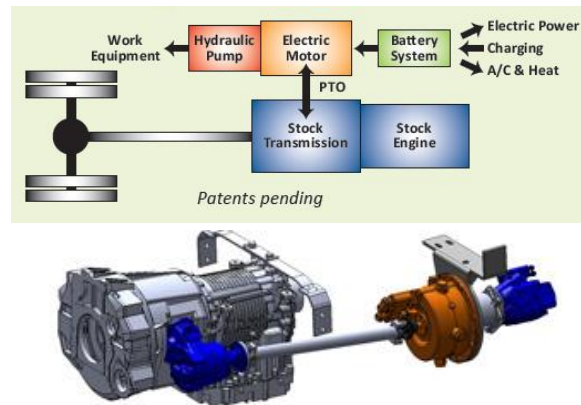


Figure IV-103: Odyne parallel hybrid architecture; compliments of www.odyne.com/

The system interfaces through the stock transmission's PTO port, which feeds power to a double-ended electric motor shaft attached to the PTO clutch on one side and the hydraulic pump on the other. The electric motor can be used to absorb or put energy back into the system for improved fuel economy when traveling to a jobsite. Once on site, the PTO clutch can be disengaged and the electric motor can drive the hydraulic work equipment, HVAC, and electric accessories without the need to idle the engine. Figure IV-104 shows two possible configurations for utility vehicles with the Odyne system installed.



Figure IV-104: Vocational vehicles with the Odyne plug-in hybrid EV system; complements of www.odyne.com/

Approach

Odyne has completed a number of vehicles and has started delivering them to final customers. Regular data uploads from Odyne to EPRI and from EPRI to NREL's FTP site are expected once these vehicles go into routine service. This is expected to start in FY 2015 and continue with increasing volume as more vehicles come online.

Results

This project is beginning in FY 2015.

Conclusions

This project is beginning in FY 2015.

Using ARRA Data in Support of Other DOE Efforts

The primary focus for the projects presented above has been on data collection, filtration, secure storage, and primary analysis for summary reporting. However, this data set has been used in support of other DOE efforts at NREL and will continue to be a valuable resource in the future. The vast amount of real-world operation in vocational duty cycles will continue to help aid the development of the next generation of hybrid and all-electric drive systems for medium- and heavy-duty vehicles. A few specific examples are highlighted below.

NREL and Frito-Lay North America are working together to better understand and quantify the current and potential benefits EVs may have on the Frito-Lay delivery fleet. At the Frito-Lay location in Federal Way, Washington, ten conventional diesel delivery vehicles were instrumented with on-board diagnostic data recorders to better understand the normal duty cycle. At the same time data from ten second-generation Smith EVs deployed at the same location were monitored for comparison. Figure IV-105 shows the daily driving distance and daily stops per mile from both sets of vehicles over the 3-week data collection period. Squares indicate an average for each vehicle over the whole period.

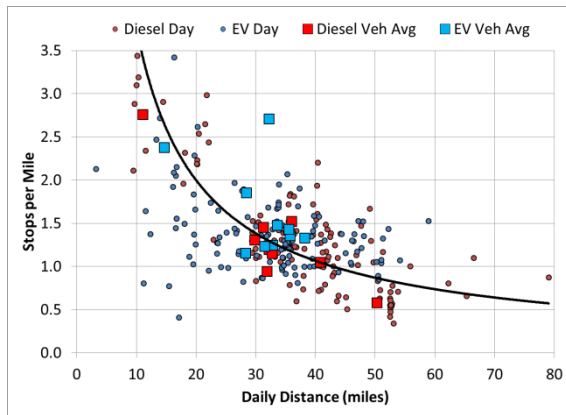


Figure IV-105: Frito-Lay delivery vehicle operation

The Smith EVs at this location are able to cover the same distance and types of routes as the conventional vehicles without sacrificing performance. Looking at the cost of operation, it was found that the diesel vehicles averaged \$0.54/mile in fuel costs as compared with the EVs, which only used an average of \$0.18/mile of electricity over similar routes, cutting the fuel cost to a third of the baseline. For more information, please refer to the FY 2014 Fleet Evaluation Milestone Report (NREL/MP-5400-62767).

The truck stop electrification data supplied by Shorepower Technologies provides booking times and energy use at 50 sites across the country. It has been used to explore the energy use requirements for other anti-idle technologies such as advanced auxiliary power units. Figure IV-106 shows a histogram of typical start and stop times along with average power use.

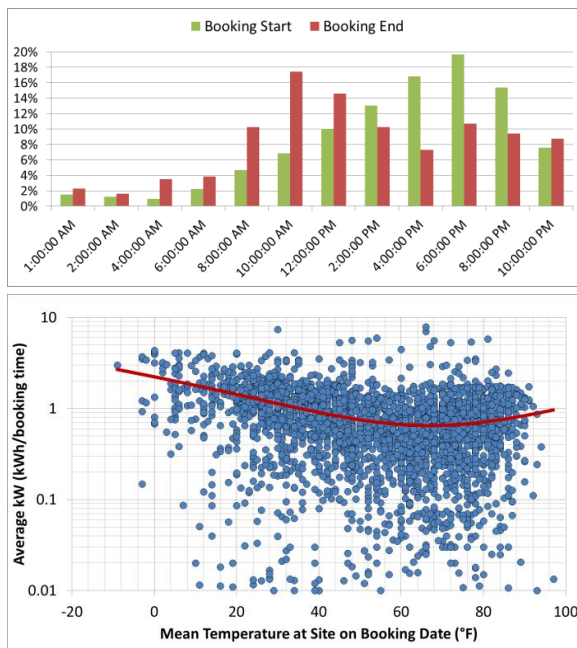


Figure IV-106: Typical truck stop booking start and stop times along with average power

The trend follows a typical truck stop nightly use of arriving in the late afternoon, spending the night, and disconnecting the following morning. The average power consumed as a function of ambient temperature shows the lowest demand when temperatures are mild and comfortable with increasing use in each direction for either heat or cooling demand as well as other accessories and appliances that may be onboard.

Finally, the ARRA data are also being used in an ongoing project looking at EV battery degradation. The data from Navistar and Smith EVs not only supply an excellent source of information on how the vehicle is being used, but also the conditions experienced by the battery. This project will monitor the behavior of these vehicles for a number of years with periodic battery capacity testing using a resistive load bank. Once a statistically significant amount of degradation has occurred, the 1-Hz battery data will be used to determine which factors are the largest contributors to early degradations. Figure IV-107 shows some examples of battery use statistics, including battery current coefficient of variance, root-mean-square current, net energy use, and minimum state of charge plotted against some basic drive cycle statistics such as kinetic intensity, driving average speed, and daily distance.

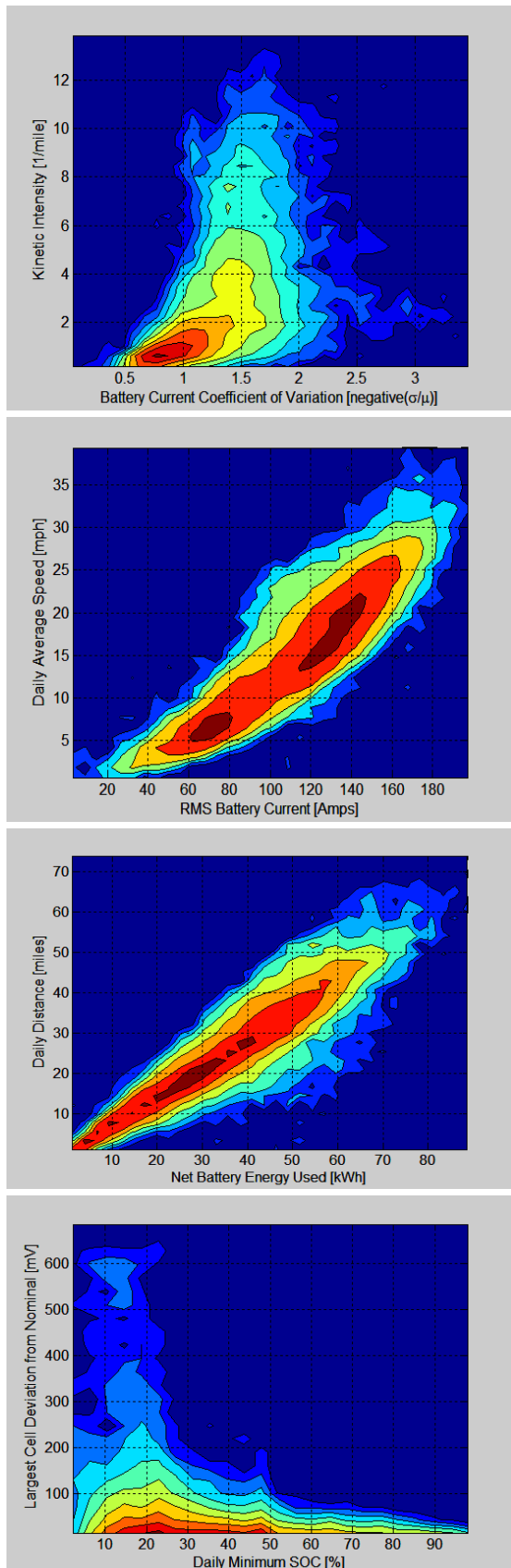


Figure IV-107: Second-generation Smith vehicle battery use

The goal of this analysis would be to develop a model that could help vehicle manufacturers and end users get the most out of their battery packs and early identification of bad cells so they can be replaced in a timely fashion before causing major problems. For more information, please refer to the FY 2014 Fleet Evaluation Report (NREL/MP-5400-62767).

Conclusions

Summary of Vehicle Data

- NREL is currently receiving usable data from 259 first-generation, and 200 second-generation Smith EVs (vehicles with data that can pass through the data filters to meet minimum usage requirements). NREL has also received data from 101 Navistar eStar vehicles through the end of June 2014. These are all battery electric delivery vehicles. The data received include over 25 parameters of 1-Hz data.
- The Smith Newton EVs have driven a total of 133,525 days, covering 3,404,958 miles, for an average of 25.5 miles per day.
- The Navistar eStar vehicles drove a total of 17,447 days, covering a combined 353,733 miles, for an average of 20.3 miles per day.
- The Shorepower Truck Electrification Project (STEP) has all 50 funded sites active with >90% uptime as of June 2014. A total of 53,979 hours booked and 41,029 kWh used were reported, offsetting an estimated 43,183 gallons of diesel fuel.
- As Odyne hybrid utility trucks come online, they will be incorporated into the automated processing and analysis routines for the ARRA project.

Reporting

- Recent quarterly and cumulative reports through June 2014 have been posted to the web for the Smith and Navistar projects. Example reports are shown below; these (and all reports) can be found at: www.nrel.gov/vehiclesandfuels/fleettest/
- Additional quarterly reports will continue to be added to the website beginning in October 2014 once all the September data are in, continuing the quarterly and cumulative report series. (see Figure IV-108).

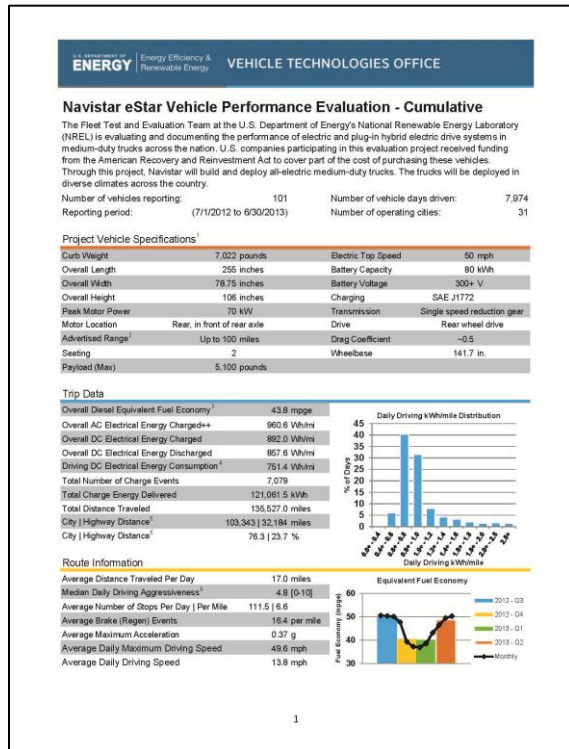


Figure IV-108: Sample cumulative report.

Publications

1. N/A

Tools and Data

1. N/A

IV.H. Commercial EV Battery Degradation Field Evaluation

Principal Investigator: Kenneth Kelly

National Renewable Energy Laboratory
15013 Denver West Parkway, MS 1633
Golden, CO 80401
Phone: (303) 275-4465
E-mail: Kenneth.Kelly@nrel.gov

DOE Program Manager: David Anderson

Phone: (202) 287-5688
E-mail: David.Anderson@ee.doe.gov

DOE Program Manager: Lee Slezak

Phone: (202) 586-2335
E-mail: Lee.Slezak@ee.doe.gov

- To date, the degradation analysis procedure has been applied to a small number of vehicle histories for which NREL's controlled degradation tests are available to validate the technique.
- Going forward, battery state of health will be estimated for the entire Smith ARRA data set through time and potentially be used to construct a life model of the pack based on in-use field data. Such a model would be of great value to fleet managers interested in pairing EVs with appropriate vocations in their fleet.



IV.H.2. Technical Discussion

Background

NREL's Fleet Test and Evaluation Team has found medium- and heavy-duty vehicle fleets to be good candidates for deploying low-emitting, advanced technologies due to their large numbers, high vehicle miles traveled—consequently high petroleum fuel consumption and emissions—and frequent operation in large population centers, as well as common return-to-base fueling regimes and consistent driving routes.

Previous testing and analysis conducted by NREL have illustrated the influence of drive cycle and vehicle usage on both energy consumption (from liquid fuels and high-voltage hybrid battery packs) and exhaust (or well-to-wheels) emissions. Drive cycle has also been shown to influence the all-electric range of battery electric vehicles (EVs), the charge depleting range of plug-in hybrid electric vehicles (PHEVs), and the potential fuel economy benefit of hybrid EVs. Accordingly, fleet customers can benefit from a further understanding of advanced vehicle technology deployment to minimize fuel consumption and emissions. It has also been shown that large-scale deployments of EVs in a localized area can lead to power quality and power cost issues.

Introduction

NREL is currently funded by the DOE to collect operational data on Smith Electric Vehicles (Smith) being deployed as part of the American Recovery and Reinvestment Act (ARRA). Data collected from these vehicles (up to 500, some of which are located at Frito-Lay North America [FLNA] facilities) will be used to understand the overall usage and effectiveness of EVs in medium-duty commercial fleet facilities and operations and also compare to operations of conventional counterparts in the same location. Through this collaboration with FLNA, NREL hopes to provide a more focused investigation to understand the implementation and performance of medium-duty EVs in a large-scale commercial facility.

IV.H.1. Abstract

Objectives

The lack of validated field data needed to predict battery life is a barrier to adoption of commercial EDVs. NREL has developed and will implement a field testing approach in an ongoing battery and drive cycle field data collection effort with Frito Lay, working with the DOE VTO Energy Storage team to build life cycle prediction capabilities for advanced transportation batteries. FY 2014 objectives included:

- Develop a protocol to acquire field data on battery life degradation and assess battery health as a factor of usage and drive cycles and share data with DOE VTO Energy Storage team to simulate battery degradation in a vehicle.
- Conduct first round of testing on Smith EVs at Frito-Lay locations with varying climates.

Major Accomplishments

- NREL validated proper operation of the test and test equipment at Smith's U.S. headquarters in Kansas City, Missouri.
- Initial battery degradation testing and preliminary analysis were conducted on 9 Smith EVs at four Frito-Lay fleet locations across the country.
- A second round of tests were conducted at Casa Grande, Arizona, and Federal Way, Washington.
- Data from the testing has undergone preliminary analysis and presented to engineers at Smith.

Future Achievements

- Battery degradation testing is currently planned to continue every six months on eight Smith EVs at 4 Frito-Lay locations throughout FY 2015 and into FY 2016.

Battery lifetime uncertainty is a major barrier to fleet manager decisions regarding the adoption of PEVs. To reduce life uncertainty, NREL, Smith, and FLNA have developed a study to perform benchmarking tests of EV batteries at regular stages throughout their life.

Approach

Battery degradation testing is currently planned to continue every six months on eight Smith Electric vehicles throughout FY 2015 and into FY 2016. To date, the degradation analysis procedure has been applied to a small number of vehicle histories for which NREL’s controlled degradation tests are available to validate the technique. Going forward, battery state of health will be estimated for the entire Smith ARRA data set through time and potentially be used to construct a life model of the pack based on in-use field data. Such a model would be of great value to fleet managers interested in pairing EVs with appropriate vocations in their fleet.

The benchmarking test results provide ground truth data that support a larger battery health trending analysis of the ARRA telemetry data set. These methods will allow NREL to quantify battery pack health and track battery performance changes over life as well as validate battery life assumptions (as envisioned in Figure IV-109) to help develop a fleet business case.

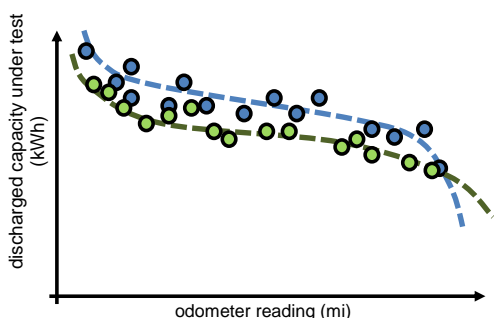


Figure IV-109 Intended data collection—collecting several points over a period of years will help to validate life models

Results

The benchmarking tests are being performed onsite at four FLNA fleet depot locations with a total of eight Smith Gen 2 trucks. Smith’s Gen 2 vehicles that Frito-Lay purchases are box trucks with two 40-kWh A123 battery pods (80 kWh total). Table IV-14 contains a list of vehicles tested.

Table IV-14: Smith EV Subjects of Battery Degradation Testing

| Location | Vehicle ID | Test Date | Average Temperature (deg C) |
|------------------|------------|-----------|-----------------------------|
| Kansas City | FE110 | 6/13/13 | 29 |
| Casa Grande, AZ | R175 | 9/11/13 | 31 |
| | | 5/6/14 | 28 |
| | R176 | 9/10/13 | 28 |
| | | 5/7/14 | 26 |
| Federal Way, WA | E123 | 9/24/13 | 18 |
| | | 4/16/14 | 21 |
| | E124 | 9/25/13 | 21 |
| | | 4/15/14 | 21 |
| Clifton Park, NY | E144 | 6/3/14 | 28 |
| | E148 | 6/4/14 | 25 |
| Manteca, CA | E157 | 6/18/14 | 28 |
| | E159 | 6/17/14 | 25 |

In 2013, NREL and Smith developed a test to perform a controlled discharge of Smith EV batteries in-situ, without removing them from the truck. NREL ships test equipment to each fleet location prior to an NREL visit, including a 14.5-kW programmable DC load bank and data recording and electrical interface boxes. Prior to the test, the truck is fully charged overnight using the normal charge protocol. NREL test engineers electrically disconnect the battery from the truck and route the electrical leads through the test equipment. The test equipment discharges the battery at a C/6 rate, with periodic rests to measure open circuit voltage and resistance. The data are recorded both from the vehicle CAN and using an independent data-logger. Following the six-hour discharge, the truck is returned to its original condition and placed on charge to resume normal service the following day. This one-day test is minimally invasive to fleet operations.

NREL validated proper operation of the test and test equipment at Smith’s U.S. headquarters in Kansas City, Missouri, in 2013 (see Figure IV-110). Data were collected at Smith headquarters on this new truck to act as a benchmark for beginning-of-life performance of Smith EV packs. During September 2013, the load bank was shipped to FLNA’s Arizona and Washington facilities, documenting battery performance for four trucks that entered service the same year. In the spring of 2014, NREL returned to the Arizona and Washington sites for follow-up testing of the same four trucks. NREL also traveled to two additional locations, Clifton Park, New York, and Manteca, California. The total number of vehicles under test is presently eight.



Figure IV-110: Load test conducted at Casa Grande, AZ (NREL PIX 29613)

Given that these vehicles are operating in their native FLNA environment, it is expected that a minimum of three years of testing may be required to discern any actionable trends in degradation from the eight vehicles under test. NREL has strong support from Smith EV and FLNA to continue the testing for several years. Each test takes less than one day per truck and is conducted without removing the battery pack from the truck. A successful outcome of the project is targeted to be the dissemination of credible, multi-year battery performance data to support increased adoption of EVs in commercial fleets.

Conclusions

At this point, results are still preliminary because all vehicles tested have relatively low mileage (6,000 to 15,000 miles) and any variations measured in capacity are still within the error margins of NREL's test equipment. Data will be presented as more data points are collected in the coming years, averaging out any errors.

Battery duty cycles harvested from large data sets of in-use operation provide an excellent opportunity to monitor and better understand the real-world aging process in EV battery packs. For this effort, the ARRA Smith EV data set is being used to identify combinations of drive cycles and climates that result in accelerated degradation.

Time series histories of pack current and voltage are applied to an electrical model of the pack that considers zero order current-resistance dynamics and a single-particle model of electrode concentration gradients (used to describe transient voltage relaxation). Modeled pack voltage is compared to the historical data, and a constrained non-linear optimization algorithm is used to minimize the root mean square of model error (usually achieving root mean square of model error values of tens of millivolts per cell). See Figure IV-111 for an example of the analysis.

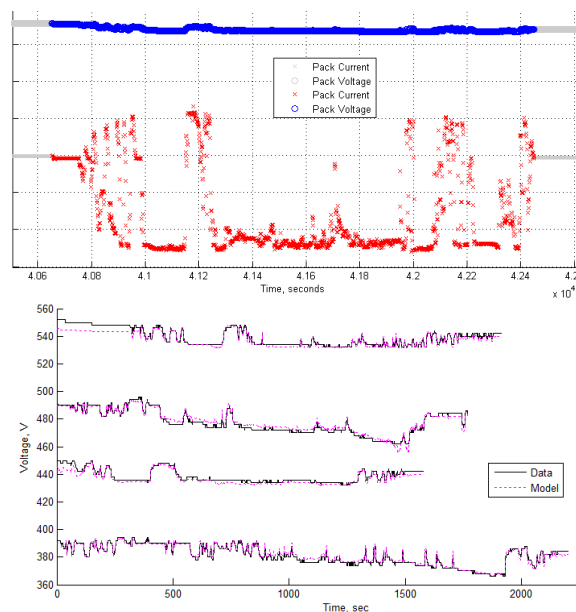


Figure IV-111: Example of sample drive cycle data from the ARRA Smith data collection project (top) used to generate models fit to a root-mean-square error of less than 6% open circuit voltage (bottom); voltages of four EVs skewed to protect intellectual property

Error is minimized by updating model parameters such as pack capacity, bulk resistance, initial thermodynamic state of charge, and multiple diffusion coefficients. Following optimization of the model over each individual drive cycle, estimated parameters used to describe pack available energy and power are reported through time and compared to controlled performance tests conducted by NREL engineers in the field.

IV.H.3. Products

Publications

Only initial data has been collected to date. No publications have been produced at this time.

IV.I. Long-Haul Truck Thermal Load and Idle Reduction

Principal Investigator: Jason A. Lustbader

National Renewable Energy Laboratory
15013 Denver West Parkway
Golden, CO 80401
Phone: (303) 275-4443
E-mail: Jason.Lustbader@nrel.gov

DOE Program Manager: David Anderson

Phone: (202) 287-5688
E-mail: David.Anderson@ee.doe.gov

DOE Program Manager: Lee Slezak

Phone: (202) 586-2335
E-mail: Lee.Slezak@ee.doe.gov

Future Achievements

- Estimate fuel use for complete-cab thermal design concepts for technologies that are selected from the conductive pathways, solar envelope, occupant environment, and efficient equipment technical focus areas.
- Develop and refine test methods to improve the direct quantification of cab heating and cooling thermal energy demands.
- Combine experimental results and analysis tools to quantify fuel use and payback period of complete-cab solutions across national weather conditions and usage patterns.



IV.I.1. Abstract

Objectives

- Demonstrate a 30% or greater reduction in long-haul truck idle climate control loads with a three-year or better payback period by 2015.
- Minimize long-haul truck rest period idling by working with industry partners to develop and apply commercially viable climate control solutions.
- Develop technologies that will help reduce the estimated 667 million gallons of fuel used annually for rest-period idling to increase national energy security and sustainability.

Major Accomplishments

- Demonstrated a complete-cab solution for rest-period idling, measuring a greater than 35.7% reduction in daily air conditioning (A/C) system energy using an ultra-white paint, a cab insulation package, and advanced curtains and shades developed by NREL.
- Measured the impact of ultra-white paint and a cab insulation package with varying curtain and shade configurations.
 - Measured an 11.6% reduction in daily A/C system energy when curtains and shades were removed.
 - Measured a 21.1% reduction when baseline stock curtains and shades were used.
- Obtained 53.9% of the maximum possible reduction in rise over ambient temperature by rotating a truck from solar-south facing to solar-north facing.
- Demonstrated the effect of an infrared reflective glazing film for soak conditions, obtaining a 22.3% reduction in rise over ambient temperature.

IV.I.2. Technical Discussion

Background

Cab climate conditioning is one of the primary reasons for operating the main engine in a long-haul truck during driver rest periods. In the United States, long-haul trucks (trucks that travel more than 500 miles per day) use approximately 667 million gallons of fuel annually for rest period idling [1]. This rest period idling is approximately 6.8% of the total long-haul truck fuel use and represents a zero freight efficiency operating condition for the truck. With the recent high prices of diesel, fuel is one of the largest trucking costs per mile, at 35% of the total [2]; therefore, the increasing cost and cost volatility of fuel provides a significant financial incentive to reduce fuel use. Recent federal, state, and city anti-idling regulations [3] are providing further incentives to reduce truck idling. One example is the idle reduction technology credit in the Heavy-Duty Greenhouse Gas Emissions Standards, which are set to begin in 2014 [4].

An opportunity exists to reduce fuel use and emissions associated with idling by reducing thermal loads and improving the efficiency of climate control systems. Enhancing the thermal performance of cab/sleepers will enable smaller, lighter, and more cost-effective idle reduction solutions. In addition, if the fuel savings from new technologies provide a one- to three-year payback period [5], fleet owners will be economically motivated to incorporate the new technologies. Therefore, financial incentives provide a pathway to rapid adoption of effective thermal load and idle reduction solutions.

Introduction

The U.S. Department of Energy's National Renewable Energy Laboratory's (NREL's) CoolCab project is researching efficient thermal management systems to maintain cab occupant comfort without the need for engine idling. The CoolCab project uses a system-level approach that addresses thermal loads, designs for occupant thermal comfort, and maximizes equipment efficiency. To advance the goals of the CoolCab project and the broader goals of increased national energy security and sustainability, the CoolCab team works closely with industry partners to develop and apply commercially viable solutions to reduce national fuel use and industry costs. To reduce thermal and resulting idle loads in long-haul trucks, NREL has identified conductive pathways, the solar envelope, the occupant environment, and efficient equipment as focus areas for potential thermal load reduction technologies. Working closely with industry partners, NREL applied modeling tools and experimental methods to identify and evaluate promising complete-cab heating, ventilating, and air conditioning (HVAC) load reduction solutions comprised of technologies in each of these focus areas. The goal of the complete-cab solutions was to exceed the project's 30% A/C load reduction goal.

Approach

NREL collaborates with original equipment manufacturers (OEMs) and suppliers to develop and implement a strategic approach capable of producing commercially viable solutions to enable idle reduction systems. NREL first conducts baseline testing of vehicles to quantify their thermal behavior. This information is then used to build and validate CoolCalc and other models. CoolCalc is NREL's rapid HVAC load estimation tool [6]. It is described in the CoolCalc section of this FY 2014 annual report. When used in conjunction with experimental screening tests, these models are used to identify promising thermal load reduction technologies. The most promising technologies are then experimentally evaluated for their impact on climate control loads. Experimental results are also used to inform model improvement as needed and gain further confidence in the models. The validated models are then used to understand the impact of the climate control load reduction technologies at the national level on thermal performance, climate control loads, and fuel consumption, spanning the wide range of use and environmental conditions that occur in the United States.

Technology Focus Areas

NREL has identified four key climate control load technology focus areas: conductive pathways, the solar envelope, occupant environment, and efficient equipment. The first three of these technologies impact the cab heat transfer and resulting thermal loads and are the focus of this paper. In contrast, the efficient equipment focus area translates the thermal loads into mechanical or electrical loads. Explanation of the four technical focus areas is provided below.

- The conductive pathways focus area addresses the heat transfer through walls and other surfaces of the cab/sleeper. While heat transfer for this focus area is largely conduction through solid bodies, it also includes convection and radiation through air gaps in the composite wall and glass structures of the cab. Technologies in this area include insulation, advanced materials, and glass.
- The solar envelope describes the interaction of surfaces with radiant energy from the sun and surrounding environment. It is predominantly driven by radiant heat transfer and is most relevant during daytime operation; however, nighttime radiation to the sky is also included. This focus area includes opaque and transparent surface properties of paints and glass, respectively. It also includes devices to modify these properties, such as window shades.
- The occupant environment includes the volume of conditioned air, occupant heat exchange with the surroundings, and human factors such as thermal sensation/comfort. Designing the thermal environment to make every occupant comfortable rather than to meet the traditional temperature based metric has a significant impact on design. Technologies in this area include sleeper curtains and microenvironmental control.
- Efficient equipment impacts the conversion of thermal loads to mechanical, electrical, or chemical loads. A range of technology options and design considerations can fall into this category. These include battery electric A/C, fuel fired heaters, and auxiliary power units. For the purposes of this study, battery electric idle-off systems were used; however, the idle thermal load reduction technologies applied to the cab/sleeper are largely independent of the equipment used.

Experimental Test Setup

The test program was conducted at NREL's Vehicle Testing and Integration Facility, shown in Figure IV-112, during the months of May through September. The facility is located in Golden, Colorado, at an elevation of 5,997 feet at latitude 39.7 N and longitude 105.1 W. The experimental setup included an NREL-owned test truck, a current model Volvo control truck, and two cab test "bucks." Both bucks were the cab section from a representative truck in current production provided by Volvo Trucks North America. One buck was utilized as the control buck; while the other was modified.

For the experimental setup, the test truck, control truck, test buck, and control buck were oriented facing solar south and separated by a distance of 25 feet to maximize solar loading and minimize shadowing effects. To keep the buck firewalls from receiving direct solar loads, a firewall shade cloth was implemented on both the control and test bucks. In each vehicle, the sleeper curtain and four shades were available for use, depending on the test being conducted. The shades available were the front privacy, cab skylight, and two bunk window curtains.



Figure IV-112: NREL's vehicle testing and integration facility

A National Instruments SCXI data acquisition system was used to record measurements at a sampling frequency of 1.0 Hz, which was averaged over 1-minute intervals. Among the four vehicles, more than 200 calibrated type K thermocouples were utilized. An isothermal bath and reference probe were used for thermocouple calibration, achieving a U95 uncertainty of $\pm 0.32^\circ\text{C}$ in accordance with American Society of Mechanical Engineers standards [7]. Air temperature sensors were equipped with a double concentric cylindrical radiation shield to prevent errors due to direct solar radiation.

Weather data were collected from both NREL's Solar Radiation Research Laboratory and NREL's Vehicle Testing and Integration Facility [8] weather station, which together feature more than 160 instruments dedicated to high-quality measurements of solar radiation and other meteorological parameters.

Thermal soak tests were conducted to evaluate the impact of technologies in an engine-off solar loading condition. This test procedure was used to characterize technology impacts on interior air temperatures in a test vehicle ($\bar{T}_{\text{modified}}$) compared to interior air temperatures in the baseline vehicle ($\bar{T}_{\text{baseline}}$). During summer operation with passive vehicle thermal load reduction technologies, the best possible steady-state performance is to reduce the interior temperature to ambient temperature. The percent of maximum possible temperature reduction (β) was developed to describe this maximum possible reduction in interior air temperature rise above ambient (\bar{T}_{ambient}), as described in Equation 1. A β value of 0% indicates that the technology under evaluation did not change the rise over ambient temperature; whereas a β value of 100% indicates that the technology reduced the interior air temperature in the modified vehicle to equal the temperature of ambient air in the environment.

Equation 1: Percent of maximum possible temperature reduction:

$$\beta = \frac{\bar{T}_{\text{baseline}} - \bar{T}_{\text{modified}}}{\bar{T}_{\text{baseline}} - \bar{T}_{\text{ambient}}} \cdot 100\%$$

To evaluate β , the interior air temperature was determined as a volume weighted average of the combined sleeper and cab air temperatures. The average interior cab air temperature was calculated by averaging six type K thermocouples with four located in accordance with the American Trucking Association Technology Maintenance Council's recommended practice RP422A [9], as shown in Figure IV-113A. Similarly, average sleeper air temperature was calculated by averaging eight type K thermocouples with six located in accordance with RP422A, illustrated in Figure IV-113B. The addition of two thermocouples located in both the cab and sleeper air spaces improved the average air temperature measurement by more accurately capturing the air temperature distribution. During testing, it was determined that the two temperature measurements made in the cab footwell air space were exposed to occasional direct solar radiation. Due to the increased variability that would occur in the calculation of average interior air temperature, these two measurements were omitted from the calculation.

For the thermal soak measurements, the sleeper curtain and all privacy shades were removed. The thermal soak performance of the vehicles in their baseline conditions were used to characterize and calibrate the inherent differences between the control buck and test vehicle. Calibration was accomplished by collecting two days of baseline data and generating a time-of-day dependent correction factor between the control and test vehicles. Solar load intensity peaked at approximately 12:00 p.m. MST daily during thermal soak testing. In addition, peak differential temperatures were found to occur within the 11:00 a.m. to 1:00 p.m. MST time interval corresponding to this peak solar load. Therefore, interior air and ambient temperatures from 11:00 a.m. to 1:00 p.m. MST were used for the calculation of β .

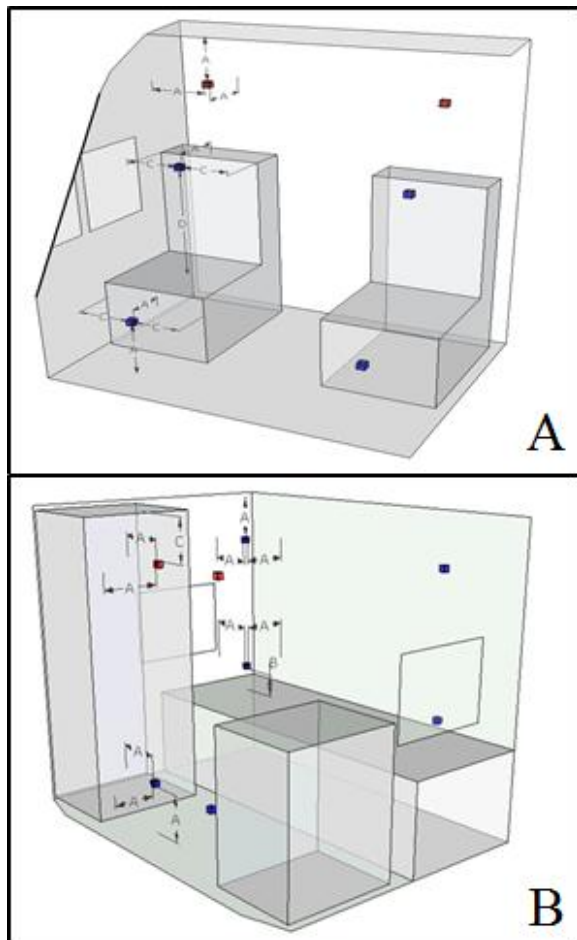


Figure IV-113. (A) Cab and (B) sleeper thermocouple locations. Dimensions: A = 12", B = 6", C = 18". Blue: TMC standard [5]; red: NREL added

For quantifying A/C system load reductions, NREL collaborated with Volvo Trucks North America, PPG Industries, and Aearo Technologies LLC, a 3M Company. Daytime rest period A/C tests were conducted to characterize thermal management technology impacts on an electric no-idle A/C system. A 2,050 W (7,000 Btu/hr) electric A/C system provided by Dometic Environmental Corporation [10] was installed in the sleeper compartment of each vehicle. For A/C experimentation, unless noted otherwise, the sleeper curtain and all four shades were utilized on the vehicles. All curtains and shades were employed to match the expected standard configuration during a rest period operation. The test period was defined as A/C system first on to last off to quantify the daily A/C energy consumption.

A/C electrical power consumption was measured using a Load Controls Incorporated model UPC adjustable capacity power sensor. The power sensor was calibrated to ± 15 W. A/C systems were controlled to a target sleeper air temperature of 22.2°C (72°F). Calibration of the modified vehicle A/C system was performed by collecting multiple days of baseline data. To determine a "High Solar Test Day," the daily clearness index

exceeded 0.525. The daily clearness index was calculated as the daily total ratio of direct normal irradiance to extraterrestrial direct normal irradiance. Due to limited high solar test days, the test procedure was expanded when appropriate to accommodate lower clearness index days. The expanded range of weather is expected to provide a conservative quantification of technologies compared to days with a high clearness index.

Technology Identification

For FY 2014, a test plan was developed based on prior experimental screening of individual technologies and CoolCalc modeling of combined packages to identify a complete-cab package for rest-period load reduction. To determine a complete-cab package, prior work at NREL identified insulation, paint color, and privacy curtains as promising technologies. Prior work on insulation has shown significant reductions in both cooling and heating tests compared to a baseline insulation package [11]. In addition, paint color has shown reductions in daily A/C load for black to white paint and blue to solar reflective blue paint [12]. An idealized sleeper curtain test identified advanced curtains as a candidate technology for A/C load reduction [13]. In addition, an idealized white film test identified advanced privacy shades as a promising technology [13].

To estimate the impact of the proposed complete-cab solution on cooling and heating thermal loads at the national level, CoolCalc modeling was performed using an Analysis of Variance (ANOVA) method to determine the contributions of each technology and their interaction effects for load reduction. The results of the ANOVA study suggested that the combination of insulation, paint, and advanced curtains and shades provide a complete package for A/C load reduction that exceeds 30% at the national level.

To quantify the impact of paint color for the complete-cab solution, an analysis was performed to estimate the national average solar-color paint. For this study, the national average solar-color paint is defined as a paint color with radiative properties that match that of the theoretical count weighted average of paint colors throughout the United States for long-haul trucks. For this analysis, truck stops were randomly selected throughout the country, and Google satellite images of the truck stops were collected. Color groupings were defined based on identifying colors that had similar radiative properties. Next, long-haul trucks for each color category were counted at each truck stop location using the satellite images. The percent of each color category was determined after classifying more than 2,600 trucks. The cumulative totals of each color category with the addition of incremental truck stop data is shown in Figure IV-114. Using the CoolColors database developed at Lawrence Berkeley National Laboratory [14], average radiative properties for each color group were calculated, and a national average solar-color was determined. Through collaboration with PPG Industries, a heavy-duty truck paint color was experimentally identified with radiative properties that matched that of the national average solar-color. This national average solar-color paint was used for experimental quantification of the baseline paint configuration.

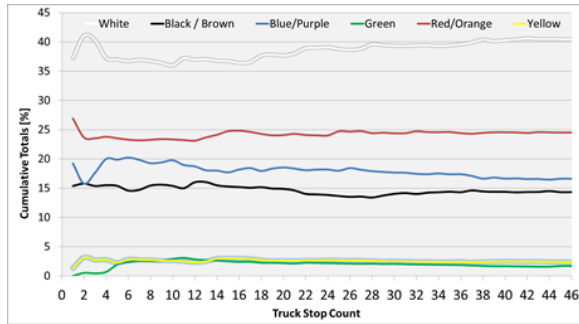


Figure IV-114. Cumulative totals of long-haul truck paint colors for the incremental addition of truck stop data

In addition to the complete-cab solution analysis, CoolCalc screening identified vehicle rotational orientation as a promising strategy for A/C load reduction and provided motivation for experimental evaluation.

Results

Baseline Testing

For the complete-cab solution experimental evaluation, an A/C system calibration was completed for the test and control trucks using the baseline configuration for the test buck, which consisted of the national average solar-color for paint, the standard OEM insulation package, and standard sleeper and privacy curtains. The calibration data for the complete-cab solution A/C baseline is shown in Figure IV-115. The figure contains daily A/C baseline data for both variable weather test days and high solar test days that exceeded the daily clearness index of 0.525. Due to the limited number of high solar test days, the entire data set was used for baseline calibration and shows a strong linear correlation with a coefficient of determination (R^2) of 0.983.

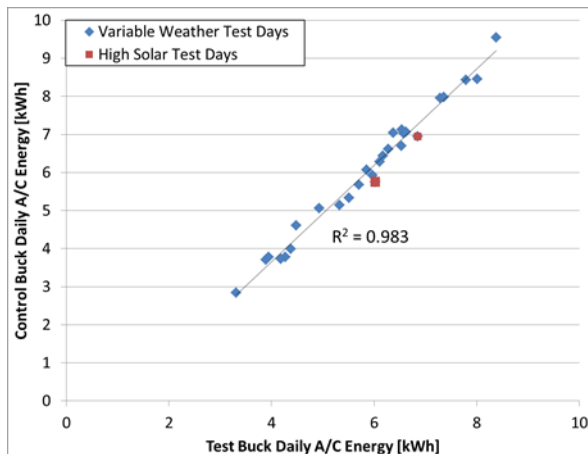


Figure IV-115. Daily A/C energy calibration data for test and control bucks

The linear trend line shown in Figure IV-116 was used to calculate a calibration curve for the baseline test buck daily A/C energy for a given test day.

To evaluate advanced glazings on solar soak performance, a time-of-day dependent soak calibration curve was created between the test truck and control truck. An average of two days of data was used for the calculation of the soak calibration curve. Prior to the calibration correction, the average interior air temperatures between the trucks varied by as much as 5.75°C. After calibration, the test truck and calibrated control truck agreed well, as shown in the calibration check day in Figure IV-116. For the check day, although scattered clouds were present, the test truck and calibrated control truck agreed to within 0.2°C during the 11:00 p.m. to 1:00 p.m. MST peak solar loading time interval.

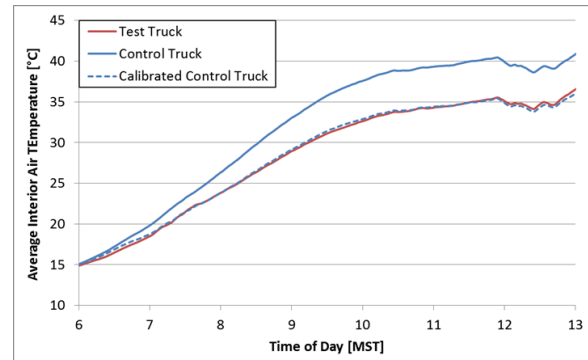


Figure IV-116. Average interior air temperature for solar soak calibration check day

Solar Envelope Technology Evaluations

In the United States, a south-facing truck rotational orientation is expected to have the highest A/C loads because of the exposure of the glazings to the sun. Preliminary investigation of the impact of rotation of a truck on cooling and heating thermal loads was investigated using CoolCalc. The CoolCalc results showed a 24.4% reduction in mean cumulative cooling degree-days from south to north vehicle orientation. The CoolCalc results prompted additional experimental evaluation.

To quantify the impact of rotation experimentally, the test truck was rotated to a north-facing orientation and compared to the baseline south-facing orientation. For the tests, three days with a clearness index greater than 0.525 from sunrise to 1:00 p.m. MST were used to calculate an average maximum possible reduction in rise over ambient temperature of 53.9%. The comparison between average interior air temperatures for north- and south-facing truck orientations for September 13, 2014, in Golden, Colorado, is shown in Figure IV-117. The results confirm a significant impact of vehicle rotation on average interior air temperatures.

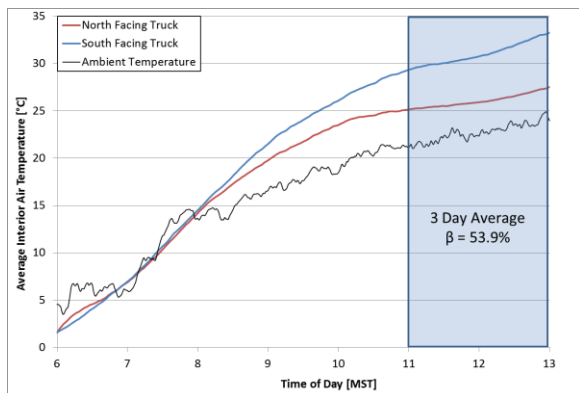


Figure IV-117. Effect of vehicle rotation on average interior air temperature—single-day temperatures with three-day average beta

A comparison between experimental and model results for the impact of rotational orientation on β is shown in Figure IV-118. For this figure, annual Golden typical meteorological year weather conditions were used as input to a validated buck model, and beta was calculated as described in the approach section. Model results were plotted for days when the clearness index exceeded the 0.525 threshold. Experimental results are those obtained from the test truck. Although the CoolCalc model and the experimental truck are different truck models and different shades of white, it is believed that the trend in β shown in Figure IV-118 is a good indicator of agreement. The reduction in β for summer conditions is due to the sensitivity of rotational orientation on solar loading and insensitivity to ambient temperature. During the winter, thermal cooling loads are driven mostly by solar loads; whereas both ambient temperature and solar loads contribute to the overall thermal cooling loads in the summer.

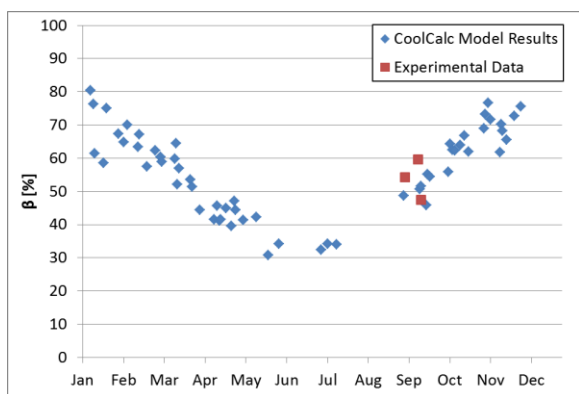


Figure IV-118. Experimental and model results for maximum possible reduction in rise over ambient temperature of a north-facing truck compared to a south-facing truck

To explore the effect of an advanced infrared reflective glazing technology on soak conditions, a glazing film was supplied by Eastman and applied to the exterior surface of all glazings on the test truck. The effect of the glazing film on the average interior air temperature is shown in Figure IV-119. For the experiment, a 22.3% reduction in rise over ambient

temperature was obtained. The reduction in rise over ambient temperature indicates that an advanced infrared reflective glazing could provide a significant benefit as a load reduction technology. Additional testing will be pursued to quantify the impact of the technology on cooling and heating thermal loads.

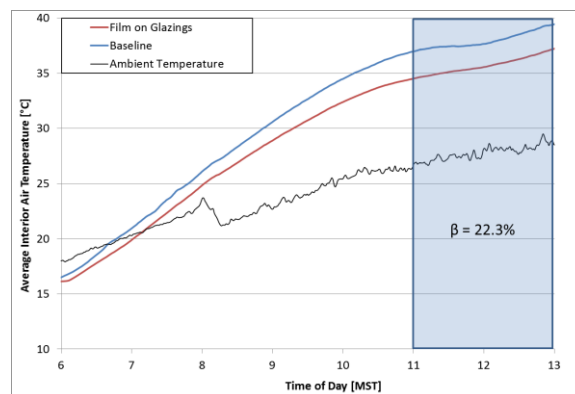


Figure IV-119. Effect of glazing film on average interior air temperature

Complete Cab Solution Evaluation

To quantify the impact of a complete-cab solution on rest-period load reduction, the test buck was painted an “ultra-white” color provided by PPG Industries, advanced privacy shades and sleeper curtains designed by NREL were installed, and a truck insulation package provided by Aearo Technologies was installed. A comparison between the complete-cab solution and baseline configurations are provided in Table IV-15. The determination of these technologies through modeling and their prior individual evaluation are discussed in the approach section and in the CoolCalc sections of the report.

Table IV-15: Technology Configurations for Baseline and Complete-Cab Package Experimental Evaluations

| | Baseline | Complete-Cab Package |
|-------------------|------------------------------|----------------------|
| Paint | National Average Solar-Color | Ultra-White |
| Curtains | Stock OEM | Advanced |
| Insulation | Stock OEM | Advanced Package |

For the complete-cab evaluation, daily A/C energy was quantified under a range of environmental conditions. The percent reduction in daily A/C energy was calculated for the complete-cab solution configuration in comparison to the baseline configuration. A plot of the percent improvement in daily A/C energy for the complete-cab solution for varying daily loads is shown in Figure IV-120. For the days tested, an improvement of at least 35.7% was obtained for the complete-cab solution. Figure IV-120 shows an increase in the percent improvement for the complete-cab solution as daily A/C energy decreased. This trend is due to seasonal variation in the results, and as the daily A/C energy was reduced for the

baseline condition, the percent improvement was expected to approach 100%. The percent improvement trend was consistent with modeling results and is expected to level out at high load conditions. The trend in the final two high load data points in the figure suggest that the improvement measured is expected to be consistent with additional increases in daily load.

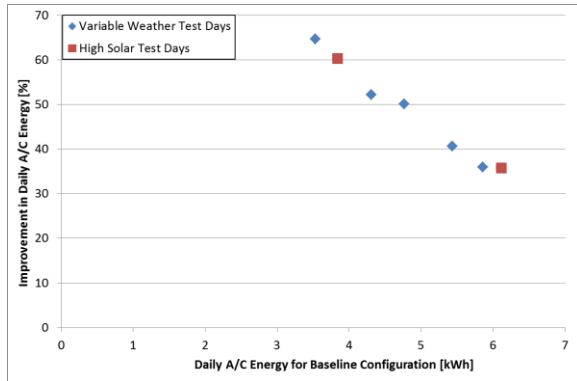


Figure IV-120. Percent improvement in daily A/C energy for the complete-cab solution for varying A/C loads and weather conditions

In addition to the complete-cab solution, the combined impact of ultra-white paint and the advanced insulation package was evaluated with both the stock OEM curtains and a configuration without curtains. For the configuration with stock OEM curtains, a three-day average was used for percent improvement over baseline. For the configuration without curtains, one day of data was collected. All test days for the comparison had a daily clearness index greater than 0.525. The effect of advanced, stock, and no curtain configurations on improvement in daily A/C load with ultra-white paint and advanced insulation is shown in Table IV-16. The results indicate that ultra-white paint and insulation combined with stock curtains provide a 21.1% improvement over baseline conditions. In addition, ultra-white paint and insulation are effective even when curtains are not used, showing an 11.6% improvement over the baseline. Finally, the results indicate that a significant improvement is obtained from the advanced curtains themselves over stock OEM curtains in the complete-cab solution, with a change in percent improvement from 21.1% to 35.7%.

Table IV-16. Percent Improvement in Daily A/C Load for Varying Curtain Configurations Combined With Ultra-White Paint and Advanced Insulation Package

| Curtain Configuration | Improvement [%] |
|--------------------------|-----------------|
| Advanced Curtains | 35.7% |
| Stock OEM | 21.1% |
| No Curtains | 11.6% |

Conclusions

Through the implementation of a complete-cab package of technologies, long-haul truck daytime rest period A/C electrical energy consumption was reduced by at least 35.7% for Colorado summer environmental conditions. The complete-cab package was composed of advanced privacy and sleeper curtains designed by NREL, an advanced insulation package provided by Aearo Technologies, and an ultra-white paint provided by PPG Industries. For the ultra-white paint and advanced insulation package, a 21.1% reduction in daily A/C electrical energy was measured when using stock curtains. Finally, an ultra-white paint and advanced insulation package with no curtains had an 11.6% reduction compared to the baseline with stock curtains.

The complete-cab experimental results obtained exceed the CoolCab goal of a 30% reduction in long-haul truck rest-period A/C loads. The technologies implemented for the complete-cab solution were determined from previous individual technology outdoor testing and national-level CoolCalc modeling. Future work is planned to quantify further technology improvements and measure the impacts on heating. These combined technologies will then be evaluated for national-level fuel use reductions and payback period estimations.

In addition to the complete-cab solution, technologies in the solar envelope focus area were screened for further study. An initial national-level CoolCalc simulation showed a 26.3% reduction in mean cumulative cooling degree days from south to north vehicle rotation. Follow-on experimental testing measured a 53.9% of maximum possible reduction in rise over ambient temperature when rotating a truck from south- to north-facing in Colorado solar soak conditions. The reduction obtained indicates that vehicle orientation could significantly reduce cooling thermal loads and represents a no-cost decision with immediate payback. Future work is planned to quantify the impact of vehicle rotational orientation on national-level fuel use for both cooling and heating conditions.

A second technology in the solar envelope focus area was evaluated experimentally. Through partnership with Eastman, an advanced infrared reflective glazing technology was investigated through the application of a glazing film to simulate the effect of the glazing technology. The results showed 22.3% of maximum possible reduction in rise over ambient temperature for Colorado solar soak conditions. This reduction identifies the advanced infrared glazing technology as a future candidate technology for idle load reduction opportunities.

By working closely with industry partners, further developing both experimental and modeling capabilities, and applying these capabilities, NREL has identified significant reduction opportunities in long-haul truck rest-period climate control loads. Implementing these technologies can improve the payback period of idle reduction systems by reducing their required capacity and therefore cost, volume, and weight. Identifying and quantifying payback periods of promising technologies reduces the risk of adoption for OEMs and fleet owners and operators and provides economic motivation for technology adoption. Improving current idle reduction technologies and providing new technologies will help to reduce the 667 million gallons used annually for long-haul truck rest period idling in the United States.

References

- Gaines, L.; Vyas, A.; Anderson, J. "Estimation of Fuel Use by Idling Commercial Trucks." 85th Annual Meeting of the Transportation Research Board, Washington, D.C., Jan. 22–26, 2006; Paper No. 06-2567.
- Fender, K.; Pierce, D. "ATRI Operational Costs of Trucking 2012." Atlanta, GA: American Transportation Research Institute, 2012.
- "Greenhouse Gas Emissions Standards and Fuel Efficiency Standards for Medium- and Heavy-Duty Engines and Vehicles, Final Rule." Federal Register 76 (15 September, 2011): 57106-57513.
- "Idling Regulations Compendium, American Transportation Research Institute." Accessed September 16, 2013: atri-online.org/2013/02/20/idling-regulations-compendium/.
- Roeth, M.; Kircher, D.; Smith, J.; Swim, R. "Barriers to the Increased Adoption of Fuel Efficiency Technologies in the North American On-Road Freight Sector." Report for the International Council for Clean Transportation. NACFE. July 2013.
- Lustbader, J.; Rugh, J.; Rister, B.; Venson, T. "CoolCalc: A Long-Haul Tuck Thermal Load Estimation Tool." SAE World Congress, April 12–14, 2011, Detroit, MI; Paper No. 2011-01-0656.
- Dieck, R.H.; Steele, W.G.; Osolobe, G. *Test Uncertainty*. ASME PTC 19.1-2005. New York, NY: American Society of Mechanical Engineers. 2005.
- NREL, Vehicle Testing and Integration Facility website, Rotating Shadowband Radiometer: www.nrel.gov/midc/vtif_rsr/.
- "Cab Insulation Testing Methodology." RP422A-1-9. *Technology and Maintenance Council's Recommended Maintenance Practices Manual*. 2010–2011 edition. Arlington, VA: American Trucking Association, p. RP422A-1.
- Accessed July 5, 2012: www.dometictruck.com/bb-hvac.php.
- Lustbader, J.A.; Venson, T.; Adelman, S.; Dehart, C.; Yeakel, S.; Castillo, M.S. "Application of Sleeper Cab Thermal Management Technologies to Reduce Idle Climate Control Loads in Long-Haul Trucks." Presented at the SAE 2012 Commercial Vehicle Engineering Congress, Oct. 2–3 2012, Rosemont, Illinois.
- Lustbader, J.; Kreutzer, C.; Adelman, S.; Yeakel, S.; Brontz, P.; Olson, K.; Ohlinger, J. "Impact of Paint Color on Rest Period Climate Control Loads in Long-Haul Trucks." SAE World Congress, April 8, 2014.
- "Vehicle and Systems Simulation and Testing 2013 Annual Progress Report." DOE/EE-1023, Section V.Q. Long-Haul Truck Thermal Load and Idle Reduction; pp. 254–260.
- Accessed May 12, 2014: coolcolors.lbl.gov/LBNL-Pigment-Database/.

IV.I.3. Products

Publications¹

1. Lustbader, J.; Kreutzer, C.; Jeffers, M.; Tomerlin, J.; Langewisch, R.; Kincade, K. "CoolCab Test and Evaluation & CoolCalc HVAC Tool Development." DOE Annual Merit Review, June 19, 2014; VSS075.
2. Lustbader, J.; Kreutzer, C.; Adelman, S.; Yeakel, S.; Brontz, P.; Olson, K.; Ohlinger, J. "Impact of Paint Color on Rest Period Climate Control Loads in Long-Haul Trucks." SAE World Congress, April 8, 2014.
3. Lustbader, J.; Kreutzer, C.; Jeffers, M.; Adelman, S.; Yeakel, S.; Brontz, P.; Kopetz, C.; Ohlinger, J.; Olson, K. "Impact of Paint Selection on Idle Climate Control Loads in Long-Haul Trucks." SAE Thermal Management Systems Symposium, Oct. 23, 2013.
4. Kreutzer, C.; Lustbader, J.; "Advanced Technologies for Long-haul Truck idle load reduction." SAE Thermal Management Systems Symposium, Sept. 24, 2014.

Patents

1. Provisional patent titled "Microenvironmental Control," NREL PROV/14-06 submitted to USPTO on April 9, 2014.

Tools and Data

1. CoolCalc rapid HVAC load estimation tool versions 2.4 and 2.5. Available only to industry and laboratory partners at this time. See CoolCalc section in this report for more information.
2. CoolSim v84 A/C modeling software for the MATLAB/Simulink software environment. See CoolSim section in this report for more information.

Acknowledgments

- Thanks to coauthor Cory Kreutzer (NREL).
- Additional thanks to Jeff Tomerlin, Matt Jeffers, John Rugh, and Lisa Fedorka (NREL).
- Special thanks to our industry partners Volvo Trucks, PPG Industries, Aearo Technologies LLC, Eastman, and Dometic Corporation's Environmental Division.

¹ Publications are listed jointly herein and in 1000181.00 CoolCalc Rapid HVAC Load Estimation Tool.

IV.J. Medium and Heavy-Duty Field Testing

Principal Investigator: Kenneth Kelly

National Renewable Energy Laboratory
15013 Denver West Parkway, MS 1633
Golden, CO 80401
Phone: (303) 275-4465
E-mail: Kenneth.Kelly@nrel.gov

DOE Program Manager: David Anderson

Phone: (202) 287-5688
E-mail: David.Anderson@ee.doe.gov

DOE Program Manager: Lee Slezak

Phone: (202) 586-2335
E-mail: Lee.Slezak@ee.doe.gov

IV.J.1. Abstract

Objectives

The main goal of this project is to test and/or validate advanced propulsion technologies in medium- and heavy-duty applications and to provide data from this activity to help facilitate transitioning these vehicles from the research and development /prototype stage into the marketplace. This will be accomplished by means of the following:

- Testing and analyzing near-term advanced technologies in vehicles and comparing them to conventional technologies in vehicles in similar service.
- Providing data and feedback to the research and development community (including other offices and programs within the U.S. Department of Energy [DOE]) to guide technology development that will lead to fuel-saving commercial products.

Major Accomplishments

FLNA Plug-In Electric Delivery Truck Case Study

- Conducted a study on Smith electric vehicles (EVs) in service with Frito-Lay North America (FLNA) in Federal Way, Washington.
- Collected and analyzed operational data, including drive cycles and fuel consumption from the EV and diesel trucks as well as facility and charging infrastructure.
- Modeled vehicle-grid integration opportunities from charge management to vehicle-to-grid energy storage.

Truck Platooning Demonstration Study

- Completed testing, data analysis, and publication of results on semiautomated line-haul truck platooning utilizing Peloton Technology's platooning system.
- Performed a series of 10 modified SAE Type II J1321 fuel consumption track tests to document fuel consumption of two platooned vehicles and a control vehicle at varying steady-state speeds, following distances, and gross vehicle weights.
- Presented results of the testing at the TRB Automated Vehicle Symposium in July 2014, and the 21st Century Truck Partnership was briefed in August 2014.
- Published detailed results of the study in an SAE paper presented at the SAE Commercial Vehicle Engineering Conference.

UPS Hydraulic Hybrid Case Study

- Completed study of Parker hydraulic hybrids in service with United Parcel Service (UPS) in Baltimore, Maryland.
- Completed field data collection and analysis of results.
- Completed chassis dynamometer testing at NREL's Renewable Fuels and Lubricants (ReFUEL) laboratory on the UPS/Parker Hannifin hydraulic hybrid, conventional gasoline UPS delivery van, and a conventional diesel delivery van.
- Published detailed results of the study in an SAE paper presented at the SAE Commercial Vehicle Engineering Conference.

Future Achievements

FLNA Plug-In Electric Delivery Truck Case Study

- In FY 2015, NREL plans to complete all testing and analysis and publish the results of the Frito-Lay study.
- NREL will continue to investigate additional charge-management strategies and renewable energy integration scenarios.
- The Federal Way depot building will be instrumented to properly time charge-management schemes to align with local minima in their daily power consumption.
- Battery degradation testing is currently planned to continue every six months on eight test vehicles.
- Battery state of health will be estimated for the entire Smith American Recovery and Reinvestment Act (ARRA) data set through time and potentially be used to construct a life model of the pack based on in-use field data.

Truck Platooning Demonstration Study

The truck platooning study conducted so far has received positive feedback from a number of industry partners. Several opportunities exist for improving the understanding and potentially optimizing the benefits of this technology. These include:

- Additional testing to confirm the trends shown here, including greater following distances to clarify the optimum configuration.
- Incorporating direct aerodynamic study into track testing (truck-mounted anemometer, smoke trails, etc.).
- Modeling computational fluid dynamics.
- Assessing current line-haul travel:
 - What percent of national line-haul miles would be conducive to platooning?
 - How often do trucks typically travel together and at what following distance?
- Designing aerodynamic aids specific to platooning to address the loss of cooling airflow over the radiator of the trailing tractor.
- Assessing any impact of platooning on criteria emissions (e.g., NOx).

UPS Hydraulic Hybrid Case Study

A final technical report and case study will be published. No further work is planned on the UPS hydraulic hybrid fleet; however, a new field study on hydraulic hybrid refuse haulers is being investigated.



IV.J.2. Technical Discussion

Background—General

DOE funds many projects to develop components and subsystems for advanced vehicles. Testing, validating, and providing data about the real-world service performance of these technologies, as well as others not funded by DOE, are necessary to help transition the technologies into widespread use in the marketplace. To accomplish this, DOE and industry need a process to document testing, validating, and benchmarking the advanced technologies to provide this data from an unbiased party. The information provided by this project is vital to original equipment manufacturers to identify areas of improvement and to fleets to aid them in making purchase decisions that will be appropriate for a vehicle's application. DOE can also utilize this information to help identify future research and development opportunities.

Approach—General

This project will cooperate with fleet and/or original equipment manufacturer partners to select, test, and validate advanced technologies in commercial vehicle applications. Specific technologies will be selected based on (1) their potential for reducing fuel consumption, (2) their potential for widespread commercialization, and (3) interest at DOE (including the 21st Century Truck Partnership and other DOE programs). After a technology area has been identified, NREL will collect vehicle data on system performance, maintenance (if applicable), and/or operational costs relative to the new technology. The data will be analyzed and sent back to DOE and the project teams, and its potential for improvement in

real-world service will be compared to baseline data if a comparable conventional technology vehicle is available.

The approach for the FY 2014 medium- and heavy-duty field evaluation projects includes:

- Working cooperatively with commercial fleets to collect operational, performance, and cost data for advanced technologies.
- Characterizing vehicle drive/duty cycles.
- Analyzing performance and cost data during a period of 6 months to 1 year or more.
- Testing and analyzing in-use performance of advanced technologies in a laboratory setting to duplicate observed real-world conditions.
- Producing fact sheets and reports on advanced heavy-duty vehicles in service.
- Providing updates on new advanced technologies to DOE and other interested organizations as needed.

FLNA Plug-In Electric Delivery Truck Case Study

Background and Introduction

NREL's Fleet Test and Evaluation Team has found medium- and heavy-duty vehicle fleets to be good candidates for deploying low-emitting, advanced technologies because of their large numbers, high vehicle miles traveled—and consequently high petroleum fuel consumption and emissions—and frequent operation in large population centers, as well as common return-to-base fueling regimes and consistent driving routes.

Previous testing and analysis conducted by NREL have illustrated the influence of drive cycle and vehicle usage on both energy consumption (from liquid fuels and high-voltage hybrid battery packs) and exhaust (or well-to-wheels) emissions. Drive cycle has also been shown to influence the all-electric range of battery EVs, the charge-depleting range of plug-in hybrid electric vehicles (PHEVs), and the potential fuel economy benefit of hybrid EVs. Accordingly, fleet customers can benefit from a further understanding of advanced vehicle technology deployment to minimize fuel consumption and emissions. It has also been shown that large-scale deployments of EVs in a localized area can lead to power quality and power cost issues.

Introduction

NREL is currently funded by DOE to collect operational data on Smith EVs being deployed as part of ARRA. Data collected from these vehicles (up to 500, some of which are located at FLNA facilities) will be used to understand the overall usage and effectiveness of EVs in medium-duty commercial fleet facilities and operations and also compared to operations of conventional counterparts in the same location. Through this collaboration with FLNA, NREL hopes to provide a more focused investigation to understand the implementation and performance of medium-duty EVs in a large-scale commercial facility.

Approach

- The technical approach for this project follows the general approach for conducting fleet evaluations described previously. The specific technical approach for the Frito-Lay project includes the following:
 - Initial fleet identification and selection
 - Initial route and in-vehicle data collection
 - 12-month fleet data collection
 - Battery life degradation study
 - Detailed results from discussion and results from each of these steps are covered in the following section.

Results

Progress to Date

Initial Fleet Identification and Selection

During FY 2013, NREL engaged with FLNA and Smith to establish a program to evaluate the performance of plug-in electric delivery vans in direct comparison to conventional diesel vehicles. Based on the availability of comparable vehicles, NREL and FLNA decided that the FLNA Federal Way, Washington, fleet depot would be the ideal target site for research.

In October of 2014, NREL contacted the Federal Way fleet and building energy managers to arrange on-site discussions and begin vehicle instrumentation. To determine an ideal vehicle set for data collection, it is often helpful to start with a list of fleet vehicles containing information about vehicle make, model, model year, gross vehicle weight rating, and fuel type. Depending on the size of the fleet, typically anywhere from 4 to 24 vehicles within the fleet should be instrumented to ensure that data captured are representative of overall fleet operating behavior.

To collect the required data for the Fleet DNA project (drive cycle and controller area network [CAN] data), it may be necessary to install onboard logging devices onto vehicles of interest. Vehicle instrumentation is a quick process—it requires only that the person installing the data recorders have access to the vehicles requiring instrumentation and approximately 30 minutes of time with each vehicle to install the necessary equipment.

Table IV-17 lists the vehicles that were instrumented.

Table IV-17: Federal Way Vehicles Monitored in Second Logger Deployment

| Manufacturer | Model | Year |
|---------------|--------------|------|
| International | 4200 SBA 4X2 | 2005 |
| International | 4200 SBA 4x2 | 2003 |
| International | 4700 4x2 | 2001 |
| International | 4200 SBA 4X2 | 2005 |
| International | 4200 SBA 4x2 | 2006 |
| Hino | HINO 238 | 2012 |
| International | 4200 SBA 4x2 | 2007 |
| International | 4200 SBA 4X2 | 2005 |
| International | 4700 4x2 | 2001 |

Initial Route and In-Vehicle Data Collection

Data collected from the nine diesel vehicles provide the baseline to which Smith EV performance was compared. NREL gathered data from the 10 Smith EVs stationed at Federal Way during the 17 days of logging in 2014 (April 16 to May 1) and found several correlations among FLNA diesel and EV operations. The routes for both sets of vehicles span similar ranges across the territory served by the Federal Way depot.

Upon closer investigation, it became evident that the FLNA delivery duty cycle fit the capabilities of Smith EVs relatively well. The kinetic intensity (a relative measure of route aggressiveness, as represented by the ratio of a drive cycle's characteristic acceleration to its aerodynamic speed) of the plug-in electric vehicles (PEVs) closely matched that of the diesels relative to daily average speed.

Traveling on similar routes as the diesel trucks, FLNA's Federal Way EVs operated at much higher fuel economies. As shown in Figure IV-121, the EVs drove nearly three times as far on the same energy as the diesels, at times exceeding 25 miles per gallon of gasoline equivalent (mpge).² The diesel trucks averaged 7.7 mpg at \$3.85/gal—roughly the average in Seattle at the time of this report—and the EVs averaged 23.3

²Fuel economy assessments for Smith EVs are represented as AC energy and thus assume a 90% charger efficiency as found in earlier ARRA data analyses for Smith's onboard chargers. A gallon of diesel fuel was assumed to contain 37.6 kWh of energy.

mpge at \$0.102/kWh³; thus, the same ratio in fuel economy applies to fuel savings for EVs. Frito Lay spent \$0.50 for every mile driven with diesel trucks compared to \$0.15 for every mile driven by an EV.

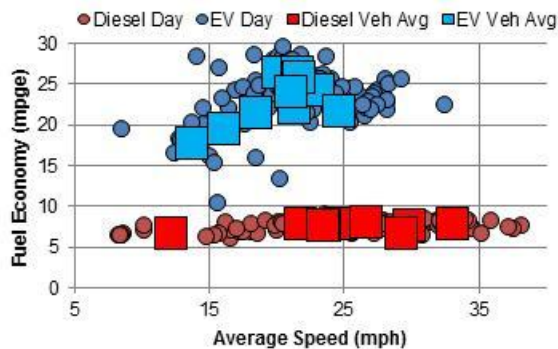


Figure IV-121: Fuel economy comparison of diesels and EVs

To further validate the onboard Smith data logger and collect more detailed information regarding grid impact from the EVs, NREL worked with one of FLNA's partners to collect the charging station power meter data. At the request of Frito-Lay, Servidyne installed a charging station energy management system. During late 2013, the ownership of the data servers for this system changed to Chateau Energy Solutions. All data were accessible via Chateau's web interface. This tool allows Frito-Lay to monitor energy consumption and power quality from each individual electric vehicle supply equipment ("charging station") and even control the stations (to one of three discrete power states: on, low, off). An additional scheduling feature is available to plan periods of controlled charging.

During the two consecutive months of continuous data collection, the charging demand from the bank of 10 vehicles peaked at slightly more than 77 kW, with 23,085 kWh (AC) delivered. This load adds \$462.77 in demand charges to the Federal Way utility bill during the months of April through September. This is a separate line item on utility bills found in the majority of commercial facilities in the United States that is proportional to the peak demand during a 15-minute period each month. The demand charge averaged \$693.77 for each month from October through March,⁴ in addition to the \$1,479.10 monthly energy charges. Electricity costs roughly

\$2,470 per vehicle each year on average; whereas Frito-Lay spent nearly \$6,000 per diesel truck in fuel costs (assuming an average of slightly more than 4 gal/day/truck found in NREL's data collection efforts at \$3.85/gal).

Figure IV-122 shows an example of the data recorded by the Federal Way charging station energy management system. Each stacked color represents the power recorded over time (energy) delivered by a single charging station. NREL found that each of the Federal Way EVs charged an average of 47.1 kWh AC per day. With an average charger efficiency of 90%, FLNA's routes consumed approximately 53% of their EV's full 80-kWh battery pack capacity each day.

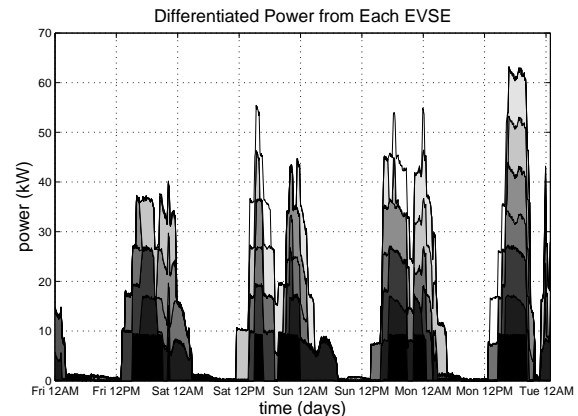


Figure IV-122: Subset of data from Chateau Energy management system

As shown in Figure IV-123, the EVs charge over night until early morning, when the delivery shifts begin. Adding load throughout the afternoon and into the early evening coincides with many facility loads and has nearly doubled the Federal Way FLNA depot's demand (see Figure IV-124). Working with the local energy management engineer at Federal Way, NREL acquired the depot's utility bills, which indicated that peak demand nearly doubled after the 10 PEVs were put into service in early 2013.

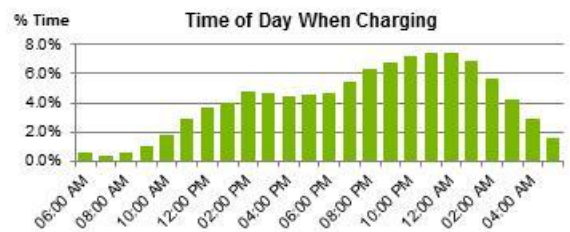


Figure IV-123: Time of day when vehicles are charging during the diesel comparison period (April-May 2014)

³ Utility bills collected from the site energy manager at the Federal Way depot during 2013 were averaged to price each kWh at \$0.102, including access and demand charges.

⁴ The FLNA Federal Way depot is on Puget Sound Energy's Tariff G rate schedule: a \$9.01/kW demand charge from October through March and \$6.01/kW demand charge from April through September. Energy costs \$0.064072/kWh above 20,000 kWh consumed.

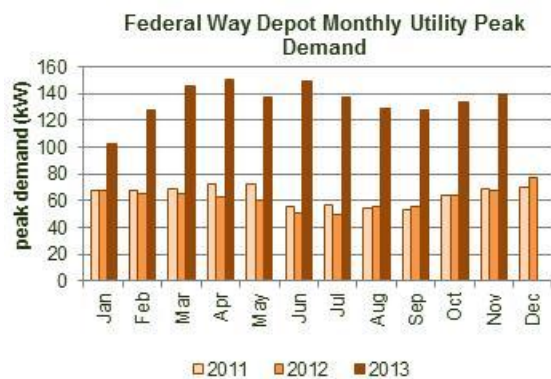


Figure IV-124: Fleet depot utility bill monthly peak demand

When analyzed in NREL’s vehicle2campus simulation tool, a slight shifting of vehicle charge times and power levels yielded an increase in the facility load by approximately 16%; however, this management also reduced net peak (vehicles + facility) by approximately 21%. Figure IV-125 shows the results of the simulations for a scenario in which the controller limited peak load with vehicles charging to no more than 120% of the original demand. In this simulation, each vehicle was ensured enough energy to fulfill each day’s driving needs.

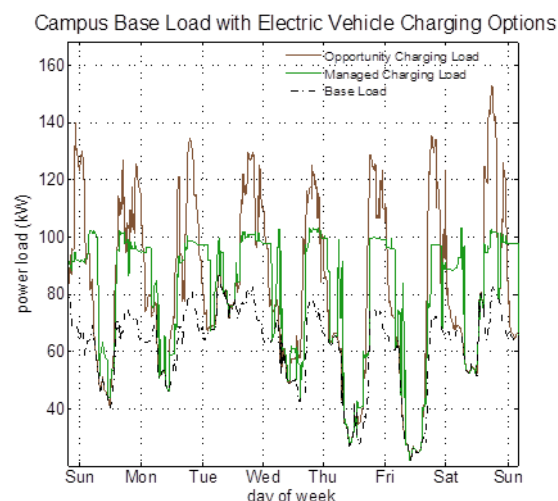


Figure IV-125: Charge management schemes developed by NREL could save FLNA in peak demand charges

12-Month Fleet Data Collection

Utilizing FLNA records and ARRA data logs throughout 2013, NREL compiled a 12-month summary comparison of performance among the diesels and EVs at Federal Way.

Conclusions

Traveling on similar routes as the diesel trucks, FLNA’s Federal Way EVs operated at much higher fuel economies. The EVs drove nearly three times as far on the same energy as the diesels, at times exceeding 25 mpg. The diesel trucks averaged 7.7 mpg at \$3.85/gal—roughly the average in Seattle at the time of this report—and the EVs averaged 23.3 mpg at \$0.102/kWh; thus, the same ratio in fuel economy applies to fuel savings for EVs. Frito Lay spent \$0.50 for every

mile driven with diesel trucks compared to \$0.15 for every mile driven by an EV.

Electricity costs roughly \$2,470 per vehicle each year on average; whereas Frito-Lay spent nearly \$6,000 per diesel truck in fuel costs (assuming an average of slightly more than 4 gal/day/truck found in NREL’s data collection efforts at \$3.85/gal).

Truck Platooning Demonstration Study

Background

Vehicle automation is a promising petroleum reduction technology, and platooning systems for heavy-duty vehicles could be an early commercial application of vehicle automation technology. These systems may employ existing technologies such as radar or laser range finders, global positioning system, dedicated vehicle-to-vehicle communications, and braking and engine torque authority to enable vehicles to follow safely in close proximity, with the goal of reducing fuel consumption through improved aerodynamics as well as reducing traffic congestion and possibly collisions. Figure IV-126 illustrates how platooning is intended to make two trucks appear more like one object to the airflow, resulting in reduced turbulence behind the lead truck and reduced forebody drag on the trailing truck. Figure IV-127 shows the actual test vehicles in platoon formation.

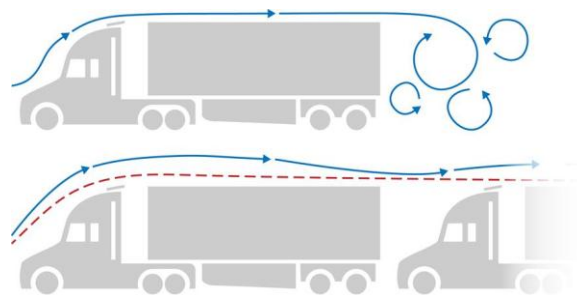


Figure IV-126: Truck platooning air flow



Figure IV-127: Trucks in platoon formation during testing. NREL #31237

Introduction

Under this field evaluation project, NREL is evaluating the fuel consumptions of two Class 8 tractor-trailer combinations platooned together compared to their standalone fuel consumptions. A series of 10 modified SAE Type II J1321 fuel consumption track tests were performed to document the fuel

consumption of two platooned vehicles and a control vehicle at varying steady-state speeds, following distances, and gross vehicle weights (GVWs). The steady-state speeds ranged from 55 mph to 70 mph, the following distances ranged from 20 ft. to 75 ft., and the GVWs were 65K lbs. and 80K lbs. All tractors involved had U.S. Environmental Protection Agency SmartWay-compliant aerodynamics packages installed, and the trailers were equipped with side skirts. Effects of vehicle speed, following distance, and GVW on fuel consumption were observed and analyzed. The platooning demonstration system used in this study was provided by Peloton Technology and consisted of radar systems, dedicated short-range communications, vehicle-to-vehicle communications, vehicle braking and torque control interface, cameras, and driver displays. Full details from the project were published at the SAE 2014 Commercial Vehicle Engineering Congress in October 2014 (paper number 2014-01-2438) and will be included in an NREL technical report in late 2014.

Approach

This research project, funded by DOE, evaluated the fuel consumption reduction of a pair of platooned Class 8 tractor-trailers on a track throughout a range of highway truck speeds, following distances, and weights that represent driving on U.S. public highway conditions under test track conditions. The matrix of test conditions is outlined in Table IV-18. The project was managed by the NREL, and the tests were performed by Intertek Testing Services NA and LINK Engineering. Testing took place at the Continental Tire Proving Grounds in Uvalde, Texas, which is an 8.5-mile (13.7-km) asphalt oval with several small-grade changes rather than a zero-grade environment. As such, the constant-speed tests were operated under cruise control and had an average speed standard deviation of ± 0.6 mph and a maximum deviation of 1.0 mph as the heavy tractors responded to the small-grade changes. The fuel consumption was measured gravimetrically, and savings were recorded through methods prescribed in SAE J1321, Fuel Consumption Test Procedure. Additional data, including emissions and the effects on engine cooling to the trailing vehicle from platooning, were recorded with data-logging devices through the use of J1939 CAN bus messages.

Table IV-18: Platooning Test Matrix

| Trailing Distance | Test Conditions | | | | |
|-------------------|--------------------|--------------------|--------------------|----------------------------|--------------------|
| | 55 mph, 65,000 lb. | 65 mph, 65,000 lb. | 70 mph, 65,000 lb. | Variable Speed, 65,000 lb. | 65 mph, 80,000 lb. |
| 20 ft. | | X | | | |
| 30 ft. | X | X | X | | |
| 40 ft. | | X | | | |
| 50 ft. | X | X | X | X | X |
| 75 ft. | | X | | | |

Results

SAE Type II Fuel Consumption Results from Platooned Tractors

Gravimetric Fuel Savings Analysis

All fuel consumption results for the 65-mph, 65K lb. GVW conditions were averaged from three baseline/test runs each. The remaining test conditions (i.e., different speeds and weights) were averaged from two baseline/test runs each because of budget limitations. Data analysis methods and the SAE spreadsheet recommended in SAE J1321, Fuel Consumption Test Procedure – Type II (2012) were used during post processing to determine the 95% confidence interval (CI) and statistical significance for each test condition. The percent fuel saved and 95% CI for each test truck individually and as a “team” are shown in Table IV-19. In addition to the constant-speed tests, a variable-speed test was conducted. As part of this effort, NREL developed an in-cab driver’s display for the drivers of the lead and control trucks to follow the variable-speed trace. The variable-speed test demonstrated no statistically significant difference from the baseline for either truck or the combined team result. A third test run may have allowed a statistical difference to be determined given this test’s higher inherent variability. The lead truck in the 80K lb. GVW condition and 65-mph, 65K lb. GVW, 75-ft. condition also resulted in no statistically significant differences. Values with no statistically significant difference from their baseline are shown in Table IV-19 as italicized and shaded grey and are not discussed further. A detailed discussion of the results is provided in the technical paper referenced at the end of this section. A summary of the results is provided below.

Table IV-19: Percent Fuel Saved (Gravimetric) of Platooned Tractors

| Test Conditions | Percent Fuel Saved (Gravimetric) | | | | | |
|---------------------|----------------------------------|--------|----------------|--------|---------|--------|
| | Lead Truck | | Trailing Truck | | “Team” | |
| | Nominal | 95% CI | Nominal | 95% CI | Nominal | 95% CI |
| 55 mph, 65k, 30 ft. | 4.33% | 0.70% | 8.38% | 1.03% | 6.38% | 0.28% |
| 55 mph, 65k, 50 ft. | 2.22% | 0.49% | 9.72% | 2.24% | 6.01% | 1.33% |
| 65 mph, 65k, 20 ft. | 5.28% | 0.34% | 2.81% | 0.71% | 4.04% | 0.52% |
| 65 mph, 65k, 30 ft. | 4.06% | 1.19% | 7.53% | 1.33% | 5.80% | 1.26% |
| 65 mph, 65k, 40 ft. | 2.69% | 0.99% | 9.10% | 0.71% | 5.91% | 0.84% |
| 65 mph, 65k, 50 ft. | 3.14% | 2.65% | 9.17% | 2.11% | 6.15% | 2.37% |
| 65 mph, 65k, 75 ft. | 1.69% | 2.35% | 9.39% | 1.93% | 5.53% | 2.12% |
| 70 mph, 65k, 30 ft. | 4.42% | 1.92% | 4.62% | 2.33% | 4.52% | 2.12% |
| 70 mph, 65k, 50 ft. | 2.23% | 0.35% | 8.36% | 1.44% | 5.31% | 0.90% |
| VAR, 65k, 50 ft. | 2.70% | 8.32% | 4.22% | 6.82% | 3.45% | 7.56% |
| 65 mph, 80k, 50 ft. | 0.55% | 3.58% | 6.67% | 4.84% | 3.68% | 2.07% |

The lead tractor consistently demonstrated an improvement in average fuel consumption reduction as following distance decreased. The fuel savings ranged from 2.7% to 5.3% at 65k lb. GVW, with a low point of 2.2% savings at both 55 mph, 50 ft. and 70 mph, 50 ft. The trailing truck achieved savings from 2.8% to 9.7%; tests with no fan-on time had savings of 8.4% to 9.7%. Engine coolant temperatures on the trailing truck generally increased as following distances decreased, resulting in engine fan-on time as high as 19% for some closer following conditions, compared to 0%–1% for longer following distances.

Statistically significant percent fuel savings with 95% CI bars for the team of two platooned tractor-trailers are shown in Figure IV-128. Team fuel savings were determined by summing both the leading and trailing vehicle fuel consumption to consider them as one vehicle. The resulting values ranged from 3.7% to 6.4% lower fuel consumption, with the best combined result documented for 55 mph, a 30-ft. following distance, and 65k lb. GVW. Closer following distances caused the engine fan on the trailing truck to engage, which appears to have negatively impacted fuel savings. Test conditions that experienced no fan-on events had nominal results that ranged in team fuel saved from 5.3% to 6.4% for the combined pair of vehicles. Other factors may have had an effect on fuel consumption at the close following distances as well. For example, an increase in the frequency of engine torque adjustments on the trailing truck was observed at the close following distances. This could potentially impact fuel consumption as well as emissions. Further testing is needed to fully understand these effects.

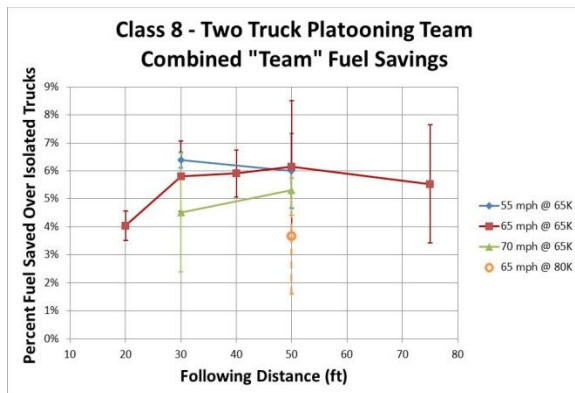


Figure IV-128: Platoon team percent fuel savings

Fuel Economy Improvement

SAE J1321 Fuel Consumption Test Procedure – Type II does not include a methodology for calculating fuel economy. To better relate the results of this testing to the trucking industry, a method was developed to calculate representative mile-per-gallon results from the fuel consumption results given above. Baseline mpg was calculated by dividing the test distance of 59.4 miles by an average of all baseline run fuel consumption results from both test trucks for each speed and load condition. For the baseline tests, reducing speed from 65 mph to 55 mph resulted in 19% improvement in mpg; whereas increasing from 65 mph to 70 mph reduced mpg by 8%.

- 7.82 mpg @ 55 mph
- 6.58 mpg @ 65 mph
- 6.07 mpg @ 70 mph

Baseline condition tests also show the effect of mass on mpg; increasing mass from 65K lbs. to 80K lbs. at 65 mph resulted in 4% lower mpg.

- 6.58 mpg @ 65 mph and 65,000 lbs.
- 6.33 mpg @ 65 mph and 80,000 lbs.

Platooning mpg is calculated by applying the SAE procedure calculated percent fuel savings to the baseline fuel consumption average and then converting to mpg using the 59.4-mile test distance. Platooning improved fuel economy at

all speeds and load conditions. Best mpg overall was platooning at 55 mph. Baseline condition tests show the effect of speed on mpg. Figure IV-129 shows the fuel economy results for the platooned team combined.

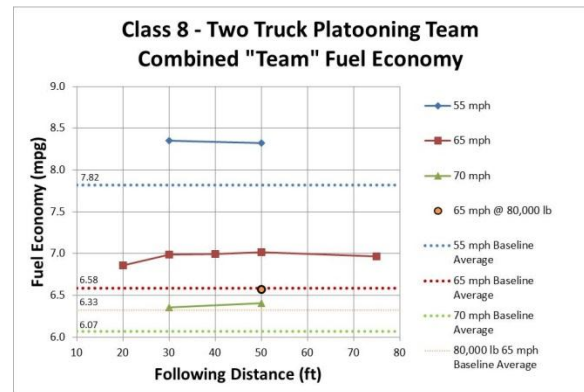


Figure IV-129: Platoon team fuel economy

Conclusions

- Platooning can result in significant fuel savings for both a leading (up to 5.3%) and a trailing (up to 9.7%) Class 8 vehicle.
- Engine coolant temperature needs to be monitored and addressed for the trailing vehicle to maximize the fuel savings for the vehicle pair by avoiding fan-on situations.
- Atmospheric conditions may play a strong role in the savings attainable because of the reduced airflow across the radiator induced by vehicle speed on the trailing vehicle.
- Heavy loads will affect the percent savings from platooning but still result in significant fuel savings, especially considering that heavily loaded vehicles consume fuel at a higher rate.
- Because the technology is expected to require a modest investment, the “team” savings of 6.4% on a pair of vehicles could end up with an attractive return on investment for the fleet without reducing safety by attempting to follow closely under driver control.

UPS Hydraulic Hybrid Case Study

Background

Parker Hannifin supplied global positioning system and fueling data from its telematics system on Baltimore hybrids for the month of April 2013 for NREL evaluation. Additionally, eight data logging devices (Isaac Instruments DRU900/908) with global positioning system antennas and J1939 controller area network bus (CANBUS) connections were deployed to the Baltimore UPS HHV fleet to capture a wider spectrum of J1939 data than were provided by Parker including Parker hybrid channels, Cummins engine reported NOx, engine torque, etc. In total, 484 days of hybrid operation were documented and evaluated by both the Parker Hannifin and NREL logging devices.

Table IV-20 presents additional details on Parker Hannifin Corporation’s Powersplit infinitely variable transmission hydraulic hybrid system, and Figure IV-130 shows a schematic of the hydraulic hybrid system. This system is not strictly parallel or series in architecture, but a combination of both styles. It is a dual path system capable of transmitting power hydraulically or mechanically or a combination of both. The system uses a gearbox to mix power input from both the diesel engine and the hydraulic motor to the wheels, to the hydraulic motor from the wheels for regeneration, or from the hydraulic motor to the engine flywheel to start the engine. The system also shuts off the diesel engine when it is not needed. UPS has custom delivery vans built to the company’s specifications. The P100 vehicles in this Baltimore field study were manufactured by Freightliner for UPS.

Table IV-20: Hybrid Propulsion-Related Systems

| Category | Hybrid System Description |
|-------------------------|--|
| Manufacturer/integrator | Parker Hannifin Corporation |
| Transmission | Parker Powersplit IVT |
| Drive mode max power | 200-hp C24 Variable Displacement Bent-Axis Hydraulic Pump/Motor |
| Regen mode max power | 200-hp C24 Variable Displacement Bent-Axis Hydraulic Pump/Motor |
| Energy storage | 22-gallon Composite Bladder Accumulator 3,500-4,000 psi nominal pressure range 5,400 psi max pressure (roughly 400 kJ of energy capture possible in normal use range) |

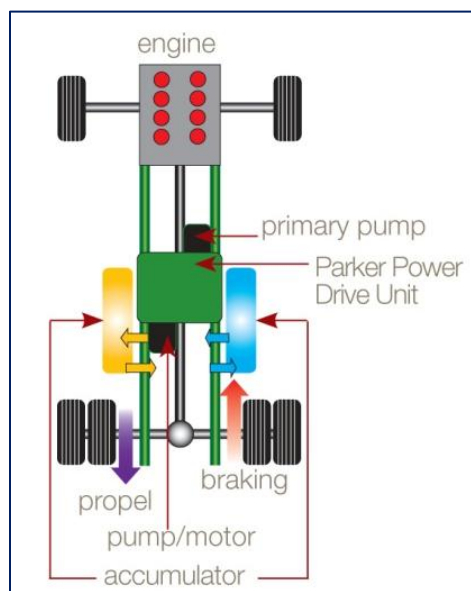


Figure IV-130: Parker IVT hydraulic hybrid schematic

Introduction

This field evaluation project discusses an in-use and laboratory evaluation of 20 MY 2012 Freightliner P10HH hybrid step delivery vans that were placed in service at UPS’s facilities in Burtonsville and Baltimore, Maryland, at the end of 2012. The new hydraulic hybrid vans (HHVs), with hydraulic drive systems manufactured by Parker Hannifin, feature an infinitely variable transmission and an integrated “engine-off at idle” feature. Conventional diesel vans of a similar emissions equipment age are not available for comparison, because in 2010 UPS started using gasoline engines for all non-hybrid delivery vans. This in-use evaluation as well the laboratory testing will be compared to gasoline-powered P100 vans. Laboratory testing also included a similar spec 2012 diesel van from another fleet. Initial duty-cycle analysis was completed in FY 2013, and in-use vehicle instrumentation and laboratory testing were completed in FY 2014. Full details from the project were published at SAE Commercial Vehicle Engineering Congress in October 2014 (paper number 2014-01-2375) and will be published in an NREL technical report in late 2014.

Host Site Profile—UPS, Burtonsville, and Baltimore, Maryland

The host site consists of two large distribution facilities serving the Baltimore area. Twenty HHVs are included in this evaluation, 10 at each facility as well as a set of comparative gasoline-powered P100s. UPS assigned the hybrid vans to routes with a mix of highway driving and urban delivery, similar to routes that were also served by gasoline vans. Dispatch and maintenance practices were the same for both facilities.

Approach

Laboratory Fuel Economy and Emissions Testing Plan

The FY 2014 focus centered on reporting the results from the on-road study conducting chassis dynamometer testing and evaluating the chassis dynamometer fuel economy and emissions. Two delivery vans were tested on the chassis dynamometer at NREL’s ReFUEL research laboratory: an HHV provided by Parker that is identical to those in service in Baltimore and a 2012 UPS gasoline-powered delivery van, which is the actual baseline vehicle UPS is currently buying for use in applications similar to those at Baltimore and Burtonsville. Testing protocol used SAE J2711 as a general guide but modified as needed to accommodate the specifics of the hydraulic hybrid system.

Chassis testing of each of the vehicles included the following elements:

1. Cargo/vehicle mass ballasting based on information from UPS regarding average daily load on these vehicles
2. Coast down testing—to determine correct dynamometer settings using SAE J2263 and J1263 procedures
3. Test cycle selection—drive-cycle metrics were examined, including average driving speed, stops per mile, kinetic intensity, and others. A highly representative set of chassis dynamometer test cycles was chosen to highlight

- shortcomings and advantages of the HHV under varying in-use duty cycles
- 4. Emissions measurements—emissions results for carbon dioxide, total hydrocarbons, carbon monoxide, oxides of nitrogen (NOx), and particulate matter were measured on at least four hot runs following at least one warm-up run. At the NREL ReFUEL laboratory, regulated emissions measurements are performed using procedures consistent with SAE J2711.
- 5. Fuel economy comparison—fuel consumption was measured using a gravimetric measurement method on at least four hot runs following at least one warm-up run.

Results

Van Duty Cycle

- The UPS Baltimore duty cycle contains more high-speed miles than are ideal for a hybrid system. Other observations from the Baltimore duty cycle include:
 - HHVs drive a much higher percentage of their miles in the 35–50 mph range than either group in the previous UPS hybrid study in Minneapolis
 - Fewer stops were made per mile and kinetic intensity was lower than ideal, which results in fewer opportunities for regeneration
 - Higher hybrid advantage could be achieved on more kinetically intense, dense urban route assignments.

Fuel Economy

- Improvements in laboratory-tested diesel-equivalent fuel economy compared to the gasoline conventional van ranged from 3% for the highway-speed California Air Resources Board (CARB) HHDDT cycle to 56% for the more urban New York Composite (NYComp) cycle (see Figure IV-131)
 - 8% (CARB HDDT) to 39% (NYComp) diesel HHV fuel cost advantage over the Gasoline Conventional vans in Renewable Fuels and Lubricants Laboratory (ReFUEL) testing

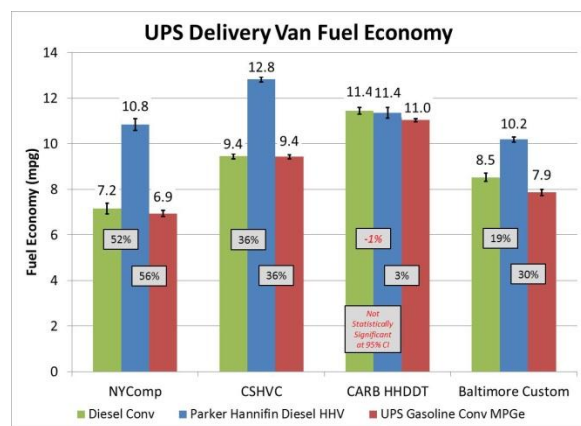


Figure IV-131: Laboratory fuel economy chart. Error bars are 95% confidence interval

- The improvement in fuel economy for the HHV ranged from 19% on the test cycle derived from the Baltimore duty-cycle data to a 52% improvement on the NYComp cycle compared to the diesel conventional van on the non-highway oriented cycles.
- When factoring in the cost of fuel, the diesel HHV showed 1% fuel cost advantage on the CARB HDDT cycle to 34% fuel cost advantage on the NYComp cycle compared to the diesel conventional vans in ReFUEL testing.
- Chassis dynamometer testing of drive cycle results: all fuel economy and emissions results presented are averaged over four test runs of each cycle. Fuel economy results, in diesel equivalent gallons (dge), for the vans are shown in Figure IV-131 with $\pm 95\%$ confidence interval error bars. While only modest improvements were observed on the low KI highway-oriented HHDDT cycle, the HHV showed a 30% to 56% improvement in fuel economy over the gasoline conventional van on the non-highway oriented cycles and a 19 to 52% improvement in fuel economy over the diesel conventional van on the non-highway oriented cycles.
- Because of the difference in fuel cost and energy density, it is also important to compare the results on a dollars-per-mile basis; the 12-month average cost for ultralow-sulfur diesel in 2013 was \$3.92 while the 12-month average cost for regular conventional gasoline in 2013 was \$3.44 (U.S. Energy Information Administration; www.eia.gov/dnav/pet/pet_pri_gnd_dcus_nus_w.htm); the HHVs showed an 8% lower fuel cost per mile on the highway-oriented HHDDT and 27%–39% lower fuel cost per mile than the gasoline conventional vans on the higher KI cycles tested and a 16% to 34% lower cost per mile than the conventional diesel on the non-highway-oriented cycles; no statistically significant difference existed on the HHDDT compared to conventional diesel vans.

Hybrid System Effectiveness

- Net fuel saved, calculated from braking energy capture in the field idle-off fuel savings, ranged from 15% to 27%, with an average of 20%.

Emissions

- Laboratory testing demonstrated an increase in NOx emissions of 52% to 140% for the hybrid compared to the conventional diesel for the range of drive cycles tested (see Figure IV-132).

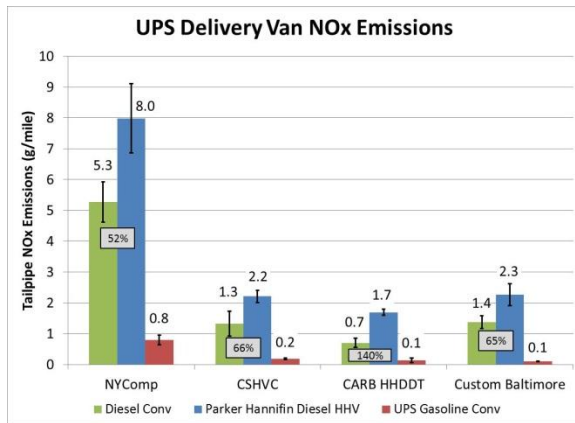


Figure IV-132: NO_x emissions chart. Error bars are 95% confidence interval

- Emissions results for oxides of nitrogen (NO_x) are shown in Figure IV-132 with ±95% confidence interval error bars; all cycles show higher emissions of NO_x from the Parker Hannifin HHV over the conventional gasoline UPS vehicle; the engines from both the hybrid and conventional vehicles were of the same engine family, model, model year, U.S. Environmental Protection Agency (EPA) NO_x certification level, and horsepower rating; heavy-duty engines are certified with the EPA engine certification test, but are not certified with the completed hybrid configuration; engine operation during a chassis dynamometer test is different than during the EPA engine certification test.

Reliability

- The hybrid vehicle group had a cumulative uptime of 98%.

Conclusions and Summary

A duty-cycle analysis of the HHVs in commercial service was carried out to design a laboratory test series to compare the potential performance improvements of a heavy-duty HHV to a conventional gasoline and a conventional diesel truck. The results were as follows:

Fuel Economy

- Laboratory testing showed a 3% to 56% improvement in diesel equivalent fuel economy compared to the gasoline conventional van on the tested duty cycles.
 - 8% to 39% diesel HHV fuel cost advantage compared to the gasoline conventional van in ReFUEL testing
- The HHV showed a 19% to 52% improvement in fuel economy compared to the diesel conventional van on the non-highway oriented cycles.
 - 0% to 34% diesel HHV fuel cost advantage compared to the diesel conventional van in ReFUEL testing

Hybrid System Effectiveness

- Net fuel saved, calculated from energy capture in the field, ranged from 15% to 27%, with an average of 20%.
- HHV demonstrated energy capture during 66% of braking distance observed in the field.

Emissions

- Laboratory testing demonstrated an increase in NO_x emissions of 52% to 140% for the hybrid compared to the conventional diesel.

IV.J.3. Products

Publications

- Lammert, M.; Burton, J.; Sindler, P.; Duran, A. "Hydraulic Hybrid and Conventional Parcel Delivery Vehicles' Measured Laboratory Fuel Economy on Targeted Drive Cycles." *SAE International Journal Alternative Powertrains* 4(1), 2015; doi:10.4271/2014-01-2375.
- Lammert, M.; Duran, A.; Burton, J.; Sindler, P. *Final Evaluation of UPS Diesel Hydraulic Hybrid Delivery Vans*. NREL/TP-5400-62814. Golden, CO: National Renewable Energy Laboratory, forthcoming.

V. MODELING AND SIMULATION

LIGHT DUTY

V.A. Analyzing the Potential of Multiple Energy Storage Systems for a BEV 300

Principal Investigators: Ram Vijayagopal, Daeheung Lee

Argonne National Laboratory
9700 South Cass Avenue, Building 362
Lemont, IL 60439
Phone: (630) 252-5386
E-mail: rvijayagopal@anl.gov, daeheung@anl.gov

DOE Program Manager: David Anderson

Phone: (202) 287-5688
E-mail: David.Anderson@ee.doe.gov

V.A.1. Abstract

Objectives

Examine the opportunity to improve battery electric vehicle (BEV) performance and cost by combining two energy storage systems with different power/energy characteristics:

- BatPaC will provide inputs on the battery technology.
- Autonomie will be used for vehicle simulation.
- Vehicle-level control models have to be developed for energy management.

Major Accomplishments

A two-battery system is found to be a cheaper alternative when high power output is necessary from the BEV:

- Lower cost is achievable.
- The power battery has lower efficiency.
- Higher energy consumption is observed.
- Current flow from the battery can be controlled.

Future Achievements

Several factors observed during this study should be explored further:

- The ability to control the current flow could be used for improving battery life.
- The impact of fast-charging requirements should be examined.



V.A.2. Technical Discussion

Background

Argonne has expertise on modeling and simulation of vehicles, as well as battery design. Autonomie and BatPaC are two tools developed by Argonne for these purposes. Linking of these tools has enabled us to study several design options. The optimization techniques that are already integrated into Autonomie are also leveraged to automate these technology evaluations.

Introduction

Current battery technologies make possible a battery electric vehicle (BEV) with a 300-mile range (BEV 300), but the cost of such a vehicle hinders its adoption by consumers. DOE has set aggressive cost targets for battery technologies. While a single technology might meet the energy and power requirements, a combination of multiple batteries with different capabilities might also meet these criteria. This study looks at how such a combination can be implemented in a vehicle simulation model and compares the vehicle manufacturing and operating costs of these options. Preliminary analysis shows that there is an opportunity to reduce BEV cost by combining a high-energy battery and a high-power battery. Argonne's battery group provided the data on battery performance and cost, while the system modeling and control group was responsible for evaluating vehicle performance and cost using those batteries.

Approach

The baseline vehicle considered in this study uses a single battery sized to meet both power and energy requirements in a BEV 300. The alternative option considered is a combination of two battery packs that are controlled by a power conditioner. The energy battery has Li-S cells, and the power battery has lithium manganese oxide (LMOG) cells. The two have different cost characteristics. While it is relatively cheaper to increase the capacity of an energy battery, adding more power to that battery is expensive. Conversely, the power battery can be given additional discharge power capability with minimal additional cost, but storing more energy in that battery is expensive.

All vehicle/technology assumptions in this study are similar to the 2020 high-case assumptions used for the recent Vehicle Technologies Office benefit analysis. This study looks at the levelized cost of driving (LCOD) for BEVs when different types of batteries and combinations of batteries are used. This cost estimate includes the cost of the vehicle and the recurring cost of operating the vehicle. The vehicle usage assumptions are based on surveys and published sources. Government Performance and Results Act (GPRA) analysis reports [1] provide a much more detailed explanation of these calculations.

Baseline vehicle

The specifications of the baseline vehicle are shown in Table V-1. The assumptions state that the progress made in component technologies and light-weighting will make the BEV lighter and more efficient. These changes help achieve an energy consumption rate of about 165 Wh/mi during the simulation analysis.

Table V-1: Overall Vehicle Specifications for BEV with One Energy Storage System (1-ESS BEV)

| Vehicle Class | midsize 2wd | |
|-----------------------------------|-------------|-----|
| All-Electric Range | 300 | mi |
| Acceleration, 0–60 | 8 | s |
| Motor Power | 120 | kW |
| Motor Maximum Efficiency | 96 | % |
| Final Drive Gear Ratio | 3.02 | - |
| Electric Accessory Load | 440 | W |
| Vehicle Mass | 1293 | kg |
| Li-S Battery Pack Usable Energy | 49.4 | kWh |
| Li-S Battery Pack Power | 97.4 | kW |
| Li-S Power-to-Energy Ratio | 1.97 | - |
| Li-S Battery Pack Nominal Voltage | 336 | V |
| Li-S Cell Capacity | 163.4 | Ah |
| Li-S Cell Nominal Voltage | 2.1 | V |
| Number of Li-S Cells | 160 | - |

The baseline battery is assumed to use Li-S cell chemistry, which can be designed to meet both energy and power requirements. When sized for high-power and high-energy requirements, the battery increases in cost, as shown in Figure V-1. Cost data are generated using the battery cost and performance models in BatPaC [2].

Results

Sizing the BEV with one battery

Autonomie has an optimization algorithm named POUNDER (developed by the Mathematics and Computer Science Division at Argonne), which can be used to size the baseline battery for the desired vehicle performance and simultaneously optimize for the vehicle cost. In this case, all other vehicle components are kept the same, so the vehicle cost will vary according to the changes in the battery cost.

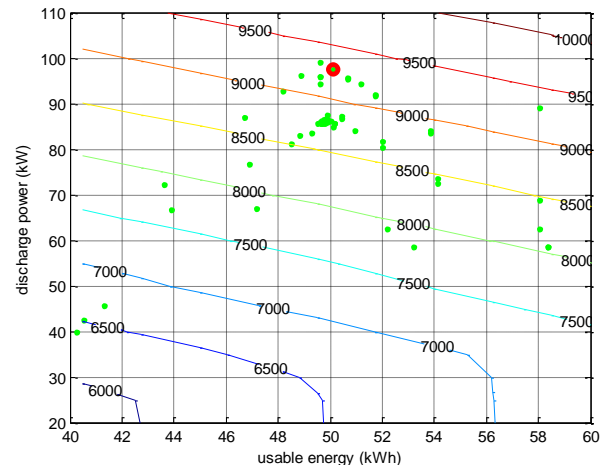


Figure V-1: Variation in battery cost with discharge power and usable energy for the Li-S single-battery option

The objective of the sizing/optimization run is to minimize the vehicle cost while maintaining a range of at least 300 miles and achieving a zero-to-60-mph acceleration time of no more than 8 s.

The cell capacity (which determines usable energy) and the maximum discharge capability of the cell (which determines the power from the battery pack) are defined as the tunable input parameters for this problem. POUNDER starts at a random point within the allowed range for these values, and over successive iterations tries to eliminate the constraint violations and achieve the minimum possible vehicle cost. This technique and its integration into Autonomie is described in earlier work [3–5].

In Figure V-1, the green dots show the evaluated points and the red circle shows the final value that satisfies the sizing requirements. As shown in Figure V-1, this battery needs about 50 kWh of usable energy and 98 kW of discharge power. The manufacturing cost of this battery, as estimated by BatPaC, is about \$9200. The overall vehicle manufacturing cost in this case is approximately \$22,800. The detailed cost values are shown in, which gives the minimum cost that will be incurred to build a vehicle using one-battery chemistry.

Alternative choice: two-battery system

There are other battery chemistries that can provide high power outputs at lower cost. However, they are not able to provide usable energy at these levels. LMOG chemistry is known to be a good option for power batteries. However, adding more energy to those batteries incurs higher cost penalties. A typical LMOG battery cost variation is shown in Table V-2 and Figure V-4.

Table V-2: Cost of Manufacturing and Owning a BEV 300 with One Battery That Provides Both Energy and Power

| Battery system | One Battery | Unit |
|------------------------------|-------------|-------|
| Electric Range (UDDS) | 300 | mi |
| Acceleration Time (0–60 mph) | 8 | sec |
| Cost of Ownership | 0.508 | \$/mi |
| Vehicle Manufacturing Cost | 22856 | \$ |
| Battery Cost | 9181 | \$ |
| Electric Consumption | 165 | Wh/mi |

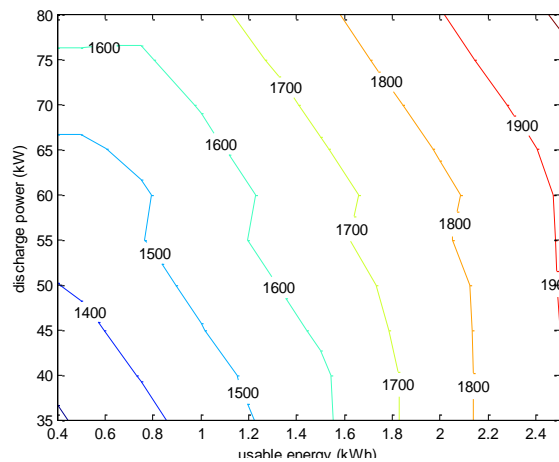


Figure V-2: Variation in battery cost with discharge power and usable energy for the LMOG battery pack

In general, it is cheaper to add energy to an energy battery like Li-S and add power to a power battery like LMOG. However, when these two chemistries are combined, the relative sizing becomes a bit complicated. There are power levels below which an energy battery does not offer any cost savings; similarly, there could be a minimum energy content required in a power battery to fully satisfy the high-power-requirement scenarios. For example, if a power battery is to provide the high power needed for an acceleration test or a quarter-mile test, then it should have enough energy to sustain the high power levels demanded over some time. So it might turn out that the power battery requires a minimum amount of energy to be a useful option. To examine all these possibilities, we need the POUNDER algorithm.

Addition of a second battery and the controller and power conditioner needed for achieving energy management makes the system less efficient and results in higher energy consumption per mile. This change increases the energy usage and adds to the battery capacity needed for the new energy storage system.

For this sizing exercise, the capacity and power of both batteries are considered as tunable input parameters. The objective is still to minimize the vehicle cost, subject to the constraints of a 300-mile all-electric range (AER) and an acceleration performance of 0–60 mph in 8 s.

The sizing output from the POUNDER algorithm is shown in Figure V-3. The baseline choice is also shown in the plot.

The red circle is the baseline one-battery system, the blue dot represents the new energy battery, and the magenta circle shows the power battery specifications. The green, cyan and yellow markers show the points that were evaluated for identifying the point with the minimum cost that satisfies the constraint criteria. The cost of each battery is shown next to the respective circle. A single battery that can provide both energy and power costs \$9.2K. In the case of the two-battery option, the energy battery will cost \$6.7K and the power battery will cost \$1.5K. An additional \$300 is added to the two-battery system to account for the cost of the controller and hardware needed to ensure appropriate energy management. It is clear that in spite of the additional cost of the controller, the two-battery system is a cheaper option. The cost details are shown in Table V-2 and Figure V-4.

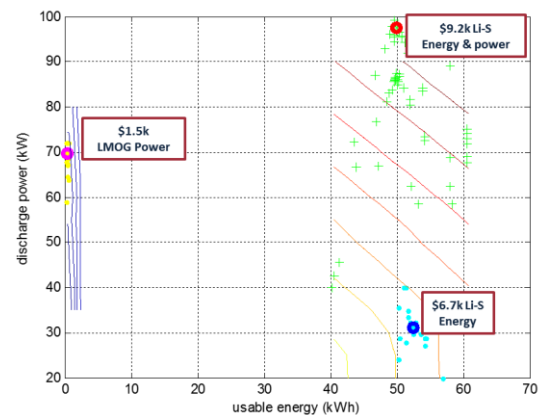


Figure V-3: Battery requirements and cost for the single-battery and two-battery options

The BEV with two energy storage systems (2-ESS BEV) has the specifications summarized in Table V-3. All the component specifications except for the battery system are the same as those of the 1-ESS BEV. The finally sized capacity and output power of each battery system were considered to analyze the LCOD and other performance metrics of the 1-ESS BEV and 2-ESS BEV.

Table V-3. Cost Comparison of Battery Systems and Vehicles

| Battery system | One Battery | Two Batteries | Unit |
|------------------------------|-------------|---------------|---------|
| Electric Range (UDDS) | 300 | 300 | mi |
| Acceleration Time (0–60 mph) | 8 | 8 | s |
| Cost of Ownership | 0.508 | 0.495 | \$/mi |
| Vehicle Manufacturing Cost | 22856 | 22143 | \$ |
| Battery Cost | 9181 | 8168 | \$ |
| Electric Consumption | 165 | 171 | Wh/mile |

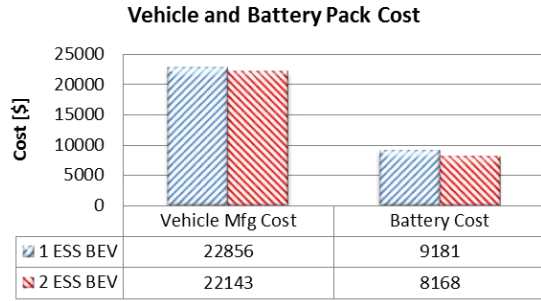


Figure V-4: Vehicle manufacturing and battery pack costs

Table V-4: Overall Vehicle Specifications for 2-ESS BEV

| Vehicle Class | midsize 2wd | |
|---|-------------|-----|
| All-Electric Range | 300 | mi |
| Acceleration, 0–60 mph | 8 | s |
| Motor Power | 120 | kW |
| Motor Maximum Efficiency | 96 | % |
| Final Drive Gear Ratio | 3.02 | - |
| Electric Accessory Load | 440 | W |
| Vehicle Mass | 1293 | kg |
| Li-S Battery Pack Usable Energy | 50.9 | kWh |
| Li-S Battery Pack Power | 30.8 | kW |
| Li-S Power-to-Energy Ratio | 1.65 | - |
| Li-S Battery Pack Nominal Voltage | 336 | V |
| Li-S Cell Capacity | 168.4 | Ah |
| Li-S Cell Nominal Voltage | 2.1 | V |
| Number of Li-S Cells | 160 | - |
| LMOG Battery Pack Usable Energy | 0.35 | kWh |
| LMOG Battery Pack Power | 69.2 | kW |
| LMOG Power-to-Energy Ratio | 197.7 | - |
| LMOG Battery Pack Nominal Voltage | 189.6 | V |
| LMOG Cell Capacity | 9.17 | Ah |
| LMOG Cell Nominal Voltage | 3.95 | V |
| Number of LMOG Cells | 48 | - |
| Power Condition Efficiency | 98.5 | % |
| Figure V-5 shows a comparison of the maximum charging/discharging powers for the various battery systems. | | |

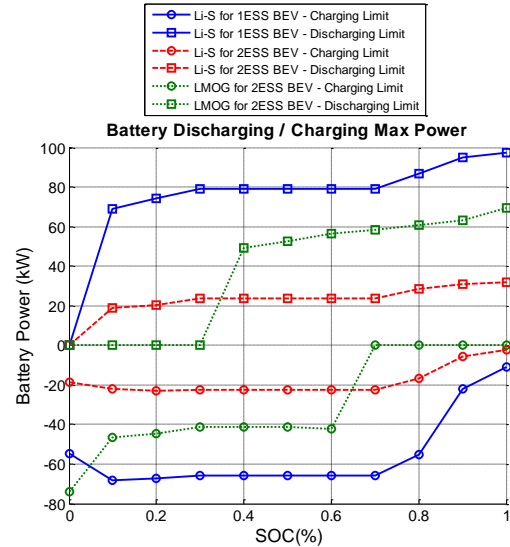


Figure V-5: Battery power required for the single-battery option

Acceleration performance prediction

In order to verify the acceleration performance of the sized BEVs, a simulation of acceleration was performed in Autonomie. Figure V-6 shows the vehicle speed and output power of each battery system to achieve a zero-to-60-mph acceleration time of no more than 8 s. The acceleration time to 60 mph is the same for both BEVs, and the electrical net power from the battery systems is very similar during the initial 10 s.

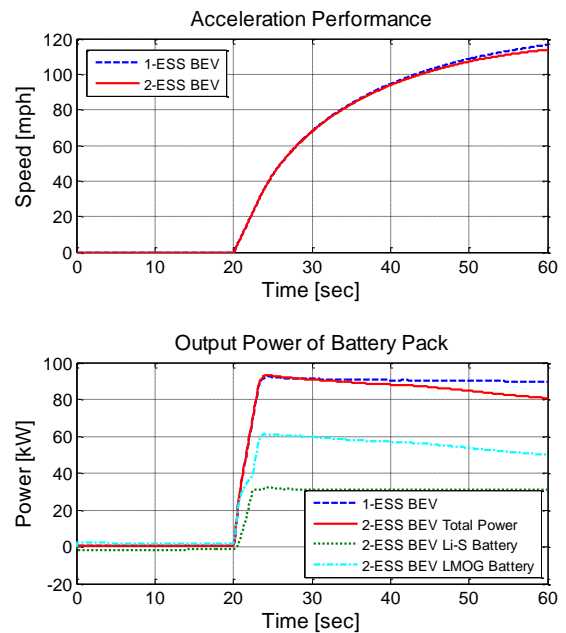


Figure V-6: Battery power comparison during performance

Simulation results for five driving conditions

To compare the electric consumption and the LCOD of the 2-ESS BEV to those of the 1-ESS BEV under various driving conditions, representative driving cycles, i.e., UDDS, HWFET,

US06, NEDC and JC08, were used in the Autonomie simulation environment.

As shown in Figure V-7, the AERs are almost the same for the 1-ESS and 2-ESS systems under the simulated driving conditions, but the AER is less than 300 miles for all cycles except the UDDS cycle, which was used to evaluate the battery capacity needed for the target AER.

The electric consumption of the 2-ESS BEV is slightly higher than that of the 1-ESS BEV, as indicated in Figure V-8. This difference in electrical consumption comes from the lower efficiency of the Li-S battery system in the 2-ESS BEV as well as the additional power electronics.

However, the estimated LCOD of the 2-ESS BEV averages about 2.5% lower than that of the 1-ESS BEV across the five cycles, as illustrated in Figure V-9 due to a higher vehicle cost for the 1-ESS BEV (about \$700 higher than that of the 2-ESS BEV).

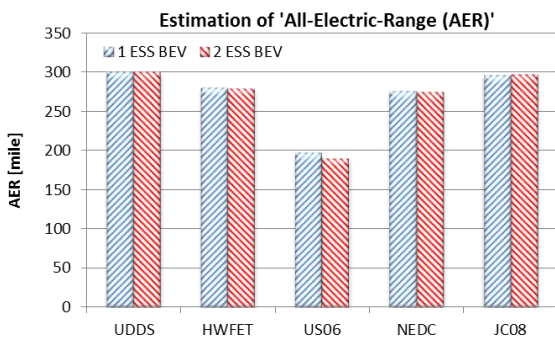


Figure V-7: All-electric range simulated for various drive cycles

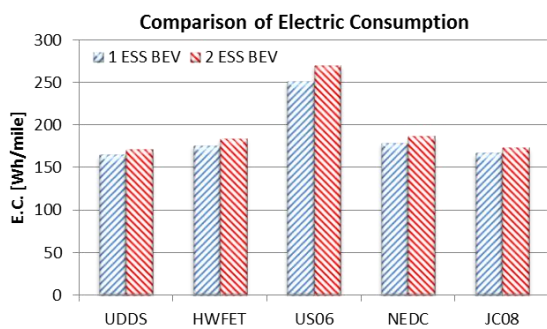


Figure V-8: Electric consumption simulated for various drive cycles

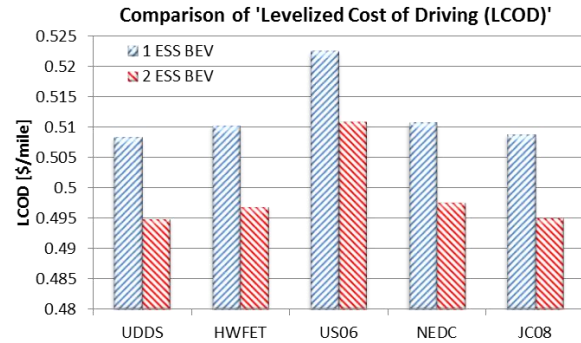


Figure V-9: LCOD simulated for various drive cycles

Conclusions

This study shows that the two-battery system is a viable option that should be explored further, as it is marginally cheaper than the single-battery design. If high-power batteries become more efficient, the two-battery system might become a significantly cheaper option. The impacts of system choice on battery life and fast-charging capabilities are not considered in this study. Those factors should be considered in assessing the selection of battery systems for future EVs.

Several exciting opportunities open up with the introduction of a cost-effective two-battery system. The power battery can be used to control the current flow from the primary energy battery. For example, Figure V-10 shows a small section of the UDDS cycle with various control parameters for regulating the current flow from the energy battery. This approach restricts the current fluctuations in the battery, at the cost of some efficiency.

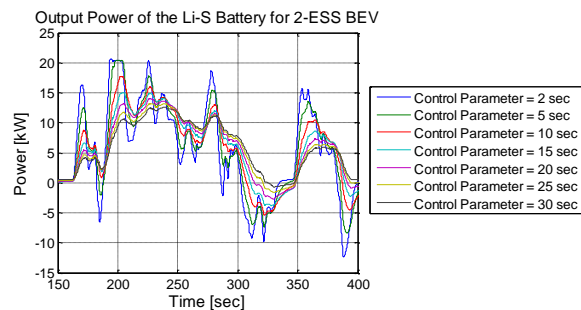


Figure V-10: Battery current from the energy battery can be controlled to a varying extent by using the power battery

Future work

There are certain disadvantages to having a high-energy battery with low power capacity. For fast charging, the battery must handle more power. The fast-charging requirements may also have to be factored into the sizing study to find an option that would be usable in future BEVs. Better integration of BatPaC with Autonomie will make such studies easier to do in the future.

V.A.3. Products

Publications

1. SAE paper in preparation.

References

1. ANL. GPRA Report for 2014.
www.ipd.anl.gov/anlpubs/2013/07/76897.pdf
2. ANL, Chemical Sciences and Engineering website.
"BatPaC: A Lithium-Ion Battery Performance and Cost Model for Electric-Drive Vehicles."
www.cse.anl.gov/batpac/
3. Wild, Stephan. "Solving Derivative-Free Nonlinear Least Squares with POUNDERS." Prepared for ANL, April 2014. www.mcs.anl.gov/papers/P5120-0414.pdf
4. Vijayagopal et al. (unpublished): Using multi-objective optimization for automotive component sizing.
5. Autonomie website. www.autonomie.net.

Tools and Data

1. Autonomie (www.autonomie.net)
2. BatPac

V.B. Evaluation of the Fuel Economy Impact of Low Temperature Combustion (LTC) using Simulation and Engine in the Loop

Principal Investigator: Neeraj Shidore

Organization: Argonne National Laboratory
 Address: 9700 South Cass Avenue
 Argonne, IL 60439
 Phone: (630) 252-7416
 E-mail: nshidore@anl.gov

DOE Program Manager: David Anderson

Phone: (202) 287-5688
 E-mail: David.Anderson@ee.doe.gov

DOE Program Manager: Gurpreet Singh

Phone: (202) 586-2333
 E-mail: gurpreet.singh@ee.doe.gov

- Quantify fuel consumption and engine-out emissions for LTC technology with EIL when steady combustion at low loads is established.



V.B.2. Technical Discussion

Background

Low-temperature combustion (LTC) technology research is being conducted by Argonne's Advanced Combustion Engines research group to improve the engine efficiency of light-duty passenger vehicles. One of the goals of the vehicle systems research at DOE is to rapidly evaluate components and systems through model-based design and component-in-the-loop. This project evaluates DOE-developed strategies for LTC of 87 anti-knock index (AKI) gasoline in a systems context by using transient vehicle drive cycles. A 1.9-L Turbo Direct Injection (TDI) engine, with diesel as the default fuel, is used for the LTC study with 87 AKI gasoline.

Introduction

LTC research performed by the Engine Research Group at Argonne National Laboratory (Argonne) with 87 AKI gasoline has shown lower fuel consumption and NO_x emissions as compared to gasoline spark ignition (SI) engines [1] (Figure V-11).

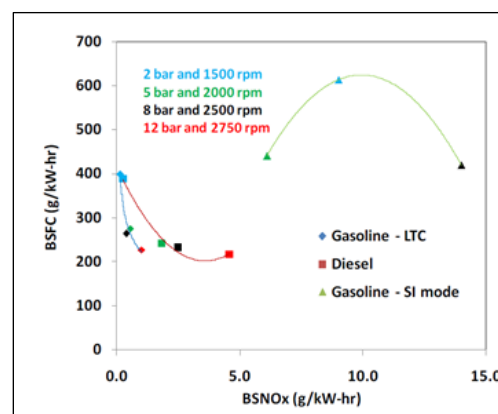


Figure V-11: Brake-specific fuel consumption and engine-out NO_x for LTC compared to gasoline SI and diesel engines

V.B.1. Abstract

Objectives

Evaluate the impacts of low-temperature combustion (LTC) technology on fuel economy and engine-out emissions using vehicle simulations and engine-in-the-loop (EIL):

- Quantify the fuel economy benefits of LTC on standard drive cycles using EIL.
- Evaluate test-to-test variability with LTC compared to diesel.
- Assess the transient behavior of LTC.
- Compare the fuel economy benefits of LTC technology to PFI (Port Fuel Injection) and SIDI (Spark Ignition Direct Injection) technologies by using simulations.

Major Accomplishments

- Completed EIL setup; demonstrated EIL operation with diesel (baseline) fuel.
- Established baseline fuel consumption and engine-out emission numbers with diesel fuel using EIL.
- Quantified the fuel economy benefits of LTC for a mild hybrid powertrain, BISG (Belt Integrated Starter Generator).
- Updated the fuel economy benefits of LTC for a conventional powertrain with improved low-load steady-state brake-specific fuel consumption (bsfc) data on LTC from the Argonne Engine Research Group.

Future Achievements

- Update the fuel economy benefits of LTC for a mild hybrid powertrain with an updated bsfc map.

This project evaluates the fuel consumption and emissions benefits of LTC over transient cycles at a vehicle system level.

Approach

The design of the experiment for the project is shown in Figure V-12. The port fuel injection (PFI) and spark-ignited direct injection (SIDI) engine technologies, which act as a baseline to which LTC will be compared, are evaluated via simulation. Fuel consumption and engine-out emissions with LTC of gasoline will be measured from engine-in-the-loop (EIL) tests. Before the EIL tests with LTC, a simulation study was conducted to compare LTC to SIDI and PFI, and EIL tests were conducted with diesel fuel to validate the system approach to reduce engine-out emissions and improve fuel consumption. For these fuels and combustion technologies, the comparison between fuel consumption and emissions is performed for a midsize sedan (conventional powertrain) over the Urban Dynamometer Drive Cycle (UDDS) and the highway drive cycle (HWFET).

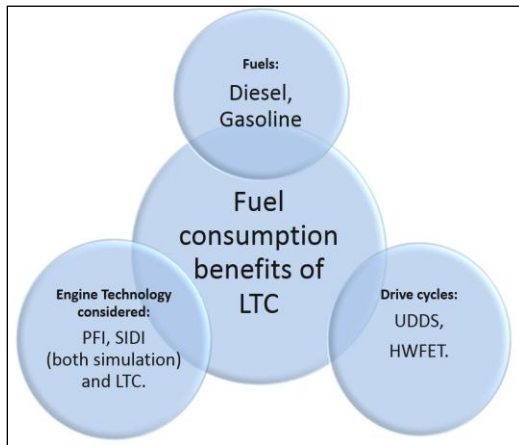


Figure V-12: Design of experiment

In order to compare the LTC technology to PFI and SIDI in simulation, a fuel rate map of LTC gasoline was generated from measured steady-state points. This was done by creating efficiency lines (willans) proportional to available efficiency curves from the steady-state data [2].

The specifications for the conventional vehicle used for the study are listed in Table V-5. The specifications are those of a MY2007 Cadillac BLS Wagon [3], which has the same diesel engine as the one used at Argonne for the LTC research.

Table V-5: Vehicle Specifications

| | |
|--------------|--|
| Vehicle | Cadillac BLS Wagon |
| Vehicle Mass | 1560 kg |
| Engine | 1.9 L TDI, 110 kW, 320 Nm peak torque, I-4 |
| Transmission | Manual, 6-speed |

For a fair comparison among SIDI, PFI, and LTC technologies, the SIDI and PFI engines were scaled in power in order to meet the vehicle technical specifications of the MY2007 Cadillac BLS Wagon. Different transmission ratios and final drives were selected for the PFI, SIDI, and LTC engines, on the basis of each engine's peak torque and maximum speed characteristics. The fuel consumption map for the SIDI engine was generated from a 2.2-L ECOTEC SIDI engine. The fuel consumption map for the PFI engine was generated from a 1.8-L Peugeot engine.

Figure V-13 shows the powertrain specifications for the conventional and the BISG powertrain with the different engines. It should be noted that the battery and electric machine specifications are valid only for the BISG configuration.

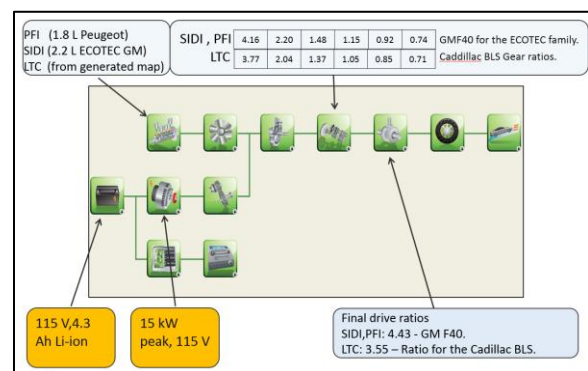


Figure V-13: Specifications of the conventional and BISG powertrains

Figure V-14 shows a conceptual representation of the EIL setup for the GM 1.9-L engine.

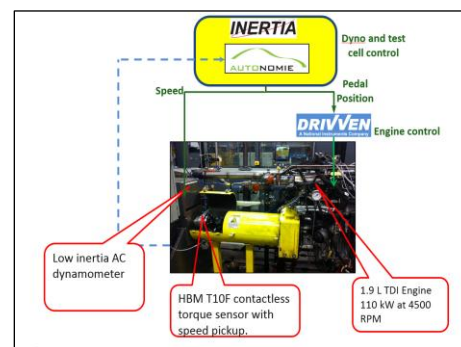


Figure V-14: Engine-in-the-loop setup with the 1.9-L TDI engine used for the LTC tests

In Q4 of FY 2014, the baseline bsfc maps for the LTC mode were updated in accordance with new results at low loads. Figure V-34 compares the fuel consumption curves for the previous and updated fuel rates at 2500 RPM. The fuel rate improvement at low and medium loads can be seen. The bsfc map used for the Autonomie simulation was updated for a speed range from 800 RPM to 2500 RPM.

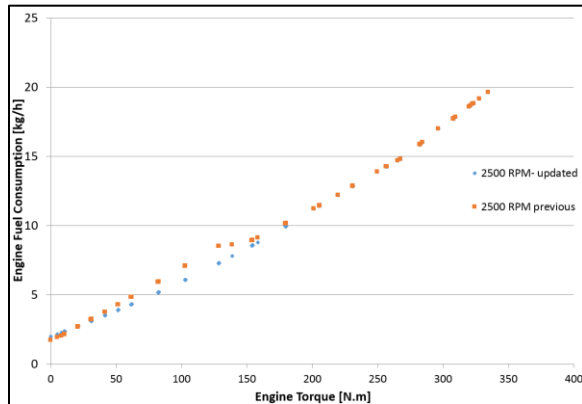


Figure V-15: Improvement in fuel consumption with updated fuel rate at low and medium loads at 2500 RPM

The conventional baseline simulations were therefore updated to account for the improvements seen at low and medium loads.

Results

Engine-in-the-loop results with baseline diesel engine

EIL capability was established with the default diesel fuel on the GM 1.9-L TDI engine. With the EIL capability established with diesel fuel, performing transient analysis on the LTC technology would require a much shorter lead time.

Table V-6 lists the mean fuel consumption and emissions (engine-out) values for the baseline diesel engine. The emissions data were recorded in ppm, and converted to a per-mile basis on the basis of published calculations [4].

Table V-6: Fuel Consumption and Emissions with Diesel Fuel for the GM 1.9-L TDI Engine, from Engine-in-the-Loop Data

| Drive Cycle | Fuel Consumption [L/100 km] | NOx [g/mi] | HC [g/mi] | CO [g/mi] |
|-------------|-----------------------------|------------|-----------|-----------|
| UDDS | 5.72 | 1.11 | 0.12 | 1.72 |
| HWFET | 4.02 | 0.40 | 0.05 | 0.88 |

Gear ratio selection and shift parameter optimization, for particular cycles, has a significant impact on fuel consumption and emissions. In FY 2013, a simulation study, based on steady-state emission maps for the 1.9-L TDI engine with diesel fuel, was conducted to evaluate the impact of shift parameters on fuel consumption and emissions [5]. In FY 2014, with the EIL setup functional with diesel fuel, the same study was repeated on hardware to validate the trends observed in simulation. Figure V-16 shows a plot of engine speed with the default and updated shift parameters. It can be seen that with the updated shift parameters, the engine operates at lower speeds, and therefore higher torque, in the time interval between 230 and 300 s.

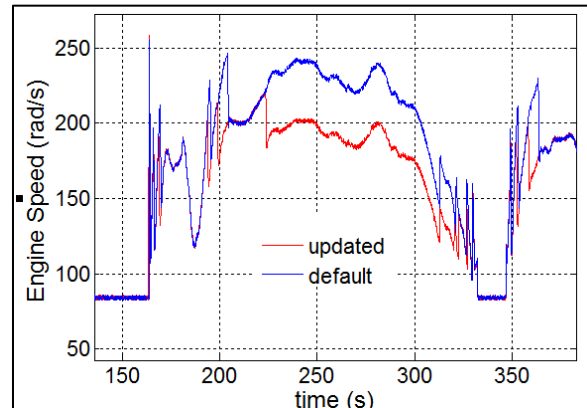


Figure V-16: Engine downspeeding via updated shift parameters during a section of the UDDS cycle

Figure V-17 shows the measured fuel rate (kg/hr) for the segment of the drive cycle between 230 and 300 s. The impact of downspeeding can be clearly seen, as the fuel rate with the updated shift parameters is lower than the default case.

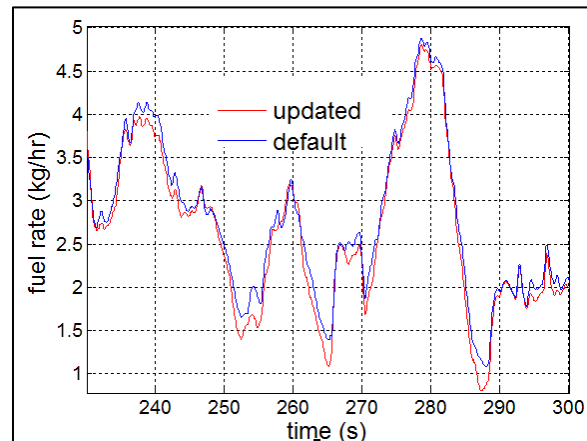


Figure V-17: Reduction in engine fuel consumption due to downspeeding

Figure V-18 shows the impact of downspeeding on instantaneous NOx emissions. As stated in last year’s annual report, simulations with steady-state NOx maps suggested a trade-off between fuel consumption and NOx due to downspeeding. As Figure V-18 shows, NOx does increase due to downspeeding and the resulting higher-torque operation of the engine. It should be noted that early in the shift regime, when the engine is in the same gear (i.e., engine speed and torque are the same) for both sets of shift parameters, the NOx emissions are very similar to each other.

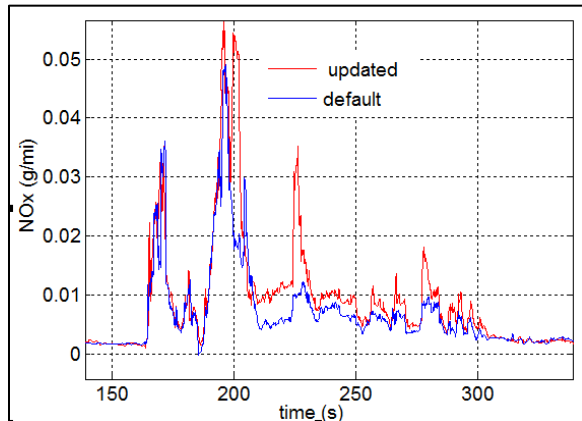


Figure V-18: Increase in NOx due to downspeeding

Table V-7 summarizes the impact of downspeeding on fuel consumption and emissions for the UDDS cycle. The mean values indicated in Table V-6 and Table V-7 are over five cycles (five with default shifting and five with shift parameters updated for downspeeding).

Table V-7: Impact of Downspeeding on Fuel Consumption and Emissions (mean values)

| Shift parameters | Fuel Consumption [L/100 km] | NOx [g/mi] | HC [g/mi] |
|------------------------|-----------------------------|------------|-----------|
| Default | 5.81 | 0.9 | 0.13 |
| Updated (downspeeding) | 5.72 | 1.11 | 0.12 |

Fuel consumption benefits of LTC for a mild hybrid powertrain using simulation (based on earlier version of bsfc maps)

As stated in the approach section, the fuel consumption benefits of LTC with gasoline were evaluated for a Belt Integrated Starter Generator (BISG). The BISG enables engine stop at idle and provides slight torque assist at low vehicle speeds. Therefore, the three engines were resized in order to have the same 0-60 mph performance.

shows the original engine peak power, the engine peak power after resizing for the conventional powertrain, and the engine peak power after resizing for the BISG powertrain.

Table V-8: Engine Resizing for the Conventional and the BISG Powertrain to Match the IVM-60 MPH Performance for the Three Engines

| Engine Type | Original (unsized) peak power [kW] | Engine peak power (resized) for conventional powertrain [kW] | Engine peak power (resized) for BISG powertrain [kW] |
|-------------|------------------------------------|--|--|
| PFI | 90 | 147 | 110 |
| SIDI | 104 | 135 | 107 |

| | | | |
|----------------|-----|-----|----|
| LTC (gasoline) | 110 | 115 | 92 |
|----------------|-----|-----|----|

For reference, the fuel economy benefit for a conventional powertrain with LTC compared to the PFI engine, based on earlier versions of the bsfc map, is 25% over the combined cycle.

Table V-9 lists the fuel economy benefits for the BISG configuration. As seen in Table V-9, for the BISG configuration, LTC technology offers a 23% improvement in fuel economy over PFI and a 7% improvement over the SIDI over the combined cycle.

Table V-9: Fuel Economy Benefits of LTC Compared to PFI and SIDI (simulation study results) for BISG Powertrain with Earlier-Generation BSFC Map

| Drive Cycle | Fuel Economy [mpg, unadjusted] | | |
|-----------------------|--------------------------------|-------|------|
| | PFI | SIDI | LTC |
| UDDS | 30 | 35.6 | 38 |
| HWFET | 34 | 42 | 46 |
| Combined [55/45] | 31.6 | 38.22 | 41.2 |
| Improvement over PFI | | 17% | 23% |
| Improvement over SIDI | | | 7% |

Fuel consumption benefits of LTC for a conventional powertrain with updated versions of the bsfc map

In Q4 of FY 2014, updated bsfc maps were generated which reflected decreased low-load fuel consumption. Figure V-18 shows the improvement in fuel consumption at low and medium loads for an engine speed of 2500 RPM. Table V-10 shows the fuel economy improvements with the conventional powertrain with the updated bsfc map.

Table V-10: Fuel economy benefits of LTC compared to PFI and SIDI (simulation study results) for conventional powertrain with updated bsfc map

| Drive Cycle | Fuel Economy [mpg, unadjusted] | | |
|-----------------------|--------------------------------|------|-------|
| | PFI | SIDI | LTC |
| UDDS | 29.1 | 32.6 | 37.6 |
| HWFET | 39.6 | 42.1 | 50.7 |
| Combined [55/45] | 33.1 | 36.3 | 42.5 |
| Improvement over PFI | | 10% | 28.7% |
| Improvement over SIDI | | | 17% |

It should be re-emphasized that the conventional fuel economy results in Table V-10 look comparable to the BISG results in Table V-9 because of the updated bsfc maps based on the latest steady-state combustion results.

Conclusions and Future Directions

1. This project evaluates a DOE-developed combustion technology (LTC with generic gasoline) in a vehicle systems context through the use of simulation and EIL.
2. The fuel consumption of a midsize sedan (conventional powertrain) with LTC was compared to the same vehicle with SIDI and PFI engines (the SIDI and PFI engines are scaled in power such that the vehicle IVM-60 mph performance is the same in each case) via simulation. In addition, fuel consumption and engine-out emissions for the said technology will be quantified by using EIL. Shift parameters will be optimized to minimize the fuel consumption and/or engine-out NO_x emissions of the LTC engine.
3. The updated simulation study on the conventional powertrain has shown that with LTC, a 28.7% improvement in fuel consumption over a PFI engine and a 10% improvement over SIDI engine technology are possible.
4. EIL has been implemented on the engine dyno test cell with the 1.9-L TDI engine. Fuel consumption and emissions with diesel fuel have been quantified with EIL.
5. The trends in the impact of shift parameters on fuel consumption and engine-out emissions, predicted through a simulation study in FY 2013, have been confirmed through EIL in FY 2014 for the baseline (diesel) fuel.
6. The improvement in fuel economy due to LTC for a mild hybrid powertrain (BISG configuration) has been quantified.
7. Once engine hardware upgrades are complete and steady engine combustion has been established across the entire engine operating map, transient evaluation with LTC will be performed using EIL.
8. The impact of LTC on the fuel consumption and emissions of an electrified powertrain will be updated in FY 2015 by using the updated bsfc map.

Presentations

N. Shidore, A. Rouseau, S. Ciatti, "Evaluation of the Fuel Economy Impacts of Low Temperature Combustion

(LTC) Using Engine in the Loop: Status Update to DOE Sponsors," demo and presentation to Ken Howden and Leo Breton.

References

1. Stephen Ciatti, Christopher Kolodziej, "Use of Low Cetane Fuel to Enable Low Temperature Combustion," DOE Annual Merit Review, June 18, 2014.

2. Phillippe Abiven, Steve Ciatti, Aymeric Rousseau, "Fuel Consumption Benefit of Low Temperature Combustion Engine for Conventional Vehicle," presentation to DOE, August 29, 2012.
3. Cadillac BLS 1.9 TiD, 2005, www.carinf.com/en/9220414062.html.
4. SAE J1003: Diesel Engine Emission Measurement Procedure.
5. Neeraj Shidore, Stephen Ciatti, Chris Kolodziej, Daehung Lee, Namdoo Kim, "Impact of Shift Parameter Turning on Fuel Consumption and NO_x for the 1.9 L TDI Engine," presentation to DOE, June 12, 2013

Tools and Data

1. Autonomie – www.autonomie.net

V.C. In-Vehicle Lower-Energy Energy Storage System (LEESS) Component Evaluation

Principal Investigator: Jeffrey Gonder

National Renewable Energy Laboratory (NREL)
15013 Denver West Parkway, MS 1634
Golden, CO 80401
Phone: (303) 275-4462
E-mail: jeff.gonder@nrel.gov

DOE Program Manager: David Anderson

Phone: (202) 287-5688
E-mail: David.Anderson@ee.doe.gov

DOE Program Manager: Lee Slezak

Phone: (202) 586-2335
E-mail: Lee.Slezak@ee.doe.gov

V.C.1. Abstract

Objectives

- Evaluate performance of lower-energy energy storage system (LEESS) devices to support power-assist or “full” hybrid electric vehicles (HEVs).
 - HEVs with lower cost or better performing energy storage systems could improve their cost-versus-benefit ratio, market penetration, and aggregate fuel savings.
- Continue OEM and supplier collaboration for conducting the project.
 - Complete shake-down testing of the reusable HEV test bed.
 - Install and test multiple LEESS devices relative to the performance of the production battery configuration.

Major Accomplishments

- Completed comparison testing between the converted Ford Fusion Hybrid test vehicle operating on its production battery pack and operating on lithium-ion capacitor (LIC) LEESS devices supplied by JSR Micro, Inc.
 - Comparisons included acceleration performance and fuel economy testing over multiple drive cycles. The evaluation also considered different LIC energy content scenarios.
 - Several of the tested LIC configurations demonstrated equivalent fuel economy and acceleration performance as the production battery configuration across all tests conducted. The lowest energy LIC scenario demonstrated equivalent

performance over most tests, though slightly higher fuel consumption on the US06 cycle.

- The overall results indicate that as long as critical attributes such as engine start under worst case conditions can be retained, considerable ESS downsizing may minimally impact HEV fuel savings.
- Completed bench testing of the second set of LEESS devices to evaluate in the vehicle—ultracapacitor modules from Maxwell Technologies.
- Removed and returned the JSR Micro LIC modules and installed the Maxwell ultracapacitor modules to prepare for in-vehicle comparison testing.

Future Achievements

- Complete in-vehicle comparison testing between the final LEESS devices under evaluation and the production vehicle battery pack.
- Consider system optimization opportunities (such as different motor or engine size) around the particular performance capabilities of LEESS devices.



V.C.2. Technical Discussion

Background

Automakers have been mass-producing HEVs for more than a decade, and the technology has proven to be very effective at reducing per-vehicle fuel use. However, the cost of HEVs such as the Toyota Prius or Ford Fusion Hybrid remains several thousand dollars higher than the cost of comparable conventional vehicles, which has limited HEV market penetration. The battery energy storage device is typically the component with the greatest contribution toward this cost increment, so significant cost reductions and/or performance improvements to the energy storage system (ESS) can correspondingly improve the vehicle-level cost-versus-benefit relationship. Such an improvement would, in turn, lead to larger HEV market penetration and greater aggregate fuel savings.

Introduction

In recognition of these potential benefits, the United States Advanced Battery Consortium (USABC) asked the National Renewable Energy Laboratory (NREL) to collaborate with its work group and analyze the trade-offs between vehicle fuel economy and reducing the decade-old minimum energy requirement for power-assist HEVs. NREL’s analysis showed that significant fuel savings could still be delivered from an

ESS with much lower energy storage than the previous targets, which prompted USABC to issue a new set of lower-energy ESS (LEESS) targets and issue a request for proposals to support their development. To validate the fuel savings and performance of an HEV using such a LEESS device, this jointly funded activity between the U.S. Department of Energy Vehicle Technologies Office Energy Storage and Vehicle Systems Simulation and Testing programs has designed a test platform in which alternate energy storage devices can be installed and evaluated in an operating vehicle.

Approach

The approach in previous fiscal years (FY 2012–FY 2013) included establishing a cooperative research and development agreement between NREL and Ford Motor Company to support the conversion of a Ford Fusion Hybrid into a test platform for evaluating LEESS devices. NREL subsequently acquired a 2012 Fusion Hybrid, designed the conversion, and entered into agreements with JSR Micro to provide (at JSR Micro’s expense) LIC modules as the first LEESS device to be evaluated in the vehicle. The LICs are asymmetric electrochemical energy storage devices possessing one electrode with battery-type characteristics (lithiated graphite) and one with ultracapacitor-type characteristics (carbon). In FY 2013, NREL completed bench testing on the LIC replacement pack compared to the production nickel metal hydride (NiMH) battery pack from the 2012 Fusion Hybrid and integrated the modules into the Fusion Hybrid test platform.

The approach in FY 2014 included troubleshooting and shakedown testing to get the vehicle fully operational with the alternative LEESS modules. Subsequently, on-road and chassis dynamometer testing were used to perform back-to-back comparisons of operation using the LIC replacement pack relative to the production NiMH configuration. While this testing was being completed (using multiple energy storage configurations of the LIC modules), NREL established agreements with Maxwell Technologies to provide ultracapacitor modules as the second LEESS device to evaluate in the vehicle (again at the supplier’s expense). In the second half of FY 2014, NREL completed bench testing on the Maxwell ultracapacitor modules, removed and returned the JSR Micro LIC modules, and integrated the Maxwell ultracapacitor modules into the vehicle test platform. The remainder of the planned in-vehicle testing will be completed in FY 2015.

Results

Figure V-19 shows a photograph of the production high-voltage traction battery (HVTB) unit, which is mounted between the rear seat and the trunk area in the Fusion Hybrid. Important components of the HVTB include the high-voltage bussed electrical center (BEC), the battery pack sensor module (BPSM), and the battery energy control module (BECM). The BEC acts as an interface between the high-voltage output of the HVTB and the vehicle’s electric motor, air-conditioning compressor, and DC/DC converter. The

BPSM measures the voltage and temperature of the NiMH cells and communicates with the BECM, which manages the charging/ discharging of the battery and also communicates with the other vehicle control modules via the high-speed controller area network (CAN) bus.



Figure V-19: Photo of the Fusion Hybrid’s HVTB. Image by John Ireland, NREL

To implement the vehicle conversion, NREL kept the production HVTB installed in its original position so that direct comparison testing could be conducted by switching back and forth between the production battery and the alternative LEESS under test. Figure V-20 shows a schematic of this configuration, in which parts from a second HVTB acquired by NREL (including the BECM, BEC, BPSM, module sense leads, and various wiring harnesses) were reconfigured to work with the alternative LEESS under test. The dSpace component represented in the schematic is a dSpace MicroAutoBox (MABx), which is used to intercept certain CAN signals pertaining to the BECM’s calculations for the production NiMH battery (state of charge, power capability, etc.) and to replace them with corresponding calculations for the alternate LEESS under test. The MABx also records data and handles safety controls during the testing.

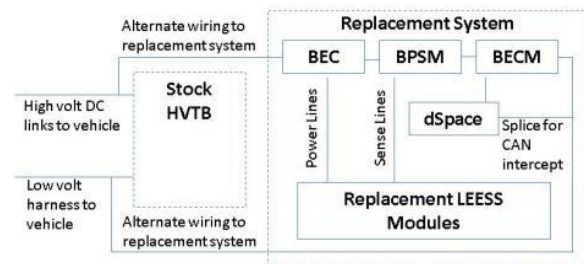


Figure V-20: Schematic of connections among replacement components and the vehicle

Prior to actually integrating the JSR LIC modules into the test vehicle, NREL first performed bench testing with the modules mounted in an environmental chamber (see Figure V-20). The purposes of the bench testing included confirming expected LIC performance, comparing the LIC pack’s operation to that of the production battery over a representative driving profile, and generating test data for calibrating the custom state estimator model to implement in the dSpace MABx. Results from the LIC module hybrid pulse power characterization (HPPC) bench testing are presented later alongside the results from the comparable testing of the Maxwell ultracapacitor modules.



Figure V-21: JSR LIC modules in an environmental chamber during bench testing, with the production 2012 Fusion Hybrid NiMH modules in the background. Image by John Ireland, NREL

Following bench testing, the LIC modules were integrated into the Fusion Hybrid test platform to enable the in-vehicle comparison testing. Figure V-22 shows a picture of the fully integrated conversion system, including LIC modules, mounted in the trunk of the Fusion Hybrid. The LIC modules and the replacement BEC are shown in the large box with the clear lid; to the side, the picture shows the MABx mounted on top of an electronics box containing a voltage divider circuit and related components.



Figure V-22: Fully integrated conversion system mounted in the trunk of the Fusion Hybrid test platform. Image by Jon Cosgrove, NREL

In addition to the physical components shown in Figure V-22, completing the vehicle integration involved validating the custom state estimator code (for calculating the LEES state of charge and charge/discharge capability at any moment in time) against the bench test data. This code was incorporated into the MABx and included temperature dependence functionality calibrated against the various temperature conditions from the bench testing (-20°C, 25°C, and 45°C).

Initial driving tests focused on confirming proper operation of the converted vehicle. This included making sure the vehicle could operate while intercepting and rebroadcasting modified signals via the vehicle CAN bus. Further shakedown tests verified proper functioning of the safety controls and the state estimator model for the alternate LEES device. After this was confirmed, NREL conducted closed-course performance testing on the vehicle in both the LIC and production configurations (see Figure V-23 and Figure V-24).



Figure V-23: Closed-road acceleration performance testing. Image by Petr Sindler, NREL

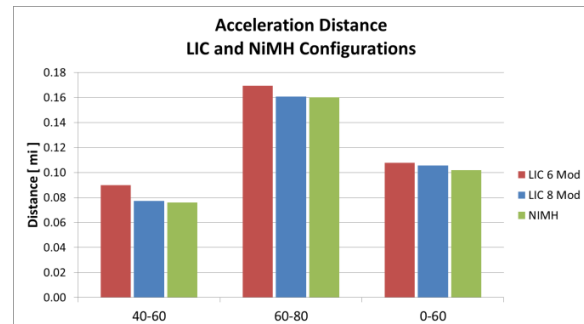


Figure V-24: Acceleration distance for NiMH, eight-module LIC, and six-module LIC configurations while performing 0–60, 40–60, and 60–80 accelerations

Figure V-24 shows the standing and passing acceleration performance from six- and eight-module configurations of the LIC replacement pack compared to the production NiMH system. NREL evaluated different configurations of the LIC storage system to examine trade-offs between size/energy content (which would ultimately influence component cost) and measured in-vehicle performance. As Figure V-25 indicates, the eight-module configuration achieved similar performance to the production system in all three of the evaluated acceleration categories. Although the six-module configuration demonstrated a slight performance penalty, it is very possible that more extensive controls calibration than was possible as part of this investigation could eliminate this difference. NREL therefore concluded that the LEES LIC configurations can support comparable level-road acceleration performance to the production configuration, but that the smallest LIC scenario evaluated may be on the edge of some small acceleration performance degradation.

For HEV fuel economy evaluation, NREL utilized chassis dynamometer testing facilities at SGS Environmental Testing Corporation in Aurora, Colorado. Tests included standard certification cycles such as the Federal Test Procedure (FTP) and its constituent Urban Dynamometer Driving Schedule (UDDS), the Highway Fuel Economy Test (HWFET), the aggressive US06, and the hot SC03 cycle (including air-conditioning). These tests allowed NREL to evaluate in-vehicle ESS performance under a variety of conditions, including moderate (24°C), hot (35°C), and cold (-7°C) temperatures.

Figure V-25 shows test results on the stop-and-go UDDS driving profile for both the production NiMH configuration and for a low-energy LIC scenario. The ESS energy profile for both storage system configurations showed oscillations in energy usage aligned with the individual microtrips in the driving

profile—i.e., when the vehicle accelerated from a stop to some nominal driving speed then later decelerated back to a stop, the ESS profile showed some amount of discharge to support accessories while stopped as well as to assist the acceleration, and then later recaptured energy through regenerative braking during the deceleration. For the low-energy LIC scenario, these oscillations remained within a 60-Wh window; whereas the production NiMH configuration showed a bulk energy swing in addition to the microtrip-scale oscillations that spanned a 170-Wh window. Comparing the cumulative fuel consumption curves for the two configurations, the NiMH case showed slightly more fuel use during the period when bulk ESS charging occurred and slightly less during the bulk discharging period, but by the end of the test cycle, the fuel use between the two cases was essentially equal.

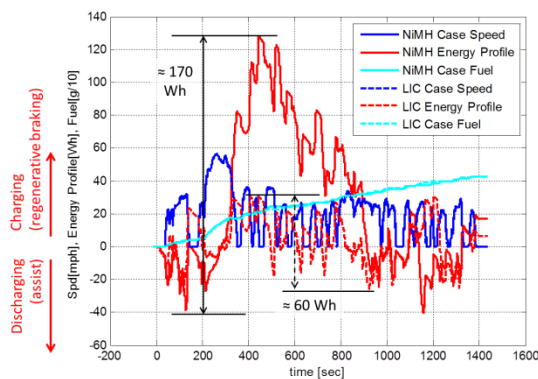


Figure V-25: ESS energy profile and fuel use for 24°C UDDS tests of production NiMH and low-energy LIC configurations

Figure V-26 shows similar results for a low-energy six-module LIC configuration compared to the production NiMH case during the 35°C SC03 cycle. This figure shows equivalent cumulative fuel use between the two scenarios, along with similar engine on/off behavior during the test cycle.

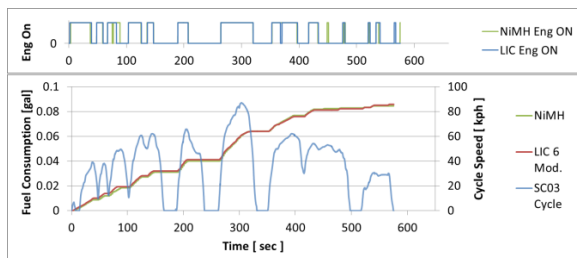


Figure V-26: Fuel consumption and engine on/off cycling during hot (35°C) SC03 testing with air-conditioning

Figure V-27 shows the ESS energy profile and cumulative fuel consumption results for the aggressive US06 cycle, which was the one test profile in which the low-energy LIC configuration showed higher cumulative fuel consumption (by approximately 4%) than the production NiMH configuration. The energy window sizes for each configuration are approximately the same as for the UDDS test shown in Figure V-27, but in the US06 test the bulk depletion of the NiMH in the middle of the cycle helped to measurably reduce the cumulative fuel consumption during that high-speed driving section. The NiMH ESS was then able to recapture

regenerative braking energy during the decelerations at the end of the cycle to remain charge-neutral during the test; whereas the low-energy LIC scenario did not have enough available capacity to capture as much energy during those braking events.

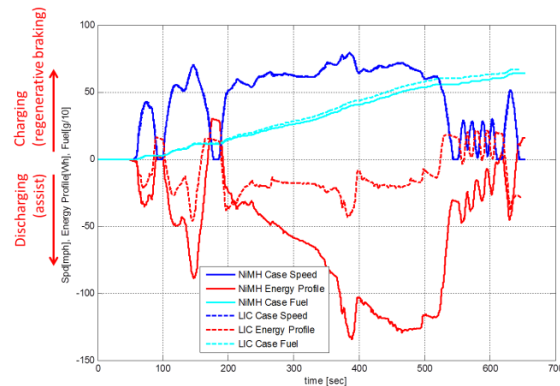


Figure V-27: ESS energy profile and fuel use for 24°C UDDS tests of production NiMH and low-energy LIC configurations

Figure V-28 summarizes the fuel consumption and energy window comparisons among multiple ESS configurations during five different test cycles. Note that the test matrix included intermediate LIC energy scenarios as well as the low-energy scenarios discussed in the previous plots. These intermediate energy scenarios still fall under the LEES category for power-assist HEV ESS, because they possess much lower nominal energy content than the roughly 1.4-kWh production NiMH ESS.⁵ Several of the relatively higher energy content LIC scenarios tested achieved energy window sizes and fuel consumption comparable to the NiMH reference case—including during the US06 cycle. For all cycles except for the US06 (including the -7°C FTP and the HWFET in addition to those already discussed), even the lowest energy LIC configurations were able to match the fuel consumption of the reference NiMH test (using roughly 60-Wh energy windows compared to energy windows closer to 200 Wh for many of the NiMH tests).

The final set of FY 2014 results involved the ultracapacitor or electrochemical double-layer capacitor (EDLC) modules provided by Maxwell Technologies. These 48-V modules underwent a similar suite of bench tests as the JSR LIC modules. Figure V-29 shows a comparison of the 2-second and 0.5-second pack level resistance for the indicated LIC and

⁵ Based on a fact sheet published by Idaho National Laboratory: www1.eere.energy.gov/vehiclesandfuels/avta/pdfs/hev/batteryfusion4699.pdf

EDLC configurations. These calculations were derived from the HPPC test results and depend on the timescale during which the measurement is taken because of the combined influence of impedance and changing energy content when measuring voltage rise/drop following each pulse. These results indicated roughly three times lower internal resistance for the LEESS devices than for the production NiMH ESS.¹

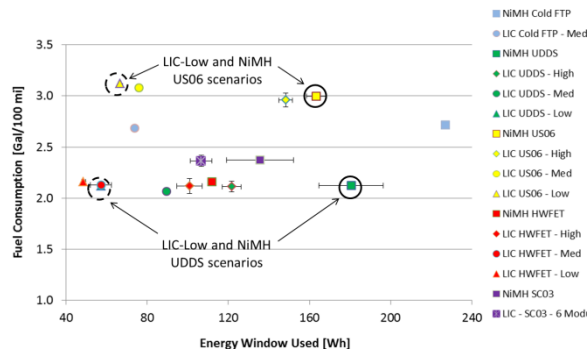


Figure V-28: Summary of fuel consumption and energy window results for multiple test cycles and vehicle configurations

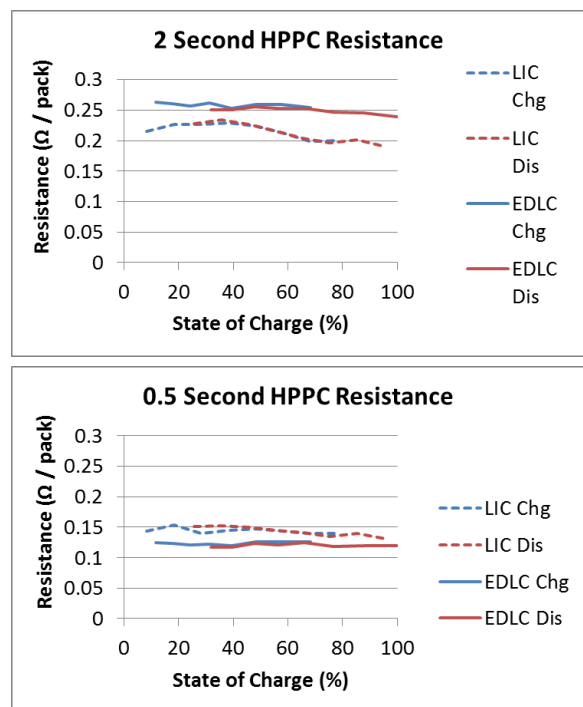


Figure V-29: Pack level 2-second and 0.5-second resistance for the ("high-energy") eight-module LIC and the seven-module EDLC configurations

The EDLC modules were also characterized for drive cycle performance and power capabilities. This data was used to calibrate the models running on the MABx in a similar manner as was used for the LIC configuration. As shown in Figure V-30, the EDLC modules have been installed in the test vehicle. In addition to conducting many of the same tests that were completed for the LIC configurations, NREL hopes to assess any operating advantage the modules may see at very cold temperatures (as low as -20°C). This testing had been

planned for the LIC configurations, but the test facility was not able to maintain such a low chamber temperature during summer testing; whereas the facility expects to be able to maintain lower temperatures during winter testing.



Figure V-30: Installed Maxwell EDLC seven-module configuration. Image by Jon Cosgrove, NREL

Conclusions

Alternate HEV storage systems such as the LIC and EDLC modules described in this report have the potential for improved life, superior cold temperature performance, and lower long-term cost projections relative to traditional battery storage systems. If such LEESS devices can also be shown to maintain high HEV fuel savings, then future HEVs designed with these devices could have an increased value proposition relative to conventional vehicles, thus resulting in greater HEV market penetration and aggregate fuel savings. This jointly funded activity between the U.S. Department of Energy Vehicle Technologies Office Energy Storage and Vehicle Systems Simulation and Testing programs developed a vehicle test platform to help validate the in-vehicle performance capability of alternative LEESS devices and identify unforeseen issues.

This report describes successful creation of the Ford Fusion Hybrid test platform for in-vehicle evaluation of such alternative LEESS devices, bench testing of the initial LIC pack provided by JSR Micro, integration and testing of the LIC pack in the test vehicle, and the bench testing and installation of a second LEESS pack from Maxwell Technologies (consisting of EDLC modules). The in-vehicle LIC testing results suggest technical viability of LEESS devices to support HEV operation. Several of the tested LIC configurations demonstrated equivalent fuel economy and acceleration performance as the production NiMH ESS configuration across all tests conducted. The lowest energy LIC scenario demonstrated equivalent performance during several tests, although slightly higher fuel consumption on the US06 cycle and slightly slower acceleration performance. However, more extensive vehicle-level calibration than was possible for this conversion project may be able to reduce or eliminate these performance differences. The overall results indicate that as long as critical attributes such as engine start under worst-case conditions can be retained, considerable ESS downsizing may minimally impact HEV fuel savings.

Ongoing work into FY 2015 will include completion of in-vehicle comparison testing between the EDLC pack and the production NiMH ESS. Other possible future work topics include evaluating the potential offered by LEESS devices with more extensive vehicle modification, such as by better matching the size of the motor in the vehicle to the LEESS power capabilities.

This project has helped demonstrate the technical viability of nontraditional technologies to compete with typical battery systems for HEV energy storage. However, some combination of systems optimization to best leverage LEESS capabilities and cost reductions on the part of suppliers will be necessary to move LEESS technology from mere technical viability to having a compelling business case for broad use in HEV energy storage.

V.C.3. Products

Publications

1. Cosgrove, J.; Gonder, J.; Pesaran, A. "Performance Evaluation of Lower-Energy Energy Storage Alternatives for Full-Hybrid Vehicles." Presentation at the Supercapacitors USA International Conference and Tradeshow, November 2013.
2. Gonder, J.; Cosgrove, J.; Pesaran, A. "Performance Evaluation of Lower-Energy Energy Storage Alternatives for Full-Hybrid Vehicles." Proceedings of the SAE 2014 Hybrid and Electric Vehicle Technology Symposium, February 2014.

3. Gonder, J.; Cosgrove, J.; Pesaran, A.; Keyser, M. "In-Vehicle Evaluation of Lower-Energy Energy Storage System (LEESS) Devices." DOE Vehicle Technologies Annual Merit Review – Project ID#: VSS129, June 2014.
4. Gonder, J.; Cosgrove, J.; Shi, Y.; Saxon, A.; Pesaran, A. "Lower-Energy Energy Storage System (LEESS) Component Evaluation." NREL Milestone Report MP-5400-62853, September 2014.

Tools and Data

1. The converted Ford Fusion Hybrid test vehicle serves as a reusable tool for evaluating multiple alternative LEESS devices.
2. Data collected from bench and in-vehicle LEESS device testing is detailed in the publications listed above.

V.D. Advanced PHEV Gen-set Development and Demonstration

Principal Investigator: Paul H. Chambon

Oak Ridge National Laboratory (ORNL)
 2360 Cherahala Boulevard, Knoxville, TN 37932
 Phone: (865) 946-1428
 E-mail: chambonph@ornl.gov

DOE Program Manager: David Anderson

Phone: (202) 287-5688
 E-mail: david.anderson@ee.doe.gov

V.D.1. Abstract

Objectives

- The objective of this project is to integrate ORNL advancements in engine and electric machine technologies to properly design, and size a gen-set for various series hybrid electric vehicle applications.

Major Accomplishments

- Expanded the study to medium duty delivery vehicles and transit buses.
- Generated and validated vehicle models for both applications
- Quantified benefits of each engine-electric machine combination for both applications.

Future Achievements

- Project concluded in FY 2014.



V.D.2. Technical Discussion

Background

The additional cost and weight associated with larger battery pack capacity forces designers to utilize smaller packs in their vehicle plans, which leads to shorter ranges of electric vehicles. The use of a range extending gen-set (engine-generator set) to convert an electric vehicle (EV) in a series hybrid electric vehicle (HEV) or series plug in hybrid electric vehicle (PHEV), can reduce battery size and cost, and alleviate “range anxiety” (fear of not completing a trip on existing battery charge), by using the gen-set to recharge the battery. Figure V-31 shows a graphical representation of gen-set architecture benefits applied to a medium duty truck: reducing BEV ESS size such that EV range drops from 70 mile range to 30 mile will dramatically reduce vehicle cost and unladen mass. Some of those savings can be invested in a

genset which can increase the PHEV vehicle range past the original BEV range of 70mile. This is particularly true for today’s ESS costs (red trace) but will remain true with 2020 target costs for batteries (blue trace).

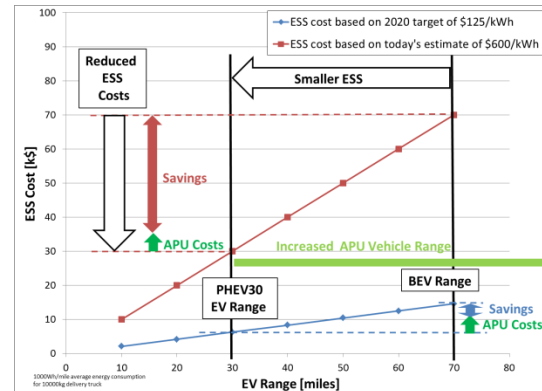


Figure V-31: Trade-off between APU costs and ESS size depending on range and ESS cost

Series HEV and PHEVs present a unique configuration when a gen-set is used to recharge the Energy Storage System (ESS). In true series architecture, the gen-set is not mechanically coupled to the drivetrain and therefore may be operated at its optimum efficiency point, regardless of driving conditions. As such, gen-sets provide unique opportunities for component sizing optimization, internal combustion engine operating regimes, exhaust after-treatment, cost effective technology components, electric machine and power electronics selection.

Introduction

This project will draw from the extensive experience in power electronics and electric machinery from the Power Electronics and Electrical Power Systems Research Center as well as the broad knowledge in advanced combustion and emissions after-treatment through the Fuels, Engines, and Emissions Research Center. Both centers are parts of the transportation section of ORNL. The emphasis will be placed on technologies currently under development in each respective center. It will attempt to focus on a modular gen-set that could have multiple applications outside of a vehicle, which would reduce cost based on high volume production.

This project will investigate several advanced technologies for each key component considering several aspects in its selection process such as efficiency, cost, strategic benefits (rare earth / non rare earth) and complementarity of the engine and motor technology.

Approach

The final year of this study will expand from passenger car applications to other applications that are well suited for hybrid electric powertrains due to the stop-and-go nature of their drive cycle. Medium duty delivery vehicles and transit buses will be considered. Models for both baseline conventional vehicles as well as series hybrid electric conversion vehicles will be generated and validated.

Fuel economy benefits of each engine-electric machine combination for both applications will be quantified.

Results

The simulation study performed during FY 2012 and FY 2013 had identified alternative fuels such as ethanol and advanced combustion as the most promising engine technologies for increased combustion efficiency, and non-rare earth induction machine as best cost and efficiency balance for electric machine technology.

The same technology matrix was considered for medium duty delivery trucks and transit buses. The following engine types were modeled during FY 2012:

- Gasoline Port Fuel Injected (PFI)
- Gasoline Stoichiometric Direct Injection (GDI)
- Ethanol Direct Injection (EDI)
- Gasoline Homogenous Charge Compression Ignition (HCCI)
- Conventional Diesel Combustion (CDC)
- Reactivity Controlled Compression Ignition (RCCI).

They were combined with the four following electric machine types:

- Interior Permanent Magnet machine (IPM)
- Wound Field machine (WF)
- Induction Machine (IM)
- Switched Reluctance Machine (SRM).

Medium Duty Delivery Truck Application

The base vehicle considered in this study was modelled after the Smith Newton BEV delivery truck, with a base weight of 10,000kg. This vehicle was selected because it could be a good candidate for hybridization in order to quantify the tradeoff between battery size and genset cost.

A model of a diesel engine powered variant of that electric truck was created to serve as a fuel economy benchmark for the PHEV version. That model was compared against a similar size diesel delivery truck that had been tested by NREL (1). Results shown on Figure V-32 show a good correlation between the model and experimental data on city and delivery route type drive cycles.

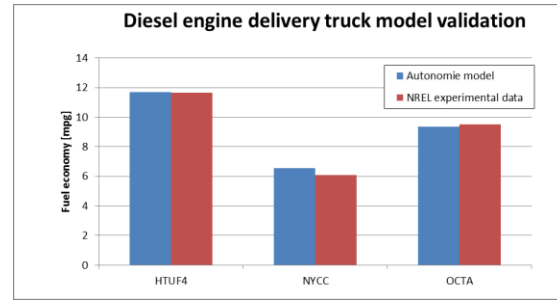


Figure V-32: Conventional diesel engine truck model validation

A model of a series PHEV variant of the same vehicle platform was then created. Its genset combined a gasoline port fuel injected engine and permanent magnet generator. This PHEV model was used to test two control strategies: thermostatic and load following. Their fuel economy numbers were very similar but the load following strategy was selected for the rest of the study as more realistic for actual implementation on a test vehicle.

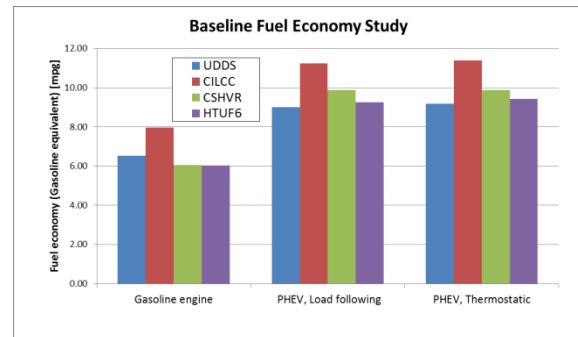


Figure V-33: Baseline fuel economy study

A sizing study was performed to determine the power of the engine and generator required for the PHEV genset to maintain vehicle performance and gradeability when in charge sustaining mode. This study yielded a genset engine power requirement of 120kW in order to for the truck to climb 2% grades at 50mph (shown in Figure V-34). Transient cycles (UDDS truck, HHDDT65, CSHVR) were also simulated to confirm that this genset size was sufficient to maintain state of charge during common drivecycles.

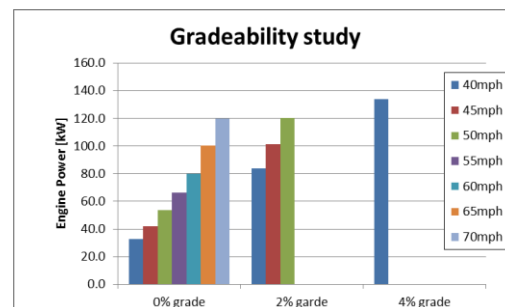


Figure V-34: Delivery truck gradeability study

The resulting model was used to conduct a parametric study to compare engine and electric machine technologies applied to a genset. Each genset combination was evaluated on four different drive cycles representative of potential use of the medium duty delivery truck: UDDS, CILCC, CSHVR and HTUF6 cycles.

Results show higher fuel economy with permanent magnet machines and induction machines over a wound field and switched reluctance machine, regardless of engine and drivecycle (Figure V-35).

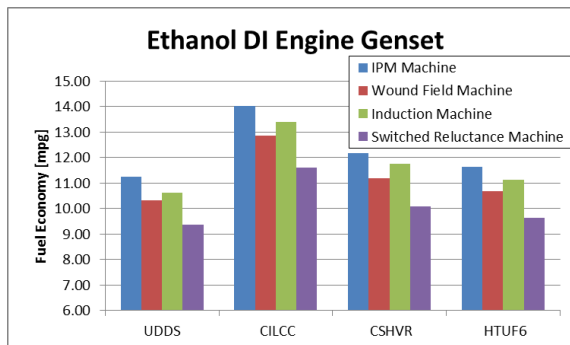


Figure V-35: Genset fuel economy results for various electric machine technologies combined with an Ethanol Direct Injected engine

For engine technology selection, fuel economy simulation results were corrected for energy content in order to allow a straight comparison. Advanced combustion engines (HCCI and RCCI) are the most efficient options but ethanol remains a competitive alternative thanks to higher efficiency than gasoline, lower after-treatment cost than diesel, and lower combustion system cost than advanced combustion engines.

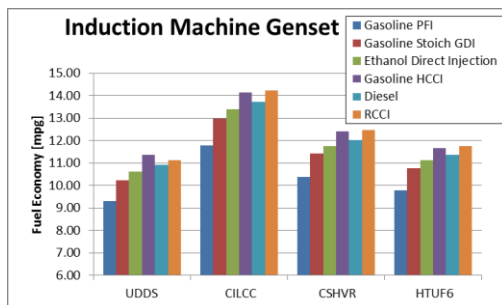


Figure V-36: Genset fuel economy results for various engine technologies combined with an induction machine

Transit Bus Application

A model of a conventional transit bus was created and validated against experimental data published by NREL for 2010 40ft Gillig transit bus equipped with a Cummins ISL 280hp on the Manhattan cycle (MAN), Orange County cycle (OCTA) and UDDS truck cycle (2) (Figure V-37)

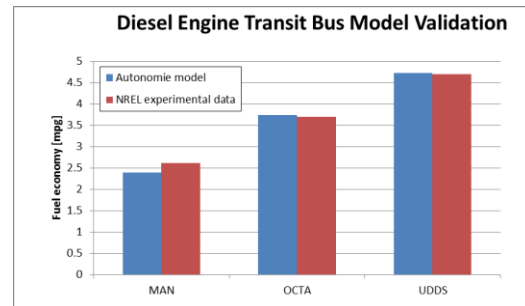


Figure V-37: Conventional powertrain transit bus model validation

A model of a series hybrid electric variant of the conventional transit bus was created to be used for the genset technology investigation. Since no series hybrid conversion of that bus (2010 40ft Gillig transit bus) exists, the benchmark for the comparison exercise was a 40ft 2004 Orion VII bus fitted with a BAE hybrid transmission whose data was published by Baltimore Metropolitan Council (3). Those platform differences can explain the discrepancies between model data and experimental data: the model fuel economy is 8 to 21% lower than experimental data.

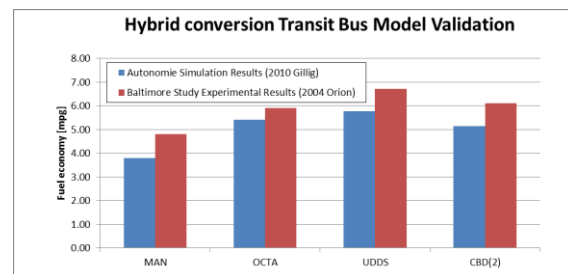


Figure V-38: Hybrid powertrain transit bus model validation

Yet the series hybrid powertrain model demonstrated 22% fuel economy improvement on a UDDS truck cycle and 45% improvements on stop and go cycles such as Manhattan and Orange County cycles, which is in line with results obtained with other series hybrid applications.

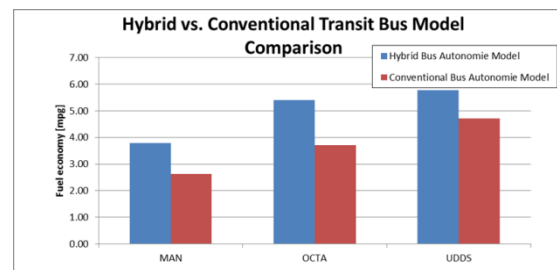


Figure V-39: Hybrid powertrain and conventional powertrain fuel economy comparison

The series hybrid bus model was therefore deemed acceptable to proceed with for the technology comparison study.

A sizing study was conducted to determine the required power level of a genset installed in this transit bus application so that its performance isn't affected. With a 200kW genset, the bus can sustain a 4% grade at 40mph and 2% grade at 50mph. Larger grades are possible thanks to the traction motor torque capabilities but they cannot be sustained because the traction power exceeds genset capabilities, so the Energy Storage System has to make up the difference. The genset size of 200kW also exceed the needs to maintain charge in charge sustaining mode on relevant transient bus cycles (UDDS truck, Manhattan, Orange County Transit and Central Business District cycles)

The resulting series PHEV transit bus model was applied to compare engine and electric machine technology combination influence on fuel economy. Each genset combination was evaluated on four different drive cycles representative of potential use of the transit bus: UDDS, Manhattan, Orange County and Central Business District cycles. Fuel economy simulation results were corrected for energy content in order to allow a straight comparison.

Permanent magnet machines and induction machines demonstrated higher fuel economy compared to wound field and switched reluctance machines.

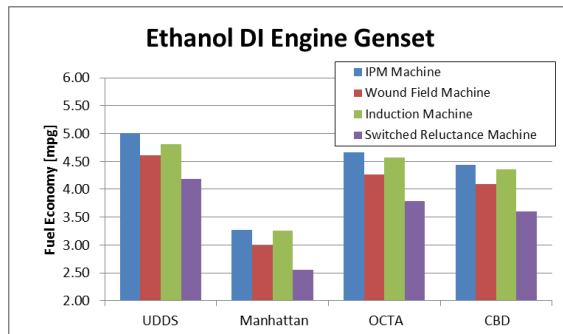


Figure V-40: Genset fuel economy results for various electric machine technologies combined with an ethanol direct injected engine

For engine technologies, advanced combustion engines (HCCI and RCCI) and conventional diesel engines performed better than others. Ethanol provided the best fuel economy out of the existing production technologies that do not require complex after-treatment like diesel combustion (Figure V-41).

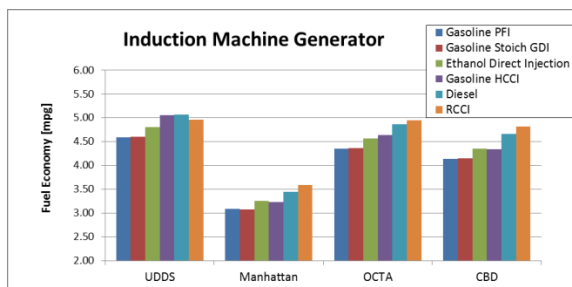


Figure V-41: Genset fuel economy results for various engine technologies combined with an induction machine

Conclusions

The use of a range extending gen-set to convert an electric vehicle into a series hybrid electric vehicle can reduce battery size requirements and cost, and alleviate “range anxiety”. A wide variety of engine and electric machine technologies can be combined in a genset and will affect the overall system efficiency. Therefore these combinations have to be carefully evaluated. The project had previously evaluated genset applied to passenger cars; it has now been expanded to medium duty delivery trucks and transit bus applications. These applications were selected for study because they might benefit from hybridization due to the stop and go nature of their duty cycles.

Models were developed and validated for both applications. They were then subjected to a parametric study to investigate the effect of different engine and electric machine genset combination on fuel economy.

The study concluded that permanent magnet machines still exhibit the best fuel economy but induction type machines offer the best non-rare earth technology fuel economy. On the engine side, advanced combustion engines (HCCI and RCCI) and conventional diesel engines performed best but alternative fuels such as ethanol provide intermediate fuel economy without the combustion system complexity and after-treatment extra cost.

References

1. Barnitt R, FedEx Gasoline Hybrid Electric Delivery Truck Evaluation: 6-Month Interim, Technical Report NREL/TP-540-47693 May 2010, National Renewable Energy Laboratory.
2. Lammert, et al. , Effect of B20 and Low Aromatic Diesel on Transit Bus NOx Emissions Over Driving Cycles with a Range of Kinetic Intensity, National Renewable Energy Laboratory, SAE 2012-01-1984.
3. Baltimore Region Hybrid Bus Tour Final Report, New West Technologies, LLC, 2006.

V.E. APEEM Components Analysis and Evaluation

Principal Investigator: Paul H. Chambon

Oak Ridge National Laboratory (ORNL)
 2360 Cherahala Boulevard
 Knoxville, TN 37932
 Phone: (865) 946-1428
 E-mail: chambonph@ornl.gov

DOE Program Manager: David Anderson

Phone: (202) 287-5688
 E-mail: david.anderson@ee.doe.gov

V.E.1. Abstract

Objectives

- Support the evaluation of current and proposed electric machine and power electronics technologies in a vehicle context to understand the applicability of a particular powertrain technology to a given vehicle and to determine areas/regions for component design improvement based upon system usage patterns.
- Enhance the current benchmarking and prototype evaluation capabilities of DOE APEEM programs with the addition of transient-capable testing facilities for power electronics and electric machinery components.

Major Accomplishments

- Procured and started the commissioning of a dynamometer suitable for electrical component characterization and validation through hardware-in-the-loop testing.
- Procured and installed electric machine suitable for test cell commissioning.

Future Achievements

- Perform hardware-in-the-loop and transient testing of electric hybrid powertrain components.



V.E.2. Technical Discussion

Background

Part of the Vehicle System Integration (VSI) Laboratory, Oak Ridge National Laboratory has commissioned a powertrain test cell capable of testing a complete heavy-duty hybrid vehicle powertrain by combining the use of two 500kW dynamometers and a 400kW e-storage unit that can emulate the behavior of a battery. It is also equipped with a hardware-in-the-loop platform to emulate vehicle components not present in the testcell, such that the powertrain behaves as if it were in a real vehicle on real world road conditions; this is referred to as Powertrain-In-the-Loop.



Figure V-42: Rendering of VSI lab with the component testcell in the foreground and the powertrain test cell in the background

Introduction

Testing electric machine and power electronics technology in the context of a vehicle using a hardware-in-the-loop approach is critical in order to understand transient, application specific, and real world conditions limitations associated with that component. These findings can be used to optimize its design and obtain a better match between the component and the vehicle application in order to achieve improved overall vehicle efficiency. This is referred to as Component-In-the-Loop.

Approach

This project will specify, procure and install key components for a testing facility suitable to characterize electric drive technologies in transient operations representative of vehicle conditions thanks to a hardware-in-the-loop set-up. That facility, called component test cell, will be part of ORNL's Vehicle System Integration laboratory.

Figure V-43 exemplifies the hardware in the loop testing of an electric machine as it will be implemented in the component testcell. The electric machine will be installed in the test cell, mechanically coupled to the dynamometer to absorb or drive torque. The inverter will be electrically connected to the battery emulator to draw or regenerate current as if the inverter were connected to an Energy Storage System. A power analyzer will be measuring DC and AC electrical energy as well as mechanical power to quantify electrical and mechanical efficiencies. A real time computer will run a model of a vehicle where the electric drive under test in the test cell could be installed. It also simulates the driver and drive cycles. Based on those models, it then controls the dynamometer and battery emulator such that they apply electrical and mechanical loads to the electric drive as if the latter were installed in the real vehicle and driving on real roads.

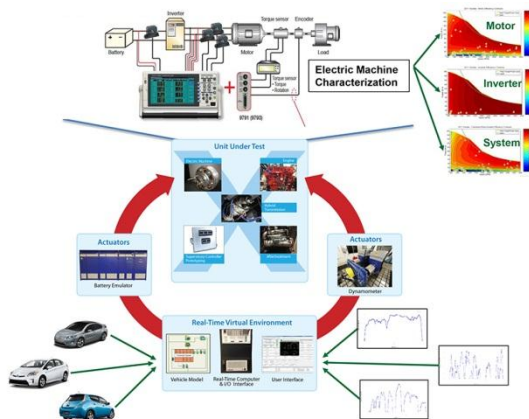


Figure V-43: Dynamic behavior characterization of electric machine using hardware-in-the-loop test configuration

Results

The procurement of a low inertia, 220kW, 12000rpm dynamometer (AVL DYNOROAD 202/12 SX) was initiated during FY 2013. It was delivered in December 2013 and moved into the testcell in March (see Figure V-44) after the installation of a bedplate to support it. The electrical installation of the dynamometer was performed in June.



Figure V-44: Component test cell bedplate and dyno

The 400kW (800V, 600A) battery emulator was integrated in the component testcell so that that it can power electric machines installed in this facility. It is controlled by a hardware-in-the-loop real time computer that emulates different battery technologies and their operating conditions based on calibrated models (see Figure V-45 for example of ESS emulation).

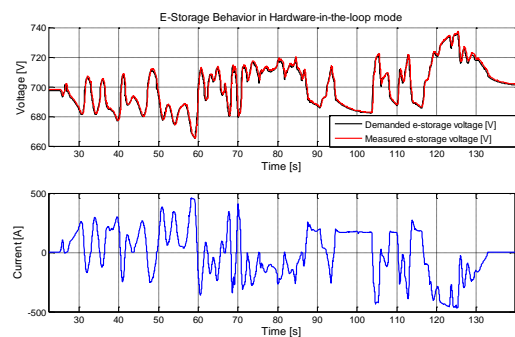


Figure V-45: Battery emulator behavior: example of voltage control when emulating a 700V nominal voltage ESS coupled to a heavy duty truck hybrid powertrain

Dynamometer commissioning could not be completed due to failure of its controller which required sourcing of a new unit. This was scheduled to early FY 2015. This delay was used to source and mechanically install a high speed electric machine that is suitable to commission the dynamometer.

Part of another CRADA that ORNL is working on with Cummins investigating medium duty and Heavy duty accessory electrification, a 50kW, 10000rpm electric machine was identified as a good candidate to commission this testcell. Cummins provided the machine and inverter as well as documentation for ORNL to install it in the component test cell.

Mechanical fixtures were designed specifically to hold the electrical machine during testing. High speed conditions required a very accurate design and expertise that was provided by the ORNL APEEM group. A riser, mounting bracket, face plate, bearings and other adapters were designed and procured (Figure V-46 shows CAD drawings of those fixtures).

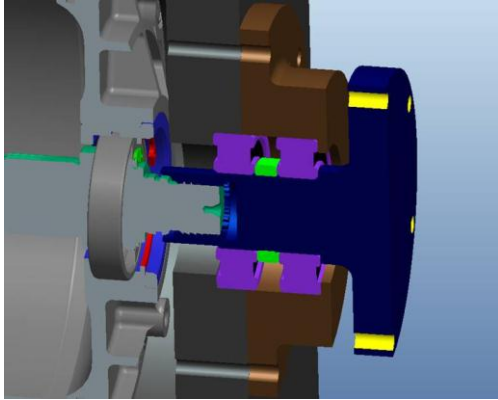


Figure V-46: Electric machine mounting bracket and bearing assembly

Also electric machine cooling requirements have been established. A new pump has been procured. All other components (hoses, heat exchanger and temperature controller) can be re-used from previous applications.

The electric machine was then installed in the testcell to commission the dynamometer with (Figure V-47).



Figure V-47: Electric machine installed in testcell

A dSPACE hardware-in-the-loop system was ordered and will be delivered in the first quarter of FY 2015. It is a duplicate of the system that controls the VSI powertrain testcell (Figure V-48) so that each cell can run concurrently and independently. It will compute real time models of virtual

vehicles and control the dynamometer to emulate road load representative of real world conditions such that the component under test (i.e. the engine or electric machine connected to the dynamometer) behaves as if it were on the road. It will also interact with the battery emulator to command the virtual battery behavior that corresponds to real world conditions.



Figure V-48: dSPACE Hardware-in-the-loop real time computer used in powertrain testcell

Conclusions

The VSI component test cell will allow enhanced evaluations of APEEM technologies by emulating transient operations and vehicle level characteristics. That test cell includes a low inertia, high speed dynamometer, a battery emulator and a hardware-in-the-loop real time system suitable to evaluate hybrid components on a test cell while still emulating real world conditions.

The electrical and mechanical installation of the high speed dynamometer has been completed in the VSI lab component testcell. The test cell commissioning is scheduled for the first quarter of FY 2015 to validate the integration and coordination of the dynamometer, battery emulator and real time platform.

An electric machine has been installed in the test cell to commission the test cell and be the first component to be evaluated in this new facility.

V.F. ACEC Technology Analysis and Evaluation

Principal Investigators: Zhiming Gao, Scott Curran, Stuart Daw

Oak Ridge National Laboratory (ORNL)
National Transportation Research Center
2360 Cherahala Boulevard
Knoxville, TN 37932-6472
Phone: (865) 946-1339
E-mail: gaoz@ornl.gov

DOE Program Managers: Lee Slezak, David Anderson

Phone: (202) 586-2335, (202) 287-5688
E-mail: lee.slezak@ee.doe.gov, david.anderson@ee.doe.gov

- Constructed hybrid and non-hybrid vehicle powertrain models using Autonomie to evaluate the impact of RCCI and other advanced combustion modes on fuel economy and emissions control.
- Simulated fuel economy and engine exhaust properties of port fuel injection (PFI), gasoline direct injection (GDI), CDC and RCCI-enabled engines in conventional and hybrid LD vehicles for both city and highway driving cycles.
- Completed preliminary simulations of the tailpipe emissions for a LD power-split hybrid vehicle equipped with a RCCI-enabled engine and a full aftertreatment train of diesel oxidation catalyst (DOC), LNT, and DPF.

Future Activities

- Continue refining and updating RCCI performance maps for assessing the fuel efficiency and emissions of RCCI-enabled engines used in conventional powertrain vehicles, hybrid electrical vehicles (HEVs) and plug-in HEVs (PHEVs).
- Utilize transient and steady-state coupled engine/aftertreatment dynamometer data to develop a DOC model capable of accurately simulating CO, HC, and NOx oxidation with RCCI exhaust.
- Assess emission control technologies that perform at low temperatures (<150°C) to enable fuel-efficient engines with low exhaust temperatures to meet current and future emission regulations.
- Evaluate “trap” material technologies that would temporarily store emissions generated during a cold start and then release and convert the emissions afterwards during high temperature conditions when conventional catalysts operate more effectively.
- Demonstrate the impact of high octane ethanol blends and other renewable fuels on the fuel economy and emissions from HEVs and PHEVs using advanced vehicle simulations.
- Update and refine a model for predicting engine transient behavior that includes detailed evaluation of the engine thermal management system and other components whose performance is not well characterized by the steady state operation.
- Coordinate closely with the USDRIVE ACEC tech team, DOE ACE/FLT/VSST R&D programs, and CLEERS to ensure access to the latest engine combustion, emissions control, and alternative fuels technology information in order to best address industry needs.



V.F.1. Abstract

Objectives

- Evaluate the merits and barriers of light-duty (LD) vehicles equipped with high efficiency clean combustion engine powertrains, leading-edge catalysts, and renewable fuels under realistic driving conditions.
- Support DOE advanced combustion engine (ACE), fuel and lubricant technologies (FLT), and vehicle systems simulation and testing (VSST) R&D programs in evaluating and identifying innovative technologies that leverage activities for assisting U.S. automakers to meet 2025 fuel economy standards and EPA Tier III emissions regulations.

Major Accomplishments

- Developed new engine maps for engines employing mixed-mode operation including reactivity controlled compression ignition (RCCI) and conventional diesel combustion (CDC) using FY 2014 experimental dynamometer measurements.
- Support of the DOE advanced combustion engine R&D program’s FY 2014 JOULE milestone, demonstrating 25% fuel economy improvement in modeled passage vehicles using a new engine map for RCCI-enabled engines.
- Support of the DOE fuels and lubricant technologies FY 2014 JOULE milestone of demonstrating 75% RCCI coverage of the non-idling portions of the city and highway drivecycles enabled by the unique properties of renewable fuels.
- Updated and refined our transient engine model to account for cold start operation, lean NOx trap (LNT) and diesel particulate filter (DPF) regeneration events, and optimal transition into and out of RCCI combustion.

V.F.2. Technical Discussion

Background

U.S. automakers are required to meet 2025 Corporate Average Fuel Economy (CAFE) standards and EPA Tier III emissions regulations. In addition, they must support the Renewable Fuel Standard (RFS), which requires the blending of 36 billion gallons of renewable fuels in the U.S. fuel supply by 2022. To meet these requirements, a broad array of individual technologies must be deployed at the vehicle level, but a coupling of technologies including high-efficiency clean combustion engines, leading-edge catalysts and renewable fuels will be necessary to achieve such challenging targets.

High efficiency clean combustion engine technologies, such as RCCI, can provide a high engine thermal efficiency while dramatically lowering engine-out nitrogen oxides (NO_x) and particulate matter (PM) emissions. Renewable fuels, including high-octane ethanol blends, can assist to increase thermal efficiency and enable downsized engines while extending the high efficiency clean combustion operating range. However, these combustion approaches inherently lead to a significantly lower exhaust temperature (typically <150°C), while the engine-out carbon monoxide (CO) and hydrocarbon (HC) emissions are considerably increased. Innovative aftertreatment devices become a necessity since the performance of conventional catalytic aftertreatment systems become inadequate in such a cool exhaust stream. Moreover, operational constraints needed to avoid mechanical damage to the engine limit the high efficiency clean combustion operation to a domain of engine speed and load where the rate of pressure rise is below a critical value. Thus, it is essential to utilize both CDC and high-efficiency combustion in mixed-mode operations. As hybridization becomes more prevalent in advanced vehicles, it is also critical to understand and evaluate the benefits and challenges associated with the integration of leading-edge engine technologies, aftertreatment systems, and renewable fuels with respect to optimization of vehicle efficiency and emissions control.

- In this project we developed and applied models for the engine, aftertreatment system, and other components to evaluate high efficiency engines, leading-edge catalysts, and renewable fuels in different vehicle configurations over realistic driving conditions. Our overall goal is to provide comprehensive vehicle system simulations that support DOE R&D efforts in evaluating and identifying innovative technologies that leverage activities for assisting U.S. automakers to meet future fuel economy standards and emissions regulations. The models and simulations rely on experimental measurements from both engines and emissions control devices in multiple facilities at ORNL. The measurement data are transformed into physically consistent computational models that can be implemented directly in simulation platforms such as Autonomie. Our models also provide guidance to experimental teams in targeting future measurements. This close interaction between simulation and experiments provides DOE with the best possible basis for

identifying promising vehicle technologies that can maximize energy efficiency and security while minimizing any negative environmental impacts from transportation.

Introduction

In FY 2014, we collaborated with ORNL colleagues and DOE ACE R&D programs to assess the impacts of RCCI operation on fuel economy and emissions from hybrid and non-hybrid vehicles using detailed vehicle system simulations. We concentrated our efforts this year on the following research topics:

- Developed new engine maps capable of the mixed-mode operation including reactivity controlled compression ignition (RCCI) and conventional diesel combustion (CDC) using FY 2014 experimental dynamometer measurements.
- Quantified the fuel economy benefit, based on passenger vehicle simulations, of the new RCCI-enabled engine relative to a 2009 PFI gasoline baseline engine, in support of DOE ACE R&D program milestones.
- Updated and refined an engine model to evaluate the initial transient fuel consumption and exhaust properties associated with various aftertreatment control strategies during cold start and the transition to mixed-mode operation.
- Developed hybrid and non-hybrid powertrain models which were used to evaluate the performance of RCCI and other advanced combustion strategies when employed in various powertrain configurations.
- Calibration and refinement of hybrid and non-hybrid powertrain models to improve the simulation of cold-starts and better predict the effects of HEV control systems on fuel consumption and emissions.
- Simulations for the comparison of fuel economy and exhaust properties of different engine technologies in LD conventional and hybrid vehicles over multiple driving cycles.
- Preliminary assessment of RCCI tailpipe emissions from modeled hybrid and non-hybrid vehicles equipped with a full aftertreatment train of DOC, LNT, and DPF devices.
 - Some results from the above have been reported in multiple journal and conference publications and at meeting presentations including SAE International, Coordinating Research Council (CRC), and the Advanced Engine Combustion Program Review. The latest results will be documented together with the most recent data and reported in the future.

Approach

The evaluation of the impact of high efficiency clean combustion engine technologies on vehicle fuel economy and emissions control requires computationally efficient and physically accurate models for different types of engines and aftertreatment devices that can maximize the energy efficiency of emission-compliant vehicles. Our transient engine models adopt a coarse representation of internal engine heat transfer and use simplified assumptions about how engine-out

emissions species change as the engine heats up. The transient exhaust properties in the model are predicted from steady-state or pseudo-steady-state engine data by applying dynamic first-order correction terms and empirical parameters that account for the inherent thermal and combustion lags in the engine as it shifts from one operating state to another. The steady-state or pseudo-steady-state engine data are typically measured in ORNL engine dynamometer cells or at the Vehicle Systems Integration (VSI) lab, or are obtained from an automotive original equipment manufacturer (OEM). The measurement data are sometimes supplemented with engine cycle simulations using highly detailed thermodynamics-based engine simulation codes such as GT Power or codes developed by ORNL specifically for the performance prediction of advanced concept engines. These data are typically used to generate engine performance maps and then integrated into our transient engine models suitable to any simulation platforms.

We also adopt physics- and chemistry-based computational models for lean and stoichiometric exhaust emissions control devices including DOC, LNT, DPF, selective catalytic reduction (SCR), and passive hydrocarbon traps. The models incorporate 1-D differential transient mass and energy balances with global reaction kinetics and heat and mass transport information to simulate the performance of each aftertreatment component. This makes it possible for the integration of engine and aftertreatment models to estimate the instantaneous properties of the exhaust stream from the engine and within each aftertreatment component during a complete drive cycle. The aftertreatment models are typically developed and refined using data for commercially available or prototype aftertreatment/catalyst material characterized at engine/catalyst/reactor labs at ORNL as well as data from OEM sources.

Consequently, ORNL engine and aftertreatment models, together with our other critical component models, are integrated into Autonomie which was developed by Argonne National Laboratory (ANL). These comprehensive vehicle powertrain, emissions and fuel economy models are capable of exploring the impact of low-temperature combustion strategies, innovative aftertreatment, and renewable fuels technologies in different vehicle powertrain configurations, including hybrids. The data and detailed information for various vehicle powertrain configurations are collected from the ORNL vehicle research laboratories and OEMs to update, refine and validate the vehicle systems models for better identifying major trends and possible ACE R&D opportunity areas that deserve more emphasis in the DOE portfolio or that can lead to specific partnerships with industry.

Results

Engine mapping

We collaborated with the DOE ACE R&D program to generate new RCCI-enabled engine maps using FY 2014 experimental dynamometer measurements at ORNL of a GM 1.9-L RCCI-enabled engine. The low- and high-reactivity fuels employed in the RCCI experiments were conventional gasoline and diesel. Detailed maps for steady-state emissions

and engine efficiency are depicted in Figure V-49. Compared to CDC, the new RCCI strategy reduces NO_x and PM emissions but generates higher CO and HC emissions. Also it increases net engine efficiency up to 6% and reduces exhaust temperatures by more than 100°C. However, compared to our previous RCCI maps generated in FY 2012 and FY 2013, the range of RCCI operation for the FY 2014 engine is reduced relative to the previous cases, particularly at high loads. The RCCI map developed in FY 2012 was generated using gasoline and 20% biodiesel for the fuel system, while the RCCI map developed in FY 2013 was based on E30 and diesel. The RCCI using gasoline and 20% biodiesel extends the low and high loads due to a higher PFI to DI ratio, and the RCCI using E30 and diesel extends the high load range due to a higher octane number and charge cooling.

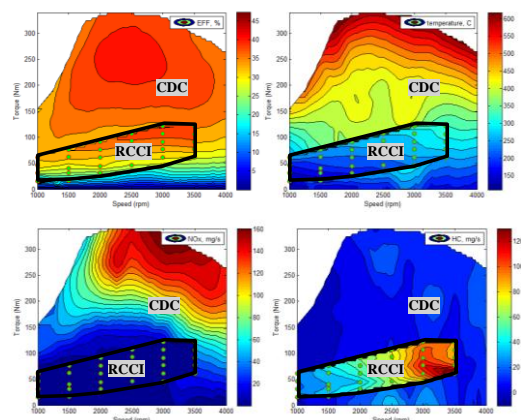


Figure V-49: Example of steady-state engine maps for the GM 1.9L engine with the RCCI-enabled zone highlighted. The green marks in both the upper and lower figures indicate operating conditions for which RCCI measurements have been made

We utilized the new RCCI-enabled engine maps to simulate the fuel economy benefit of a multi-mode implementation of RCCI with conventional gasoline and diesel in mid-size sedans operating over city and highway driving. This activity supported the DOE ACE R&D program FY 2014 JOULE milestone to demonstrate the benefits of RCCI-enabled engines compared to 2009 conventional 2.4-2.7L PFI gasoline and 2.0L DI diesel engines. The results indicate that implementation of RCCI can improve fuel economy by 5.8-7.6% relative to conventional diesel operation. Compared to stoichiometric gasoline engines, utilization of RCCI can boost fuel economy by 25%, consistent with the DOE FY 2014 milestone.

Additional, we used the RCCI maps developed in FY 2012 to demonstrate 75% RCCI coverage of the non-idling portions of the city and highway drive cycles enabled by the unique properties of renewable fuels in support of the DOE fuels and lubricant technologies FY 2014 JOULE milestone.

Vehicle powertrain and engine models updating

Models of both non-hybrid and hybrid powertrain configurations were constructed using Autonomie. The non-hybrid powertrain architecture was established based on the 1701kg 2012 Ford non-hybrid Fusion, powered by a 3.0-L V6 stoichiometric gasoline engine and a 6-speed automatic

transmission; the hybrid powertrain architecture was based on the 1814kg 2010 Ford Fusion hybrid powered by a 2.5-L stoichiometric gasoline engine and a power-split planetary gear. To account for the different weights of the various drive train options related to different combustion engines, we selected the weight of engine and other vehicle components based on the peak power demand and recommendations from the ORNL automotive system cost model. Thus, the simulated vehicle weight is appropriate for the specific engine type and powertrain configuration used in each case.

In the hybrid vehicle model, a sustained-charge control strategy was adopted to eliminate the need for off-board charging. In addition, we developed an optimal brake specific fuel consumption (BSFC) line for high efficiency engines in order to maximize the fuel savings for the power-split configuration. This optimal efficiency line is determined by calculating the speed at which the minimum BSFC occurs for each incremental power level. To address the impact of cold and warm starts on RCCI-enabled engines, we added a specific constraint that allows the engine to (1) run at its optimal CDC efficiencies at cold start; and (2) run at its optimal RCCI efficiencies during sufficiently warm operations and appropriate loads for RCCI. In the latter case, the engine reverts to CDC operation if the temperature falls below a critical threshold or the demanded load is outside the RCCI operating range.

The vehicle models have been validated with chassis dynamometer measurements made by ANL of the Ford Fusion vehicles. Since we did not have access to engine maps for the particular Ford vehicles, we simulated these by resizing available 2.7L stoichiometric gasoline engine maps to approximate the 3.0L and 2.5L engines. We conducted drive cycle simulations to compare with the ANL measurements for three EPA drive cycles, including the urban dynamometer driving schedule (UDDS), the highway fuel economy test (HWFET), and the US06 supplemental federal test procedure. The predicted fuel economies are reasonably close to the measurements, with not more than 5.4% and 7.2% errors in predicted fuel economy for the non-hybrid and hybrid cases, respectively. Figure V-50 compares the predicted and measured transient fuel consumption for a UDDS drive cycle. These comparisons demonstrate that our simulations of the conventional and hybrid vehicle configurations can reasonably approximate the fuel economy of the actual vehicles.

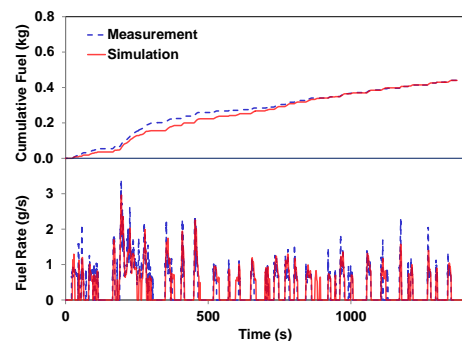


Figure V-50: Comparison of the simulated fuel economy with measurements for the 2010 Ford Fusion power-split hybrid operating over the hot UDDS drive cycle

Our transient engine model was also updated to account for cold start, aftertreatment control activities, and the transition into and out of RCCI other advanced combustions. Experience at ORNL indicates that it is impossible to successfully initiate RCCI at engine block temperatures below 80°C. Thus, in the engine model, we quantified the engine thermal state with a warm-up index, which characterizes the degree to which the engine has warmed as a function of the difference between its fully cold and final steady-state operating temperatures. In order to initiate RCCI in the model, a warm-up index of 80% is required, which represents an estimated engine block temperature of 80°C for a steady-state hot engine block temperature of 95°C and an ambient temperature of 20°C. Further experimental studies are required to determine the critical temperature for initiating RCCI in partially heated engines to refine the modeling approach employed.

Fuel economy simulations

To evaluate and compare the impacts of high efficiency combustion engines on LD vehicle fuel economy and emissions during city and highway driving, we used the available engine maps from a SAAB 2.0-L PFI engine, a BMW 2.0-L GDI engine, and a GM 1.9-L diesel engine operating with or without RCCI. The studied RCCI operation employed the FY 2013 E30/ULSD RCCI map. These 2007-2008 engine models were selected since they are representative of current and future trends in engine technology, even though they are not the most recent models. Each case was simulated using an initial cold-start of 20°C. Figure V-51 shows the simulated fuel economies of both the non-hybrid and hybrid vehicles powered by the discussed engine technologies. We observed that the lean GDI engine gives significant gains over PFI engine fuel economies, but the RCCI engine gave the highest simulated fuel economies for all drive cycle cases in both non-hybrid and hybrid configurations.

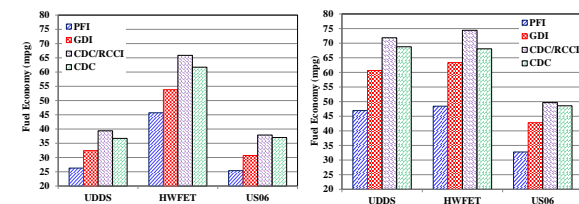


Figure V-51: Fuel economies in the simulated vehicles powered by different combustion engine technologies over various city and highway drive cycles

Figure V-52 shows the hybrid vehicle’s engine speed vs. load operating conditions depicted on the steady-state engine maps for the studied PFI, lean GDI, CDC/RCCI and CDC-only engine configurations over a UDDS cycle. In the Figure, the white curve is the optimal engine efficiency for each engine power level across the map. Hybridization enables engines to better meet the required vehicle power at different operating conditions while maintaining peak efficiency. For example, hybridization allows more RCCI operation over the simulated drive cycles. The results also indicate that the drive distance and engine-on time percentages with RCCI are significantly increased in the hybrid case. Figure V-52 also reveals that the RCCI operation region meets most hybrid vehicle drive conditions over the UDDS cycle except for cold-starts which

are marked by a red circle with an internal green color. As mentioned earlier, the cold-start operations ran with an optimal CDC efficiency curve is shown with grey color in Figure V-52.

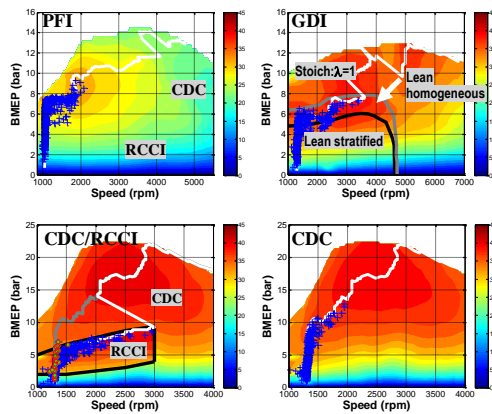


Figure V-52: Hybrid vehicle engine speed vs. load operating points depicted on the steady-state engine maps for PFI, lean GDI, CDC/RCCI and CDC-only over a UDDS cycle. Each blue cross represents the engine state at 1s intervals. The red circle with internal green color in RCCI represents cold-start CDC operation

Figure V-53 compares the simulated exhaust temperatures of the PFI, lean GDI, CDC/RCCI and CDC-only engines in hybrid vehicles over the cold-start FTP cycle. As shown, exhaust temperatures for the lean GDI gasoline engine are nearly 150°C lower than for the stoichiometric engine but still considerably higher than CDC-only and CDC/RCCI cases. The RCCI-enabled engine’s exhaust temperature is 50-70°C less than the CDC-only engine. RCCI gives the lowest exhaust temperatures, which are below 200°C during a significant portion of the drive cycle. For these exhaust temperatures, oxidation of HCs becomes very difficult for conventional oxidation catalysts. Thus, the reduced exhaust temperatures may significantly hamper the performance of conventional aftertreatment devices.

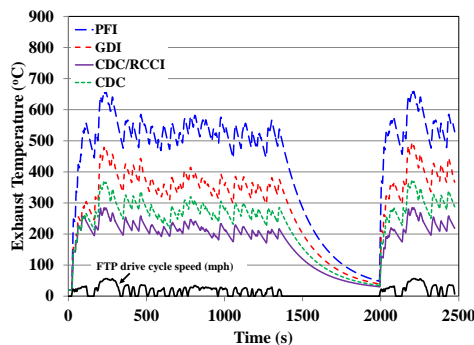


Figure V-53: Simulated exhaust temperatures of the PFI, lean GDI, CDC/RCCI and CDC-only engines in the simulated vehicles under the cold-start FTP cycle

Emissions simulations with aftertreatment

We conducted city and highway drive cycle simulations to evaluate the impact of aftertreatment emissions control devices on the fuel penalty and tailpipe emissions with a 1.9-L

RCCI-enabled engine and a full aftertreatment train in a LD hybrid vehicle configuration. The simulated aftertreatment train consists of a 0.6-L DOC, a 2.4-L LNT, and a 2.4-L DPF. Many details of RCCI exhaust properties are unknown, and this situation will require some significant modifications to our current device models and their operating strategies. To begin, we made preliminary studies to determine basic trends and we continue to update the simulations as more experimental data becomes available about the interactions of aftertreatment devices with RCCI exhaust. For example, in typical simulations, we assumed a highly simplified control strategy for LNT regeneration (for NOx reduction using aftertreatment) which consists of alternating the engine fueling in such a manner that there is at least 60s of lean-NOx storage, followed by a short (3s) rich pulse for LNT regeneration. However, such a strategy can be far from optimal for RCCI operation, because engine-out NOx is greatly reduced and the CO/HC emissions (which can effect catalyst regeneration) are greatly increased. Therefore, to investigate the impact of the regen control strategy parameters, we studied an alternative strategy with an even shorter rich pulse (1.5s) while maintaining at least 60s of lean operation for NOx storage.

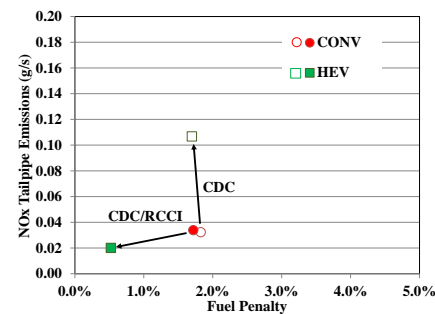


Figure V-54: Modeling results of the potential tradeoff between the LNT regen fuel penalty and NOx tailpipe emissions from hybrid and non-hybrid vehicles powered by either CDC only or CDC/RCCI engines over a FTP cycle with 20C cold start. The solid markers are CDC/RCCI and the unsolid markers are CDC

Figure V-54 shows the potential trade-off between modeled NOx tailpipe emissions and the associated fuel penalty for both hybrid and non-hybrid vehicles equipped with the new LNT operating strategy. The simulated drive cycle is a FTP cycle with a 20°C cold start. While these results imply that implementing RCCI in hybrid vehicles could achieve significant NOx reductions with a reduced fuel penalty, it is important to recognize that additional experimental data on LNT performance with RCCI exhaust needs to be obtained for validation. In the absence of such data, these results need to be considered as encouraging, but speculative. However, we still expect that the results can provide a general trend and guidance to future RCCI experiments. We will continue to update and refine the simulations with future findings from RCCI experiments.

Conclusions

- RCCI-enabled engine maps with conventional gasoline and diesel used as low- and high- reactivity fuels used in the RCCI operating mode were constructed from FY 2014 experimental measurements of a GM 1.9-L engine and implemented in Autonomie to support simulations of different powertrain configurations of LD vehicles.
- The RCCI operation space in the new map is less than previous RCCI maps generated with renewable fuels, but still increases net engine efficiency up to 6% and reduces the exhaust temperature more than 100oC compared to CDC.
- We have developed and validated models of non-hybrid passenger car powertrains that account for the different weights of the various drive train options related to different combustion engines and powertrain configuration.
- We have assessed the simulated fuel economy and engine exhaust property results from PFI, GDI, CDC and RCCI-enabled engines in conventional and hybrid LD vehicle configurations for city and highway driving cycles.
- Simulations indicate that the RCCI-enabled engine yields significant fuel economy improvements for all drive cycle cases in both non-hybrid and hybrid configurations.
- Hybridation increases the opportunity for high efficiency RCCI operation and dramatically decreases engine-out NOx.
- RCCI lowers exhaust temperatures with significant time during drive cycles below 200°C where oxidation of CO and HCs is very difficult for conventional oxidation catalysts.
- Preliminary simulations of tailpipe emissions for the hybrid vehicle equipped with a full aftertreatment train system shows that implementing RCCI in hybrid vehicles could achieve significant NOx reductions with a reduced fuel penalty.

V.F.3. Products

Publications

1. Z. Gao, S. Curran, J. Parks, D. Smith et al., Drive cycle simulation of high efficiency combustions on fuel economy and exhaust properties in light-duty vehicles, Applied Energy Journal, under review.
2. S. Curran, Z. Gao, R. Wagner, Reactivity controlled compression ignition drive cycle emissions and fuel economy estimations using vehicle systems simulations with E30 and ULSD, SAE International Journal of Engines, 7(2), 2014.
3. S. Curran, Z. Gao, R. Wagner, Fuel Economy Estimates of RCCI/Diesel Multi-Mode Operation Using Vehicle System Simulations, Advanced Engine Combustion Program Review, Southfield, MI, Aug. 2014.
4. S. Curran, Z. Gao, J. Szybist, D. Smith et al., Fuel effects on RCCI combustion: performance and drive cycle considerations, 2014 CRC Workshop on Advanced Fuels and Engine Efficiency, Baltimore, MD, Feb. 25, 2014 (Invited).
5. S. Curran, Z. Gao, C. Daw, V. Prikhodko et al., Opportunities and challenges for integrating future engine concepts into hybrid electric vehicle powertrains, SAE 2014 Hybrid and Electric Vehicle Technologies Symposium, San Diego, CA, Feb. 2014 (Invited).

Patents

1. None

Tools and Data

1. All the data and simulation tools described above are summarized in the cited publications [1-5].

V.G. Prius PHEV Thermal Vehicle Model Validation

Principal Investigator: Namwook Kim

Argonne National Laboratory
9700 South Cass Avenue
Argonne, IL 60439-4815
Phone: (630) 252-2841
E-mail: nakim@anl.gov

DOE Program Manager: David Anderson

Phone: (202) 287-5688
E-mail: David.Anderson@ee.doe.gov

- Use the validated vehicle thermal models to evaluate the impact of temperature on multiple use cases (i.e., real-world driving cycles).



V.G.2. Technical Discussion

Background

Argonne has analyzed the control behaviors of advanced vehicles, such as hybrid electric vehicles (HEVs), PHEVs, and battery electric vehicles (BEVs), to develop simulation models and reproduce vehicle performances with simulation techniques [1–3]. Since many studies related to transportation technologies conducted at Argonne rely on simulation techniques [4], validated models are critical.

This project leverages the Argonne vehicle testing facility, which is able to test vehicles under different thermal conditions, such as -7°C or 35°C . Once analyzed, the results are used to develop individual thermal component models. One of the main reasons to develop thermal models is that the impact of temperature on vehicle performance is significant, especially for electrified vehicles. For instance, engine and battery efficiencies decrease at low temperature, or the battery is not be able to provide enough power if the battery is very cold or very hot. Further, the climate control system demands additional energy consumption under very cold weather conditions, because the engine might not provide any waste heat.

In order to analyze the impact of thermal conditions, thermal component models were developed by analyzing the test data obtained from the APRF at Argonne [5, 6]. As part of its ongoing effort to keep developing thermal models for the advanced vehicles [2,3], the Toyota Prius PHEV was tested in the environmental thermal chamber, and the test data were analyzed to understand the control strategies for different thermal conditions.

Introduction

The Prius PHEV shares the same configuration as the Prius HEV, as shown in Figure V-55. The engine and the electric machine technologies implemented in the PHEV are the same as those of the HEV. However, the battery technology has been upgraded from a 1.3-kWh nickel-metal hydride battery to a 4.4-kWh lithium-ion battery, so that the vehicle is able to run in EV mode on U.S. Environmental Protection Agency (EPA) driving cycles.

V.G.1. Abstract

Objectives

- Understand the impact of temperature on vehicle control and performance using test data. Develop and validate the vehicle thermal model reproducing the control and performance behaviors of the vehicle.
- Import test data obtained in an environmental chamber under different thermal conditions.
- Analyze the vehicle-level control algorithm and the performances of the vehicle components from the test data.
- Develop the plug-in hybrid electric vehicle (PHEV) model for the Prius PHEV and validate it using Argonne National Laboratory's (Argonne's) Advanced Powertrain Research Facility (APRF) test data.
- Improve existing component thermal models and the analysis process.

Major Accomplishments

- Analyzed vehicle test data for the Toyota Prius PHEV, including the impacts of component temperatures on control and performance.
- Developed a vehicle-level controller for the PHEV.
- Completed a vehicle thermal model for the PHEV and validated the model with test data (simulations calculated the energy consumption within the test to test repeatability).
- Developed a battery thermal model.

Future Achievements

- Develop systematic processes to estimate thermal parameters for components using test data.
- Release all developed thermal vehicle models with generic parameters in Autonomie.
- Apply an optimal control concept, such as Pontryagin's Minimum Principle, to establish the control philosophy.

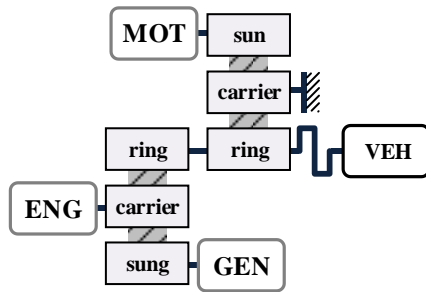


Figure V-55: The configuration of the Toyota Prius PHEV is the same as that of the Prius HEV

The PHEV has a different operating mode according to the battery state-of-charge (SOC), as the vehicle is expected to drive in EV mode when it is fully charged. For instance, the vehicle tries to consume electric energy as much as possible if the SOC is higher than 28%, whereas the control behavior is very similar to the Prius with a low SOC [2]. On the other hand, there is more opportunity for the engine to be cooled down due to the longer electric driving than in the case of the HEV, or to be turned on to provide heat to a passenger compartment under the cold ambient test. In this study, the control behaviors were analyzed, and, based on the analysis results, a vehicle-level controller for the Prius PHEV was developed and integrated into the vehicle model. The comparative study shows that the simulated fuel consumptions are close to the measured ones from the tests. The data and analysis results provided in this study should be very useful to other researchers in developing thermal models in their own studies.

Approach

This study included four major steps.

1. Test data were obtained from bench dynamometer tests in an environmental thermal chamber.
2. The data were imported into Autonomie and used to analyze control strategies and component performances.
3. A control model and component models were developed based on the analyzed results.
4. The model was validated with the test data.

The vehicle was mounted on a dynamometer in the APRF, as shown in Figure V-56, in order to obtain the test data. The tests are designed to operate the vehicle on a number of driving cycles for different temperatures (i.e., -7°C, 21°C, or 35°C). Argonne also provides some vehicle test data on a website for public use [7]. In the second step, the test data obtained from the APRF are imported into Autonomie for analysis, as shown in Figure V-57 [8].



Figure V-56: Toyota Prius PHEV loaded on a dynamometer in the APRF

| Test Name | Test Unit | Unit Type | Matching Attribute | Converted Name | Converted Unit (SI) |
|--------------------------------|------------|---------------|--------------------|-----------------------------|---------------------|
| IGNM_Cur_Prim_1(S) | A | current | A | ign2_cur_prim_1st_meas | A |
| IGNM_Vol_Prim_1(S) | V | voltage | V | ign2_vol_prim_1st_meas | V |
| IGN_On | | normalized | (S,T) | ign2_ign_on_1st_meas | (S,T) |
| IGN_Compressor_Cur_Helm_1(S) | A | current | A | ign2_ign_com_1st_meas | A |
| IGN_Compressor_Engne | rpm | normalized | (S) | ign2_ign_com_engne_1st_meas | (S) |
| IGNComp_Spd_Acc_CAR1(S) | rpm | rotational_sp | rpm | ign2_ign_acc_1st_meas | rpm |
| IGNTemp_Temperature | C | temperature | C | ign2_ign_acc_1st_meas | C |
| IGNTemp_Pressure | pressure | pressure | | ign2_ign_acc_1st_meas | pressure |
| IGNM_Torque_Lat1(S) | Nm | torque | Nm | ign2_ign_lat1_1st_meas | Nm |
| IGNM_Torque_Fwd1(S) | Nm | torque | Nm | ign2_ign_fwd1_1st_meas | Nm |
| IGNM_Cur_Cat_1(S) | A | current | A | ign2_ign_cat_1st_meas | A |
| IGNM_Cur_Helm_2(S) | A | current | A | ign2_ign_helm_2_1st_meas | A |
| IGNM_Temp_Lat_Drives_Temp1(C) | C | temperature | C | ign2_ign_lat_1st_meas | C |
| IGNM_Temp_Lat_Drives_Temp2(C) | C | temperature | C | ign2_ign_lat_1st_meas | C |
| IGNM_Temp_High_Drives_Temp1(C) | C | temperature | C | ign2_ign_high_1st_meas | C |
| IGNM_Temp_High_Drives_Temp2(C) | C | temperature | C | ign2_ign_high_1st_meas | C |
| IGNM_Vol_1(S) | V | voltage | V | ign2_ign_vol_1st_meas | V |
| BatteryBankVol_1(S) | V | voltage | V | ign2_ign_vol_1st_meas | V |
| BoostRatio | | | | ign2_ign_boost_1st_meas | |
| BrakeBank_CAR1(S) | Nm | torque | Nm | ign2_ign_bank_1st_meas | Nm |
| Brake_Bank_CAR1(S) | Nm | torque | Nm | ign2_ign_bank_1st_meas | Nm |
| Brake_Sig_CAR1 | normalized | (S,T) | (S,T) | ign2_ign_bank_1st_meas | (S,T) |
| Cabin_Temp1(C) | C | temperature | C | ign2_ign_cabin_1st_meas | C |
| Cabin_Vol_1(S) | C | temperature | C | ign2_ign_cabin_1st_meas | C |
| CalculateLoad | | | | ign2_ign_calculate_1st_meas | |

Figure V-57: Importing process in Autonomie (all test data are imported into Autonomie, and signals required for the analysis are calculated in the importing process)

During the import process, the measured signals units are converted to standard international (SI) units when needed, and additional signals are calculated for later analysis. For instance, an index parameter that represents the charge depleting (CD) mode or charge sustaining (CS) mode is generated because it is usually not measured from the test. When the data are successfully imported into Autonomie, they are analyzed to understand the control behaviors and the performance behaviors, as shown in Figure V-58.

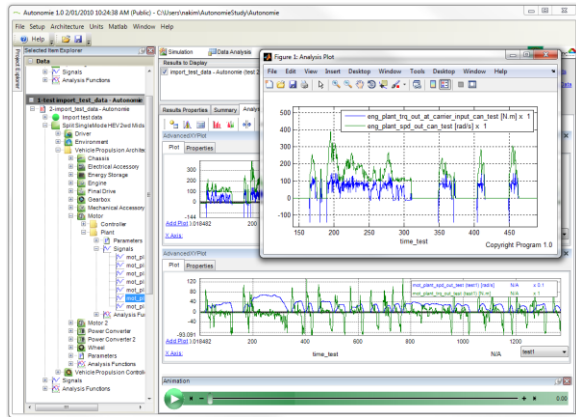


Figure V-58: Analysis process (Autonomie provides functions to analyze the control behaviors from the imported test data)

The performance analysis results provide direct or useful information to estimate parameters required when component models are developed. For instance, the tire efficiencies according to the thermal condition analyzed in this step are used to obtain the coefficients of the wheel loss model. In the third step, simulation models for the controller and the components are developed in Autonomie, as shown in Figure V-59, on the basis of the analyzed results.

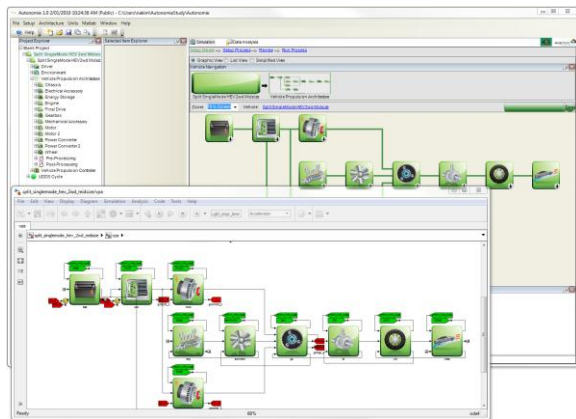


Figure V-59: Running simulation model in Autonomie (the simulation results are validated with the test data obtained from the APRF)

In the last step, the developed model is validated with the test data. Through the validation work, the development work is completed if the vehicle model appropriately calculates vehicle performances, such as fuel economy, but also reproduces the operating behaviors of the vehicle components.

Results

Performance Analysis for Components

Argonne has collaborated with other national laboratories, vehicle manufacturers, and component suppliers to develop component thermal models [2,3], where performances of components have been analyzed through various studies. In

this study, the impact of the component temperature on their efficiency is investigated for multiple components.

Engine Efficiencies According to Engine Coolant Temperature

The engine control is affected by the engine coolant temperature. For instance, the engine should be turned on if it needs to provide waste heat to warm up the passenger compartment. The additional fuel consumed lowers the fuel economy. On the other hand, engine efficiency is also affected by engine temperature, which is not easy to characterize from the test data. Figure V-60 shows the overall change of the engine efficiency according to the engine coolant temperature, where the efficiency, η_{eng} , can be calculated as:

$$\eta_{eng} = \frac{S_{eng} \cdot T_{eng}}{\dot{m}_{fc} \cdot LHV} \quad (2)$$

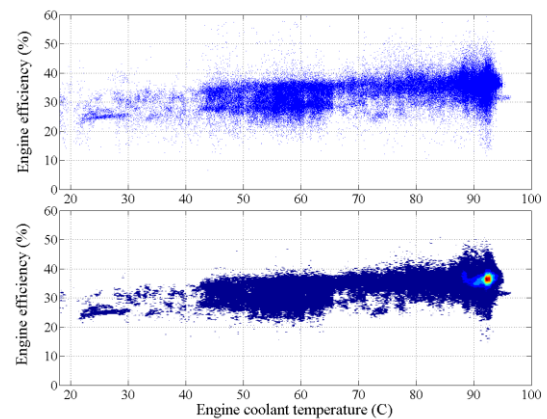


Figure V-60: Engine efficiency change according to engine coolant temperature

In Equation (1), S_{eng} and T_{eng} are the engine speed and the engine output torque, and \dot{m}_{fc} and LHV are the fuel consumption rate and the lower heating value of the fuel.

The engine coolant system tries to maintain the coolant temperature below 92°C, so the density of operation in Figure V-60 (b) is very high at the temperature of 92°C, at which the efficiency is around 37%. However, one notices that engine efficiency continuously decreases with lower engine coolant temperature. Although Figure V-60 only shows the tendency of the efficiency according to the coolant temperature, an engine map can be generated from the test data as shown in Figure V-61, which is used for the engine thermal model.

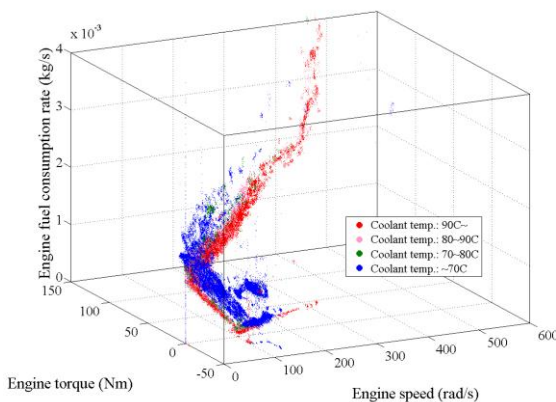


Figure V-61: Engine fuel consumption rate according to the engine coolant temperature

Battery Efficiencies According to Battery Temperature

Although round-trip efficiencies can properly represent the battery efficiency, it is not easy to evaluate the battery round-trip efficiency in PHEVs because round-trip efficiency is exact only when the initial SOC is the same as the final SOC. Therefore, segments of SOC trajectories that have no difference between the initial SOC and the final SOC are selected to calculate the round-trip efficiencies, where the efficiency, η_{bat} , can be calculated as:

$$\eta_{bat} = \frac{E_{out}}{E_{in}} \tag{3}$$

E_{in} is the energy that flows into the battery, and E_{out} is the energy that flows out from the battery where the flow direction is determined by the flow direction of the current.

Figure V-62 shows the overall behavior of the battery efficiency according to its temperature. The parameters used for the battery model can be developed from the test data similarly to the engine map. For instance, the battery internal resistance has been estimated from the test data, as shown in Figure V-63.

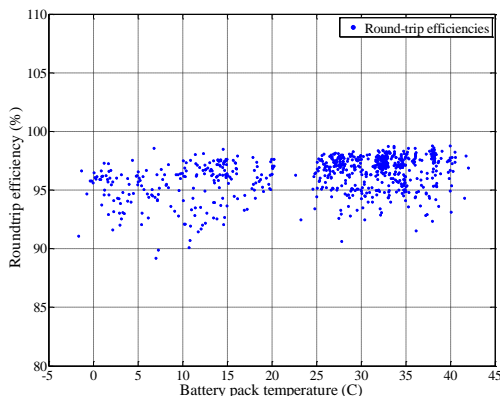


Figure V-62: Battery Round-Trip Efficiencies

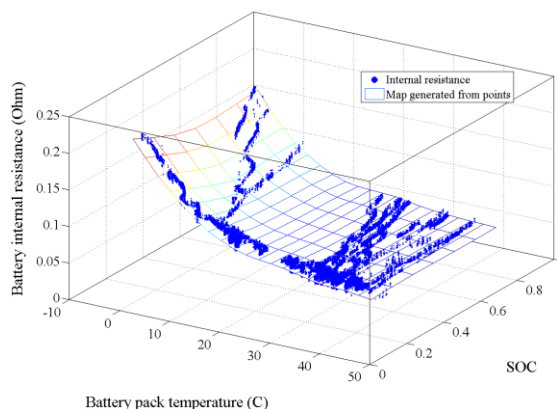


Figure V-63: Internal resistance of the battery according to the SOC and battery pack temperature

In addition to the internal resistance, the open circuit voltage or the parameters for the polarization effect have been estimated as well.

Wheel Torque Loss According to Tire Temperature

The tire is also a component significantly affected by the operating temperature. Figure V-64 shows the wheel torque loss according to the tire temperature obtained from the test data.

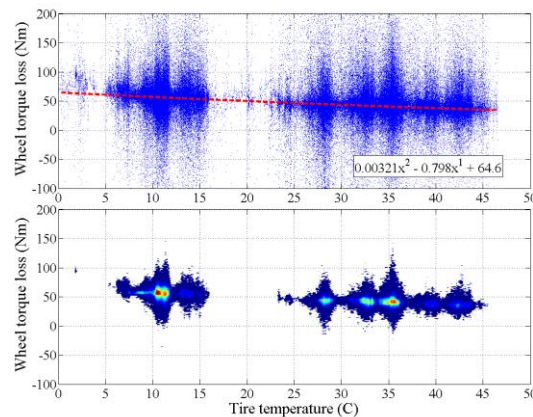


Figure V-64: Wheel loss according to tire temperature (the torque loss significantly increases as tire temperature decreases)

In Figure V-64, the torque loss changes according to the tire temperature. Because of the wheel loss, the input energy required at the wheel is very different according to the test condition, although the vehicle is tested on the same Urban Dynamometer Driving Schedule (UDDS) cycle, as shown in Figure V-65.

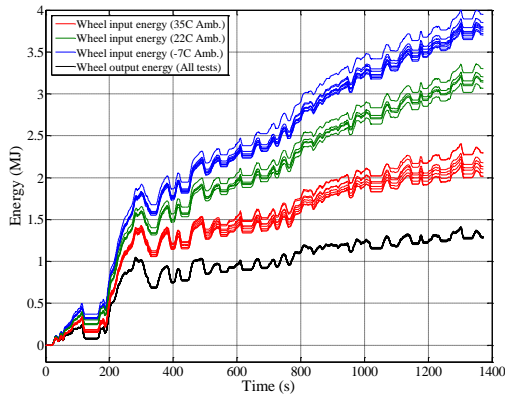


Figure V-65: Variation of input energy at the wheel (all test results were obtained from the UDDS cycle, and the output energy at the wheel did not show any difference, whereas the input energy was significantly different according to the ambient temperature)

In Figure V-65, the black lines in the bottom are the output energy trajectories of all UDDS tests calculated from the torque and the speed measured at the chassis dynamometer, which shows that all output energy trajectories are, of course, similar on the cycle. However, the energy that should be transferred from the powertrain is much larger when the ambient temperature is low. The difference increases compared with the Prius HEV [3]. It cannot be directly compared, however, because the tire used in the test for the Prius HEV is not the same as the tire used in the test for the Prius PHEV.

Control Analysis

The goal of this study was to develop a simulation model that reproduces the vehicle’s performance under different thermal conditions. In order to reproduce the behaviors, the controller should be designed to appropriately control the components and should be validated with the test data. In this section, the analysis results for control behaviors are introduced, including the thermal impacts on the control.

Engine On/Off Control According to Operating Mode

PHEVs are able to operate in EV mode if the SOC is high enough and the demand power does not exceed the power limit of the motor and the battery. Figure V-66 shows all points when the engine is turned on.

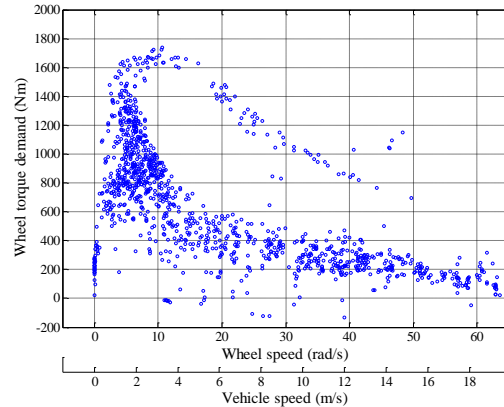


Figure V-66: Wheel speed and demand torque when the engine is turned on (points on the high power demand line are obtained when the vehicle is under CD mode)

In Figure V-66, the points crowded on the lower line are the points when the vehicle is under CS mode, and the points grouped on the upper line are obtained when the vehicle is under CD mode. For the CS mode, the overall trend shows that the engine is primarily turned on if the demand torque exceeds a given threshold torque, which is the same as the on/off strategy of the Prius HEV [2]. On the other hand, in CD mode, it is observed that the engine is not turned on unless the motor is not able to provide all demand power, which means that the vehicle tries to use the electrical energy first without the blended mode control as long as the motor and the battery are able to provide the demand torque and the demand power. The threshold line for the CD mode in Figure V-66 is constrained by the battery power limitation, while the motor torque constraint is activated only on low vehicle speed. Although, the main control idea for the engine on/off is described by the demand torque and the demand power, it is also affected by the engine coolant temperature if the engine needs to provide waste heat to the cabin system.

Figure V-67 shows several trajectories of the engine coolant obtained from tests on the UDDS cycle. In CD mode, if the ambient temperature is 22°C or above, the engine might not be turned on (see red solid lines). However, the engine is forced to be turned on at the launch of the vehicle and is forced to be turned on again if the coolant temperature is below 40°C (see blue solid lines). This is because the heater core connected to the engine coolant loop does not appropriately provide heat to the passenger compartment without the engine’s operation.

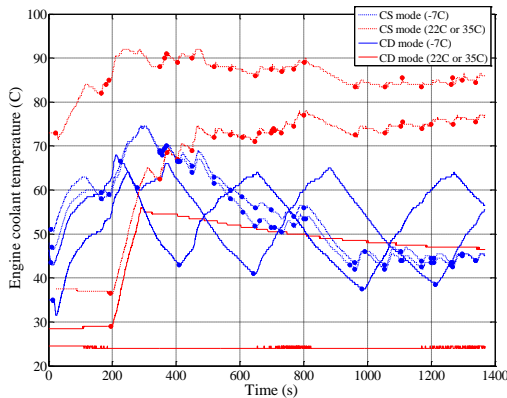


Figure V-67: The engine is forced to be turned on if it needs to provide waste heat to the passenger compartment (dots represent the moments when the engine is turned on)

One interesting thing is that the threshold temperature is lower than the temperature of the Prius HEV, which was about 53°C [3]; the coolant temperature does not go below 40°C in CS mode even when the ambient temperature is -7°C, as shown in Figure V-67 (see blue dashed lines). The lowered threshold might keep the engine turned off longer than for the HEV and save more fuel on the UDDS cycle than the HEV.

SOC Balancing

Another control strategy is necessary to distribute the power between the engine and the battery, which determines the behaviors of SOC on the hybrid driving mode. Figure V-68 shows the overall control strategy to manage the SOC according to the CD or CS mode.

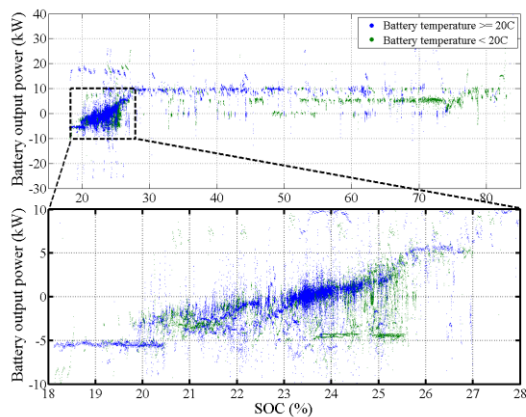


Figure V-68: Output power of the battery for SOC balancing (the points were obtained only when the engine is turned on)

In Figure V-68, the points only shows the output power of the battery during the hybrid driving mode whereas all operating points are plotted in Figure V-69. First, the battery provides no power or constant power under the CD mode if the SOC is greater than 28%. The engine is turned on under the CD mode when the battery does not provide all the demand power, and the engine provides all demand power. However, if the vehicle speed exceeds 100 km/h, the battery provides about 10 kW of constant power, or 6 kW when the battery temperature is low. With the 10 kW of constant power,

the CD driving range could be around 26 km if the vehicle runs with 100 km/h, and the usable energy of the CD mode is 60% of 4.4kWh. The range is similar to the all-electric driving range claimed by Toyota. It seems that this control is designed to constantly consume electric energy under the CD mode, so that drivers have similar experiences in the driving range in the CD mode. In contrast, the control strategy to manage the SOC in the CS mode is similar to the Prius HEV [2], where the desired power of the battery decreases as the SOC decreases. Further, rapid recuperation is also observed in the very low SOC range, like below 20%, and there is no specific control for the SOC balancing according to the battery temperature just as for the Prius HEV.

Whereas the battery power is significantly limited by the battery temperature, especially when the temperature is above 50°C in the Prius HEV [9], the Prius PHEV controls the battery temperature so as not to exceed 45°C. In Figure V-69, the power constraints are observed in the regenerative operation because the electric machine must provide the demanded propulsion torque over the constraints until the engine is turned on, whereas the mechanical brake is able to quickly respond to compensate for the required braking torque.

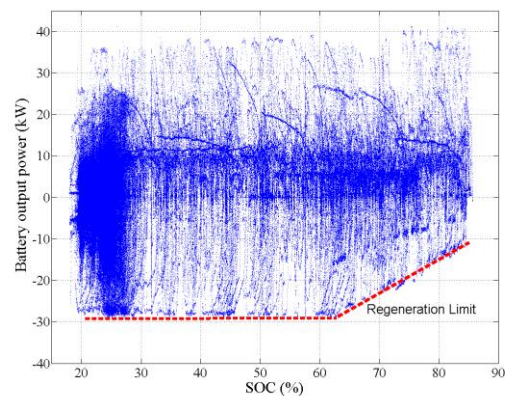


Figure V-69: Battery output power according to SOC (the recuperating power is constrained by the SOC)

Component Operation

If the engine is turned on and the desired battery power is calculated according to the strategies in the previous two sections, the desired engine power can be calculated by the demand power and the desired battery power. However, the engine operating target is not fixed because the engine could operate at a number of operating points to produce the same power. Therefore, the operating target of the engine should be controlled as well as a function of temperature.

Figure V-70 shows the two different engine operating targets according to the coolant temperature, which are almost the same as the operating targets of the Prius HEV [9]. The line that can be inductively assumed from the red points in Figure V-70 shows that the desired torque and speed can be determined if the desired power is given. However, the engine speed is constrained if the engine coolant temperature is not hot enough, as shown in Figure V-71.

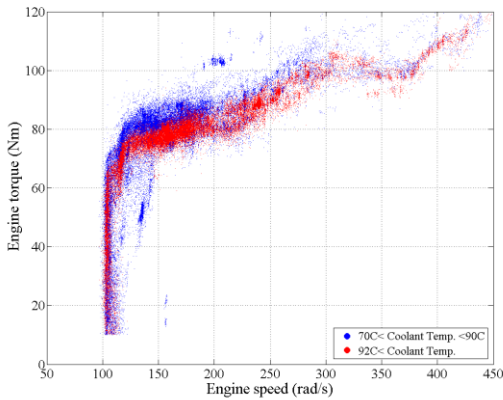


Figure V-70: Engine operating target (red points are the engine operating points when the engine is hot enough and the blue points are the points when the engine is not hot enough)

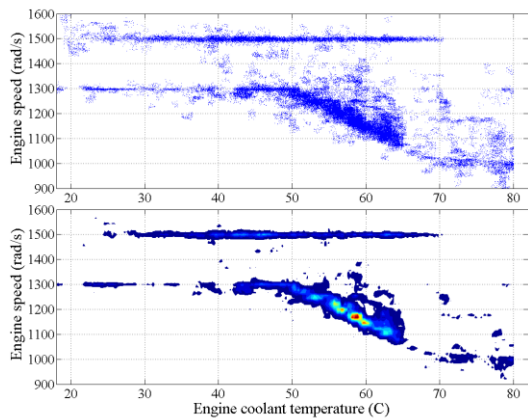


Figure V-71: Engine speed constraint by engine coolant temperature

In Figure V-71, the engine speed is maintained at about 1500 rpm if the engine does need to provide any propulsion power or is controlled from 1000 to 13000 rpm according to the engine coolant temperature if the engine needs to provide power. The speed constraints make the engine operate in a higher torque region than the normal operation, and so the higher operation torque under low engine coolant temperature is observed in the test data.

Three main supervisory control ideas were analyzed based on the obtained test data, by which the status of the engine is determined, the desired power of the engine is calculated, and the desired torque and speed of the engine are determined. Other operating targets, such as motor torque or generator torque, can be calculated by the demand torque and the desired engine torque, which will be discussed in detail in the following sections.

Model Development and Validation

Control Model

The control model is developed based on the analysis results, which are similar to the Prius HEV controller, as shown in Figure V-72.

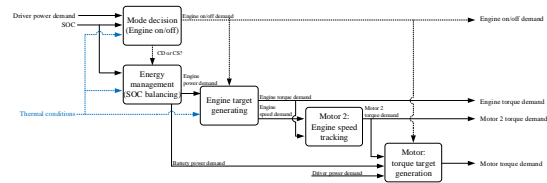


Figure V-72: Control flows for the Prius PHEV (the mode decision for CD or CS mode is added in the engine on/off control compared with the control of the HEV [12])

First, the controller determines the operating mode (CD or CS) according to the SOC and whether or not the engine should be ON or OFF based on a threshold power. Second, the controller calculates how much energy should be provided from the engine if the engine is turned on, based on the desired battery power. Then, the engine target speed and torque are selected from the target operating line in Figure V-69, and the target speed of the generator is calculated by the engine speed. Once the target speeds are determined, the motor and the generator target torques are calculated. In addition, the engine temperature and the battery affect the engine on/off conditions and the battery power limit as described previously.

System Validation

The component and models developed in this study were integrated into Autonomie, as shown in Figure V-72.

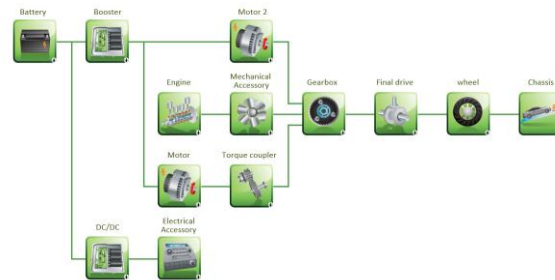


Figure V-73: Vehicle Configuration of 2010 Toyota Prius in Autonomie

Because the Prius PHEV has very similar component specifications compared with the Prius HEV, except for the battery, most components developed for the Prius HEV are used for the Prius PHEV model. The vehicle model has been validated in Autonomie with the test data, and the comparative studies show the results, as presented in Figure V-72 and Figure V-73.

For the comparative study, the simulation results and the test data obtained under the cold ambient temperature, -7°C, are used when the vehicle is tested on the UDDS cycle. In Figure V-72, the simulated engine speed, torque, and coolant temperature match well with the test data. Figure V-73 shows that the simulation model reproduces the cumulated fuel consumption and SOC.

Table V-11 summarize the comparative results on HWFET cycles, respectively. The results show that the simulation model is able to evaluate vehicle performance within 4% in most cases.

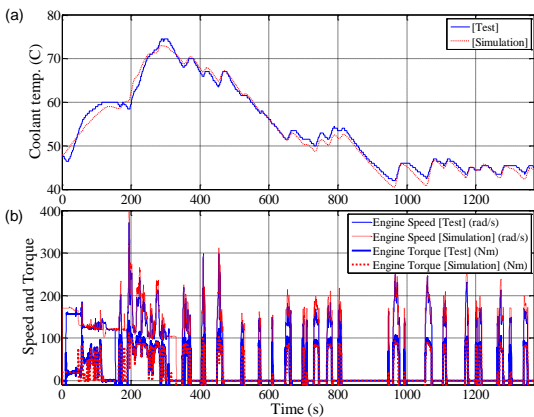


Figure V-74: Comparison between the test and the simulation on the UDDS cycle under cold ambient conditions: (a) engine coolant temperature; (b) engine speed and engine torque

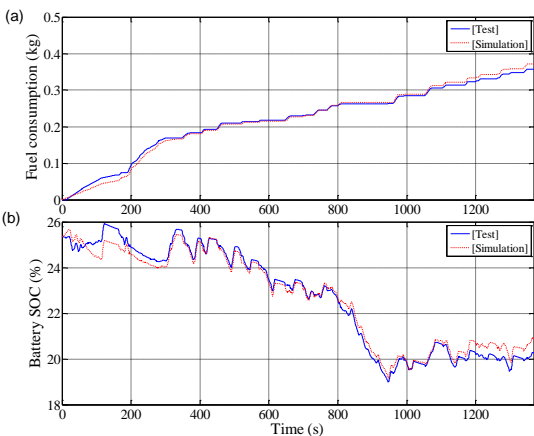


Figure V-75: Comparison between the test and the simulation on the UDDS cycle under cold ambient conditions: (a) fuel consumption; (b) battery SOC

Table V-11: Comparative Results for Fuel Consumption and Final SOC between Test Data and Simulation Results on the HWFET Cycle

| Amb. Temp. | Driving mode | Fuel Consumption (g) | | Final SOC (%) | |
|------------|--------------|----------------------|-----------------|---------------|-------------|
| | | Test | Simulation | Test | Simulation |
| 22C | CD | 0 | 0 (-) | 39.9 | 40.8 (2%) |
| | CS | 442.3 | 443.9 (-0.370%) | 25.2 | 25.8 (2.1%) |
| 35C | CD | 0 | 0 (-) | 30.6 | 32.6 (6.4%) |
| | CS | 521.3 | 527.4 (-1.17%) | 25.3 | 25.2 (0.7%) |
| -7C | CD | 413.9 | 413.7 (0.045%) | 63.4 | 62.2 (2%) |
| | CS | 497.1 | 516.5 (-3.76%) | 26.1 | 25.6 (2%) |

Conclusions

Vehicle test data for the Toyota Prius were obtained from the Argonne APRF under different driving cycles and

temperatures. The data were analyzed to understand the vehicle-level control and component performance.

Detailed thermal models were developed and validated for each main component, with specific focus on engine, battery, and tire losses.

The vehicle-level control was developed to take into account temperature. The main rules include:

- Mode control (engine on/off): engine on/off determined by demand power, SOC, and engine coolant temperature.
- Energy management (SOC balancing): desired battery power is zero or constant under the CD mode and is proportionally controlled according to the SOC under the CS mode.
- Component operating target (engine target): engine operating target line is predefined, and the speed of the engine is constrained when the engine coolant temperature is low.

A complete vehicle thermal model for the PHEV has been developed and validated within a test to test repeatability for different ambient conditions. The thermal model will be used to evaluate the impact of thermal conditions on vehicle energy consumption.

V.G.3. Products

Publications

1. Kim, N., Rask, E., and Rousseau, A., "Control Analysis under Different Driving Conditions for Peugeot 3008 Hybrid 4," Society of Automotive Engineers (SAE) Technical Paper 2014-01-1818, 2014.
2. Kim, N., Rask, E., and Rousseau, A., "Control Analysis under Different Driving Conditions for Peugeot 3008 Hybrid 4," *SAE Int. J. Alt. Power*, 3(1):44–55, 2014.

Tools and Data

1. Autonomie; available at www.autonomie.net.

References

1. Rousseau, A., Kwon, J., Sharer, P., Pagerit, S., et al., "Integrating Data, Performing Quality Assurance, and Validating the Vehicle Model for the 2004 Prius Using PSAT," SAE Technical Paper 2006-01-0667, 2006.
2. Kim, N., Rousseau, A., and Rask, E., "Vehicle-level Control Analysis of 2010 Toyota Prius Based on Test Data," *IMEchE Part D: J. Automobile Engineering*, 226(11):1483–1494, Nov. 2012.
3. Kim, N., Rousseau, A., Lee, D., and Lohse-Busch, H., "Thermal Model Development and Validation for 2010 Toyota Prius," SAE Technical Paper 2014-01-1784, 2014.
4. Government Performance and Results Act; available at www.whitehouse.gov/omb/mgmt-gpra/index-gpra.

5. Lohse-Busch, H., Duoba, M., Rask, E., Stutenberg, K., et al., "Ambient Temperature (20°F, 72°F and 95°F) Impact on Fuel and Energy Consumption for Several Conventional Vehicles, Hybrid and Plug-In Hybrid Electric Vehicles and Battery Electric Vehicle," SAE Technical Paper 2013-01-1462, 2013, doi:10.4271/2013-01-1462, 2013.
6. Rask, E., Duoba, M., Lohse-Busch, H., and Bocci, D., "Model Year 2010 (Gen 3) Toyota Prius Level-1 Testing Report, ANL/ES/RP-67317, Argonne National Laboratory, 2010.
7. Data available at www.transportation.anl.gov/D3/.
8. Information available at www.autonomie.net.
10. Kim, N., Rousseau, A., and Lohse-Busch, H., "Vehicle Level Control Analysis for Toyota Prius HEV under Different Thermal Conditions," submitted to *IMEchE*.

V.H. Analysis for Improving Efficiency with Connected Vehicles

Principal Investigator: Andreas Malikopoulos

Oak Ridge National Laboratory
National Transportation Research Center (NTRC-2)
2370 Cherahala Boulevard
Knoxville, TN 37932-6472
Phone: (865) 946-1529
E-mail: andreas@ornl.gov

DOE Program Manager: David Anderson

Phone: (202) 586-8055
E-mail: david.anderson@ee.doe.gov

V.H.2. Technical Discussion

Background

Fossil fuels are an unsustainable resource and our planet has only a finite number of deposits. Two-thirds of the oil used around the world currently goes to power transportation vehicles, of which half goes to passenger cars and light trucks [1]. Incomplete carbon reactions, unburned hydrocarbons, or other elements present in the fuel or air during combustion all create pollution. Studies have shown that tailpipe emissions from cars and trucks account for almost a third of the air pollution in the United States [1]. Transportation will contribute about 25 percent of incremental carbon emissions over the next two decades as the total number of vehicles on the roads increases [2]. In emerging Asia alone, the total number of vehicles is expected to rise from 55 million in 2003 to 420 million in 2030.

The typical US highway capacity is 2,200 vehicles per hour per lane, or 750 trucks per hour per lane [3] and the vehicles occupy only 5% of road surface at the maximum capacity [4]. Congestion is created by drivers' response to various disturbances. In 2011, congestion caused people in urban areas to travel 5.5 billion hours more and to purchase an extra 2.9 billion gallons of fuel resulting at a total cost estimated to 121 billion [5]. This traffic time leads to an increase in the energy consumption and vehicle emissions. Furthermore, according to the US National Highway Traffic Safety Administration (NHTSA) in 2012 there were 5.615 million crashes in the United States leading to 33,561 deaths [4]. Connected vehicle technologies can enable various users including individual vehicles and traffic control centers to better monitor transportation network conditions and make better operating decisions to improve safety and reduce pollution, energy consumption, and travel delays.

Introduction

Recognition of the necessity for connecting vehicles to their surroundings is gaining momentum. Many stakeholders intuitively see the benefits of multiscale vehicle control systems and have started to develop business cases for their respective domains, including the automotive and insurance industries, government and service providers. It seems clear that the availability of vehicle-to-vehicle (V2V) communication has the potential to reduce traffic accidents and ease congestion by enabling vehicles to more rapidly account for changes in their mutual environment. Likewise, vehicle-to-infrastructure (V2I) communication, e.g., communication with traffic structures, nearby buildings, and traffic lights, should allow for individual vehicle control systems to account for unpredictable changes in local infrastructure. Widespread adoption of these technologies requires streamlined use of the

V.H.1. Abstract

Objectives

- The objective of this project was to summarize the development and research trends in connected vehicle technologies that have been reported in the literature to date. The main applications of these technologies have been also identified, including driver assist systems, predictive vehicle control, autonomous vehicles, and multivehicle routing and control.

Major Accomplishments

- Completed an extensive literature review of more than 100 archival publications covering key state-of-the-art connected vehicle technologies and reported the outcome in a survey paper submitted in the International Journal of Powetrain.
- Developed a simple decentralized control algorithm that can coordinate vehicles with respect to fuel economy.

Future Achievements

- The project was completed.



radio channel resources. Backof [6] presented an extensive historic journey on vehicular communication systems from the beginning of the twentieth century to the present.

Connected vehicle technologies can provide shorter gaps between vehicles, faster responses while it can improve the highway capacity by identifying appropriate target speeds. In 1970, Fenton [7] reported the state of the art in vehicle automatic guidance and control, and emphasized its significance in addressing both traffic-related problems and accidents. A few years later, Pue [8] investigated communication requirements in the longitudinal control of vehicles for the allocation of control computation and the associated trade-offs for maintaining an acceptable level of vehicle performance in automated guideway transit systems. The same year, Caudill, Kornhauser, and Wroble [9] discussed the hierarchy of controller functions in vehicle management for an automated vehicle system and provided the economics of system-owned communication and control packages for AHS.

By the mid-1980s, it had become apparent that to increase traffic flow the intervehicular spacing had to decrease. Forming a platoon of vehicles traveling at high speed that would allow vehicles to accelerate or brake simultaneously was a popular system-level approach to address traffic congestion that gained momentum, as packing the vehicles tightly together yielded significant improvements in highway capacity. Rajamani et al. [10] reported the integrated control system used in National Automated Highway Systems Consortium in August 1997 that was implemented in eight fully automated vehicles traveling together as a platoon. The demonstration used 7.6-mile highway segment consisting of two lanes.

The goals of automated highway systems (AHS) is to alleviate congestion, reduce energy use and emissions, and improve safety. One of the ways these can be achieved is through significantly higher traffic flow as a result of closer packing of automatically controlled vehicles in platoons. The vehicles need to be able to communicate with each other and exchange information. Namely, they need to be connected. Matsumoto [11] proposed a guidance cable for automatically driving vehicles that could be used as a communication medium between the highway authority and vehicles on it. Tank and Linnartz [12] proposed a statistical model aimed at clustering the interests of car drivers, increasing the throughput in V2V environments. Kato et al. [13] presented various technologies for cooperative driving with automated vehicles and intervehicle communication (IVC). Fax and Murray [14] addressed the problem of cooperation among a collection of vehicles performing a shared task using IVC.

The international Society of Automotive Engineers (SAE) reported a taxonomy for on-road vehicles automation ranging from no automation to full automation (SAE, 2013). “On-road” refers to public roadways that collectively serve users of vehicles of all classes and automation levels (including no automation), as well as motorcyclists, pedal cyclists, and pedestrians. So according to this SAE report, we have the following levels of automation:

- *Non-automated*: when full time performance of all aspects of the dynamic driving task, even when enhanced by

warning or intervention systems, is conducted by the human driver.

- *Assisted*: when the driving mode-specific execution is performed by a driver-assistance system of either steering or acceleration/deceleration using information about the driving environment and with the expectation that the human driver perform all remaining aspects of the dynamic driving task, e.g., adaptive cruise control or lane keeping assistance.
- *Partial automation*: when the driving mode-specific execution is performed by one or more driver-assistance systems of both steering and acceleration/deceleration using information about the driving environment and with the expectation that the human driver perform all remaining aspects of the dynamic driving task, e.g., adaptive cruise control and lane keeping assistance, traffic jam assist.
- *Conditional automation*: when the driving-specific performance of all aspects of the driving task is conducted by an automated driving system with the expectation that the human driver will respond appropriately to a request to intervene, e.g., traffic jam pilot, automated parking.
- *High automation*: when the driving mode-specific performance of all aspects of the dynamic driving task is conducted by an automated driving system, even if a human driver does not respond appropriately to a request to intervene, e.g., highway driving pilot, driveless shuttle, valet parking.
- *Full automation*: when full time performance of all aspects of the dynamic driving task is conducted by an automated driving system under all roadway and environmental conditions that can be managed by a human driver, e.g., automated taxi, car-share repositioning system. These levels can be used to describe the automation of (1) on-road vehicles, (2) particular systems within those vehicles, and (3) the operation of those vehicles.

Vehicle collision warning systems (CWSs) provide warning signals to alert the driver when potential collisions are detected. Typical CWSs are based on the information obtained by the vehicle using radar, acoustic and vision sensors. The sensors yield relative information about the vehicle and moving or stationary obstacles. This information is then processed to determine the likelihood of a collision and to estimate the time to collision. A warning is issued if the estimated time to collision is smaller than the specific threshold under the specific scenario. Tan and Huang [15] explored the engineering feasibility of a cooperative CWS (CCWS) where vehicles are equipped with a DGPS and basic motion sensors. Car-to-car overlay networks for enhancing safety in a group of cars has been also investigated for CCWS [16].

Advanced driver-assistance systems (ADASs) provide essential information to the driver aimed at automating difficult or repetitive tasks and thus can lead to an overall increase in safety and an enhanced driving experience. Ambuhl and Guzzella [17] investigated the contribution of IVC in ADASs and compared it with traditional safety sensors. A continuous human-kinetic traffic-flow model for the explorative analysis of ADASs presented in [18]. Slowdown warning systems aim to

simultaneously provide information to all drivers in a platoon of vehicles when a vehicle abruptly decelerates. This advance information gives the drivers more time to react in preparation for the impending slowdown, and as a result, it increases the distances between them and the cars immediately ahead of them. Various scenarios aimed at providing advance warnings to enhance safety in the context of IVC were presented in [19]. Chiara, Deflorio, and Diwan [20] investigated the use of V2V and V2I communication systems to reduce secondary accidents whose occurrence is often due to low visibility and/or poor weather conditions where conventional safety features/systems such as brake lights are not effective. Torrent-Moreno et al. [21] analyzed V2V communication from an active-safety perspective and identified the challenges and associated strategies for improving performance through packet-level interference management. A detailed survey of the development and research trends in connected vehicle technologies that have been reported in the literature to date can be found in [3].

Approach

There is a solid body of research now available that has aimed at enhancing our understanding of vehicle system optimization [22]. Many different approaches have been proposed to address the fundamental vehicle performance challenges. The biggest remaining uncertainties are related to external factors including the driver's driving style, the surrounding traffic environment, and driving terrain. It appears that research needs to be devoted to considering the vehicle as part of a larger system, which can be optimized at an even larger scale. Such larger-scale optimization will require the acquisition and processing of additional information from the driver and conditions outside the vehicle itself. This is likely to require addition of new sensors and/or better utilization of information generated by existing sensors. However the processing of such multi-scale information will require significantly new optimization and control approaches in order to overcome the curse of dimensionality.

Connected vehicle technologies can enable various users including individual vehicles and traffic control centers to better monitor transportation network conditions and make better operating decisions to improve safety and reduce pollution, energy consumption, and travel delays. The problem of scheduling automated traffic in a city with the intention to improve efficiency by decreasing delays, increasing capacity and easing congestion has attracted considerable attention. Giridhar and Kumar [23] addressed this problem by constructing a discrete-space and -time model for the movements of vehicles assuming a minimum safe distance between vehicles, and they derived a class of scheduling algorithms that are provably deadlock free given a certain sufficient condition associated with the configuration of vehicles on the road network. The requirements of information exchange between vehicle and roadside units in highways were discussed in [24]. In this work, the authors described a model of the roadside for ITS data buses providing a better communication service on intelligent highways. Du and Barth [25] introduced a low-cost automated vehicle location system able to determine vehicle lane position in real time. The

system was developed based on an in situ driving method and high-resolution aerial image technique. A connected vehicle infrastructure for ITS that exploits vehicular mobility and builds stable vehicular clusters for ITS network infrastructure was discussed [26]. The authors presented a VANET clustering algorithm that helps nodes dynamically adapt to mobility changes and regroup in order to form stable, long-lasting vehicle clusters. Baskar et al. [27] provided a survey of traffic control frameworks for IVHS aimed at improving traffic performance and discussed the potential application of control design methods that are available for traffic control.

To assess potential benefits in fuel economy with connected vehicles, it is necessary to explicitly formulate the relation between the impact of the major driving factor, defined as coefficient of power demand, on fuel economy. Such a formulation could be used to develop a competent interface to “translate” the optimal coordination among the vehicles. In this context, we quantified the impact of this driving factor and constructed a set of polynomial metamodels that formulates explicitly its relationship with fuel consumption.

The coefficient of power demand is a driving factor that provides an indication of the transient engine operation since it is proportional to power demanded by the driver. This power is the work done by the vehicle over time, which is equal to the total force acting on the vehicle multiplied by the distance traveled. The forces acting on the vehicle in the longitudinal direction consist of (a) tractive force, (b) drawbar force, (c) aerodynamic force, (d) rolling resistance force, and (e) the component of vehicle weight in this direction. The power demanded by the driver is proportional to the product of the vehicle speed and acceleration.

Figure V-76 illustrates the variation in fuel consumption per meter for several driving cycles with respect to the average speed of each driving cycle [28]. The resulting trend indicates that those driving cycles with lower average speed tend to have higher fuel consumption per meter, which might be associated with frequent transient engine operation. HWFET exhibits the lowest fuel consumption as it represents highway driving conditions and, thus, steady-state engine operation at high average vehicle speed. The Japan 10-15 and FTP driving cycles exhibit the highest fuel consumption per meter, deemed characteristic of their low average speeds. Thus, these three driving cycles were used to investigate further the impact of the coefficient of power demand on fuel consumption.

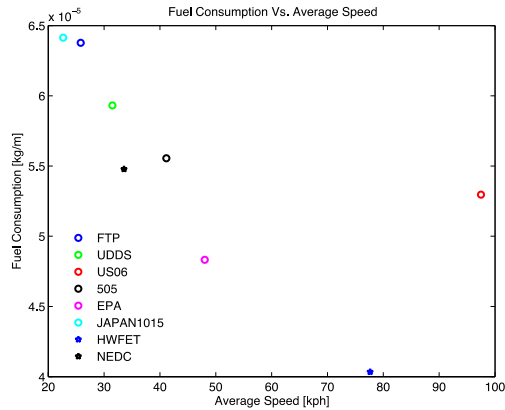


Figure V-76: Fuel consumption versus average speed for various driving cycles [28]

To reduce computation time a set of polynomial metamodels was constructed. These models can reflect the responses in fuel consumption produced by changes in the coefficient of power demand, e.g., vehicle speed and acceleration. A metamodel is a “model of a model” that is used to approximate a usually expensive analysis or simulation process; metamodeling refers to the techniques and procedures of constructing such a model. In this framework, fuel consumption was evaluated through simulation in Autonomie over a grid of values for vehicle speed and acceleration in a particular driving cycle. Then multivariate polynomial functions were fit to the data using the least squares method.

For the problem formulation considered here, a quadratic metamodel turned out to provide an appropriate fitting to the discrete simulation data points of fuel consumption with respect to vehicle speed and acceleration. We also investigated a higher order polynomial metamodel, but this appeared to “overfit” the data. Likewise, a lower order polynomial was not adequate to accurately estimate fuel consumption.

Different sets of discrete simulation data points consisting of a grid of vehicle speed and acceleration for three driving cycles (Japan 10-15, combined FTP and HWFET, and FTP) were derived by running a vehicle model in Autonomie. The fuel consumption estimated by the polynomial metamodel [28] for the FTP driving cycle is illustrated in Figure V-77. Such polynomial metamodels can be used to estimate fuel consumption for any different type of vehicle.

Results

Vehicle communication technologies are the key enabler to encompass connected vehicles and intelligent transportation systems. The goals of automated highway systems are to alleviate congestion, reduce energy use and emissions, and improve safety. One of the ways these can be achieved is through significantly higher traffic flow as a result of closer packing of automatically controlled vehicles in platoons. The vehicles need to be able to communicate with each other and exchange information. Namely, they need to be connected.

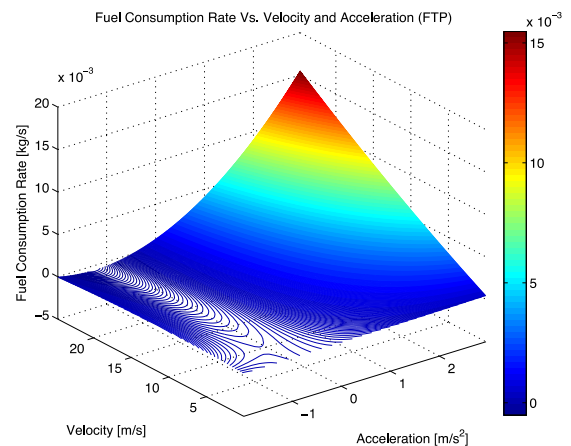


Figure V-77: Fuel consumption metamodel corresponding to the FTP driving cycle

Connected vehicle technologies can provide shorter gaps between vehicles, faster responses while it can improve the highway capacity by identifying appropriate target speeds. The problem of scheduling automated traffic in a city with the intention to improve efficiency by decreasing delays, increasing capacity and easing congestion has attracted considerable attention. Some studies addressed this problem by constructing a discrete-space and -time model for the movements of vehicles assuming a minimum safe distance between vehicles, and they derived a class of scheduling algorithms that are provably deadlock free given a certain sufficient condition associated with the configuration of vehicles on the road network.

We developed a decentralized control algorithm that can coordinate vehicles with respect to fuel economy. The research hypothesis here is that the solution of a stochastic control problem formulation can efficiently address the problem of optimizing these vehicles when V2V and V2I communication is available. The vehicles are treated as autonomous intelligent agents. The agents attempt through their interaction to jointly maximize overall their own operation. In this framework, each vehicle interacts with other vehicles and obtains information, using the metamodels presented in the previous section, enabling it to improve its future performance; namely, optimizing the specific performance criteria while satisfying the system’s physical constraints. In a simulation example involving two vehicles approaching an intersection at the same time, the algorithm provided instructions to the driver of one of the vehicles to reduce speed, and thus avoiding a full stop at the intersection (Figure V-78–Figure V-80). More specifically, two vehicles (one red, one blue) arrive at an intersection at the same time. Suppose the blue vehicle is approaching a “yield” sign; hence, the driver will have to come to a full stop and let the red vehicle proceed. In this case, the algorithm promotes the following optimal outcome: the blue vehicle should decelerate precisely enough to allow the red vehicle to reach the intersection first and proceed without braking. The blue vehicle will not have to come to a full stop, thereby conserving momentum and fuel while also improving travel time. By avoiding a full stop, the

vehicle essentially doesn't have to decelerate, idle while being at stop, and then accelerate again, which has significant implications in fuel economy improvement.

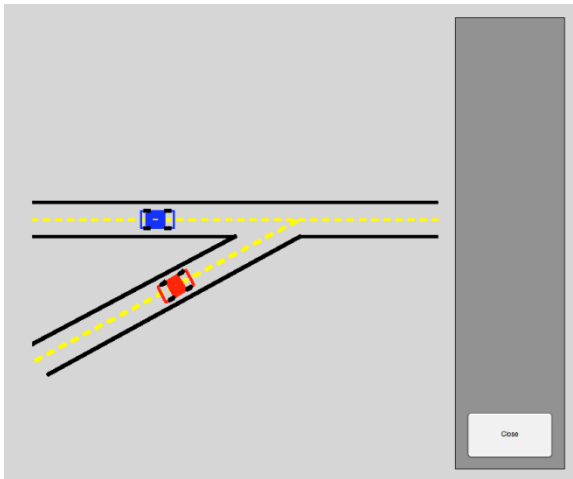


Figure V-78: Two vehicles with V2V communication while approaching the intersection at the same time

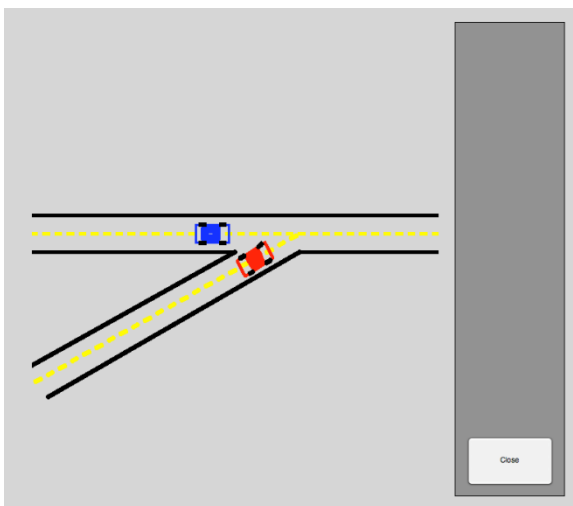


Figure V-79: The blue vehicle reduces speed through the decentralized control to avoid full stop at the intersection

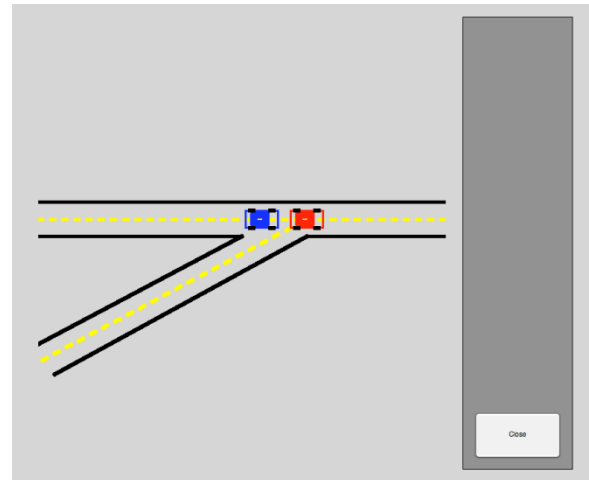


Figure V-80: Both vehicles pass the intersection avoiding stop-and-go driving

Conclusions

There is a solid body of research now available that has aimed at enhancing our understanding of power control optimization in HEVs and PHEVs. Many different approaches have been proposed to address the fundamental vehicle system performance challenges using both offline and online analytical algorithms. The biggest remaining uncertainties are related to external factors, including the driver's driving style, the surrounding traffic environment, and the driving terrain. It appears that future research studies need to be devoted to considering the vehicle as part of a larger system, which can be optimized at an even larger scale. Such large-scale optimization will require the acquisition and processing of additional information from the driver and conditions outside the vehicle itself. This is likely to require addition of new sensors and/or better utilization of information generated by existing sensors. However, the processing of such multiscale information will require significantly new approaches in order to overcome the curse of dimensionality. One particular area where new sensors will be needed is in vehicle-to-vehicle communication. It seems clear that the availability of this information has the potential to reduce traffic accidents and ease congestion by enabling vehicles to more rapidly account for changes in their mutual environment that cannot be predicted by deterministic models. Likewise, communication with traffic structures, nearby buildings, and traffic lights should allow for individual vehicle control systems to account for unpredictable changes in local infrastructure.

Recognition of the necessity for connecting vehicles to their surroundings is gaining momentum. Many stakeholders intuitively see the benefits of multiscale vehicle control systems and have started to develop business cases for their respective domains, including the automotive and insurance industries, government, and service providers. The main focus is on safety and how accidents could be potentially prevented by developing multiscale systems based on V2V and V2I communications to alert drivers. Thus, we can assume that these technologies will be available in a few years. The question is whether we could take advantage of these

technologies and optimize the power management control in HEVs and PHEVs. What if we would consider the problem of optimizing fuel economy and emissions for a fleet of vehicles rather than a single vehicle, thus eliminating the uncertainty related to traffic? What would be the appropriate conceptual approaches for modeling and optimization?

Investigating a new optimization framework that considers a fleet of vehicles could aim to compute the most efficient vehicle speed in centralized locations and communicate this with driver information systems to the driver to avoid congestion, thus improving overall efficiency and reducing emissions in conventional vehicles. In HEVs and PHEVs, the power management controller would have to account for limited uncertainty about surrounding traffic and commute and be able to optimize fuel economy, pollutant emissions, as well as battery lifetime and range. The detailed investigation of these issues could provide policymakers with unique new tools to assess the implications in promoting the development of technologies and infrastructure in new directions.

References

1. www.ftc.gov/. Federal Trade Commission.
2. web.mit.edu/mitei/index.html. MIT Energy Initiative.
3. Malikopoulos, A.A., H. Borhan, and S.A. Toran, *Connected Vehicle Technologies for Safety and Efficiency: A Survey*. International J. Powertrains (in review), 2014.
4. DOT, www.its.dot.gov. 2014.
5. Schrank, D., B. Eisele, and T. Lomax, *TTI's 2012 Urban Mobility Report*. 2012, Texas A&M Transportation Institute.
6. Backof, C., *Vehicle communications before 1950*. IEEE Vehicular Technology Magazine, 2006. **1**(1): pp. 3–7.
7. Fenton, R.E., *Automatic vehicle guidance and control: A state of the art survey*. IEEE Transactions on Vehicular Technology, 1970. **19**(1): pp. 153–161.
8. Pue, A.J., *Implementation trade-offs for a short-headway vehicle-follower automated transit system*. IEEE Transactions on Vehicular Technology, 1979. **28**(1): pp. 46–55.
9. Caudill, R.J., A.L. Kornhauser, and J.R. Wroble, *Hierarchical vehicle management concept for automated guideway transportation systems*. IEEE Transactions on Vehicular Technology, 1979. **28**(1): pp. 11–21.
10. Rajamani, R., et al., *Demonstration of integrated longitudinal and lateral control for the operation of automated vehicles in platoons*. IEEE Transactions on Control Systems Technology, 2000. **8**(4): pp. 695–708.
11. Matsumoto, S., *Highway communication system using guidance-cable*. IEEE Transactions on Vehicular Technology, 1969. **20**: pp. 46–49.
12. Tank, T. and J.-P.M.G. Linnartz, *Vehicle-to-vehicle communications for AVCS platooning*. IEEE Transactions on Vehicular Technology, 1997. **46**(2): pp. 528–536.
13. Kato, S., et al., *Vehicle control algorithms for cooperative driving with automated vehicles and intervehicle communications*. IEEE Transactions on Intelligent Transportation Systems, 2002. **3**(3): pp. 155–161.
14. Fax, J.A. and R.M. Murray, *Information flow and cooperative control of vehicle formations*. IEEE Transactions on Automatic Control, 2004. **49**(9): pp. 1465–1476.
15. Tan, H.-S. and J. Huang, *DGPS-Based Vehicle-to-Vehicle Cooperative Collision Warning: Engineering Feasibility Viewpoints*. IEEE Transactions on Intelligent Transportation Systems, 2006. **7**(4): pp. 415–428.
16. Aoyama, M. and H. Takeichi, *Adaptive Self-Organizing Overlay Network for Car-to-Car Communications*, in *Proceedings of the Ninth ACIS International Conference on Software Engineering, Artificial Intelligence, Networking, and Parallel/Distributed Computing*. 2008. pp. 605–610.
17. Ambuhl, D. and L. Guzzella, *Predictive Reference Signal Generator for Hybrid Electric Vehicles*. IEEE Transactions on Vehicular Technology, 2009. **58**(9): pp. 4730–4740.
18. Tampere, C.M.J., S.P. Hoogendoorn, and B. van Arem, *Continuous Traffic Flow Modeling of Driver Support Systems in Multiclass Traffic With Interverhicle Communication and Drivers in the Loop*. IEEE Transactions on Intelligent Transportation Systems, 2009. **10**(4): pp. 649–657.
19. Chakravarthy, A., K. Song, and E. Feron, *Preventing Automotive Pileup Crashes in Mixed-Communication Environments*. IEEE Transactions on Intelligent Transportation Systems, 2009. **10**(2): pp. 211–225.
20. Chiara, B.D., F. Deflorio, and S. Diwan, *Assessing the effects of inter-vehicle communication systems on road safety*. IET Intelligent Transport Systems, 2009. **3**(2): pp. 225–235.
21. Torrent-Moreno, M., et al., *Vehicle-to-Vehicle Communication: Fair Transmit Power Control for Safety-Critical Information*. IEEE Transactions on Vehicular Technology, 2009. **58**(7): pp. 3684–3703.
22. Malikopoulos, A.A., *Supervisory Power Management Control Algorithms for Hybrid Electric Vehicles: A Survey*. IEEE Transactions on Intelligent Transportation Systems (in press), 2014.
23. Giridhar, A. and P.R. Kumar, *Scheduling Automated Traffic on a Network of Roads*. IEEE Transactions on Vehicular Technology, 2006. **55**(5): pp. 1467–1474.
24. Cai, H. and Y. Lin, *A Roadside ITS Data Bus Prototype for Intelligent Highways*. IEEE Transactions on Intelligent Transportation Systems, 2008. **9**(2): pp. 344–348.
25. Du, J. and M.J. Barth, *Next-Generation Automated Vehicle Location Systems: Positioning at the Lane Level*. IEEE Transactions on Intelligent Transportation Systems, 2008. **9**(1): pp. 48–57.
26. Koulakezian, A. and A. Leon-Garcia, *CVI: Connected Vehicle Infrastructure for ITS*, in *Proceedings of the 2011 IEEE 22nd International Symposium on Personal Indoor*

and Mobile Radio Communications (PIMRC). 2011. pp. 750–755.

27. Baskar, L.D., et al., *Traffic control and intelligent vehicle highway systems: a survey*. IET Intelligent Transport Systems, 2011. **5**(1): pp. 38–52.
28. Malikopoulos, A.A. and J.P. Aguilar, *An Optimization Framework for Driver Feedback Systems*. IEEE Transactions on Intelligent Transportation Systems, 2013. **14**(2): pp. 955–964.

V.H.3. Products

Publications

1. Malikopoulos, A.A., Borhan, H., Toran, S., "Connected Vehicle Technologies for Safety and Efficiency: A Survey," *International Journal of Powertrain*. (*in review*)

V.I. Trip Prediction and Route-Based Control Using Digital Maps

Principal Investigator: Dominik Karbowski

Argonne National Laboratory
9700 South Cass Avenue
Argonne, IL 60439-4815
Phone: (630) 252-5362
E-mail: dkarbowski@anl.gov or nkim@anl.gov

DOE Program Manager: David Anderson

Phone: (202) 287-5688
E-mail: David.Anderson@ee.doe.gov

V.I.1. Abstract

Objectives

- Demonstrate that route-based control for plug-in hybrid electric vehicles/hybrid electric vehicles (PHEVs/HEVs) is possible thanks to trip prediction using digital maps.

Major Accomplishments

- Processed and quality-checked a database of real-world speed recordings to create transition probability matrices.
- Packaged previous algorithm for better useability and greater maintenance flexibility.
- Created a graphical user interface (GUI) allowing the generation of speed profiles.
- Improved execution speed and accuracy of the speed profile generation tool.
- Analyzed the effect of stochastic trip-to-trip variability (for a given itinerary) on optimal tuning of a route-based controller.

Future Achievements

- Improve modeling of intersections in speed profile generation tool.
- Evaluate route-based control in a broad range of driving situations.



V.I.2. Technical Discussion

Background

Detailed maps of the road network, increased on-board computing capabilities, connectivity to cloud-based computing resources, and ever-increasing inclusion of global navigation satellite systems (GNSSs) make route prediction more and more conceivable. One of the main applications of route prediction is energy efficiency: knowledge of future driving conditions, if used effectively, can contribute to improving the efficiency of advanced vehicles, such as HEVs and PHEVs.

Several optimization techniques that use some form of route prediction as an input already exist. The most theoretical is dynamic programming, which provides a global optimum. It is highly computer-intensive and is hardly implementable because of the very nature of the algorithm, which runs backwards (i.e., starting from the end). Stochastic dynamic programming uses a probabilistic distribution of drive cycles, rather than a single cycle.

An alternative and easier to implement online optimization technique relies on the Pontryagin's Minimum Principle (PMP), which under certain assumptions can be simplified to an Equivalent Consumption Minimization Strategy (ECMS) method. In this case, global optimality is not guaranteed, but it generally leads to good results. However, the outcome of using this method highly depends on one constant, the initial co-state in one case, or equivalence factor in the other, that is chosen for the online implementation. Finding the optimal factor for a given trip can be done by predicting the route.

Many studies assume the speed profile is given and do not explore two major hurdles of real-world implementation of trip-based control optimization: (1) how to predict the vehicle speed profile for the trip, and (2) how well the optimization works when the predicted and the actual speed differ — which invariably can happen in the real world, given drivers unpredictability.

One approach to trip prediction is to model vehicle speed as a Markov Chain. This model relies on a database of real-world vehicle speeds, from which transition probabilities can be computed. This allows the generation of stochastic speed profiles. However, this method per se does not provide a prediction for a particular itinerary.

Introduction

In this research, we investigated a method of obtaining a stochastic vehicle speed profile for a given itinerary using real geographical data and then demonstrated how this could be used for PHEV optimization by using a PMP-based controller.

This project involves two core activities: development of an algorithm for robust vehicle speed and terrain grade

prediction using digital maps on the one hand, and development and analysis of a route-based control strategy for a PHEV on the other hand. The latter requires the inputs of the former in order to be implementable in the real-world. These two activities were started in fiscal year (FY) 2013.

Figure V-81 shows how the two activities would relate in the context of an in-vehicle application. A module would provide detailed segment-by-segment information about the future itinerary, all of which can be known thanks to digital maps, user input, global positioning system (GPS) position, and traffic information. That information would then be processed by a speed prediction module, which would produce naturalistic speed and grade predictions; an optimization module would then compute the optimal tuning of the vehicle controller.

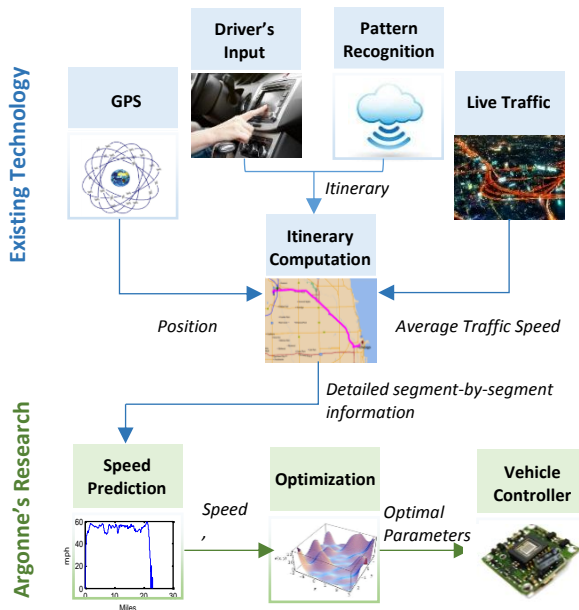


Figure V-81: Conceptual view of speed prediction and route-based control in the context of a vehicle

Our guiding principle is to accurately represent the causalities and uncertainties of the real world, from the powertrain chosen to the flow of information. In particular, we rely on digital map information currently available in modern cars; HERE is such a provider. We use its desktop tool, ADAS-RP (Advanced Driver Assistance Systems Research Platform), for accessing this data in our research.

Approach

Creating a Transition Probability Matrix

The transition probability matrix (TPM) is at the heart of our trip prediction algorithm. The TPM is used in a Markov Chain to compute the next state, given the current one. The TPM is built from counting state transitions in a database of real-world speed recordings. In order to produce naturalistic speed profiles, it is of paramount importance to ensure that the database itself is free of erroneous data points.

To that end, we processed the dataset from the 2007 Chicago travel survey using a multiple step approach. First,

we identified the stops, which led to the segmentation of each trip into micro-trips. Some micro-trips were removed, either because of unusual low speeds or the absence of correlation between “GPS” distance and “integral of speed” distances.

The remaining trips often included abnormalities that could be corrected using filters or interpolations. However, we wanted to ensure that we did not keep micro-trips with too many “bad” points. So we computed a “correction index”: if a correction factor was below a threshold, the corrected trip was deemed valid; otherwise it was rejected. We filtered for the following abnormalities:

- *Missing points.* Sequences within trips with no recorded data, despite moving vehicle.
- *Speed variation.* Sections of the recorded data in which the speed stayed exactly the same.
- *Trajectory variation.* Improbable variations of GPS coordinates resulting in bad speed acquisition.
- Unusual speeds or accelerations.

The last step was smoothing the speed signal using a Butterworth filter. Based on the correction index, the micro-trips with too many abnormal points were considered not valid and were not used in the final database.

After processing, 47% of the trips were considered valid, representing 59% of the original data points. The acceleration and speed distribution of the processed database is shown in Figure V-82. The envelope of the distribution is comparable to that of the most aggressive standard drive cycles, such as US06.

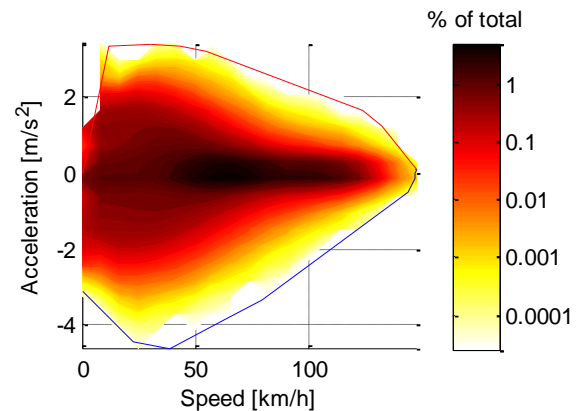


Figure V-82: Distribution of speed and acceleration of the processed Chicago database

Preparing the Trip Prediction Code to Be More Widely Used

In FY 2014, we worked on making the initial exploratory tools developed in FY 2013 more robust, easier to use for the end user, and also more capable of receiving further upgrades.

As part of this effort, we reorganized the code, dividing it into specific functions, moving many of the hard-coded values into parameters. Each function was carefully documented. In the process, we were able to identify many bugs and solve them. Furthermore, we developed an application programming interface (API), so that it is easy to call the various components of the code. All these steps were necessary to

ensure the tool can be efficiently maintained and developed in a team.

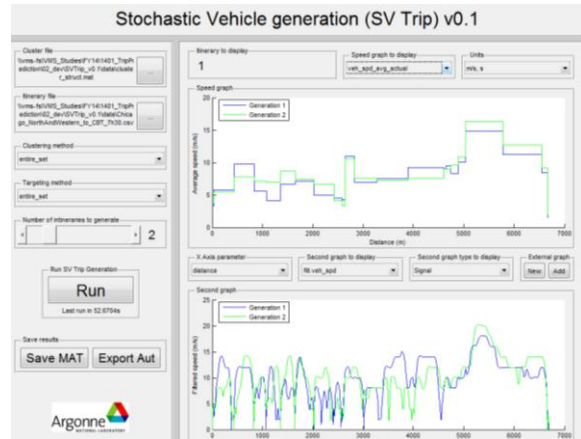


Figure V-83: Screenshot of SVTrip

Thanks to the API, it was also possible to create a GUI, which was given the temporary name of “SVTrip” — for Stochastic Vehicle Trip prediction. Figure V-83 is a screenshot of one of the first versions. This interface was used to create speed profiles for the route-based control study.

Reducing the Execution Time of the Trip Prediction Algorithm

If the speed prediction algorithm is to be implemented in a vehicle, it needs to be computationally efficient. We noticed that it tended to be slow when there was a stop at the end of the segment. In such a situation, it was very difficult to obtain a speed profile that matched the target speed and that ended at exactly zero speed at the desired distance.

To circumvent that issue, we implemented a bi-directional Markov Chain, as illustrated in Figure V-84. Two speed profiles are simultaneously generated: one forward, starting from the initial speed on that segment and using the standard TPM; one backward that starts from zero speed at the end of the segment, moving toward the start and requiring a TPM intended for backward generation. When the two speed profiles match, we can build a new one made from two pieces: the initial part of the forward profile, and the initial (if looked at from the end) of the backward part.

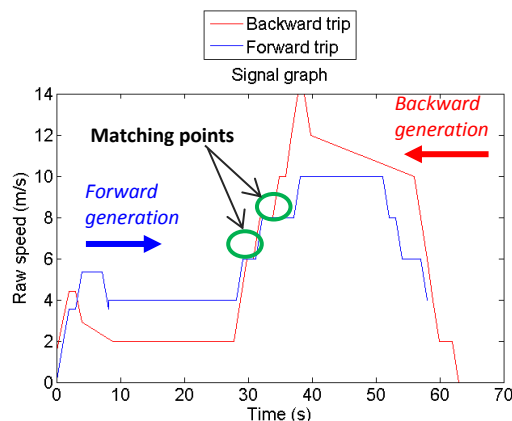


Figure V-84: Bi-directional Markov Chain

Using the Trip Prediction Algorithm for Vehicle Performance Prediction

One application of our speed prediction tool is forecasting the value of a parameter related to the use of a vehicle on a particular trip, for example, fuel consumption. Because of the stochastic nature of the prediction, it is possible to generate N speed profiles (e.g., N = 10) that would all be different, yet still specific to the selected itinerary. A vehicle model, such as Autonomie, can then be run on each one of them. The result can then be analyzed using statistical tools: average value, kernel distribution, etc. Consequently, the results are more likely to reflect the unavoidable variability of actual driving.

Application to Analysis Route-Based Control

In FY 2013, we developed a vehicle controller for Autonomie that incorporates the PMP for a PHEV modeled after the Toyota Prius PHEV 2012. The goal is to show that route-based control is more fuel efficient on longer trips than the conventional strategy — “electric vehicle” mode followed by a “charge-sustaining” mode (EV+CS).

In essence, PMP consists of comparing the weighted sum of battery power and fuel power for each control option, and picking the one with the lowest overall power. The summation of the two powers, of different natures (thermal and electrical), is done through the use of an equivalence factor (EQF). According to the PMP, such control is optimal given the initial and final state-of-charge (SOC). The challenge is to find the EQF such that the battery is fully depleted at the end of the trip, but not too much time before the end. The challenge of PMP is to find the appropriate EQF that will lead to that situation. This can be done using the predicted speed and grade profiles from our algorithm.

Results

Execution Time Reduction

The bi-directional Markov Chain technique used on segments ending with a stop significantly reduced the number of iterations needed to find an appropriate solution. We compared the improved algorithm against the original one on a set of 12 standard itineraries with varied driving conditions. For each itinerary, 20 different speed profiles were generated. As shown in Table V-12, there was a 20% reduction in execution time.

Sensitivity to the Speed Profile of Vehicle Operations

We evaluated how the stochastic variations between synthesized speed profiles generated for the same itinerary affect key operations of vehicles.

Table V-12: Performance of original algorithm and improved one with bi-directional Markov Chains

| | Original Algorithm | Bi-directional Markov Chains |
|--------------------------------|--------------------|------------------------------|
| Average number of iterations | 57.15 | 30.80 (-46 %) |
| Average time of generation (s) | 0.915 | 0.722 (-21 %) |

We generated 50 stochastic speed profiles for a 25-km itinerary in the Chicago area and ran two default Autonomie vehicles: a conventional car and an HEV with a powertrain very similar to that of the Toyota Prius.

The fuel consumption is shown in Figure V-85. The coefficient of variation was 2.3% and 3.7%, respectively, for the conventional vehicle and the HEV — which is to be expected because HEVs are more sensitive to driving cycles than conventional vehicles. Two parameters important in control analysis are the number of gear shifts for the conventional vehicle and the number of engine starts for the HEV. Their distributions are shown in Figure V-85.

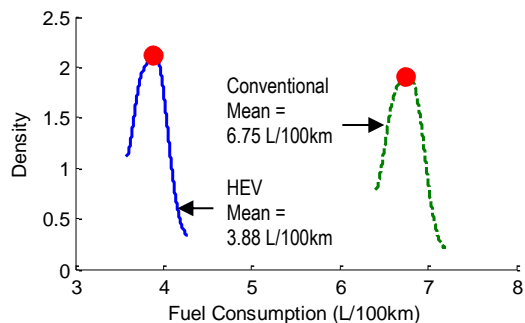


Figure V-85: Probability density function of fuel consumption for HEV and conventional vehicle (using kernel density estimation)

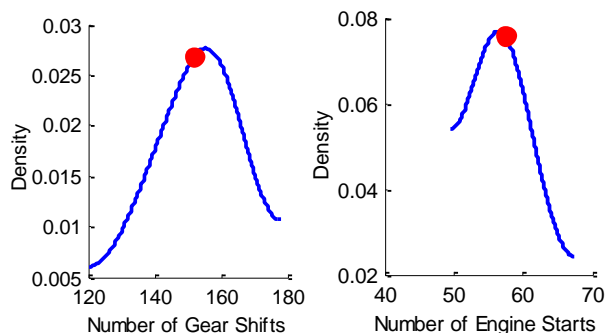


Figure V-86: Probability Density of Powertrain-Specific Variables: Number of Gear Shifts for the Conventional Car (left) and Number of Engine Starts for the HEV (right)

Sensitivity of PMP Controller to Trip Prediction

Using a 36-km itinerary and 10 generated speed profiles, we evaluated how sensitive the optimal value of the EQF is to each trip prediction; that is, if an optimal EQF for one particular speed profile would also be optimal on a speed profile generated for the same itinerary.

If the EQF is too high, battery energy is too expensive, and as a result, the final SOC is too high: there is battery energy left at the end of the trip that could have been used to displace fuel consumption. In that case, the performance of the PMP controller vehicle is actually worse.

On the other hand, if the EQF is too low, the battery will be discharged prematurely, and the fuel consumption will

approach the reference case. As a result, the benefits of PMP will diminish.

Figure V-86 shows the fuel savings achieved on all speed profiles (called “trips”) for a range of EQFs. The reference is the EV+CS control strategy. The solid line shows the average fuel savings for all trips as a function of the EQF. Average savings peak at 3.3% at an EQF of 2.805. At that value, there is a big variance (from less than 1% to nearly 6%); however, a closer look shows that for EQF = 2.8, fuel savings of at least 2% would occur in all cases. On the other hand, EQF = 2.81 seems to be the best value if we count the top 8 savings out of 10: savings range from 3.5% to 5.8%. This sensitivity suggests that an adaptive EQF updating algorithm should be investigated to ensure reliable and maximum fuel savings in each situation.

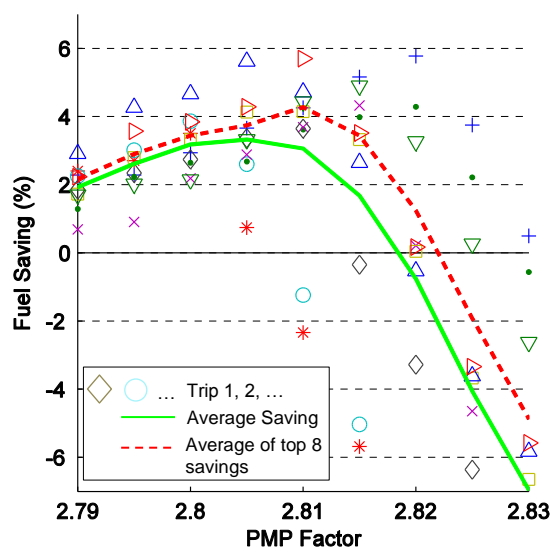


Figure V-87: Fuel savings as a function of EQF for all 10 trips

Conclusions

This project includes two areas of research, trip prediction and route-based control. In FY 2014, we built upon to the achievements of FY 2013 in both areas.

The speed profile generation tool was significantly improved at multiple levels: more robust algorithm, better flexibility to test and maintain the code, faster execution thanks to bi-directional Markov Chains, and a GUI. Because of these improvements, the tool is closer to being used more broadly for route-based control. As a side benefit of this project, it is also found to be useful to other U.S. Department of Energy (DOE) studies by providing sets of naturalistic speed and grade profiles and allowing more realistic results.

We also reused the route-based PHEV controller developed in FY 2013 to better understand how the stochastic speed predictions affect the optimal tuning of the controller. In the future, the analysis will be expanded to a larger number of driving situations.

V.I.3. Products

Publications

1. Karbowski, D., Smis-Michel, V., and Vermeulen, V., "Trip Prediction Using GIS for Vehicle Energy Efficiency," presented at the 2014 Intelligent Transport Systems World Congress, Sept., 2014, Detroit, MI, 2014.
2. Karbowski, D., Kim, N., and Rousseau, A., "Route-Based Online Energy Management of a PHEV and Sensitivity to Trip Prediction," presented at the 2014 Vehicle Power and Propulsion Conference, Oct. 2014, Coimbra, Portugal, 2014.
3. Karbowski, D., Smis-Michel, V., and Vermeulen, V., "Using Trip Information for PHEV Fuel Consumption Minimization," presented at the 27th International Electric Vehicle Symposium (EVS 27), Nov. 2013, Barcelona, Spain, 2013.

Tools and Data

1. Autonomie; available at www.autonomie.net.
2. Method to filter, process, and quality check a large database of real-world vehicle speed recordings, and turn it into a transition probability matrix.
3. A tool to generate a stochastic vehicle speed profile for an itinerary defined in ADAS-RP.
4. A route-based PHEV controller in Autonomie.

References

1. Lee, T., Bareket, Z., Gordon, T., and Filipi, Z., "Stochastic Modeling for Studies of Real-World PHEV Usage: Driving Schedule and Daily Temporal Distributions," in *IEEE Transactions on Vehicular Technology*, 61(4), 2012.
2. André, M., "Real-World Driving Cycles for Measuring Cars Pollutant Emissions – Part A: The ARTEMIS European Driving Cycles," Laboratoire Transports et Environnement (LTE), Report No. 34-40, 2004.
4. Karbowski, D., Pagerit, S., and Calkins, A., "Energy Consumption Prediction of a Vehicle along a User-Specified Real-World Trip," presented at the 26th International Electric Vehicle Symposium (EVS 26), 2012.
5. Moura, S.J., Fathy, H.K., Callaway, D.S., and Stein, J.L., "A Stochastic Optimal Control Approach for Power Management in Plug-In Hybrid Electric Vehicles", in *IEEE Transactions on Control Systems Technology*, 19(3), May, 2011.
6. Wu, G., Boriboonsomsin, K., and Barth, M., "Development and Evaluation of Intelligent Energy Management Strategies for Plug-In Hybrid Electric Vehicles," 2012, University of California Transportation Center website, www.uctc.net/research/papers/UJCTC-FR-2012-09.pdf, accessed July 2012.

7. Kim, N., Cha, S., and Peng, H., "Optimal Control of Hybrid Electric Vehicles Based on Pontryagin's Minimum Principle," in *IEEE Transactions on Control Systems Technology*, 19(5):1279–1287, Sept., 2011.
8. Paganelli, G., Delprat, S., Guerra, T.M., and Rimaux, J., "Equivalent Consumption Minimization Strategy for Parallel Hybrid Powertrains," in *Proceedings of the 55th IEEE Vehicular Technology Conference*, pp. 2076–2081, 2002.
9. Serrao, L., Onori, S., and Rizzoni, G., "ECMS as a Realization of Pontryagin's Minimum Principle for HEV Control", in *Proceedings of the American Control Conference — ACC*, pp. 3964–3396, 2009.
10. Musardo, C., Rizzoni, G., and Staccia, B., "A-ECMS: An Adaptive Algorithm for Hybrid Electric Vehicle Energy Management," presented at the 44th IEEE Conference on Decision and Control, 2005.
11. *Travel Tracker Survey*; available at www.cmap.illinois.gov/data/transportation/travel-tracker-survey, accessed July 2013.

V.J. Impact of Advanced Vehicle Technologies on Engine Operation and Vehicle Energy Consumption Benefits

Principal Investigator: Neeraj Shidore

Argonne National Laboratory
9700 South Cass Avenue
Argonne, IL 60439-4815
Phone: (630) 252-7416
E-mail: nshidore@anl.gov

DOE Program Manager: David Anderson

Phone: (202) 287-5688
E-mail: david.anderson@ee.doe.gov

V.J.1. Abstract

Objectives

- Evaluate the impact of advanced technologies (i.e., engine, transmission, electrification) on targets developed by the Advanced Combustion and Emissions (ACEC) tech team.
- Compare the impact of advances in powertrain technology on ACEC/U.S. Drive engine targets for the following:
 - Engine part load and full load efficiency operation.
 - Areas of engine operation on the engine map.
- Quantify the energy consumption and cost benefits of advanced engine technologies for different component and powertrain configurations.

Major Accomplishments

- Developed engine fuel rate maps for 16 incremental engine technologies using high fidelity GT-Power models.
- Developed rules for engine operation, gear ratio selection, and shifting algorithm based on a literature review and chassis dynamometer vehicle test data for conventional and mild hybrid vehicles.
- Developed progressive gear ratios, representing 6 speed automatic, 8 speed automatic, and 8-speed dual clutch transmissions (DCTs), to meet engine operation and transmission ratio rules.
- Evaluated fuel economy benefits of the advanced engines, in combination with the 6 speed automatic, 8 speed automatic, and 8 speed DCT for a representative compact car in 2020.

Future Achievements

- Optimize the gear ratio design and shifting algorithm for each of the 16 engines to maximize the fuel economy potential of each engine.



V.J.2. Technical Discussion

Background

Recent advances in spark ignition (SI) engine technology (i.e., variable valve lift [VVL], gasoline direct injection [GDI], cylinder deactivation), turbocharging, and engine friction reduction have resulted in significant improvements in engine part load and full load efficiencies. Recent trends in transmission technology for light duty vehicles show an increase in the number of gears and a reduction in final drive ratios. This results in engine operation at lower speeds and higher torques (engine downspeeding); that is, the engine operates in a higher efficiency region. DCTs are more efficient than automatic transmissions but result in slower accelerations due to the absence of the torque converter. Mild hybridization (belt integrated starter generator [BISG]) enables a reduction in the final drive ratio because of additional torque provided by the starter motor.

Introduction

The study evaluated the impact of advances in transmission design (number of gears, gear span), transmission technology (DCT), lightweighting (model year 2020), and mild hybridization (BISG) on engine operating region for each of the engine technologies outlined below. In addition, the impact of engine technology, in combination with transmission technology, electrification, and lightweighting, on vehicle fuel economy was quantified.

Approach

Gasoline brake specific fuel consumption (bsfc) maps, representing incremental improvements in engine and friction technology were developed by IAV International under contract with Argonne National Laboratory (Argonne). The maps were developed using GT-Power.

Figure V-88 shows the naturally aspirated (NA) engine technologies considered. The baseline engine map (port fuel injection [PFI], variable-valve timing [VVT]) was based on measured engine test data. In addition, engine maps representing various levels of turbocharging were also developed using GT-Power, as shown in Figure V-89. The bsfc map for the 1.6-L 18-bar peak brake mean effective pressure (BMEP) engine was also developed from test data.

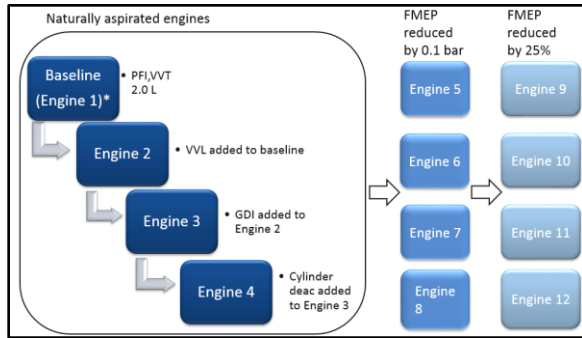


Figure V-88: Naturally aspirated engine maps with incremental engine and friction improvements

| | |
|------------|--|
| Engine 13* | 1.6 L , 4 cylinder , 18 bar BMEP |
| Engine 14 | 1.2 L , 4 cylinder , 24 bar BMEP |
| Engine 15 | 1.2 L , 4 cylinder , 24 bar BMEP, cooled EGR |
| Engine 16 | 1.0 L , 4 cylinder , 27 bar BMEP, cooled EGR |
| Engine 17 | 1.0 L , 3 cylinder , 27 bar BMEP, cooled EGR |

* Map generated from test data.

Figure V-89: Turbocharged engine maps

To properly evaluate the engine operation for different component technologies and powertrain configurations, a rigorous selection of transmission gear ratios, final drive ratio, and gear shift parameters is important.

On the basis of a literature review [1], [2], [3], [4], [5] and chassis dyno test data [6,] the following criteria were selected for transmission (gear ratio), final drive, and shift parameters.

1. The vehicle should shift to top gear around 45 mph.
2. In top gear, the engine should operate at about 1250 rpm to prevent engine lugging.
3. The number of gear shifts for a 6 speed transmission, Urban Dynamometer Driving Schedule (UDDS) cycle, should be around 110 to 120.
4. Gear span and final drive ratios should be based on industry trends for the compact vehicle class.
5. Engine operation will be restricted in the low speed high torque region, to prevent noise, vibration, and harshness (NVH) issues and ensure drive quality.

On the basis of industry trends in gear spans, top gear and final drive progressive gear ratios [7] were designed for 6 speed and 8 speed automatic transmissions using the following formula:

$$i_n = i_z \left[\frac{Span}{\phi_2^{0.5(z-1)(n-1)}} \right]^{\frac{z-n}{z-1}} \quad z \neq 1$$

where

z = total number of gears,

n = gear number in consideration for design (varies from 1 to z),

ϕ_2 = progression factor (independent variable — normally between 1 and 1.2),

i_z = top gear ratio, and

i_n = nth gear ratio.

The independent variable ϕ_2 was chosen for each transmission type so as to maximize the fuel economy over a combined (UDDS, Highway Fuel Economy Test [HWFET]) cycle.

Figure V-90 shows the design of the experiment for the study. The simulations are shown in the left column, and the anticipated analysis is shown in the right column.

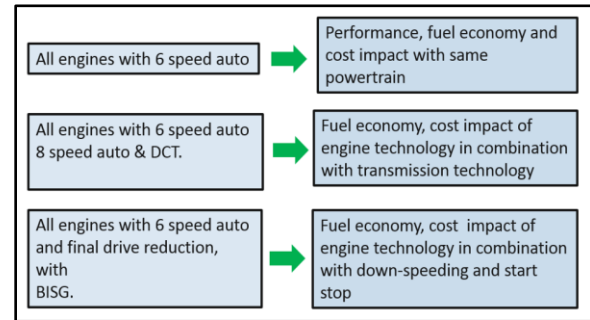


Figure V-90: Design of experiment

Table V-13 lists the powertrain assumptions for the compact car for 2020.

Table V-13: Vehicle Specifications

| | |
|--|----------------------------------|
| Vehicle Mass | 1118 kg (6 speed automatic) |
| Cd | 0.27 |
| Af | 2.25 |
| Transmission | Auto, 6 speed |
| BISG battery | Li-ion, 115 V, 32 cells, 4.34 Ah |
| BISG electric machine | 15 kW |
| Additional transmission weight for 8 speed AU | 25 kg |
| Additional transmission weight for 8 speed DCT (over 6 speed AU) | 45 kg |

Table V-13 also lists the battery and electric machine assumptions used for the BISG configuration, and the additional vehicle weight associated with the 8 speed automatic and 8 speed DCT transmissions [8].

Results

Validation of the Gear Ratio Design Algorithm

As stated previously, the gear ratio design algorithm was used to design progressive gear ratios, with the gear span, top gear, and final drive as inputs to the algorithm. Validity of the algorithm was evaluated against several 6 speed automatic transmissions in the market today. For example, Figure V-91 and Figure V-92 show the gear ratio output of the algorithm for a Volkswagen Golf and Mazda 3, respectively, when the span, top gear, and final drive ratio were entered as inputs. The independent variable ϕ_2 was iterated in order to obtain gear ratios close to the actual.

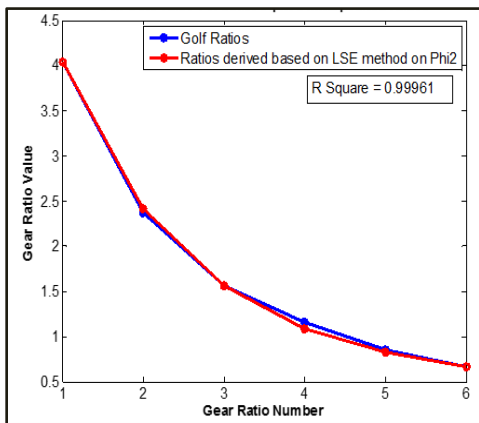


Figure V-91: Golf gear ratios (actual versus algorithm design)

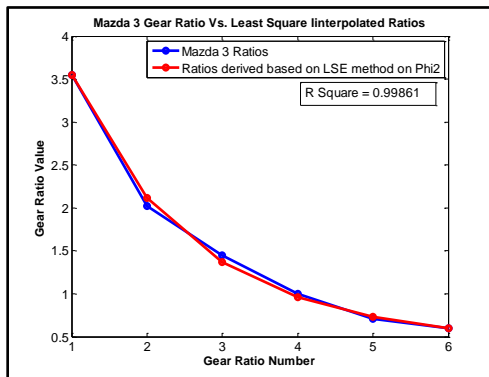


Figure V-92: Mazda gear ratios (actual versus algorithm design)

Figure V-91 and Figure V-92 show that the gear ratios designed using the algorithm are close to industry gear ratios.

Table V-14 shows the transmission gear ratios and final drive ratio designed for the 6 speed automatic, 8 speed automatic, and 8 speed DCT, which, along with proper selection of shift algorithms, meet all the criteria listed previously. Currently, the 8 speed automatic and DCT transmissions are rarely seen for the compact car segment.

Also, the gear span of the 8 speed DCT is slightly higher than the 8 speed automatic, such that the acceleration performance

Table V-14: Transmission and Final Drive Ratios

| | Span | FD | G 1 | G 2 | G 3 | G4 | G 5 | G 6 | G 7 | G 8 |
|-------|------|------|------|------|------|------|------|------|------|------|
| 6 AU | 6 | 3.74 | 3.89 | 2.37 | 1.55 | 1.08 | 0.81 | 0.65 | | |
| 8 AU | 7.5 | 3.5 | 4.72 | 2.97 | 1.98 | 1.40 | 1.05 | 0.84 | 0.70 | 0.63 |
| 8 DCT | 7.8 | 3.5 | 4.91 | 3.16 | 2.14 | 1.52 | 1.13 | 0.89 | 0.73 | 0.63 |

of the DCT matches the acceleration performance of the 8 speed automatic. For the same gear span, the 8 speed automatic results in better performance on account of the initial torque multiplication provided by the torque converter.

Impact of Transmission and Mild Hybridization (start-stop) on Engine Operation

Figure V-93 shows the engine operation for a 6 speed transmission. As shown in the figure for the UDDS cycle, the engine predominantly operates in a speed range between 1200 and 1700 rpm. The green star and the red star represent the part load engine efficiency target points defined by the engine tech team at the United States Council on Automotive Research (USCAR) [9].

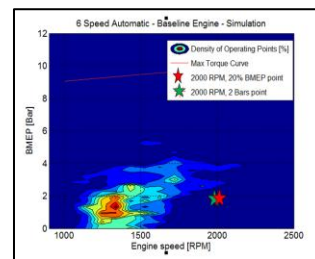


Figure V-93: Engine operation with a 6-speed automatic transmission

Figure V-94 and Figure V-95 show engine operation with an 8 speed automatic and an 8 speed DCT transmission.

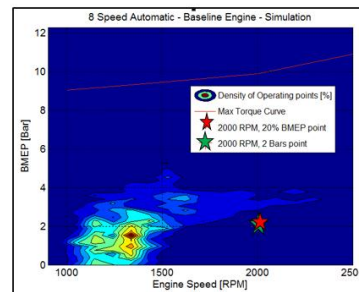


Figure V-94: Engine operation with an 8-speed automatic transmission

As shown in Figure V-94, because of the larger gear span of the 8 speed automatic (when compared with the 6 speed automatic), the engine operates in a narrower speed range when compared with a 6 speed automatic transmission (apart from the one high speed excursion above 2000 rpm). The speed range for the 8 speed DCT (Figure V-95) is slightly narrower than the 8 speed automatic. This is because, as stated previously, by design, the span of the 8 speed DCT is slightly larger than the 8 speed automatic, in order that the performance of the 8 speed DCT matches the performance of the 8 speed automatic.

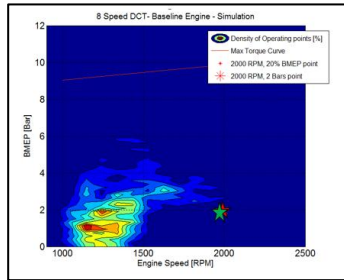


Figure V-95: Engine operation with an 8-speed DCT

Figure V-96 depicts the engine operation without the lightweighting (higher vehicle mass), representing a car currently in the market.

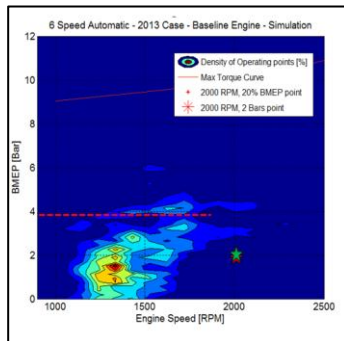


Figure V-96: Engine operation with a 6-speed automatic, without lightweighting

The hashed horizontal line in Figure V-96 at 4-bar BMEP can be used to compare the engine operation with the vehicle with lightweighting (Figure V-93). It can be seen that the engine operates at higher loads with the heavier vehicle.

Figure V-97 shows the engine operation for the 1-L, 4-cylinder turbo engine. It can be seen that the engine operates at a higher BMEP for the turbo engine, which results in better engine efficiency and higher fuel economy. The maximum engine torque is also significantly higher with the turbo engines.

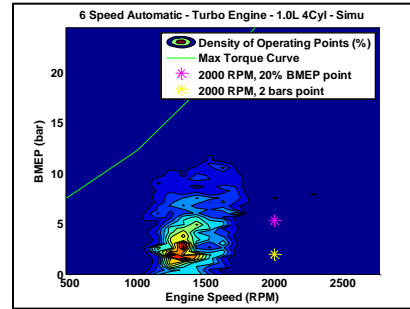


Figure V-97: Engine operation for the 1-L turbo engine, with a 6-speed automatic transmission

As stated previously, with a BISG system, the motor provides additional torque, which helps with vehicle acceleration. Thus the final drive ratio of the vehicle can be reduced to further aid in engine downspeeding and fuel economy improvement. Figure V-98 shows a comparison of the engine speed for the same engine for a conventional powertrain with a 6 speed automatic and a BISG powertrain with a 6 speed automatic, for the highway cycle. The

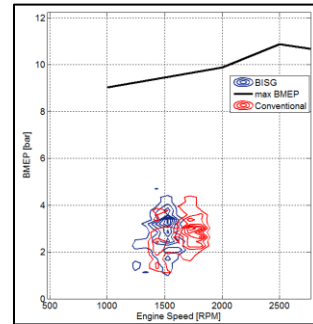


Figure V-98: Engine operation for the conventional and BISG powertrain, HWFET cycle

downspeeding achieved on account of a lower final drive ratio of the BISG powertrain can be clearly seen.

Impact of Engine Technology on Fuel Economy and Performance

Figure V-99 shows the impact of engine technology on vehicle fuel economy, for a 6 speed automatic transmission. Cylinder deactivation (in combination with VVL, GDI) reduces the unadjusted fuel consumption by 11% over the baseline PFI engine for a combined (UDDS and HWFET) cycle.

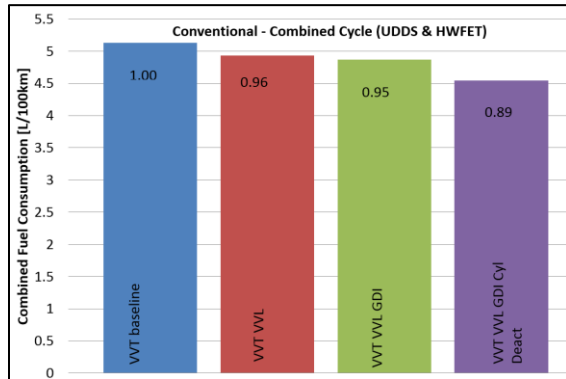


Figure V-99: Impact of engine technology on fuel consumption

Figure V-100 shows the impact of engine technology on vehicle performance. Direct injection and VVL contribute to higher engine peak torque and therefore improved engine performance.

Figure V-101 shows the impact of friction reduction on vehicle fuel economy. The fuel consumption can be significantly reduced by reducing engine friction. In Figure V-101

, the fuel consumption fraction (5th bar) shows that by reducing the friction mean effective pressure (FMEP) by 0.1 bar, the fuel consumption is reduced by 3.5%. The last bar shows the impact of reduction in FMEP by 25%. The fuel consumption reduction (over the 0.1 bar FMEP reduction) is an additional 2.3%. Overall, friction reduction and cylinder deactivation offer the most significant fuel economy improvement.

Figure V-102 shows the variation in fuel consumption on account of transmission technology. The fuel consumption with DCT is about 5% lower than the 6 speed automatic, for the NA baseline engine (2-L PFI with VVT).

Turbocharging results in significant fuel economy and performance improvement. Figure V-103 shows that with a 1-L, 3-cylinder turbo engine, the fuel consumption is about 20% lower than the baseline 2-L NA engine with PFI technology. For performance and fuel economy simulations with turbo engines (Figure V-104), turbo lag is taken into account by modelling it as a single pole first-order transfer function, with the time constant varying with speed and load [10], [11].

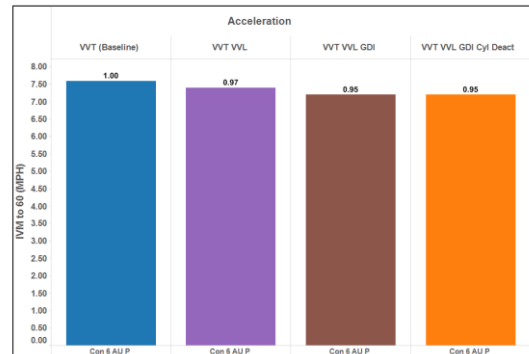


Figure V-100: Impact of engine technology on performance

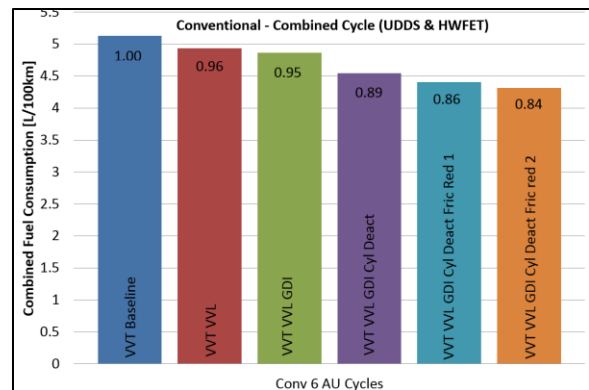


Figure V-101: Impact of friction reduction on vehicle fuel consumption

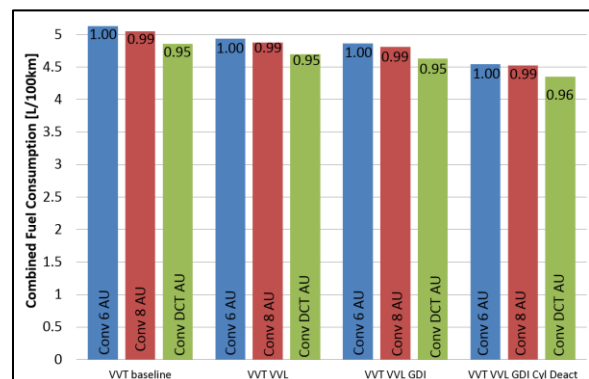


Figure V-102: Impact of transmission technology on vehicle fuel consumption

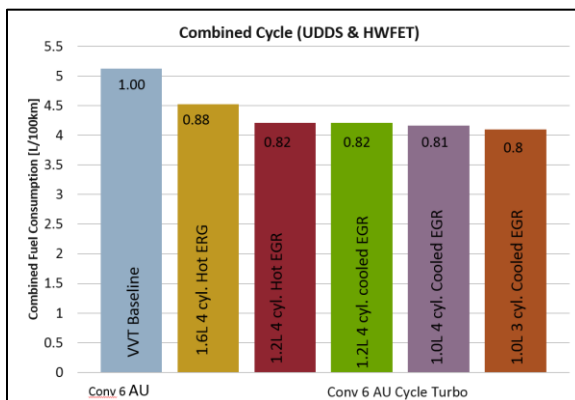


Figure V-103: Impact of turbocharging on vehicle fuel consumption

Figure V-105 shows the gains due to mild hybridization (BISG). The fuel consumption impact is constant over the four NA engine types due to engine downspeeding and idle fuel off.

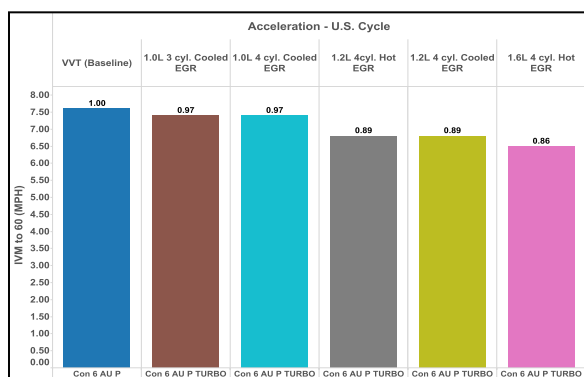


Figure V-104: Impact of Turbocharging on Performance

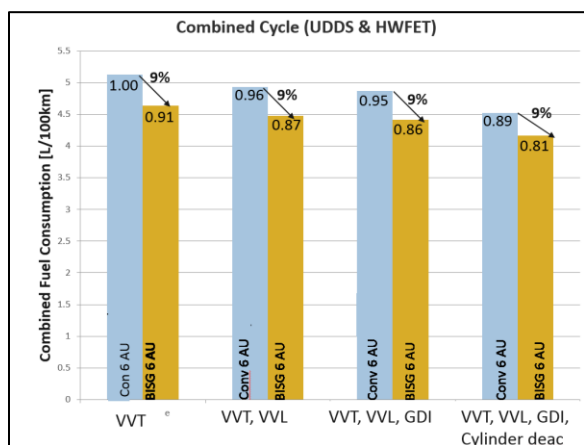


Figure V-105: Impact of mild hybridization (BISG) on fuel consumption

The leveled cost of driving (LCD in \$/mile [12]) for the combined, unadjusted results for the different engine technologies was calculated. As can be seen from Figure V-106, a reduction in fuel consumption compensates for the additional technology cost. The engine with VVT, VVL, GDI, and cylinder deactivation (4th bar) has a LCD value which is

the same as the baseline engine, inspite of having better fuel consumption.

Optimization of Shift Parameters for Each Engine/Transmission Pair

Using Argonne’s optimization algorithm “Pounder,” which is available for use through the Autonomie User Interface [13], shift parameters were optimized for NA engines to evaluate the potential for shift parameter optimization, to further reduce

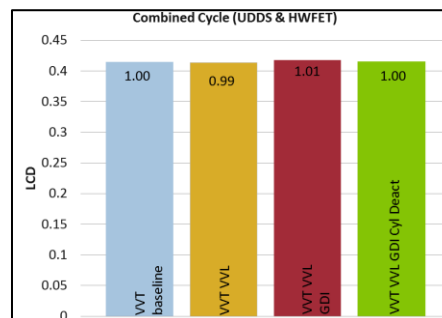


Figure V-106: Decrease in fuel consumption compensates for increased technology cost

the fuel consumption of each engine technology over a combined (UDDS + HWFET) cycle. Figure V-107 shows the shift map and the shift parameters selected for optimization using Pounder.

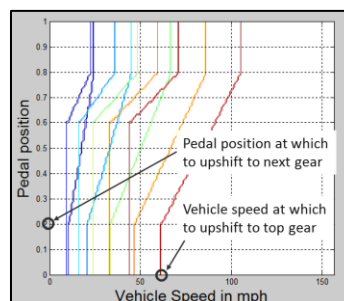


Figure V-107: Shift map and parameters selected for optimization for each engine transmission pair

Figure V-108 shows the results space for a parametric sweep of all possible combinations of the above parameters, with the baseline engine and the 6 speed transmission, for the UDDS cycle. The data points in red represent fuel consumption results which are unacceptable, based on the criteria laid out in the assumptions section. The green data points are a set of acceptable results.

The points in blue show the trajectory taken by the Pounder optimization algorithm, as it locates the minimal fuel consumption, and the recommended pedal position for upshift (0.42) and vehicle speed for top gear upshift parameter (43 mph) for minimal fuel consumption, for the baseline engine with the 6 speed automatic transmission. The parametric sweep is used to validate the success of the optimization algorithm. Several iterations of the optimization were

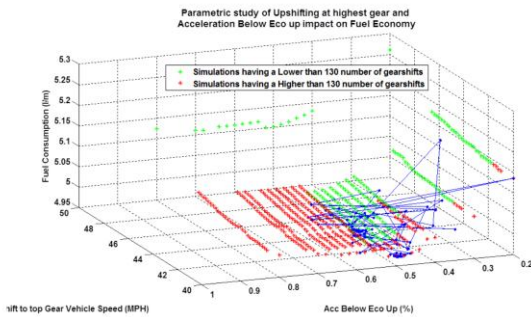


Figure V-108: Fuel consumption as a function of the parametric sweep of shift parameters and the trajectory of the optimization algorithm

repeated, and the algorithm always settled on the same values for the parameters. Thus, the robustness of the algorithm was also validated.

Figure V-109 shows the comparison of fuel consumption for the VVT, VVT with VVL, and VVT, VVL, and GDI engines with and without optimization.

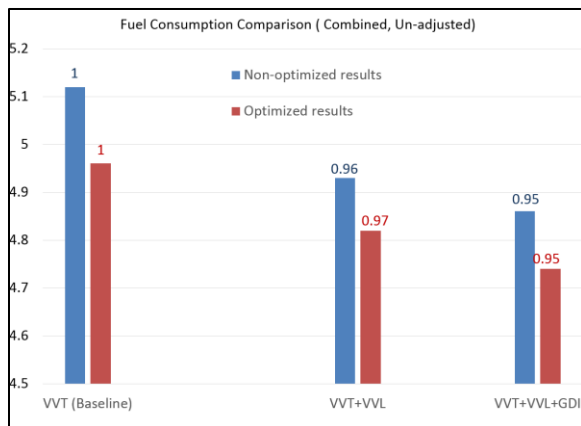


Figure V-109: Comparison of fuel consumption benefits (l/100km) with and without the use of shift parameter optimization

As can be seen from the plot, fuel consumption is reduced with the optimization of the shift parameters. However, it can also be seen that the relative fuel consumption decrease between engines is the same in both cases. Therefore, the results stated for impact of engine technology on fuel consumption (Figure V-99, Figure V-101) are still valid.

Conclusions and Future Directions

This project quantified the impact of advances in engine and drivetrain technology on fuel consumption and LCD for conventional and start-stop powertrains. The study also analyzed the impact of advances in drivetrain and electrification on future engine operation.

Advances in drivetrain and electrification will result in engine downspeeding and lower the speed range of engine operation.

Engine operating points for part load efficiency targets need to be recalibrated for future target setting exercises (around 1500 rpm).

Friction reduction and cylinder deactivation offer the most significant fuel economy benefits over the U.S. Environmental Protection Agency (EPA) standard combined cycle.

Fuel economy benefits of downsizing and turbocharging are higher than improvements in NA engines through VVL and GDI.

Based on cost assumptions, extreme friction reduction, in addition to VVL, DI, and cylinder deactivation, can result in lower LCD than the current (PFI, VVT) engine technology.

Optimization of shift parameters for each engine and transmission pair results in lower fuel consumption when compared with default shift parameter settings for all the engines.

The design of progressive gear ratios can be coupled with shift parameter optimization to provide maximum fuel consumption benefits of each technology.

In addition to fuel consumption, important aspects for consideration when deciding engine operation are NVH and engine out emissions. The above process for gear ratio and shift parameter selection can be extended to consider emissions through actual hardware-in-the-loop (HIL) testing, or use of quasi-static emission maps in modelling.

In this project, the powertrain types were limited to conventional and start-stop. The impact of engine technology will be significantly different for powertrains with significant hybridization (e.g., pre-transmission parallel). The entire process should be repeated for strong hybrid powertrains.

The locus of engine operating points on standard drive cycles differs with vehicle class. Similarly, the locus of engine operating points varies with drive cycle. To get a complete picture of the locus of engine operating points, numerous drive cycles should be considered over different vehicle classes and powertrain types.

V.J.3. Products

Presentations

1. Shidore, N., Lemazurier, L., Wallner, T., Rousseau, A., Bonkoski, P., and Schilling, H., "Impact of Advanced Technologies on Engine Targets," presentation at the U.S. Department of Energy Annual Merit Review, June 2014.
2. Shidore, N., Lemazurier, L., Kim, N., Moawad, A., and Rousseau, A., "Impact of Advanced Engine and Powertrain Technologies, update to U.S. Department of Energy, August 5, 2014.

Tools and Data

1. Autonomie; available at www.autonomie.net.

References

1. Thring, R.H., "Engine Transmission Matching to Improve Passenger Car Fuel Economy," Society of Automotive Engineers (SAE) paper 820167, presented at SAE International Congress & Exhibition, Detroit, February 1982.
2. Celli, C.A., "The Fuel Efficiency Improvement through a Six Speed Manual Transmission Application in Passenger Vehicles with Low Displacement Engines," SAE paper 2011-01-1430, 2011.
3. Kasseris, E.P., and Heywood, J.B., "Comparative Analysis of Automotive Powertrain Choices for the Next 25 Years," SAE paper 2007-01-1605, 2007.
4. Amendola, C.H.F, and Alves, M.A.L., "Gear Shift Strategies Analysis of the Automatic Transmission in Comparison with the Double Clutch Transmission," SAE paper 2006-01-2872, 2006.
5. Meetings and phone conversations with Chrysler.
6. Naunheimer, H., Bertsche, B., and Novak, J.R.W., *Automotive Transmissions – Fundamentals, Selection, Design and Application*, 2nd edition, Springer, ISBN 978-3-642-16213-8, 2010.
7. GETRAG Products, accessed at www.getrag.com/en/products/products.html.
8. U.S. Drive, Advanced Combustion and Emission Control (ACEC) Tech Team presentation, U.S. Drive All Tech Team Meeting, October 25, 2011.
9. Lefebvre, A., and Guilain, S., "Modelling and Measurement of the Transient Response of a Turbocharged SI Engine," SAE paper 2005-01-0691, 2005.
10. Stoffels, H., Quiring, S., and Pinggen, B., "Analysis of Transient Operation of Turbo Charged Engines," SAE paper 2010-32-0005, 2010.
11. Ward, J., "VTO Analysis Portfolio," presentation at the U.S. Department of Energy Annual Merit Review, May 16, 2013.
12. Kannan, A., and Wild, S.M., POUNDERC example for AUTONOMIE, accessed at www.mcs.anl.gov/~wild/codes/pounderaut/index.html.
13. Autonomie; available at www.autonomie.net.

V.K. Autonomie Maintenance and MBSE Enhancements

Principal Investigator – Shane Halbach

Argonne National Laboratory
9700 South Cass Avenue
Argonne, IL 60439-4815
Phone: (630) 252-2853
E-mail: shalbach@anl.gov

DOE Program Manager – David Anderson

Phone: (202) 287-5688
E-mail: David.Anderson@ee.doe.gov

V.K.1. Abstract

Objectives

- Enhance and maintain Autonomie as needed to support the U.S. Department of Energy and the user community.
- Enhance Autonomie to expand its model-based system engineering scope.

Major Accomplishments

- Modeling Enhancements
 - BatPaC Linkage
 - Hydraulic Hybrid Vehicles
 - Series-Parallel PHEV Multi-Mode (2-Motor)
 - New Shifting Calibrations
 - Physical Models
 - Thermal Models
 - Continuously Variable Transmission and Dual Clutch Transmission Models
- User Interface Enhancements
 - “Quick Launch”
 - HTML Reports
 - Graphical Configuration Editor
- Model Based System Engineering (MBSE) Enhancements
 - Cosimate Linkage Updates
 - Functional Mock-up Interface Integration
 - Model Parallelization with Message Passing Interface
 - New Optimization Algorithms

Future Achievements

- Continue to enhance Autonomie to support DOE and technology transfer.



V.K.2. Technical Discussion

Background

Autonomie is a plug-and-play powertrain and vehicle model architecture and development environment that supports the rapid evaluation of new powertrain/propulsion technologies for improving fuel economy through virtual design and analysis in a math-based simulation environment. Autonomie has an open architecture to support the rapid integration and analysis of powertrain/propulsion systems and technologies. This architecture allows rapid technology sorting and evaluation of fuel economy under dynamic/transient testing conditions.

Introduction

To better support the U.S. Department of Energy (DOE) and its user community, several new features have been implemented in Autonomie. Some of the most significant accomplishments are described below.

Approach

There are always more ideas for new Autonomie features and enhancements than time to actually implement them. Feedback on which items to prioritize and include is collected in several ways.

First, users of Autonomie register suggestions for improving the software or models by email, in person, or through our online issue-tracking system at www.autonomie.net. Second, direct interaction with partners and sponsors while working on shared projects also contributes to collecting new requirements. Finally, DOE studies often drive the improvement of existing capabilities and /or the development of new ones.

MBSE enhancements focused on longer-term strategies for the future of vehicle modeling and simulation, such as an emphasis on parallelization for running larger number of simulations. Another emphasis was the integrating of tools which themselves integrate tools, increasing the Autonomie ecosystem.

Results

Modeling Enhancements

BatPaC Linkage

The Argonne Battery Performance and Cost Model (BatPaC) has been integrated with Autonomie (Figure V-110) to provide detailed battery inputs for the simulation.

Autonomie provides inputs to BatPaC based on the characteristics of the selected vehicle (chemistry, number of cells, energy and power information, etc.), and BatPaC feeds information back to Autonomie for simulation initialization or post-processing (cost, mass, volume, etc.).

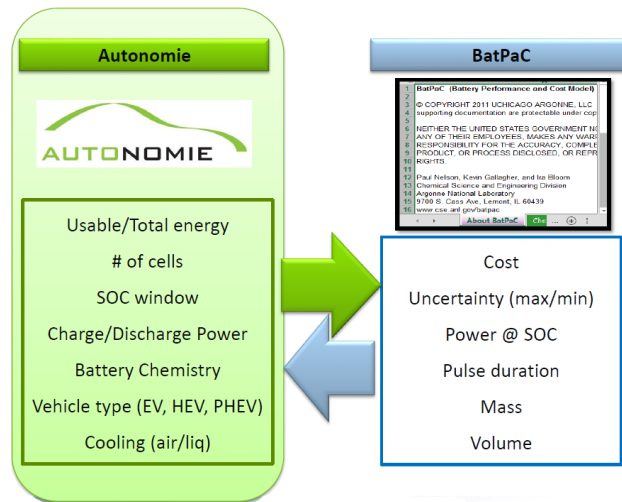


Figure V-110: BatPaC model integration

Hydraulic Hybrid Vehicles

Hydraulic hybrid vehicles (HHVs, Figure V-111) can achieve higher powertrain efficiencies (wheels to storage) during regenerative braking owing to hydraulic machine efficiency at high loads. Therefore, HHVs can provide some advantages when used as heavy vehicles with aggressive drive cycles and numerous start/stop conditions, such as parcel delivery trucks or refuse trucks.

Four HHVs were developed and sized as Class 6 vehicles, and the appropriate vehicle control strategies were developed and included in Autonomie:

- Parallel PostTrans HHV AutoManualTrans 2wd Class 6;
- Parallel PostTrans HHV AutoTrans 2wd Class 6;
- EREV HHV FixedGear 4wd Class 6; and
- Series Engine HHV AutoManualTrans 2wd Class 6.

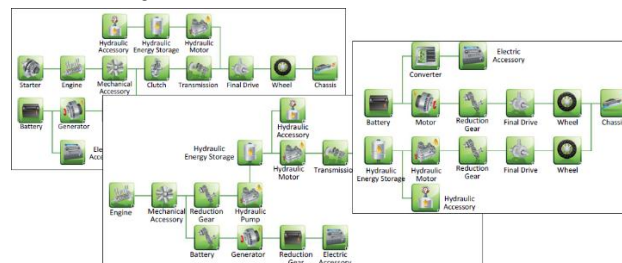


Figure V-111: HHV configurations

Series-Parallel PHEV Multi-Mode (2-Motor)

A series-parallel PHEV multi-mode configuration was developed for Autonomie (Figure V-112). A default vehicle, Series-Parallel FixedGear PHEV 2wd Midsize (similar to the Honda 2 Motor PHEV), was created and included in the release.

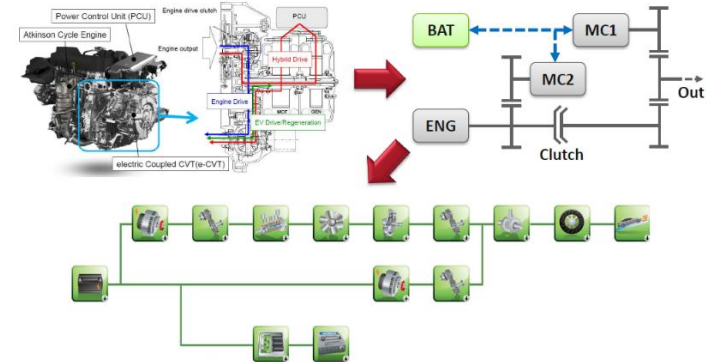


Figure V-112: Development of series-parallel PHEV 2-motor configuration

New Shifting Calibrations

In addition to our existing shifting calibrations, new calibrations (Figure V-113) were created using vehicle test data to better represent state-of-the-art technologies.

The new shifting calibrations are also heavily parameterized to provide the user greater access to the control parameters.

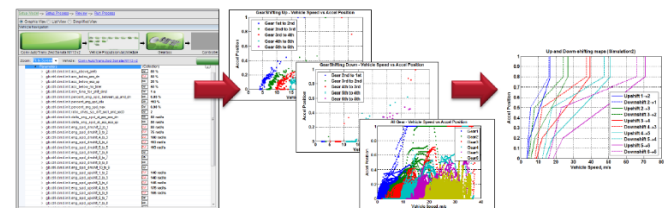


Figure V-113: New shifting calibrations

Thermal Models

Thermal component models have been developed (Figure V-114), using data from the ANL Advanced Powertrain Research Facility (APRF) thermal cell to represent the impact of thermal conditions on energy consumption.

Test data were collected under various thermal conditions (-7°, 21°, and 35° Celsius). These data were used to validate the plant models, as well as to develop the control strategies (engine on/off, SOC balancing, powertrain mode decisions, engine operating points, etc.).

Finally, the components were imported into Autonomie, and the full vehicle models were validated against the test data.

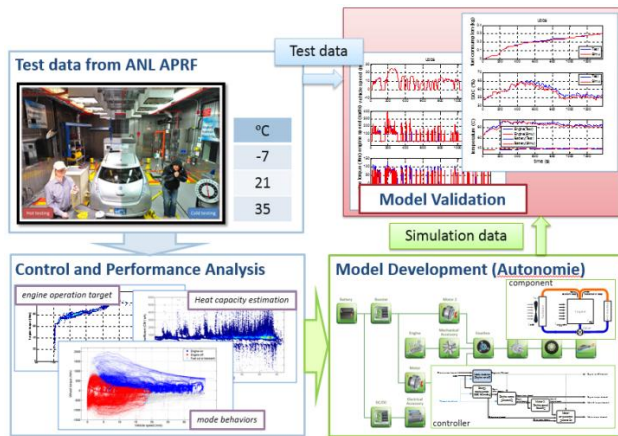


Figure V-114: Thermal model development

Continuously Variable Transmission Model

New continuously variable transmission (CVT) plant and control models have been developed (Figure V-115) to replace the legacy CVT models.

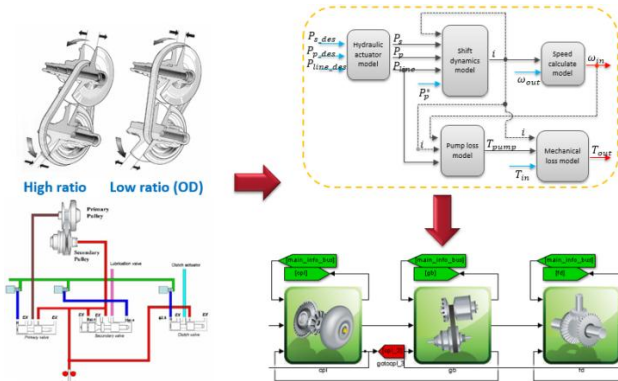


Figure V-115: CVT transmission model development

Dual Clutch Transmission Model

Dual clutch transmission (DCT) plant and control models have been developed (Figure V-116) and included in the Autonomie release. Models were validated with APRF test data from vehicles that included the 2013 VW Jetta TDI conventional vehicle (6 speed DCT) and the 2013 VW Jetta HEV (7 speed DCT).

Physical Models

Physical modeling allows developers to graphically create components that are physics-based rather than equation-based. This approach allows the user to build the model without worrying about the underlying equations. In theory, this allows the solver to optimize those equations for faster execution time.

Support for physical modeling was added to Autonomie. Now, models produced using the Matlab Simscape™ or SimDriveline™ toolbox can be incorporated seamlessly into simulations with the same automatic building and compatibility checking afforded to non-physical models (Figure V-117).

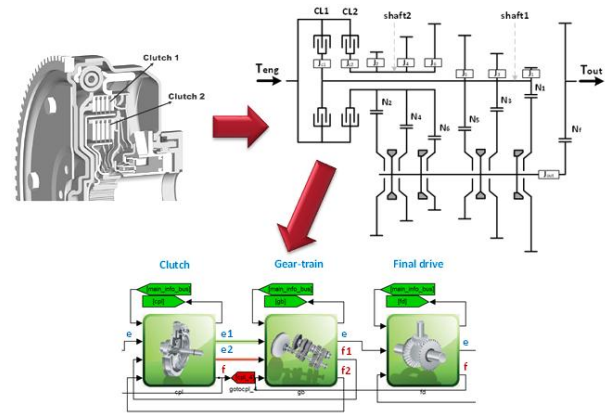


Figure V-116: DCT transmission model development

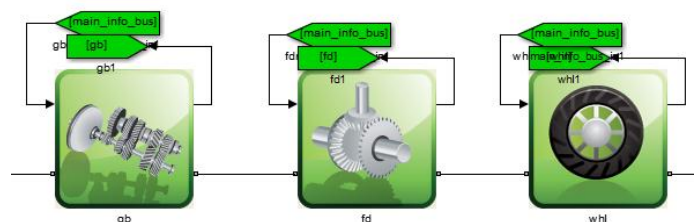


Figure V-117: Gearbox, final drive, and wheel models connected via physical ports

User Interface Enhancements

“Quick Launch”

During installation, Autonomie now registers some Autonomie-specific file types, so that double clicking on the file will open it in Autonomie directly (Figure V-118). For example, double-clicking on a vehicle file will open Autonomie and load the vehicle in the main user interface.

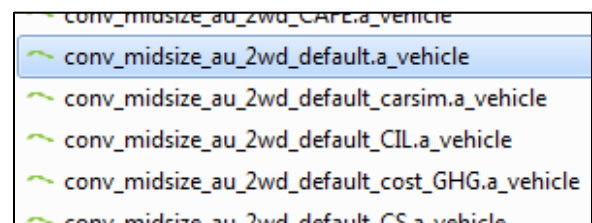


Figure V-118: Double clicking on the vehicle will open it directly in Autonomie

Autonomie run files are registered to open Autonomie in “Developer Mode.” Developers do their work in the Simulink environment. The “Work in Simulink” functionality allows Simulink developers to set up their Matlab environment as quickly as possible, so they can begin their work (i.e., test/modify/ test/modify component models) directly in Simulink, or continue work where they left off.

Depending on what types of information are present in the run file, and which files are co-located in the directory, the dialog will be initialized to do different things. Using this functionality, a user has the ability to

- Open the correct Matlab version (if a specific version is required by the model).
- Set up the path, including any libraries or extra directories.

- Open the model.
- Initialize the workspace (run initialization files, load .mat files, etc.).
- Run any extra scripts required.

The user can preview this information before any action is taken. Any information on this screen is saved for an even quicker start next time. Afterwards, Autonomie closes and the user is free to work in Simulink directly (Figure V-119).

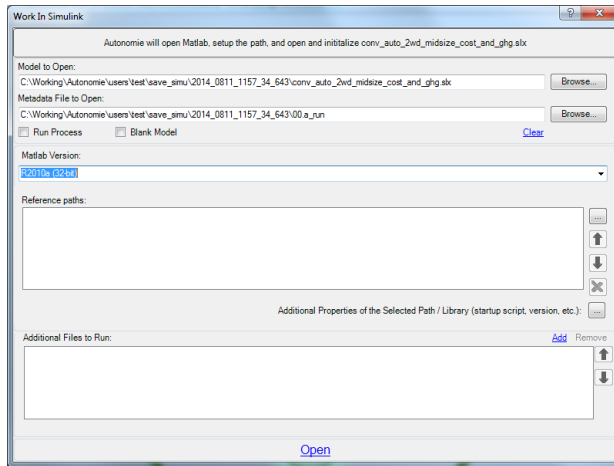


Figure V-119: Work in Simulink

HTML Reports

A new Report tab in Data Analysis allows users to view and edit custom HTML reports based on the simulation (Figure V-120).

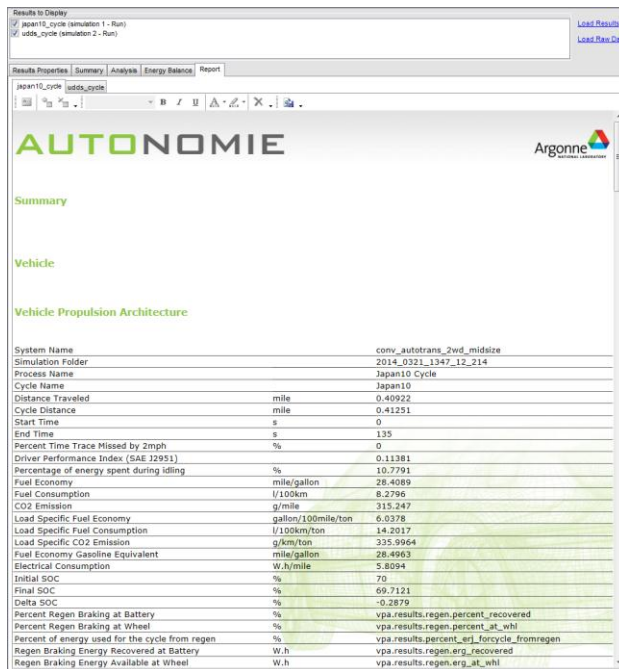


Figure V-120: HTML report of simulation results

Sections can be added or removed and text can be edited, including font, forecolor, back color, etc. Parameter value tables and plots can be added via drag and drop.

Finally, the report can be exported to a single HTML file for sharing.

Additionally, the report can be saved as a template. This feature allows a custom report to be loaded with a different set of simulation results, and all of the values, plots, etc., will be specific to that result set. In this manner, a user can create detailed, attractive, reusable HTML reports that can be quickly selected and exported across any number of simulation results.

Graphical Configuration Editor

Previously, configurations could be created for Autonomie by using Simulink as a graphical editor. Simulink models could be “captured” to create the necessary configuration files for Autonomie.

However, this could be a difficult process. Simulink allowed users to create and connect blocks, but it was cumbersome for the user to provide some information, such as connection types. The user required detailed documentation to understand how to enter the information as annotations.

Autonomie now provides a graphical user interface (Figure V-121) to create new configurations. For example, users can now add or modify powertrain components or provide additional sub-levels for greater fidelity of modeling (i.e., breaking the engine plant from a monolithic model into sub-component models, which are each versioned separately).

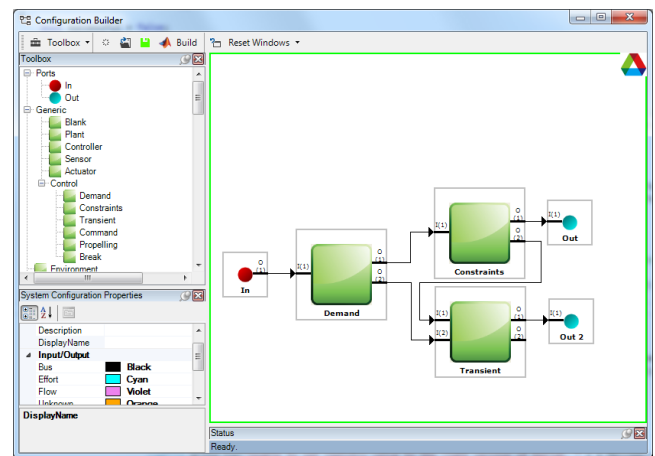


Figure V-121: Graphical configuration editor

Systems can be dragged and dropped to set up the block layout (Figure V-122). Properties of those blocks, such as input and output numbers and connection types, can be edited directly in this user interface. Configurations can be saved and re-loaded later for additional work.

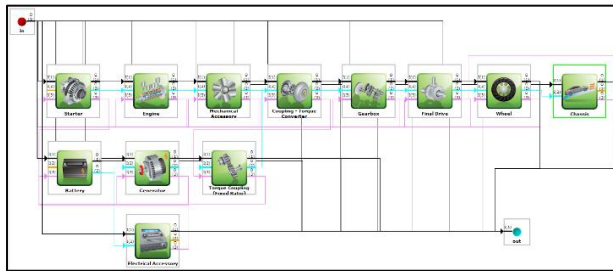


Figure V-122: Conventional vehicle architecture built in the configuration builder

Users can still create configurations via Simulink if they prefer.

MBSE Enhancements

CosimMate Linkage Updates

Integration with CosimMate allows users to distribute pieces of a vehicle to multiple machines and/or co-simulate pieces of a vehicle in their native tools. Autonomie integration allows users to run these distributed simulations from a single user interface.

Once a CosimMate-enabled model is imported into Autonomie, its use is completely transparent. Autonomie will check for a valid CosimMate license during its model compatibility checking. Users can control the CosimMate parameters through the editor on the CosimMate process step editor, as shown in Figure V-123.

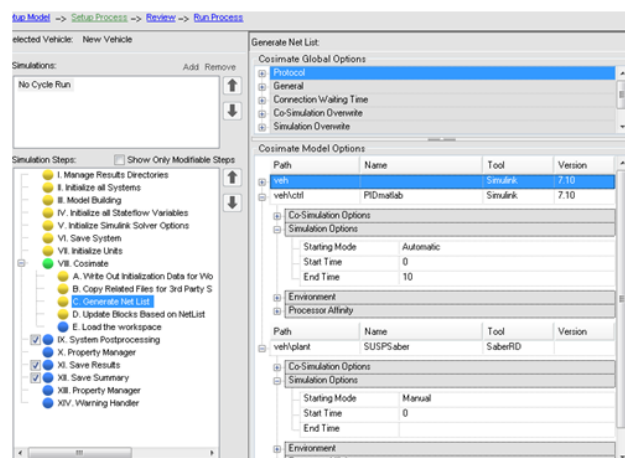


Figure V-123: Setting up CosimMate options

In this release, the CosimMate integration has been updated to work with the latest version of CosimMate. Additionally, an example has been added demonstrating co-simulation between Saber™ and Simulink.

Functional Mock-up Interface Integration

Functional Mock-up Interface (FMI) is a tool-independent standard that is used to exchange and/or co-simulate models. Integrating with FMI allows Autonomie to integrate any modeling tool that is exportable to FMI, greatly widening the scope of models allowable in Autonomie.

Autonomie integrates FMI in two ways:

- 1) By using CosiMate, the tool already allows co-simulation via FMI, which means that by integrating CosiMate, we already have the ability to integrate FMI models.
- 2) By using Functional Mock-up Units (FMUs) directly in Simulink via the Modelon toolbox. Users create a Simulink model with the Modelon S-Function to interface with the FMU file. Then the model is imported into Autonomie (Figure V-124). Autonomie is able to pre-fill some of the fields on the basis of information in the FMU file.



Figure V-124: FMU integration using the Modelon toolbox

Model Parallelization with Message-Passing Interface

A new message passing interface (MPI) algorithm was written to allow simulations to be distributed across multiple cores of a single computer (Figure V-125). Most desktop computers today come with 4, 8, or even 16 cores. Using this technique, vehicle simulations can be run in parallel across these cores without the use of additional hardware and expensive software, such as clusters or distributed computing toolboxes.

Some of the procedures in Autonomie have been retrofitted to call the MPI algorithm automatically, so the runs will be distributed without the user needing to do anything.

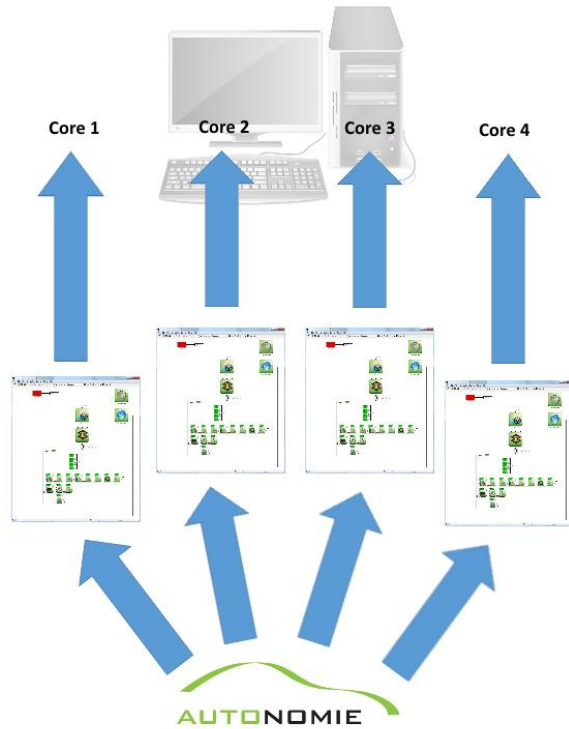


Figure V-125: Autonomie MPI distributes simulations across cores

New Optimization Algorithms

A generic optimization process was developed that will allow users to substitute their own optimization implementation. The provided editors (Figure V-126) allow users to generically define optimization problems independently of the optimization algorithm.

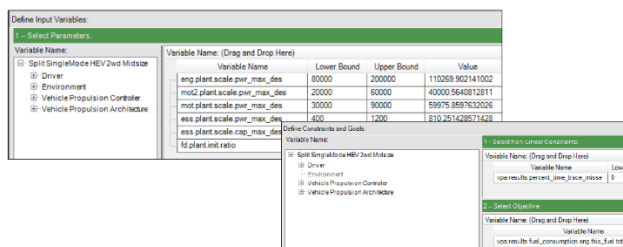


Figure V-126: Generic Optimization Editors

Two example optimization algorithms, “Pounder” and “Modified Random Search.” were developed for Autonomie by the Argonne Mathematics and Computer Science Division. These algorithms can be used out of the box with the Autonomie release.

Pounder is an example of a single objective optimization technique. This optimization could be used, for example, to maximize the potential savings from a PHEV by optimizing the battery size .

Random Search is an example of a full, multi-objective optimization. It could be used, for example, to identify the best possible trade-off between two conflicting objectives, such as fuel economy and performance .

Conclusions

Several versions of Autonomie were released this year; these include numerous new features developed on the basis of the feedback from DOE and the user community.

5.9.1 Products

Publications

1. L. Michaels, “Increasing the Robustness of Hybrid Electric Vehicle Controls via System Simulation,” presented at the SAE 2013 Hybrid Powertrain Complexity and Maintainability Symposium, Dearborn, MI, Oct. 22, 2013.
2. A. Rousseau, Y. Ding, “Impact of Worldwide Test Procedures on Advanced Technology Fuel Efficiency Benefits,” presented at EVS27, Barcelona, Spain, Nov. 17–20, 2013.
3. A. Rousseau, “Fuel Efficiency Benefits of Electrified CNG Vehicles,” presented at EVS27, Barcelona, Spain, Nov. 17–20, 2013.
4. N. Kim, E. Rask, A. Rousseau, “Control Analysis under Different Driving Conditions for Peugeot 3008 Hybrid 4,” 2014-01-1818, SAE World Congress, Detroit, Apr. 8–10, 2014.
5. D. Lee, A. Rousseau, E. Rask, “Development and Validation of the Ford Focus Battery Electric Vehicle Model,” 2014-01-1809, SAE World Congress, Detroit, Apr. 8–10, 2014.
6. N. Kim, A. Rousseau, H. Lohse–Busch, “Advanced Automatic Transmission Model Validation Using Dynamometer Test Data,” 2014-01-1778, SAE World Congress, Detroit, Apr. 8–10, 2014.
7. S. Pagerit, P. Sharer, A. Rousseau, “Complex System Engineering Simulation Through Co-Simulation”, 2014-01-1106, SAE World Congress, Detroit, Apr. 8–10, 2014.
8. L. Michaels, “Model–Based Systems Engineering at Argonne National Laboratory,” presented at the 2014 NAFEMS Americas Conference, Colorado Springs, CO, May 28–30, 2014.
9. L. Michaels, “Future of Automotive Simulation Software: What Capabilities Should One Expect?,” Panel Discussion, IEEE Transportation Electrification Conference, Dearborn, MI, June 16–18, 2014.
10. A. Rousseau, S. Halbach, L. Michaels, N. Shidore, Na. Kim, N. Kim, D. Karbowski, M. Kropinski, “Electric Drive Vehicle Development and Evaluation using System Simulation,” Journal of the Society of Instrument and Control Engineers, Vol. 53, 2014 (www.sice.jp).
11. N. Shidore, N. Kim, R. Vijayagopal, D. Lee, A. Rousseau, J. Kwon, B. Honel, E. Haggard, “Battery in the Loop: Battery Evaluation in a Systems Context,” presented at

the IEEE Transportation Electrification Conference
(ITEC), Beijing, China, Aug. 31–Sept. 3, 2014.

Tools and Data

1. Autonomie (www.autonomie.net)

V.L. Internal Combustion Engine Energy Retention (ICEER)

Principal Investigator: Jeffrey Gonder

National Renewable Energy Laboratory (NREL)
 15013 Denver West Parkway, MS 1634
 Golden, CO 80401
 Phone: (303) 275-4462
 E-mail: jeff.gonder@nrel.gov

DOE Program Manager: David Anderson

Phone: (202) 287-5688
 E-mail: david.anderson@ee.doe.gov

V.L.1. Abstract

Objectives

- Collaborate with ANL on effort to better understand real-world fuel penalties associated with engine cold start.
- Develop and apply broad analysis methodology taking into account:
 - Thermally sensitive engine fuel rate maps,
 - Large-scale, representative driving behavior, trip length, and dwell time distributions, and
 - Seasonal ambient temperature variation.

Major Accomplishments

- Validated simplified model of vehicle fuel consumption based on driving demand and temperature.
 - Calibrated against test data from ANL.
- Exercised model over broad distribution of driving profiles and annual temperature variations in three regions.
 - Included roughly 40 million miles of simulations.
- Estimated that cold-start fuel penalties related to engine friction and enrichment could account for 7.5% of real-world fuel use.
 - NREL’s initial assessment also indicates that mitigation techniques may have greater real-world fuel savings than what standard certification cycle testing would suggest.

Future Achievements

- Incorporate additional relevant effects into the modeling, such as cabin climate control loads, and thermal effects on other driveline components, such as the transmission.
- Exercise approach in collaboration with automakers to evaluate potential real-world fuel economy impacts of technologies for which 5-cycle standardized testing may not fairly represent on-road benefits.



V.L.2. Technical Discussion

Background

Internal combustion engines (ICEs) are presently included in over 99% of U.S. light-duty (LD) vehicle powertrains, and are anticipated to remain in the majority of vehicles for many years to come. Cold start effects are widely understood to cause reduced efficiency during the time period from initial vehicle start to when a vehicle powertrain comes up to its optimal operating temperature. These effects include higher lubricant viscosity, and fuel enrichment for catalyst light off. Basic analysis of existing test data shows cold start fuel penalties on the order of 10% over standardized driving cycles. Improved understanding and mitigation of cold start fuel penalties under real-world driving conditions could thus lead to significant fuel savings if implemented on a large scale. (Note that a broad efficiency improvement of just 1% in light-duty conventional vehicles would have the equivalent fuel use impact to taking 2.5 million cars off of the road).

Introduction

NREL collaborated with Argonne National Laboratory (ANL) on this effort to better quantify real-world LD vehicle fuel penalties due to cold start, and to explore fuel penalty mitigation opportunities. The techniques developed and implemented through this activity may be of interest to automobile manufacturers and regulators as a means to help quantify expected impacts from such technologies that have different real-world impacts than what can be estimated from standard certification tests.

Approach

Chassis dynamometer testing at ANL’s Advanced Powertrain Research Facility (APRF) provided the data basis for the modeling conducted at NREL. Tests were performed on a highly-instrumented 2011 Ford Fusion (2.5L, 6-speed automatic) over a broad range of temperatures and drive cycles. Table V-15 presents the full matrix of conditions included in the testing.

Table V-15: Matrix of Test Conditions Run at APRF (16 tests in total)

| | |
|-----------------------|---|
| Drive Cycle | UDDSx2, US06x2, non-operational cool down |
| Start Condition | Hot Start, Cold Start |
| Test Cell Temperature | -17°C, -7°C, 20°C, 35°C |

Component Model Development

While many modeling approaches exist to estimate road load as a function of vehicle speed coupled with powertrain component efficiency maps as functions of engine power, less effort has been expended characterizing the efficiency of internal combustion engines with respect to thermal state. It was the intent of this work to develop a simplified methodology to understand thermal effects in real-world driving conditions without using extremely complex and data-intensive high-fidelity vehicle models dependent upon accurate measurement of comprehensive component data. Not only is such data not generally available, but computation through hundreds of thousands of real-world drive cycles from around the country may be time prohibitive.

The following simplified component models provide a means for predicting component warm-up times and steady-state operating points sensitive to ambient conditions. The generalized approach involves response surface methodology type models coupled with simplified lumped capacitance parameter-based models. Application of the Nelder-Mead non-linear optimization method solves for the unknown coefficients to minimize model error to measured results of fuel consumption over the cycles.

Engine Efficiency

To simplify the modeling approach, a model of the engine fueling rate as a function of engine power and catalyst light-off was developed. The engine power is a third-order response surface model as a function of engine power and engine oil temperature. The oil temperature in this case is a differential between the initial engine oil temperature and the current oil temperature state. The catalyst model is a simplified exponential decay equation that takes into consideration the catalyst temperature until light-off. This equation adds a decaying amount of fuel until a certain catalyst temperature is reached. The engine fueling equations are shown here for reference:

$$fuel = f_1(P_{out}, T_{oil}) + f_2(T_{cat}) \tag{1}$$

$$f_1(P_{out}, T_{oil}) = a_0 + a_{1,1}P_{out}^3 + a_{1,2}P_{out}^2 + a_{1,3}P_{out} + a_{2,1}dT_{oil}^3 + a_{2,2}dT_{oil}^2 + a_{2,3}dT_{oil} + a_{3,1}P_{out}^3 dT_{oil}^3 + a_{3,2}P_{out}^2 dT_{oil}^2 + a_{3,3}P_{out} dT_{oil} \tag{2}$$

$$f_2(T_{cat}) = \max(0, a_1 * (e^{a_2*(T_{cat}-a_3)} - 1)) \tag{3}$$

$$dT_{oil} = T_0 - T_{oil} \tag{4}$$

Following the Nelder-Mead solution of the coefficients, plots of the engine efficiency as a function of the engine oil temperature and power output were generated, as well as the time-based comparison between the model-predicted fuel flow and the actual measured data. In the case of the time-based comparison, results are shown for a 250-second segment only of a UDDS cycle conducted at -17°C. This was done to show relative model accuracy relative to the actual fuel flow measurements recorded during testing. These results may be seen in Figure V-127 and Figure V-128.

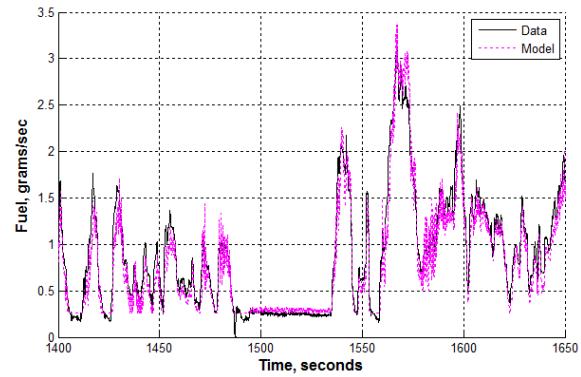


Figure V-127: Example time series data of engine fueling rate (250-second section of UDDS); measured test data from chassis dynamometer (solid black) overlaid with the model estimate (dashed magenta)

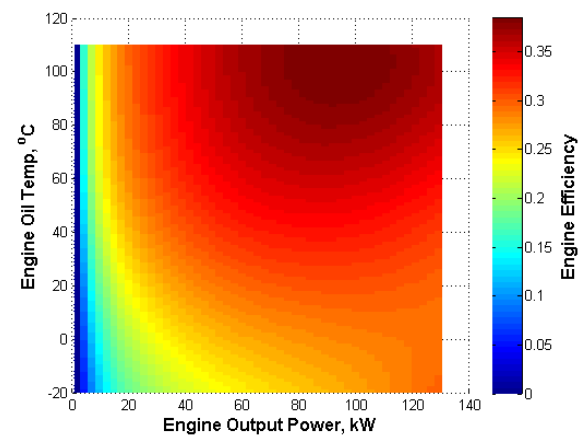


Figure V-128: Best-fit engine efficiency map as function of output mechanical power and engine oil temperature (considering operation over 16 test cycles)

Finally, calculations were done to determine the relative accuracy of the simplified models to predict overall drive cycle fuel consumption for the various drive cycles and temperatures used to develop the model. The results listed in Table V-16 show that the maximum predicted deviation from the measured results is 5.2%. The average cumulative error from the measured results of all the cycles is 2.2%, which falls within the range of experimental cycle-to-cycle deviation.

Table V-16: Cumulative fuel error between measured test data and the model estimate (positive error indicates model overestimation)

| Ambient Temp | UDDS | | US06 | |
|--------------|------------|-----------|------------|-----------|
| | Cold Start | Hot Start | Cold Start | Hot Start |
| -17°C | -3.9% | 1.5% | -5.0% | 2.5% |
| -7°C | 0.5% | 1.9% | 2.5% | 5.2% |
| +22°C | -1.7% | -1.3% | -0.5% | -0.9% |
| +35°C | -4.1% | -2.0% | -0.5% | -2.8% |

Engine Oil Temperature

A simplified lumped capacitance model of engine oil temperature was developed, the parameters of which were fit to the experimental data. The model includes convective heat transfer from the oil to environment, convective transfer between the oil and coolant (the coolant also contains a thermostat open/closed logic), and the difference between the power in (fuel times mass flow) and power out (brake torque and speed) of the engine. Additionally, the convective heat transfer term for the engine oil includes a vehicle velocity based function to more accurately reflect forced convection as the vehicle velocity changes. The equations and relative predicted model accuracy are shown below and in Figure V-129.

$$\dot{T}_{oil} = \frac{h_1(T_{amb}-T_{oil})+h_2(T_{cool}-T_{oil})+\alpha(P_{out}-P_{in})}{m_{oil}} \quad (5)$$

$$h_1 = a_1 v_{veh} + a_2 \quad (6)$$

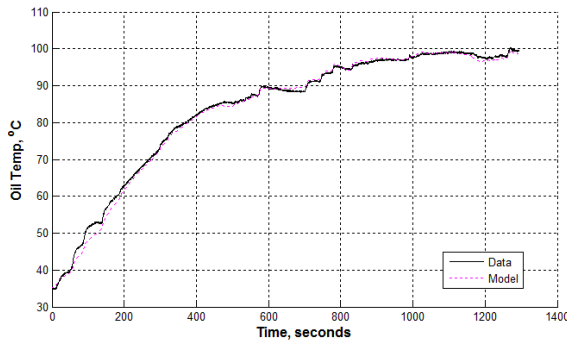


Figure V-129: Example time series data of engine oil temperature (measured at dipstick). Measured test data from chassis dynamometer (solid black) overlaid with the model estimate (dashed magenta)

Additionally, root-mean-square error analysis of the instantaneous model predicted engine oil and actual measured temperature were conducted. Results to this analysis are listed in Table V-17. From these results it is shown that the average of the instantaneous root-mean-square error deviation from the actual temperature is 5.3°C. These deviations do not last the entirety of the simulation, but rather for short durations of the simulated cycle.

Table V-17: Root-mean-square error for engine oil temperature between measured test data and the model estimate

| Ambient Temp | UDDS | | US06 | |
|--------------|------------|-----------|------------|-----------|
| | Cold Start | Hot Start | Cold Start | Hot Start |
| -17°C | 5.2 | 7.2 | 5.4 | 2.0 |
| -7°C | 4.9 | 4.1 | 5.5 | 1.9 |
| +22°C | 5.7 | 6.1 | 8.5 | 2.5 |
| +35°C | 6.3 | 8.1 | 6.7 | 4.6 |

Engine Coolant Temperature

Similar to the engine oil model, a simplified lumped capacitance model of engine coolant temperature was developed. This model includes convective heat transfer from the coolant to the environment, between the coolant and the oil, and (similarly to the oil) the difference between the power in and power out of the engine. Shown here is the logic included that accounts for the thermostat opening, which greatly increases the heat transfer from the coolant to the ambient environment, and accounts for vehicle velocity and forced convective heat transfer. The equations and relative predicted model accuracy are shown below and in Figure V-130.

$$\dot{T}_{cool} = \frac{h_1(T_{amb}-T_{cool})+h_2(T_{oil}-T_{cool})+\alpha(P_{out}-P_{in})}{m_{cool}} \quad (7)$$

$$\text{if } T_{cool} < T_{set}: h_1 = a_1 v_{veh} + a_2, \text{ else: } h_1 = a_3 v_{veh} + a_4 \quad (8)$$

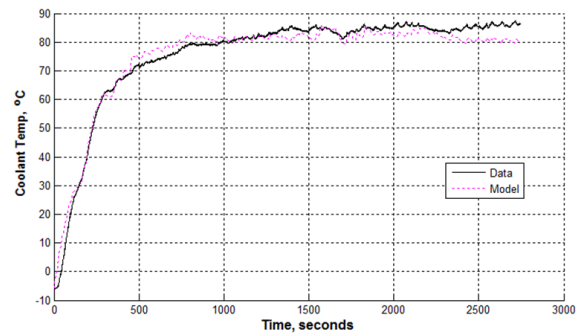


Figure V-130: Example time series data of engine coolant temperature (measured at heater core inlet). Measured test data from chassis dynamometer (solid black) overlaid with the model estimate (dashed magenta)

Similar to the oil, root-mean-square error analysis of the instantaneous model coolant and actual measured temperature were conducted. The results of this analysis are listed in Table V-18. From these results, it is shown that the average of the instantaneous root mean square error deviation from the actual coolant temperature is 6.9°C. As was the case for engine oil temperature, these deviations do not last the entirety of the simulation, but rather for short durations of the simulated cycle.

Table V-18: Root mean square error for engine coolant temperature between measured test data and the model estimate

| Ambient Temp | UDDS | | US06 | |
|--------------|------------|-----------|------------|-----------|
| | Cold Start | Hot Start | Cold Start | Hot Start |
| -17°C | 7.0 | 9.2 | 7.4 | 3.9 |
| -7°C | 5.1 | 5.4 | 6.9 | 3.3 |
| +22°C | 6.8 | 4.3 | 12.5 | 5.9 |
| +35°C | 6.5 | 6.0 | 10.9 | 9.1 |

Real-World Simulations

Vehicle modeling done in this analysis was performed using NREL’s Future Automotive Systems Technology Simulator (FASTSim). FASTSim is a vehicle simulation tool developed by NREL to evaluate the impact of various technologies on vehicle performance, cost, and utility in conventional and advanced technology powertrains. FASTSim calculates the power necessary to meet a given speed trace and overcome road loads (rolling, aerodynamic, kinetic, and potential) while considering component limitations, system losses, and auxiliary loads. Given required engine output power at each time step from FASTSim, engine fuel use is calculated per a thermally sensitive efficiency map (previously discussed), and differential equations describing the thermal response of engine oil, engine coolant, and exhaust catalyst are evaluated.

Real-world drive cycle data for this study are sourced from NREL’s Transportation Secure Data Center (TSDC). Specifically, 1-Hz travel histories 1 to 7 days in duration are queried from vehicles across the United States. These data represent a composite of several data collection efforts from Metropolitan Planning Organizations across the country as documented on the TSDC website (www.nrel.gov/tsdc).

Ambient temperature data are assembled from NREL’s Typical Meteorological Year Database (TMY3). The TMY3 database contains hourly ambient temperature and solar irradiation data for 1,020 distinct U.S. weather stations. Typical meteorological patterns are synthesized from representative days across historical data from the 1991–2005 time frame to form a 365-day history with hourly values for each site. Figure V-131 shows a map of average yearly ambient temperatures across the continental United States.

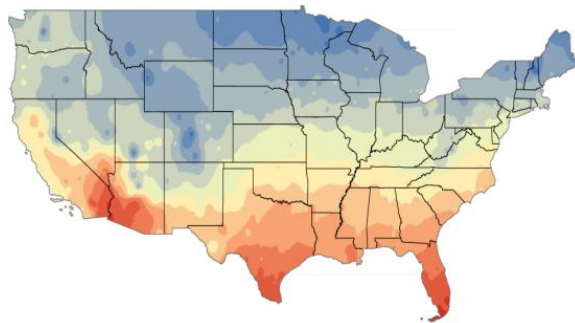


Figure V-131: Map of average ambient temperatures for the contiguous United States (hot climates in red, cold in blue) as sourced from NREL’s database of typical meteorological years

By bringing global positioning system travel histories into a shared computing environment with the TMY3 data, it is possible to align real-world drive cycle data with representative ambient temperature data from any major U.S. city at any time of year. This flexibility enables realistic evaluations of simulated thru-life vehicle efficiency relative to large amounts of drive cycle and climate data.

Results

Example Results

Introductory analysis was conducted to investigate the effects ambient conditions coupled with real-world drive cycle data have on vehicle fuel consumption. As an example, one vehicle from the TSDC dataset was selected to demonstrate the effects. In Figure V-132, a time series of this vehicle driving a one-week period, January 2 to January 9, as well as a one-hour magnified trip occurring on January 2, are shown.

This figure plots vehicle speed along with oil, coolant, and ambient temperatures, and illustrates the modeled response of coolant and oil temperature relative to the power requirements of the trip—both the initial rise at the start of each trip segment, and the cooling-down period once the vehicle is keyed off. Note that the coolant temperature rise leads the oil temperature rise (as is the case in the experimental data). Given the relationship between oil temperature and viscosity, this means that viscous friction losses would be underestimated during warm-up if engine coolant were instead used as the sole temperature indicator. Additionally, the modeled connection between coolant and engine oil allows the model to capture the increased heat transfer losses as the thermostat opens, reducing the thermal load on the engine oil.

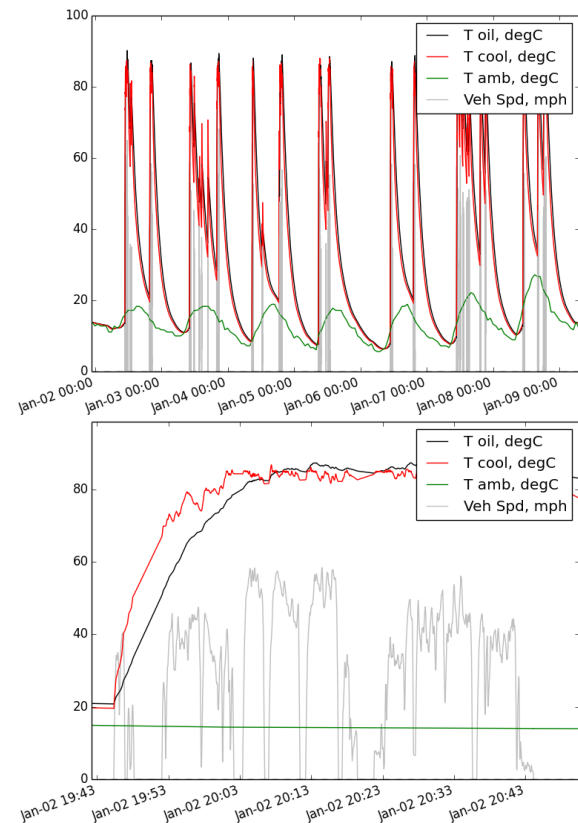


Figure V-132: Time series examples of thermal simulations predicting engine oil and coolant temperatures. Real-world drive cycle data overlaid with TMY climate data. Results are shown at two horizontal zoom windows: 1—one week (top) and 2—one hour (bottom)

Fleet Statistics

Having established a modeling framework for quantifying real-world efficiency impacts of engine cold-start events, approximately 40 million miles of driving were simulated given combinations of drive cycles (recorded from thousands of U.S. vehicles), local ambient temperature profiles (three representative climates), and weeks of the year (52 in total). Ambient temperature statistics were compiled for U.S. cities from the TMY3 database, and climates representing extreme hot and cold scenarios were identified as Phoenix, Arizona, and Minneapolis, Minnesota, respectively. Baltimore, Maryland, was selected as a nationally representative average climate scenario.

Figure V-133 shows simulation results with distance-weighted, fleet average fuel economy (units of miles per gallon of gasoline, MPG) plotted by climate and week of year. The first trend identified is the intuitive fluctuation of fuel economy with season. Average fuel economy is shown to decrease by 1–3 MPG during cold winter months as a result of increased viscosity from cooler engine oil temperatures and more frequent fuel enrichment events to accelerate catalyst heating. These are likely conservative estimates of reduced fuel economy during cold weather months as additional effects including increased transmission oil viscosity, decreased tire pressure, increased air density, and changes in road surface resistance (e.g., snow-covered roads) are not considered in this analysis.

Equally intuitive is the variation between generally hot and cold climates. Simulated Minneapolis fuel economy is shown to be approximately 8% lower during winter months relative to Phoenix, and 2% lower during summer months. In reality, fuel economy during summer months is potentially greater in Minneapolis than in Phoenix as incremental mechanical loads associated with belt-driven cabin air conditioning systems have not been included in this analysis.

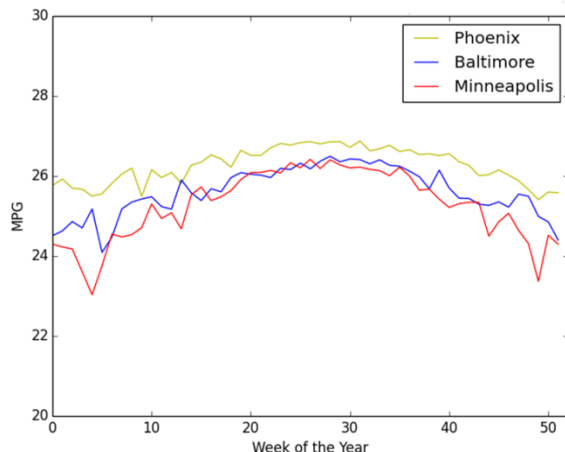


Figure V-133: Distance-weighted fleet average MPG by week of year for three U.S. climates

To highlight variation in fuel economy between drivers, Figure V-134 presents efficiency results for all vehicle histories simulated in the Baltimore climate with individual box plots for each week of the year. In addition to the aforementioned seasonal fuel economy fluctuation, these box plots reveal

significant variation between different drive cycle histories with 25th and 75th percentile drivers differing by approximately 5 MPG (~19%). Drive cycle characteristics such as driving speeds, acceleration rates, and percent idle times have been shown to significantly impact simulated fuel economy in previous studies. The featured modeling aspect of this work (engine efficiency sensitivity to thermal state) further contributes to driver-to-driver fuel economy variation. For example, a driving pattern with several short trips in a week would experience depressed fuel economy as a result of the engine spending a large percentage of operational time under “cold” conditions. These effects are magnified in driving patterns with extended dwell times between trips as components are afforded ample time to decay to ambient temperatures.

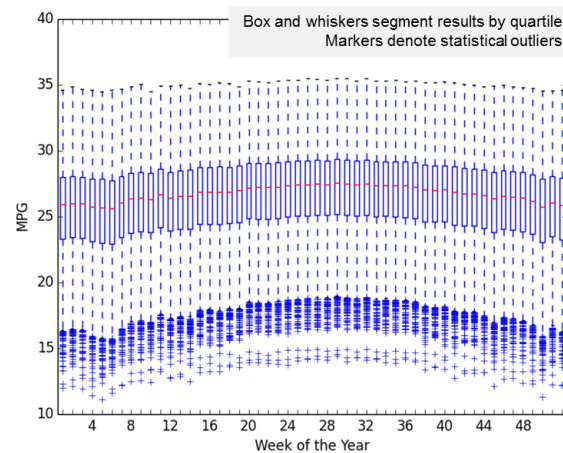


Figure V-134: Distribution of simulated vehicle history MPG by week of year (approximately 50% of data is bounded between 23 and 28 MPG)

Simulated vehicle efficiency data are aggregated into nine distinct combinations of drive cycle data sets and climate scenarios in Figure V-135 to highlight the incremental energy impacts of modeling engine cold starts. The large composite drive cycle data set presented in Figure V-133 and Figure V-134 is now geographically grouped and anonymously named as drive cycle sets 1, 2, and 3. The relatively more aggressive drive cycle characteristics of set 1 result in the highest fleet fuel consumption, while set 3 on the whole features less aggressive driving and results in lower fuel consumption. Each of the drive cycle datasets is overlaid with ambient temperature data from the three selected climates with familiar trends of increased fuel consumption with low average ambient temperature operation.

Figure V-135 further shows that the incremental fuel consumption contributions from engine thermal state and enrichment effects account for 4.8% and 2.7% of total simulated fuel use, respectively. Taken in aggregate, this is an increase of 7.5% on average and underscores the importance of considering thermal effects in analysis of real-world fuel economy.

Using FASTSim in combination with engine efficiency and thermal models specific to the Ford Fusion under test, the full EPA 5-cycle test procedure is simulated (including cold FTP and SC03), weighted, and scaled per EPA documentation to

determine the modeled vehicle’s certification fuel economy. Not surprisingly, the range of simulated real-world fuel consumption values generally falls short of the EPA estimate. This result is likely a byproduct of several real-world effects presently unaccounted for in the modeling environment, including cabin air conditioning loads and additional powertrain thermal sensitivities (transmission, rear differential, etc.). Accounting for these remaining real-world effects remains a goal of future research.

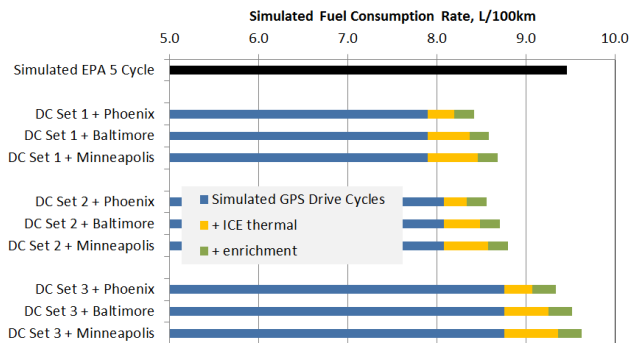


Figure V-135: Relative fuel consumption model contributions shown for various combinations of drive cycle datasets and year-long TMY climate data. Results are compared with the simulated EPA 5-cycle test procedure

Conclusions

To better understand real-world thermal and driving effects on vehicle efficiency, this effort developed and implemented a novel approach of simplifying experimental data into a predictive model. The approach employed lumped capacitance and response surface modeling methodologies to predict vehicle fuel consumption as a function of velocity and thermal state. On average, the approach proved able to predict UDDS and US06 fuel consumption from -17°C to 35°C to within 2.2% of the actual test measured values. These simplified models were then run through a large data set of 1 Hz travel histories 1 to 7 days in duration that were collected from vehicles across the United States. The models and travel histories were coupled with a typical meteorological year database such that vehicle longitudinal, latitudinal, and elevation histories were coupled with seasonal average ambient temperatures.

Using Phoenix, Baltimore, and Minneapolis as regional examples, three different fleet data sets were modeled to better understand the seasonal fuel consumption. Results show significantly higher fuel consumption in the colder Minneapolis climate relative to Phoenix. Future work will include addition of cabin climate control loads along with thermal effects from other components to even more accurately capture real-world fuel efficiency. On-going activities will also include evaluating cold start mitigation strategies—where simulation results have shown greater estimated real-world than 5-cycle fuel economy benefit. This evaluation approach could prove to be a useful assessment method when considering potential off-cycle credits that manufacturers might receive for implementing thermal

retention techniques (which do not necessarily show 5-cycle benefits due to the nature of the certification tests).

V.L.3. Products

Publications

1. Gonder, J., Wood, E., Lopp, S. “Internal Combustion Engine Energy Retention.” DOE Vehicle Technologies Annual Merit Review - Project ID#: VSS126, June 2014, Washington, DC.
2. Wood, E., Gonder, J., Lopp, S., Jehlik, F. “Simulated Real-World Energy Impacts of a Thermally Sensitive Powertrain Considering Viscous Losses and Enrichment.” Proceedings of the SAE Thermal Management Symposium, Sept 2014, Denver, CO.
3. Jehlik, F., Wood, E., Gonder, J., Lopp, S. “Simulated Real-World Energy Impacts of a Thermally Sensitive Powertrain Considering Viscous Losses and Enrichment.” Submitted to the SAE World Congress, April 2015, Detroit, MI.

Tools and Data

1. ANL’s Advanced Powertrain Research Facility (www.transportation.anl.gov/facilities/aprf.html). Testing in support of this project was led by Forrest Jehlik of ANL. Additional thanks to Mike Duoba for APRF support.
2. Future Automotive Systems Technology Simulator (www.nrel.gov/fastsim). FASTSim operation and associated thermal model development and implementation were led by Eric Wood of NREL. Additional thanks to Sean Lopp and Aaron Brooker for modeling support.
3. Transportation Secure Data Center (www.nrel.gov/tsdc).

V.M. Impact of VTO Technologies on Energy Consumption and Cost Using Large-Scale Simulation

Principal Investigator – Ayman Moawad

Argonne National Laboratory
9700 South Cass Avenue
Argonne, IL 60439-4815
Phone: (630) 252-2849
E-mail: amoawad@anl.gov

DOE Program Managers: David Anderson, Jacob Ward

Phone: (202) 287-5688, (202) 586-7606
E-mail: david.anderson@ee.doe.gov,
jacob.ward@ee.doe.gov

V.M.1. Abstract

Objectives

- Develop a database and analysis tool to analyze data generated by large-scale simulations.
- Analyze the impact of U.S. Department of Energy (DOE) Vehicle Technologies Office (VTO) technologies on component operating conditions, component size, vehicle energy consumption, and cost.

Major Accomplishments

- Developed a database and plotter tool to facilitate the analysis of large-scale simulation data.
- Analyzed the impact of VTO component targets on battery requirements and operating conditions.

Future Achievements

- Further enhance the large-scale simulation process to improve post processing on sets of simulations and conduct additional quality assurance.
- The VTO benefits will be reassessed based on the latest component and vehicle data.



V.M.2. Technical Discussion

Background

Through the Office of Planning, Budget, and Analysis, the DOE Office of Energy Efficiency and Renewable Energy (EERE) provides estimates of program benefits in its annual Congressional Budget Request. The Government Performance and Results Act (GPRA) of 1993 provided the basis for assessing the performance of federally funded programs. Often referred to as “GPRA Benefits Estimates,” these estimates represent one piece of EERE’s GPRA implementation efforts — documenting some of the economic, environmental, and security benefits (or outcomes) that result from achieving program goals.

Introduction

Any large-scale simulation study focused on vehicle energy consumption requires the user to tackle two complicated problems simultaneously:

- A vehicle simulation tool must be used to quickly and properly estimate energy consumption of extremely large numbers of specific vehicles, powertrain, and component technologies.
- The user must easily access and analyze specific information across large amounts of data.

A process for performing large-scale simulation with Autonomie is now in place. With it, a simulation can be quickly validated, or any discrepancies in the results can be examined in details. In addition, Autonomie is fully integrated with distributed computing, making extremely large numbers of simulations, such as the quantity required for full VTO benefit analysis, feasible.

However, Autonomie was not originally designed to analyze such large sets of data. Such analyses impose data management concerns (numbers of files, disk sizes, access times); require the ability to run post-processing calculations without the time cost of rerunning all of the simulations; and involve plots, calculations, and other analytical tools to look at high-level indicators and spot overall trends. In response, Argonne National Laboratory’s (Argonne’s) new process allows the detailed simulation results provided by Autonomie to either be distilled into a format that can be easily distributed and analyzed horizontally across many simulations, or examined via a deep, vertical dive into one simulation. Both aspects are critical for the full-scale vehicle analysis that VTO benefit analysis requires.

The process is composed of two distinct phases. The objective of the first phase is to set up the simulations to be performed, and launch all the runs through a distributed computing toolbox and be able to perform analysis of individual results to ensure the simulations are performed properly as shown in Figure V-136.

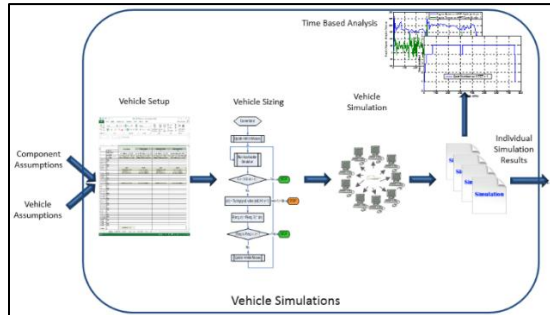


Figure V-136: Running Large-Scale Simulations Using Autonomie

The simulations outputs include everything necessary for Autonomie to analyze or recreate an individual simulation, including the Simulink model representing the vehicle; a metadata file containing simulation results, *.a_result file; and a data.mat file containing all of the time-based signal data. These results can be archived for full traceability and reproducibility of all simulations.

However, it is currently not feasible to share or analyze these data. For example, 7503 simulation results consumed 296 GB of disk space. It is simply not scalable to pass this much information around, much less the number of simulations required for the VTO benefit analysis. In addition, each simulation has individual files storing the results, so just managing or indexing the sheer number of files becomes an issue. Most of the information contained in those results files, however, is not necessary for the analysis (i.e., second-by-second fuel or electrical consumption values). Therefore, a subset of the data is collected into a portable, user-friendly database.

As a result, the second phase of the process allows users to analyze a limited number of parameters from the individual simulations to perform large-scale analysis. As shown in Figure V-137, this process starts with the development of a standardized query language (SQL) database based on a list of parameters defined by the users. The objective of the database analysis tool is then, for example, to select the most cost-beneficial technologies and understand uncertainties.

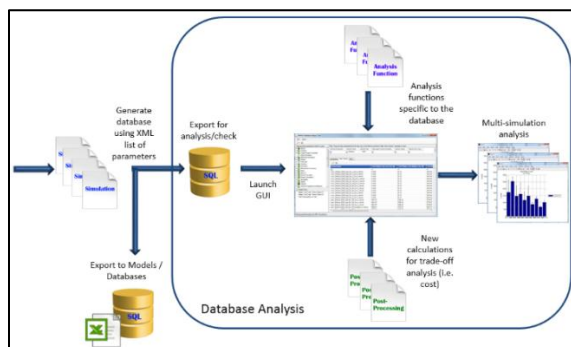


Figure V-137: Analyzing Large-Scale Simulations Data

Approach

To evaluate the fuel efficiency benefits of advanced technologies, the vehicles are designed based on individual component assumptions. To properly assess the benefits of future technologies, options are considered for the following categories:

- Different vehicle classes (e.g., compact, midsize, small sport utility vehicle [SUV], medium SUV, pickup truck).
- Different time frames (e.g., 2015, 2020, 2030).
- Different powertrain configurations (e.g., conventional, hybrid electric vehicle [HEV], plug-in HEV [PHEV], fuel cell HEV, EV)
- Different fuels (e.g., gasoline, diesel, compressed natural gas [CNG], ethanol).

Also, to address uncertainties, a triangular distribution approach (low, medium, and high) was employed. For each component, assumptions regarding efficiency, power density, and so forth were made, and three separate values were defined to represent the (1) 90th percentile, (2) 50th percentile, and (3) 10th percentile. A 90% probability means that the technology has a 90% chance of being available at the time considered. For each vehicle considered, the cost assumptions also follow the triangular uncertainty. Each set of assumptions is, however, used for each vehicle, and the most efficient components are not automatically the least expensive ones. As a result, for each vehicle considered, we simulated three options for fuel efficiency. Each of these three options also has three values representing the cost uncertainties.

In order to address all of these combinations, the VTO benefit analysis requires the definition and simulation of more than 4,000 vehicles (Figure V-138).

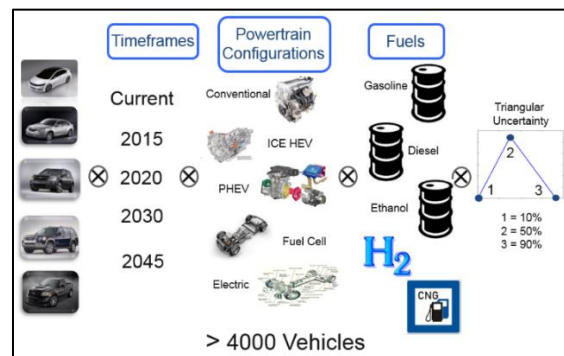


Figure V-138: The Number of Required Runs Accumulates Quickly

Vehicle Creation

The first step in the process is to generate the vehicles based on the individual assumptions gathered from the component experts, such as the U.S. Drive technical teams.

In order to facilitate this, a template Excel document is used to quickly define the required parameters needed to characterize the vehicles. Excel was chosen for its familiar, tabular format. This Excel document is used to create and populate all of the .a_vehicle files needed by Autonomie to run the actual simulations.

Next, the vehicles are run over a custom sizing process which imposes recurrence and iteration/looping. This adjusts the vehicle parameters to meet certain characteristics, such as acceleration times, gradeability profiles, or other performance requirements.

Finally, the vehicles are ready to be run on the various simulations, such as cycles and combined or PHEV procedures.

Distributed Computing

With the multitude of technology combinations to simulate, the usual computing resources are no longer practical. Running all of the simulations on one computer would take several months before any analysis could be completed. Fortunately, advances in distributed computing have greatly reduced simulation time. One of the biggest advantages of distributed computing is that it facilitates the quick rerun of simulations, which occurs many times during any study.

Among the computing resources available at Argonne is a cluster of 128 worker nodes dedicated to the System Modeling and Control Group. A larger computing facility could be used in the future to further accelerate the simulations.

System Modeling and Control Group researchers use Autonomie as the simulation framework, synchronized by a cluster head node computer. An algorithm optimizes the distribution of jobs for vehicle simulations and parametric studies.

Database Creation

Each simulation run by Autonomie creates a separate directory of output files. As mentioned in the introduction, these files are difficult to manage effectively and take a significant amount of disk space. Therefore, the full results are archived at this point, and an easier to manage database is generated for distribution and analysis.

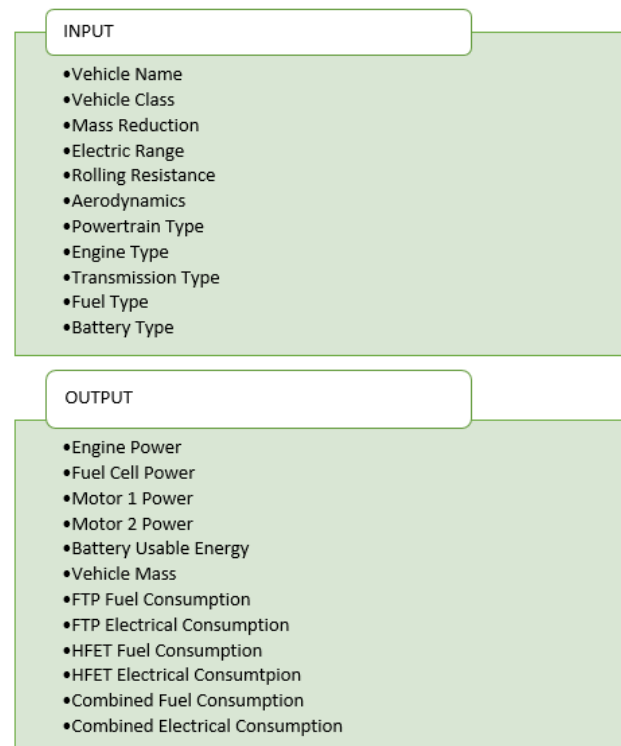


Figure V-139: Example Autonomie parameters to add to the database

Argonne's database creation process relies on an input sheet that specifies the input and output parameters (Figure V-139) to be included in the database. The process scans all of the simulation results files, extracts the specified parameters, and stores them in a single, specialized database file. This allows us to exclude irrelevant information not needed for cross-cutting analyses, while leaving the full results archived.

A single database file is easy to redistribute. The aforementioned 296 GB of data was compressed into 30.4 MB of data, and took only 27 minutes to generate from the original simulation results. In addition, the database is developed using the MS SQL Express 2012 format, which is free and easily accessed by standard SQL tools.

Database Structure

The database is structured to be generic, so that any simulation input parameter, result, or descriptive property can be stored. This allows maximum flexibility in the type of data that can be stored. The tables are structured to allow logical grouping of data, maximize retrieval speed, and minimize disk space.

Each parameter stores name, description, data type (i.e., string, double, integer, Boolean), and unit (Figure V-140). The values themselves are organized into tables by data type for disk size optimization.

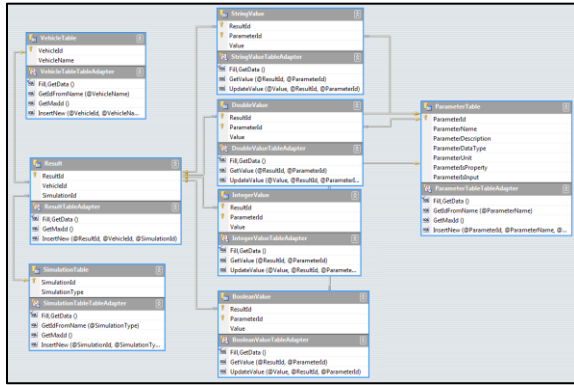


Figure V-140: Database structure

Not all vehicles and simulations have the same parameters; for example, motor parameters are only available for a vehicle with an electric power path (e.g., EVs, HEVs, PHEVs), and fuel consumption is only available for simulations with an engine or fuel cell, which excludes EVs.

User Interface

Although the database is accessible by any tool or programming language that can interact with databases, Argonne has also developed a tool to easily visualize and analyze the data. This tool provides a quick and intuitive way for users to quickly select subsets of simulation results of interest, select which parameters to view, modify assumptions, perform additional post-processing calculations on the data retrieved from the database, and view plots to better visualize the data (Figure V-141, Figure V-142, and Figure V-143).

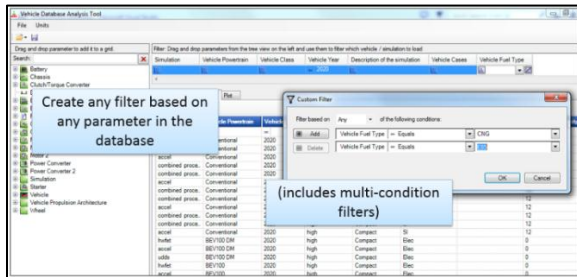


Figure V-141: Quickly filter data

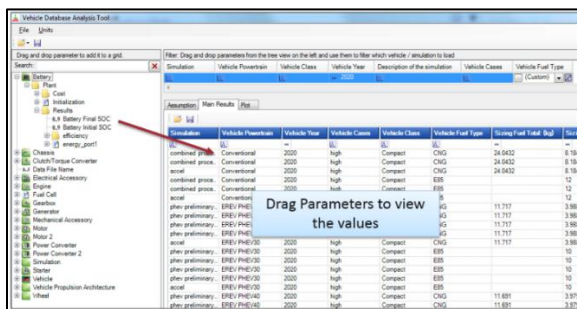


Figure V-142: View simulation parameters

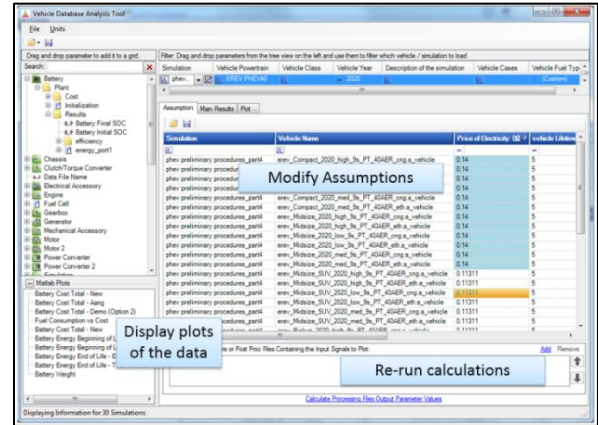


Figure V-143: Scenario analysis with data recalculation

The user interface also provides some advanced features that allow users to import their own plots and analysis functions; save “projects” of filters, parameters, and overridden assumptions; or export subsets of the data to Excel for additional data analysis or redistribution (Figure V-144).

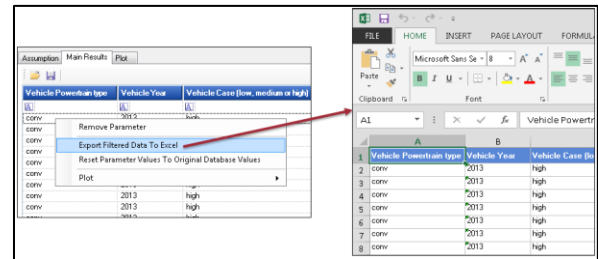


Figure V-144: Export data to Excel

This tool allows users who are not familiar or comfortable with direct database access to perform the analysis necessary for large-scale simulations.

In addition to the database tool, a plotter tool has been developed in MATLAB which enables easy plotting of standard analysis plots through the database user interface. Figure V-145 shows an example of standard plots being tabulated in the database graphical user interface (GUI).

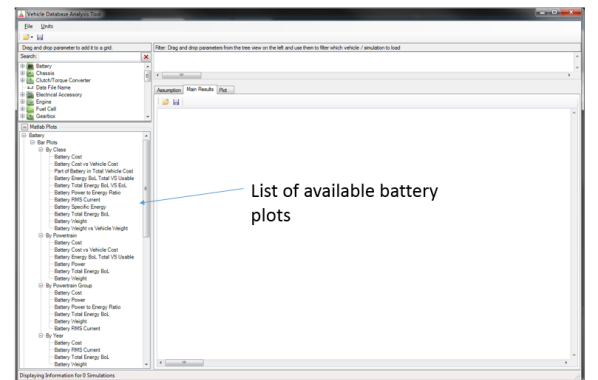


Figure V-145: Available plots for battery analysis in the database GUI

With the plotter tool, results in the database can be plotted with easy swapping of the reference variable, plotting of absolute or relative values, and categories of sorting. Bar plots or scatter plots can be generated for analysis (Figure V-146). Examples of use of the database tool and the plotter tool are discussed in the results section.

In addition to the GPRA study, the database tool is used for many studies at Argonne that require analysis of a large number of results [1], [2].

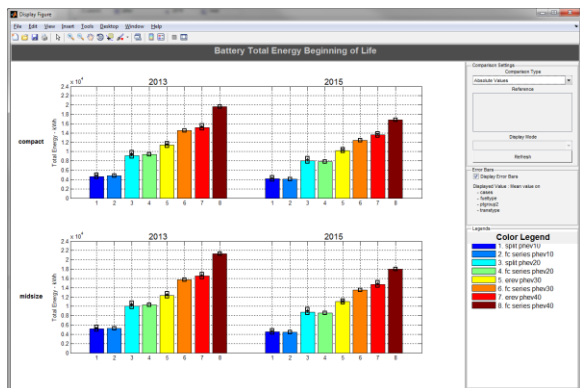


Figure V-146: Standard plots for the battery generated through the plotter tool

Results

For the VTO benefit analysis study, a thorough analysis of the VTO targets' impacts on battery requirements and operating conditions, amongst other powertrain components, was performed [3]. The plotter tool was used to generate plots from the parameters in the database to analyze the battery results.

Figure V-147 shows a plot of battery total energy (beginning of life [BOL]) for the EV with a 100-mile range (EV-100) for different classes across the different time frames. It can be seen that due to VTO-aided battery technology development, there is a steady decrease in battery energy requirement, compounded with improvements in the rest of the powertrain as well as vehicle lightweighting.

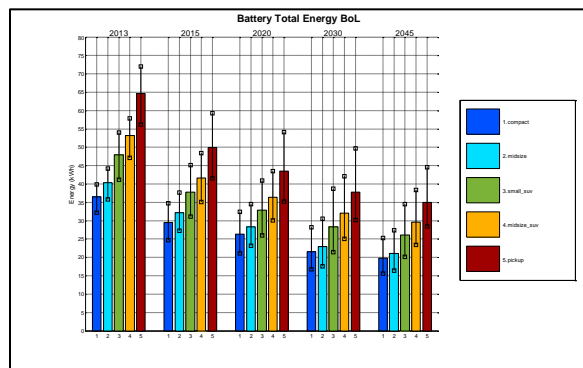


Figure V-147: Battery energy requirements decrease with time (for all vehicle classes)

Similarly, peak power requirements also decrease with time (Figure V-148). For example, the battery EV (BEV) 100 average power requirement for the compact car in 2013 is around 120 kW; it decreases to 70 kW in 2045.

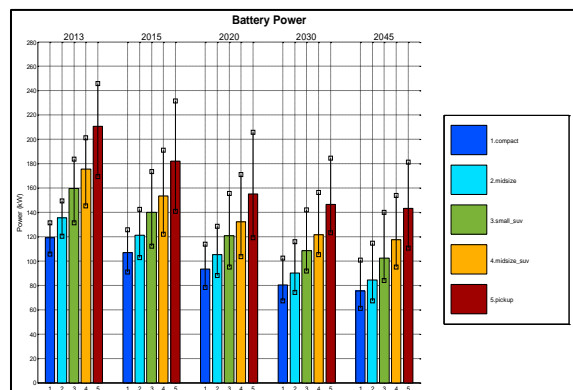


Figure V-148: Battery peak power requirements decrease significantly with time

This effect is due to the higher energy density of the batteries, in addition to the compounding effects of improvements in component efficiencies and vehicle lightweighting.

Vehicle-level impacts of VTO technology improvements were also analyzed. Figure V-149 shows the trends in fuel consumption for a midsize 10-mi, 20-mi equivalent electric range PHEV for the Urban Dynamometer Driving Schedule (UDDS) and Highway Fuel Economy Test (HWFET) cycles. The 10-mi and the 20-mi PHEVs have a power split powertrain configuration.

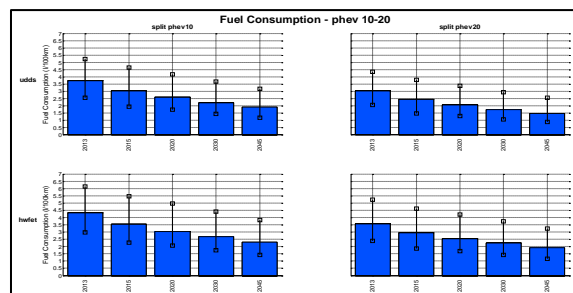


Figure V-149: Fuel consumption trends for PHEV 10 and 20 for UDDS and HWFET

Figure V-150 shows the trends in ratios of hydrogen and electric (battery) fuel energy carried on board for a conventional, electric, and fuel cell hybrid powertrain. Here, the ratio on the Y axis is defined as:

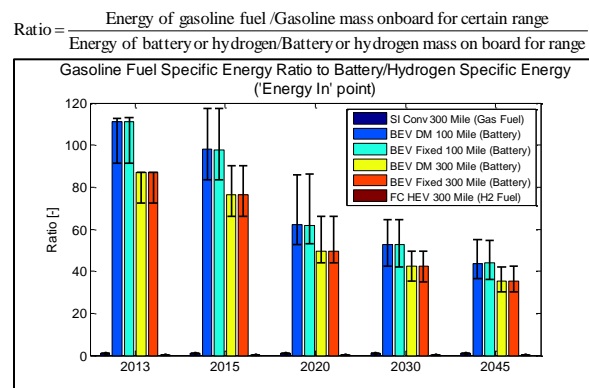


Figure V-150: Trends in the ratio of fuel-specific energy to battery-specific energy

The ratio decreases because the decrease in battery energy or hydrogen energy required for 300 mi decreases faster than the decrease in gasoline energy required. The decrease in battery energy required for 300 mi is because of higher battery-specific energy and improvement in battery and powertrain efficiency. The decrease in hydrogen energy required for 300 mi would similarly be on account of improvement in fuel cell efficiency, compounded by improvements in powertrain efficiency and vehicle mass reduction due to VTO technology developments. It can be seen that the ratio decreases by a factor of 2 by 2030.

The ratio at the energy source (gasoline/battery/fuel cell) can be contrasted with the ratio at the wheel as shown in Figure V-151. Here, the ratio is defined as:

$$\text{Ratio} = \frac{\text{Energy at wheel for certain range with gasoline / Conventional Powertrain mass with gasoline}}{\text{Energy at wheel for certain range with FC or battery / Powertrain mass with FC or battery}}$$

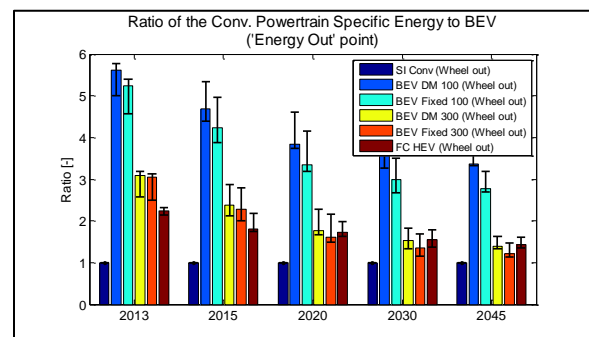


Figure V-151: Specific energy ratio of the powertrain at the wheel

It can be seen from Figure V-150 and Figure V-151 that even though the “fuel energy ratio” is high (and decreases with time), the “powertrain energy at the wheel ratio” is significantly lower (ranges from 1.1 to 5.7) and would be the correct metric for powertrain comparison among different types of energy sources [4].

Conclusions and Future Directions

More than 4000 vehicles were simulated to analyze the benefits of the VTO program and developed technologies on vehicle energy consumption and cost.

A process to run such large-scale simulations in Autonomie has been developed. To support thorough analysis of such large-scale simulation results, Argonne has developed a process to generate a database of all the results and other important simulation parameters.

The database can be accessed through a database GUI, and standard as well as customizable plots can be generated for analysis of VTO developed technologies.

The database tool and the plotter were used to analyze the impact of VTO targets on battery requirements and operating conditions.

A similar analysis was conducted on other component/fuel technologies supported by the VTO.

The process will be repeated next year with enhancements and modifications to the VTO technology assumptions, based on feedback from DOE technology managers and other stakeholders such as U.S. Drive partners.

The simulation and analysis process will be further enhanced through the development of dedicated post processing for a large database (large-scale database analysis) and development of quality assurance/quality control (QA/QC) methods.

V.M.3. Products

Tools and Data

1. Autonomie; available at www.autonomie.net.

References

1. Kim, N., Moawad, A., Shidore, N., and Rousseau, A., “PHEV Powertrain Benefit Comparison,” presentation to the U.S. Department of Energy, Washington D.C., August 5, 2014.
2. Shidore, N., Lemazurier, L., Moawad, A., Kim, N., and Rousseau, A., “Impact of Advanced Technologies on Engine Targets and Vehicle Fuel Economy – Status Update,” presentation to the U.S. Department of Energy, Washington, D.C., August 5, 2014.
3. Moawad, A., Judalet, N., and Rousseau, A., “Impact of VTO Targets on Battery Requirements and Operating Conditions,” presentation to the U.S. Department of Energy, Washington, D.C.
4. Lee, D., Gallagher, K., Vijayagopal, R., and Rousseau, A., “BEV Powertrain Specific Energy Compared to Conventional Vehicles”, presentation to the U.S. Department of Energy, Washington D.C., February 28, 2014.

V.N. Advanced PHEV Powertrain Benefit Comparison

Principal Investigator: Namdo Kim

Argonne National Laboratory
 9700 South Cass Avenue
 Argonne, IL 60439-4815
 Phone: (630) 252-2843
 E-mail: nkim@anl.gov

DOE Program Manager: David Anderson

Phone: (202) 287-5688
 E-mail: david.anderson@ee.doe.gov

V.N.1. Abstract

Objectives

While numerous plug-in hybrid electric vehicle (PHEV) powertrain options have been introduced into the market, there is currently no clear understanding or agreement within the industry regarding which option is the most fuel and cost effective. Study objectives are to:

- Evaluate the energy consumption and cost of different PHEV architectures using different component technologies.
- Leverage vehicle-level controls developed for power split and pre-trans with two clutches.
- Develop generic Honda two-motor hybrid system and control models.
- Design PHEVs with similar Vehicle Technical Specifications (VTS) for different powertrain configurations.
- Evaluate the fuel economy impacts of combinations of advanced powertrain and component technology with cost considerations.

Major Accomplishments

- Developed the powertrain and control for the Honda PHEV in Autonomie [1]. The driving mode selection rule was defined by maps developed using a brute-force algorithm.
- Completed sizing and simulation for midsize vehicle simulations for three risk levels: low, average, and high.
- Repeated the study for different component technologies (i.e., variable valve timing (VVT) engine versus turbo).
- Quantified the energy consumption and cost of different PHEV powertrain options for standard and stochastic cycles.
- Integrated the new model and controller into the Autonomie R14 release after modifying the model and initializing the files with generic parameters.

Future Achievements

- Assess the impact of advanced powertrain and accurate evaluation of U.S. Department of Energy (DOE) Vehicle Technologies Office (VTO) benefits and targets to guide future research and development (R&D).
- Develop and validate models to understand and quantify the impact of cold and hot ambient temperature on the vehicle energy consumption for new PHEV powertrain configurations.
- Set the baseline to evaluate DOE VTO benefits under different thermal conditions.



V.N.2. Technical Discussion

Background

In order to meet environmental targets for fuel economy and emissions, automakers have no choice but to develop PHEVs or battery electric vehicles (BEVs). Several automakers have been focusing on developing competitive PHEVs by introducing a variety of system architectures, as shown in Figure V-52. In 2011, General Motors (GM) introduced the Volt, which had a series-power split system with one planetary gear and three clutches. In 2013, Honda released the Accord PHEV with a series-parallel system.

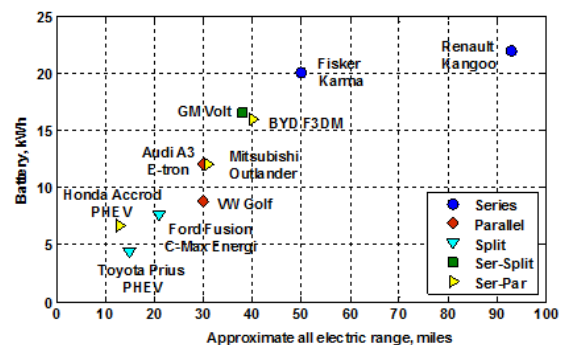


Figure V-152: PHEV models

While series configurations have a high system efficiency in electric driving mode with low mechanical loss, they demonstrate low efficiency in the hybrid driving mode because of electric machines loss. Consequently, in order to overcome low system efficiency in the hybrid driving mode, the series system needs to have an additional transmission mode by adding a clutch or gearset. The additional modes provide higher system efficiency since the engine directly connects to the output shaft. However, mechanical elements should be added, which lead to increased mechanical losses. Therefore, electric transfer loss as well as mechanical element loss should be considered to properly evaluate plug-in systems' system efficiency.

Introduction

PHEVs have demonstrated the potential to provide significant fuel displacement across a wide range of driving cycles. Companies and research organizations are involved in numerous research activities related to PHEVs. One of the current unknowns is the impact of driving conditions on the true benefits of PHEVs from a worldwide perspective. To address this issue, five different PHEV powertrain configurations (input split, parallel, series, series-output split and series-parallel) with four all electric range (AER) vehicles were analyzed under different standards (i.e., Urban Dynamometer Driving Schedule [UDDS], Highway Fuel Economy Test [HWFET], New European Driving Cycle [NEDC]) cycles. Component sizes, manufacturing cost, and fuel consumption were analyzed for a 2020 midsize car through the use of vehicle system simulation. These configurations represent current mass-production vehicles, including the Toyota Prius PHEV, Chevrolet Volt, and Honda Accord PHEV.

In addition, this study examined the impact of the transmission mechanical losses, and especially the planetary gear losses modelled using power split ratio analysis. The powertrain components were sized to meet AER, performance, and grade-capacity requirements. The impact of different driving behavior was analyzed through fuel consumption benefits and manufacturing cost. The PHEV system analysis in this study will provide insight into how PHEVs can be designed to support market introduction of a limited number of vehicle options to maximize market penetration.

Approach

To evaluate the fuel-efficiency benefits of advanced PHEVs, each vehicle was designed from the ground up on the basis of component assumptions. Each vehicle was sized to meet the same VTS, such as performance and gradeability. The energy consumption was then simulated using the different driving cycles. The vehicle costs were calculated from the components' characteristics (e.g., power, energy, weight).

To properly assess the benefits of future technologies, several options were considered, as shown in Figure V-153:

- One time frame: 2020 (U.S. Drive R&D portfolio)

- Five powertrain configurations for several AER vehicles: input split, parallel, series, series-output split, and series-parallel.
- A conventional vehicle as well as HEVs (parallel and split configuration) for reference.



Figure V-153: Vehicle configuration, AER, and risk levels considered

- Two engine technologies: VVT baseline versus variable valve lift (VVL) VVT turbo engine.
- Three risk levels: low, average, and high. These correspond, respectively, to 10% uncertainty, 50% uncertainty, and 90% uncertainty (aligned with aggressive technology advancement based on the DOE VTP. Hereafter, this uncertainty will be represented in the figures with an error bar.

Results

Series-Parallel PHEV (Honda Multi-Mode) Development

A series-parallel PHEV has two paths for engine output. One is a mechanical transmission path directly connected to a driveshaft, and the other is an electric transmission path through a generator. A representative example on the market of this system is the Honda Accord PHEV. Figure V-154 shows the configuration and operation modes of this system.

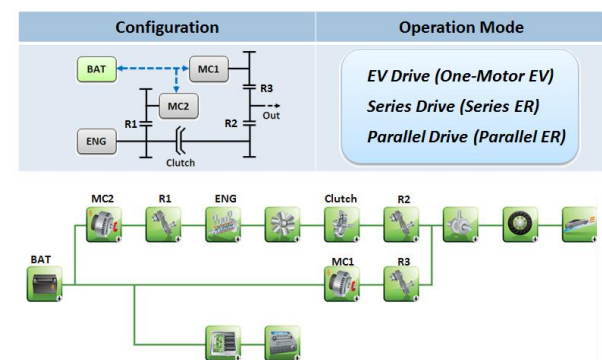


Figure V-154: Configuration of series-parallel system and vehicle model in Autonomie

This system can be operated in three operation modes. In "EV Drive," the traction motor which is physically connected to the drive shaft propels the vehicle by using the electric energy stored in the battery. In "Series Drive," the traction motor is driven by the power produced by the generator using the engine output. The battery is charged or discharged depending on its state-of-charge (SOC) and driver demand. In "Parallel Drive," the engine-drive clutch located between the engine and the wheels is engaged, and the vehicle is directly propelled by the engine. Fuel efficiency of all driving conditions is maximized by selecting these modes properly.

Supervisory Controller Development

The supervisory controller computes the torque demands or states of all actuators so that the vehicle fulfills the driver's demand safely and efficiently. The controller includes a rule-based energy management strategy that optimizes the energy source and controls the powertrain mode (EV/series/parallel), the battery SOC, as well as the torque split to meet the driver's request.

To understand when the series mode is the most beneficial, we compared the efficiency of both modes as a function of vehicle speed and output wheel torque. Efficiency here is defined as the ratio of mechanical power at the input of the wheel and engine fuel power.

Figure V-155 shows the efficiency for parallel and series modes, as well as their differences. Series mode will not be used for efficiency but only to alleviate the shortcomings of the parallel mode. The three main operating ranges are as follows:

- At low speed (<38 mph), series is the only possible mode because the engine speed would be below idle if operated in parallel mode.
- At high speed (>60 mph), the series mode is outperformed by the parallel mode both in terms of available power and efficiency; the parallel mode should be used.
- In between, the parallel mode should be used at low power demands to preserve efficiency.

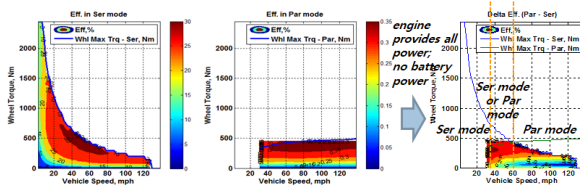


Figure V-155: Fuel-to-wheel efficiency in parallel mode, series mode, and difference of efficiency

Transient Controller Development

The operating logic was defined based on the operation modes of this system, and the low-level controller was also developed. The transient controller overwrites the torque and clutch demands when shifting from series to parallel mode, so that engine speed and final drive speed are synchronized before the clutch gets locked. Figure V-156 shows the vehicle speed, engine speed, and electric motor torque for shifting from series to parallel mode.

Simulation Results

The developed plant models and controllers were integrated into the series-parallel PHEV model. Vehicle speed, SOC transition, and component power in a highway driving cycle with the developed supervisory controller are shown in Figure V-157. Vehicle speed is indicated in three different colors: "EV Drive (green)," "Series Drive (blue)," and "Parallel Drive (gray)." Series drive is selected if strong acceleration is required, and EV drive is selected during slight acceleration or deceleration. As mentioned previously, intermittent operation between parallel and EV drive is performed during slight acceleration or cruise in a high speed situation.

Component Assumptions

Engine

Data for three different engines were used as reference in the study: gasoline port fuel injection (PFI) VVT, gasoline turbo VVT VVL, and gasoline Atkinson. The engines used for split, series, series-parallel, and series-split configuration are based on Atkinson cycles generated from test data collected at Argonne National Laboratory's (Argonne's) dynamometer testing facility [2].

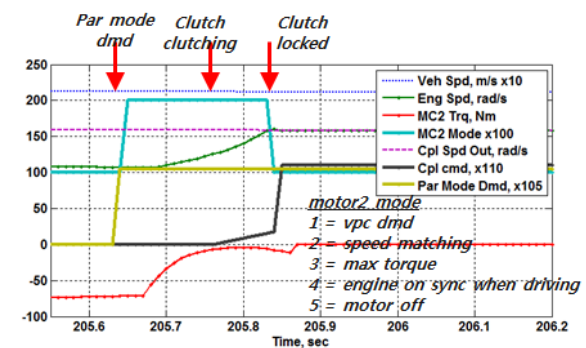


Figure V-156: Detailed component performances when shifting from series to parallel mode

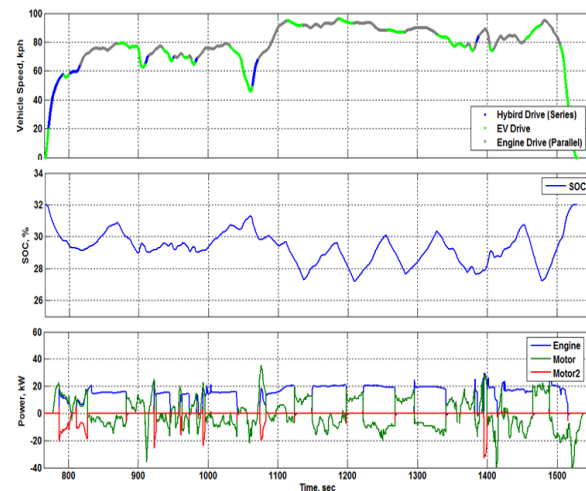


Figure V-157: Simulation results on the UDDS

Table IV-19 shows the peak efficiencies for the different technologies.

Table V-19: Engine Peak Efficiencies for Gasoline

| SI PFI | | | SI Atkinson | | |
|--------|------|------|-------------|------|------|
| High | Med | Low | High | Med | Low |
| 0.45 | 0.44 | 0.38 | 0.46 | 0.45 | 0.41 |

Electric Machine

Two different electric machines were used as references in the study:

- The split configurations use a permanent-magnet electric machine (similar to that used in the Toyota Camry [3]).
- The series-configuration and EVs use an induction electric machine.

Table V-20 shows the electric machine specific power and peak efficiencies, respectively.

Table V-20: Electric Machine Assumptions

| Specific Power, kg/W | | | Peak Efficiency, % | | |
|----------------------|------|------|--------------------|-----|-----|
| High | Med | Low | High | Med | Low |
| 1700 | 1600 | 1500 | 96 | 84 | 92 |

| System Cost, \$/kW | | | Charger Efficiency, % | | |
|--------------------|-----|-----|-----------------------|-----|-----|
| High | Med | Low | High | Med | Low |
| 7 | 10 | 13 | 98 | 95 | 92 |

Energy Storage

The battery used for the PHEV is a lithium-ion model from Argonne. Table V-21 shows the energy density and cost term for high energy application.

Table V-21: Battery Energy Density and Cost for High Energy Applications

| | Energy Density, Wh/kg | | | Cost Term, \$/kWh | | |
|----------|-----------------------|-----|-----|-------------------|-----|-----|
| | High | Med | Low | High | Med | Low |
| PHEVs 10 | 176 | 144 | 95 | 325 | 351 | 416 |
| PHEVs 40 | 220 | 180 | 120 | 250 | 270 | 320 |
| BEVs | 225 | 200 | 150 | 150 | 220 | 270 |

Vehicle

Light weighting, reductions in rolling resistance, frontal area, and drag coefficient have the potential to improve fuel consumption significantly, as these factors also lead to a reduction in the force required at the wheels (Table V-22).

Table V-22: Glider Weight, Aerodynamic, and Tire Assumptions

| Glider Weight, kg | | | Frontal Area, m2 | | |
|-------------------|-----|-----|------------------|-------|-------|
| High | Med | Low | High | Med | Low |
| 717.4 | 759 | 930 | 2.29 | 2.362 | 2.434 |

| Drag | | | Rrr | | |
|--------|-------|-------|-------|--------|-------|
| High | Med | Low | High | Med | Low |
| 0.2293 | 0.299 | 0.305 | 0.007 | 0.0075 | 0.008 |

Transmission Loss Modelling

Among the mechanical losses, three primary elements — gaset, clutch, and oil pump losses — are considered. The split configuration normally has two planetary gears; one as a power split device and one as a motor reduction gear. Series-split has one planetary gear and three clutch elements, and series-parallel has three spur gears and one clutch element. Detailed transmission models were developed by using SimDriveline, as shown in Figure V-158. Such a level of detail is necessary to properly assess the trade-off between complexity and efficiency.

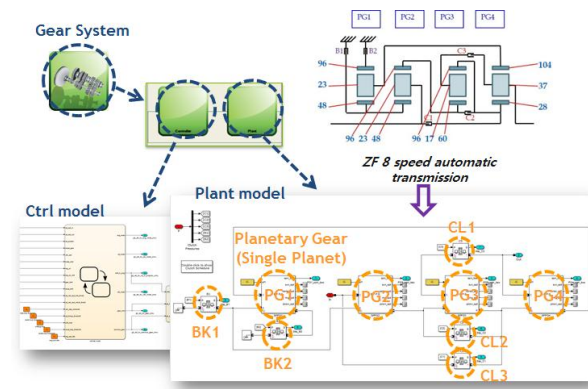


Figure V-158: Transmission loss modeling

Vehicle Technical Specifications

All the vehicles have been sized to meet the same requirements:

- Initial vehicle movement (IVM) to 60 mph in 9 s +/-0.1 s.
- Maximum grade of 6% at 65 mph at gross vehicle weight (GVW).

Several automated sizing algorithms were developed to provide a fair comparison among technologies. These algorithms are specific for each powertrain (i.e., conventional, blended type PHEVs, range-extender PHEVs) and application. The main assumptions for the sizing algorithms are:

- Engine sized to meet 70% of peak power required to meet VTS.
- Blended type PHEVs (split PHEV, par PHEV)
 - Battery energy sized to meet AER on UDDS based on unadjusted values.
 - Electric machine and battery powers sized to follow the UDDS in EV mode at low SOC (beginning of charge-sustaining [CS] mode).
- Range-extender PHEVs (ser PHEV, ser-par PHEV, ser-split PHEV)
 - Battery energy sized to meet AER on UDDS based on unadjusted values.
 - Electric machine and battery powers sized to be able to follow the US06 in EV mode at low SOC (beginning of CS mode).

Vehicle Sizing

This section describes the vehicle weight and manufacturing cost of the different vehicles after sizing. Figure V-159 shows the vehicle curb weight for all powertrains over different AERs. Split PHEVs have smaller weights across AERs. The weights of all PHEVs are higher than the conventional vehicles by 5% to 10% except for split PHEVs.

In Figure V-160, parallel PHEVs show the lowest total embedded power, whereas it shows the highest engine power for all of the powertrains. The component power is higher when the AER increases because components are sized based on acceleration and grade. Different PHEVs also vary from one another mainly due to a larger battery.

The electric machines used for the split and parallel configuration cases are sized to be able to follow the UDDS drive cycle in electric mode, while those used for the series, series-parallel, and series-split configuration cases allow the vehicles to follow the US06 drive cycle. It is important to note that during the simulations to estimate vehicle energy

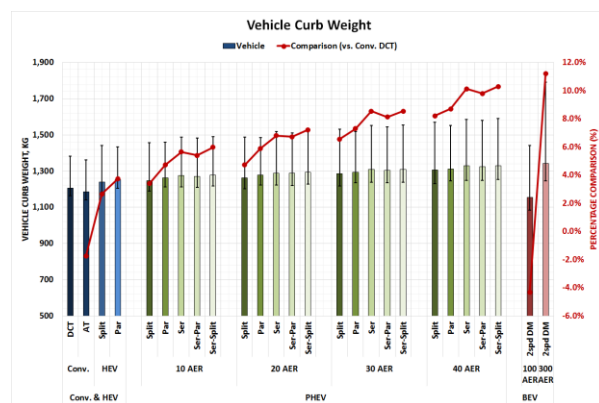


Figure V-159: Vehicle curb weight

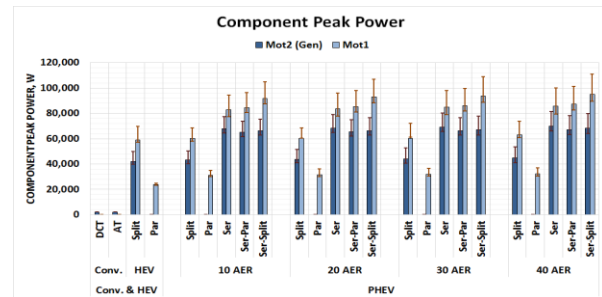
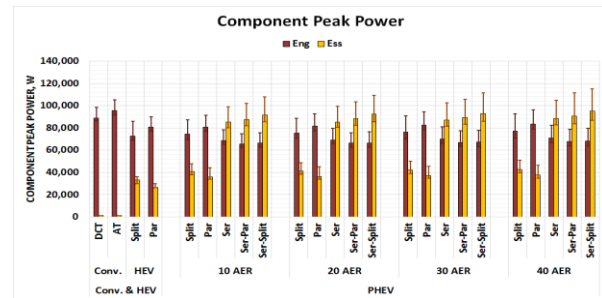


Figure V-160: Vehicle component power

consumption, the vehicles with a 10- and 20-mi AER have the ability to drive the UDDS cycle in blended mode.

Figure V-161 shows the vehicle manufacturing cost for all powertrains. Parallel PHEVs are cheaper than other configurations since they use only one electric machine and need relatively smaller battery power. The difference in cost compared with conventional vehicles increases with higher AER.

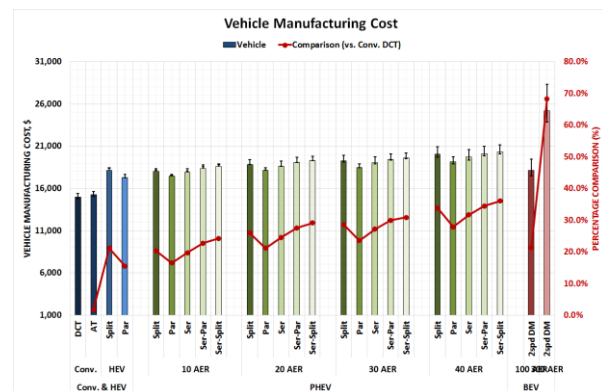


Figure V-161: Vehicle manufacturing cost

Energy Consumption Results

Charge-Sustaining Fuel Consumption Results

Figure V-162 shows the fuel consumption, in charge-sustaining mode, compared with the reference conventional vehicle for the combined procedure. One can see that most of the electric drive powertrains considered lead to fuel consumption reduction.

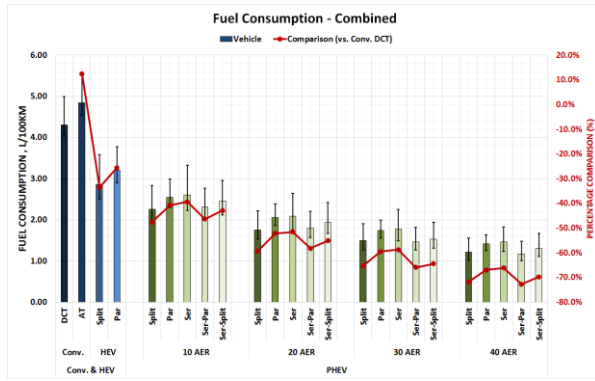


Figure V-162: Charge-sustaining fuel consumption – combined

Most of the powertrain configurations achieve a similar fuel consumption ratio, but split, series-parallel, and series-split PHEVs get more competitive as the AER increases due to simple or additional operation modes.

Results on U.S. Standard Procedures

Figure V-163 shows the fuel and electrical consumption for the different electric drive vehicles considered. Since the standard procedures do not provide a single energy value, both consumptions have been plotted on different axes.

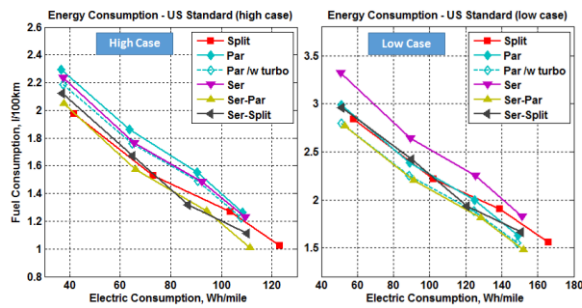


Figure V-163: Fuel and electricity consumption results on U.S. standards

The series-split PHEV and series-parallel PHEV configurations consistently demonstrate the highest powertrain efficiencies regardless of the AER considered. But the split PHEVs also show the advantage of a short AER. The series and parallel configurations provide close results for the high case. The series configuration, however, demonstrates significantly higher losses than any other configuration for the low case, due to the relatively low electric efficiency.

Figure V-164 shows the trade-offs of incremental manufacturing cost versus fuel consumption for PHEVs compared with the reference conventional gasoline vehicles. Overall, the vehicles on the bottom right would provide the best fuel consumption for the least additional cost. Parallel PHEVs are more likely to improve in cost than in fuel benefit,

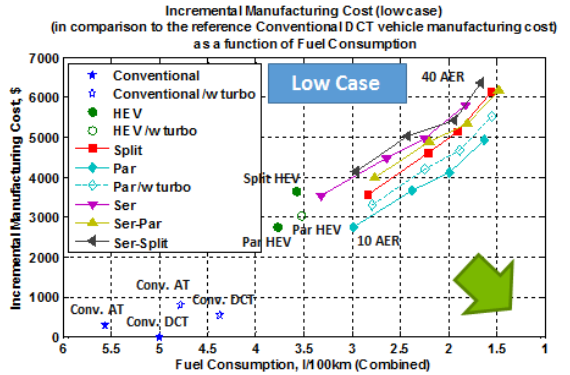
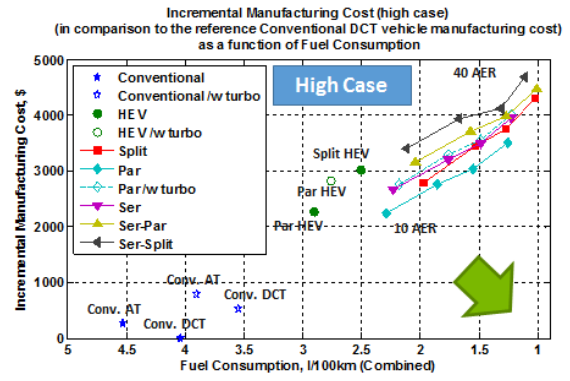


Figure V-164: Incremental manufacturing cost as a function of fuel consumption for all powertrains

whereas the higher the fuel consumption level, the more the improvement focuses on cost.

Results on Certified Cycles

Different cycles have been used to represent the fuel displacement potential of each powertrain configuration under different driving conditions. Figure V-165 shows the energy consumption for different cycles. Note that the consumption values significantly vary based on the type of trip compared with the standard drive cycle.

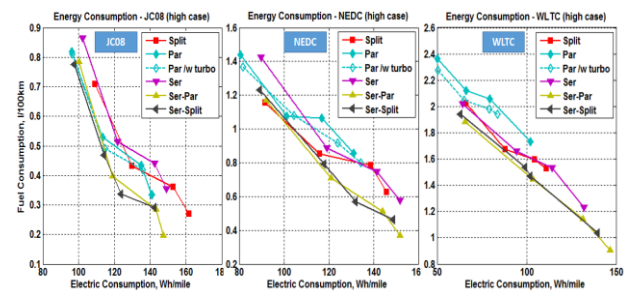


Figure V-165: Fuel and electricity consumption results on certified cycles

In the majority of cases, the series-parallel and series-split configurations consistently demonstrate the highest powertrain efficiencies regardless of the driving cycles. But split PHEVs have higher efficiency on NEDC and Worldwide harmonized Light vehicles Test Procedures (WLTC) cycles, and parallel PHEVs also have higher efficiency on the JC08 cycle for a short AER.

Conclusions

- A complete vehicle model similar to the Honda PHEV powertrain and control was developed in Autonomie. The mode selection rule was defined by maps computed using a brute-force algorithm.
- Five different PHEV powertrain configurations (input split, parallel, series, series-output split, and series-parallel) with four AERs were sized and simulated under different standards cycles.
- The uncertainty due to component technologies (i.e., engine) was evaluated.
- The energy consumption and cost of the different PHEV powertrain options was quantified for multiple driving cycles.
 - For long AERs, series-parallel and series-split PHEVs demonstrated the lowest energy consumption. For short AERs, split PHEVs also have an advantage on U.S. standards.
 - Parallel PHEVs achieve the lowest cost.
 - For low uncertainty, parallel PHEVs also have the lowest energy consumption for short AER on certified cycles.
 - A turbocharged engine leads to fuel consumption decrease for conventional and parallel PHEVs, but it leads to higher cost.

V.N.3. Products

Publications

1. Kim, N., Moawad, A., Shidore, N., and Rousseau, A., "Fuel Consumption and Cost Potential of Different Plug-in Hybrid Vehicle Architectures," 2015 Society for Automotive Engineers (SAE).

Tools and Data

1. Autonomie; available at www.autonomie.net.

References

1. Autonomie; available at www.autonomie.net.
2. Wallner, T., and Lohse-Busch, H., "Performance, Efficiency, and Emissions Evaluation of a Supercharged, Hydrogen-Powered, 4-Cylinder Engine," SAE paper 2007-01-0016, 2007.
3. Olszewski, M., *Evaluation of the 2007 Toyota Camry Hybrid Synergy Drive System*, Report for the U.S. Department of Energy, 2008.
4. Higuchi, H., and Shimada, H., "Efficiency Enhancement of a New Two-Motor Hybrid System," EVS27 Conference, 2013.
5. Kim, I., and Kim, H., "Configuration Analysis of Plug-in Hybrid Systems Using Global Optimization," EVS27 Conference, 2013.
6. Da Costa, A., et al., "Fuel Consumption Potential of Different Plug-in Hybrid Vehicle Architectures in the European and American Contexts," EVS26 Conference, 2012.

V.O. Vehicle Thermal System Model Development in MATLAB/Simulink

Principal Investigator: Jason A. Lustbader

National Renewable Energy Laboratory
15013 Denver West Parkway
Golden, CO 80401
Phone: (303) 275-4443
E-mail: Jason.Lustbader@nrel.gov

DOE Program Manager: David Anderson

Phone: (202) 287-5688
E-mail: David.Anderson@ee.doe.gov

DOE Program Manager: Lee Slezak

Phone: (202) 586-2335
E-mail: Lee.Slezak@ee.doe.gov

V.O.1. Abstract

Objectives

- Develop flexible, publicly available tools in MATLAB/Simulink for vehicle thermal systems modeling that can co-simulate with Autonomie and apply these tools with industry partners for research and development.
- Develop analysis tools to assess the impact of technologies that reduce thermal load, improve climate control efficiency, and reduce vehicle fuel consumption and range.
- Develop an open, accurate, and transient thermal system modeling framework using the MATLAB/Simulink environment for both standalone and co-simulation with Autonomie.

Major Accomplishments

- The National Renewable Energy Laboratory's (NREL's) CoolSim MATLAB/Simulink modeling framework was expanded for predicting physical processes in liquid coolant loops of vehicle thermal systems. This enables the simulation of state-of-the-art vehicle thermal management systems, including combined refrigerant and liquid coolant loop designs.
- The modeling method developed is very flexible. It is capable of predicting the flow rates of the coolant and the heat transfer rates in and out of the coolant in liquid coolant cooling systems of any practical complexity.
- Using component data from an industry partner, the combined loop thermal system model was applied to an experimental electric drive vehicle (EDV) thermal system test bench built at NREL. The model had the flexibility to simulate all five identified operating modes of the system.
- Predicted system parameters for 10 steady-state system operating points were compared to measurement data

obtained on an experimental test bench, and good agreement was found between them. The root mean square (RMS) error between predicted and measured coolant temperatures was found to be 1.62 K, and the RMS of the errors between predicted and measured heat exchanger capacities was found to be 8.1%.

- Both Distributed-Parameter and Mapped Performance heat exchanger models were implemented, allowing trade-offs between model accuracy and speed to be made.

Future Achievements

- Improve models, adding more detailed components, and validate to different systems. Apply tools to advanced light- and heavy-duty vehicle thermal management system research.
- Use models to identify design improvement opportunities and estimate the impact of advanced thermal management systems on vehicle performance, fuel use, and range.
- Update and improve integration with Autonomie.



V.O.2. Technical Discussion

Background

With improving vehicle efficiency, thermal systems are increasingly important for effective and efficient heavy- and light-duty vehicle design. Developing flexible and cost-effective tools to understand vehicle thermal trade-offs at the system level is critical to designing advanced electrified traction drive systems and their associated thermal controls.

When operated, the air conditioning (A/C) system is the largest auxiliary load on a vehicle. A/C loads account for more than 5% of the fuel used annually for light-duty vehicles in the United States [1]. Climate control loads can have an even larger impact on hybrid electric vehicle, plug-in hybrid electric vehicle, and electric vehicle performance. Hybrid electric vehicles have 22% lower fuel economy when the A/C is on [2]. For pure EDVs, the effect of the climate control can be even more severe. Due to the relative shortage of waste heat, heating the passenger cabin in electric vehicles is difficult. Cooling the cabin can take a high portion of the energy available in the battery, significantly reducing vehicle efficiency and range. Mitsubishi reports that the range of the i-MiEV can be reduced by as much as 50% on the Japan 10–15 cycle when the A/C is operating [3]. The advanced powertrain research facility at Argonne National Laboratory has reported a 59.3% and 53.7% reduction in range in max heating and max cooling, respectively, for the Ford Focus EDV operating on the UDDS cycle [4]. In addition to these climate control

impacts, EDVs may have additional cooling requirements for the electric traction drive system components, including batteries, power electronics, and electric machines.

Therefore, compared to internal combustion engine-driven vehicles, different heating methods and more efficient cooling methods are needed for hybrids and EDVs. These methods often involve running the A/C system in heat pump mode for sufficient heating of the cabin. In some advanced concepts, the traditional liquid coolant based thermal management is supplemented with the refrigerant based cooling system, which can make the thermal management system more complex. When developing an internal combustion engine vehicle thermal management system, it has traditionally been sufficient to run models of the A/C system and the liquid coolant based cooling system separately. For advanced vehicles, especially for hybrid and electric vehicles, the interconnectedness of the thermal systems requires a more integrated simulation approach.

The more complex thermal management systems of advanced vehicles typically allow for various alternative modes of operation that can be selected based on driving and ambient conditions. Investigating a number of system alternatives and determining the best ranges for the various operating modes with experimental methods can be very time consuming. A good system simulation tool can greatly reduce the time and expense spent developing these complex systems. A simulation model should also be able to efficiently co-simulate with vehicle simulation programs, and it should be well-suited for evaluating various control algorithms. The MATLAB/Simulink dynamic system simulation environment is well suited for such system simulation models, because it is widely used in the automotive industry and effectively meets these criteria.

Introduction

To meet the needs of advanced vehicle thermal system simulation, NREL is building on previously developed Simulink A/C models, adding liquid coolant loops to enable integrated system simulation. Simulink is a common engineering platform that allows for co-simulation with Autonomie [5]. NREL previously developed CoolSim, an A/C system simulation modeling framework in MATLAB/Simulink, and validated its performance against test bench data. To match the wide range of A/C modeling needs, NREL developed models with three different levels of detail: the Fully-Detailed, Quasi-Transient, and Mapped-Component, illustrated in Figure V-166.

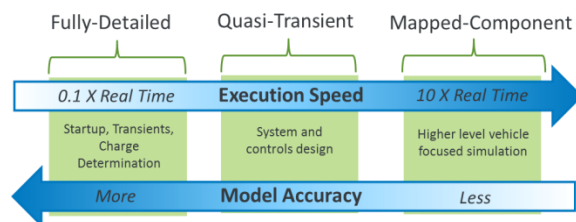


Figure V-166: Available A/C system simulation versions

In the trade-off of speed and accuracy, the three models occupy very different parts of the scale and meet a wide range of modeling needs. The Fully-Detailed model captures the detailed system transient behavior but runs at 0.1 real-time speed [6]. The Quasi-Transient and Mapped-Component models make progressively more simplifications while trying to maintain accuracy and run at real-time speed and greater than 10 times real-time speed, respectively [7]. The goal of these new model versions was to provide faster simulation tools for less-detailed, vehicle-focused, drive-cycle based evaluation of A/C systems. For steady state conditions, the Quasi-Transient model provides essentially the same accuracy as the Fully-Detailed model. The Mapped-Component model does lose some accuracy in steady-state conditions. For the SC03 cycle, the averaged results of power and heat exchange rates obtained with the Quasi-Transient model are within 3% of the results of the Fully-Detailed model. The Mapped-Component model results are within 15% of the results of the Fully-Detailed model. Short transients, such as those occurring during compressor cycling, produce the most deviation from the Fully-Detailed model for both simplified models. Conversion from one A/C system model approach to another (Fully-Transient, Quasi-Transient, and Mapped-Component) is relatively simple. This allows a new system model to be developed in a faster version before the results are refined using a slower, more detailed solution method as needed.

As outlined in the Background section, there is a need for full thermal system simulation due to the interconnectedness of the refrigerant and liquid coolant circuits utilized in advanced thermal management systems, especially for electric vehicles; therefore, in FY 2014, NREL's refrigerant-circuit simulation model was extended with liquid-coolant-circuit simulation capability. The Quasi-Transient and Mapped-Component model versions of the A/C system simulation work were used as the basis of the extension, because they are the best fit in terms of model execution speed and accuracy. The new model was applied to an experimental advanced electric vehicle thermal management system. A comparison of simulated results to measured data validated this particular system model and also the modeling methodology in general.

Approach

Liquid Coolant Circuit Model Methodology

Solving the single-phase liquid coolant circuit model requires determining the coolant flow through the various branches in the system and the heat transfer of the components.

Solving for liquid coolant flow rates in the system

A lot of processes in the liquid coolant part of the thermal management system take place over minutes and longer time periods. Therefore, it is important that the simulation model is able to run at least in real-time speed or faster. The two-phase refrigerant circuit model is already difficult to keep at such speed; therefore, it is important that the liquid coolant simulation run as fast as possible on its own so that, together, the full system model has adequate speed. Pressure wave line dynamics are not important in the liquid coolant flow; therefore an incompressible flow formulation was selected.

This allows for a larger simulation time step. The Mapped-Component refrigerant circuit simulation can also use this larger time step. In Simulink, it is difficult to have two parts of the model run at different simulation time steps; therefore, it makes sense to have the two model formulations be optimal with approximately the same time steps.

During the development of a thermal system, various options for system design and operating modes may be investigated; therefore, providing model flexibility is important. To achieve this coolant circuit flexibility, the liquid coolant fluid of the thermal system was modeled as a generic fluid network with loops and branches in which the flow rates are determined by the pressure changes (losses and rises) through various components (e.g., transport lines, heat exchangers, valves, pump) in the system (Figure V-167).

To solve for the flows in a complex fluid network, there are two main sets of equations to consider: nodal continuity and loop equations. One continuity equation is written for each node that states that the sum of the incoming flow rates should equal zero. For each fluid loop, an equation is written that states that the sum of pressure changes in each branch around the fluid loop should equal zero. These equations are analogous to the Kirchhoff laws for electric circuit theory, in which they are written for the total incoming current in the nodes and for the sum of electric potential drop around conductor loops. The unknowns are the flow rates in the branches. To have the right number of equations, the numbers of loops needed is determined according to certain rules. To be able to solve for the branch flows, the loops have to be selected such that the loop equations are independent. One way to achieve this is to be sure each loop has at least one branch that belongs to only that one loop. There is still some freedom in how to select the loops, and it makes sense to select them according to how the system is intended to work.

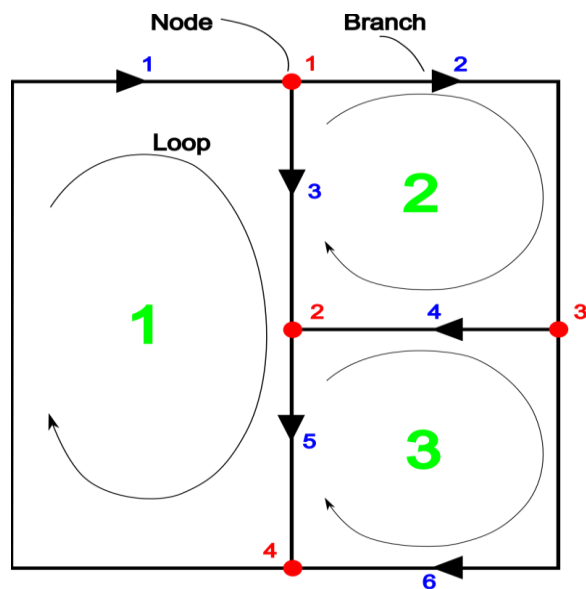


Figure V-167. Fluid network example—green marker: loops; red marker: nodes; blue marker: branches

After a valid set of independent flow loops is defined, the flow rates in the branches can be written as a superposition of the flow rates in the loops. Note that with this method the

nodal continuity equations are automatically satisfied, and we reduced the number of unknowns in the system from the number of branches to the number of loops. The number of equations equals the number of unknowns, and the system can be solved.

The numerical process can be summarized as follows: assume a flow rate for each loop; calculate the branch flow rates from the loop flow rates with consideration of which loops each branch is a part of, then calculate the loop pressure drops, which are the total of the branch pressure drops around each loop. If these loop pressure drops are not all zero within a small error, then iterate on the loop flow rates until they are. This process is summarized in Figure V-168 using the notations from Figure V-167.

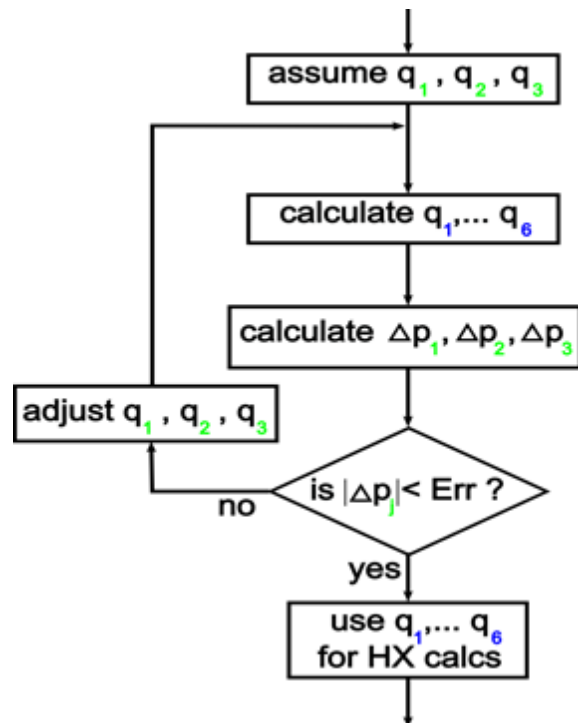


Figure V-168. Coolant flow rate calculation flow chart

The iteration can be done to convergence within one simulation time step; therefore, the accurate flow rates can be obtained in each time step. However, in order to increase execution speed, only the first iteration of this flow rate calculation process is executed at each time step. If boundary conditions on the system change slowly (over a second or longer), the flow rates will approach the accurate flow rates quite well within a few simulation time steps, and the overall error over time will be small. The advantage in model execution speed, however, is quite significant.

When modeling the loops, it is important to consider what happens when valves close. The best way to structure the loop network is to ensure that a branch with a valve in it is part of a single loop only; then, when the valve is closed, the flow rate in that loop does not have to be solved for, it can simply be set to zero. This will then result in zero flow through the valve.

Solving for component heat transfer rates in the liquid coolant based system

Because most heat transfer occurs in heat exchangers, the focus of this section is on the heat exchanger models. Other system components, such as transport lines, however, can be treated similarly. For the heat exchanger models, two levels of detail are available: Distributed-Parameter and Mapped models. The Distributed-Parameter model provides more detail and flexibility; whereas the Mapped model provides faster execution time.

Distributed-Parameter component models

The Distributed-Parameter modeling method is described here with an example of a two-pass liquid coolant radiator. Figure V-169 shows how this radiator is represented in such a model. The flow of coolant and the air flow across each of the flat tubes in a pass are assumed identical; therefore, the total coolant mass flow rate is divided by the number of flat tubes in the passes, and the flow in only one flat tube in each pass is calculated using that flow rate. In other words, all flat tubes in one of the radiator passes are represented by only one “liquid-coolant line with heat transfer” simulation block, and all flat tubes in the other radiator pass are represented by another simulation block of the same type. The total heat transfer rate is then the sum of the heat transfer rates in the two passes; each is the number of flat tubes in the pass times the heat transfer rate in just one tube of the pass.

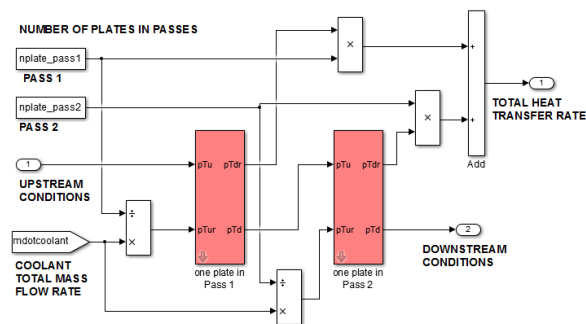


Figure V-169. Distributed-Parameter model example for two-pass liquid coolant heat exchanger

In the “liquid coolant line with heat transfer” simulation block, the tube is split into a number of segments. In each segment, the coolant flow parameters, air flow parameters, wall temperature, and heat transfer rates are calculated individually with a “marching” scheme starting from the inflow boundary. Because this is a cross-flow heat exchanger, the air inflow parameters are the same on all segments. The coolant mass flow rate is also the same in all segments, because the steady-state flow rate of an incompressible liquid is assumed. The heat transfer rates, wall temperature, coolant-in temperature, and coolant-out temperature, however, will be different for each segment. The effectiveness–number of transfer units (E-NTU) method is used for each segment [8]. The Chang correlation [9] for heat transfer coefficient on louvered fins is used on the air flow side, and the Dittus-Boelter correlation [8] is used on the internal liquid coolant side. The coefficients used in these correlations are typically adjusted in a calibration process.

Mapped component models

To increase the speed of model execution for long simulations, the Distributed-Parameter model can be used to generate a Mapped model. The process is similar to the one applied for generating the Mapped-Component A/C system model using the Quasi-Transient A/C system simulation model [7]. The steps in this mapping process are as follows. First, create a Distributed-Parameter model of the heat exchanger with sufficient detail. Next, calibrate this model with available experimental data for a reasonably large set of measurement points. Then, map out the heat transfer rate over the entire operating range of the component. Implement this map into a lookup table in the thermal system management simulation model so that the heat exchange rate can be determined for any air and coolant inflow conditions over the entire operating range. Finally, use the inflow conditions and the heat exchange rate to determine the air and coolant outflow conditions for the heat exchanger.

Application of Model for Combined Cooling Loops, Integrated Thermal Management

NREL’s combined fluid loop (CFL) EDV thermal management system test bench, shown in Figure V-170, was selected for the validation and demonstration of the modeling method. This test bench allows for testing a wide range of advanced A/C, heat pump, and cooling loop configurations [10].

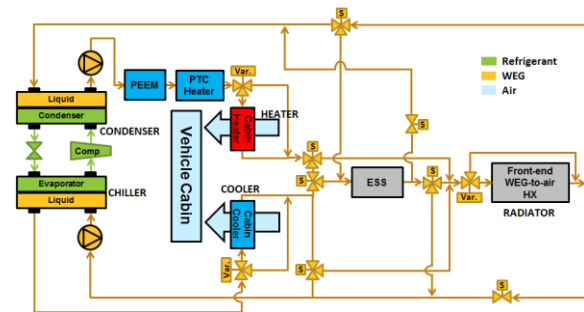


Figure V-170. Schematic of NREL’s CFL EDV Thermal Management System

In this system, a refrigerant circuit operating on the vapor compression cycle is used as both an A/C unit (providing cooling) and as a heat pump (providing heating). The refrigerant loop heat exchange is with the liquid coolant in the chiller and in the condenser. The liquid coolant is used to provide cooling and heating to the cabin. With proper setting of the valves, various modes of operation can be achieved. For example, the system can be reduced to Active Heating (Figure V-171) and Active Cooling (Figure V-172). Passive cooling and heating is also available when the refrigerant compressor is not operating and there is no refrigerant flow through the system. Further details about this system are described in a separate report [10].

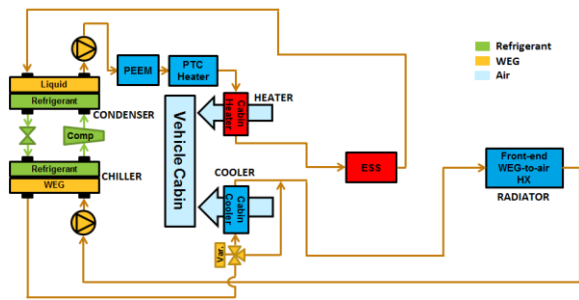


Figure V-171. CFL active heating mode

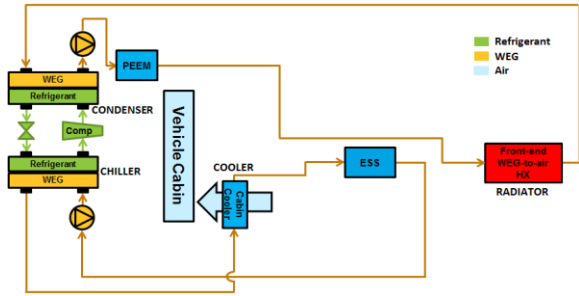


Figure V-172. CFL active cooling mode

Figure V-173 shows the top level of the Simulink model that represents the above system. Note that the entire refrigerant circuit is incorporated into one subsystem model. This subsystem is essentially the same as the Quasi-Transient A/C system model from previous work [7], except that the evaporator and condenser have been modified to now use liquid coolant instead of air for heat transfer in and out of the refrigerant. Therefore, the refrigerant-to-liquid evaporator is now called a chiller.

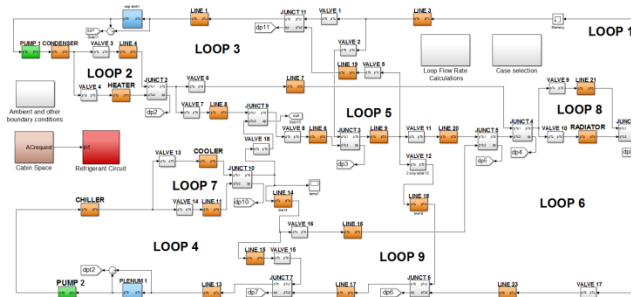


Figure V-173. Top-level view of the Simulink model of the CFL system

This simulation model can be used to predict processes in the experimental system for any combination of valve settings. The way the coolant loops were selected is shown in Figure V-174. The activated loops for the active heating mode are shown in Figure V-175, and the activated loops for the active cooling mode are shown in Figure V-176.

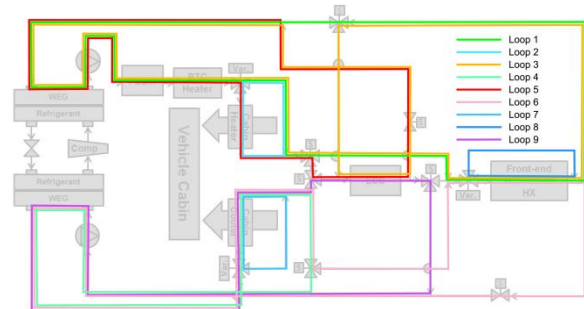


Figure V-174. Selected coolant loops for modeling purposes

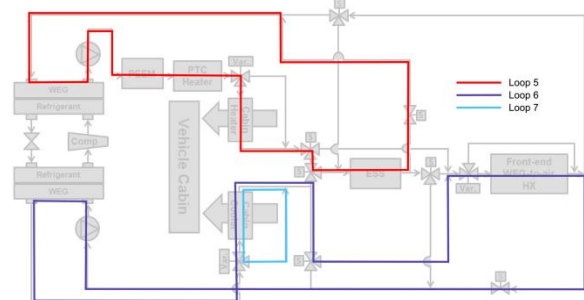


Figure V-175. Activated loops for active heating mode

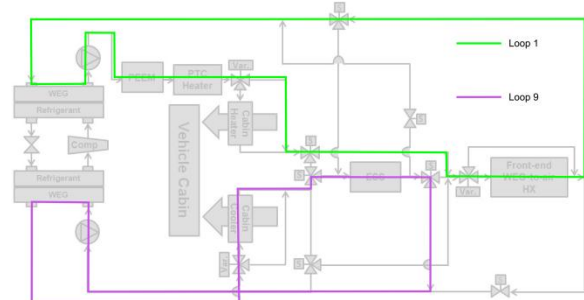


Figure V-176. Activated loops for active cooling mode

Component information was provided by Delphi Automotive Systems, Halla-Visteon Climate Control, and measurements for 10 different system operating conditions were conducted at NREL [10]. Component models were built and a calibration process for all heat exchangers was carried out using this data. For calibration of the refrigerant-based heat exchangers, that is the chiller and the condenser, the appropriate component models from the Quasi-Transient A/C system sub-model were used. As an example, the result of the calibration for the chiller is shown in Figure V-177.

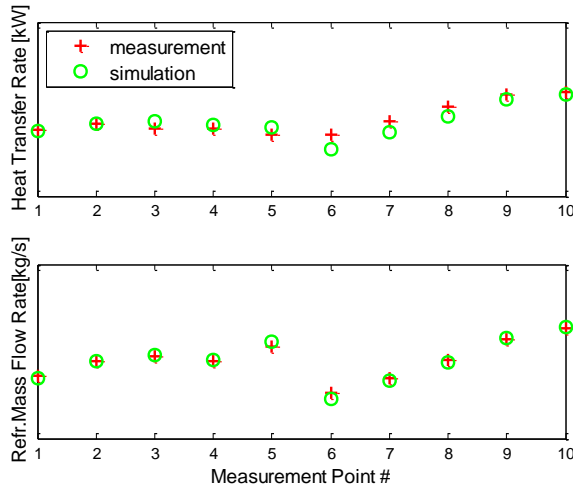


Figure V-177. Calibration results for the chiller model

On all three liquid-coolant-based heat exchangers in the system, Distributed-Parameter component models of the heat exchangers were created and calibrated. As an example, the result of this calibration for the radiator is shown in Figure V-178.

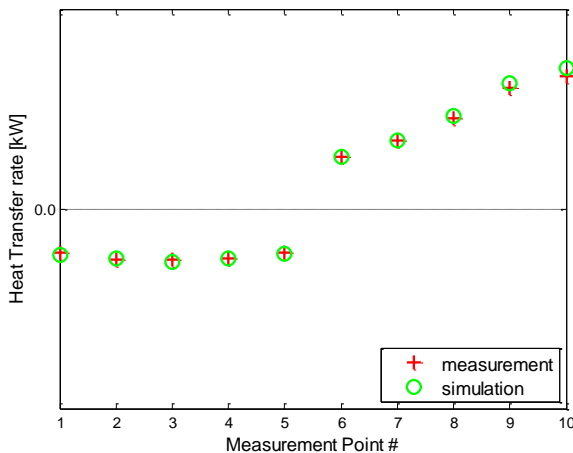


Figure V-178. Heat transfer calibration for the radiator

The calibrated Distributed-Parameter models of the liquid-coolant-based heat exchangers in the system were then used to generate maps of heat exchanger performance. These maps are four-dimensional, and they use the inlet liquid coolant mass flow rate and temperature and the air mass flow rate and temperature as the input parameters (Figure V-179). Note that instead of heat transfer rate, the effectiveness values calculated from the heat transfer rates and thermal mass flows were used for the lookup table, because it was believed that the interpolation between and possible extrapolation beyond the grid points would be more accurate by doing so.

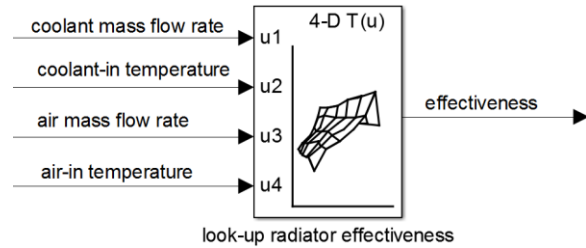


Figure V-179. Simulink lookup function (with labels) for obtaining the effectiveness of the radiator

These lookup tables were then used in the Mapped model, as shown in Figure V-180, for the example of the radiator.

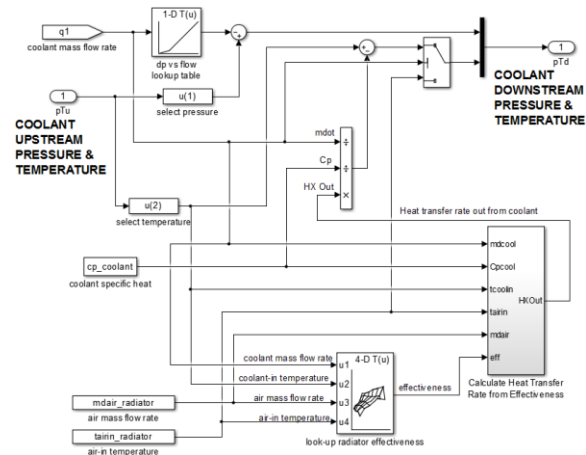


Figure V-180. Radiator Mapped Component model

Results

Steady-state results for the CFL system in active heating and active cooling modes (Figure V-171 and Figure V-172) were available from NREL’s experimental test bench [10]. The ambient temperature of the system was swept between -2°C and $+43^{\circ}\text{C}$. A total of five points were below an ambient of 20°C , for which the active heating mode was used. Another five points were above the 20°C ambient, for which the active cooling method was used. The simulated data compared to the measured data was plotted as a function of the ambient temperature. The predicted and measured refrigerant flow rates for all measurement points are shown in Figure V-181. Note that the measured data for 18°C , Point 5, is an outlier. It is believed this data point is erroneous. The RMS error for refrigerant mass flow rate is 7.0% for the remaining 9 data points. The capacities of the condenser and chiller, the refrigerant-to-liquid coolant heat exchangers, are shown in Figure V-182. The RMS error for these capacities is 4.3%. Note the drop-off of the capacities for heating as the ambient temperature increases above 8°C (points 3–5). This behavior is caused by the controller reducing the compressor RPM to avoid exceeding the system maximum refrigerant pressure limit. The capacities of the liquid coolant heat exchangers are shown in Figure V-183. Note that the actual heat transfer rate on the radiator changes sign when the operating mode is switched from heating to cooling. When active heating mode is

used, the radiator accepts heat from the ambient; and when active cooling mode is used, the radiator rejects heat to the ambient. The RMS of errors for the heat exchange rates in the liquid coolant just upstream of the heat exchangers is 3.6%. The coolant temperatures just upstream of the heat exchangers are shown in Figure V-184. The RMS of the errors is 1.20 K. The RMS values of errors indicate that the simulated results match the measured ones well.

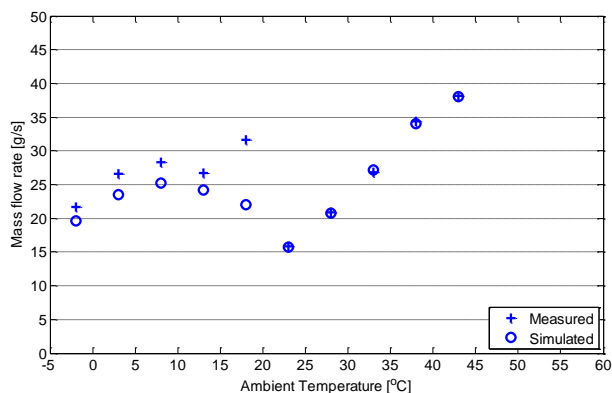


Figure V-181. System refrigerant mass flow rates

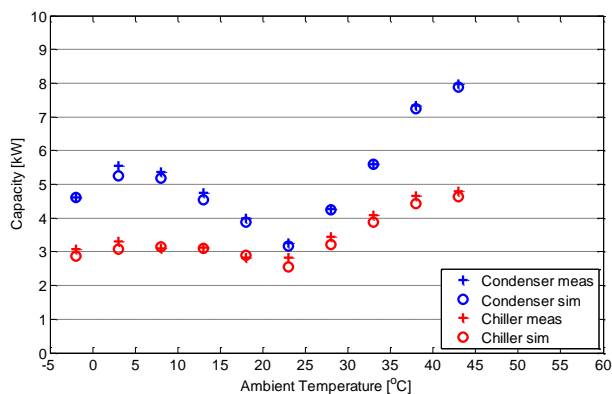


Figure V-182. Capacities of chiller and condenser

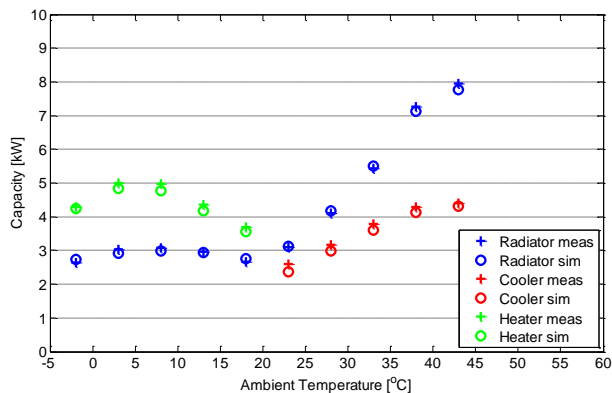


Figure V-183. Capacities of liquid-coolant-based heat exchangers

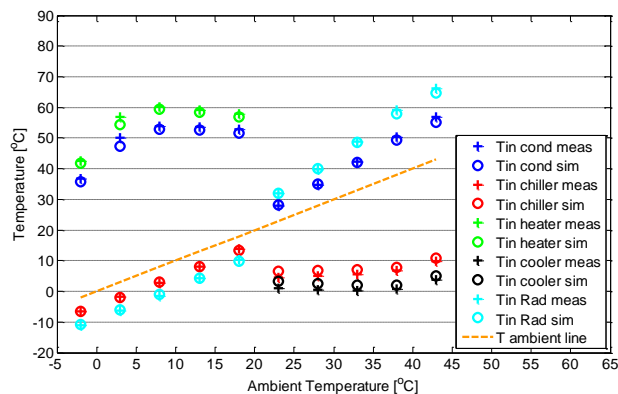


Figure V-184. Coolant temperatures just upstream of heat exchangers

Conclusions

NREL's MATLAB/Simulink A/C modeling tool set, CoolSim, was extended to incorporate the simulation of liquid coolant subsystems. This enables the simulation of an entire electric vehicle thermal management system. This new modeling methodology is especially useful for the simulation of thermal management systems in which the refrigerant and liquid-coolant-based thermal subsystems can be highly influenced by one another, such as in advanced hybrid and electric vehicles.

The new simulation capabilities were applied to an advanced combined cooling loop electric vehicle thermal management system concept. Predicted system parameters for 10 steady-state system operating points were compared to measurement data obtained on an experimental test bench, and good agreement was found between them. The RMS error between predicted and measured coolant temperatures was found to be 1.62 K, and the RMS of the errors between predicted and measured heat exchanger capacities was found to be 8.1.

The CoolSim model can be an effective tool to evaluate the various operating modes possible for complex thermal management systems, thereby aiding the pairing of the most effective and efficient operating mode to any given driving and ambient conditions.

References

1. Rugh et al. Earth Technologies Forum and Mobile Air Conditioning Summit. 2004.
2. Francfort, J.; Murphy, T. "Operational and Fleet Testing, A. Hybrid Electric Vehicle Testing." Chapter V. *Advanced Vehicle Technology Analysis and Evaluation Activities: FY 2007 Annual Report*. Washington, D.C.: Vehicle Technologies Program, U.S. Department of Energy, 2007; p. 145.
3. Umezu et al. SAE Automotive Refrigerant and System Efficiency Symposium. 2010.
4. Rask, E. et al. "Ford Focus BEV In-depth (Level 2) Testing and Analysis." Presentation. DOE Annual Merit Review. 2014.
5. "Autonomie." www.autonomie.org.

6. Kiss, T.; Chaney, L.; Meyer, J. "A New Automotive Air Conditioning System Simulation Tool Developed in MATLAB/Simulink." *SAE International Journal of Passenger Cars—Mechanical Systems* 6(2), 2013; doi:10.4271/2013-01-0850.
7. Kiss, T.; Lustbader, J. "Comparison of the Accuracy and Speed of Transient Mobile A/C System Simulation Models." *SAE International Journal of Passenger Cars—Mechanical Systems* (7), August 2014; pp. 739–754; doi:10.4271/2014-01-0669.
8. Incropera, F.P.; DeWitt, D.P. "Fundamentals of Heat and Mass Transfer." 2nd edition. New York: John Wiley and Sons, Inc., 1985.
9. Chang, Y.J.; Wang, C.C. "A Generalized Heat Transfer Correlation for Louver Fin Geometry." *International Journal of Heat Mass Transfer* (40:3), 1997; pp. 533–544.
10. Leighton, D.; Rugh, J. "Electric Drive Vehicle Range Improvement Using a Combined Fluid Loop Thermal Management Strategy." Presentation. SAE Thermal Management Systems Symposium, Sept. 22–24, 2014, Denver, CO.
2. Kiss, T.; Lustbader, J. "Development of a New Vehicle Thermal System Simulation Tool for MATLAB/Simulink." Presentation. SAE Thermal Management Systems Symposium. Sept. 22–24, 2014, Denver, CO; 14TMSS-0079.
3. Kiss, T.; Lustbader, J. "Vehicle Thermal System Modeling in Simulink." Poster. DOE Annual Merit Review, April 6, 2014; VSS134.

Tools and Data

1. CoolSim v84, thermal system modeling tool for MATLAB/Simulink environment

Acknowledgements

1. Coauthor Tibor Kiss (NREL)
2. Additional thanks to John Rugh and Lisa Fedorka (NREL)
3. Special thanks to our partners Delphi Automotive Systems, Halla-Visteon Climate Control, Daimler Trucks, and Argonne National Laboratory

V.O.3. Products

Publications

1. Kiss, T.; Lustbader, J. "Comparison of the Accuracy and Speed of Transient Mobile A/C System Simulation Models." *SAE International Journal of Passenger Cars—Mechanical Systems* (7), August 2014 7; pp. 739–754; doi:10.4271/2014-01-0669.

V.P. Advanced Transmission Impact on Fuel Displacement

Principal Investigator: Namdoo Kim

Argonne National Laboratory
9700 South Cass Avenue, Building 362
Lemont, IL 60439
Phone: (630) 252–2843
E-mail: nkim@anl.gov

DOE Program Manager: David Anderson

Phone: (202) 287–5688
E-mail: David.Anderson@ee.doe.gov

V.P.1. Abstract

Objectives

- The objective is to update current transmission models and shifting algorithms as well as develop new ones to represent state-of-the-art technologies.
 - In FY 2013, Argonne developed and validated new model and control algorithms for advanced transmissions (8+-speed automatic transmission and dual-clutch transmission (DCT) for conventional vehicles). The objective in FY 2014 was to develop DCTs for hybrid electric vehicles (HEVs) and continuously variable transmissions (CVTs).
 - Validated models will be used to evaluate Vehicle Technologies Office (VTO) benefits and guide future R&D.
 - The project will provide a solid foundation for assessing the impact of advanced transmissions on component requirements (power, energy, etc.) and operating conditions as well as vehicle energy consumption, performance and cost.
 - Control algorithms and component models will be included in future Autonomie releases.

Major Accomplishments

- Developed plant model and low-level controller for a DCT in Simulink, based on the original system schematic.
- Validated the conventional vehicle and HEV with the DCT model, using test data from the Argonne Advanced Powertrain Research Facility.
- Produced a model for a vehicle with a metal V-belt CVT. This model consists of a mechanical and hydraulic control system, a drive train, and the gear ratio dynamics
- Developed and integrated the low-level controller to define the operating mode on the basis of the principle of CVT operation.
- Developed vehicle models for the Nissan Altima conventional vehicle with CVT and the Honda Civic HEV

with CVT. Validated the vehicle models with test results in Autonomie.

- Integrated the generic vehicle model and controller into the Autonomie R14 release.

Future Achievements

- Assess the impact of advanced transmissions and accurate evaluation of VTO benefits and targets to guide future R&D.
- Develop transmission selection (gear selection, gear spread, final drive ratio, etc.) for specific component technologies and powertrain configurations.
- Evaluate the impact of emissions on gear shifting optimization using engine in the loop.



V.P.2. Technical Discussion

Background

As a result of more stringent regulations and customer expectations, auto manufacturers have considered numerous technology options to improve vehicle fuel economy. One example is transmission technology, since transmission improvements are one of the most cost-effective options. Over the past few years, transmissions have evolved significantly and have impacted both performance and fuel efficiency. This study validates the shifting control of advanced transmission technologies in a vehicle systems context by using Autonomie.

Introduction

Transmission innovations are one of the most cost-effective ways to reduce vehicle energy consumption. Various types have been introduced in the marketplace, such as the 8+-speed automatic transmission, dual-clutch transmission (DCT), continuously variable transmission (CVT), and power split type transmission. Among these, DCTs provide reduced shift shocks and better driver comfort compared to manual transmissions, in addition to higher top speeds and torques. CVTs are also known to have many advantages, providing optimal engine operation with high thermal efficiency regardless of the vehicle speed.

In this study, the DCT model and the shifting algorithm are validated using Argonne Advanced Powertrain Research Facility (APRF) test data from a conventional Volkswagen Jetta TDI vehicle with a 6-speed DCT and a Jetta HEV with a 7-speed DCT. New CVT plant and control models have been developed to replace the legacy CVT models.

The CVT model was developed by considering hydraulic and mechanical loss. The hydraulic loss constitutes the majority of the total loss at low vehicle speeds, while the mechanical loss is the main source of inefficiencies at high speeds. In addition, CVT ratio control and clamping force control strategies, including the CVT shift dynamics, were developed. By analyzing the vehicle test results, the engine optimal operating line (OOL) was constructed for the two vehicles on the basis of the engine brake-specific fuel consumption. The battery state-of-charge (SOC) range and battery characteristics (i.e., maximum charging and discharging power) were investigated. Using the analysis results, vehicle operation control strategies were developed for acceleration, cruising, deceleration and idling modes. Control algorithms were also developed for each vehicle operation mode. Finally, the shifting control algorithms were verified by comparing the simulation results with the test results for several certificated cycles.

Approach

The project workflow is shown in Figure V-185. This study leverages numerous vehicle test data collected at the APRF (i.e., fuel economy or time from 0 to 60 mph, based on several signals). With the results obtained from various driving schedules with several types of transmissions, we analyzed the advanced powertrain system. We also developed and validated the advanced transmission model and shifting algorithm in Autonomie.

Results

Development of Dual Clutch Transmission Controller for HEVs

A model of a DCT was developed in Simulink on the basis of the original system schematic and a bibliographic search. Figure V-186 shows a schematic diagram of the DCT model. The powertrain is based on a parallel hybrid drive, which is the type used in the Volkswagen Jetta HEV. The electric machine, clutch and flywheel are a single hybrid component. The electric machine is located between the internal combustion engine and transmission. The parallel hybrid powertrain with DCT enables full hybrid functionality.

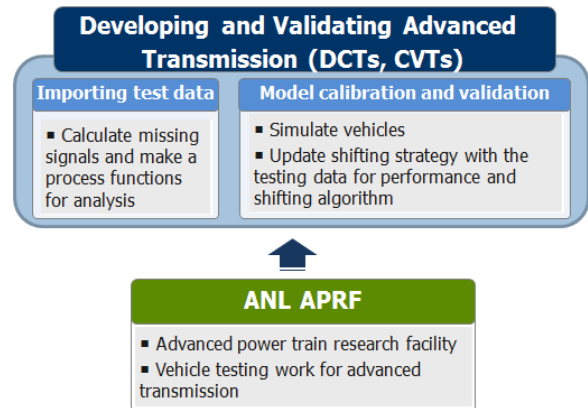


Figure V-185: Study process for developing advanced transmission models and shifting algorithm

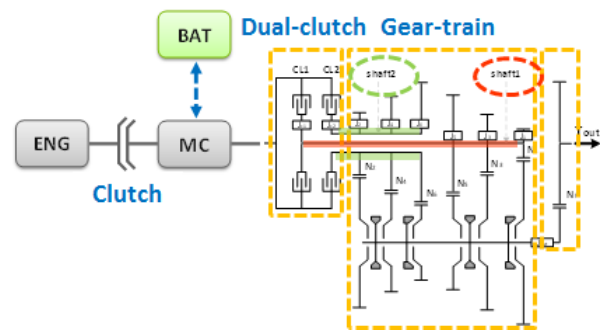


Figure V-186: Schematic of DCT powertrain for HEVs

DCT Controller Development

The operating logic was defined on the basis of the principle of DCT operation, and a low-level controller was also developed. This gearbox transient block coordinates all components during transient phases, as shown in Figure V-187.

The component modes (i.e., engine mode, clutch mode, and electric motor mode) and signals of gear demand (odd/even) are generated when a gear shift is required or the engine turns on. The gear selection control (synchronizer control) algorithm is unique to DCT systems. Once the gearshift schedule algorithm generates a new desired gear command, the gear selection control algorithm controls the synchronizer actuators to pre-select the desired gear.

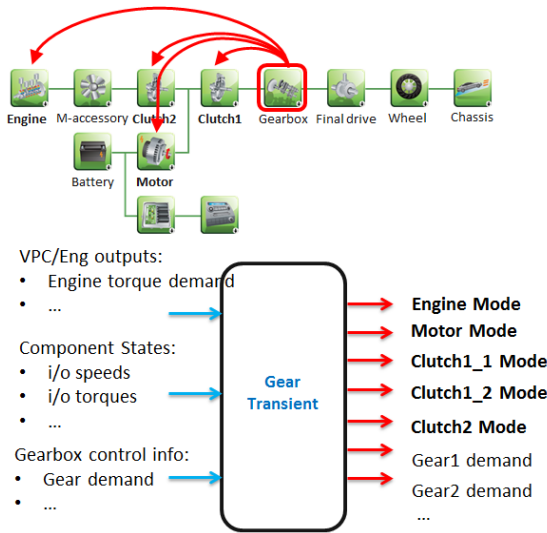


Figure V-187: DCT controller development for HEVs

Simulation Results

A parallel HEV with a DCT was built and simulated to demonstrate proper behavior. The vehicle speed, engine speed, and electric motor torque for the engine start-up are compared with the vehicle test results for $t=21-24$ s in Figure V-188. The single clutch (CPL2) is located inside the electric machine, between the engine and the electric machine. The clutch is engaged when starting the internal combustion engine.

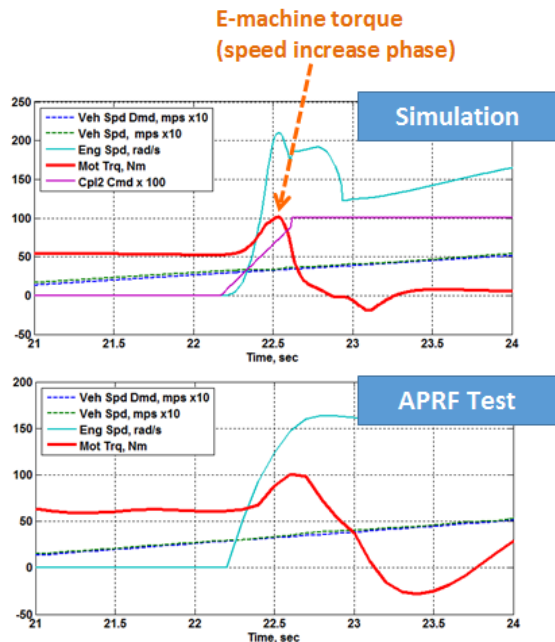


Figure V-188: Detailed component performance for the DCT

The electric machine torque is also controlled to quickly synchronize the clutch input and output speed. The controller reacts by setting a torque-increasing intervention that is added to the torque of the electric machine in the speed increase phase.

DCT Validation Results

Two DCT vehicles (2013 Volkswagen Jetta TDI conventional vehicle and HEV) with the above-mentioned model and controller for the DCT were simulated and validated with test data.

Vehicle Model in Autonomie

Autonomie provides reliable component models that have been validated from a number of testing results, and so our approach is to load the necessary components, build the DCT vehicles, and apply the shifting logic in the vehicles (Figure V-189).

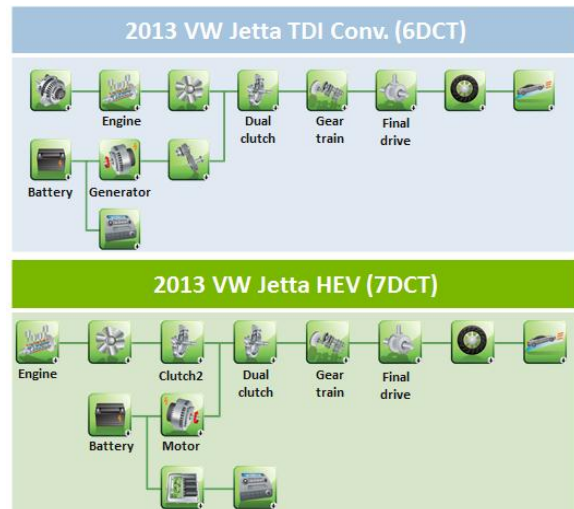


Figure V-189: The vehicle systems in Autonomie

The specifications for each component in the two vehicles are shown in Table V-23.

Table V-23: Vehicle Specifications

| Specification | 2013 VW Jetta TDI Conv. | 2013 VW Jetta HEV |
|-----------------------|---------------------------------------|---|
| Test weight | 1,595 kg | 1,647 kg |
| Engine size and power | 2.0 L, 104 kW | 1.4 L, 110 kW |
| Battery | Pb | 1.1-kWh li-ion |
| Motor power | - | 20 kW |
| Transmission ratio | 3.46 2.05 1.30 0.90 0.91 0.76 | 3.50 2.09 1.34 0.93 0.97 0.78 0.65 |
| Final drive ratio | 4.12 (for 1,2,3,4) /3.04 (for 5,6) | 4.44 (for 1,2,3,4) /3.23 (for 5,6,7) |

Test Data Analysis for the Jetta HEV

The vehicle control behaviors for the Jetta HEV are interpreted on the basis of the analyzed results in order to understand the overall control behaviors.

Figure V-190 (upper panel) shows the vehicle speed and wheel demand torque when the engine is turned on. The lower panel shows the operating area of pure electric driving in the same index.

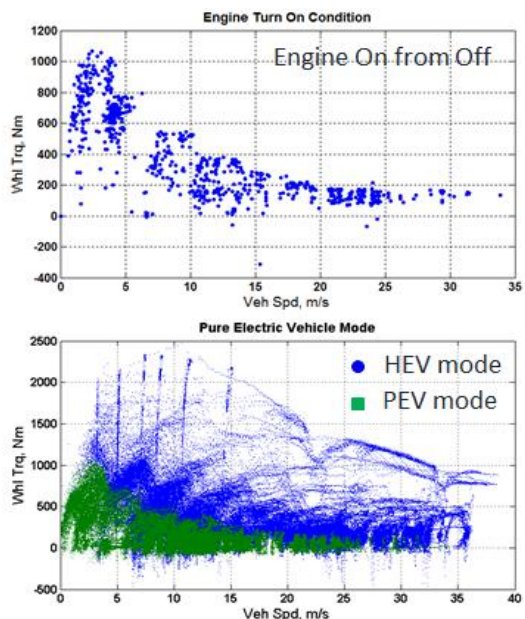


Figure V-190: Wheel torque vs. vehicle speed in Autonomie

One other important control concept at the vehicle level is how to manage the battery SOC within the appropriate range. Figure V-191 (upper panel) shows the battery SOC target when the engine is turned on. Under the engine on/off condition, the proportional demand power for the battery sustains the SOC level at an appropriate range near 55%.

Comparison between Simulation and Test Data

Simulation of the DCT was done with four certified driving schedules, and the simulation results were compared with the test results. First, simulation results for the vehicle speed, engine speed, engine torque, and gear number for the conventional vehicle on the UDDS cycle were compared with test results, as shown in Figure V-192. The simulation results for engine torque and speed were similar to the test results. Next, the simulation results for battery SOC and gear number for the HEV were compared with test results, as shown in Figure V-193. The gear number simulation result and test result were similar, implying that the DCT control algorithm is accurate.

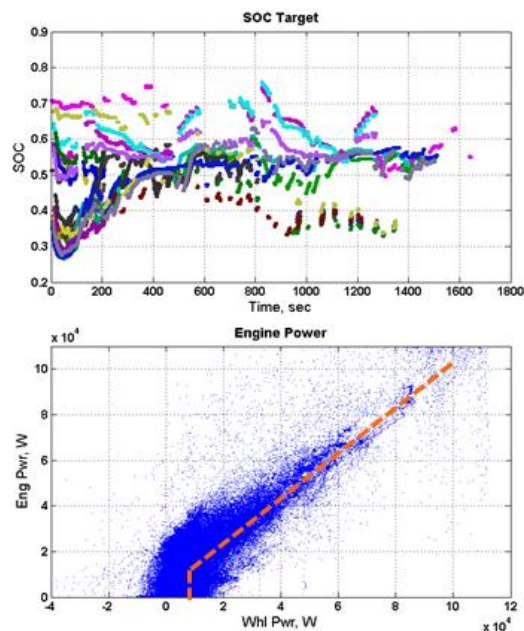


Figure V-191: (Upper panel) SOC vs. time and (lower panel) engine power vs. wheel power in Autonomie

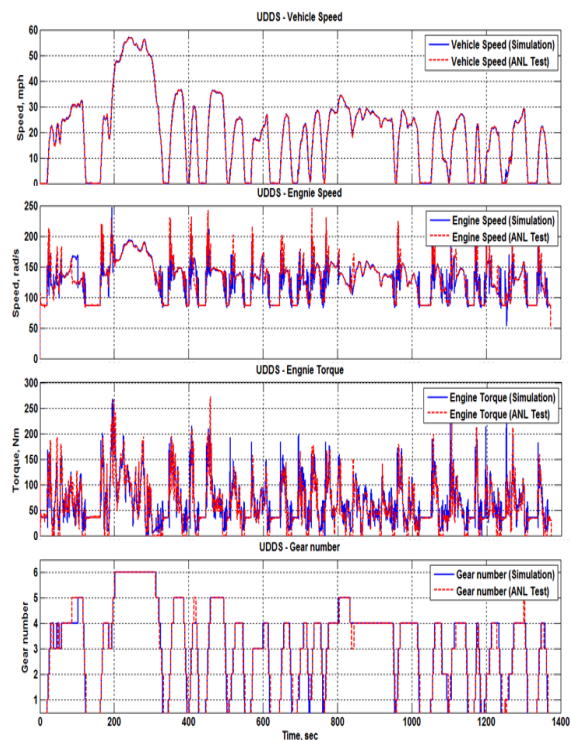
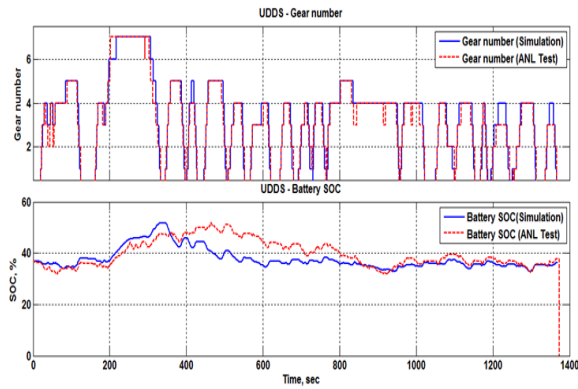
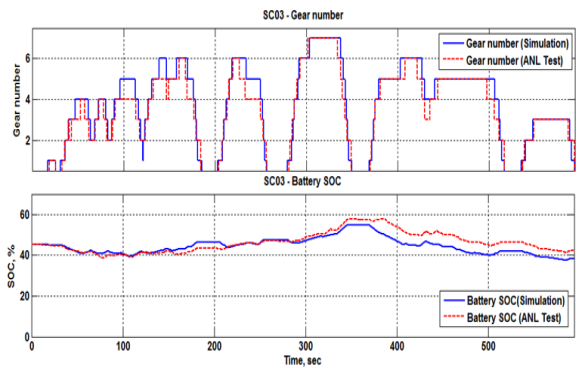


Figure V-192: Simulation and test results for the 2013 VW Jetta conventional vehicle with 6-speed DCT on the UDDS cycle



(a) UDDS



(b) SC03

Figure V-193: Simulation and test results for the 2013 VW Jetta HEV with 7-speed DCT on the (a) UDDS cycle and (b) SC03 cycle

Table V-24 shows the normalized cross correlation power (NCCP) values for the simulations reported here. The values of NCCP for the simulations shown in boldface are above 0.93 across all cycles, showing that a high level of correlation exists and that these results are very close to the test results.

Table V-24: Shifting Algorithm Model Validation for 2013 VW Jetta Conventional Vehicle and HEV

- 2013 VW Jetta Conventional Vehicle with 6-speed DCT

| | UDDS | HWFET | NEDC | LA92 |
|---------------------|--------------|--------------|--------------|--------------|
| Gear number | 0.984 | 0.998 | 0.992 | 0.979 |
| Engine Speed | 0.973 | 0.994 | 0.983 | 0.989 |
| Engine Torque | 0.925 | 0.966 | 0.928 | 0.911 |
| Fuel Rate | 0.897 | 0.943 | 0.895 | 0.887 |

- 2013 VW Jetta HEV with 7-speed DCT

| | UDDS | HWFET | WLTC | SC03 |
|--------------------|--------------|--------------|--------------|--------------|
| Gear number | 0.962 | 0.993 | 0.962 | 0.925 |
| Engine Speed | 0.864 | 0.904 | 0.859 | 0.840 |
| SOC | 0.937 | 0.952 | 0.950 | 0.958 |

Continuously Variable Transmission Model Development

A metal V-belt CVT model was developed by considering hydraulic and mechanical loss. The hydraulic loss constitutes

the majority of the total loss at low vehicle speed, whereas the mechanical loss is the main source of inefficiency at high speed, as shown in Figure V-194.

The CVT model was improved to consider the oil pump efficiency as a function of the line pressure and input speed. The mechanical loss map collected from experimental data was also used in the improved model as a function of the speed ratio, input torque, and vehicle speed.

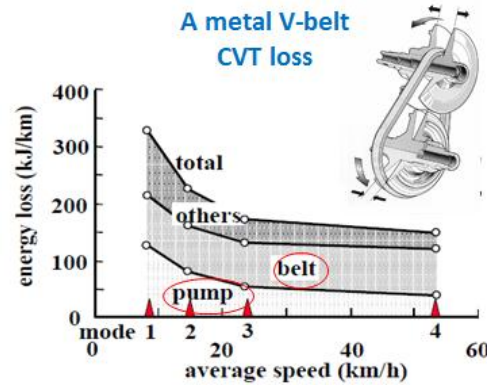


Figure V-194: Hydraulic pump loss and mechanical loss for metal V-belt CVT [2]

Generally, the operating conditions of the metal V-belt CVT system can be described by the following five parameters:

- Primary clamping force (FP) or primary pressure (PP);
- Secondary clamping force (FS) or secondary pressure (Ps);
- Primary revolution speed (ω_p);
- Input torque (TIN); and
- Pulley ratio (i).

On both the primary and the secondary pulleys, the belt is clamped by the forces produced by the hydraulic pressures in the cylinders. These two clamping forces, F_p and F_s , counteract each other. Therefore, when the pulley ratio is constant, there is a balance between F_p and F_s . A ratio change occurs when their balance is lost. In the next subsection, the relation between F_p and F_s in a state of balance is discussed. After that, di/dt is considered.

Variator Clamping Force Model

In the CVT system, the pulley ratio is controlled by the primary pulley. Therefore, it is convenient to consider that the state of balance is produced by the primary clamping force FP. The necessary primary clamping force for counterbalance is denoted by FP^* , and the corresponding primary pressure is denoted by PP^* .

The secondary actuator pressure PS can be obtained for the given input torque TIN and CVT ratio i from Fujii's formula:

$$F_s = \frac{T_{IN}}{2\mu R_p} \cos \frac{\alpha}{2}, \quad (1)$$

where μ is the friction coefficient between the belt and the pulley and R_p is the pitch radius of the primary pulley. In the CVT system design, F_s should be controlled to prevent slippage between the belt and the pulley.

The primary pressure PP at steady state can be determined from the thrust ratio map. The thrust ratio shows the relationship between the steady-state primary force FP and the secondary force FS with respect to the speed ratio i and the torque ratio, as shown in Figure V-195. The thrust ratio FPFS is represented as

$$F_p F_s = \frac{F_p}{F_s} = f\left(i_{CVT}, \frac{T_{IN}}{T_{max}}\right). \quad (2)$$

For the given speed ratio i and the input torque TIN, the secondary pressure PS is calculated from equation (1). The primary actuator force FS is determined from the thrust ratio map for the given i and ratio FPFS. The primary pressure can be calculated from equation (2).

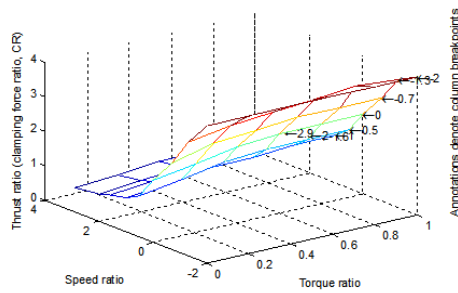


Figure V-195: $F_p F_s$ ratio map

CVT Shift Dynamics Model

In order to obtain the dependency of the ratio changing speed di/dt on the five above-mentioned parameters, one needs to consider the Ide's experiment formula, which is based on a test rig using only the belt and pulley set. The deviation of PP from PP* is denoted by ΔPP . Then, di/dt is expressed by the following equation:

$$\frac{di}{dt} = \beta(i) \cdot \omega_p \cdot (P_p - P_p^*). \quad (3)$$

The parameters of Ide's formula were determined from experiments reported in the literature. The linear relation is also obtained for all pulley ratios. Herewith, from the five parameters (PP, PS, ω_p , TIN, i), the effect of PP on di/dt is obtained. This formula shows that di/dt is in a proportional relation with ΔPP under loaded conditions as well, and the slope β hardly changes even if TIN changes.

CVT Control Algorithm

In addition, CVT ratio control and clamping force control strategies, including the CVT shift dynamics, were developed. The following improvements are needed in the low-level controller:

- The demanded CVT ratio should be determined from the engine OOL;
- The secondary pressure should be determined for the given input torque and CVT ratio; and
- The primary pressure needs to be controlled to meet the demanded CVT ratio.

Figure V-196 shows a block diagram of the model-based ratio control.

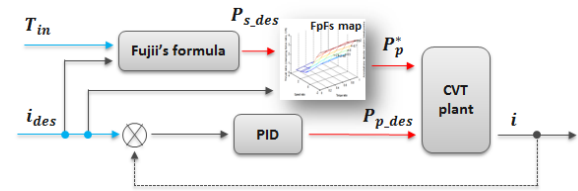


Figure V-196: Block diagram of model-based ratio control

CVT Validation Results

Vehicle Model in Autonomie

All the developed CVT plant models and controllers were integrated into the 2013 Nissan Altima conventional vehicle and the 2013 Honda Civic HEV system, and the vehicle models were validated under different driving cycles in Autonomie. The vehicles' main characteristics are shown in Table V-25.

Table V-25: Vehicle Specifications

| Specification | 2013 Nissan Altima Conventional Vehicle | 2013 Honda Civic HEV |
|-----------------------|---|----------------------|
| Test weight | 1,588 kg | 1,455 kg |
| Engine size and power | 2.5 L, 110 kW | 1.5 L, 82 kW |
| Battery | Pb | 0.675 kWh li-ion |
| Motor power | - | 17 kW |
| Transmission ratio | 0.39–2.35 | 0.529–3.172 |
| Final drive ratio | 4.828 | 3.94 |

The vehicle control behaviors for the Honda HEV are interpreted on the basis of the analyzed test results. For example, Figure V-197 shows the OOL from test data as a function of engine demand power. To achieve the lowest fuel consumption, the engine operation should be maintained close to the OOL by the CVT ratio control.

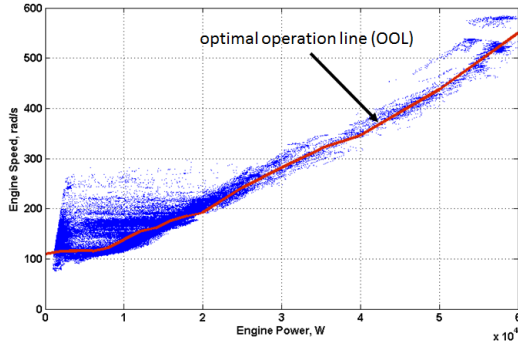


Figure V-197: Optimal operation line from test data

Comparison between Simulation and Test Data

An example of a comparison between the simulation results and the test data for engine operating parameters and gear ratio is shown in Figure V-198 and Figure V-199; Table V-26 shows the NCCP values for the simulations reported here. The values of NCCP for the simulations shown in boldface are above 0.93 across all cycles, showing that a high level of correlation exists and that these results are very close to the test results.

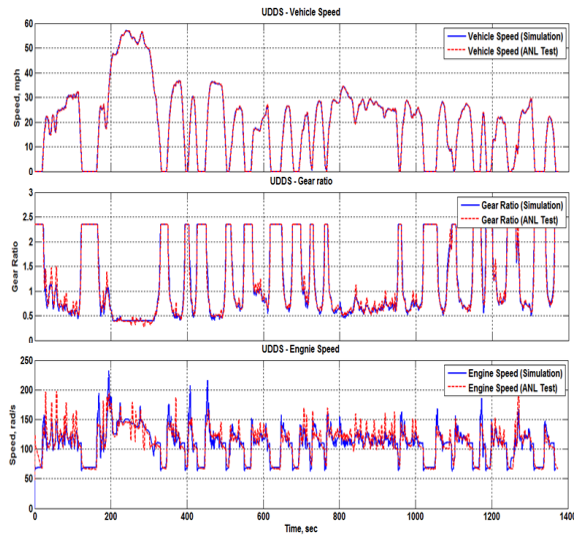


Figure V-198: Simulation and testing results for the 2013 Nissan Altima conventional vehicle on the UDDS cycle

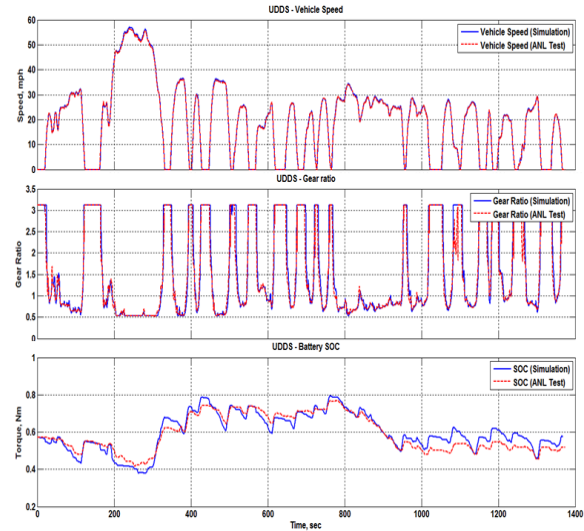


Figure V-199: Simulation and testing results for the 2013 Honda Civic HEV on the UDDS cycle

Table V-26: Shifting Algorithm Model Validation for 2013 Nissan Altima Conventional Vehicle and 2013 Honda Civic HEV

- 2013 Nissan Altima Conventional Vehicle

| | UDDS | HWFET | NEDC | LA92 |
|---------------------|---------------|---------------|---------------|---------------|
| Gear number | 0.9925 | 0.9882 | 0.9910 | 0.9880 |
| Engine Speed | 0.9803 | 0.9912 | 0.9600 | 0.9522 |
| Engine Torque | 0.9594 | 0.9361 | 0.9221 | 0.9343 |
| Fuel Rate | 0.9331 | 0.8847 | 0.9073 | 0.9321 |

- 2013 Honda Civic HEV

| | UDDS | HWFET | US06 | SC03 |
|--------------------|--------------|--------------|--------------|--------------|
| Gear number | 0.954 | 0.982 | 0.991 | 0.969 |
| Engine Speed | 0.902 | 0.990 | 0.875 | 0.966 |
| SOC | 0.983 | 0.982 | 0.704 | 0.860 |

Conclusions

- The controller for the DCT was developed for a pre-transmission HEV.
- Two DCT vehicles were simulated and validated with the test data (VW Jetta TDI conventional vehicle and HEV).
- The plant and controller for the CVT were developed by leveraging data from the literature and testing.
- Vehicle models of the Nissan Altima conventional vehicle and Honda Civic HEV with CVT were developed and validated using APRF test results.
- The plant models and controllers have been integrated into the Autonomie R14 release.

5.9.2 Products

Publications

1. N. Kim, H. Lohse-Bush, and A. Rousseau, *Development of a model of the dual clutch transmission in Autonomie and validation with dynamometer test data*, International Journal of Automotive Technologies, 15(2), 263–271, March 2014.
2. N. Kim, A. Rousseau, and H. Lohse-Bush, *Advanced automatic transmission model validation using dynamometer test data*, SAE 2014-01-1778, SAE World Congress, Detroit, April 2014.
3. H. Son, N. Kim, S. Ko, A. Rousseau, and H. Kim, *Development of performance simulator for a HEV with CVT and validation with dynamometer test data*, EVS28 conference, 2015, submitted.

Tools and Data

1. Autonomie.

References

1. www.autonomie.net
2. V. Francis, *Fuel consumption potential of the pushbelt CVT*, presented at the FISITA World Automotive Congress, 2006.
3. W. Ryu, *A Study on Metal Belt CVT Control for System Efficiency Improvement*, Dissertation, Sungkyunkwan University, 2006.
4. T. Ide, A. Udagawa and R. Kataoka, *Simulation approach to the effect of the ratio changing speed of a metal V-Belt CVT on the vehicle response*, Vehicle System Dynamics, 24(4), 377–388, 1995.
5. J. Park, *A Study on Shift Control Algorithm for a 2 Stage CVT*, Dissertation, Sungkyunkwan University, 2012.
6. T. Fujii, T. Kurokawa and S. Kanaehara, *A study of a metal pushing V-belt type CVT—Part 1: Relation between transmitted torque and pulley thrust*, SAE Tech. Paper Series 930666, 1993.

HEAVY DUTY

V.Q. CoolCalc Rapid HVAC Load Estimation Tool

Principal Investigator: Jason A. Lustbader

National Renewable Energy Laboratory
15013 Denver West Parkway
Golden, CO 80401
Phone: (303) 275-4443
E-mail: Jason.Lustbader@nrel.gov

DOE Program Manager: David Anderson

Phone: (202) 287-5688
E-mail: David.Anderson@ee.doe.gov

DOE Program Manager: Lee Slezak

Phone: (202) 586-2335
E-mail: Lee.Slezak@ee.doe.gov

V.Q.1. Abstract

Objectives

- Develop modeling tools to help quantify the impact of advanced load reduction technologies and show progress toward at least a 30% reduction in long-haul truck idle climate control loads with a three-year or better payback period by 2015.
- Reduce the risk of advanced technology adoption by improving the quantification of thermal load reduction technology impacts for both design points and in-use estimation.
- Investigate opportunities to reduce truck cab thermal loads through modeling and simulation to decrease the estimated 667 million gallons of fuel used for truck rest period idling.

Major Accomplishments

- Incorporated new features into CoolCalc, including: simplified heating, ventilating, and air conditioning (HVAC) system, revision of animation and rendering settings/controls, model process tool, curtain creation tool, and post-processing tool. Released versions 2.4 and 2.5 to industry partners.
- Developed and released a long-haul truck cab example model that is independent of truck geometries or parameters specific to original equipment manufacturers (OEM).
- Predicted with CoolCalc a 24.4% reduction for cooling and an 8.7% increase in heating degree-days when rotating a truck from solar-south facing to solar-north facing during

rest-period solar soak conditions, indicating a need for testing.

- Predicted a 44.1% and 23.2% reduction in national 95th percentile daily A/C cooling and heating thermal loads using a complete-cab thermal package with ultra-white paint, advanced insulation, and advanced curtains and shades. Typical annual weather at 161 cities was used for the analysis.
- Developed a method to combine CoolCalc with an auxiliary power flow distribution model for estimating auxiliary A/C system battery size. The method was used to demonstrate CoolCalc as an engineering tool for system design.

Future Achievements

- Provide industry with estimations of individual and combined technology design impacts on fuel use and payback period for design point and in-use weather conditions for the United States.
- Continue to improve CoolCalc models, validate against experimental data, use CoolCalc to inform testing, and extrapolate thermal load reduction impacts to the regional and national level.
- Begin development, validation, and application of medium- and light-duty vehicle models.
- Complete a stand-alone version of CoolCalc and improve integration of CoolCalc with NREL's thermal systems models and full vehicle models, such as Autonomie.



V.Q.2. Technical Discussion

Background

Heating and air conditioning (A/C) are two of the primary reasons for long-haul truck main engine operation when a vehicle is parked. In the United States, trucks that travel more than 500 miles per day use 667 million gallons of fuel annually for rest period idling [1]. Including workday idling, more than 2 billion gallons of fuel are used annually for truck idling [1]. By reducing thermal loads and improving efficiency, there is an opportunity to reduce the fuel used and emissions created by idling. Enhancing the thermal performance of cab/sleepers will enable cost-effective idle-reduction solutions. If the fuel savings from new technologies can provide a one- to three-year payback period, fleet owners will be economically motivated to incorporate them. This provides a pathway to the rapid adoption of effective thermal and idle load reduction solutions.

The U.S. Department of Energy's (DOE's) National Renewable Energy Laboratory (NREL) CoolCab project is researching efficient thermal management strategies that keep the vehicle occupants comfortable without the need for engine idling. To achieve this goal, NREL is developing tools and test methods to assess idle-reduction technologies. The heavy-duty truck industry needs a fast high-level analysis tool to predict thermal loads, evaluate load-reduction technologies, and calculate their impact on climate control fuel use over a wide range of temperatures and use conditions.

To meet the needs of industry, NREL developed CoolCalc, a software tool, to assist the industry in reducing climate control loads for heavy-duty vehicles. CoolCalc is a simplified HVAC load estimation tool that enables the rapid exploration of idle reduction design options for a range of climates.

Introduction

CoolCalc is an easy-to-use, simplified, physics-based HVAC load estimation tool that requires no meshing, has flexible geometry, excludes unnecessary detail, and is less time intensive than more detailed computer-aided engineering (CAE) modeling approaches. For these reasons, it is ideally suited for performing rapid trade-off studies, estimating technology impacts, and sizing preliminary HVAC designs. CoolCalc complements more detailed and expensive CAE tools by providing the ability to explore the design space to identify promising technologies and specific parameters that require deeper investigation.

CoolCalc, described in more detail in [2], was originally built on NREL's OpenStudio platform as a plug-in extension for Trimble's SketchUp three-dimensional design software, and it has since been adapted to better suit the transportation industry. DOE's EnergyPlus software (developed for building energy modeling) is used as the heat transfer solver for CoolCalc.

CoolCalc fills an important role in the CoolCab project's suite of experimental and analytical tools. It enables the rapid evaluation of technologies over a range of weather types and locations to help understand their impacts as they will be used on long-haul trucks. CoolCalc also provides industry partners with a valuable and cost-effective research and design tool.

Approach

The goals of the CoolCab research project are to reduce thermal loads, improve occupant thermal comfort, and maximize equipment efficiency to eliminate the need for rest period engine idling. To accomplish these goals, NREL is closely collaborating with OEMs and suppliers to develop and implement commercially viable thermal management solutions.

CoolCalc is a critical tool for achieving the CoolCab project goals. It enables the rapid evaluation of thermal load reduction technologies, not only at extreme design points, but also over the wide range of weather and use conditions that the vehicles will experience. Each phase of the CoolCab project approach leverages CoolCalc. After baseline testing is

completed, CoolCalc models of the test vehicles are built, starting from computer-aided design (CAD) models and other information provided by OEMs and suppliers. Best engineering estimations are used when data is not available. Next, models are validated against test data collected at NREL's Vehicle Testing and Integration Facility (VTIF). Local weather data collected at the VTIF are input into the CoolCalc simulation to ensure that the model behaves similarly to the test vehicle under the same weather conditions. CoolCalc is then leveraged to identify opportunities to reduce thermal loads via rapid simulation of technologies and thermal management strategies. Top candidates from parametric simulations are selected for further investigation through outdoor testing.

After testing of promising thermal load reduction technologies is completed, the information is used to improve CoolCalc models as needed and verify the accuracy of the model results. CoolCalc simulations are then used to analyze cab thermal performance at a national-level under typical weather conditions. Results can be coupled with HVAC and vehicle models to understand the impact on system performance. CoolCalc supplies thermal loads to CoolCab's A/C model, which calculates the required A/C system power. In upcoming work, the model will then couple with Autonomie to predict fuel use for weather and use conditions. This analysis will provide industry with the necessary information to adopt solutions that reduce or prevent engine idling and save fuel.

To capture weather conditions throughout the United States for the national-level analysis, the three most populous cities in each of the contiguous U.S. states were selected. Additional cities are also included to improve the national contour map spatial resolution and interpolation, resulting in typical meteorological year (TMY) weather data for 161 cities used for simulations. TMY weather data consist of actual hourly weather information representative of typical local climatic conditions on a monthly basis concatenated into an entire year [3]. Due to location and technology combinations, national-level simulations can have thousands of individual simulations. To increase the simulation speed of large parallel runs, NREL coupled CoolCalc with a Windows based high-performance computer using 96 cores to quickly complete analysis.

Results

CoolCalc Improvements and New Features

A number of enhancements were made to the CoolCalc HVAC load estimation tool to improve functionality and usability. The major enhancements are listed below.

1. CoolCalc source code was updated to retain compatibility with the new version of EnergyPlus (v8.1).
2. A "simplified" HVAC system option was added to the HVAC tool. This simplified system does not require modeling an entire HVAC system; therefore, it requires much fewer EnergyPlus objects than the previously implemented "detailed" version. The simplified system still provides the flexibility and control needed to simulate a basic HVAC system for most modeling scenarios. The

HVAC tool now provides the option to implement either simplified or detailed HVAC systems, depending on the user's requirements.

3. The rendering and animation settings/controls were redesigned to improve both stability and usability. These controls visually display simulation surface data through the use of color animation during post-processing. The improvements included consolidation of the animation settings and controls into a single, expandable interface, along with stability improvements to the existing rendering and animation tools. The CoolCalc Rendering toolbar was also restructured to provide streamlined access.
4. The CoolCalc Process Tool (Figure V-200) was implemented to aid users in the creation of a CoolCalc project through the use of interactive documentation. The Process Tool provides a hierarchical list of both common and required steps needed for the completion of a model. Each element in the list describes the step and how it can be completed, along with a status icon that represents if the step is incomplete, has been correctly completed, or is optional. This provides a visual representation of the steps needed for a functional model that is ready for simulation execution.

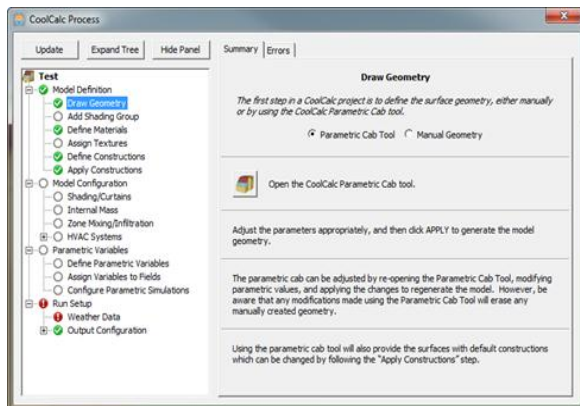


Figure V-200: CoolCalc process tool

5. A Curtain Creator tool was implemented to simplify the task of adding shades to windows within a model. The Curtain Creator provides a single interface to easily define and create shades of variable thermal and geometric properties that control the functionality of the curtain. After a curtain is created, it can be applied to any window existing in the model. In addition, the Curtain Creator allows for defined curtains to be quickly removed or deployed in a model, helping to assess the impact of technologies with and without curtains.
6. The Post-Processing tool (Figure V-201) was developed to allow rapid display of simulation results. The tool offers an interface for importing simulation output (EnergyPlus *.csv files), selecting variables from the imported data sets, and plotting the data using a number of different configuration settings. Within the Post-Processing Viewer, the plots can be displayed with one, two, or four plots to a page for easily comparing multiple plots to one another.

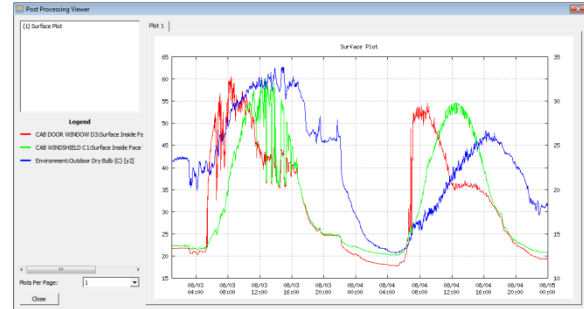


Figure V-201: CoolCalc post-processing tool

Preliminary Development of VTCAB

Vehicle Thermal Cabin Simulator (VTCab), a SketchUp-independent version of CoolCalc, is currently under development. CoolCalc was initially developed and continues to exist as a plug-in to the SketchUp program environment. For rapid preliminary tool development and the demonstration of CoolCalc, the use of the SketchUp environment was very beneficial; however, this dependency is also a disadvantage because of updates that are required for CoolCalc to remain compatible with SketchUp as the SketchUp product changes over time. For this reason, development of VTCab has been initiated.

The primary purpose of VTCab is to retain and improve upon existing CoolCalc functionality with stand-alone execution of the software. VTCab is currently being developed to use EnergyPlus as the thermal solver; however, future development could include the addition of a thermal solver developed in the MATLAB/Simulink environment. VTCab provides additional programming flexibility and control while eliminating unnecessary SketchUp tools and features that were unused in a CoolCalc project. VTCab also simplifies the installation process with a single installer, providing a more rapid and simple procedure for new users. A comparison of the VTCab and CoolCalc graphical user interfaces are shown in Figure V-202.

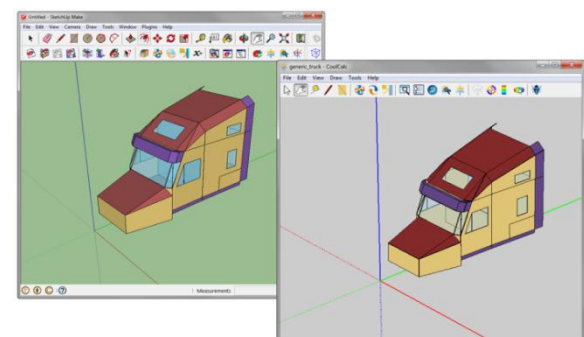


Figure V-202: (Left) CoolCalc and (right) VTCab graphical user interfaces

The following features have been included in VTCab:

1. VTCab was integrated with EnergyPlus (v8.1). A VTCab project can now interact with EnergyPlus by parsing the EnergyPlus Data Dictionary (.idd), creating/modifying/deleting EnergyPlus objects, and as executing EnergyPlus simulations.
2. A number of rendering features were added to VTCab. For example, EnergyPlus surface objects are now visually displayed in the drawing window. This provides the user with a visual representation of the model in geometric space. Along with the ability to visually display the model, tools for panning, rotating, and zooming were added to provide a flexible 360-degree view.
3. The Object Browser was implemented in VTCab. This tool is the primary tool to view, edit, add, or delete EnergyPlus objects. Although similar in design to CoolCalc's Object Browser, the VTCab version contains improvements, such as highlighting invalid/incomplete fields. The ability to add and edit "libraries" was also implemented in the VTCab Object Browser, allowing users to define custom collections of EnergyPlus objects for use in projects.
4. The Run Simulation window was redesigned and implemented for use in VTCab. The portions of the Run Simulation window used to configure weather files, design days, and output variables were simplified by a new checklist style design. In addition, populated output variables can now be filtered using a text based search tool. Stability improvements were made to ensure that VTCab is responsive during simulation execution. Users now have the ability to hide/show the EnergyPlus simulation output and can now easily cancel a simulation that is in progress.
5. The design of the project file structure was refactored to include the main project file in its corresponding project folder. In addition, the new file structure better separates information used by VTCab from information that could involve user interaction.
6. To allow the use of models drawn in other CAD programs, especially SketchUp, functionality was added to VTCab to import a COLLADA file. A COLLADA file (.dae) is a universal format for reading and writing three-dimensional models, and it is used by many modeling programs. VTCab is now capable of reading a COLLADA file and converting the geometry to EnergyPlus surface objects. This allows a user to draw geometry in another program (e.g. SketchUp), export the model to a COLLADA file, and import the model into CoolCalc.

Generic Long-Haul Truck Model Development

To provide the user with a framework for rapid model evaluation without the need for time-consuming model development, a full CoolCalc model of a generic Class 8 long-haul truck with sleeper was developed and integrated into CoolCalc. The CoolCalc generic truck cab model was created to represent a typical long-haul truck in order to produce relevant simulation results that are independent of OEM-specific truck geometries or parameters.

The generic truck cab model was released with CoolCalc Version 2.5 as two separate templates. The first template was

configured as a long-haul truck with a functional HVAC system in the sleeper compartment. The second template was configured as a long-haul truck with curtains open in a solar soak configuration. Model inputs for both templates can be adjusted to meet the user's specific simulation needs.

Example applications of the generic truck cab model include quantification of the sensitivity of truck orientation relative to the sun, impact estimations for paint and glazing property changes on HVAC loads and soak profiles, and the impact of HVAC control settings on thermal load profiles.

The generic truck cab model was developed and compared against three reference CoolCalc models of long-haul trucks. Each reference model was built from individual truck cab CAD geometry. When available, information from OEM's or measurements was used for model parameters. Otherwise, engineering estimates were made for the material properties, surface constructions, surface boundary conditions, internal mass, air flow, and exterior paint color. The geometry of the generic truck cab is shown in Figure V-203 and was simplified to exclude specific features and styling of the reference models. The primary dimensions and major features, however, are representative of a modern Class 8 truck with sleeper to ensure accurate thermal behavior.

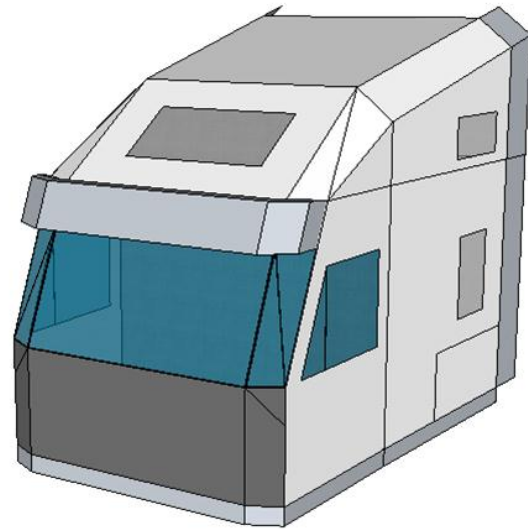


Figure V-203: CoolCalc geometry of the generic long-haul truck model

Prior to release, the generic truck cab model was compared against simulation data from the three OEM-specific CoolCalc models. Comparison included thermal soak as well as heating and cooling performance for a variety of realistic ambient conditions. Example comparison results are shown in Figure V-204. The comparison results show that the thermal behavior of the generic truck cab is similar to that of the OEM models. Specifically, diurnal trends match closely and are within the range of the three models.

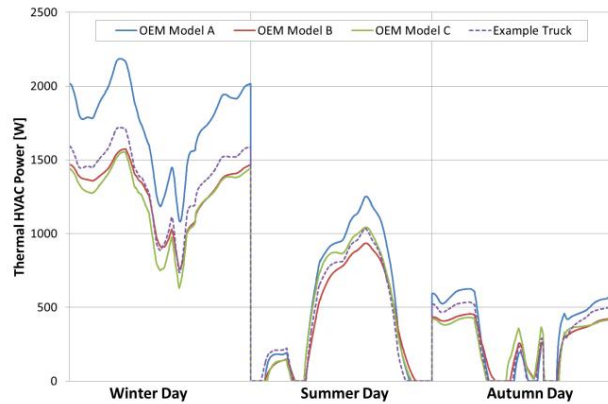


Figure V-204: Thermal HVAC loads of the generic truck cab model compared to three validated CoolCalc models

Truck Orientation Study

For the United States, a south-facing truck is expected to receive the highest amount of solar load relative to other orientations. A south-facing truck therefore, represents the worst-case orientation for evaluating thermal loads on the vehicle. To explore the effect of truck orientation on cooling and heating thermal loads, a national-level rotational analysis was performed with a previously validated sleeper cab model.

For the national rotational analysis, typical meteorological data for 161 locations throughout the 48 contiguous United States were used as input to the model. For each location, the orientation angle of the cab was varied in 22.5-degree increments. Annual cumulative cooling and heating degree days were used as a surrogate metric for cooling and heating thermal demand on the sleeper compartment. Cooling and heating degree-days were calculated as the integration of sleeper air temperature above the respective reference climate control set point temperature of 25°C and 20°C. The effect of orientation angle on cooling degree days normalized to the south orientation at the national level is shown in Figure V-205. The figure indicates a strong effect of vehicle orientation on cooling degree-days, with a 24.4% reduction in mean cumulative cooling degree-days from south to north vehicle orientation. Similarly, modeling results for heating showed an 8.7% increase in the mean cumulative heating degree-days from south to north vehicle orientation.

The model results identified vehicle orientation as a promising method for load reduction, and preliminary experimental results are presented in the CoolCab section of this FY 2014 annual report.

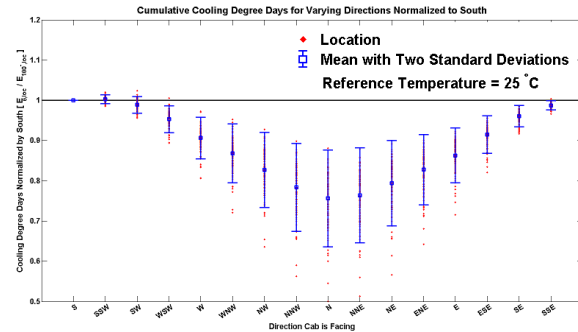


Figure V-205: Effect of normalized cooling degree-days with respect to truck cab orientation angle

Complete-Cab Solutions Study

Based on prior experimental and CoolCalc model results, a combination of individual technologies were identified to meet the overall project goal of achieving 30% or greater reduction in rest-period climate control loads. Prior to experimental evaluation, the technologies were combined and modeled at the national level to estimate their impact. In addition, an analysis of variance (ANOVA) was performed to quantify the interaction of individual technologies with respect to load reduction.

For the complete-cab solution study, the technologies evaluated were paint color, insulation, and curtain with shades. For the analysis, black, mid-tone and white paint colors were selected to cover the full range of options. The black and white paint solar and thermal absorptance properties were based on experimental data; whereas the mid-tone paint properties were selected to be the mid-point value between the black and white paints. Ideally, the mid-tone paint color would have the properties of the national long-haul truck fleet average paint color. An analysis was performed to estimate the national average solar-color, and a detailed description of the analysis is provided in the CoolCab experimental test section of this report. The solar absorptance of the mid-tone paint and the national average solar-color paint are 0.66 and 0.63, respectively. Therefore, the mid-tone paint in the analysis provides an estimate of a vehicle painted with a national average solar-color.

For insulation, a baseline package as well as half thickness and full thickness advanced insulation packages were modeled. In addition to the thickness changes of the insulation, the thermal conductivity and density of the insulation was changed for the half and full thickness advanced insulation configurations to more closely reflect the change in materials.

For curtains, the standard sleeper curtain and privacy shades were compared to that of an advanced curtain and shade package. The advanced package included improvements to the solar reflectivity and conductivity of the curtains, in addition to changes in the shade-to-glass distance and a reduction in air exchange rate between the cab and sleeper compartments for the sleeper curtain.

The complete-cab solution study used typical meteorological data for 161 locations throughout the 48 contiguous United States as environmental inputs. Combining 161 locations with three paint colors, three insulation levels, and two curtain configurations resulted in 2,898 individual model simulations. NREL’s high performance computer was leveraged for increased throughput of the analysis.

The relative effects of each technology on the global mean for both national-level cooling and heating at the 95th percentile is shown in Figure V-206. The global mean is defined as the average cooling or heating thermal load for all of the possible technology combinations evaluated. To simplify the study and more closely match the expected national average truck behavior, black paint was removed and only mid-tone and white paint were considered. For cooling, curtains and shades showed the strongest impact, followed by insulation, and ending with paint color. However, the relative impact of paint becomes the largest impact of the technologies when black paint is included in the analysis. For heating, insulation showed the strongest impact followed by curtains. As expected for heating, paint color has a relatively small but negative impact going from mid-tone to white paint.

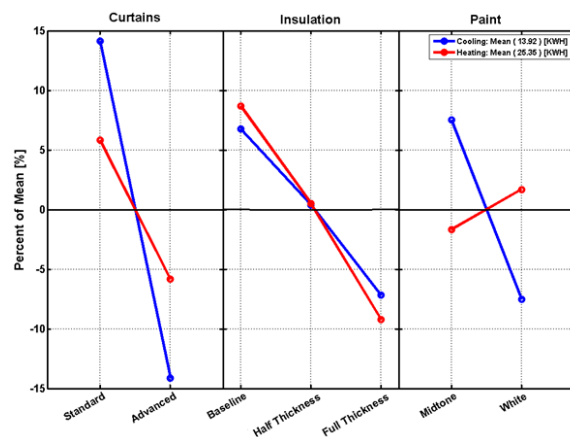


Figure V-206: Relative impact of individual technologies for both cooling and heating thermal loads

Table V-27: Percent Improvement for Technology Combinations for Cooling and Heating Daily Loads at the 95th Percentile

| Configuration | | | Improvement [%] | |
|---------------|----------------|----------|-----------------|----------|
| Paint Color | Insulation | Curtains | Cooling | Heating |
| Mid-tone | Baseline | Standard | Baseline | Baseline |
| White | Baseline | Standard | 13.7 | -3.4 |
| Mid-tone | Half Thickness | Standard | 5.8 | 7.3 |
| White | Half Thickness | Standard | 17.9 | 4.4 |
| Mid-tone | Full Thickness | Standard | 12.6 | 16.0 |
| White | Full Thickness | Standard | 22.9 | 13.5 |
| Mid-tone | Baseline | Advanced | 22.5 | 10.9 |
| White | Baseline | Advanced | 35.1 | 7.5 |
| Mid-tone | Half Thickness | Advanced | 28.0 | 17.7 |
| White | Half Thickness | Advanced | 39.2 | 14.6 |
| Mid-tone | Full Thickness | Advanced | 34.6 | 25.8 |
| White | Full Thickness | Advanced | 44.1 | 23.2 |

The percent improvements for both cooling and heating thermal loads at the national 95th percentile for each technology combination are provided in

Table V-27. The baseline configuration used for percentage improvement calculations is listed at the top of the table and consists of the mid-tone paint, baseline insulation package, and standard curtain package. As shown in the table, a 44.1% improvement in cooling thermal loads over the baseline case was obtained for the combination of white paint, full thickness insulation, and advanced curtains with shades. In addition, this configuration showed a 23.2% improvement in heating thermal loads compared to the baseline configuration.

National-level contour plots of normalized daily cooling thermal load at the 95th percentile are shown in Figure V-207 for both baseline and complete-cab solution analyses. The figure shows a strong reduction in cooling thermal load for the complete-cab solution and also shows a decrease in sensitivity to environmental conditions throughout the United States.

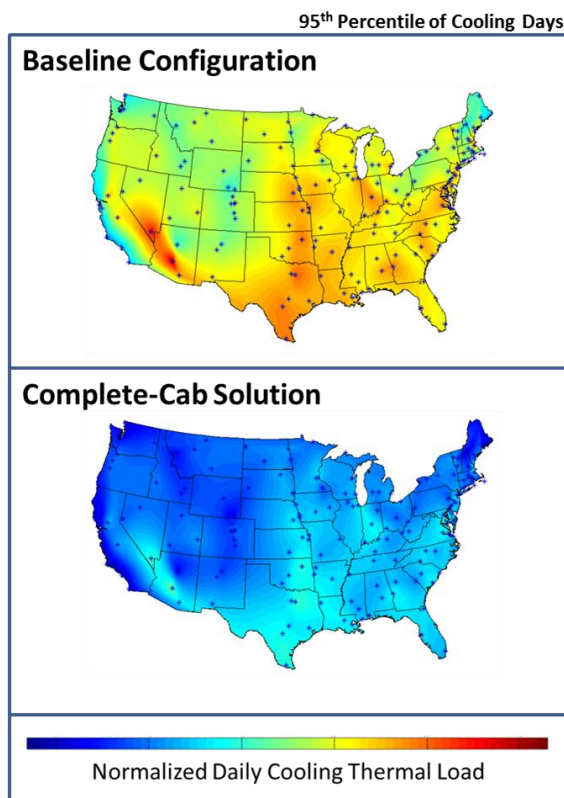


Figure V-207. National contour plots of normalized daily cooling thermal load for both baseline and complete-cab solution CoolCalc analysis results

Battery Sizing for Auxiliary Electric A/C Systems

Required battery size for a long-haul truck auxiliary A/C system was modeled using CoolCalc analysis coupled with an electrical flow distribution model developed in MATLAB. A diagram of the discharge and charge states of an electric A/C system is shown in Figure V-208. For fuel use estimation, evaluation of both the charge and discharge state of the battery is required; however, to determine the battery size for an auxiliary A/C system, only the discharge state is characterized, and the sizing is therefore dependent on the HVAC system inverter efficiency as well as the A/C system model.

For the analysis, TMY data for 161 locations throughout the 48 contiguous United States were used as input to the model. As an example technology, black and white paint colors were evaluated. Thermal loads were calculated for each location and paint color. To account for the coefficient of performance of the A/C system, a preliminary A/C system map was created using NREL’s CoolSim software with overall energy use as a function of thermal energy demand and ambient temperature. A/C system energy use was then calculated for each time step. Finally, the HVAC system inverter was modeled as having a fixed efficiency independent of electrical load and was set at 90%.

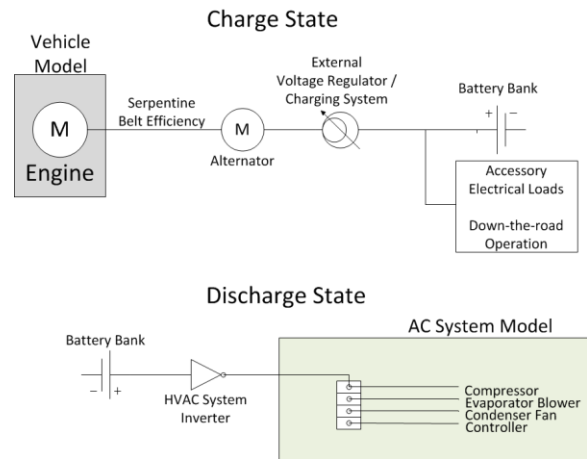


Figure V-208. Battery charge and discharge states for electric A/C systems

Figure V-209 shows the daily maximum 10-hour battery load for both black and white trucks as a function of the percent of the total number of cooling days for the United States. In addition, Figure V-209 contains a table of battery sizes needed to meet 95%, 99.7%, and 100% of the cooling days for black and white painted trucks. The battery analysis shows the use of CoolCalc as a tool for engineering evaluation of HVAC system and component design. In addition, battery sizing is an important step in the complete evaluation of an electric A/C system for fuel use estimation.

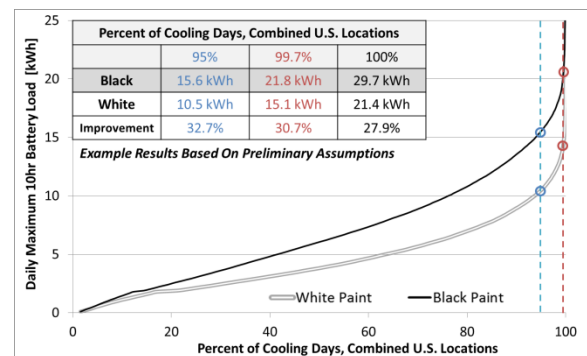


Figure V-209. Effect of paint color national results on electric A/C battery size requirements

Fuel Use Estimation

Significant progress has been made on the development of a method for the quantification of fuel use and payback

period. Figure V-210 shows a schematic of the fuel use estimation modeling process. The power flow model developed for the battery sizing study provides the critical link between cab thermal and vehicle accessory loads for more complex configurations, such as battery electric HVAC systems that are recharged during down-the-road operation of the vehicle.

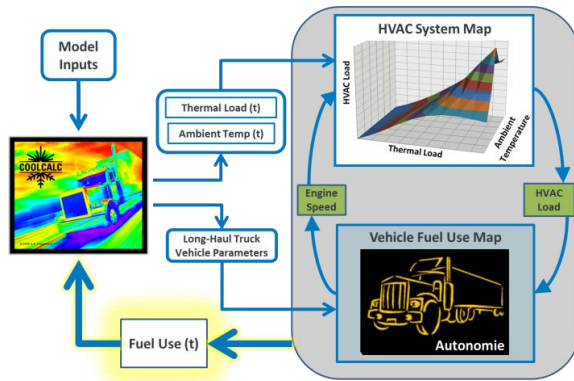


Figure V-210. Fuel use estimation modeling process

Conclusions

CoolCalc was enhanced with the addition of a simplified HVAC system option, improvements to rendering and animation capabilities, the addition of the Process Driven tool, a graphical user interface to aid in the implementation of curtains and shades, and the addition of the Post Processing tool. CoolCalc was also updated to retain compatibility with EnergyPlus version 8.1. In addition, initial development progress has been made on VTCab; a stand-alone version of CoolCalc that is independent of SketchUp. Development on VTCab has consisted of the addition of model rendering capabilities, implementation of the Object Browser, an improved Run Simulation graphical user interface, an improved project file structure, and the ability to import geometry from the Collada file structure.

A typical long-haul truck sleeper cab model, the generic truck cab, was developed to provide the user with a functional model to reduce development time for technology evaluation. The generic truck cab model was constructed to represent a typical long-haul truck sleeper cab geometry and construction while omitting OEM-specific information. The generic truck cab showed good agreement when compared to CoolCalc results of actual cabs. The validated model shows close agreement with the reference models throughout a range of example weather conditions, including both heating and cooling applications. The generic truck cab has been implemented in CoolCalc as two separate template projects: a solar soak model with curtains open and a model containing a rear HVAC system and closed curtains.

CoolCalc national-level modeling capabilities were used to evaluate the impact on vehicle orientation on heating and cooling HVAC loads. The results show a 24.4% reduction in cooling degree-days going from a south-facing to north-facing vehicle and an 8.7% increase in heating degree-days. These

results identified vehicle orientation as a no-cost method for load reduction, and preliminary experimental results are provided in the CoolCab section of this FY 2014 annual report.

CoolCalc modeling and parametric run capabilities were also used to explore and identify technologies for a complete-cab rest-period idle load reduction solution. An ANOVA technique was used to identify advanced curtains, insulation, and paint as opportunities for improving cooling loads from a baseline condition. The study also showed improvements in heating loads using advanced curtains and insulation, with a minor detrimental impact for paint. The combined technologies reduced the 95th percentile national daily cooling thermal load by 44.1% and heating loads by 23.2%. The results of this study were used to inform outdoor testing, and experimental results are presented in the CoolCab section of the report.

The use of CoolCalc as an engineering design tool was demonstrated through a preliminary national-level analysis of auxiliary electric A/C system battery sizing for black and white painted long-haul trucks. Battery size estimates were obtained through the coupling of CoolCalc with a power flow distribution model that included an example A/C system efficiency map generated in CoolSim. The results indicate that a significant reduction in battery size is obtained when going from a black to white painted truck. In addition, the results indicate a strong sensitivity to battery size when capturing 95%, 99.7%, and 100% of the combined national cooling loads.

CoolCalc is being used effectively to guide testing efforts through preliminary technology performance evaluation. The development of tools to aid in the application of CoolCalc across a wide variety of weather conditions contributes to the overall goal of quantification of fuel savings and payback periods for potential thermal and idle load-reduction technologies. Providing industry with the tools and information necessary to select and quantify the impact of idle load reduction solutions dramatically reduces their risk, which creates a pathway for the rapid adoption of technologies. CoolCalc was used to assist partners, including Volvo Trucks, the Daimler SuperTruck project, Aearo Technologies/E-A-R, and PPG on DOE- and industry-funded projects.

References

1. Gaines, L.; Vyas, A.; Anderson, J. "Estimation of Fuel Use by Idling Commercial Trucks." 85th Annual Meeting of the Transportation Research Board, Washington, D.C., Jan. 22–26, 2006; Paper No. 06-2567.
2. Lustbader, J.; Rugh, J.; Rister, B.; Venson, T. "CoolCalc: A Long-Haul Truck Thermal Load Estimation Tool." SAE World Congress, April 12-14, 2011, Detroit, MI; Paper Number 2011-01-0656.
3. Accessed September 2014: redc.nrel.gov/solar/old_data/nsrdb/1991-2005/tmy3/.

V.Q.3. Products

Publications

1. Lustbader, J.; Kreutzer, C.; Jeffers, M.; Tomerlin, J.; Langewisch, R.; Kincade, K. "CoolCab Test and Evaluation & CoolCalc HVAC Tool Development." DOE Annual Merit Review, June 19, 2014; VSS075.
2. Lustbader, J.; Kreutzer, C.; Adelman, S.; Yeakel, S.; Brontz, P.; Olson, K.; Ohlinger, J. "Impact of Paint Color on Rest Period Climate Control Loads in Long-Haul Trucks." SAE World Congress, April 8, 2014.
3. Lustbader, J.; Kreutzer, C.; Jeffers, M.; Adelman, S.; Yeakel, S.; Brontz, P.; Kopetz, C.; Ohlinger, J.; Olson, K. "Impact of Paint Selection on Idle Climate Control Loads in Long-Haul Trucks." SAE Thermal Management Systems Symposium, Oct. 23, 2013.
4. Kreutzer, C.; Lustbader, J. "Advanced Technologies for Long-haul Truck idle load reduction." SAE Thermal Management Systems Symposium, Sept. 24, 2014.

Tools and Data

- CoolCalc rapid HVAC load estimation tool versions 2.4 and 2.5. Only available to industry and laboratory partners at this time.
- CoolSim v84 A/C modeling software for the MATLAB/Simulink software environment. See CoolSim section in this VSST FY 2014 Annual Report for more information.

Acknowledgements

- Coauthors Cory Kreutzer, Matthew Jeffers, Kameron Kincade, and Ryan Langewisch (NREL).
- Additional thanks to William Hamilton, Dustin Crouse, John Rugh, and Lisa Fedorka (NREL).
- Special thanks to our industry partners Volvo Trucks, Daimler Trucks, EAR Thermal Acoustic Systems, and PPG Industries.

V.R. Advanced Heavy Duty Engine Systems and Emissions Control Modeling and Analysis

Principal Investigators: Zhiming Gao, Stuart Daw

Oak Ridge National Laboratory
National Transportation Research Center
2360 Cherahala Boulevard
Knoxville, TN 37932-6472
Phone: (865) 946-1339, (865) 946-1341
E-mail: gaoz@ornl.gov, dawcs@ornl.gov

DOE Program Manager: David Anderson

Phone: (202) 287-5688
E-mail: David.Anderson@ee.doe.gov

DOE Program Manager: Lee Slezak

Phone: (202) 586-2335
E-mail: Lee.Slezak@ee.doe.gov

- Compared simulated fuel economy and component energy loss of parallel, series and dual-mode hybrid powertrain configurations on Class 8 trucks over freeway-dominated driving conditions.
- Evaluated the expected impact of technology options in six HD target areas identified by the 21st Century Truck Partnership (21CTP) program: engine systems, heavy-duty hybrids, power demands in vehicle technology, idle reduction, safety and operational efficiency.

Future Achievements

- Further activities on this project have been suspended at the end of FY 2014. Models developed in this project will be documented and adapted for use in simulations of other HD hybrid powertrains in separate projects.



V.R.1. Abstract

Objectives

- Develop powertrain component models that can be used to accurately simulate and optimize the overall fuel efficiency and emissions control of advanced medium (MD) and heavy-duty (HD) hybrid powertrain systems powered by current and leading-edge combustion engines with exhaust aftertreatment over transient driving conditions.
- Reduce U.S. dependence on imported fuels by collaborating with industry partners to identify and overcome major technical barriers to commercial implementation of hybrid MD and HD powertrains.

Major Accomplishments

- Developed a transient auxiliary load model accounting for mechanical and electrical power consumption of the accessory components for HD conventional and hybrid trucks.
- Constructed models for different MD and HD hybrid powertrain configurations integrated with a comprehensive component system model describing fuel consumption, emissions control, and accessory power demand interactions.
- Simulated fuel economy, component energy loss, and emissions control of series hybrid powertrain configurations in transit city buses over city driving cycles and Class 8 trucks over both city and highway driving conditions.

V.R.2. Technical Discussion

Background

The U.S. transportation sector consumes nearly 13.5 million barrels of petroleum per day, more than 22% of which goes to MD and HD vehicles. Thus, MD and HD vehicle hybridization could play a vital role in reducing the overall greenhouse gas generation and imported oil consumption in the U.S. Typically lean-burn diesel engines offer a significant fuel efficiency advantage over stoichiometrically fueled engines. This is one of the reasons why current MD and HD vehicles are overwhelmingly powered by diesel engines. However, emissions control challenges are higher for diesels because aftertreatment of lean engine exhaust requires utilization of special catalysts and aftertreatment devices to remove nitrogen oxides (NO_x), particulate matter (PM), unburned hydrocarbons (HCs), and carbon monoxide (CO). Unlike the three-way catalyst technology used to control stoichiometric gasoline engine exhaust, the technology for diesel emissions control is still under intense development. As advanced diesel engines become even more efficient, their exhaust temperatures are becoming even cooler, and this is challenging the limits of current diesel catalyst technology. Thus it is important that simulations of advanced MD and HD diesel hybrid vehicles accurately account for the current and expected trends in both diesel engine and aftertreatment technology, linking to other critical component models. Even though models for both advanced diesel combustion engines and diesel exhaust aftertreatment are still under active development, simulations using the best current models are helpful in identifying future opportunities and guiding and focusing experimental research and development.

In this project we are specifically concerned with developing and implementing engine, aftertreatment, and accessory load component models that allow comparative simulations of different vehicle configurations, operating strategies, and component hardware. Our overall goal is to provide preliminary full system simulations that help support DOE's vehicle systems R&D efforts by providing the most accurate possible predictions to guide the selection and experimental validation of the most promising candidate MD and HD hybrid technology options. To build our models, we rely heavily on the most recent available experimental measurements from both engines and emissions control devices made in multiple facilities at Oak Ridge National Laboratory (ORNL). We transform these measurement data into physically consistent computational models that can be implemented directly in simulation platforms such as Autonomie. In some cases, the available data are incomplete, requiring assumptions to be made based on the best available information of the controlling physics and chemistry. Thus we continually strive to update component models as new data become available. By noting where key model sensitivities occur, we also provide guidance to experimental teams in targeting future measurements. This close interaction between simulation and experiments provides DOE with the best possible basis for identifying promising technologies that can address the country's strategic needs for maximizing energy efficiency and security while minimizing negative environmental impacts.

Introduction

In FY2014, we continued collaborations with partners at ORNL, industry, and other national labs to develop and refine component engine, aftertreatment, and peripheral system models needed to simulate drive cycle fuel consumption, emissions, and accessory power demands for advanced MD and HD hybrid vehicles. The updated models included transient auxiliary load models accounting for mechanical and electrical power consumption of the accessory components in HD trucks. The models were integrated with reference MD and HD hybrid vehicle powertrain configurations in Autonomie, enabling simulations of multiple advanced vehicle system scenarios that included:

- The simulated fuel economy, component energy loss, and emissions of series versus parallel hybrid city buses over city driving cycles.
- The fuel economy and component energy losses for parallel, series and dual-mode hybrid configurations of Class 8 trucks.
- The relative impact of six HD hybrid technology targets identified by the 21CT Program on fuel economy.

Results from the above simulations have been reported in multiple journal and conference publications and presentations at meetings of the Society of Automotive Engineers (SAE), the Transportation Research Board Annual Meeting, and Cross-Cut Lean Exhaust Emissions Reduction Simulations (CLEERS) Workshop. Additional manuscripts documenting the major findings from the hybrid city bus and HD truck studies are still under preparation.

Approach

Engine Simulations

Because of the inherent complexity of internal combustion engines under transient conditions, most previous simulations of vehicle drive cycles have relied on approximating fuel consumption and engine exhaust properties by interpolating steady-state maps generated from engine dynamometer measurements. We have modified that approach to account for transients by including a correction to the steady-state engine maps based on a first-order approximation of the overall engine heat balance to account for the impact of transient changes in speed and load. The result is expressed in the form of an experimentally parameterized transient correction term that is applied to steady-state or pseudo-steady-state engine-dynamometer data. While this approach is admittedly crude, we have validated it with chassis dynamometer measurements for LD engines as described in previous journal publications. For all the MD and HD cases evaluated so far, this methodology has produced reasonable trends in the fuel consumption and engine-out exhaust characteristics for both conventional and advanced combustion modes under drive cycle conditions. Nevertheless, we are continually working to improve the accuracy of these estimates as additional transient and advanced combustion engine data become available. The availability of highly controlled transient measurements from HD engines studied in the ORNL Vehicle Systems Integration (VSI) Lab will be a major step in this direction.

Aftertreatment Simulations

We have also continued to develop and refine low-order, physically-based computational models for diesel emissions control devices including diesel oxidation catalysts (DOCs), lean NOx traps (LNTs), diesel particulate filters (DPFs), selective catalytic reduction (SCR), and passive hydrocarbon traps. To increase computational efficiency and speed, our aftertreatment device models typically incorporate 1-D differential transient mass and energy balances with the most recent available global reaction kinetics and heat and mass transport information. These models make it possible to simulate the performance of each aftertreatment component based on its past history and the input streams it is exposed to at each point in the drive cycle, while maintaining reasonable execution speeds.

Auxiliary Load Simulations

Auxiliary loads in HD trucks are typically very complex and their measurement can be extremely challenging. As a starting point for this project, we collected auxiliary load data from open literature and utilized these to develop simple models for both mechanical (ME) and electrical energy (EE) consuming components (see Figure V-211). For a conventional truck, the auxiliary ME loads include power for the belt-drive of the air-brake compressor, the engine fan, the air-conditioning compressor, the lubricant oil pump, the power steering, the engine coolant pump, and the transmission-fluid pump. All these mechanical loads are considered as functions of engine speed, driving conditions, driver response for load demand, and 'on' time required for each accessory component. For the

HD simulations in this project, we assumed a constant electrical load of 600W electricity for conventional trucks, based on estimates from SAE J1343.

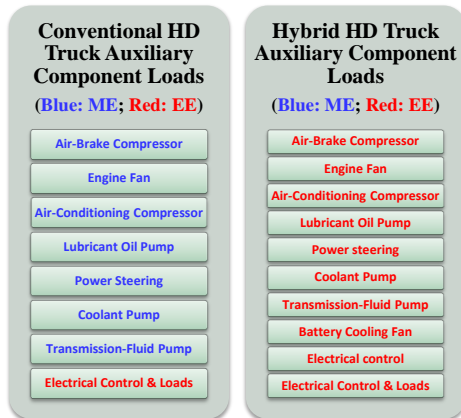


Figure V-211: Auxiliary-load comparison between conventional and hybrid trucks; ME and EE represent mechanical and electrical energy consumption, respectively

For hybrid trucks, we assumed that all of the ME auxiliary loads are replaced with EE loads, and these are not considered as functions of engine speed any more. Additionally, for hybrid trucks there is additional EE consumption for cooling the battery and electrical devices.

The ‘on’ time required for each component also depends on the drive cycle. As an initial starting point, we assumed a set of simple on/off duty cycles for each auxiliary device based on the estimated power demands for each cycle.

The models have been integrated with the previously described engine and aftertreatment models in Autonomie, in order to comprehensively explore the effects of a wide range of technology options in different MD and HD hybrid vehicles.

Hybrid Bus Simulations

We established and simulated both parallel- and series-hybrid transit buses assuming they were powered by a 5.9-L diesel engine and a full aftertreatment-train, which included a 2.3-L DOC, a 9.7-L catalyzed DPF, and a 7.7-L urea-SCR catalyst. The parallel-hybrid MD bus had a pre-transmission hybrid configuration with a 5-speed gearbox, and included a 120 kW permanent magnet electric motor and a 9kWhr Li-Ion battery. The series-hybrid bus was assumed to have a fixed gear ratio. The electric drivetrain included a 202 kW permanent magnet electric motor and a 208kW generator. In the series hybrids, we evaluated 12kWhr and 24kWhr Li-Ion batteries, corresponding to two different series hybridization levels: (1) Series_HH mode: a ‘high hybridization’ scheme where the electric drive was used extensively and the engine used mainly to maintain battery state of charge (SOC), and (2) Series_LH mode: a ‘low hybridization’ scheme where the engine was the primary propulsion source.

Hybrid Truck Simulations

We assumed three powertrain models for Class 8 hybrid truck simulations, including a pre-transmission parallel configuration with a 220 kW motor and a 35 kWh battery, a non-transmission series configuration with a 420 kW motor and a 64 kWh battery, and a pre-transmission parallel-series configuration with two motors (i.e. 220kW and 75kW, respectively) and a 35 kW battery. All the hybrid HD truck models were powered by the Cummins 2010-certified, 15-L engine with a full aftertreatment train consisting of a 5.8-L DOC, a 19-L catalyzed DPF, and a 24-L urea-SCR catalyst. For hybrid truck simulations we assumed sustainable charge strategies, where no vehicle speed constraints were imposed. For the dual-mode hybrid, the hybrid was assumed to operate in series mode below 15mph and parallel mode at highway speeds. Meanwhile, to account for the effects of different loads, three different fully loaded weights were considered, and the weight of the electric motor, the battery, and accessory components were also included.

Results

Accessory Load Effects

The above accessory load models were implemented in Autonomie to carry out drive cycle simulations. In some of these simulations, we evaluated the relative accessory load of hybrid HD trucks compared to conventional trucks. All the simulated trucks were assumed to be powered by 2010 complaint 15-L diesel engine. The truck weights were varied from 16,000-35,000kg to evaluate the impact of cargo load. Figure V-212 compares the estimated accessory loads between the simulated conventional and parallel-hybrid trucks over a UDDS truck cycle. The predicted trend implies that electrification of accessories can significantly reduce the peak accessory power demand. Simulations for different drive cycles (not shown here) also revealed that hybridization benefits should be higher for trucks operating under city driving conditions (over a UDDS cycle) compared to freeway driving, where electric propulsion is limited and the engine runs most of the time.

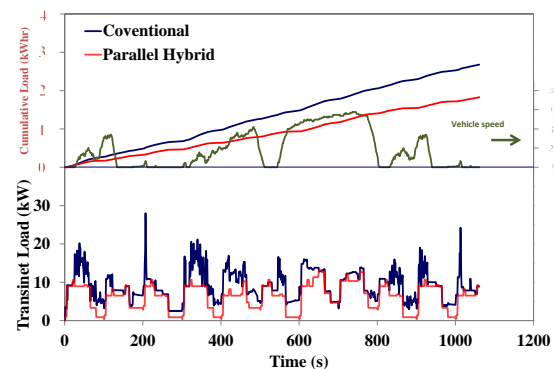


Figure V-212: Comparison of the simulated accessory load for the Class 8 conventional and parallel-hybrid trucks UDDS truck cycle; the simulated truck weight is 25,000 kg

Hybrid Bus Results

We simulated hypothetical parallel- and series-hybrid transit buses for five city driving cycles, including the Washington Metropolitan Area Transit Authority (WMATA) cycle, the New York Bus Cycle (NYBC), and the Knox Area Transit (KAT) cycles. Both the parallel- and series-hybrid buses had better estimated engine efficiencies compared to the conventional bus, with the series hybrid having the highest efficiency of all. This appeared to be a consequence of the series hybrid engine operating more of the time near maximum efficiency. We also observed that the series hybrids with larger batteries had the highest engine efficiency. However, the engine efficiency trends were not necessarily mirrored by fuel economy. As indicated in Figure V-213, the fuel economies of the series and parallel hybrids were not much different. Thus the engine efficiency alone was not a controlling factor for fuel economy.

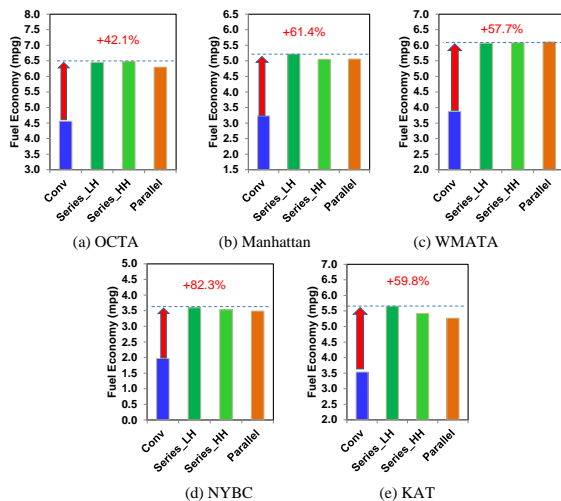


Figure V-213: Comparison of simulated fuel economy for the conventional and hybrid buses over five different city drive cycles; Series_LH and Series_HH refer to the same two series-hybrid cases described above

The estimated component energy losses for the buses reveal that the efficiency penalty associated with mechanical (i.e. engine energy) to electric to mechanical (i.e. motor energy) in the series- hybrid powertrain offsets the higher engine efficiency, reducing any benefit to fuel economy.

Our simulated results also reveal that both parallel- and series-hybrids have significantly reduced engine-out emissions compared to the conventional bus. However, their tailpipe emissions are not consistent with the engine-out trends, probably because their lower exhaust temperatures reduce the effectiveness of aftertreatment. Figure V-214 compares the change in simulated CO, HC, and NOx emissions for the conventional versus hybrid buses.

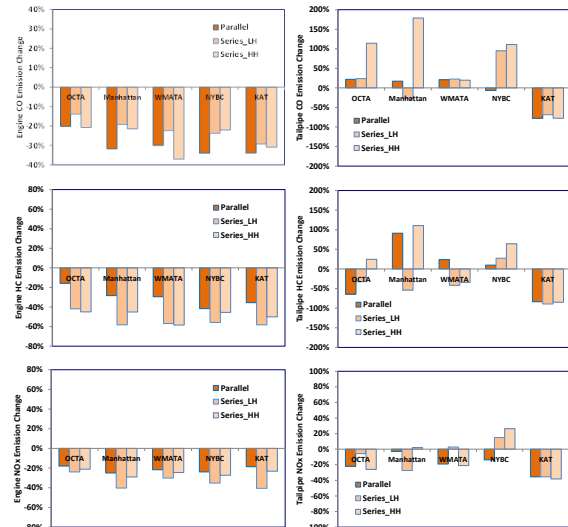


Figure V-214: Comparison of simulated engine-out and tailpipe emissions change for CO, HC, and NOx for parallel- and series-hybrid buses; Series_LH and Series_HH refer to the same two series-hybrid cases described above

Hybrid Truck Results

We simulated parallel, series, and dual-mode hybrid Class 8 trucks over both city and highway driving conditions. For city driving conditions, the simulations indicated that hybridization can improve fuel economy, with the series hybrid benefit being the least significant.

In highway driving, the series hybrid truck configuration resulted in a loss in fuel economy. However, as illustrated in Figure V-215, both parallel and dual-mode hybrid powertrains appear to be capable of improving fuel economy by 7-8%. Compared to the parallel configuration, the dual-mode hybrid achieves nearly 0.5% better fuel economy. The slightly higher dual mode hybrid energy saving appears to be associated with a slightly higher energy utilization efficiency during the short stop-and-go intervals in the highway driving cycle. It should be noted that for the highway simulations depicted here, we did not consider any vehicle speed constraints. In other simulations we found that applying a 50 mph speed constraint can reduce the fuel economy benefit from hybridization to 2-4%.

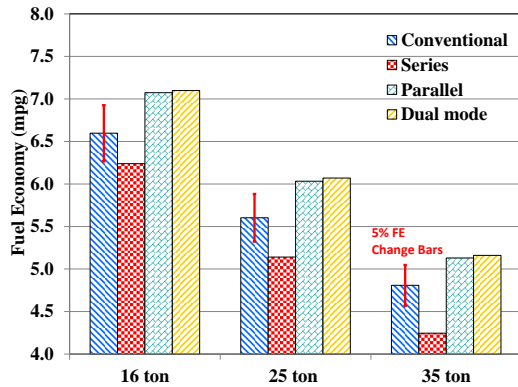


Figure V-215: Comparison of fuel economy among the conventional and hybrid trucks over the freeway-dominated heavy-duty driving cycle

Analysis of component energy losses reveals that the opportunity for kinetic energy recovery (regenerative braking) is very limited for long-haul trucks over the highway. The fuel economy improvement of parallel and dual-mode hybrid powertrains results from more optimal engine operation (at more efficient speeds and loads) and reduced engine demands during low load and idle. On the other hand, Figure V-216 reveals that there are also large energy losses for long-haul trucks due to aerodynamic drag and rolling resistance. Thus, it is particularly important for improving long-haul truck fuel economy to minimize these factors as well. The results in Figure V-215 indicate that hybrid powertrains could also reduce accessory loads, resulting in a fuel economy boost of around 2%.

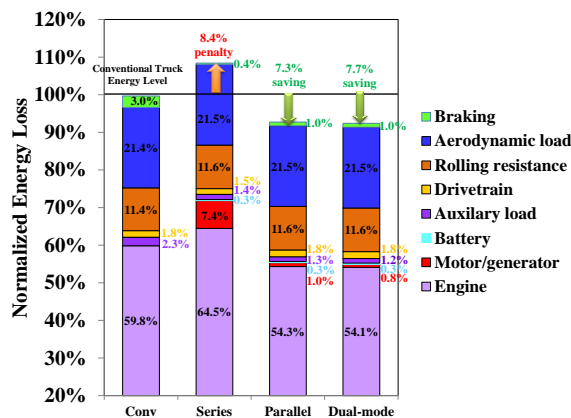


Figure V-216: Energy loss distribution for the 25ton conventional and hybrid trucks operating over the freeway-dominated heavy-duty driving cycle; the energy losses are shown relative to the conventional truck's overall energy use

The sensitivity of HD truck fuel economy to aerodynamic drag and rolling resistance can be seen by reducing these factors by 30% and 35%, respectively, as suggested in targets set by the 21st Century Truck Partnership. Figure V-217 illustrates the predicted impact on fuel economy for both conventional and parallel hybrid trucks in our simulations. We observed that, compared to the non-hybrid trucks with the same improvement in aerodynamics and rolling resistance, the hybrid technology increased fuel economy more than 15%, which is about 7-8% greater improvement than the cases

without the targeted aerodynamic drag and rolling resistance reductions. This indicates that long-haul hybrids with significant aerodynamic drag and rolling resistance reduction can minimize heavy engine loads, recover more kinetic energy, and make greater use of engine-off operation. In particular, the engine load cutoff in the case of aerodynamic drag and rolling resistance reductions is significantly higher than the baseline cases. This shows that hybrid technology has the potential to provide even better fuel savings in future long-haul trucks with load reduction technologies than for current truck technologies.

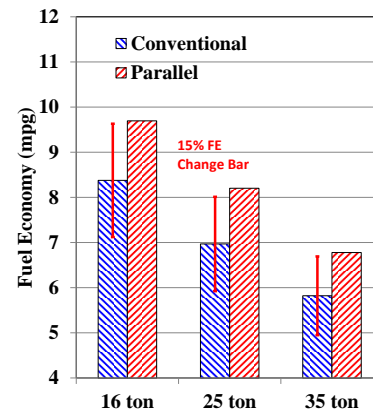


Figure V-217: Comparison of fuel economy of the conventional and parallel hybrid trucks with the targeted aerodynamic drag and rolling resistance reductions over the freeway-dominated heavy duty driving cycle

The 21CTP program also identified other key HD R&D target areas besides electric hybridization, aerodynamic drag, accessory power demand, and rolling resistance, including waste heat recovery, and advanced engine combustion modes. We simulated the collective impact of the combined 21CTP targets by simulating the potential benefits of HD trucks with advanced combustion engines operating with 50% peak efficiency, waste heat recovery, 50% auxiliary loads reduction, 35% rolling resistance reduction, 30% aerodynamic drag reduction, and 10% empty truck weight reduction in both conventional and hybrid long-haul trucks. Again, these simulations confirmed the major importance of reduced aerodynamic drag and rolling resistance for improving fuel economy, but the levels of their benefits were very sensitive to weight loads. Also, the increased peak engine efficiency also had high impact. Fuel economy benefits from reducing truck weight and waste heat recovery were much more limited (near 2%). All these results are summarized in Figure V-218. If achieved simultaneously, they could potentially result in a more than 60% improvement in fuel efficiency.

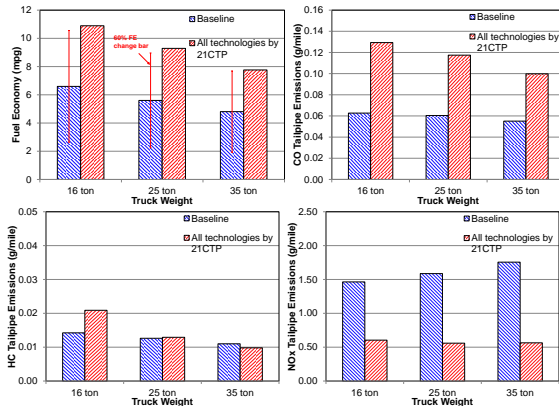


Figure V-218: Predicted fuel economy and emissions impact of the combined technology target goals identified by the 21CTP over a freeway-dominated heavy-duty truck cycle

In regard to tailpipe emissions, hybrid powertrains tended to have lower NOx but higher CO and HC. This is also reflected in Figure V-218. The higher CO and HC appears result from the low activity of the diesel oxidation catalysts with the lower exhaust temperatures. Therefore, the interaction of oxidation catalysts used in combination with other fuel saving measures would appear to be an important area for future computational and experimental hybrid vehicle systems investigations.

Conclusions

- Transient auxiliary load models have been developed to account for mechanical and electrical power consumption of accessory components in both conventional and hybrid HD trucks and implemented in Autonomie.
- Multiple types of hybrid powertrain configurations for MD and HD buses and Class 8 trucks have been set up in Autonomie and integrated with component models for transient engine and emissions control performance as well as the above accessory power demand models.
- Simulations of conventional, series-hybrid, and parallel-hybrid city buses with a fully integrated aftertreatment trains operating over five city driving cycles reveal that series-hybrid buses had the best average engine efficiency. But this was not reflected in the fuel economy due to inefficiencies in the mechanical-to-electrical-to-mechanical energy conversion in the series-hybrids.
- Both the parallel- and series-hybrid city buses have significantly reduced engine-out emissions compared to the conventional bus, but their tailpipe emissions are not consistent with the engine-out trends.
- Simulations of parallel, series and dual-mode hybrid Class 8 trucks on the highway powered with a full aftertreatment trains revealed that parallel and dual-mode hybrids (without any vehicle speed constraint) are capable of improving fuel economy by 7-8% through more optimal engine operation at higher speeds and loads with less idle. However there was no observable fuel economy benefit for the series hybrid truck.
- HD technology targets identified by 21CTP were found to have high potential impact on fuel economy. The greatest

impacts were observed for aerodynamic drag reduction, reduced rolling resistance, higher peak engine efficiency, and lower auxiliary loads.

- Final documentation of the results and models generated by this project is underway in anticipation of project termination.

V.R.3. Products

Publications

1. Z. Gao, T.J. LaClair, D.E. Smith, C.S. Daw, Fuel Saving Potential of Hybrid Technology in Long-Haul Trucks, TRB-15-3136, 94th Transportation Research Board Annual Meeting, January 2015.
2. Z. Gao, C.E.A. Finney, C.S. Daw, T.J. LaClair, D.E. Smith, Comparative Study of Hybrid Powertrains on Fuel Saving, Emissions, and Component Energy Loss in HD Trucks, SAE Int. J. Commer. Veh., 7(2):2014, doi:10.4271/2014-01-2326.
3. Z. Gao, T.J. LaClair, C.S. Daw, D.E. Smith, et al., Simulations of the Fuel Economy and Emissions of Hybrid Transit Buses over Planned Local Routes, SAE Int. J. Commer. Veh., 7(1):216-237, 2014, doi:10.4271/2014-01-1562.
4. Z. Gao, C.S. Daw, Advanced Heavy-Duty Engine Systems and Emissions Control Modeling and Analysis, U.S. DOE Hydrogen Program and Vehicle Technologies Program, Annual Merit Review and Peer Evaluation Meeting, Washington DC, June 19, 2014.
5. Z. Gao, T.J. LaClair, C.S. Daw, D.E. Smith, Hybridization Technology Impact on Transit Bus Fuel Economy and Emissions Control, DOE Crosscut Workshop on Lean Emissions Reduction Simulation, Dearborn, MI, April 29, 2014.
6. Z. Gao, C.S. Daw, Advanced HD Engine Systems and Emissions Control Modeling and Analysis, 2013 Annual Report, October, 2013.

Patents

1. None

Tools and Data

1. All the data and component models described above are summarized in the cited publications [1-6].

VI. CODES & STANDARDS

VI.A. EV–Smart Grid Interoperability Center

Principal Investigator: Keith Hardy

Director, EV-Smart Grid Interoperability Center
Argonne National Laboratory
6900 S. Cass Ave., Bldg. 362, Lemont, IL
Phone: 630-816-7383
E-mail: khardy@anl.gov

DOE Program Manager: Lee Slezak

Phone: (202) 586-2335
E-mail: Lee.Slezak@ee.doe.gov

VI.A.1. Abstract

Objectives

- Support the development of **standards to promote universal interoperability** between PEVs, EV supply equipment (EVSE) and the electric power supply infrastructure. Note that both EV and PEV refer to plug-in hybrid and electric vehicles.
 - Directly participate in and/or lead committees established by international standards definition organizations to develop EV-grid connectivity and communication standards.
 - Develop test procedures and tools to verify compliance with the standards.
- Develop **enabling technologies** to verify and implement grid connectivity, communication, sensing and measurement.
- Facilitate **international cooperation** through coordination with industry and government-sponsored initiatives in Europe and Asia.
- Equip the EV–Smart Grid Interoperability Center (IOC) to **support DOE initiatives** in grid integration and modernization.

Major Accomplishments

- SAE J2953 EV interoperability standard**; interoperability requirements and verification test procedures developed by Argonne were issued as recommended standard practices via the SAE consensus based process with industry and other stakeholders.
- AC InterOP Test Fixture (version2)** to verify compliance with the SAE J2953 standard; the first test fixture was transferred to a DOE project to test production EVs and EVSE.
- PEV Compliance Test Tool**; smart Level 2 AC EVSE, based on Argonne’s SpEC module, that tests for compliance with the SAE J1772 charge coupler standard.

- Industrial applications of the SpEC module**; communication controllers for a DC fast charging power system (to emulate a vehicle and/or EVSE) and combined AC/DC charging. Commercialization of the SpEC module was recognized with a Federal Lab Consortium (FLC) Award for Technology Transfer.
- Global InterOP Team**; established with major automakers and the EC Joint Research Center (JRC) to develop global interoperability requirements, procedures and test equipment.
- Enhancements to Argonne IOC facilities**; initiated design and development of additions to the embedded controls and vehicle-grid integration labs.

Future Achievements

- Universal EV interoperability requirements; release a non-proprietary spec for a ‘global test device’ applicable to AC/DC charging (with the Global InterOP Team).
- Developmental applications of the SpEC module; as a ‘smart’ adaptor for ‘dumb’ EVSE and a platform for agent-based control of grid-connected systems.
- Wireless charging test fixture; automated positioning and data acquisition system to verify compliance with SAE J2954.
- Electric fuel delivery measurement device; to verify EVSE compliance with NIST HB44.
- Compact metrology; End Use Measurement Devices (EUMDs) packaged in formats for sub-metering EVs and grid-connected devices.
- Reference vehicle testing at Argonne and JRC; to harmonize PEV test procedures.
- Grid Innovation Lab; expansion of the embedded controls lab to enable hardware-in-the-loop testing in a 100 kW emulated grid.
- Smart Energy Plaza; expansion of the vehicle-grid integration lab to test components, software and standards for energy and transaction management in an integrated dynamic network of EVSE, building systems, distributed energy resources (DERs) and energy storage.



VI.A.2. Technical Discussion

Background

The interoperability centers were established in an agreement between the U.S. Department of Energy (DOE) and the European Commission’s Joint Research Centre

(JRC), signed in November 2011, with the intent of harmonizing EV and battery test procedures as well as EV interoperability. The agreement stipulated the following activities:

- Establish state-of-the-art facilities for development and testing of EV-grid interface technologies.
- Play an active role in standardization.
- Undertake projects to enhance interoperability.
- Participate in inter-laboratory round-robin testing.

Argonne had been involved in standards and technology development at the time of the agreement, but the launch of the center was delayed until FY 2013 when funding became available to equip the vehicle laboratory for grid connectivity and communication development.

Test procedures and tools to verify EV interoperability, as well as related technology, were developed in FY 2013, including the first AC interoperability test tool and the SpEC modules. Subsequent testing found instances of incompatible production EVs and EVSE, though they presumably complied with applicable standards (Figure VI-1).

| PEV | Tier | Test | EVSE 1 | EVSE 2 | EVSE 3 | EVSE 4 | EVSE 5 |
|-----|------|------------|--------|--------|--------|--------|--------|
| 1 | 1 | Mechanical | Green | Green | Green | Green | Green |
| | | Charging | Yellow | Yellow | Green | Green | Green |
| | | Safety | Yellow | Yellow | Yellow | Yellow | Yellow |
| | 2 | Indefinite | Green | Green | Green | Green | Green |
| | | Dynamic | Green | Green | Green | Green | Green |
| 2 | 1 | Mechanical | Green | Green | Green | Green | Green |
| | | Charging | Yellow | Red | Green | Green | Yellow |
| | | Safety | Yellow | Red | Yellow | Yellow | Yellow |
| | 2 | Indefinite | Yellow | Red | Green | Green | Yellow |
| | | Dynamic | Yellow | Red | Green | Green | Green |

■ EVSE and EV completed testing; passed all requirements
■ EVSE and EV completed testing; did not pass all requirements
■ EVSE failed to establish a charging session with the EV

Figure VI-1: Argonne AC interoperability test matrix

In the meantime, JRC gathered European automotive manufacturers and equipment suppliers to get their input on the testing requirements to verify EV-EVSE interoperability. Based on this input, potentially acceptable test equipment was identified and a project was launched in FY 2014 to assess their capabilities to perform the interoperability tests.

The status and accomplishments of the JRC and Argonne centers were documented in early FY 2014 [1] and the results of interoperability testing will be published in Q1 FY 2015 [3].

Introduction

This report covers all the activities in the EV-Smart Grid Interoperability Center (or 'Argonne IOC'), including standards and technology development, grid integration and international cooperation; separate reporting of interdependent tasks in FY 2013 led to unnecessary duplication. Figure VI-2 shows current tasks and the relationship to FY 2015 activities.

Standards

Argonne chaired the SAE J2953 committee and led the development of EV interoperability requirements and test procedures that were issued as standard practices (SAE J2953/1 and J2953/2, respectively).

Technology Development

The SpEC module was further refined and licensed for commercial use as a combined communication controller for AC/DC charging and DC fast charge emulation. It was also the basic component of the PEV Compliance Test Tool.

Grid Integration

Argonne is participating in the NREL-led Multi-lab EV-Grid Integration Study to identify technical interface issues and recommend solutions (i.e., technology development and/or harmonization of standards).

Enhancements to the embedded controls and vehicle labs were initiated to enable hardware-in-the-loop testing of sensing and communication technology in a realistic workplace charging environment.

International Cooperation

Collaboration in Europe focused on efforts with the JRC to compare interoperability requirements, test procedures, equipment and preliminary test results; the objective was to identify differences and recommend specific steps to harmonize. Ensuing interaction with the auto industry led to the formation of an international team to harmonize requirements and specify/develop universal test tools to verify compliance; the target date for requirements and specifications is Q2 FY 2015.

Establishing a cooperative activity with China progressed slower than planned; however DOE and China's Ministry of Industry and Information Technology (MIIT) agreed in July to cooperate on EVs and EV interoperability in particular. This is expected to lead to a cooperative interoperability center at the China Automotive Technology and Research Center (CATARC) in FY 2015.

In addition, China and the US proposed establishing a similar center under the auspices of the Asia Pacific Economic Cooperation (APEC).

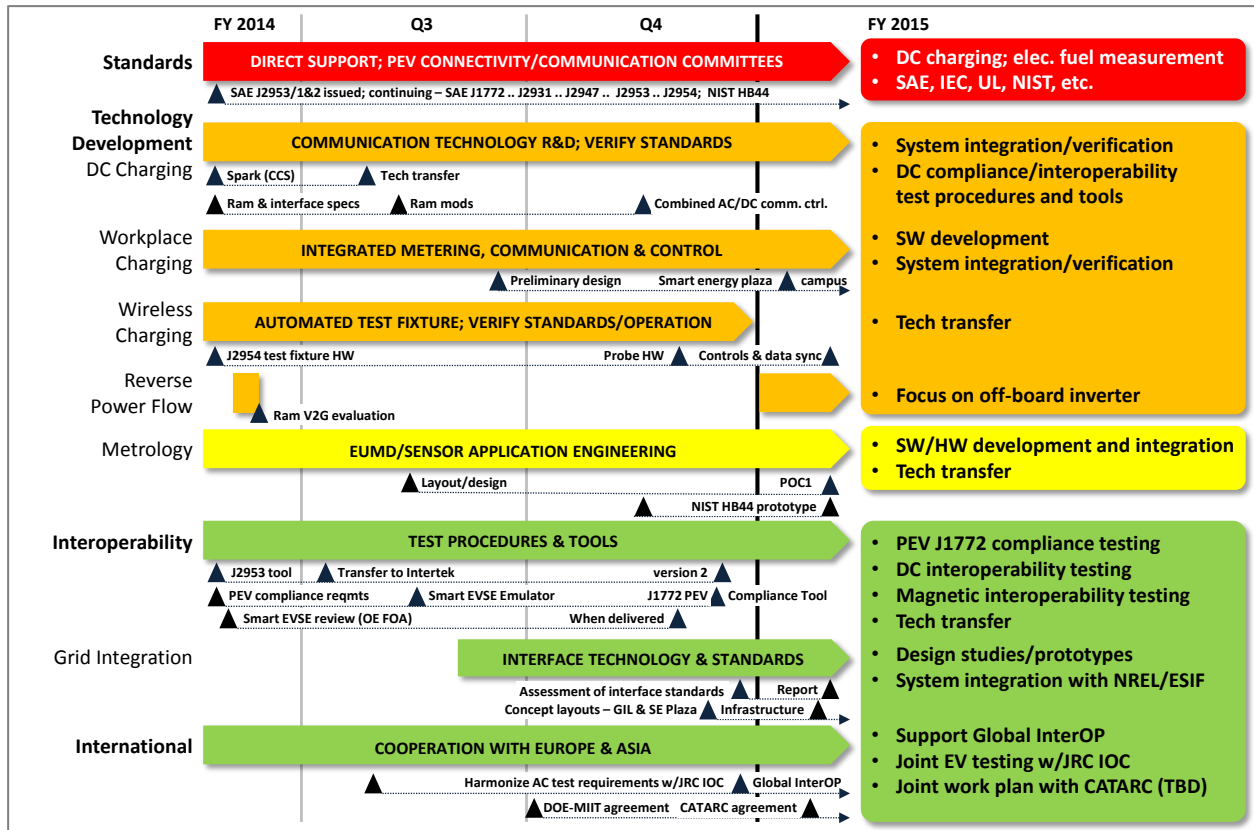


Figure VI-2: Argonne IOC task schedule

Approach

The approach to harmonizing EV testing, battery testing and interoperability are described in this section.

Harmonization of EV Test Procedures

The EV dynamometer testing facility at the JRC IOC in Ispra, Italy was commissioned at the end of FY 2014; hence the efforts to harmonize vehicle test procedures and protocols will begin in FY 2015. The first task will be comprehensive assessment of a PEV at Argonne’s Advanced Powertrain Research Facility (APRF); testing should be completed in Q2 FY 2015. The vehicle will be transported to Ispra for comparable dynamometer testing; this eliminates variables associated with the vehicle and instrumentation – allowing the effort to focus on pre-test preparations, test procedures, analysis and reporting protocols. The BMW i3 with a range extender (Figure VI-3) was chosen because it will allow testing in electric/hybrid modes and it is capable of DC charging using the SAE Combo Coupler System, or CCS, connector.

Harmonization of Battery Test Procedures

Comparison of battery test procedures awaits completion of the enhancements of the JRC-IET battery laboratory in Petten, NL, expected in mid-2015, and development of a joint work plan with the DOE/Argonne battery testing activities.



Figure VI-3: Reference vehicle – BMW i3 with range extender

Harmonization of EV Interoperability Standards

EV interoperability is being addressed holistically, including direct support to standardization efforts by industry (domestically and internationally), research, analysis and testing. The task areas listed below and described in the following sections are interdependent; sharing personnel, facilities and industry involvement. They are regularly reviewed within the SAE standards committees and/or the U.S. DRIVE Grid Interaction Technical Team as well as in DOE’s Annual Merit Review. This approach insures that industry needs and perspectives are reflected at the Argonne IOC.

- Direct support to EV standards committees
- Standards-related R&D
- International collaboration
- EV-smart grid integration requirements study
- Facility enhancements for grid integration

Direct Support to EV Standards Committees

SAE J1772 Conductive Charge Coupler standard

Argonne developed the DC charging sequence diagrams to harmonize the timing requirements of SAE, DIN, and ISO/IEC. Five timing/sequence diagrams were updated and a new timing requirements table was developed for J1772 v6.

SAE J2953 EV interoperability standard

The focus was on interoperability for AC charging, i.e., the requirements and procedures required to verify compliance with the SAE J1772 EV charge coupler standard. Argonne chaired the SAE J2953 committee, drafted and managed the J2953/1 (requirements) and J2953/2 (test procedures) documents through the review process prior to balloting.

In addition, Argonne developed a MATLAB simulation to provide the necessary timing requirements for rise, fall and settling times in SAE J2953/1; the script was included as an appendix to allow simulation using different combinations of variables. Development of the standard was documented in a 2014 SAE technical paper [3].

SAE J2954 wireless charging standard

The SAE J2954 wireless charging committee has not released a draft standard or defined requirements and test procedures. However, Argonne continued work with the subcontractor to finalize the design of the positioning systems for the field probe, vehicle and transmitter coil as well as data acquisition and synchronization. The integrated and automated system is expected to be commissioned in Q1 FY 2015.

NIST Handbook 44 standard

Argonne chaired a subcommittee of the NIST HB44 committee related to sub-meter definitions and standard measurement of electric fuel delivery; a prototype tool for EVSE testing was designed this year and will be fabricated in FY 2015.

Standards-related R&D

AC Interop Test Fixture (Version 2)

The first version of the AC interoperability test tool, which was designed and fabricated by Argonne in FY 2013, was transferred to a DOE contractor in Q1 FY 2014 to evaluate the interoperability of production EVs and EVSE because off-the-shelf equipment does not support testing according to the standard.

Argonne designed the second version of the test fixture to be more portable and user-friendly (Figure VI-4) by replacing the analog scope with an internal digital scope and adding wireless communication.

SAE J1772 PEV Compliance Test Tool

EV compliance with the SAE J1772 connector standard is a prerequisite for standard EV-EVSE interoperability; Argonne defined the test procedures and, leveraging the SpEC module, developed a smart AC Level 2 EVSE that provides the functions required for the PEV Compliance Test Tool.



Figure VI-4: Argonne's AC Interop Test Fixture (Version 2)

The tool features a touchscreen LCD and an interactive LabVIEW GUI; a LabVIEW iPad app was developed for wireless control of the tool (Figure VI-5).



Figure VI-5: Argonne's PEV Compliance Tool

Combining the reporting capabilities of the AC Interop Test Fixture with the PEV Compliance Test Tool results in a compliance/interoperability tool set that will contribute substantially to the development of a universal interoperability test tool in FY 2015.

Industrial applications of the SpEC module

Chrysler Ram DC Charging Pilot Project – Argonne and Chrysler collaborated on modifications to the RAM DS PHEV pickup to enable both DC Level 1 and Level 2 DC fast charging. This activity leveraged previous DOE projects; the Ram pickup, developed in an ARRA project to demonstrate reverse power flow (vehicle-to-home), and the SpEC module.

The effort required close collaboration with Chrysler to design hardware and software to enable DC fast charging on the RAMs using the CCS connector. Results of this activity will

be used to support the FY 2015 efforts to define DC interoperability requirements.

DC fast charge emulator – Argonne demonstrated in FY 2013 that two SpEC modules could be combined with an Aerovironment ABC-170 to emulate DC fast chargers and/or PEVs capable of fast charging. The effort in FY 2015 focused on software security and development of the necessary documentation to make the SpEC modules truly “plug ‘n play.” The latest version of the SpEC module is shown in Figure VI-6.



Figure VI-6: Argonne's SpEC communication controller module

International collaboration

International efforts focused on cooperation with the JRC IOC to work toward common EV interoperability requirements, test procedures and test tools to verify compliance. With these objectives in mind, the labs in the US and Europe took different approaches to the problem. Argonne had led the development of the SAE AC interoperability standard and, therefore, developed test procedures and equipment to verify compliance accordingly.

The ISO/IEC had not developed a specific interoperability standard, so the JRC IOC gathered automotive manufacturers and test equipment suppliers to develop a comprehensive list of interoperability requirements. The 'EU InterOP' project was then formed by the German automotive manufacturers (Audi, BMW, Ford of Europe, GM, Opel, Porsche and VW) and the JRC IOC to launch a program that would evaluate available test equipment versus the test requirements. Comparison of the requirements to those of SAE J2953 implied substantial agreement as well as some gaps from a global perspective.

In the spring of 2014, the German Ministry of Transport, along with automakers BMW, Daimler, Porsche and VW plus the utility EnBW, launched the "Schnellladenetz für Achsen und Metropolen" (SLAM) project to install 400 DC quick charging points across Germany by 2017. One element of the project is development of a test tool to verify EV interoperability at these charge points.

Since the DOE, JRC and German initiatives share objectives, German automotive manufacturers in EU Interop proposed joining forces and a 'Global InterOP Team' was formed by adding Argonne and representatives of the SLAM project. Key objectives of the team are definition of universal interoperability requirements and development of a non-proprietary specification for a 'golden test device' applicable

for AC and DC charging. The preliminary set of requirements is scheduled to be completed this year and the target for completion of a prototype tool is mid-CY 2015.

Discussions regarding cooperation in Asia are being coordinated with DOE International Affairs to ensure Argonne IOC activities are consistent with ongoing policy discussions between the US, China and APEC. Activities in FY 2014 included participation in the bi-annual US-China EV/battery technology workshop and contributions to strategic documents and proposals to China (MIIT/CATARC) and APEC by DOE Policy and/or International Affairs.

EV-smart grid integration requirements study

The NREL-led Multi-lab EV-Grid Integration Study was initiated in mid- FY 2014; Argonne's role is assessing technology and standards for hardware and software interfaces with the grid, with the objective of recommending technology development and/or refinement of connectivity or communication standards to insure EV interoperability.

Various smart grid architectures were reviewed as well as standards for physical connectivity, communication, information exchange and cyber security. Comparison of the EVSE- and grid-related standards identified barriers to integration for the communication and information layers that will need to be addressed by harmonizing interface standards or developing technology such as protocol translators or gateways. The final report is planned for Q1 FY 2015.

Facility enhancements to support grid integration

The Argonne IOC relies on the embedded controls and vehicle-grid integration labs for development and testing of components designed for EV-EVSE connectivity and communication to standard grid interfaces such as meters. Comprehensive grid integration will require communication between vehicles, the charging infrastructure, buildings, distributed energy resources and energy storage (or some combinations of these) to support intelligent energy and transaction management. Argonne's contribution to the Multi-Lab EV-Grid Integration Study is to assess these interfaces and identify technical needs for integration and 'standard' communication; the facility enhancements are intended to facilitate development based on the recommendations.

The enhanced facilities will provide a more comprehensive development and testing environment to support grid integration. The embedded controls lab is being expanded to allow flexible hardware-in-the-loop testing in a 100 kW simulated/emulated grid. This 'grid innovation lab' will be comprised of technology kiosks with EV/EVSE components, building systems, DERs and grid storage ... all linked by a common power bus and control system. These networked systems will facilitate control system integration, power quality studies and energy management system demonstrations emulating integrated workplace energy management.

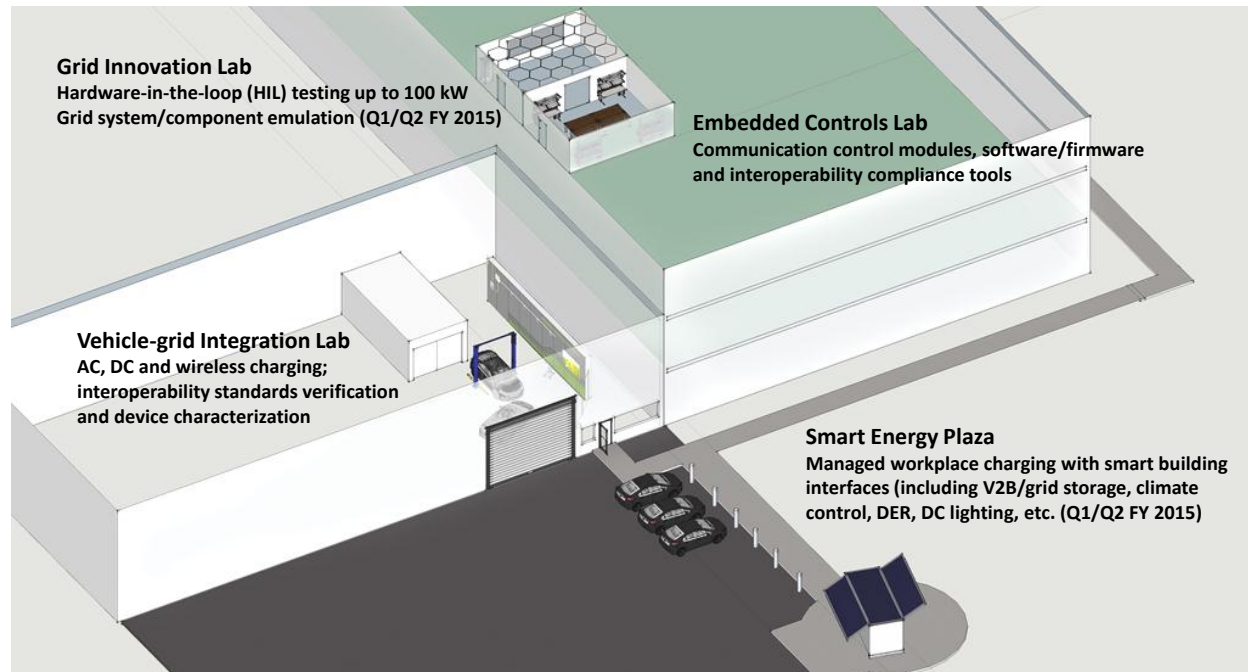


Figure VI-7: Laboratories and capabilities of the Argonne EV-Smart Grid Interoperability Center

The vehicle-grid integration lab is being expanded to include an outdoor 'smart energy plaza' with networked EVSE, building systems, DERs and energy storage. This dynamic environment will enable integrated control system development for energy and/or transaction management, i.e., a venue for development and/or testing of sensing and measurement devices, communication controllers, translators/gateways, agent-based control systems and the requisite interface standards. Figure VI-7 provides an overview of existing facilities of the IOC and enhancements underway.

Results

Notable results this year include issuance of key parts of the SAE J2953 interoperability standard, development of test tools to verify compliance with the standard, commercial applications of the SpEC module and formation of an international team to work toward global interoperability requirements and common test tools.

SAE J2953 Interoperability Standard

SAE J2953/1, which establishes requirements and specification by which a specific PEV and EVSE pair can be considered interoperable, was issued in Q1 FY 2014.

SAE J2953/2, which establishes the test procedures to ensure the interoperability of PEV and EVSE for multiple suppliers, was issued in Q2 FY 2014.

Interoperability Test Tools

The AC InterOP Test Fixture (version 2) implements the test procedures specified in SAE J2953/2 to evaluate the connectivity and communication of an EV-EVSE pair versus the interoperability requirements specified in SAE J2953/1; the tool was completed in Q4 FY 2014.

The PEV Compliance Test Tool implements test procedures defined by Argonne to evaluate the connectivity of a PEV versus the requirements of SAE J1772; the tool was completed in Q4 FY 2014.

Industrial Applications of the SpEC Module

Argonne collaborated with Chrysler to incorporate the SpEC module in the RAM DS PHEV pickup to enable both DC Level 1 and Level 2 DC fast charging using the CCS connector. Lessons learned in this project will support the Global InterOP team and SAE J2953 committee as they define and standardize EV interoperability requirements and procedures.

Argonne's FY 2013 development efforts with the SpEC module paid off in FY 2014; it was licensed for use with an Aerovironment ABC-170 to emulate DC fast chargers and/or PEVs/batteries capable of fast charging. In addition, the module was licensed for use in a production-intent DC smart charger. Hence, efforts this year focused on embedded software security and documentation.

International Cooperation

The 'Global InterOP Team' was formed by the major automotive manufacturers in the EU (with the cooperation of their US counterparts), JRC, the German SLAM project and Argonne to work together on global EV interoperability requirements and a universal 'golden test device' to verify compliance. The team's schedule calls for completion of preliminary interoperability requirements and an 'open' specification for the test tool by Q2 FY 2015.

Conclusions

Cooperation between Argonne and the US automotive industry resulted in substantial contributions to the definition of

standard practices, tools to verify compliance and technology to implement EV interoperability standards.

Cooperation between the US and European IOCs led to substantive joint activities and collaboration with industry to develop global interoperability requirements and test tools.

Investments by the US DOE and EC JRC in the IOCs are paying off, both domestically and internationally. Programmatic and technical relationships between government and industry have produced measurable results in terms of program coordination, standard practices, tech transfer and commercialization.

Publications

1. Hardy, K., Bohn, T., Slezak, L., Krasenbrink, A. and Scholz, H., US-EU Joint EV-Smart Grid Interoperability Centers, EVS27 Symposium, Barcelona, Nov. 2013.
2. Hardy, K., Scholz, H., Dobrzynski, D., Lajtkep, A. and Selle, W., "Progress toward Harmonization of EV Interoperability Requirements in Europe and the US", EEVC, Brussels, Dec. 2014.
3. Dobrzynski, D. and Harper, J., "Development and Implementation of SAE J2953 for AC Charging," SAE Int. Journal of Passenger Cars – Electronic & Electrical Systems 7(1):85-94, 2014, doi:10.4271/2014-01-0184.

Tools and Data

1. AC InterOP Test Fixture (compliance of an EV-EVSE pair with the SAE J2953 AC interoperability standard)
2. PEV Compliance Tool (compliance of a PEV with the SAE J1772 charge coupler standard)

VI.B. Codes and Standards and Technical Team Activities

Principal Investigator: James Francfort

Idaho National Laboratory
P.O. Box 1625, Idaho Falls, ID 83415-2209
(208) 526-6787
James.francfort@inl.gov

DOE Program Manager: Lee Slezak

(208) 586-2335
Lee.slezak@ee.doe.gov

VI.B.1. Abstract

Objectives

- To contribute vehicle, component, and fueling infrastructure testing knowledge gained by Idaho National Laboratory (INL) staff from 232 million miles of benchmarking to industry and government groups developing and modifying standards, codes, best practices, and regulations.

Major Accomplishments

- Recognition as an industry expert and being a voting member of these industry and government committees is a major accomplishment in itself.
- The current committees/organizations that INL staff are contributing to include the following:
 - Society of Automotive Engineers (SAE) J2954 Wireless Charging Task Force
 - SAE J2894 Power Quality Requirements for Plug-in Electric Vehicle Chargers
 - National Institute of Standards and Technology's U.S. National Work Group on Measuring Systems for Electric Vehicle Fueling and Submetering
 - U.S. Drive: Vehicle Systems Analysis Tech Team
 - U.S. Drive: Grid Integration Tech Team
 - Electric Power Research Institute – National Electric Transportation Infrastructure Working Council.

Future Achievements

- Continued future participation on various committees and panels, representing U.S. Department of Energy (DOE) interests and providing expertise and testing results from testing of cutting edge advanced technologies.



VI.B.2. Technical Discussion

Background

DOE's Advanced Vehicle Testing Activity (AVTA) is part of DOE's Vehicle Technologies Office, which is within DOE's Office of Energy Efficiency and Renewable Energy. AVTA is the only DOE activity tasked by DOE to conduct field evaluations of fueling infrastructure and light-duty vehicle technologies that use advanced technology systems and subsystems in light-duty vehicles to reduce petroleum consumption. A secondary benefit is reduction in exhaust emissions.

Most of the advanced technology vehicles, subsystems, and fueling infrastructure that AVTA tests include the use of electric drive propulsion systems and advanced energy storage systems. However, other vehicle technologies that employ advanced designs, control systems, or other technologies with production potential and significant petroleum reduction potential are also considered viable candidates for testing by AVTA. AVTA and INL's first priority is providing DOE feedback on the performance of advanced technologies that DOE has made funding investments in.

The AVTA light-duty activities are conducted by INL for DOE. INL has responsibility for AVTA's execution, direction, management, and reporting. INL is supported in this role by various subcontracts for specific tasks when greater value can be achieved for DOE if INL conducts research in partnerships with other organizations.

The AVTA sections of the FY 2014 Annual Program Report jointly cover the testing work performed by INL and any subcontractor conducting work that INL manages. When appropriate, AVTA partners with other governmental, public, and private sector organizations to provide maximum testing and economic value to DOE and the United States' taxpayers via various cost-sharing agreements.

Introduction

DOE's AVTA is evaluating grid-connected plug-in electric drive vehicle (PEV) technology in order to understand the capability of electric grid-recharged electric propulsion technology to significantly reduce petroleum consumption when vehicles are used for transportation. In addition, many companies and groups are proposing, planning, and have started to introduce PEVs into their fleets.

Knowledge that INL staff has gained from 20 years of testing electric drive and other vehicle technologies and fueling infrastructure for more than 232 million miles is used by INL staff to contribute to various industry and government groups that are primarily interested in developing policies,

standards, codes, and regulations that ensure safety and interoperability within technologies sectors.

Approach

As a member of a technical committee or industry group, participation is intended to contribute to the common body of knowledge being applied to develop standards and other industry practices. Participation is also intended to represent DOE interests.

Results

SAE International

SAE J2954 Wireless Charging Task Force: INL supports the SAE J2954 committee as a full voting member and by providing detailed test results from wireless charging systems. The test results detail system efficiency and EM-field strength. Additionally, multiple factors (such as misalignment, coil gap, component temperature, and debris tolerance; all of which impact the system efficiency and EM-field strength) are tested and detailed to the SAE J2954 committee in order to support the safety and test procedures sections of the document.

INL has performed the only independent testing of a wireless power transfer technology and published the testing results. The testing was conducted under a non-disclosure agreement with Evatran; Evatran has graciously allowed INL to publish very detailed testing results. The detailed results are provided elsewhere in this annual report. From the information learned from the Evatran test results, INL has provided numerous revisions to the SAE J2954 document.

SAE J2894 Power Quality Requirements for Plug-in Electric Vehicle Chargers: The SAE J2894 committee is developing requirements and test procedures to ensure that PEV chargers do not cause power quality issues and that the PEV can continue to function properly in the presence of power quality issues caused by adjacent loads. Because both conductive and wireless power transfer systems testing are being conducted at INL, INL staff participation as a committee member and INL input is considered as a valuable resource of expertise and hands-on experience for the committee.

National Institute of Standards and Technology

U.S. National Work Group on Measuring Systems for Electric Vehicle Fueling and Submetering: This National Institute of Standards and Technology committee is developing a draft standard of rules and regulations that electric vehicle supply equipment (EVSE) must adhere to if the EVSE sells power and they are the point of metering. INL staff participation in this meeting is important, because in the future, EVSE will need to be tested to ensure they are following the standard. By participating in this standard development, INL staff engineers are helping to direct future EVSE testing needs, methods, and procedures.

U.S. Drive (United States Driving Research and Innovation for Vehicle efficiency and Energy Sustainability)

Vehicle Systems Analysis Tech Team: INL is a long-time member of the Vehicle Systems Analysis Tech Team because of the history of the testing INL performs for DOE. INL staff contributes, via presentations and papers, the results of benchmarking advanced automotive powertrain components and subsystems from INL's whole vehicle system and component testing. This testing includes fuel use, efficiencies, auxiliary loads, and energy storage results that are subsequently used by other team members as modeling inputs.

Grid Integration Tech Team: INL is a founding member of the Grid Integration Tech Team by nature of the infrastructure testing INL performs for DOE. This includes wireless power transfer and conductive charging, including DC fast charging and INL's data collection, analysis, and reporting as to how 8,000 PEV drivers utilize 16,000 Level 2 EVSE and DC fast chargers.

Electric Power Research Institute – National Electric Transportation Infrastructure Working Council

Infrastructure Working Council: INL is a 20-year member of the Infrastructure Working Council, which is sponsored by the Electric Power Research Institute and is a group of individuals whose organizations have a vested interest in the emergence and growth of the electric vehicle and plug-in hybrid and electric vehicle industries, as well as the electrification of truck stops, ports, and other transportation and logistics systems. Infrastructure Working Council members include representatives from electric utilities, vehicle manufacturing industries, component manufacturers, government agencies, related industry associations, and standards organizations. The various committees meet several times a year to address the main areas of electric vehicle, plug-in hybrid electric vehicle, truck stop and port electrification, and infrastructure research and development. INL supports the Plug-in Hybrid and Electric Vehicle Working Group and the Transportation Electrification Committee, as well as serving on the Infrastructure Steering Committee. The results from INL's testing of vehicles and infrastructure, as well as data collection from 24,000 vehicles and charging infrastructure units, with data loggers, is of great interest and support to the Infrastructure Working Council's decision processes.

Conclusions

The intent of the work that is described in this section is to leverage the benchmark testing results and staff knowledge gained as a resource to various industry groups that are putting in place either industry-led or government-led codes, standards, requirements, or best practices.

VI.B.3. Products

Publications

The intent of this work is decidedly not to publish results as products of INL because the outcomes are usually the sole intellectual rights of other organizations, such as SAE.

Patents

The work that is described in this section will not result in INL patents. The intent of this work is to provide technical support to DOE and industry in the development of standards.

Tools and Data

Whenever possible, INL leverages its data and testing capabilities to support the development of codes and standards.

VI.C. Model Reusability

Principal Investigators: Chuck Folkerts (Project Leader), Larry Michaels, and Aymeric Rousseau

Argonne National Laboratory
9700 South Cass Avenue
Argonne, IL 60439-4815
Phone: (630) 252-7261
E-mail: cfolkerts@anl.gov

DOE Program Manager: Lee Slezak

Phone: (202) 586-2335
E-mail: Lee.Slezak@ee.doe.gov

VI.C.1. Abstract

Objectives

- Establish dynamical modeling and simulation standards.
- Facilitate dynamical modeling and simulation of automotive systems.
- Make dynamical models universally reusable using plug-and-play technology.

Major Accomplishments

- Defined, refined, validated, and completed the architectural partitioning of a ground vehicle system model into a hierarchical organized set of fundamental subsystem building blocks.
- Defined the interfaces for all of the fundamental subsystem building blocks for a ground vehicle system simulation model.
- Summarized and documented work by writing a draft of SAE Standard Recommended Practice J-3049 (Task 2), called "Model Architecture and Interfaces Recommended Practice for Ground Vehicle System and Subsystem Dynamical Modeling and Simulation."

Future Achievements

- Submit the draft of SAE J-3049 to the Dynamical Modeling and Simulation Technical Committee for approval vote.
- Submit SAE J-3049 to SAE for formatting.
- Submit to SAE Motor Vehicle Council for final voting approval and adoption as a standard.
- Publish SAE J-3049 in first quarter of CY15.



VI.C.2. Technical Discussion

Background

The complexity of automotive ground vehicle systems (as used in passenger cars, heavy-duty trucks, military vehicles, and agricultural, mining, and construction equipment) is increasing at a rapid rate, as are competitive pressures to reduce product development cycle times. Development of these modern automotive systems requires highly coordinated collaboration between the disciplines of engineering and physics within organizations, and among a network of original equipment manufacturers, suppliers, research laboratories, and universities across the industry and around the globe.

To keep up with technology changes and competitive pressures, these global teams need virtual engineering methods to enable responsive, cost-effective, and efficient collaborative development. To make global enterprise and cross-enterprise virtual engineering methods cost-effective, efficient, and robust, automotive-industry-wide standards for virtual engineering of dynamical modeling and simulation are required.

Introduction

Background

Future development of automotive systems will continue to be driven by the same forces and trends that drive it today: continual improvements in fuel efficiency, quality and reliability, emissions performance, and safety, with more value to the customer for a lower cost. To minimize costs and time, automotive systems will be developed by global teams collaborating across an industry network using virtual engineering processes and methods with minimal physical builds to confirm designs and performance only. Virtual engineering of automotive systems will require dynamical modeling and simulation that integrate models with varying levels of abstraction (fidelity and complexity) from different companies and disciplines. Such models will enable global teams to engineer and develop automotive systems rapidly, efficiently, and effectively and facilitate an integrated development process that seamlessly flows between all processes from research to production.

The Dynamical Modeling and Simulation Technical Committee (DM&S TC), a committee of experts from industry, academia, and the national laboratories, was formed to address these issues and requirements by developing standard recommended practices for dynamical modeling and simulation of a ground vehicle system.

Objective

The objective of the committee is to establish modeling and simulation standards to facilitate dynamic modeling and simulation of automotive systems. These standards will facilitate integrated and multidisciplinary virtual engineering processes for highly coordinated and collaborative engineering work. SAE Standards, Recommended Practices, and Information Reports (standards) will be established and published to facilitate and promote the following:

- 1) Cost-effective, efficient, and robust model and data sharing and reuse;
- 2) Seamless modeling, simulation, and analysis workflows;
- 3) Virtual engineering processes;
- 4) Interoperability in modeling and simulation tools; and
- 5) Portability across simulation tools.

Scope

The committee will focus on developing standards for dynamical models and simulations that mathematically describe an automotive system's time-varying response and behavior and the interactions of its subsystems and components. These standards will include processes, methods, performance metrics, and analyses related to improving the reusability and effectiveness of dynamic modeling and simulation for automotive systems. The goals are to make models reusable and simulation results predictable and repeatable across engineering and physics disciplines, application tools, and the automotive industry.

Benefits

The established standards will improve the overall efficiency of development processes by providing a "common language" and a means for sharing and reusing data and mathematical simulation models of dynamic systems across engineering disciplines within companies and across the industry network. Hence, these standards will facilitate virtual engineering of automotive systems, resulting in optimized performance, improved process efficiency, and reduced development time and costs for the automotive industry and individual companies. Such process enhancements will accelerate the rate of development and adoption of new technologies, thereby providing improvements in fuel economy, efficiency, and displacement.

Approach

The committee developed a charter and a work plan for developing standards to enable and facilitate model reusability. After defining its charter, the committee identified and prioritized four main standards development projects (tasks), to be developed in the following order.

- 1) Model Description Documentation Project (Task 1)
 - Define the content of documentation necessary to decide whether a model is appropriate for a given task.
 - Define model uses or applications for which the model is appropriate.

- Define what the model does; what principles, theories, and/or equations it is based upon; and what approximations or assumptions were made.
 - Provide any verification and validation work performed (i.e., test data and reports).
 - Provide technical specification and development history for model maintenance and upgrades.
- 2) Model Architecture and Interfaces Definition Project (Task 2)
 - Define a model architectural structural partitioning into subsystems and their interfaces for any ground vehicle system and the associated subsystems, including the location of system and subsystem controls in the architecture.
 - Define the architecture interfaces to support any form of simulation, such as MIL, SIL, RCP, and HIL interfaces to controls models.
 - 3) Model Data Dictionary Information Project (Task 3)

Define the file format for the metadata needed to describe the fundamental information required to support import/export reuse of models between simulation models of ground vehicle systems through plug-and-play for a given simulation tool. The model information metadata include the following:

- Model classification type, version, creator, fidelity, accuracy, computational workload, tool version compatibility, and other model classification characteristics.
- Model interfaces (inputs, outputs, and buses), variables, and parameters, including names, data types, data ranges, and meanings of interfaces, variables, and parameters.

- 4) Model Portability and Interoperability between Tools Project (Task 4)

Define the methods, procedures, and file formats needed to support plug-and-play import/export reuse of models between software applications by means of interoperability (e.g., co-simulation or wrapped-code) or porting of models between tools with repeatable results. The methods and procedures for model portability and interoperability include the following:

- Define model simulation requirements needed to make the model function in the simulation of a system with repeatable results.
- Define simulation details related to precision of arithmetic, integration interval, integration type (fixed or variable), required sampling interval, and required ordinary differential equation solvers.
- Define task scheduling for models of control algorithms.
- Define model simulation initialization processes or methods for establishing initial conditions.

The four project tasks are designed to be developed sequentially, with some overlap between them. Each project is dependent upon the projects that precede it. Hence, as one project approaches a sufficient level of maturity, the succeeding project can be ramped up. The sequentially interdependent relationship between the projects is shown in

Figure VI-8, where the increasing capabilities to enable or facilitate model reusability by each project are summarized.

How: To Make Dynamical Simulation Models Reusable

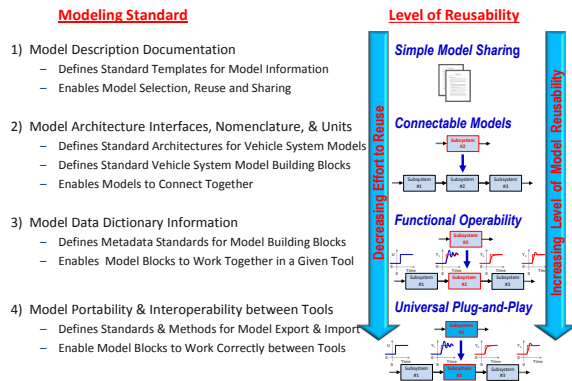


Figure VI-8: Relationship between the four major projects for enabling and facilitating model reusability

The Principal Investigator for this project is the chair of the SAE DM&S TC. He develops proposals for each of the projects. These proposals are submitted to the committee for review, comment, revision, and refinement. As they approach maturity, the proposals are submitted to the committee for a vote to ensure that the committee is reaching a consensus. Once the proposals are approved, the materials are used to produce a draft standards document, which is then reviewed and revised by the committee. Next, the draft is submitted to the DM&S TC for an official approval vote. After approval, the draft is sent to SAE for final formatting before it is submitted to the Motor Vehicle Council for approval and adoption as an official SAE standard.

Results

Ground Vehicle System Model Architectural Structure

The committee has developed a model of the architectural structure for a ground vehicle system. The architecture is a hierarchical structure showing the interconnection of the fundamental subsystem building blocks. The architecture and subsystem partitioning have been validated against all known or proposed alternative vehicle and propulsion configurations for automotive, trucking, military, agricultural, mining, construction, and off-road equipment applications. A ground vehicle system architecture was proposed, modified, and refined through an extensive validation process (using a total of 22 configurations) that included a number of propulsion alternatives— combustion engines, electrics (battery and fuel cell), hybrids (parallel and series), hydraulic hybrids (parallel and series), and flywheel hybrids—and the following chassis alternatives: front-wheel drive, rear-wheel drive, all-wheel drive, tractor trailer, tandem or double-bottom trailers, and trailer trains.

The results of this validation process demonstrated that any ground vehicle system can be described by the hierarchical model architecture structure shown in Figure VI-2 through Figure VI-10. The first level of the hierarchy or top-level view of the model for a ground vehicle system consists of three major subsystems, as depicted in Figure VI-2. The four

main components of the second level of the vehicle subsystem hierarchy are shown in Figure VI-3. Next, Figures Figure VI-4, Figure VI-5 and Figure VI-6 present some of the third level in the hierarchy, which defines the internal structure of the power, chassis, and trailer subsystems. Figure VI-7 shows an example of the trailer architecture for a tandem trailer, where trailer 1 would connect to a trailer 2 at the far right of the diagram. The internal architecture of trailer 2 is the same as that of trailer 1, so it is not shown. An example of a trailer train is displayed in Figure VI-8, where the internal architecture of the *i*-th trailer in the train, which is identical to the architecture of any trailer, is shown. Finally, the internal architecture of the body-frame subsystem and the trailer *i* body-frame subsystem are shown in Figure VI-9 and Figure VI-10, respectively, which reveal some of the fourth level of the architecture.

The internal architecture of the power subsystem architecture is shown in Figure VI-4 as being composed of, at most, eight subsystems. The internal architecture for the chassis subsystem is defined in Figure VI-5 and is composed of, at most, seven subsystems. The trailer subsystem internal architecture is defined in Figure VI-6 as being composed of, at most, seven subsystems, where internal architectural partitioning of the trailer is the same as that of the chassis. The architectural structures of the chassis and the trailer subsystems have the same functional partitioning, since they perform the same fundamental functions: (1) as enclosures for transporting people and their goods, and (2) as support structures for work equipment (i.e. power take-off powered accessories that are used by people to perform work functions).

This layered approach to organizing models in a hierarchy can continue further for each of the subsystems to reveal their internal subsystem architecture until the lowest subsystem level is reached; at that level, the internal architecture of each subsystem is composed of components. Each component would be described at the lowest level of the hierarchy by a mathematical model of its dynamic behavior.

This discussion demonstrates that complete definition of a ground vehicle system hierarchical model to the equation level would require several hundred models. Therefore, the scope of the current Model Architecture and Interfaces Project is limited to defining the architecture and interfaces for the top four levels, as described in Figure VI-9 through Figure VI-17, to establish a standard for plugability of ground vehicle subsystems.

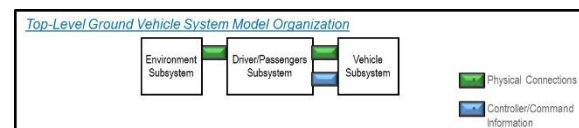


Figure VI-9: Top-level ground vehicle system model organization

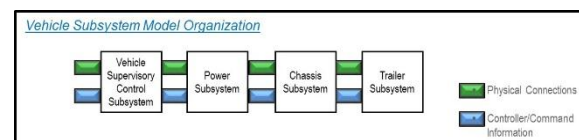


Figure VI-10: Vehicle subsystem model organization

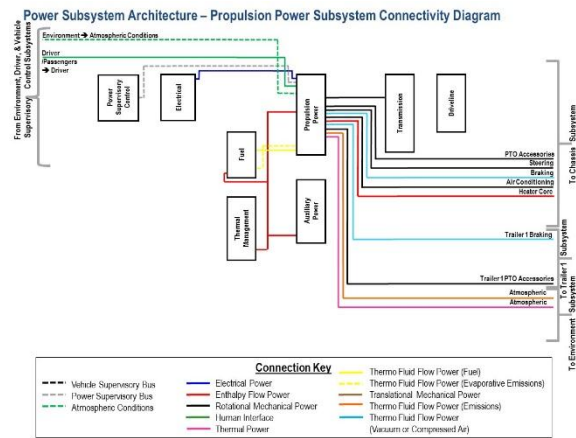


Figure VI-19: Example of a Single Subsystem Connectivity Diagram for the Propulsion Power Subsystem

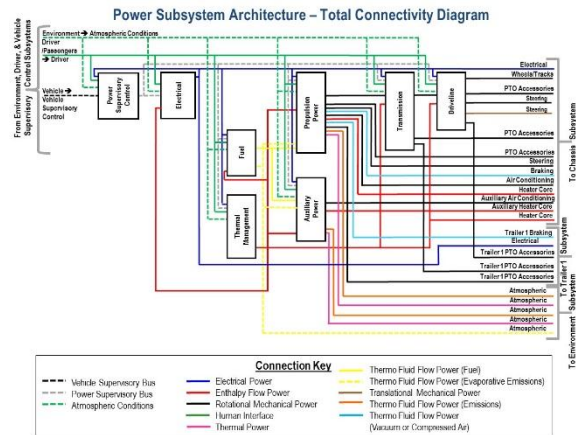


Figure VI-20: Total Connectivity Diagram for the Power Subsystem

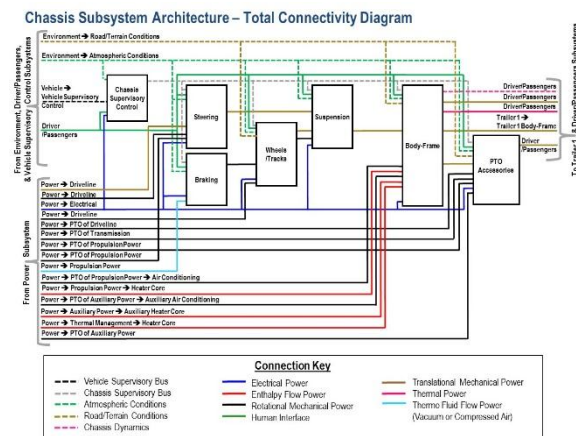


Figure VI-21: Total Connectivity Diagram for the Chassis Subsystem

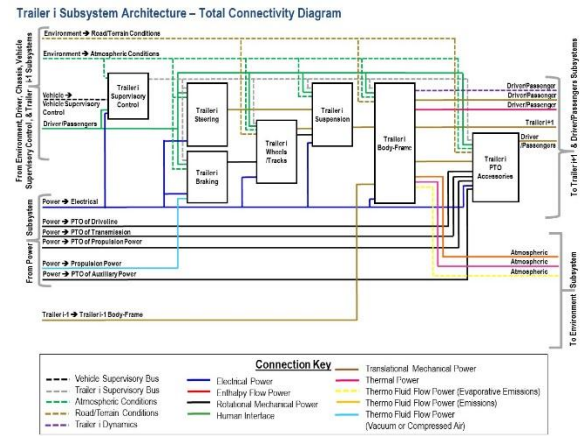


Figure VI-22: Total Connectivity Diagram for the Trailer Subsystem

The standards for the model architecture and interfaces for subsystems in the first four levels are defined. Next, the plan was to shift to the development of standards for playability, portability, and inter-operability, as described in the "Approach" section above under the Task 3 and Task 4 projects. However, these projects will not be pursued, since the tasks have already been adequately covered by a large multi-year European initiative, ITEA 2 (Information Technology for European Advancement 2), which endorsed, initiated, and completed a project called Modelisar. This project has developed (1) a Functional Mock-up Interface that provides a solution for a data dictionary and interface between tools as described in Task 3, and (2) a Functional Mock-up Unit specification that provides a method to package models, data, and solvers for porting models between tools as described in Task 4.

The development of model architecture and interface standards for other lower-level subsystems and components is beyond the scope of the current effort. The intention of the current project is to lay a foundation for model reusability through standards that establish plugability and playability of dynamic models for ground vehicle systems. This foundational methodology could be extended to lower-level subsystems and components in the future. However, in doing so, care must be taken not to specify details that would limit the flexibility of the architecture to address the modeling of any ground vehicle system.

Conclusions

The definition of the system architectural structure and the partitioning of a ground vehicle system model into subsystems have been completed. Subsystem model interfaces have been defined for the 44 fundamental subsystem building blocks that define a hierarchical ground vehicle system model.

During this year, a draft for an SAE Standard (J-3049), called "Model Architecture and Interfaces Recommended Practice for Ground Vehicle System and Subsystem Simulation," was developed by the SAE DM&S TC. The standard is in the process of final revision and will be submitted to the DM&S TC for a vote in October 2014. After the standard is approved and formatted by SAE, it will be

submitted to the SAE Motor Vehicle Council for review, voting, and approval as an official SAE standard recommended practice.

VI.C.3. Products

Publications

1. SAE J-3049: Model Architecture and Interfaces Recommended Practice for Ground Vehicle System and Subsystem Dynamical Modeling and Simulation (to be submitted to SAE DM&S TC for approval in October 2014, with publication expected in the first quarter of 2015).
2. DOE Annual Project Report 100161.00: Model Reusability.

VI.D. SAE Standards Development Support

Principal Investigator (Rick Pratt)

Organization: Pacific Northwest National Laboratory
 Address: P.O. Box 999, M/S: K5-17
 Phone: (509) 375-3820
 E-mail: rmpratt@pnl.gov

DOE Program Manager (David Anderson)

Phone: (202) 287-5688
 E-mail: David.Anderson@ee.doe.gov

Future Achievements

- Complete technical reviews of J2836/5 - Customer to Vehicle communications use cases
- Support development of J2847/5 - Customer to Vehicle communications messages
- J2847/3 – Communication for Plug-in Vehicles as a Distributed Energy Resource messages
- PEV / Grid Integration Charging Economic tool development for quantifying regional value propositions
- Complete Multi-Lab PEV Smart Grid Integration Requirements and Opportunities Study and collaborate conducting high value PEV Charging / Grid integration demonstration.



VI.D.1. Abstract

Objectives

- PNNL will contribute to accelerating the development and harmonization of vehicle to grid communication standards by supporting the SAE, ANSI and NIST/SGIP technical working groups to develop use cases and technical requirements in the development of the following standards:
- J2847/3 - Communication for Plug-in Vehicles as a Distributed Energy Resource
- J2836/5 - Customer to vehicle communication
- PNNL will provide leadership to the Smart Grid Interoperability Panel (SGIP) vehicle to grid domain expert working group (V2G DEWG) to identify and address high priority industry needs for standardization.

Major Accomplishments

- PNNL submitted use cases, performed technical reviews, and helped SAE committees develop the following standards. J2836/3 has completed committee preparation and is in the review and approval process.
- J2847/3 – Communication for Plug-in Vehicles as a Distributed Energy Resource.
- J2836/5 – Use Cases for Customer Communications with the Electric Vehicle.
- PNNL prepared and presented use cases for J2836/5 – Customer to Vehicle communications standard.
- PNNL evaluated the economics of using PEV & V2G charging as a grid resource, provided recommendations for additional investigation, and tested foundational capabilities needed to develop a realistic PEV / Grid Integration Value proposition.
- PNNL coordinated with industry stakeholders to develop a new priority action plan (SGIP/PAP-22) for developing submetering requirements for EV fueling.
- PNNL completed providing leadership to the NIST V2G DEWG and transitioned the leadership.

VI.D.2. Technical Discussion

Background

EV Standards Development

The interoperability between vehicles, charging stations and electric utilities is critical to the success of electric vehicle deployment. SAE, ISO and IEC are leading the US standards development to define the communication architectures, protocols and messages.

To expedite the standards development process DOE / EERE / VSST has been funding national laboratories (PNNL, ANL, ORNL and INL) to provide technical support for the SAE, ANSI, and NIST standards development process.

FY 2014 SAE communications standards development began with a recognition that standards needed to be updated (i.e., J2847/2), several needed to be completed (i.e. J2847/3 and J2836/5), and contributing to the gap analysis of standardization efforts.

Introduction

In order to promote the widespread adoption of electric vehicles, interoperable charging infrastructure must be made available. While the majority of electric vehicle charging events currently take place at home using residential AC Level 1 or Level 2 charging equipment, the availability of public and commercial (such as workplace and retail) charging infrastructure may alleviate “range anxiety,” increasing driver confidence and the overall utility of electric vehicles.

Approach

PNNL participates in the monthly committee meetings and actively contributed to the development and technical review of SAE EV/EVSE communication standards J2847/3 and J2836/5. PNNL prepared and presented use cases to the J2836/5 committee.

PNNL led and contributed to the ANSI Electric Vehicle Standards Panel working groups and NIST SGIP Vehicle to Grid domain working group on smart charging communications and related standards and roadmap development activities.

PNNL evaluated international research conducted to identify the economic benefits of intelligent vehicle charging for the consumer and the utility and tested foundational capabilities needed to develop a realistic PEV / Grid Integration Value proposition.

Results

PNNL participated in the SAE Hybrid committees to review and finalize the J2836/5 standard and support development of the J2847/3 standard. Further, PNNL led the NIST Smart Grid Interoperability Panel (SGIP) vehicle to grid domain expert working group (V2G DEWG) and contributed to the formulation of a priority action plan (PAP-22) for EV fueling submetering requirements. Several new use cases including sub-metering and vehicle telematics have been developed for inclusion in the SAE J2836/5 standard.

In addition to the standard support, PNNL analyzed international reports to identify potential economic and grid impact of Intelligent Charging including:

- The potential system constraints if vehicle charging patterns observed through Transportation Electrification deployment projects are scaled up.
- The types of grid services a fleet of V2G PEVs provide an Intelligent Vehicle Charging (IVC) infrastructure.
- The potential value of the grid services that PEVs could provide.
- The PEV (Plug-in Electric Vehicle), EVSE (Electric Vehicle Support Equipment), and smart grid communication needed for IVC implementation.
- The IVC optimization strategies that would maximize the benefits to the PEV owner and the grid, while minimizing costs.

The analysis concluded:

- Continued or accelerated PEV sales growth will lead to an emerging grid load that with adequate coordination and communications can offer valuable load-shifting and ancillary services to the grid. The degree to which this new PEV load will be enabled depends on specific regional and local needs as well as policies and standards that enable PEVs to become responsive to pricing and other signals.
- Grid services for individual PEVs will be limited to integration with residential home energy management

system primarily due to the current minimum aggregation limits. Adding PEV charging rate control to the home energy management system can level home demand, enable effective load shifting, and mitigate demand charges.

- Grid services for aggregated loads of PEVs have the potential for business model development. These aggregated PEV loads must be capable of dynamically adjusting to changing grid services requirements to maximize customer benefit. These grid services must be customized to the local region.

Conclusions

The value of electric vehicle communications standards includes five necessary electric vehicle and charging infrastructure capabilities:

1. EVSE and EV interoperability between vendors.
2. International markets for U.S. vehicle manufacturers.
3. International vehicle and EVSE manufacturers compliant to U.S. standards.
4. PEV charging generates value to the electric power grid that is monetized for the PEV customer.
5. Renewable energy resource challenges mitigated and utilization enhanced.

Optimizing PEV charging must integrate customer needs, grid needs, local electricity markets, and utility requirements. A tool is needed to perform this regional economic analysis. The tool used in the PEV / Grid Integration report was adapted from energy storage applications. When PEV optimization characteristics are added, it could provide a method to quantify the value proposition for PEV / Grid integrated charging and develop a range of use cases for IVC communication development.

VI.D.3. Products

Publications

1. Pratt, R.M., Kintner-Meyer, M., & Stanton, N.E., "PEV / Grid Integration: Value Proposition and Charging Optimization," Pacific Northwest National Laboratory, October 2014.
2. RM Pratt, 2014. "Vehicle to Grid Communications and Field Testing." Presented by Rick Pratt (Invited Presenter) at DOE Office of Vehicle Technology - Annual Merit Review 2014, Washington, DC on June 16, 2014. PNNL-SA-102785.
3. RM Pratt, 2014. "Vehicle Communications and Charging Control." Presented by Rick Pratt (Invited Presenter) at DOE Office of Vehicle Technology - Annual Merit Review 2014, Washington, DC on June 17, 2014. PNNL-SA-102303.

VI.E. HEV, PHEV, EV Test Standard Development and Validation

Principal Investigator: Michael Duoba

Argonne National Laboratory
9700 South Cass Ave, Argonne, IL, 60439
Phone: (630) 252-6398
E-mail: mduoba@anl.gov

DOE Program Manager: Lee Slezak

Phone: (202) 586-2335
E-mail: Lee.Slezak@ee.doe.gov

emissions are judged. Historically, vehicle testing procedures have typically been developed with traditional conventional vehicles in mind. Such test methods may not be suitable for new advanced powertrain technologies. This is a critical issue, as the introduction of electrified powertrain technologies could be derailed if their advantages are under- or over-reported by test evaluation. Argonne National Laboratory, along with many other partners, has been developing new, robust analytical testing techniques for close to two decades. This important standards work protects the substantial investments made by the US DOE VTO into advanced vehicle propulsion technologies.

VI.E.1. Abstract

Objectives

- Organize and chair an SAE standards task force to define test methods for hybrid vehicle system power rating.
- Collaborate and communicate with several international entities also involved with vehicle system power definition.
- Leveraging existing vehicles, instrumentation, hardware and test equipment, invent new approaches for testing system power rating.

Major Accomplishments

- Completed “neck-down” of possible system power testing approaches and defined the document scope which includes 4 parameters to investigate.
- Completed preliminary validation testing using existing Argonne test vehicles and test cells.
- Hosted collaborative peer-review meetings for the Japan Automobile Research Institute (JARI) and Korea Automobile Testing and Research Institute (KATRI) – two institutions also working in this area.

Future Achievements

- Validation of the system power ratings using both a chassis dynamometer and an axle hub dynamometer.
- Based upon test results and input from committee and international partners, write procedures into SAE J2908 and successfully ballot.



VI.E.2. Technical Discussion

Background

Standards Relevance

Testing standards provide the information by which achievements in vehicle efficiency, performance, and

Existing Engine Power Rating

The SAE has issued and reissued engine horsepower standards for many decades. Engineers and customers compare conventional vehicle performance based on SAE engine horsepower ratings. However, as more hybrid vehicle models (including plug-in variants) are now available, they are increasingly being compared to conventional vehicles and other hybrids. The current engine rating practice, which only considers engine output, leaves out the important contribution from the electric propulsion components. Currently there is no standard approach to addressing power ratings for an entire powertrain system (hybrid or otherwise). In the absence of a standard, each manufacturer is using their engineering judgment to rate their hybrid vehicle product line. Until a standard approach is recognized, a fair comparison among manufacturers and among different hybrid vehicle types is not possible. This research program addresses this standards gap by arbitrating all the viewpoints from a large number of stakeholders into consensus, resulting in procedures and definitions that are fair and practical.

Introduction

Challenges from Legacy Power Ratings

The engine power rating at the flywheel is not compatible with a system rating that can only be defined at the axle or wheel hub. This issue can only be reconciled by one of the following approaches:

- A) All vehicle power ratings are changed to reflect power at the axle or wheel (a diminished value from current ratings) or
- B) The HEV power rating is determined without being reduced by losses in the transmission and transaxle systems (reflecting a similar “flywheel” power level).

More J2908 Definitions for Incentive Programs

In addition to the system power rating, other parameters describing HEVs or PHEVs would be extremely useful in government incentive programs or credit systems. If a new law or credit system is to be proposed, it should be based upon a

careful and analytical standard. This document could provide that function if the need arises in the future.

Approach

Neck Down and Scope Definition

Standards work for new advanced vehicles frequently involves revising existing standards by adapting them to the unique aspects of HEVs, PHEVs and BEVs. In this case, a completely new document, SAE J2908, was required and the task force started with a clean sheet.

The approach to defining J2908 began by first investigating simple and inexpensive test methods, then moving on to more involved and accurate methods. The fundamental approaches investigated are the following:

- On-road acceleration test determining powertrain power using fast GPS sensors and knowledge of road load losses and vehicle mass.
- Using a chassis dynamometer with torque measurements taken at the axle or wheel (see Figure VI-23).
- Using a hub dynamometer measuring torque and speed directly from dynamometer at each driven wheel (see Figure VI-24).

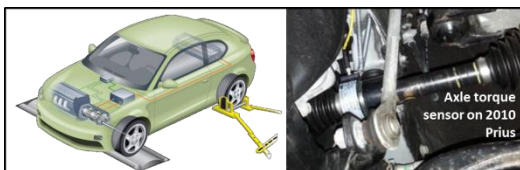


Figure VI-23: Chassis Dynamometer Approach to Measure System Power Using Axle Torque Sensors



Figure VI-24: Axle Hub Dynamometer Approach to Measure System Power

In addition to the system power rating, other useful power ratings unique to HEVs were identified by the committee. Currently, four (4) testable parameters for SAE J2908 are being investigated, they are the following:

- Hybrid System Power (kW)
- Battery assist power (DC kW)
- Electric-only peak power levels for PHEVs in depleting mode (mechanical kW)
- Regenerative braking power (DC kW from drive inverter system).

The two basic approaches to determine peak powertrain power are either to run a full-power acceleration (in road load

dynamometer mode), or to command full power at a fixed dynamometer speed. Investigating choices like these are the top priorities of this research.

Results

On-Road Testing

The on-road method for system power was initially investigated because it could potentially be performed with the least expense in testing facilities and equipment. Using only high-speed GPS and a flat long track, an attempt was made to infer power at the wheel of a Volt PHEV. Full-power acceleration is followed by a coast-down phase (in neutral gear) that measures the resistive load on the vehicle for any given speed. The acceleration data is processed knowing the resistive load from the coast-down and the vehicle weight to provide a power versus vehicle speed result.

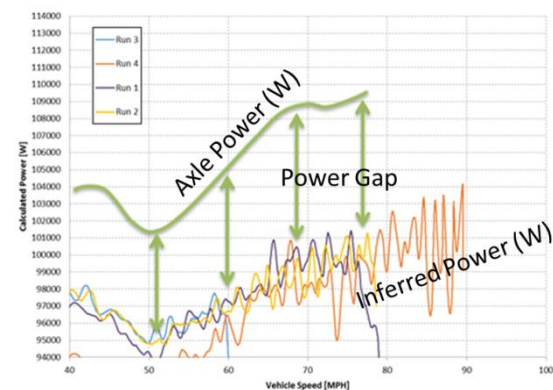


Figure VI-25: Results of Road Test Showing Power Gap

The results of the inferred power calculations are compared to the more accurate axle power made by direct measurement in Figure VI-25. Evidently, the inferred power shows a significant shortfall missing additional loads (perhaps in the tire and brakes). It was concluded from these results that the on-road GPS approach is inadequate for the standard.

Chassis Dynamometer Testing

The next testing phase investigated the feasibility of using a standard chassis dynamometer to test vehicles fitted with axle torque sensors. An example of a system power test for the Volt PHEV is shown in Figure VI-26 with power plotted against vehicle speed. Like the on-road approach, unknown losses in the tire prevent us from using measured dynamometer power as a representative measurement method for powertrain system power rating.

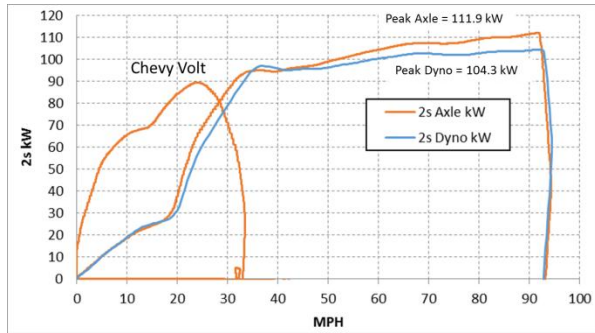


Figure VI-26: Initial Chassis Dynamometer Testing of Volt System Power Test

Transient Issues

During testing, several important issues arose related to power transients that will be important in the final procedure. They are:

- 1) Battery peak power out occurring of phase with engine peak power, and
- 2) The selection of an appropriate filtering window.

Out of Phase Battery and Engine Peak Power

A method currently used by some manufactures in reporting hybrid system total power prescribes adding the peak component powers (engine plus battery, or engine plus motor). However a significant gap in the timing between when peak battery and engine power was found in acceleration tests (0 to 80 mi/hr). The engine power (measured directly with a torque sensor) and axle power data for three acceleration runs are overlaid in Figure VI-27. This phasing issue was not unique to the Prius, two other hybrid vehicles also exhibited out-of-phase peak component powers. In order to prescribe test methods that are more in line with the respective peak component powers, experimentation with test conditions was made.

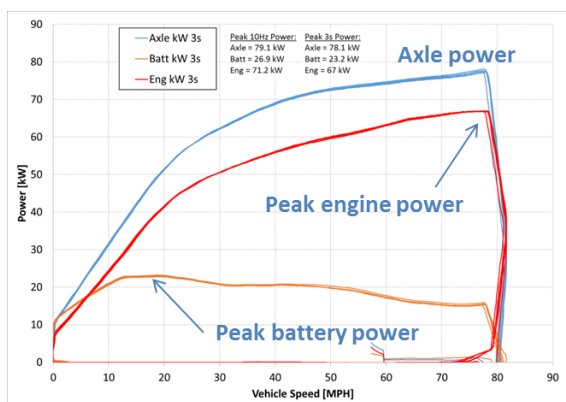


Figure VI-27: Initial Chassis Dynamometer Testing of Volt System Power Test

Employing lessons learned during engine component power testing, component speed change transients can be controlled to a degree by running the tests at fixed vehicle speeds. A chassis dynamometer can be commanded to maintain a fixed vehicle speed while absorbing the powertrain’s full power output. If a fixed vehicle speed where

peak power occurs can be found, then the test can be run at that speed for a robust powertrain power measurement.

A comparison of the peak powertrain power at three different fixed vehicle speeds is shown in Figure VI-28. Following this test, the procedure was refined to start from an intermediate power level before commanding 100% accelerator pedal. This method reduces the tip-in transient operation compared to a 0 % to 100% tip-in test. It is evident from the results that the measured sum of the engine and battery power is significantly higher than the measured axle power, thus reflecting the expected losses that exist in the powertrain rating method that are absent in the engine-only power rating test method.

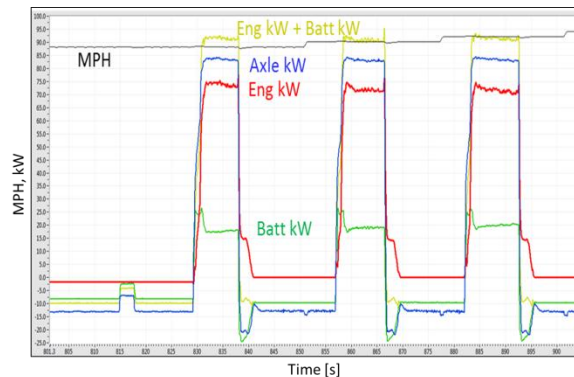


Figure VI-28: MY2010 Prius System Power Tests at Fixed Dynamometer Speeds

Appropriate Transient Filter Window

Note in Figure VI-28 the shape of the battery assist plot line (in green). The initial peak of around 26 kW lasts for only about one second. However, the axle power curve is essentially stable in that same period of time. It can be concluded from the figure that not all battery power is employed in propulsion at the wheels, instead some batter power is diverted to other functions.

Indeed by looking at the engine power curve, the 1-second peak battery was employed quickly speed up the engine to peak power as opposed to using the motor to power the drivetrain directly. In order to define a battery peak power that represents the hybrid system’s contribution to propulsion, the measurement would need to encompass a time window of sufficient length to remove short-lived transient events. An appropriate time window is still the topic of ongoing research. Currently, the development the committee and our international collaborators are looking at filtering windows of 2 to 3 (or maybe more) seconds in time.

Other Power Ratings in J2908

As mentioned earlier, as many as a total of four ratings will be part of SAE J2908. In addition to the “Hybrid System Power Rating” discussed so far in this report, the three others still under investigation are:

Battery Assist Power

Currently, the plan is to integrate this test into the Hybrid System Power Rating test. Results so far have been very promising. The results of this test are the most sensitive to choices taken in window filter options.

Electric-Only Power Rating

This test would only be useful to help describe capabilities of PHEVs operation in charge-depleting mode. Test methods currently being explored are speed ramp cycles driven on a dynamometer in “road load” mode. Speed ramp cycles are still being optimized to achieve a power profile with the least number of test time.

Regenerative Braking Power Rating

Based upon initial testing, finding the peak regenerative braking power appears to be possible with a very simple braking test on the dynamometer in “road load” mode starting from a high speed (~80 mi/hr).

Conclusions

New or revised standards typically take roughly two years to complete, and include the following phases of development: organize, scope, experiment, propose, write and validate. After one year of progress, this standard, SAE J2908 has completed the “organizing” and “scoping” tasks, and is finishing up the “experimental” phase.

The organizing task for entirely new standards development involves collecting a substantial amount of opinions and past experience from many stakeholders. Due diligence in collecting and sharing input is critical to having a final standard that will fully satisfy objectives and users alike.

Early in the next year of this project, experimentation will continue and a substantial amount of validation testing will be conducted. During a three month period starting in February 2015, a hub dynamometer be rented to validate this third measurement approach.

Finally, following completion of the scoping tasks and initial testing, the group will be ready to move on to the “proposal” phase. Herein, the results from initial experimentation will be used to propose a set of procedures that will be written up in a first draft. If specific parts need further definition or refinement, more experiments will be conducted.

VI.E.3. Products

Publications

1. SAE Draft J2908, “Hybrid Electric Powertrain Power Test Methods and Definitions”

VI.F. Green Racing Technical Support

Principal Investigator P.T. Jones

Senior Technical Lead: Bob Larsen (OboTech)

Oak Ridge National Laboratory
2360 Cherokeela Boulevard
Knoxville, TN 37932
Phone: (865) 946-1472
Email: Jonespt@ornl.gov

DOE Program Manager Lee Slezak

Phone: (202) 586-2335
E-mail: Lee.Slezak@ee.doe.gov

VI.F.1. Abstract

Objectives

- Incentivize vehicle manufacturers to develop, validate, and promote advanced technologies relevant to production vehicles through motorsport participation.
- Increase the use of renewable fuels and petroleum alternatives in racing, and provide an avenue to introduce new fuels or bio-fuel blends.
- Establish a link between BioEnergies Technologies Office (BETO) and Green Racing Initiative.
- Increase the use of electric drive technologies in racing.
- Use racing as a platform to educate the public:
 - On the benefits of using renewable fuels and the concept of well-to-wheels fuel life cycles.
 - On the performance and efficiency benefits and capabilities of advanced vehicle technologies.
- Diversify the success of the Green Racing Initiative beyond the TUDOR United Sportscar Championship (TUSC) to include other racing series with the final goal of establishing advanced transportation technologies as a foundation for all motorsports.
- Gain the support of the automotive industry in the validation of "green racing" in the United States and internationally.
- Maintain collaborative partnership with the U.S. Environmental Protection Agency (EPA) and SAE International.
- Complete the revisions to SAE J2880 Green Racing Protocols and publish an updated version of this Recommended Practice for Green Racing.

Major Accomplishments

- All of the full season GTLM class cars racing with the TUSC used E85R fuel with cellulosic ethanol sourced from INEOS, a DOE grant recipient. This fuel reduced oil consumption by over 62% and provided more than 65%

reduction in GHG emissions compared to conventional racing fuels with no renewable content. (For IMSA this would be a 2005 baseline.)

- Extended the partnership with IMSA through 2019 with a new MOU signed into place by DOE and IMSA leadership at the Daytona race in 2014.
- HEVs from Audi and Toyota dominated at the 24 Hours of Le Mans in 2014, and have won every World Endurance Championship (WEC) race to date in the 2014 season. Four different HEV architectures competed at Le Mans in 2014.
- Porsche returned to the LMP1 category in the WEC with an advanced HEV powered by a downsized, boosted V-4 SI engine with waste heat recovery and multiple electric drives.
- Each of the three factory HEV entries in the WEC LMP1 uses different forms of energy storage illustrating the diversity of technical solutions relevant to road cars: Audi with an electro-mechanical flywheel, Toyota with ultracapacitors, and Porsche with Li-Ion batteries.
- Nissan raced an experimental lightweight HEV at Le Mans in 2014, and was the first vehicle competing in the iconic 24 hour race to complete an entire lap of the 8.5 mile circuit at racing speeds using only electric propulsion. Nissan also announced a full factory effort in the WEC LMP1 for 2015 aiming to bring advanced HEV technology to the race track to further their development of HEV technology for road cars.



Figure VI-29: Formula 1 introduced new powertrains in 2014 emphasizing efficiency, energy recovery, and significantly more hybridization (photo: espn.f1.com)

- Formula 1 (F1) introduced new HEV powertrains in 2014 that specified small turbocharged V6 engines with waste heat recovery and greatly expanded electric drive capabilities. In addition, an energy allocation was established (100kg of fuel) and maximum fuel flow set to limit potential engine power with real-time fuel flow metering for monitoring compliance to the rules. These efficiency-encouraging steps have long been a part of the Green Racing Initiative philosophy and resulted in a 30% reduction of energy consumption with competitive performance. Improvements in the first season of the new formula, show further speed potential while those teams that have been able to most efficiently use the available

energy have had competitive advantages. With these changes, F1 has become eligible for a Green Challenge Award starting in the 2015 season.

- The light weight, downsized engine - Elan DeltaWing coupe raced in 6 rounds of the TUSC, finishing as high as fourth place in the LMP class.
- Mazda competed with their street-based diesel engine in the TUSC Prototype category in 2014. The engine uses the production block and head along with more than 50% of stock components. A 100% renewable synthetic diesel fuel with a cetane of 75 was made available to Mazda through the DOE's Green Racing program technical support. The engine was able to more than triple its output, when compared to a stock engine, to over 450 hp.
- Increased visibility for the "Clean, Fast, Efficient" Green Challenge tagline was achieved with international television coverage, race teams and media.
- Completed the revisions to the Green Racing Protocols and published a substantially revised and updated version of SAE J2880. Conducted multiple discussions with INDYCAR about becoming a Green Challenge race series in 2015; offered to supply 2nd Generation (cellulosic) ethanol in support of the series and options to incorporate energy recovery technologies in future powertrains.
- Monitored the adoption of the HySpy fuel flow meter as the FIA-approved approach to limit power and implement fuel allocations for the 2014 Formula 1 and LMP1 category in the World Endurance Championship. Followed the development of a second generation fuel flow sensor with greater accuracy and reliability for possible field test in TUSC in the 2015 season.
- Transported and displayed the Green Racing Simulator (E85 CORVETTE HEV race car simulator) at three TUSC races and planned for several additional events around the country next year with EPA and BETO support.

Future Achievements

- Work with TUSC to incorporate fuels with a higher percentage of renewable content into additional classes in 2015 and advanced technology into racing in 2016 and beyond.
- Continue to make advanced renewable fuel sources available to TUDOR USCC and INDYCAR for SI and CI engines.
- Develop Green Racing integration plan with INDYCAR as they qualify as a Green Racing series for the first time in 2015, and help them move towards achieving Green Challenge status and recognition from DOE, EPA, and SAE International.
- Work with the FIA to establish a Green Challenge Award in Formula 1 in 2015 or 2016. Under the revised J2880, F1 qualifies for recognition and award status starting in 2015.
- Work with the ACO to recognize the LMP1 category in WEC as a Green Racing series in 2015. Support discussions within the ACO on new formats for LMP2 and the GTE/GTLM classes to embrace Green Racing content.

- Support and incentivize the use of energy recovery technology in race cars, and identifying methods available to properly limit and/or record use of technologies to allow for performance balancing.
- Expand working relationship with BETO including additional biofuels suppliers and inclusion of BETO information on the Green Racing website update.
- Move towards a scoring system based on energy allocation, working with industry partners to develop fuel flow measurement technologies applicable in a racing vehicle.



VI.F.2. Technical Discussion

Background

Green Racing History

The Green Racing Initiative (GRI) started in 2006 with a working group of industry, government and national lab representatives. The team sought to take advantage of the efforts and opportunities in motorsports to further develop advanced transportation technologies that could be applied to street vehicles. This effort focused on providing a proving ground for petroleum displacement and technology advancements in a competitive setting. Once the working group had built the foundation for GR, a set of protocols was approved through SAE and in 2008 the J2880 'Recommended Green Racing Protocols' were established.

The American Le Mans Series (ALMS) acknowledged these protocols and awarded the first Green Challenge Award in October 2008.

The Green Challenge Award and the Michelin Green X Challenge soon became an integral part of SportsCar racing, where Michelin recognized the teams and the DOE, EPA, and SAE recognized the manufacturers who perform best when evaluated using the Green Racing formula for competition. The scoring formula takes into account measured performance and fuel consumption to determine a total score: Clean, Fast and Efficient terms are calculated in real time for each lap for each vehicle in the appropriate racing categories.

Introduction

The 2014 racing season in the US came to an end right after the end of FY2014 generating a record that showed sustainable motorsports activities advanced both technology and performance in the multiple racing series they were adopted in. The 2014 season has been extremely competitive in the renewable fuel-powered GTLM class of the TUSC. Teams have applied new technologies and sanctioning bodies have confirmed future rules which incorporate sustainable practices and require advanced technologies for future racing vehicles. INEOS, a cellulosic ethanol producer who has received DOE funds to develop their process, provided fuel to IMSA through a relationship with VP Racing fuels which was established through the Green Racing

Initiative. The Green Racing Initiative seeks to coordinate the strategies and guide motorsports requirements to optimize efforts within motorsports to highlight advances in transportation technologies.

Approach

Motorsports are the only professional sport that can directly help attain national energy and environmental objectives. The rapid developmental cycles in racing, the focused development of advanced technologies and alternative fuels, and the search for more efficient and capable vehicles inherent in racing, all tie directly with our national transportation goals. These efforts reduce our dependence on petroleum and lower the carbon footprint of vehicles – and still provide the entertainment and drama that has made racing one of the most followed forms of sports around the world. Racing is one of the best platforms for reaching a large audience with the message that through advanced vehicle technologies and renewable fuels we can maintain the personal mobility and performance customers want while moving toward the energy security and sustainable transportation the country needs.

Racing brings out the best in automotive technology and places it in a demanding competitive environment allowing a technology showcase that resonates with the public. Racing also inherently values efficiency as successful teams operate in alignment with sanctioning body rules to optimize fuel use with other racing parameters, like distance between required tire changes. Efficiency and petroleum displacement are attributes that underpin our national energy and environmental objectives. Building on core values in racing and adding renewable fuels and advanced transportation technologies as ways to improve sustainability, we have developed the Green Racing Initiative with our partners.

Results

The 2014 racing season had a number of highlights in advancing transportation technologies through motorsports. Of particular interest was the domination of hybridized racing vehicles in the world's most important sporting event, the 24 Hours of Le Mans. Audi, Porsche and Toyota each brought hybridized Le Mans Prototype (LMP1) vehicles to the event, with the Audi's diesel HEVs taking the pole and finishing in first and second place.



Figure VI-30: An Audi R18 e-tron quattro diesel HEV took first and second place in the 2014 24 Hours of Le Mans in (photo: Audi Sport)

Toyota's ultra-capacitor and Porsche's Li-Ion battery SI HEVs often matched the pace of the Audis but ultimately finished in third and eleventh places respectively at the world's most famous endurance race. At the end of FY2014 with three races to go, Toyota holds a small lead in the driver's and manufacturer's championships in the 2014 World Endurance Championship (WEC), illustrating the close competition within this elite category of the most technologically-advanced racing vehicles in the world. The Automobile Club de l'Ouest (ACO) refined their 2014 rule package for the LMP1 premiere category vehicles in the WEC expanding the size and type of energy recovery and hybrid technologies by a factor of 4 as well as allowing a limited amount of energy (fuel) per lap depending on the level of hybrid technologies applied to each car. These ACO rules were developed to enhance efficiency and not performance in consultation with the Green Racing Initiative. The rules are remarkably open with regards to technologies allowing the factory teams to be innovative in creating and applying advanced technologies. This shift of motorsports to using energy allocations, rather than purely speed, as a way to structure future competition represents a substantial change in the perspective of sanctioning bodies, and places a renewed relevance in the sport, as energy efficiency is something the manufacturers deal with in every vehicle they produce. WEC also moved to E20 cellulosic as the base fuel for all its categories, lowering its WTW GHG emissions by 18.5% and boosting its oil displacement to 19.5%.

The Green Racing Initiative has become an integral part of the TUSC in its first year of operation. TUSC was formed from the merger of the American Le Mans Series and the GRAND AM sportscar racing series into a major new unified Sportscar racing series for North America. Green Racing content will spread to other classes in TUSC over the next several years. Working in close collaboration with TUSC and the ACO from which a significant amount of the sporting regulations are drawn, the Green Racing Initiative continues to explore ways where advanced technologies can be showcased and renewable fuels utilized for racing in the future.



Figure VI-31: DeltaWing Coupe continues its development in 2014 (photo: deltawingracing.com)

The experimental DeltaWing from the innovative Garage 56 at the 2012 Le Mans race returned in updated form in the TUSC in 2014. A completely new chassis and ongoing developments made the car competitive by the end of the 2014 season. The DeltaWing led the Petit Le Mans race and placed fourth in the LMP class in 2014 after an early shot at winning the race. It remains a fan favorite due to its innovative, light weight design and tiny front wheels.

The 2014 TUSC season continued to offer advanced renewable fuels for use by its competing teams. In the GTLM class, E85R dominated as the fuel of choice in this ultra-competitive category. All the top three finishers in all the races used E85R fuel. The GT class is based on cars that are on the road today and puts rival teams in door-to-door competition that may be the most competitive class in racing anywhere in the world. All the BMW, Corvette, Dodge, Ferrari, and Porsche factory cars and most of the privately entered cars used this renewable fuel with great success. The wholesale movement to E85R was primarily motivated by the performance potential of this excellent fuel, but the message with respects to its upstream impact and its energy security and environmental advantages have provided an excellent outreach opportunity for DOE goals. The Green Challenge scoring system accurately reflects each fuel's characteristics in terms of its greenhouse gas and oil replacement attributes without rewarding a team's selection of bio-fuels over conventional fuels. That makes this switch to renewable fuels at this level of motorsports all the more impressive and significant. This noteworthy accomplishment demonstrates that these fuels are capable of outstanding performance, reliability, and capable of widespread use in street vehicles.



Figure VI-32: Green Challenge Awards were given in all ten TUSC races in 2014 (photo: press.porsche.com)

In the LMP class in TUSC, Mazda's commitment to their diesel-powered prototype race car was a major story. The remarkable performance from a production-based diesel engine was highlighted by its use of 100% synthetic renewable diesel fuel made from waste vegetable oil thanks to the Green Racing program. Its high cetane, zero sulfur content allowed impressive power density – achieving more than three times the production engine's power - and virtually no PM emissions. This engine's performance became better and better as the season unfolded, now producing in excess of 450 hp. Mazda also made a major contribution to STEM education by bringing a race car to local high schools near the race tracks to show how important STEM education was to open exciting futures for high school students. Using their commitment to racing as their model, they explained how practical and specific applications of science and technology will shape the future and offered real-life examples of how that knowledge can be put to work.

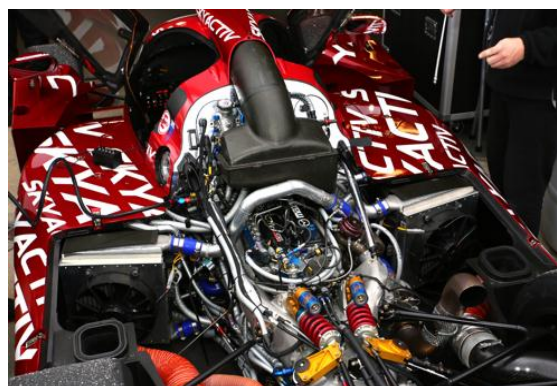


Figure VI-33: Mazda Skyactiv-Diesel production-based race engine competed in all ten TUDOR United SportsCar Championship races using 100% renewable synthetic diesel fuel (photo by mazdamotorsports.com)



Figure VI-34: Fans and professional racing drivers alike try their hand at the GRS; Tommy Milner of Corvette Racing puts the simulated E85/Hybrid Corvette to the test

Due to the success of last years Green Racing Simulator (GRS), the mobile outreach simulator was deployed again this season for the Green Racing program. The GRS, developed by Argonne National Laboratory, incorporates a program that calculates the amount of regenerative braking energy captured and fuel used during two laps of simulated racing. This simulator was set up at three IMSA races in 2014. It served as a notable means of disseminating the DOE's Green Racing key message that the use of renewable fuels and hybrids can displace a substantial amount of imported petroleum to over 1000 racing fans.

Conclusions

Motorsports in FY2014 was a year that showed significant world-wide acceptance of Green Racing content in the premier racing series around the world: WEC LMP1, F1, TUSC, and INDYCAR. Significant petroleum reduction was recorded in the GTLM class in TUSC of 62.5% with a 65.5% reduction in GHG emissions when compared to a baseline of the 2005 series. All vehicles in GTLM class are running on E85 racing fuel, while the Mazda LMP team has successfully employed an advanced synthetic renewable diesel fuel to power their two-car team in the TUSC. Green Racing continues to expand in the elite levels of racing, illustrating how advanced

transportation technologies and renewable fuels are leading the way to sustainable transportation through motorsports.

Important accomplishments regarding the incorporation of energy recovery systems into world class racing were showcased multiple times during the year. The adoption in F1 of both exhaust and kinetic energy recovery was an important part of reducing energy consumption in that series by 30%. The domination of HEVs in the WEC LMP1 class with competitive vehicles fielded by three major OEMs shows that recovering energy is an essential element in the future of racing at the highest levels. Making advanced renewable fuels available to TUSC and INDYCAR shows that using these fuels is the easiest and most cost-effective way to reduce the carbon emissions and oil consumption of race series.

The adoption and publications of the updates to SAE J2880, the Green Racing Protocols, provides a flexible set of guidelines for racing series around the world to adopt elements of Green Racing that fit their situation. In addition, the new J2880 contains a set of recognitions and rewards that incentivize series' progressing to greater levels of Green Racing content and sustainability. The Protocols form a solid foundation for advancing the development of technologies and fuels used in future road vehicles.

The relationship between DOE, IMSA and partners at EPA and SAE International is strong and there are many opportunities for building acceptance of Green Racing principles contained in the Green Racing Protocols. The Green Racing Initiative continues to impact the future of motorsports in alignment with DOE's transportation goals.

VI.F.3. Products

Publications

1. SAE J2880 Protocols for Green Racing (standards.sae.org/j2880_201406)

Tools and Data

During FY2014, proprietary data and opportunities to be included in test/development were made available to the Green Racing Working Group representatives. As these are projects in process reports will be generated in FY2015.

1. Flowsonic fuel flow measuring systems ability to enable enforcement of energy allocation regulations.
2. Advanced energy storage device (flywheel simulink model) was obtained from a Green Racing partner and will be used in HEV analysis in FY2015.

VII. VEHICLE SYSTEMS EFFICIENCY IMPROVEMENTS

VII.A. Cummins MD& HD Accessory Hybridization

Principal Investigator: Dean Deter

Oak Ridge National Laboratory
 2370 Cherahala Boulevard
 Knoxville, TN 37932
 Phone: (865) 946-1580
 E-mail: DeterDD@ornl.gov

DOE Program Manager: David Anderson

Phone: (202) 287-5688
 E-mail: david.anderson@ee.doe.gov

VII.A.1. Abstract

Objectives

- Analytically verify novel heavy truck accessory hybridization and electrification approaches, and experimentally validate prototype hardware utilizing the ORNL Vehicle Systems Integration (VSI) Laboratory's component and powertrain test cells.
- Develop and validate medium/heavy duty accessory models by means of data collection on a test vehicle and extraction from Cummins' preexisting models.
- Using the project's generated models and market research, choose and develop an electric or hybrid architecture and controls for one or more accessories depending on fuel consumption reduction and perceived market acceptability.

Major Accomplishments

- Typical vehicle level models use a "lumped" mechanical and electrical accessory structure that is not detailed enough to represent dynamic accessory behavior. ORNL has integrated Cummins' accessory models into Autonomie's vehicle architecture to capture these behaviors at a vehicle level.
- Using test vehicle data the power steering model been validated within the acceptable system assumptions.
- Exercised three different vehicles to determine which vehicle application would have the most impact of fuel consumption; a MD pickup/delivery truck, an HD class 8 bus, and an HD class 8 line haul sleeper cab.
- Validated the class 8 line haul sleeper cab to be accurate within 5% of a chassis tested vehicle.
- Using results from the simulation study as well as data from literature reviews, the CRADA team was able to

determine that while line haul sleeper cabs made the smallest impact with hybrid accessories for driving when compared to MD P&D or HD bus, they made the biggest impact when looking into idle mitigation and overnight hotel loads.

- Based on the findings from the literature review and simulation study ORNL proposed and designed a hybrid Auxiliary Power Unit (h-APU) architecture that would allow for hybridization for the air conditioning, electrification of the vehicles fans, and energy storage for other electrical hotel loads. This will allow for the truck to eliminate or greatly reduce all over night idling by providing hotel loads from a battery pack that utilizes regenerative braking for charging.
- The baseline controls and system architecture have been designed and implemented in Autonomie for further testing and controls development.

Future Achievements

- Providing NREL with the proper resources, we will use their CoolSim Quasi-Transient air conditioning model for both the simulation portion of the project as well as the Hardware-In-the-Loop (HIL) portion of the project. This will provide a much needed high fidelity model for reliable testing and results.
- Cummins is currently designing the hardware required to build the proposed h-APU system.
- It will first be tested in ORNL's Vehicle Systems Integration (VSI) Laboratory in the component test cell to provide a safer and controlled environment to protect the prototype equipment.
- It will be tested in the VSI lab's powertrain test cell on a Cummins' ISX 450 engine that is typically found in class 8 line haul vehicles as a proof of concept.



VII.A.2. Technical Discussion

Background

Medium and heavy duty trucks are a growing market and integral part of our society. From the home delivery of goods by medium duty trucks to the freight hauling of heavy duty line haul trucks, they are the main source of material and goods transport. Due to these trends, there is an overwhelming need to quickly address key problems with excess fuel usage and emissions production of these diesel vehicles.

Modern trucks have become much more advanced in terms of engine, aftertreatment, and transmission technologies which greatly reduced both fuel consumption and emissions. Due to these improvements focus of truck OEMs has shifted to start looking at what other aspects of MD and HD trucks can be impacted by advanced technologies.

Introduction

There are many areas of MD and HD vehicles that can be improved by new technologies and optimized control strategies out of which two need to be addressed near term: component optimization and idle reduction; this is best done by a two part approach that includes selecting the best component technology, and/or architecture, and optimized controls that are vehicle focused. While this is a common focus in the light duty industry it has been gaining momentum in the MD and HD market as the market gets more competitive and the regulations become more stringent.

When looking into systems optimization and idle reduction technologies, affected vehicle systems must first be considered, and if possible included in the new architecture to get the most benefit out of these new capabilities. Typically, when looking into idle reduction or component optimization for MD/HD, the vehicle's accessories become a prime candidate for electrification or hybridization. While this has already been studied on light duty vehicles (especially on hybrids and electric vehicles) it has not made any head way or market penetration in most MD and HD applications. If hybrids and electric MD and HD vehicles begin to break into the market this would be a necessary step into the ability to make those vehicles successful.

Approach

ORNL and Cummins began this project by discussing which approach would be most successful in reducing fuel consumption, but also which approach would gain acceptance by the market to enable this technology to penetrate the market more quickly. A two phased approach was selected due to ORNL's test cell capabilities and Cummins market resources and access to vehicle data.

The first phase is a modeling/simulation/data collection and market study phase that is focused on determining, which accessories would be feasible to hybridized/electrify, what accessories have fuel consumption benefits if hybridized/electrify, the ideal vehicle application which would benefit most from these new technologies, and what architecture on the selected vehicle type would have the most impact on fuel consumption.

Phase one of the project started by collecting all of the data and resources ORNL and Cummins had to begin the modelling and simulation. Cummins was able to supply base models for the four major accessories that the project would be looking at: the engine's cooling fan, the vehicle air conditioning system, the power steering system, and the vehicle's air compressor and air brake system. ORNL opted to use Argonne National Laboratory's Autonomie as the platform for simulation work on a vehicle level.

With the necessary models and accessory structures in place we began to start the examination of different vehicle types. Three vehicle types were suited for this project and study. A HD transit bus and MD pickup and delivery (P&D) vehicle were chosen due to their extremely transient drive cycles and time spent in idle between pickups and drop offs. Neither Cummins nor ORNL had access to high level data on vehicle parameters and opted to use Autonomie's included class 8 HD transient bus as well as their class 6 P&D vehicle (Figure VII-1).

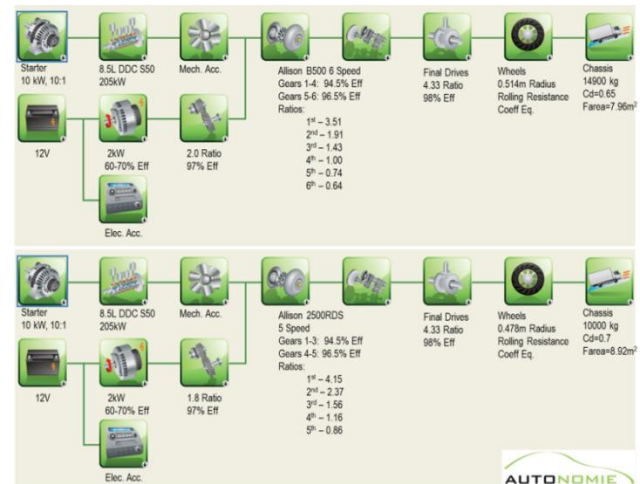


Figure VII-1: HD transit bus and MD P&D Autonomie vehicle models

The last vehicle chosen was a HD class 8 line haul (LH) sleeper cabin. This vehicle was assessed due to its overwhelming market size and total amount of fuel consumed per year compared to the other two vehicles. Additionally, sleeper cabs spend a large amount of time idling, especially during the driver's overnight hoteling in the warm months of the year. ORNL had access to parameters and data on this vehicle type. The engine and transmission for this vehicle has been tested in ORNL's VSI lab as well as had access to vehicle parameters for a Kenworth T700 to further increase the fidelity of this vehicle model (Figure VII-2)

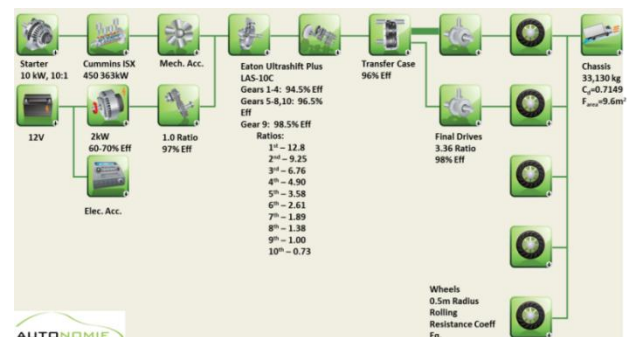


Figure VII-2: HD class 8 line haul sleeper cab based on a chassis tested Kenworth T700

The second phase of the project will be a prototype development and component/powertrain/vehicle testing phase which will be used to validate the developed component and vehicle models, develop and build a prototype system based on simulation findings, create and test prototype controls in ORNL's VSI component test cell using HIL practices, and test the finished system in ORNL's powertrain test cell as a final system validation.

In order further develop and validate the accessory and vehicle models Cummins was able to leverage a test vehicle from another project in order to instrument the accessories and get real world data from most of the accessories. Phase two of this project has begun, but currently the selected architecture and prototype are protected under the CRADA agreement. Once the prototype reaches a fully validated phase more information will be available. It is currently in the final design phases and will begin the testing phase during first months of 2015.

Results

After the first round of baseline accessories models were developed and integrated into the Autonomie, Cummins and ORNL checked the behavior of the models against the limited data available at the time. The models also needed further tweaks and adaptations in order to have all the necessary interactions with all of the vehicle systems. Figure VII-3 through Figure VII-8 show the first round of expected accessory behavior for the HD line haul truck while driving the HHDT65 drive cycle. The HHDDT65 cycle and line haul truck was chosen do to ORNL and Cummins have access to chassis roll data for the modeled line haul vehicle, the results was reviewed and found to be within a 5% average of the chassis tested vehicle (Table VII-1).

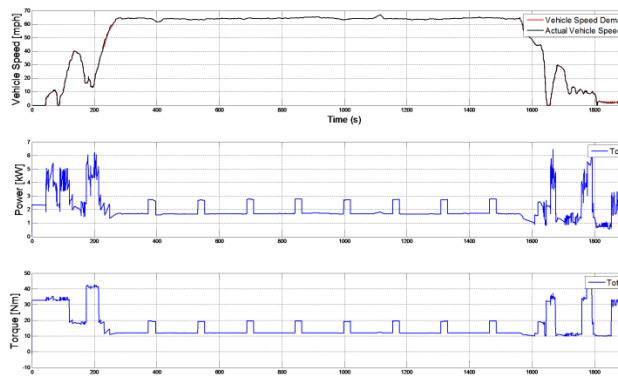


Figure VII-3: Vehicle speed trace, total accessory power consumption, and total engine drag torque from the accessories

Table VII-1: Modelled vehicle vs chassis roll data (HD class 8 line haul sleeper cabin)

| Chassis Vehicle vs. Simulation Fuel Economy | | | | | |
|---|------|---------|----------------|--------------|--------------|
| Data | WHVC | Utility | CARB Transient | 55mph Cruise | 65mph Cruise |
| Chassis Summary (mpg) | 5.40 | 4.78 | 3.90 | 8.17 | 6.54 |
| Model (mpg) | 5.41 | 5.08 | 4.26 | 7.77 | 6.67 |
| Percent Error | 0.19 | 6.28 | 9.23 | 4.90 | 1.99 |
| Percent Error Average | 4.52 | | | | |

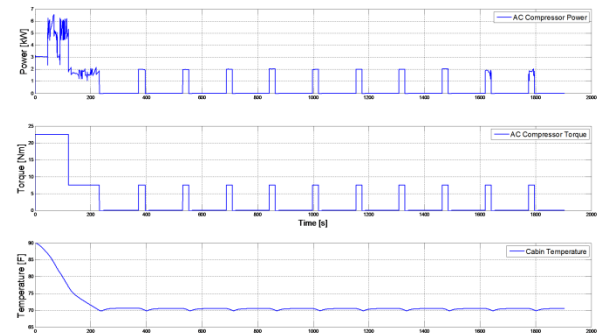


Figure VII-4: Air conditioning system traces; power, torque, and cabin temperature

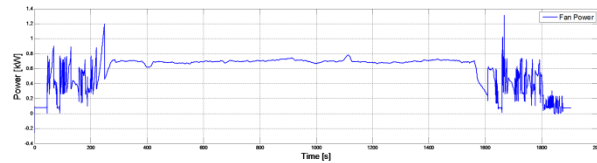


Figure VII-5: Engine cooling fan system traces; power and torque

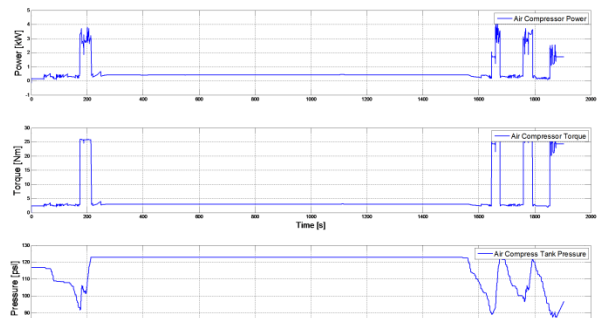


Figure VII-6: Air compressor and brake system traces; power, torque, and tank pressure

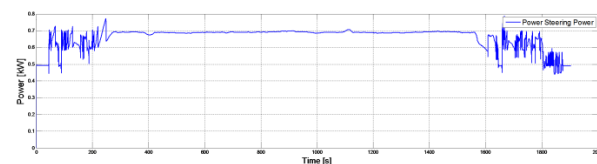


Figure VII-7: Power steering system traces; power and torque

With the baseline accessory models responding with the expected behavior, ORNL began to exercise all of the vehicle models to start analyzing vehicle types to determine which had the most promising returns on hybridizing or electrifying.

This was completed by choosing one drive cycle that best represented the duty cycle of each of the test vehicles and then eliminating the accessories completely one-by-one to find the entitlements for each. For the HD bus, the Manhattan Bus Cycle (Figure VII-8) was used, for the MD P&D vehicle it was the HTUF6 Cycle (Figure VII-9), and for the HD line haul truck it was the Cummins proprietary line haul drive cycle (not pictured).

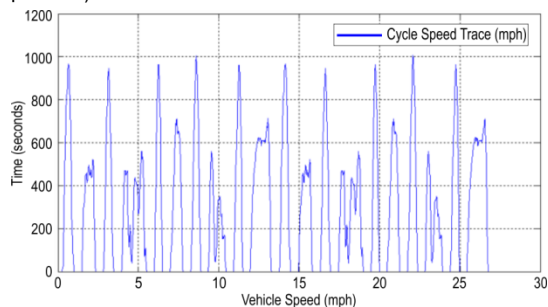


Figure VII-8: Manhattan Bus Cycle

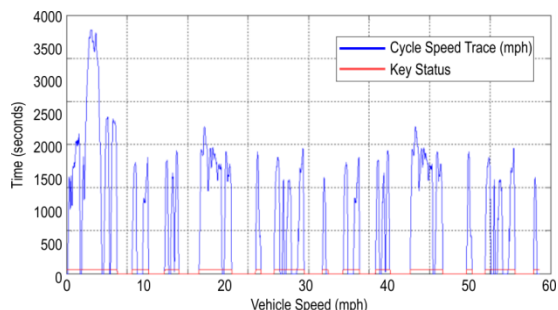


Figure VII-9: HTUF6 cycle with key on and off events

The results indicate that while bus and P&D vehicle have a large potential for fuel economy improvement during on road cycles, showing two or more accessories with greater than 2% improvement (Table VII-2 and Table VII-3), the line haul truck shows less than 1% for all accessories (Table VII-4). This is due to two main effects: first a line haul truck’s engine’s power output of around 300-400kW is much larger than the power used by accessories, and second, the typical line haul drive cycle keeps a vehicle speed that typically holds a steady speed of 65mph which is the operating point that accessory manufacturers design the systems to run most efficiently at.

Table VII-2: Accessory entitlements for the Manhattan Cycle (HD Class 8 transit bus)

| Manhattan Fuel Consumption Entitlements | |
|---|-----------------------------|
| Data | Fuel Consumption % Decrease |
| A/C Out | 6.209 |
| Cooling Fan Out | 0.674 |
| Air Comp Out | 1.309 |
| Power Steering Out | 10.129 |

Table VII-3: Accessory entitlements for the HTUF6 Cycle (MD Class 6 P&D vehicle)

| HTUF6 On/Off Fuel Consumption Entitlements | |
|--|-----------------------------|
| Data | Fuel Consumption % Decrease |
| A/C Out | 2.756 |
| Cooling Fan Out | 0.848 |
| Air Comp Out | 8.104 |
| Power Steering Out | 8.528 |

Table VII-4: Accessory entitlements for the Cummins Proprietary Cycle (HD Class 8 line haul sleeper cabin)

| Fuel Consumption Entitlements | |
|-------------------------------|-----------------------------|
| Data | Fuel Consumption % Decrease |
| A/C | 0.123 |
| Power Steering | 0.438 |
| Brake Air Compressor | 0.282 |
| Cooling Fan | 0.344 |

The on road portion of the vehicle utilization is only one factor that has to be taken into account when looking at accessory hybridization or electrification. When examining the amount of fuel burned during overnight hoteling in a sleeper cab, researchers found that the amount of fuel consumed was larger than any other application for saving during the on road entitlement studies.

An idling line haul truck consumes between 0.4–0.88 gallons an hour. Required driver rest period is at least 10 hours which translates into 4-9 gallons consumed during idling not including idling that might incur during freight drop-off and pick up which may also be an extended period of time at distribution hubs. Cummins and ORNL have chosen and developed an architecture that will allow for idle reduction or elimination during these distribution hub times as well as overnight idling

Conclusions

Phase one of the project is largely completed. As more data from Cummins test vehicle becomes available the models will continually be updated to provide more realistic results as well as continue to improve both ORNL and Cummins model libraries for future projects. Phase one has allowed Cummins and ORNL to create tools to evaluate future accessory technologies as well as discover the current landscape in accessory technologies and idle reduction devices.

After reviewing the results of the study Cummins and ORNL determined that an accessory architecture which will either reduce or eliminate the need for idling, in HD Class 8 trucks is the best solution for maximized potential in reducing emissions and fuel consumption. This allows the project to address issues of idling for extended periods while accessory loads are still needed, as in overnight hoteling and idling while in queue at distribution hubs. An architecture for this has been chosen and developed but is protected under the CRADA agreement.

VII.B. Powertrain Controls Optimization for HD Hybrid Line Haul Trucks

Principle Investigator: David E. Smith

Oak Ridge National Laboratory
2370 Cherahala Blvd.
Knoxville, TN 37932
Phone: (865) 946-1324
E-mail: smithde@ornl.gov

DOE Program Manager: David Anderson

Phone: (202) 586-8055
E-mail: david.anderson@ee.doe.gov

VII.B.1. Abstract

Objectives

- Develop and validate accurate component models for simulating integrated engine, hybrid energy storage, emissions control, and supervisory control systems in Class 8 trucks.
- Evaluate the merits of specific alternative technologies and control strategies under realistic MD and HD drive cycle conditions.
- Investigate Reactivity Controlled Compression Ignition (RCCI) advanced combustion coupled with series hybrid electric operation
- Introduce emissions controls to minimize criteria pollutants, with emphasis on challenges of low temperature combustion
- Integrate actively controlled hybrid energy storage systems (battery plus ultracapacitor) for enhanced regenerative braking energy capture
- Experimentally verify advanced combustion, hybrid energy storage, and aftertreatment systems utilizing actual hardware and virtual vehicle systems.

Major Accomplishments

- Completion of baseline hybrid vehicle model supervisory control algorithms for Powertrain Controls Optimization for HD Hybrid Line Haul Trucks
- Identification and integration of preliminary hybrid energy storage system component data and baseline control strategy for Powertrain Controls Optimization for HD Hybrid Line Haul Trucks
- Completion of first generation energy management strategy involving hybrid energy storage system, RCCI operation, and emissions control for Powertrain Controls Optimization for HD Hybrid Line Haul Trucks

Future Achievements

- Development and integration of RCCI engine model into vehicle simulation for estimated drive cycle efficiencies
- Baseline powertrain testing of system in ORNL VSI Laboratory to establish reference point
- Completion of baseline active control strategies for hybrid energy storage system
- Integration of baseline emissions control strategies into overall supervisory controls
- Conversion of current Cummins ISX 15L engine to RCCI operation (installation of instrumented cylinder head and engine control hooks)
- Baseline engine mapping of the RCCI engine
 - Population of new RCCI engine model with engine map for use in supervisory controls development
 - Emissions data collected will provide insight into proper emissions control strategy variations due to low temperature combustion
 - Revise series hybrid engine operating region to better utilize RCCI
- Powertrain testing of improved system incorporating hybrid energy storage system



VII.B.2. Technical Discussion

Background

Hybrid medium and heavy-duty (MD and HD) powertrains offer large potential reductions in fuel consumption, criteria pollutants, and greenhouse gases. In addition to powertrain electrification, advanced combustion regimes could further reduce the fuel consumption for these vehicles. The most fuel-efficient MD and HD combustion engines are advanced diesels, which require aftertreatment for compliant emissions control. Diesel hybridization is challenging because the integrated aftertreatment, engine, and battery systems must be optimized to meet efficiency targets and simultaneously satisfy drive cycle and emissions constraints.

Introduction

This is a vehicle system level project, encompassing analytical modeling and supervisory controls development as well as experimental verification/validation testing at the component, powertrain, and full vehicle system level. This project supports the goal of petroleum consumption reduction for medium and heavy trucks through the development of advanced hybrid technologies and control systems. VSST has invested previously in R&D to support hybrid energy storage

systems (Li-ion plus ultra-caps) for light duty, passenger car applications. This research will be extended to the MD and HD sector where current battery technology is not mature enough to handle the substantial regenerative braking power levels these trucks are capable of producing. With this hybrid energy storage system, substantial gains in overall vehicle efficiency are possible. In addition, advanced combustion technologies, such as RCCI, will be implemented into an advanced hybrid powertrain for a Class 8 line haul application. This powertrain, leveraged from other VSST work (Meritor, a current ORNL/VSST partner), is ideal for taking advantage of the benefits of RCCI operation due to its series hybrid mode of operation. Emissions control is also a focus of this project, especially due to the fact that RCCI creates a low temperature exhaust stream that must be addressed.

Approach

The project seeks to leverage multiple research areas into a single vehicle platform. The chosen hybrid powertrain is a fully capable Class 8 powertrain designed for line haul applications, and has the ability to be operated as an all-electric vehicle, series hybrid electric vehicle (at low to moderate speeds), and a parallel hybrid electric vehicle at moderate to highway speeds. This powertrain offers itself to improvement by the technologies investigated in this project.

There are four focus areas for this project, ranging from advanced combustion regimes and engine control strategies, emissions control technologies, pulsed energy storage systems (dual energy storage systems), and advanced energy management and supervisory controls. These four areas are shown graphically in Figure VII-10, and are summarized below.

Advanced engine control strategies

Research in this area is being leveraged with on-going projects at ORNL and being co-sponsored by the DOE VTO Advanced Combustion and Emissions Control program. ORNL has been engaged in the area of Reactivity Controlled Compression Ignition (RCCI) on multi-cylinder engines for improved fuel efficiency and reduced emissions.

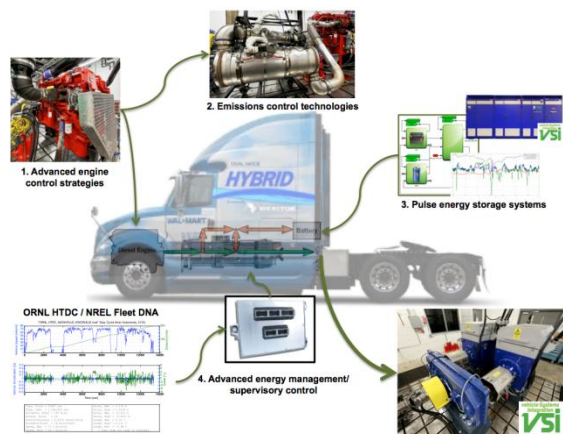


Figure VII-10: Project focus areas

This mode of combustion offers increased fuel efficiency at the sacrifice of a narrow operating window and reduced exhaust gas temperatures. For this reason, a series HEV would be a good operating environment for this type of engine control, due to the ability to maintain complete control over the operating envelope of the engine.

Emissions control technologies

Emissions control is essential for the success of RCCI due to lower exhaust temperatures. To further exacerbate the problem, the hybrid powertrain has the ability to operate solely on electric power, as well as intermittent engine start/stop operation. This leads to increased importance of coordinating engine operation and emissions control in order to maximize the benefits of powertrain electrification and advanced combustion.

Pulse energy storage systems

Perhaps the greatest opportunity for powertrain efficiency improvement is new approaches for increased regenerative braking energy collection for Class 8 line haul hybrid trucks. Current battery technology, while reasonably mature for light duty applications, is not capable of absorbing the large amounts of energy that is necessary to slow these trucks down. One approach that has been researched in the past for light duty applications is dual energy storage systems, or the combination of batteries with ultra-capacitors. This section of the research builds upon past research from Argonne National Laboratory that was done for light-duty vehicles. The approaches developed as part of that work will be adapted/extended to this heavy-duty line haul vehicle application.

Advanced energy management/ supervisory control

In order for each of the previous technologies to function seamlessly at the vehicle level, appropriate energy management strategies must be developed that will fully realize the compound benefits of all the candidate technologies being investigated in this project. Past HD HEV supervisory control experience will be leveraged and expanded to incorporate these new technologies in a meaningful and cohesive manner.

Results

Supervisory controls baseline established

Powertrain supervisory controls software was leveraged from a previous program that utilized the Meritor DMHP. This approach kick-started the project by allowing the baseline supervisory control system to be rapidly completed. The baseline supervisory control model was developed for the single ESS case with no advanced combustion or emissions control strategies.

In order to exercise the model, “real world” drive cycles were created. Data was mined from the ORNL Heavy Truck Duty Cycle (HTDC) database (now integrated with the NREL Fleet DNA database) and was used to develop custom real world drive cycles. All of these “real world” drive cycles include grade, which is a key parameter in evaluating hybrid benefits of line haul trucks. An example of primary cycles to be used for this project is shown in Figure VII-11. This drive cycle represents an approximately 170-mile trip along Interstate I-40 eastbound from Nashville, TN to Knoxville, TN.

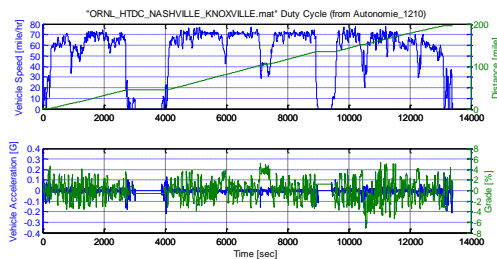


Figure VII-11 ORNL HTDC "real world" drive cycle from Nashville, TN, to Knoxville, TN

System and component models completed

ORNL has implemented past transient engine modeling experience to develop a transient model of a Cummins ISX-450 15 liter engine. The model has been validated against actual test data from a Cummins ISX450 15 liter engine. A graphic of the engine installed in the ORNL VSI laboratory is shown in Figure VII-12.



Figure VII-12 Cummins ISX-450 installed in the ORNL VSI laboratory

In addition, a full aftertreatment suite of models has been “built” and is currently being validated against experimental data from the same engine. Figure VII-13 outlines the high level Autonomie implementation of the transient engine model, including a snapshot of the aftertreatment models.

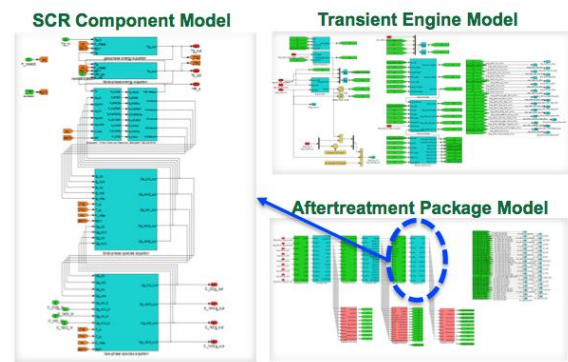


Figure VII-13 ORNL transient engine model and associated aftertreatment models

The baseline dual energy storage system model has been completed. This model builds upon the previous work performed by ANL in light duty systems, and utilizes the model framework currently available in the public release of Autonomie. The control system has been completely changed, with most of the active control relocated to the supervisory control model outlined earlier in this text. The li-ion battery model is based upon proprietary data from Meritor on an actual vehicle energy storage system (ESS), but is sized such that the ESS can provide sufficient energy capacity to power all electrified accessories for during the normal hoteling period. The ultra-capacitor model is being reviewed and modified based upon input from an industry subject matter expert. Once complete, the ultra-capacitor bank will be sized appropriately for the project. Figure VII-14 gives an overview of the model architecture being used for the dual energy storage system.

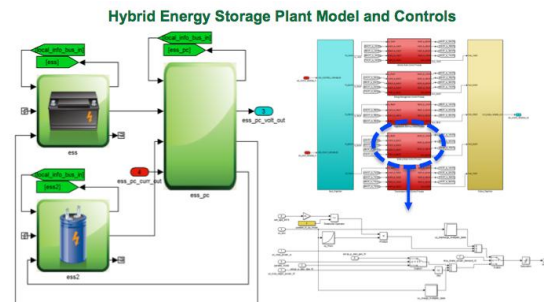


Figure VII-14 Model framework for the dual energy storage system model

Conclusions

The project is focused on advanced heavy-duty powertrain systems that will reduce energy consumption and criteria emissions for Class 8 line haul vehicles. A multi-faceted approach is being taken to minimize the fuel consumption and emissions of a Class 8 line haul powertrain utilizing advanced combustion, hybridization, and dual energy storage systems. Progress on the project includes establishing reference supervisory controls based upon experimental powertrain results for ORNL VSI Laboratory, a completed literature review of various approaches to hybrid energy storage systems, as well as development of a transient engine and aftertreatment modeling “package,” as well as an actively controlled hybrid energy storage system model.

FAST AND WIRELESS CHARGING

VII.C. INL Wireless Power Transfer and EVSE Charger Testing

Principal Investigator: James Francfort

Idaho National Laboratory
P.O. Box 1625, Idaho Falls, ID 83415-2209
(208) 526-6787
James.francfort@inl.gov

DOE Program Manager: Lee Slezak

(208) 586-2335
Lee.slezak@ee.doe.gov

VII.C.1. Abstract

Objectives

- Provide the U.S. Department of Energy (DOE) with independent and unbiased benchmarked testing results by evaluating technologies in which DOE and industry have invested.
- Benchmark the efficiencies and safety of wireless power transfer (WPT) systems, conductive electric vehicle supply equipment (EVSE), and DC fast chargers (DCFC).
- Benchmark the cyber security of charging systems.
- Benchmark DCFC and EVSE Level 2 compatibility with new generations of plug-in electric vehicles (PEVs).
- Continue to provide testing results to other DOE programs and national laboratories, as well as several U.S. Drive technical teams of which Idaho National Laboratory (INL) staff are members.

Major Accomplishments

- Completed initial vehicle-level testing for the Evatran pre-production WPT system. Results were compared to the previously published laboratory testing of the Evatran pre-production WPT system in an effort to quantify the impact of the vehicle's steel chassis on Electromagnetic field strength as well as system efficiency.
- Detailed test results from both vehicle-level and laboratory open-air testing of the pre-production Evatran WPT system supported improvements in design and efficiency for the production Evatran WPT system.
- Provided significant support to Society of Automotive Engineers (SAE) J2954 in their development of WPT codes and standards.
- In support of SAE J2954 test procedure development, numerous inanimate objects were evaluated for temperature response when positioned close to a wireless charger during operation.

- In support of SAE J2954 test procedure development, open-air testing was conducted on a wireless charger using a proposed mock floor pan design intended to emulate the steel vehicle chassis floor.
- Test facility was augmented to enable the testing of WPT systems both as installed on a vehicle as well as open-air test conditions.
- Completed efficiency and functionality testing of the GE smart grid capable EVSE. The EVSE is the final deliverable from GE for FOA-554 (development of smart grid capable EVSE funded by the DOE Office of Electricity Delivery and Energy Reliability).
- Completed cyber security testing of the GE smart grid capable EVSE.
- Continued joint SAE, Intertek, and INL charging compatibility / interoperability testing of approximately 40 EVSE and vehicles.
- Additional NDAs have been signed and are being signed in anticipation of additional testing candidates.

Future Achievements

- Continue identifying WPT, DCFC, and EVSE test partners and obtaining test systems.
- Conduct efficiency, functionality, and cyber security testing on three smart grid enabled EVSE developed with funding from DOE Office of Electricity Delivery and Energy Reliability.
- Continue close coordination with the SAE J2954 committee.
- Conduct charging compatibility / interoperability testing of DCFC, EVSE, and vehicles.
- Conduct additional efficiency and EM field strength testing of the production Evatran WPT system both as installed on a Chevy Volt and in open-air test conditions.



VII.C.2. Technical Discussion

Background

DOE's Advanced Vehicle Testing (AVTA) is part of DOE's Vehicle Technologies Office, which is within DOE's Office of Energy Efficiency and Renewable Energy. AVTA is the only DOE activity tasked by DOE to conduct field evaluations of vehicle technologies and fueling infrastructure that use advanced technology systems and subsystems in light-duty vehicles to reduce petroleum consumption. A secondary benefit is reduction in exhaust emissions.

Most of these advanced technologies include the use of electric drive propulsion systems and advanced energy storage systems (ESS). However, other vehicle technologies that employ advanced designs, control systems, or other technologies with production potential and significant petroleum reduction potential are also considered viable candidates for testing by AVTA.

Charging infrastructure for electric drive vehicles is also a study area of focus, because there is no singular successful business model that has been developed for public charging. In addition, there is much discussion within both the vehicle and charging infrastructure industries as to what the appropriate level of charging (kW) will be in the future and where will that placement occur (e.g., public, workplace, and/or residential?). In support of this uncertainty, INL is testing the efficiencies, standby power, unit power during charging, and mis-alignment (for wireless power transfer) impacts on efficiency and electro-magnetic field emissions.

The AVTA light-duty activities are conducted by INL for DOE. INL has responsibility for AVTA's technical execution, direction, management, and reporting, as well as data collection, analysis, and test reporting.

The current AVTA staff has 20+ years of experience testing grid-connected PEVs and PEV charging infrastructure. This experience includes significant use of DCFCs with various battery chemistries since the middle 1990s; that important legacy of experience is still available today. In addition, INL has significant experience performing cyber security testing for various Federal agencies and that experience is also being used for this project. During this reporting period, AVTA collected performance and use data from more than 16,000 Level 2 EVSE from the two largest providers of EVSE, as well as several additional EVSE manufacturers.

Introduction

With the expanding introduction and use of grid-connected PEVs by fleets and individual taxpayers, there is continuing development of both private and public PEV charging infrastructure, collectively known as conductive EVSE. EVSE currently takes the form of Level 1 (110 Volt) and Level 2 (240 Volt) levels that safely supply AC electricity to the vehicle and the charger that resides onboard the vehicle. The third type of EVSE is the DCFC, which provides DC electricity to the vehicle and the power electronics equipment onboard the vehicle. For DCFC, the charger is actually located off board the vehicle in the DCFC unit itself. Level 1 and 2 EVSE may either be in the form of "smart" EVSE, with functionalities such as revenue grade electricity meters, bidirectional communication capabilities, and other smart features. The opposite of this is "dumb" EVSE, which only provide electricity with minimal communication and metering capabilities. Regardless if an EVSE is smart or less than optimally smart, its basic function is to safely transfer AC electricity from the consumers' side of the electric utility meter to a PEV, which has an onboard vehicle battery charger and power electronics. By nature of its design, DCFC are also at least somewhat smart units to ensure a minimal amount of communication

between the DCFC charger and the vehicle's battery control system.

Normally, the term EVSE will refer to Levels 1 or 2 and DCFC will be referred to by its acronym. It should be noted that most installed EVSE are Level 2 units, which provide significantly shorter charge times than Level 1.

Adding to the complexity of charging infrastructure selection and placement is the introduction of wireless charging systems, which transfer power without having the conductive connector of today's EVSE and DCFCs (thus the term wireless power transfer or WPT). To support the introduction of safe and efficient wireless charging systems, DOE and AVTA are conducting a series of activities to test and benchmark WPT systems. These activities include grants to support development of smart EVSE and wireless charging, as well as benchmarking the efficiencies of the different charging options and testing for the vehicle-to-charging infrastructure compatibility. The activities discussed here detail the support activities being conducted by INL and some of the benchmarked results.

Approach

INL has created a process to benchmark wireless charging systems developed with DOE technology funding and with other wireless providers. Initial testing has been conducted and the results for the first system tests will be discussed in the next section. Of significant importance is the creation of NDAs in order to support the development of test procedures and sharing of protected proprietary information, while protecting the release of the proprietary information. This is currently ongoing with several NDAs signed to date.

INL has developed a testing regime for benchmarking Level 1 and 2 conductive EVSE efficiencies and this is being used to quantify grid-to-vehicle energy transfer efficiencies. This work is being leveraged to support benchmarking of the DOE Office of Electricity Delivery and Energy Reliability developed smart grid EVSE. Testing was completed on the first smart grid EVSE which was produced by GE. The other three smart grid EVSEs are scheduled for delivery in late 2014 / early 2015 and testing will commence then.

INL has benchmarked the cyber security of the GE smart grid EVSE. This is not an area that will receive significant disclosure due to the nature of the subject.

Much discussion has occurred regarding efficiency of emerging wireless systems. For this reason, INL obtained, tested, and provided the first independent test results for a WPT system. The WPT system is a pre-production version of the *PLUGLESS* wireless charger from Evatran. INL continued with this effort by testing this WPT as installed on a Chevy Volt to determine the interaction of the wireless charger and the vehicle as well as quantify the performance (efficiency, and EM field strength) as compared to operating off-board the vehicle in open-air test condition.

Of concern to industry and DOE is the compatibility of both DCFC and EVSE Level 2 equipment with original equipment manufacturer vehicles. AVTA has already benchmarked some compatibility problems with the new generations of PEVs; therefore, this task has been expanded

and a test regime has been designed and initiated in conjunction with SAE, Intertek, and Argonne National Laboratory. In total approximately 40 vehicles, EVSE, and DCFC will be compatibility / interoperability tested by AVTA under the supervision of INL engineering staff.

In accordance with AVTA’s normal process, fact sheets and reports are used to document benchmarking procedures and results and the quantitative results are published, with the exception of cyber security findings.

Results

EVSE Testing

There have been 14 Level 1 and 2 EVSE that have completed benchmark testing and the results are available at: avt.inel.gov/evse.shtml. A single fact sheet is published for each EVSE and the documented results include the following:

- Features
- Specifications
- Model tested
- Test conditions
- Test vehicle used
- Test results, including the following:
 - AC watt energy consumption prior to charge, during steady-state charge, and at post charge
 - Steady-state charge efficiency
 - Charge start and end profiles.

The most recent EVSE tested was the GE smart grid enabled EVSE. The results were published in both a detailed technical document and a fact sheet. Figure VII-15 is a photo of the GE EVSE.



Figure VII-15: GE smart grid enabled EVSE

EVSE testing was conducted in the laboratory for both the left and right J1772 plug (i.e., Plug 1 and Plug 2). Energy testing was done at four EVSE output power levels (i.e., 0.05 kW, 1.1 kW, 3.3 kW, and 6.5 kW), where each power level was tested for 10 minutes. EVSE standby power consumption also was tested to determine the amount of energy the EVSE uses while in a passive, non-charging state. Various power levels were chosen because they represent typical charge rates for a wide range of plug-in vehicles such as Level 1 and Level 2. The highest output power tested was limited to 6.5 kW, because of the 32-amp input continuous current limit of the 40-amp circuit breaker with 20% safety factor. The nominal input voltage was 208 VAC.

Table VII-5 details the EVSE efficiency while operating at the various charge power test conditions. Table VII-6 details the standby (not charging the vehicle) power consumption of the EVSE in the various operational states. Note, State D is an operational state that is not compatible with this EVSE since State D requires a ventilation fan for operation per the operational codes and standards. The response of the GE EVSE to the requested of State D is correct and expected.

Table VII-5: GE smart grid enabled EVSE efficiency testing

| Test Condition | Average EVSE Efficiency (Output Power/Input Power) |
|----------------|--|
| 50 watts | 71.9% |
| 1.1 kW | 97.8% |
| 3.3 kW | 98.7% |
| 6.5 kW | 98.5% |

Table VII-6: EVSE standby power (watts)

| J1712 State | Left Plug | Right Plug |
|-------------|------------|------------|
| State B | 17.7 Watts | 17.8 Watts |
| State C | 19.8 Watts | 19.9 Watts |
| State D | N/A | N/A |

The EVSE internal energy meter was tested during a 6.5 kW charge event over 10 minutes. The EVSE output power measured by the Hioki laboratory grade power meter and the IQ 250 laboratory grade watt-hour meter are very close (red and yellow lines). The purple dots indicate the energy measurement displayed on the EVSE front panel. This curve looks like stairs steps rather than a straight line because the EVSE measurement display is rounded to the nearest 100 watt-hours (0.1 kWh).

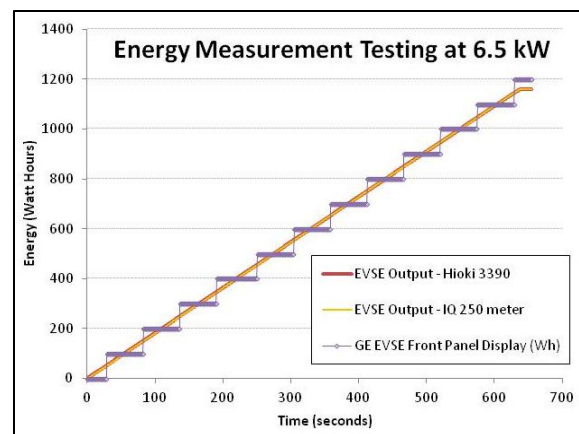


Figure VII-16: Energy measurement testing from the GE smart grid enabled EVSE

Conductive Interoperability Charger Testing

Testing is underway on 13 EVSE and 15 plug-in vehicles in an effort to identify EVSE to plug-in vehicle interoperability issues. Products have been supplied from vehicle and EVSE manufactures for the purpose of testing. The vehicles are being tested with each of the EVSE for functionality and compatibility per SAE J2953. Table VII-7 lists the EVSE participants and Table VII-8 lists the vehicle participants.

Table VII-7: EVSE Participants

| | EVSE Participants |
|----|--|
| 1 | Eaton Marina |
| 2 | Clipper Creek CS-100 |
| 3 | Clipper Creek LCS-25 |
| 4 | GE |
| 5 | Siemens |
| 6 | Schneider Electric |
| 7 | ChargePoint |
| 8 | Merit Charge LLC |
| 9 | AddEnergie CoRe+ |
| 10 | AddEnergie Smart Two |
| 11 | Aerovironment |
| 12 | Bosch |
| 13 | EVSE LLC (A division of Control Module Inc.) |

Table VII-8: Vehicle Participants

| | Vehicle Participants |
|-------|-------------------------------|
| 1 | Mitsubishi i-MiEV |
| 2,3 | Toyota Prius Plug-In, RAV4 EV |
| 4 | Nissan Leaf |
| 5 | Kia Soul EV |
| 6,7 | Ford C-MAX Energi, Focus EV |
| 8 | VW eGolf |
| 9 | BMW i3 |
| 10 | Chevrolet Volt |
| 11,12 | Honda Fit EV, Accord PHEV |
| 13 | Fiat 500e |
| 14,15 | Smart Fortwo ED (B-Class EV?) |

With EVSE interoperability testing complete on eight (8) of the fifteen (15) vehicles, the findings are being directly disseminated to the SAE J2953 committee at monthly meetings. SAE then communicates the results to the individual vehicle and EVSE manufacturers. Several main findings are as follows. The vehicle and EVSE pairs have been able to successfully charge the vehicle battery packs, but there have been failures according to J2953 criteria; therefore, most vehicle EVSE pairs have received “soft passes” rather than full passes. The mechanical test that is part of Tier 1 of J2953 is too arbitrary and dependent upon the individual test personnel. One EV failed during testing. The cause is unknown. This vehicle was recalled by the OEM and has been re-scheduled for an open slot late in 2014. Figure VII-17 shows a few of the EVSE used for the vehicle to EVSE interoperability testing.



Figure VII-17: Several of the thirteen EVSEs for interoperability testing with production plug-in vehicles

Wireless Charger Testing

Testing was completed on the pre-production wireless charger from Evatran as installed on a Chevy Volt as shown in Figure VII-18. The testing evaluated the system efficiency and EM field emissions at various power levels, coil-to-coil alignment, and coil gap. The results were compared to the previous open-air testing (off board the vehicle) of the same pre-production Evatran wireless charger. The impact on the results by the variation of charge power, coil gap, and coil to coil misalignment during vehicle testing was nearly the same as with the open-air testing. But there is a notable difference in the magnitude of results between the vehicle testing and open-air testing due to the interaction of the steel chassis floor and the magnetic field created by the wireless charger.



Figure VII-18: Vehicle-level testing of the pre-production Evatran wireless charger operation on a Chevy Volt

With the known differences between open-air testing and vehicle-level testing, INL evaluated a proposed SAE J2954 mock floor pan for use with open-air testing to closer replicate the vehicle-level testing conditions. The mock floor pan design is comprised of sheet steel of specific dimensions and thickness. One side is coated with a thin foil of aluminum. Testing was conducted with the mock floor pan (both aluminum side up and down) to determine the efficiency and EM field correlation to vehicle testing results and open-air test results. Figure VII-19 shows the proposed SAE J2954 mock floor pan design during testing with a wireless charger.

INL conducted evaluations of various inanimate objects for temperature increase when placed in close proximity to the EM field produced by a wireless charger during charge events. For the SAE J2954 test procedures, a small list of standard test objects is desired. At INL the objects were tested for rate of temperature rise and peak temperature after 5 minutes.

Table VII-9 and Figure VII-20 show the items evaluated in support of SAE J2954 test procedure development.



Figure VII-19: Open-air testing of the pre-production Evatran wireless charger using the proposed SAE J2954 mock floor-pan design

Table VII-9: Standardized debris test items

| |
|--|
| Paper Clips (various shapes and sizes) |
| 3/8" Rebar |
| Soda can |
| Steel toe shoe |
| Aluminum foil |
| Various coins (international and domestic) |



Figure VII-20: Debris items evaluated in support of SAE J2954 test procedure development

The test facility was augmented to improve testing capabilities to include in-laboratory vehicle-level testing of wireless and conductive charging systems. This will enable direct laboratory comparison between open-air testing and vehicle-level testing. Additionally the lab improvements will enable reduced testing time and higher quality of results. Figure VII-21 shows the new laboratory test facility called the INL Electric Vehicle Charging Infrastructure Test Facility.



Figure VII-21: Vehicle-level testing of conducting and wireless charging systems in INL's Electric Vehicle Charging Infrastructure Test Facility

Conclusions

INL will be testing additional wireless and conductive charging technologies with industry participation during the next 12 months. Industry, DOE, and INL are also conducting research into dynamic vehicle charging technologies that will use wireless power transfer technologies for possibly charging vehicles while they are driven on roadways.

With the importance of charging infrastructure to the successful adoption of grid connected vehicles, there are multiple key factors to the successful integration of vehicles and charging infrastructure. This includes interoperability, safety, test methodology, and efficiency. Therefore, AVTA is working with industry to develop robust testing methodologies for evaluation of wireless and conductive charging systems.

The augmentation of INL Electric Vehicle Charging Infrastructure Test Facility to enable laboratory testing of charging system, both integrated into a vehicle as well as a standalone sub-system, is an important accomplishment. This enables precise measurement of efficiency and EM field for both vehicle-level and open-air testing in a controlled laboratory environment.

VII.C.3. Products

Publications

1. Carlson, et. al. Results from the Operational Testing of the General Electric Smart Grid Capable Electric Vehicle Supply Equipment (EVSE), Idaho National Laboratory, INL/EXT-13-30929, 2014.
2. Electric Vehicle Supply Equipment (EVSE) Test Report: GE Smart Grid Enabled EVSE, INL/EXT-11-23986, Idaho National Laboratory, Idaho Falls, ID, November 2014.
3. INL Testing of Wireless Charging Systems, 2014 DOE Annual Merit Review, avt.inl.gov/pdf/prog_info/vss096Carlson2014.pdf, Idaho National Laboratory, 2014.

4. Testing Results: PLUGLESS Wireless Charging System by Evatran Group, Inc., Dec 2014 IWC meeting, avt.inl.gov/pdf/prog_info/WirelessChargingResultsVSATTDecember2013.pdf, Idaho National Laboratory, 2014.
5. Testing Results: PLUGLESS Wireless Charging System by Evatran Group, Inc., Plug-in 2013 conference, avt.inl.gov/pdf/phev/WirelessChargingPlugIn2013.pdf, Idaho National Laboratory, 2014.
6. Carlson, et. al., Test Results of the PLUGLESSTM Inductive Charging System from Evatran Group, Inc., SAE World Congress 2014-01-1824, INL/CON-13-29939, 2014.

Patents

1. This is a test program that is not designed to develop patents. The intent is to provide independent testing and feedback to DOE and industry on DOE and other funded technologies and technology improvements.

Tools and Data

The data generated by this testing are used to populate publications in the form of testing fact sheets, reports, and industry-referred papers.

VII.D. Wireless Power Transfer (WPT) Systems Optimization

Principal Investigator: Jeffrey Gonder

National Renewable Energy Laboratory (NREL)
15013 Denver West Parkway, MS 1634
Golden, CO 80401
Phone: (303) 275-4462
E-mail: jeff.gonder@nrel.gov

DOE Program Manager: David Anderson

Phone: (202) 287-5688
E-mail: david.anderson@ee.doe.gov

Future Achievements

- Present and publish work details, including on quasi-static WPT application along transit bus routes, and on market penetration impact analysis for passenger vehicles.
- Further examine power demand fluctuations and implications for the electric roadway infrastructure and the utility grid.



VII.D.1. Abstract

Objectives

- Building on previous efforts, analyze the potential future opportunity for wireless power transfer (WPT) to vehicles during a driving trip.
 - Focus on optimized deployment for incremental amounts of WPT infrastructure.
 - Examine personal as well as commercial vehicles, considering cost vs. benefit and relative market penetration potential for WPT-equipped vehicles.

Major Accomplishments

- Demonstrated strong leveraging potential for WPT-equipped light-duty (LD) hybrid vehicles over incremental urban WPT infrastructure roll out.
 - In-motion WPT on 1% of infrastructure in a given urban area enables LD hybrids to reduce their fuel consumption by 25% within the corresponding area.
- Identified strong leveraging potential as well for WPT-enabled heavy-duty (HD) hybrid trucks over incremental WPT deployment on sections of interstate highway with road grades greater than 1.5%.
 - This approach enables engine downsizing in the HD hybrid that would not otherwise be feasible.
 - Estimated enabled fuel savings of 9% relative to the baseline hybrid truck (without WPT) over a national driving distribution (where uphill interstate highway segments represent roughly 0.3% of all roads).
 - An initial cost vs. benefit analysis suggests that the resulting lifetime fuel savings could offset the incremental hybridization and WPT costs relative to a conventional truck, if spread across both LD and HD infrastructure users.

VII.D.2. Technical Discussion

Background

Significant advances in wireless power transfer (WPT) technology in recent years have led to the development of many prototype and even some commercial products for stationary wireless charging of plug-in electric vehicles (PEVs). In the fairly near future, companies such as Qualcomm, WiTricity and Evatran hope to increase the convenience of garage and parking lot PEV charging through the use of WPT. As the technology continues to advance, WPT has the long-term potential to transform PEV deployment by enabling power transfer during a driving trip or during a series of trips. This could take the form of stationary charging at intermittent stops, such as along a bus route—a strategy that companies such as WAVE are pursuing. Others, such as OLEV Technologies, are extending the concept of charging at intermittent stops to enable in-motion inductive power transfer. Siemens and Volvo are similarly pursuing the concept of in-motion conductive power transfer (using catenary lines and in-roadway conductive tracks, respectively).

Introduction

Previous National Renewable Energy Laboratory (NREL) analyses of potential long-term impacts for in-motion WPT found significant benefits for both light-duty (LD) and heavy-duty (HD) vehicles. The analyses estimated that in-motion WPT on the entire Interstate System (roughly the top one percent of most heavily travelled roads nationally) could reduce LD gasoline use by 20% and HD line-haul truck diesel use by over 75%.

Various advanced powertrain technologies derive different benefits from in-motion WPT. Hybrid electric vehicles (HEVs) equipped to receive power from such an electrified roadway could gain lower cost electric operation while on the system—effectively realizing the operating benefits of a PEV without the upfront battery cost. Battery electric vehicles (EVs) could have their range limitations all but eliminated through electrification of the entire Interstate System. Plug-in hybrid electric vehicles (PHEVs) could achieve incrementally longer operating range on

low-cost electricity, producing a corresponding cost savings for the vehicle owner.

The optimization analyses summarized here build on the previous investigation of in-motion WPT deployment across the national Interstate System. The analyses focus on initial incremental infrastructure deployment within a defined urban area or along sections of road that could provide the greatest fuel displacement benefit. The incremental in-motion WPT analyses consider both LD and HD vehicles, and additional analyses (not included in this summary report) are exploring LD vehicle market penetration implications as well as quasi-static WPT deployment at stops along a transit bus route.

Approach

Light-Duty Modeling Approach

Although the Interstate System comprises a relatively small fraction of all roads, the scenario from the previous impact study of electrifying the entire national Interstate System represents a very significant undertaking that would necessarily roll out incrementally if it were ever to occur. The approach for this analysis examines an incremental deployment scenario within a defined urban area. Reasons for focusing on incremental urban deployment include the travel overlap potential for a given population of vehicles considering that 80% of people reside in concentrated urban areas. Urban areas can be defined using the 2010 U.S. Census Combined Statistical Area (CSA) geographic boundaries, which create convenient delineations for analyzing road and travel distances within vs. outside an analysis region. Datasets from NREL's Transportation Secure Data Center (TSDC) can also be paired with a specific CSA in the region corresponding with the original travel survey. This section describes the analysis performed within seven CSA regions using corresponding second-by-second global positioning system (GPS) driving profiles from the TSDC, although the analysis has been framed such that a

similar approach could be applied to other regions without the need for detailed GPS driving data.

Three of the CSAs investigated, Kansas City, Chicago and Atlanta, were paired with TSDC data originally collected by metropolitan planning organizations from those regions. A separate California survey provided similar data on a statewide level. To ensure the statewide survey aligned with the regional surveys, it was broken up into subsets corresponding to four CSAs within California: Los Angeles, San Francisco, Sacramento, and Fresno. Altogether, the available GPS data within these seven CSAs included 5,342 vehicle driving profiles totaling nearly one million miles of on-road data. Candidate infrastructure sections considered for roadway electrification within these CSA boundaries included both interstates and highways—defined as Functional Class (FC) 1 and FC2 roads by a NAVTEQ/Nokia/HERE data layer of the underlying road network. Figure VII-22 highlights these candidate roads alongside lower capacity FC3 and FC4 roads within each of the seven CSAs.

As described earlier, HEVs can experience some of the greatest vehicle-level operating differences when using vs. not using an electrified roadway (driving on electricity vs. on gasoline). The initial urban analysis therefore focused on HEVs. NREL used its Future Automotive Systems Technology Simulator (FASTSim) to simulate the fuel consumption that would be expected from five different HEV models operated over the million miles of GPS driving profiles. Subsequent analysis of the simulation results can then quantify the total HEV fuel consumption on each road segment within the CSAs. An ordered ranking beginning with the segments showing the highest fuel consumption can then prioritize electric roadway rollout so that fuel displacement is maximized for a given amount of WPT infrastructure.

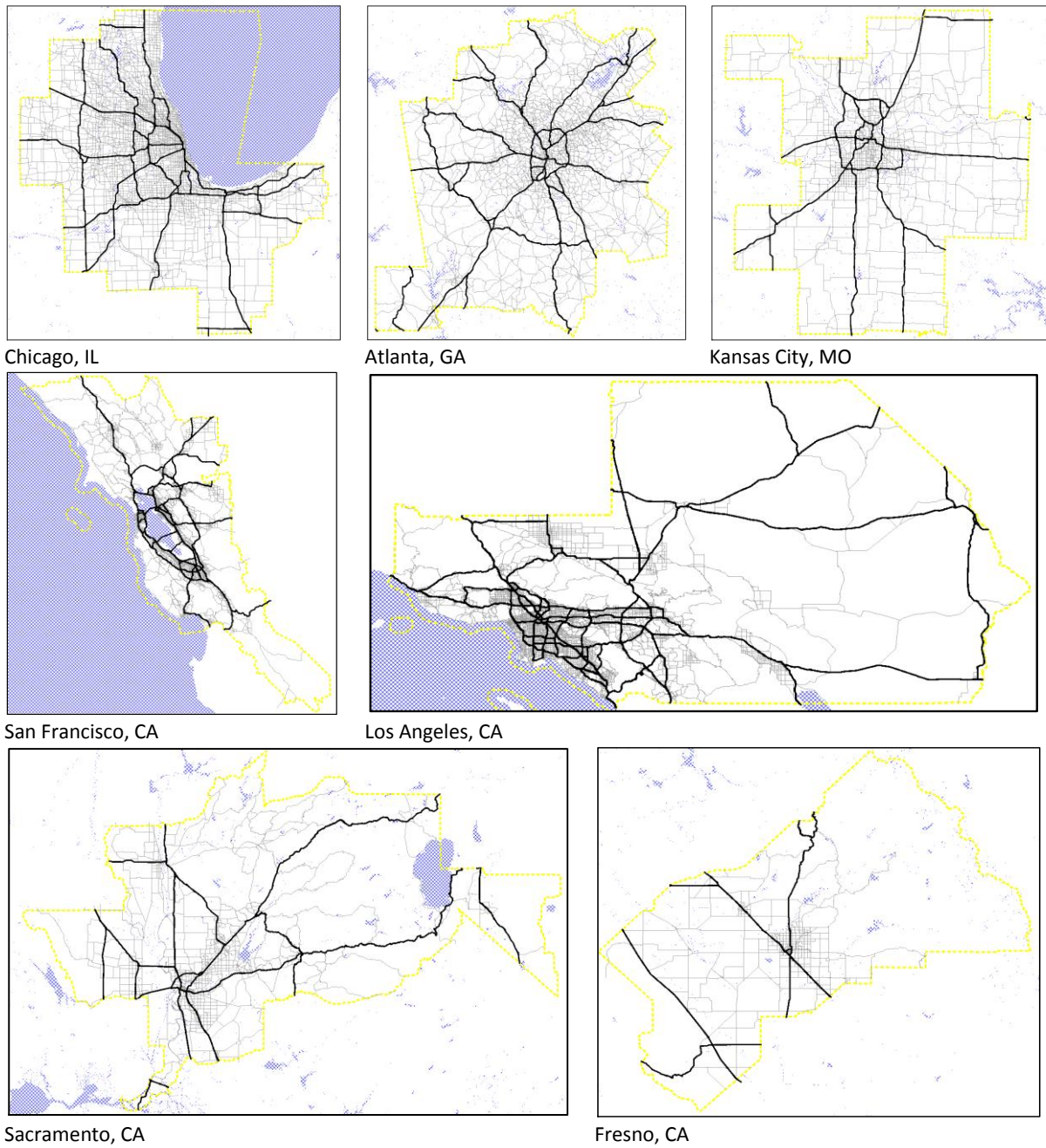


Figure VII-22: Roads identified as options for in-motion WPT (black lines) within defined CSAs (yellow lines)

Heavy-Duty Modeling Approach

For the HD-focused optimization analysis of incremental electrified roadway rollout, NREL investigated moderate-power WPT deployment at road locations where the trucks experienced the highest power demands. In addition to directly offsetting some amount of fuel consumption with the WPT, this approach could enable greater engine downsizing in a hybrid electric line-haul truck by ensuring satisfactory performance over long-duration high-power demands (i.e., demand durations longer than could be supported by the on-board HEV battery). NREL anticipated road sections containing substantial grade to be a primary location where such sustained power demands occur, and selected a five-day line-haul truck GPS driving profile that traversed a variety of terrain to explore this hypothesis.

To help quantify the power demand characteristics and fuel displacement opportunities, NREL leveraged a conventional and an HEV line-haul tractor-trailer model, both originally from studies at Oak Ridge National Laboratory. These models were input into FASTSim and simulated over the GPS driving cycles.

Results

Light-Duty Modeling Results

As an initial analysis, Figure VII-23 examines the amount of overlap with respect to driving miles on the FC1 and FC2 infrastructure considered as candidates for WPT within the CSAs. The figure organizes the FC1 and FC2 road segment data by CSA, with the four California CSAs combined and represented as a single curve. Each curve illustrates results for the FC1 and FC2 road segments traversed by the vehicle driving profiles, beginning with the ones that supported the most vehicle miles traveled (VMT) from the driving sample and ending with the segments that supported the least amount of VMT. The x-axis of the figure gives the cumulative amount of FC1 and FC2 infrastructure represented at any given point along the curves, calculated as a percentage of the total miles of roadway within the CSA. The y-axis indicates the cumulative VMT occurring on those road segments, calculated as a percentage of the total VMT from the driving profiles that occurred within the CSA.

The curves in Figure VII-23 reinforce the previously identified trend that relatively small percentages of road miles support much larger fractions of overall travel. For instance, the most heavily used 1.0%-1.5% of road segments (that are FC1 or FC2) in each region are able to support one fifth of the miles traveled by the driving profiles within the CSA. The cumulative profiles for the four California CSAs show the greatest amount of road overlap, with roughly 50% of urban VMT supported by only 3% of urban road infrastructure.

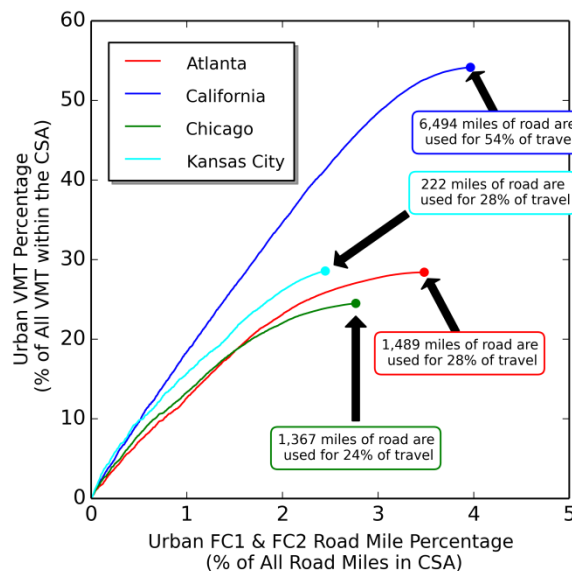


Figure VII-23: analysis of overlapping FC1 and FC2 travel within each CSA

For the fuel consumption analysis, NREL simulated five HEV models over the GPS driving profiles. While the models represented a range of vehicle sizes and powertrain designs, each showed very similar proportions of simulated fuel use as the results shown in Figure VII-24 for a vehicle model with similar characteristics as the third-generation Toyota Prius. Relative to the total simulated fuel consumption over the full extent of the GPS driving profiles, roughly 70% of the fuel consumption took place within the designated CSA analysis boundaries, and roughly 30% occurred on FC1 and FC2 road segments within the CSAs.

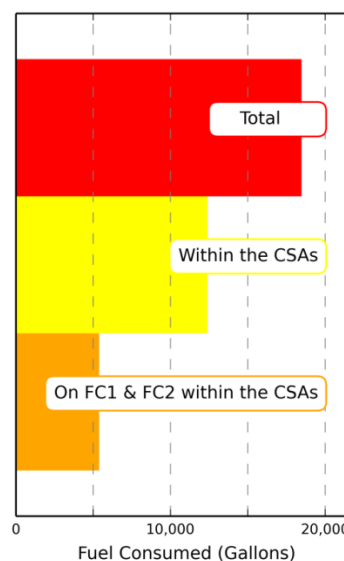


Figure VII-24: Simulated HEV fuel consumption over the GPS driving profiles

Figure VII-25 shows the fuel consumption analysis in each region, with FC1 and FC2 road segments ordered by the amount of fuel consumption occurring on them. The charts include individual curves for all five of the simulated HEVs, but show no significant differences between the results for each vehicle model. The charts on the right side of Figure VII-25 show trends similar to those in Figure VII-23, but suggest that the leveraging opportunity from a small percentage of infrastructure may be even greater when considering fuel consumption than when considering VMT overlap. For instance, across all regions, electrifying the top 1% of road infrastructure (that are FC1 or FC2) shows the potential to displace close to 25% of HEV fuel consumption within the CSA. The slightly higher leveraging outcome when considering fuel consumption likely relates to HEVs' slightly lower fuel economy on highways than they exhibit in stop-and-go city driving. HEVs also tend to show less benefit relative to conventional vehicles on highway-intensive drive profiles, so roadway electrification could provide a path for HEVs to deliver significant benefits independent of driving type.

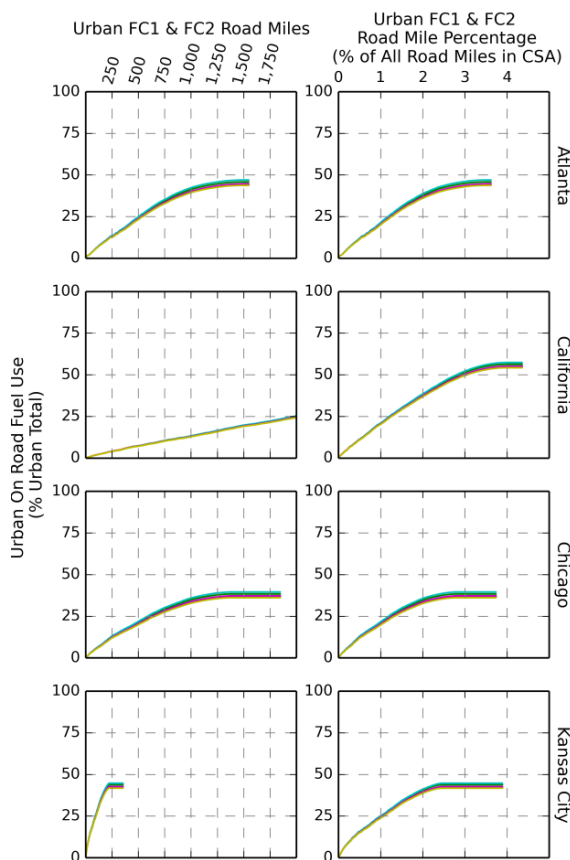


Figure VII-25: Fuel consumption reductions by WPT rollout for five HEV models

The charts on the left side of Figure VII-25 indicate the actual number of FC1 and FC2 road miles required to achieve a given percentage of simulated HEV fuel use within each region. These graphs highlight the significant regional differences on the road miles required to reach 1% of CSA road infrastructure. The Kansas City CSA requires less than 100 miles of FC1 and FC2 infrastructure to reach 1% of urban

road miles, whereas the combined California dataset would require over 1,600 mi of road infrastructure to achieve the same 1% of urban road miles.

Finally, each of the charts in Figure VII-25 shows a roughly linear trend of increasing fuel displacement potential out to about 2.5% of urban road coverage. Beyond that the curves level off, largely due to the sparse coverage of the GPS driving profile sample on those particular FC1 and FC2 road segments. Planned future work includes establishing correlations between the simulated HEV fuel consumption from the GPS driving profiles and the characteristics of roads on the network. This correlation will permit extension of the analysis to any road segment and any area with road network flow data to get around the GPS driving profile coverage limitations. Nevertheless, it is interesting to see the current results' linear trend in fuel displacement potential (out to nearly 50% of fuel use in the CSA) over the roughly 2.5% of road segments with sufficient GPS driving profile coverage.

Heavy-Duty Modeling Results

Table VII-10 shows the average engine power outputs by roadway type for the baseline HEV simulations. The results are summarized for all driving and just for the driving that occurred on FC1 and FC2 roads (though this subset represented over three quarters of the driving). As expected, the results show higher overall power demands on the FC1 and FC2 roads relative to all driving, and steeply increasing power demands as road grade increases. Altogether, about 21% of the miles from the 5-day (and roughly 720 mile) driving sample contained road grades over 1.5%, and hence higher average power requirements. NREL selected this fraction of the sample over which to evaluate potential impacts from incremental WPT rollout.

Table VII-10: Class 8 Truck Power Level Characterization Over Sections of the 5-Day Driving Sample with Positive Grade

| | Average Power (kW) | Percent of Distance | Average Power (kW) | Percent of Distance |
|--|--------------------|---------------------|--------------------|---------------------|
| | 124 | 25.8 | 199 | 24.8 |
| | 261 | 5.9 | 266 | 5.7 |
| | 317 | 11.8 | 324 | 10.9 |
| | 353 | 5.8 | 368 | 4.7 |

Table VII-11 summarizes the results for various line-haul truck scenarios simulated over the real-world driving profiles. The table includes results for the conventional baseline truck and for the HEV truck with different levels of engine downsizing, both with and without roadway electrification. The scenario in Table VII-11 showing the largest fuel savings potential included a hybrid powertrain with its engine downsized to 305 kW and roadway electrification at a 100 kW

power level on FC1 and FC2 road sections with grades larger than 1.5%. Relative to the baseline conventional vehicle this scenario achieved a 22% fuel economy improvement. Relative to the hybrid vehicle with no engine downsizing and no roadway electrification this scenario achieved a 14% fuel economy improvement.

For the 305 kW engine HEV case with no roadway electrification the vehicle experienced cumulative small misses of the target trace such that the total simulated driven distance was slightly less than 99% of the target distance (all the other scenarios traveled within 1% of the target distance). This observation is consistent with the expectation that substantial engine downsizing scenarios would be unable to maintain acceptable performance without the support of roadway electrification in areas of high power demand.

Table VII-11: Class 8 Truck Fuel Economy Results

| Scenarios | Engine Power (kW) | WPT Power (kW) | Total Fuel (Gallons) | FE (mpg) | Improvement (%) |
|------------------------|-------------------|----------------|----------------------|----------|-----------------|
| Conventional baseline | 391 | 0 | 145 | 5.5 | 0 |
| Hybrid baseline engine | 391 | 0 | 138 | 5.9 | 7 |
| | | 100 | 125 | 6.5 | 18 |
| Hybrid Downsize1 | 350 | 0 | 135 | 5.9 | 8 |
| | | 100 | 123 | 6.6 | 20 |
| Hybrid Downsize2 | 305 | 0 | 133 | 6.1 | 10 |
| | | 100 | 121 | 6.7 | 22 |

NREL next conducted a cost vs. benefit analysis for widespread deployment of the greatest fuel saving scenario from Table VII-11. Examination of the national NAVTEQ/Nokia/HERE road layer data indicated that roughly 14% of FC1 and FC2 nationwide miles have grades greater than 1.5% (out of the total FC1 and FC2 distance of 194,600 miles). Because this percentage is less than the comparable 21% of FC1 and FC2 road miles figure from the 5-day GPS sample, for the cost vs. benefit analysis NREL reduced the estimated fuel economy improvement over the HEV case with no roadway electrification from 14% to 9%. Table VII-12 lists the assumptions for annual truck operating miles (tapering over the assumed 19-year life) as well as other inputs used in the analysis.

Figure VII-26 shows the net present cost and lifetime fuel savings results. For the baseline assumptions, the HEV reduces lifetime diesel use by about 6% relative to the 259,000 gallon lifetime consumption estimate for the conventional truck. In spite of the dominance of diesel expenditures in the lifetime cost calculation, the estimated HEV savings are insufficient to totally offset its upfront cost increment, resulting in a 2.3% higher cost estimate for the

HEV relative to the \$857,000 lifetime cost estimate for the conventional truck. For the incremental HEV electric roadway scenario (i.e., 100 kW on interstate highway sections with grades of 1.5% or greater), the WPT-enabled HEV consumes less fuel (14% lower lifetime fuel use than the conventional truck) and does so at an estimated 0.3% lower lifetime net cost than the conventional truck.

Table VII-12: Assumptions for Class 8 Truck Cost vs. Benefit Analysis, With In-Motion WPT on Interstate Highway Road Segments Having Grades of 1.5% or Greater

| Inputs | Assumption |
|--|--------------|
| Vehicle Life (years) | 19 |
| Beginning of Life Annual Miles | 120,000 |
| End of Life Annual Miles | 30,000 |
| Conventional Vehicle Cost | \$110,000 |
| Hybridizing Cost Increment | \$61,450 |
| Additional WPT Cost per Vehicle | \$10,000 |
| Diesel Price | \$3.88 / gal |
| Electricity Price | \$0.08 / kWh |
| Sales Tax | 7.8% |
| Discount Rate | 4.2% |
| Vehicle Electricity Consumption on the WPT Infrastructure (kWh/mi) | 1.47 |
| WPT Cost Per Mile | \$3,000,000 |
| WPT Infrastructure Life (years) | 8 |
| Total Length of All FC1 and FC2 Roads (miles) | 194,600 |
| Total Fuel Use on All FC1 and FC2 Roads (k gallon) | 169,049,277 |

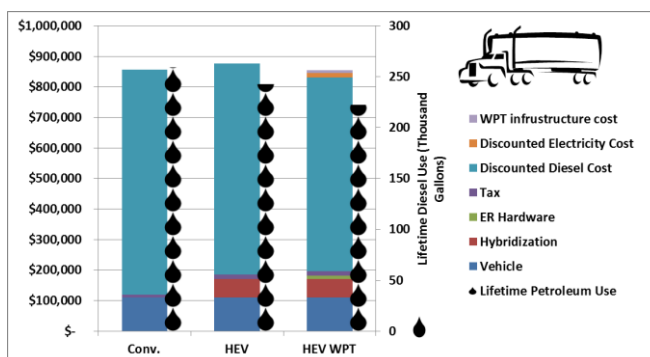


Figure VII-26: Net present lifetime cost and fuel savings of in-motion WPT scenario relative to baseline conventional and HEV truck scenarios

The cost vs. benefit results obviously depend strongly on the input assumptions, for which there are many uncertainties. With diesel expenditures being the largest contributor to the lifetime cost calculations, important factors include the relative fuel economy of the three scenarios as well as future diesel price projections. For instance, assuming a diesel price of \$5.10/gallon (EIA's high fuel price scenario estimate for the year 2023), the lifetime cost savings increases to \$35,000 for the HEV WPT scenario relative to the conventional baseline.

The results also depend on the hardware and infrastructure cost assumptions, though the WPT infrastructure costs could be a small fraction of the overall lifetime expenses if spread over all potential WPT users, which was the approach taken here. As an illustration of the relative sensitivities under this approach, for the \$5.10/gallon diesel price assumption the cost for the WPT infrastructure installation could rise as high as \$14 million per mile and still achieve lifetime cost parity with the conventional truck case.

Conclusions

The analyses in this report suggest cost and petroleum reductions for both LD and HD vehicles from incremental rollout of WPT. Installing in-motion WPT on 1% of infrastructure in a given urban area enabled LD HEVs to reduce their fuel consumption by 25% within the corresponding area. Additional analysis has shown that extending the 1% of infrastructure coverage across the nation would significantly increase HEV and PEV sales estimates.

For HD Class 8 trucks, incremental rollout also had benefits. Assuming in-motion WPT on interstate highway road segments with grades greater than 1.5% (approximately 0.3% of the roads in the nation), petroleum use was reduced and the vehicle's net cost was similar to that of a conventional vehicle. As WPT infrastructure rollout increases further, so do the estimated benefits.

VII.D.3. Products

Publications

1. Gonder, J., Brooker, A., Burton, E., Wang, L., and Konan, A. "Advanced Wireless Power Transfer Vehicle and Infrastructure Analysis." DOE Vehicle Technologies Annual Merit Review – Project ID#: VSS130, June 2014.
2. Brooker, A., Burton, E., Gonder, J., Konan, A. and Wang, L. "Analysis of Wireless Power Transfer Systems Optimization Scenarios." Vehicle Systems Optimization Focus Area Report, September 2014.
3. Burton, E., Brooker, A., Gonder, J., and Konan, A. "Fuel Savings Potential from Future In-Motion Wireless Power Transfer." Submitted to the 3rd Conference on Electric Roads & Vehicles (CERV), February 2015.
4. Wang, L., Brooker, A., Burton, E., and Gonder, J. "Wireless Power Transfer System Optimization for Heavy-Duty Trucks." Submitted to the 3rd Conference on Electric Roads & Vehicles (CERV), February 2015.

Tools and Data

1. Transportatoin Secure Data Center (www.nrel.gov/tsdc)
2. FASTSim model (www.nrel.gov/fastsim)
3. Fleet DNA Project Database (www.nrel.gov/fleetdna www.nrel.gov/vehiclesandfuels/fleettest/research_fleet_dna.html)

FRICION AND WEAR

VII.E. DOE/DOD Parasitic Energy Loss Collaboration

Principal Investigator: George Fenske
Co-Investigators: Aaron Matthews (Aerotek),
Nicholaos Demas, Robert Erck

Argonne National Laboratory
 9700S. Cass Ave.
 Argonne, IL 60439
 Phone: (630) 252-5190
 E-mail: gfenske@anl.gov

CRADA Contact: Ricardo, Inc.

DOE Program Manager: Lee Slezak
 Phone: (202) 586-2335
 E-mail: lee.slezak@ee.doe.gov

- Completed preliminary parametric study of asperity friction for commercial and advanced friction modifiers.

Future Achievements

- Complete parametric study of FMEP for a midsized diesel engine as functions of engine speed, load, lubricant viscosity, asperity friction, and surface finish.
- Complete parametric study of asperity friction for commercial and advanced lubricant friction modifiers.



VII.E.2. Technical Discussion

Background

Multiple approaches are being pursued to improve the fuel economy of vehicles, including the development of advanced tribological systems involving lubricants, materials, coatings, and engineered surfaces to reduce parasitic friction losses in engines (and drivelines). This project focuses on the development of a user friendly, web-based calculator to predict the impact of tribological parameters such as the boundary friction coefficient, lubricant viscosity, temperature, surface finish, speed, load, and visco-piezo properties on the fuel economy of engines typically used for ground transportation vehicles.

Introduction

Friction, wear, and lubrication affect fuel economy, durability, and emissions of engines used in ground transportation vehicles. Total frictional losses in a typical engine may alone account for more than 10% of the total fuel energy (depending on the engine size, driving condition, etc.). The amount of emissions produced by these engines is related to the fuel economy of that engine. In general, the higher the fuel economy, the lower the emissions. Higher fuel economy and lower emissions in future diesel engines may be achieved by the development and widespread use of novel materials, lubricants, and coatings. For example, with increased use of lower viscosity oils (that also contain lower amounts of sulfur- and phosphorus-bearing additives), the fuel economy and environmental performance of future engine systems can be dramatically improved. Furthermore, with the development and increased use of smart surface engineering and coating technologies, even higher fuel economy and better environmental soundness are feasible.

VII.E.1. Abstract

Objectives

- Develop a web-based toolkit based on FMEP (friction mean effective pressure) maps to predict the impact of key tribological engine parameters on vehicle fuel economy.
- Identify pathways to reduce parasitic friction losses in engines.
- Develop high-fidelity database on key tribological parameters (boundary friction) for use in a toolkit for identifying low-friction solutions.
- Validate mechanistic models by performing instrumented, fired-engine tests with single-cylinder engines to confirm system approaches to reduce friction and wear of key components.
- Identify common issues associated with commercial and military ground vehicles on the ability of low-friction lubricant technologies to reduce parasitic friction losses and vehicle efficiency.

Major Accomplishments

- Completed parametric study of combustion chamber FMEP as a function of engine load (indicated mean effective pressure) and speed for a small spark-ignited engine.
- Developed engine 3D finite element models of power cylinder components for a medium-sized diesel engine.
- Analyzed FMEP simulation data using a linear-regression approach to develop an analytical tool that will predict FMEP and fuel consumption scaling factors as functions of load, speed, and lubrication properties.

Integration of advanced lubricant chemistries, textured surfaces (plateau-honed, fine-honed, etc.), and advanced component materials and coatings necessitates pursuing a systems approach. Changes in one system component can readily change the performance of other components. For example, application of a hard coating on a liner to improve its durability may decrease the durability of the mating rings. Also, lowering the oil viscosity will cause certain components (e.g., bearings) to operate under boundary lubrication regimes not previously encountered, resulting in accelerated degradation. A systems approach is required to not only identify the critical components that need to be addressed in terms of energy savings, but also to identify potential pitfalls and find solutions.

The main goal of this project is to use advanced models of engine-component friction and contact loading to predict the impact of advanced surface engineering technologies (e.g., laser dimpling, near frictionless carbon, and superhard coatings) and energy-conserving lubricant additives on parasitic energy losses from diesel engine components. The project also aims to develop more realistic databases on the boundary or asperity friction that are used in advanced codes to predict total (asperity and hydrodynamic) friction losses and, in the future, to validate the predictions in tests using fired engines. Such information will help identify critical engine components that can benefit the most from the use of novel surface technologies, especially when low-viscosity engine oils are used to maximize the fuel economy of these engines by reducing churning and/or hydrodynamic losses. The long-term objective of the project is to develop a database that provides a “look-up” capability to predict the impact of lubricant viscosity, asperity friction, and surface finish on FMEP and contact severity at different engine operating modes.

Approach

Under the Argonne/Ricardo CRADA, multiple codes (PISDYN, RINGPAK, VALVDYN, and ENGDYN) will be integrated to calculate from first principles the parasitic friction losses (FMEP) under prescribed engine conditions (load and speed) for a range of tribological parameters (asperity friction, lubricant viscosity, surface finish, and pressure-temperature-viscosity coefficients). The information will be provided in a series of spreadsheets that will enable users to calculate changes in FMEP and fuel consumption scaling factors (FCSFs) to predict changes in fuel consumption for different driving cycles.

For a given engine type (diesel or gas) and size (small, medium, or large), the database will consist of FMEP contributions from the ring pack, piston skirt, engine bearings, and valve train as a function engine mode (load and speed) for different lubricant viscosities, asperity friction, type (mineral or synthetic), and component surface finish. The database users will employ a recommended baseline configuration (viscosity, asperity friction, surface finish, and oil type), or users can specify their own baseline configuration and a new (variant) configuration. The users will also specify the engine modes (speed and load) and weighting factors. The web-based calculator will utilize the FMEP database to calculate

differences in the FMEP (relative to the baseline), which will be used to scale the fuel consumption at each specified engine mode (speed and load) and thus predict the change in fuel consumption from the baseline.

Our primary task for this project is to perform FMEP calculations for the following range of parameters: engine type [spark ignition (SI) or compression ignition (CI)], engine size, engine mode (speed and load), lubricant viscosity, asperity friction, surface finish, oil type (mineral or synthetic), and additive (friction modifier), as discussed previously [1].

The codes used to model the FMEP allow detailed calculations of the dynamic forces on the engine components and, in the process, provide information on the severity of the contact loading between moving components (e.g., between the rings and cylinder liner). Such information will also be tracked and used to predict changes in the contact severity for different tribological conditions as well as changes in the minimum oil film thickness. This information can, to a first approximation, be used to estimate the impact of the parameters on component durability (gradual wear) and reliability (sudden catastrophic failure, e.g., scuffing) and the need for improved wear resistance and/or surface finishes to accommodate a given low FMEP strategy.

A second task focuses on developing a high-fidelity database on asperity friction for use in the calculator. Our approach in this effort utilizes laboratory-scale tribometers to simulate engine conditions to measure asperity friction for a range of conventional and experimental material and lubricant combinations.

Results

Results presented in previous progress reports [1,2] discussed the concept of FMEP maps and their use to calculate Δ FMEP maps for different operating conditions utilizing FMEP simulation data typical of a large (9-12 L) in-line diesel engine [3-6]. Figure VII-22 is a Δ FMEP map that shows the change in FMEP for a SAE 20 WT lubricant with a low friction interface representing a 90% decrease in asperity friction relative to an SAE 40WT oil with nominal asperity friction values.

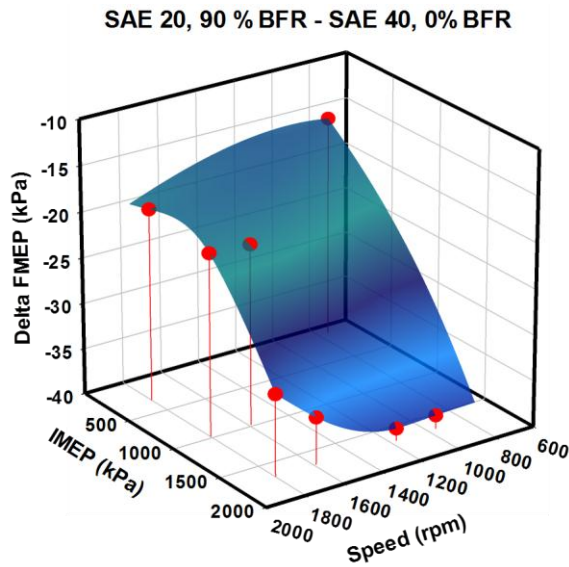


Figure VII-27: Map showing ΔFMEP between an SAE20 WT (90% reduction in asperity friction) and an SAE 40WT oil (with baseline asperity friction) as function of speed and load (BFR = boundary friction reduction)

The ΔFMEP maps were used to calculate FCSFs for the different cases using the following equation:

$$(1) \text{ FCSF} = (\text{IMEP} + \Delta\text{FMEP})/\text{IMEP}$$

where IMEP is the indicated mean effective pressure. This relation can be used to develop FCSF maps for different lubrication conditions (viscosity and asperity friction), which together with fuel consumption data (as functions of load and speed and drive-cycle weighting factors) can be used to predict fuel consumption.

During FY 2014, linear-regression protocols were developed to analyze FMEP and fuel consumption data, and these results were used to calculate FMEP simulation data at different lubrication conditions (viscosity and asperity friction).

For each lubrication condition, the engine FMEP data (consisting of contributions from ring/liner interactions, piston/liner and wrist pin friction, valvetrain friction, and engine bearing friction) for different engine load and speed conditions were fitted to the polynomial:

$$(2) \text{ FMEP} = F_0 + A*\text{IMEP} + B*\text{Speed} + C*\text{IMEP}^2 + D*\text{Speed}^2$$

The leading coefficients (F₀, A, B, C, and D) were then fitted to a polynomial as functions of viscosity at 100°C and BFR (ranging from 0.1 for a 90% reduction in asperity friction to 1.6 for an increase in asperity friction of 60%). The linear regressions for F₀, A...D, are of the form:

$$(3) F_0 = f_0 + a_{f0}*BFR + b_{f0}*\eta + c_{f0}*BFR^2 + d_{f0}*\eta^2$$

$$(4) A = a_0 + a_A*BFR + b_A*\eta + c_A*BFR^2 + d_A*\eta^2$$

.....

$$(5) D = d_0 + a_D*BFR + b_D*\eta + c_D*BFR^2 + d_D*\eta^2$$

where BFR is the boundary friction reduction (0.1 to 1.6), and η is the kinematic viscosity (in cSt) at 100°C. The results of the linear regression for a heavy-duty diesel engine (HDDE) are given in Table VII-13.

Table VII-13: Linear Regression Coefficients of FMEP for a HDDE

| | * ₀ | a _* | b _* | c _* | d _* |
|----------------------|----------------|----------------|----------------|----------------|----------------|
| F₀ | 4.9E+00 | -8.2E+00 | 9.8E-01 | | |
| A | -6.2E-02 | -3.9E-02 | 1.0E-02 | -5.5E-18 | -2.6E-04 |
| B | 4.5E-02 | 6.2E-02 | 3.3E-04 | 3.8E-17 | -1.1E-04 |
| C | 4.7E-05 | 3.3E-05 | -7.2E-06 | 2.7E-21 | 1.8E-07 |
| D | -1.5E-05 | -2.9E-05 | 9.2E-07 | -1.1E-20 | 2.3E-08 |

* - refers to a_A, a_B, a_C..., b_A, b_B..., etc.

Additional linear-regression analysis of the regression-based FMEP predictions vs. the Ricardo code simulation data was performed to develop secondary correction factors (as functions of BFR and η) to the liner-regression polynomial data. An example of the final linear regression of the FMEP simulation for an SAE 40WT oil (baseline friction) is shown in Figure VII-28.

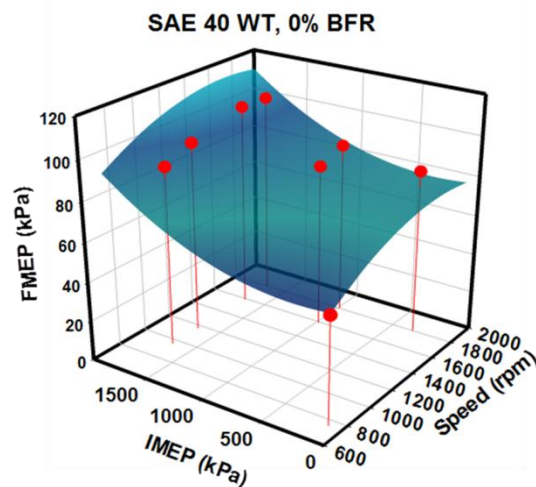


Figure VII-28: Comparison of FMEP simulation data (red circles) to linear-regression fit (mesh)

For the SAE 40WT case shown in Figure VII-28, the maximum deviation of the regression fit from the FMEP simulation data was (-)9%. Overall, the deviation typically was in the range +/- 20%. However, the deviation from simulated FMEP for the 60% increase in asperity friction (1.6 BFR) was higher, and thus, the predictions for this case are not as accurate.

The FCSFs were calculated from the relation given in Eq. 1. Figure VII-29 shows an example of the FCSC factor map for the case of an SAE 20WT oil with a 90% BFR compared to the baseline case of an SAE 40WT oil with nominal baseline asperity friction.

FCSF - SAE 20WT, 90% BFR - SAE 40WT 0% BFR

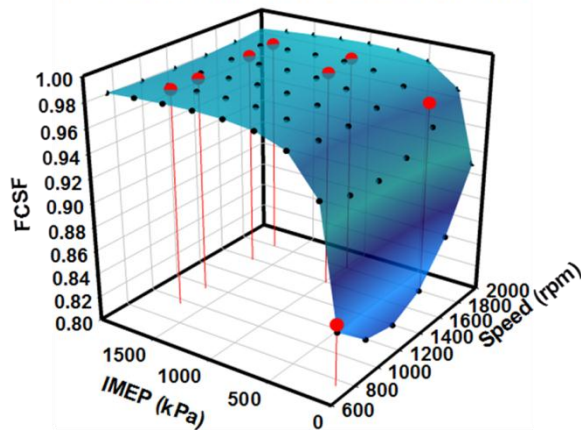


Figure VII-29: FCSF for an SAE40WT oil (with a 90% BFR) relative to an SAE 40WT oil with baseline asperity friction

The next step in the calculation requires information on the fuel consumption rate as a function of engine load and speed. Figure VII-30 shows a 3D map of the fuel consumption rate (kg/hr) used to model the impact of lubrication conditions on fuel economy. In this case a Lorentzian fit to IMEP and speed was employed. The red data points represent the fuel burn rate for the eight engine points for the baseline case (SAE 40 WT, baseline asperity friction), and the mesh is a Lorentzian fit to the data.

Lorentzian Fit to Fuel Consumption Rate

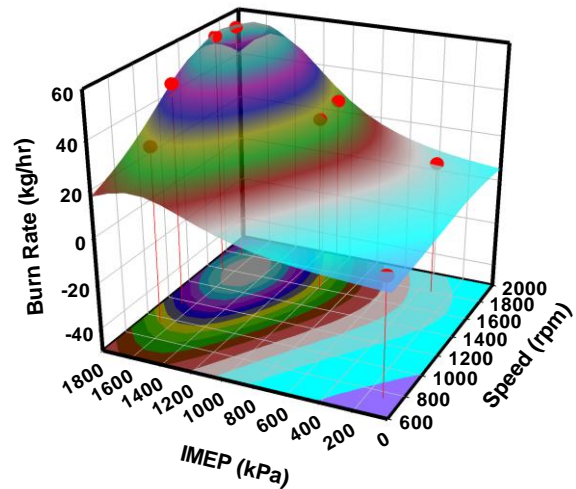


Figure VII-30: Lorentzian fit to fuel consumption rate

The last piece of information required to estimate the impact of lubrication parameters on fuel economy is drive cycle weighting factors. As the name implies, the weighting factors represent the fraction of the overall time spent at a given engine condition (load and speed). The sum of the weighting factors is unity. Weighting factors for the example considered below are given in Table VII-14 along with data on the IMEP, BMEP (Brake Mean Effective Pressure), fuel mass, and engine speed for the 8-mode Ricardo FTP (Federal Test Procedure) drive cycle.

Table VII-14: Engine Conditions

| FTP Mode | Engine Speed (rpm) | Fuel Mass (kg) | IMEP (kPa) | BMEP (kPa) | Weight |
|----------|--------------------|----------------|------------|------------|--------|
| 1 | 750 | 1.77 | 104 | 0 | 0.52 |
| 2 | 960 | 28.08 | 1683 | 1565 | 0.03 |
| 3 | 1170 | 48.42 | 1683 | 1565 | 0.04 |
| 4 | 1590 | 28.79 | 983 | 783 | 0.15 |
| 5 | 1590 | 58.14 | 1683 | 1565 | 0.08 |
| 6 | 1800 | 10.22 | 325 | 157 | 0.06 |
| 7 | 1800 | 31.09 | 983 | 783 | 0.08 |
| 8 | 1800 | 57.31 | 1683 | 1565 | 0.05 |

The improvement in fuel economy (FE) was calculated from the following relation:

$$(6) \quad FE = \frac{\text{Weighted Burn Rate}_{\text{case 1}} - \text{Weighted Burn Rate}_{\text{ref case}}}{\text{Weighted Burn rate}_{\text{ref case}}}$$

where

$$(7) \quad \text{Wt'd Burn Rate} = \sum_i \text{Wt Factor}_i \times \text{FCSF}_i \times \text{Burn Rate}_i$$

Figure VII-31 summarizes the calculations of the fuel economy change one would expect relative to a reference case for SAE 40WT oil with baseline friction.

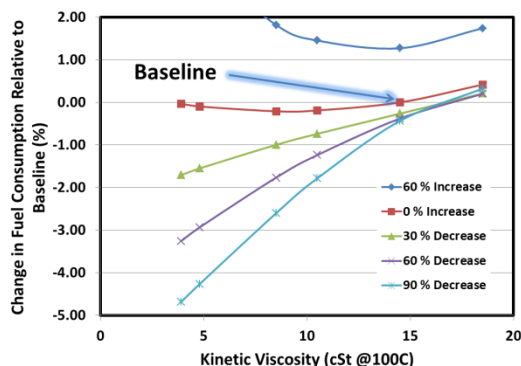


Figure VII-31: Predicted change in fuel consumption for a HDDE vehicle as function of viscosity and change in asperity friction

The results illustrate three interesting trends:

- Reducing or even eliminating all asperity friction alone will save at most 1/2% in fuel consumption.
- Reducing viscosity, while keeping asperity friction fixed at the nominal values, will again save at most ½ % in fuel consumption.
- Incorporating low boundary friction surfaces (low friction coatings or low friction additives) in conjunction with a low viscosity oil will produce significant reduction in fuel consumption.

Work is currently underway on modeling parasitic friction losses of power cylinder components for a small SI engine (500 cc displacement/cylinder). Tribological parameters include lubricant viscosity, asperity friction, and surface finish.

Task 2 of the CRADA addresses developing a high fidelity database on asperity friction for use in the models. As reported previously [1, 2], Argonne has established a number of laboratory-scale test protocols to simulate engine conditions and to quantify asperity friction coefficients for different lubricant packages, temperatures, and surface finishes. The protocols utilize reciprocating ring-on-liner and ball-on-flat configurations as well as a unidirectional (rotating) ball-on-flat configuration to measure friction during 1- to 3-hour long tests. The protocols include speed ramps at the start and end of the tests to obtain speed-dependent data.

During this past year, results of a series of reciprocating ball-on-flat experiments performed with different lubricants at room temperature (RT) to 125°C were analyzed. An example of the frictional data as a function of time for mineral-based fully formulated lubricant (minus the factory-supplied friction modifier) with molybdenum dialkyldithiocarbamate (MoDTC) and zinc dialkyl dithiophosphate (ZDDP) additives is shown in Figure VII-32.

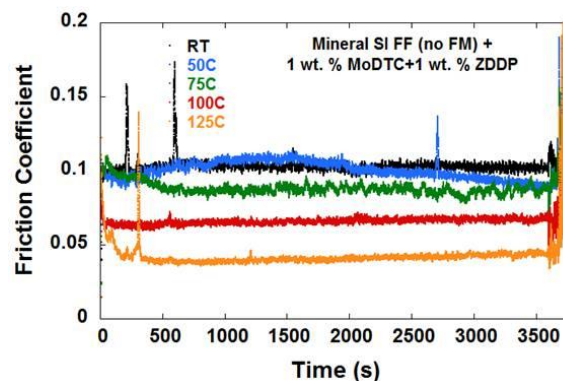


Figure VII-32. Friction vs. time for 1-hour ball-on-flat tests at different temperatures

The main portion of the tests was performed at a relatively low sliding rate (1 Hz, 20-mm stroke), and the friction is representative of boundary lubrication (not mixed or hydrodynamic). For this particular combination, the asperity friction decreased from 0.10-0.11 at room temperature to 50°C to 0.04 at 125°C.

Figure VII-33 summarizes the trends for different variations of lubricants and friction modifiers examined in this limited study – with asperity friction ranging from 0.04 to 0.11 depending on temperature and chemistry.

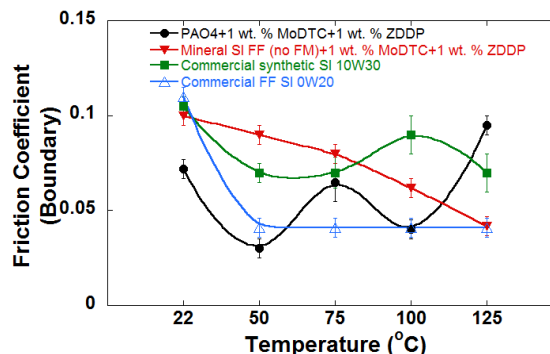


Figure VII-33: Asperity friction as a function of temperature for four lubricants

Conclusions

The Parasitic Energy Loss Reduction project is examining the effects that tribological variables such as viscosity, boundary friction, and surface finish have on the friction losses in an engine and the overall vehicle fuel economy. Utilizing data for a large heavy-duty diesel engine, we applied a linear-regression method to develop polynomial fits to the FMEP as functions of load, speed, viscosity, and asperity friction. We developed FMEP difference maps and applied them to calculate fuel consumption scaling factors, which were combined with fuel consumption data to predict the impact of viscosity and asperity friction on fuel consumption.

Studies on a high-frequency reciprocating rig and pin-on-disk rig indicate that more realistic information on boundary friction coefficients can be achieved as functions of temperature and composition. Several candidate additive

approaches have been identified that show significant improvements in friction. The results suggest that asperity friction can be reduced up to 60%.

Future activities will focus on CRADA activities to model parasitic friction losses for a medium-sized diesel engine using OEM engine models. Work will continue to “data mine” existing friction data for a range of tribotests performed during the past 5-10 years at Argonne, as well as to identify novel friction modifiers under development. Efforts to further define a cohesive collaboration with the U.S. Army Tank Automotive Research, Development and Engineering Center (TARDEC) are in progress under a formal memorandum of understanding developed between the Departments of Energy and Defense to pursue advanced vehicle power technologies.

References

1. G. Fenske, N. Demas, and R. Erck, “DOE/DOD Parasitic Energy Loss Collaboration,” *FY 2012 Annual Progress Report*, DOE/EE-0834.
2. G. Fenske, A. Matthews, N. Demas, R. Erck, “DOE/DOD Parasitic Energy Loss Collaboration,” *FY 2013 Annual Progress Report*, DOE/EE-1023.
3. George Fenske, “Parasitic Energy Loss Mechanisms,” *FY 2006 Progress Report for Heavy Vehicle Systems Optimization* (2006).
4. George Fenske, “Parasitic Energy Loss Mechanisms: Impact on Vehicle System Efficiency,” U.S. Department of Energy Heavy Vehicle Systems Review, Argonne National Laboratory, Argonne, IL, April 18-20, 2006.
5. G. Fenske, O. Ajayi, R. Erck, C. Lorenzo-Martin, A. Masoner, and A. Comfort, “Reliability of Powertrain Components Exposed to Extreme Tribological Environments,” *Proceedings of the 2010 Ground Vehicle Systems Engineering and Technology Symposium*, Dearborn, MI, 2010.
6. George Fenske, Nicholas Demas, and Robert Erck, “Efficiency Improvements through Parasitic Loss Reduction,” *FY2011 Annual Progress Report for Vehicle Systems Optimization* (2011).
3. DOE/DOD parasitic energy loss collaboration, G. Fenske, A. Matthews, and N. Demas, U.S. Department of Energy Vehicle Technologies Office Annual Merit Review and Peer Evaluation Meeting, June, 16-20, 2014, Washington D.C.
4. Tribological evaluation of piston skirt/cylinder liner contact interfaces under boundary lubrication conditions, N. G. Demas, R. A. Erck, and G. R. Fenske, *Lubrication Science*, 22:3, 73–87, 2010.
5. Tribological studies of coated pistons against cylinder liners in laboratory test conditions, N. G. Demas, O. O. Ajayi, R. A. Erck, and G. R. Fenske, *Lubrication Science*, DOI: 10.1002/lis.1175, 2012.
6. Tribological effects of BN and MoS₂ nanoparticles added to polyalphaolefin oil in piston skirt/cylinder liner tests, N. G. Demas, E. Timofeeva, J. L. Routbort, and G. R. Fenske, *Tribology Letters*, 47:1, 91-102, 2012.
7. Influence of surface texture on micro EHL in boundary regime sliding, R. A. Erck, O. O. Ajayi, C. Lorenzo-Martin, and G. R. Fenske, *Extended Abstract, ASME/STLE 2012 International Joint Tribology Conference*, October 8-10, 2012.
8. Effect of hard coatings on tribochemical film behavior in lubricated sliding contact, N. G. Demas, A. Navratil, O. O. Ajayi, and G. R. Fenske, *35th International Conference and Exposition on Advanced Ceramics and Composites (ICACC'12)*, Daytona Beach, FL, January 22-27, 2012.
9. Tribological behavior of Ti-based thin film coatings under boundary lubrication regime, C. Lorenzo-Martin, N. G. Demas, and O. O. Ajayi, *STLE Annual Meeting*, St. Louis, MO, May 6-10, 2012.
10. Investigation of MoS₂ and BN nanolubricants and their effect on the tribological behavior of combustion engine parts, Poster, N. G. Demas, E. Timofeeva, J. L. Routbort, and G. R. Fenske, *APS/CNM/EMC Users Meeting*, Argonne National Laboratory, 2012.
11. Tribological effects of BN and MoS₂ nanoparticles added to polyalphaolefin oil in piston skirt/cylinder liner tests, N. G. Demas, E. Timofeeva, J. L. Routbort, and G. R. Fenske, *ASME/STLE International Joint Tribology Conference*, Denver, CO, October 8-10, 2012.
12. Effect of coating thickness on tribological performance of CrN in dry sliding contact, C. Lorenzo-Martin, O. O. Ajayi, S. Torrel, N. G. Demas, A. Erdemir, and R. Wei, *ASME/STLE International Joint Tribology Conference*, Denver, CO, October 8-10, 2012.

VII.E.3. Products

Publications

1. Application of FMEP maps to model the impact of friction technologies on fuel economy, G. Fenske, A. Greco, and D. Dascalescu, presentation at 2014 STLE Tribology Frontiers Conference, October 26-28, 2014.
2. Engine friction reduction technologies, G. Fenske, O. Ajayi, N. Demas, R. Erck, C. Lorenzo-Martin, A. Erdemir, and O. Eryilmaz, U.S. Department of Energy Vehicle Technologies Office Annual Merit Review and Peer Evaluation Meeting, June, 16-20, 2014, Washington D.C.

Tools and Data

Software tools that are provided for use in this project as part of the CRADA with Ricardo, Inc., include: RINGPAK, PISDYN, ENGDYN, and VALDYN.

VII.F. Development of High Power Density Driveline for Vehicle Efficiency Improvement

Oyelayo Ajayi, Cinta Lorenzo-Martin, Aaron Greco and George Fenske

Argonne National Laboratory
9700 South Cass Avenue, Argonne, IL 60439
Phone: (630) 252-9021
E-mail: ajayi@anl.gov

DOE Program Manager: Lee Slezak

Phone: (202) 586-2335
E-mail: lee.slezak@hq.doe.gov

Future Achievements

- Complete contact fatigue evaluation of appropriate lubricant and coating technologies individually and in combination for required increase in fatigue life for HPD driveline systems.
- Integrate materials, lubricant, and surface technologies to produce adequate simultaneous increase in wear, scuffing, and contact fatigue lives to enable at least 25% size reduction in driveline systems.



VII.F.1. Abstract

Objectives

- Enable significant reduction in transportation vehicle weight and consequent fuel savings through size and weight reduction of driveline systems, such as transmission and axles.
- Develop materials, surface finishes, and lubricants to enable development of durable and reliable high-power-density (HPD) driveline systems that are smaller and lighter than current systems.
 - Increase wear, scuffing, and contact fatigue lives for HPD driveline to facilitate up to 25% size reduction in gears and bearings.

Major Accomplishments

- Completed preliminary analysis of the contact kinematics for specific size reduction in a simple planetary gearbox.
- Assessed the effect of new contact kinematics in terms of Hertzian contact stresses, effect of surface velocities of meshing gear teeth on wear, and scuffing and contact fatigue lives.
- Identified potential synergy between thin-film coatings and lubricant additives resulting in low friction and more than twofold improvement in wear life under the boundary lubrication regime.
- Evaluated scuffing performance attributes of lubricant and surface coatings individually and in combination to achieve greater than fivefold increase in scuffing life.
- Developed a new lubricant additive blend that interacts with many commercially available coatings and steel surfaces for substantial reduction in friction and a significant increase in both wear and scuffing lives under severe contact conditions.

VII.F.2. Technical Discussion

Background

DOE Goal

One of the main goals, perhaps the ultimate goal, of the U.S. Department of Energy's Vehicle Technologies Program (DOE-VTP) is the dramatic reduction of the amount of petroleum oil used in transportation vehicles. This would reduce the nation's dependence on foreign oil, thereby enabling greater energy independence and homeland security. In addition, consumption of less oil in vehicles would reduce environment-degrading emissions, such as greenhouse gases and particulates. Such emissions have been associated with climate change and detrimental effects on human health.

Project Goal

The ultimate objective of this project is the development of technologies that will enable original equipment manufacturers (OEMs) and their suppliers to successfully develop smaller, lighter, and more efficient driveline system for transportation vehicles by increasing the power density without sacrificing reliability and durability. Such a system will result in significant vehicle weight reduction and concomitant increase in fuel savings. Furthermore, an HPD driveline may enable the downsizing of the powertrain system, resulting in further fuel savings.

Introduction

Significant fuel savings can be achieved in all classes of transportation vehicle through weight reduction. Numerous analyses have shown that 2-5% reduction in fuel consumption is possible with a 10% reduction in automobile weight. Table VII-15 shows such a calculation for three classes of vehicles based on the New European Drive Cycle (NEDC) for both gasoline- and diesel-fueled internal combustion engines

commercially available gear oil, and a low-viscosity formulation developed at ANL.

Figure VII-36 shows the average scuffing load for many different coatings tested with the three lubricants. Compared to the average scuffing load of about 700 N for the baseline material and lubricant combination, the combined coating and lubricant technologies enabled 2-5 times increase in scuffing life. Such an improvement meets the target of 2X increase in scuffing life for 20% reduction in size.

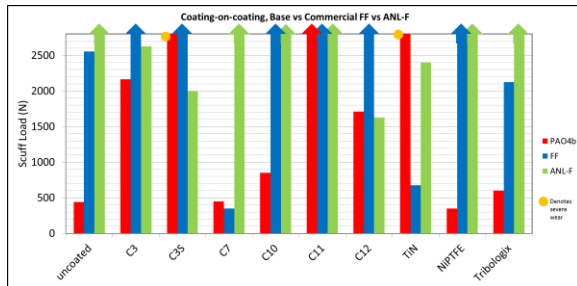
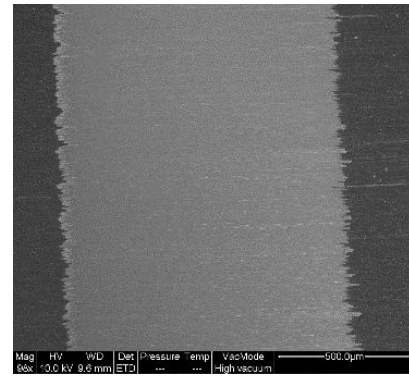
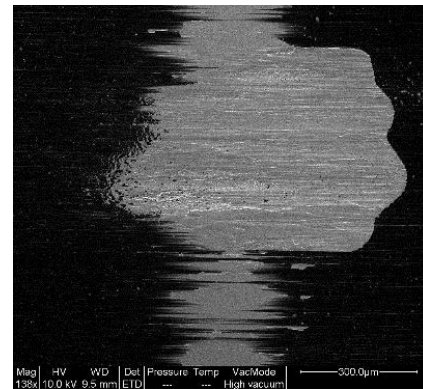


Figure VII-36: Average scuffing load for different coatings in three lubricants

In all contact combinations that involved coated surfaces, scuffing occurred only after the coating had been worn as shown by the scanning electron microscopy (SEM) images in Figure VII-37. Once the coating was removed, scuffing occurred in the steel substrate due to severe plastic deformation. The scuffed steel surfaces showed features that are typical of shear instability, as indicated by the characteristic shear serration in Figure VII-38. The same typical features are characteristic of scuffed uncoated steel surfaces. Based on this observation, one plausible way of further enhancing the scuffing resistance of coated surfaces is by increasing its wear resistance. The wear mechanisms of the coatings during the scuffing test were assessed by different levels of microscopy. In some of the coatings, especially the amorphous ones (diamondlike carbon or carbon-based coatings), wear occurred by a series of micro-spalling processes within the coating, until eventually the substrate was reached. Figure VII-39 shows an SEM micrograph of the wear mechanism at different stages. For this class of coating, increasing its toughness and reduction of the coating residual stress (often tensile) are expected to reduce the wear rate by the micro-spalling process.



(a)



(b)

Figure VII-37: SEM micrographs showing coating wear through prior to scuffing failure in coated surfaces

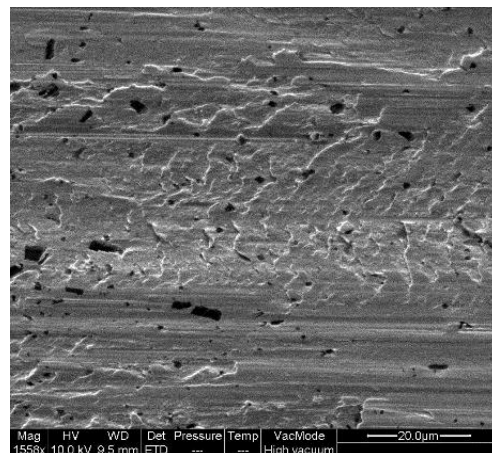


Figure VII-38: SEM micrograph of scuffed substrate surface showing shear instability indicated by serration

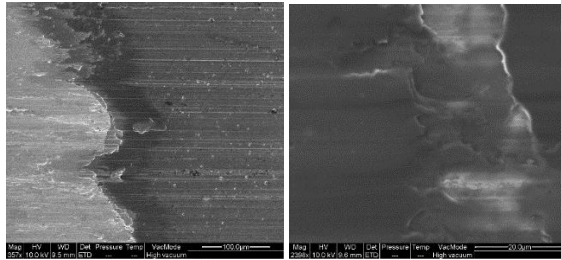


Figure VII-39: SEM micrographs showing micro-spalling wear mechanism of coatings

During this reporting period, efforts were also devoted to the evaluation of possible improvements in contact fatigue life by surface and lubricant technologies. The initial contact fatigue tests were conducted with the test rig (PCS three-ring-and-roller assembly) shown in Figure VII-40. The roller contact kinematics can simulate the meshing gear teeth kinematics, ranging from pure rolling to different levels of slide-to-roll ratios. The load range of the rig, which is up to 1250 N (3 GPa), covers the range of all possible gear contacts. Similarly, the speed and slide-to-roll ratio as well as the temperature range of the test rig are more than adequate to cover typical gear operating conditions. Two of the rings are partially submerged in the oil bath, thereby ensuring adequate lubrication of the roller-ring contact interface during testing.

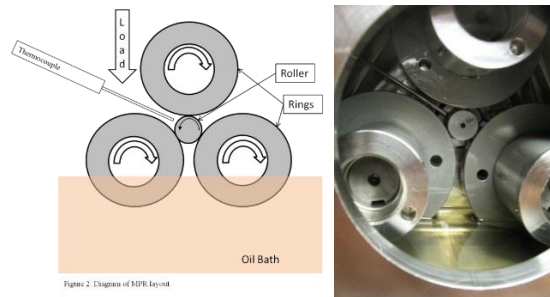


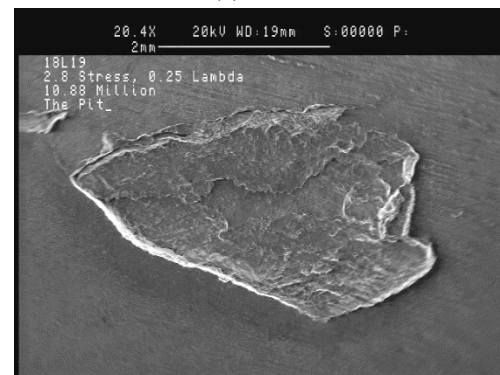
Figure VII-40: Schematic and picture of fatigue test configuration with PCS three-ring-and-roller contact

The initial contact fatigue test was conducted with a baseline gear material consisting of case carburized and hardened AISI 4620 steel. The test lubricant was commercially available, fully formulated gear oil. In order to accelerate the contact fatigue testing, a relatively high contact pressure of 2.84 GPa was applied. The typical design contact pressure for the transmission gear was between 1.0 and 2.0 GPa. The entraining (rolling) velocity was 2.5 m/s, which produces a λ ratio (i.e., the ratio of lubricant fluid film thickness to the composite roughness of the ring and roller contacting surfaces) of 1.7. The temperature was maintained at 80°C, which is typical of the gearbox, and a 30% slide-to-roll ratio (SRR) was also applied to the contact. The test rig has a vibration sensor to indicate the initiation and propagation of contact fatigue damage. After 1.6 million cycles of testing, the vibration sensor signal jumped from 250 to about 1300 in less than 100 sec, which is an indication of a rather sudden failure instead of the normal progressive damage typical of a fatigue mechanism. Examination of the roller surface indicated the occurrence of case crushing, as shown in Figure VII-41a rather than a typical contact fatigue damage illustrated in

Figure VII-41b. When the contact condition was made less severe, more wear and prevention of contact fatigue crack propagation after over 80 million cycles (15 days of testing) were observed. The contact fatigue test protocol is under refinement to provide adequate, but timely assessment of impacts of lubricant and coating technologies on contact fatigue life.



(a)



(b)

Figure VII-41: (a) Optical micrograph of case crushing failure mode under severe contact conditions and (b) SEM micrograph of a typical contact fatigue failure on a gear tooth

Conclusions

In order to reduce the size and weight of the vehicle driveline system by 20-25%, analysis showed that the wear life must be increased 2X, the scuffing life by 2X, and the contact fatigue life by 3X. Unfortunately, because of their complementary nature and mechanisms, it is difficult to simultaneously increase these three tribological performance attributes, which is the main objective of the present project. In previous reporting periods, the project successfully demonstrated 4-5X increase in wear life using a combination of lubricant and coating technologies. In this reporting period, 2-4X improvement in scuffing life was demonstrated, again with combined lubricant and coating technologies. Analysis of the scuffing failure mechanisms in the coated surface showed that removal of the coating by wear is a necessary condition for scuffing to occur. Once the coating is worn through, scuffing occurs by a shear instability mechanism characteristic of the uncoated surface. Consequently, the best approach to further enhance the scuffing life of coated surfaces is through

increase in the coating's wear resistance and adhesion to the substrate. Initial evaluation of the contact fatigue life showed that an attempt to accelerate the failure process resulted in a different failure mode of case crushing, while a less severe contact condition resulted in more wear without contact fatigue. Work is in progress to refine the contact fatigue test protocol to adequately assess the impact of lubricant and coating technologies on contact fatigue life.

VII.F.3. Products

Publications

1. O. O. Ajayi, C. Lorenzo-Martin, and A. Korenyi-Both. "Tribological performance evaluation of complex bonded coatings." Presented at 69th STLE Annual Meeting, May 18–22, 2014, Lake Buena Vista, Florida, USA.
2. O.O. Ajayi, C. Lorenzo-Martin, R. A. Erck, and G. R. Fenske. "Analytical predictive modeling of scuffing initiation in metallic materials in sliding contact." *Wear* 301 (2013), 57–61.
3. C. Lorenzo-Martin, O.O. Ajayi, R. A. Erck, and G. R. Fenske. "Thermal limit of tribochemical surface films from fully formulated lubricants." Presented at the 69th STLE Annual Meeting, May 18–22, 2014, Lake Buena Vista, Florida, USA.
4. C. Lorenzo-Martin, O. O. Ajayi, S. Torrel, and G. R. Fenske. "Friction and wear behavior of thin-film ceramic coatings under lubricated sliding contact." *Thin film Solid* 569 (2014) 70–75.

5. C. Lorenzo-Martin and O. O. Ajayi. "Effect of SiC particle impact texturing on tribological performance of 304L stainless steel." *Applied Surface Science* 315 (2014), 287–291.
6. C. Lorenzo-Martin and O.O. Ajayi. "Surface layer modification of 6061 Al alloy by FSP and second phase hard particles for improved friction and wear performance." *ASME Journal of Tribology* 136 (2014) 044501, pp. 1–5.
7. O. Ajayi, C. Lorenzo-Martin, S. Torrel, A. Erdemir, and R. Wei. "Effect of microstructure and thickness on the friction and wear behavior of CrSiCN coatings." 38th International Conference and Exposition on Advanced Ceramics and Composites (ICACC), Daytona Beach, FL, Jan. 26–31, 2014. (Invited Talk)

Patents

1. O. O. Ajayi, C. Lorenzo-Martin, and G. R. Fenske, "A tribochemical synthesis method for producing low-friction surface film coatings," Pending.

Tools and Data

1. N/A

GRID INTEGRATION

VII.G. PEV Integration with Renewables

Principal Investigator: Tony Markel

National Renewable Energy Laboratory
 1617 Cole Blvd
 Phone: (303) 275-4478
 E-mail: tony.markel@nrel.gov

DOE Program Manager: David Anderson

Phone: (202) 287-5688
 E-mail: david.anderson@ee.doe.gov

VII.G.1. Abstract

Objectives

- EV Grid Integration Strategies
 - Renewables and the Grid
 - Charging and discharging in sync with RE generation or grid ancillary services needs
 - Integration with Buildings and Campuses
 - Maximize use of local renewable generation improving overall system efficiency
 - Minimize peak demand (and resulting costs) with charge management and export power functions.

Major Accomplishments

- Collected and analyzed electric vehicle charging station usage data for 18mo. from the NREL parking garage.
 - The data confirms initial expectations of workplace charging patterns and energy demands (typically 2–4 hours and ~5–8 kWh per vehicle).
- Completed an analysis of typical commercial buildings highlighting an opportunity for 1 million–2.5 million vehicles with modest 6kW interfaces to extract vehicle to building demand charge reduction value.

Future Achievements

- Implement interface tools linking, driver, vehicle, building, and renewables information streams together and enabling intelligent management of vehicle charging.



VII.G.2. Technical Discussion

Background

NREL has conducted research in the PEV grid integration area for ~5 years. This research leverages expertise in multiple technology spaces. The current research addresses three specific challenges:

- Advancing communication between vehicles and load management tools
- Understanding alignment of grid and building loads with vehicles utilization
- Development of low-cost infrastructure options enabling V2G functions.

The impetus for doing this research is to create additional savings and or revenue generation from PEVs that complements their fuel saving value.

Introduction

The integration of renewables in the electricity grid provides the opportunity for significant greenhouse gas emissions reduction. Policies and incentives, in addition to technologic and economical advances are accelerating the growth and adoption of renewable generation.

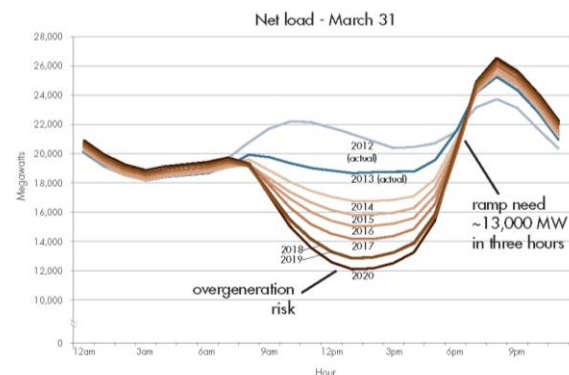


Figure VII-42: Forecasted typical trends in aggregate net load profile in California ISO with high penetration of solar generation (www.caiso.com/Documents/FlexibleResourcesHelpRenewables_FastFacts.pdf)

In California, the Independent System Operator (ISO) forecasts that the growth of renewables, in particular solar will significantly change the long-term load shape trends. Figure VII-42 shows that moving from 2012 with a mid-day peak around 10 a.m., there will then be a mid-day valley around 1pm by 2020. It may be difficult for typical grid generation resources to satisfy the dramatic ramp rate that could materialize.

The NREL South Table Mountain (STM) campus already sees many of the trends expected to become prevalent in California. In addition to low net load mid-day due to solar production, the dynamic nature of solar can result in dramatic peak demand events that are costly for a facility.

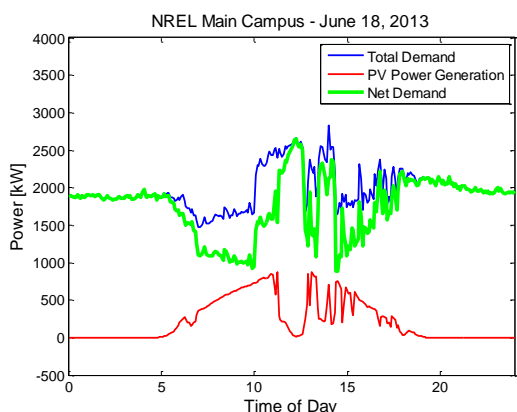


Figure VII-43: Under high-penetration scenarios, solar production dynamics can lead to net demand peak event; data are one representative day on the NREL South Table Mountain Campus

Figure VII-43 provides a one day snapshot of data from the NREL STM campus in which net demand spikes at ~noon due to intermittent cloud cover.

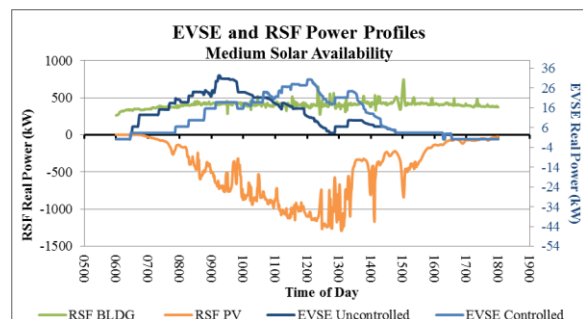


Figure VII-44: Scenarios demonstrating the management of PEV charging in aggregate aligned with solar production

Previous modeling results have shown how electric vehicle charging loads in a commercial facility could be managed to align with local solar production that in the long-run could reduce the depth of the California net load valley shown in Figure VII-42. Figure VII-44 shows actual load data from EV charging stations at NREL (dark blue) and a managed scenario of EV charging (light blue) in which the timing of the charge events have been manually rearranged to align with the solar production on the same building.

Taking these analyses one step further will highlight that with export power capability, vehicles could be used as a resource to reduce local electrical peak demand charges through an intelligent discharge event strategy.

Approach

To address the industry needs, this project has worked to collect data that can be used for scenario analysis along with the development of some early demonstration hardware supporting export power in commercial buildings settings.

The data leverages NREL’s facility data streams including total demand, net demand, solar production, and EVSE demand.

Hardware partners include Ideal Power, Inc for bi-directional EVSEs based on solar inverter technology and Aeroironment and GE for controllable level 2 EVSEs.

Results

Data collected under DOE’s EV Project has confirmed several early assumptions about PEV usage. A majority of PEV recharging could be done at a person’s residence. There are often many hours for this charging to be completed. From Figure VII-45, it is apparent that the charging needs of the uncontrolled vehicles (peaking at ~10 p.m.) do not require the entire evening. Those using time-of-use rates (peaking at ~12:30 a.m.) seem to require even less time. These both suggest much opportunity for shifting load away from typical peak times to early morning hours through charge management strategies.

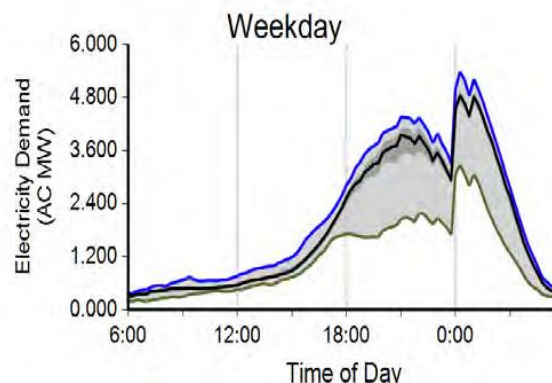


Figure VII-45: Residential charging load profile from EV project through Q2 2013; highlights evening starts and TOU impacts

Likewise, in public charging situations (shown in Figure VII-46), the load shape would ideally have a shift away from 8am and more toward 1pm to align with available renewable generation. It is unknown at this time how much opportunity there is to enact such policies.

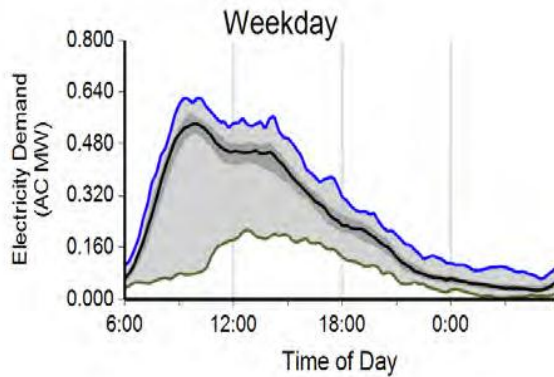


Figure VII-46: Public charging load profile from EV project through Q2 2013; highlights morning and mid-day loads that could be shifted to align with solar production
www.theevproject.com/cms-assets/documents/127233-901153.q2-2013-rpt.pdf

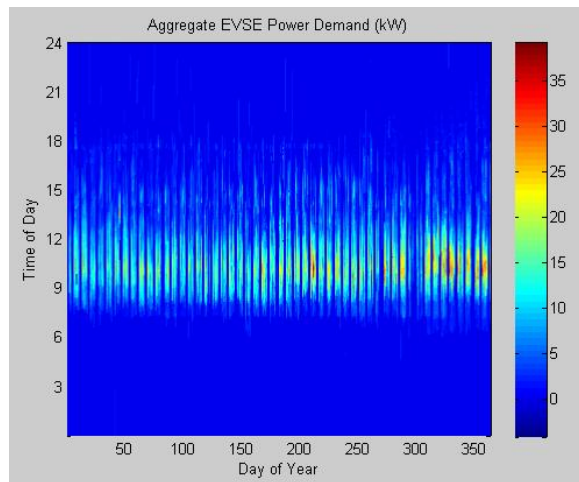


Figure VII-47: One year of aggregate EVSE power demand (kW) for 36 EVSEs installed in the NREL parking garage (03/05/2013-03/04/2014)

In Figure VII-47, one complete year of power demand data for PEV charging on the NREL STM campus is shown by day and hour of the year. The load peak occurs around 10am and is mostly complete by ~1 p.m. Given the normal working hours of 8 a.m.–5 p.m. the current trend offers plenty of opportunity to modify this uncontrolled load shape to be more aligned with solar production trends and campus net load. Research is planned to continue to develop the information tools needed to ensure necessary charging is completed and the facility achieves the most from flexible load integration.

In Figure VII-43, it was highlighted that with high local PV penetration, peak demand events may occur in cases where intelligent load control is not implemented in concert with renewable generation growth. Peak demand charges vary from utility to utility across the country. Costs have been found to range from as low as \$4/kW to \$28/kW with a typical charge in the \$10/kW range. At \$17/kW on the NREL campus, each 6 kW vehicle could be worth as much as \$100/mo. in savings to the facility if capable of short discharge events.

Using the attributes of commercial building stock, vehicle-to-building (V2B) load balancing scenarios were analyzed to determine the number of vehicles required to significantly reduce related national commercial electricity expenditures (~\$132 billion each year). Approximately 30%–40% of these expenditures result from local peak demand charges. The analysis revealed that application of V2B technologies to 20% of commercial buildings could require as many as 1 million–2.5 million vehicles, each capable of delivering 6 kW (Figure VII-48). Break-even projections for the technology required to implement these systems and diminish monthly loads by 5% demonstrated the greatest potential with installation of low-cost elements in small commercial buildings of 25,000 square feet or less. Conclusions suggest that even with low power (6–10 kW) systems, value creation is possible.

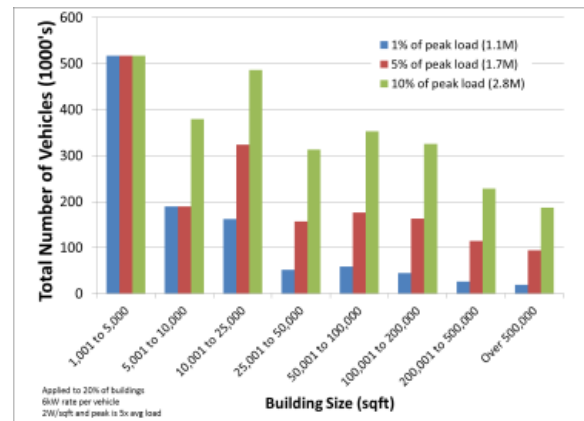


Figure VII-48: Commercial building attributes analysis suggests market opportunity for 1 million–2.5 million vehicles with 6 kW bi-directional power interface to generate peak demand reduction value



Figure VII-49: Implementation of 20 kW bi-directional vehicle power management system for building and renewables integration

Finally, to begin to consider how the V2B systems would be made to function, a technology demonstration platform was developed. This hardware built upon previous V2G work supporting the DOD efforts to integrate vehicles with microgrid operations. The testing platform is depicted in Figure VII-49. The battery pack of the Ford Transit Connect Electric (TCE) is charged and discharged using the Ideal Power Converters (IPC) inverter. The interface is managed and monitored through an SCADA-controlled electrical distribution

bus installed in NREL's Vehicle Testing and Integration Facility (VTIF). Future efforts will highlight the automatic charge and discharge functions of this system coordinated with the VTIF net demand.

Conclusions

The future electricity grid is expected to have a much higher level of renewable generation in the overall energy mix. Having flexible loads and resources, like PEVs, distributed throughout the grid suggests opportunities for creating a well-balanced and active system that provides value for all involved.

The work conducted in FY2014 focused on collecting and analyzing data streams and system attributes that would highlight opportunistic pathways forward. At this point, it seems viable to link charge management to local and potentially system-wide solar generation to shift load shapes and relieve grid operations stress. Furthermore, the integration of charge demand profile information and vehicle storage capabilities at the local building level offer financial opportunities if infrastructure and implementation costs can be minimized. Further research is needed to quantify the potential impacts on vehicle components including batteries, EVSEs, and charging power electronics of these alternative operating strategies.

VII.G.3. Products

Publications

1. Markel, T. "PEV Integration with Renewables." Presented at the DOE Annual Merit Review June, 2014, energy.gov/sites/prod/files/2014/07/f17/vss114_markel_2014_o.pdf.
2. Markel, T. "PEV Integration with Renewables: Vehicles, Buildings, and Renewables Working Together." Presented at EPRI EV Infrastructure Working Council Meeting June 2014, www.nrel.gov/docs/fy14osti/62244.pdf.

Patents

1. N/A

Tools and Data

1. 18 months of 1-minute resolution data on power demand from 36 EVSEs in the NREL parking garage

VII.H. PEV Smart Grid Requirements Study

Principal Investigator: Tony Markel

National Renewable Energy Laboratory
1617 Cole Blvd
Phone: (303) 275-4478
E-mail: tony.markel@nrel.gov

DOE Program Manager: David Anderson

Phone: (202) 287-5688
E-mail: david.anderson@ee.doe.gov

VII.H.1. Abstract

Objectives

- Leverage the expertise of multiple national laboratories to evolve the implementation scenarios and requirements for PEV integration with smart grid systems.
- Produce a guidance document for DOE that details PEV grid integration system implementation methods and remaining research gaps.

Major Accomplishments

- Project kick-off held between NREL, ANL, INL, ORNL, PNL, LBNL sharing areas of expertise, interests, and draft report content recommendations.
- Delivered interim report structure with individual laboratory roles and responsibilities detailed.

Future Achievements

- Final smart grid integration requirements study report to be delivered that highlights challenges, opportunities, and remaining research needs.



VII.H.2. Technical Discussion

Background

Multiple national laboratories support the DOE Vehicle Technologies program. Each of these laboratories provides unique and complimentary knowledge on PEV integration with the grid.

This project was created to bring together the experts from each laboratory to provide insights toward next steps in the DOE program on vehicle to grid integration.

As an outcome, the team will establish a PEV smart grid requirements document that provides a discussion of the current knowledge and gaps to enable vehicle to grid power

flow and communications. The project outcome will be used to focus the future research efforts at NREL's Energy Systems Integration Facility (ESIF) and those related facilities at the other national labs.

Introduction

For a vehicle to be considered smart grid-enabled, it is expected that there will be a limited number of functional and interface requirements. The objective of this project is to pull from individual laboratory knowledge and industry experience to define structure for what a vehicle could do and what it will need to be capable of to participate in the future smart grid such that it has access to the associated value streams.

DOE composed a team of engineers from each of 6 national laboratories to contribute to this project. The group is expected to produce a guidance document for DOE to use in defining future research efforts to be conducted at ESIF and other DOE laboratory facilities that would address these gaps.

The gaps are likely to include both technical and policy aspects. Although smart grid features are not yet a necessity, the work is intended to lay the foundation such that vehicles will be ready to take advantage of grid integration opportunities as they arrive.

Approach

A working group of national lab technical experts was convened by DOE. NREL has the project leadership role and is guiding the collaborative content development of the final product to support the PEV Smart Grid Requirements Study.

The project has been planned to include an Interim Report deliverable that frames the expected final report content. A Final Report deliverable is planned for December, 2014.

The output from this project will 1) highlight the laboratory resources and expertise that DOE has available to them for continuing research in this area, 2) provide a status update on industry collaboration toward PEV smart grid integration, and 3) offer guidance on priority issues and gaps that need further research to support long-term PEV smart grid integration.

Results

The PEV Smart Grid Requirements Study is a collaborative project among the national lab participants and was initiated in March 2014 (Figure VII-50). It was funded mid-year FY2014. The team meets regularly to discuss progress toward the deliverable report.



Figure VII-50: Multi-lab collaboration meeting to design the PEV smart grid requirements study (photo credit: Ted Bohn)

The expertise of the individual labs is being leveraged in several areas as detailed in Table VII-16.

Table VII-16: EV Smart Grid Lab Roles and Responsibilities

| Lab | Core Contributions |
|------|--|
| NREL | Overall project coordination, reports on existing V2G systems, high penetration renewables scenario framing |
| ANL | Vehicle to grid communications and controls standards evolution |
| INL | EV Project data analysis and real-time systems simulation |
| ORNL | Grid integration of wireless power transfer to vehicles |
| PNL | Grid operations functions for vehicles and associated value potential, leveraging Voltron and Gridlab-D tools |
| LBNL | Reporting on system level demonstrations and simulations leading to grid function values; leverages V2G-Sim tool development |

The following are some of the key questions the multi-lab team is working to answer:

- What are the future grid services that are relevant to electric vehicles?
- What are the potential costs and benefits of candidate grid and EV services?
- What are the metrics and key performance parameters relevant to quantifying the cost and benefits of candidate EV grid services and technology solutions?
- What are the grid-centric and EV-centric opportunities and perspectives?
- How might achieving these future integrated systems influence the petroleum consumption and energy benefits of the overall system?
- What steps would stand in the way of growing PEV adoption and what actions can be taken to enable the growth of grid-integrated features?

As the project team continues to work together, early conversations and conclusions are suggesting that the following are core scenarios for EV smart grid integration that should be enabled through requirements definition:

- Vehicle to home for local solar and emergency backup
- Vehicle to building for peak demand reduction
- Vehicle to grid participation in aggregation and ancillary service markets.

Conclusions

The PEV Smart Grid Requirements Study project is a collaboration among 6 national labs to provide the DOE Vehicle Technologies program with technology status and guidance on future research to enable vehicles to participate in smart grid functions. The goal is to highlight remaining research challenges and gaps that both the NREL ESIF and other national laboratory facilities could be and should be used to address. The project is expected to provide a final report in December 2014 and further project development guidance into the FY 2016 planning cycle.

VII.H.3. Products

Publications

1. N/A

Patents

1. N/A

Tools and Data

1. N/A

VII.I. VT INTEGRATE

Principal Investigator: Tony Markel

National Renewable Energy Laboratory
1617 Cole Blvd
Phone: (303) 275-4478
E-mail: tony.markel@nrel.gov

DOE Program Manager: David Anderson

Phone: (202) 287-5688
E-mail: david.anderson@ee.doe.gov

VII.I.1. Abstract

Objectives

- Develop INTEGRATE - Integrated Network Testbed for Energy Grid Research and Technology Experimentation.
- Enable EERE technologies to increase the hosting capacity of the grid by providing grid services in a holistic manner using an open source, interoperable platform
- Characterize the grid services and grid challenges. associated with energy efficiency (EE) and renewable energy (RE) technologies when integrated into the grid at scale.
- Utilize an open-sourced, interoperable platform that enables communication and control of EE and RE technologies both individually and holistically.
- Develop and demonstrate high-value grid services that EE and RE technologies can provide holistically at a variety of scales.

Major Accomplishments

- Implemented coordination between technology experts representing 5 program areas at NREL including, vehicles, buildings, solar, wind, and hydrogen.
- Created a vehicle specify execution strategy focused on four grid integration aspects:
 - Managed Charging
 - Local Power Quality Enhancement
 - Export Power to Independent Loads
 - Bi-direction powerflow with building and grid interactivity.
- To support characterization efforts, the following grid interactive vehicle systems have been installed:
 - Dual-headed GE Wattstation providing remote charge management functions
 - Mini-E EV with Milbank EVSE providing full bi-direction V2G functions
 - Transit Connect EV with an Ideal Power Converters off-board inverter for bi-directional power management.

Future Achievements

- Development and implementation of device characterization test plans for the breadth of grid functions
- Details of current and future open architecture communications and controls approaches related to vehicles
- Research of potential system level value streams from more functional PEVs and the life impacts on batteries and components of several usage scenarios



VII.I.2. Technical Discussion

Background

Integration of renewables into the electricity grid have the potential to dramatically change future greenhouse gas emissions trends. The flexibility of both generation resources and demands will play a role in determining the cost of electricity in a high renewables penetration scenario. It is envisioned that significant value exists for devices and systems at multiple levels to participate in systems management and coordination.

Plug-in electric vehicles (PEVs) are devices at the end of the electrical grid that may have opportunity to provide system level value if unique functions and capabilities are enabled. There is also a need to understand how PEV functions can be coordinated with the characteristics of other EERE technologies to provide holistic system scenarios.

Introduction

To support the objectives of the INTEGRATE initiative, the Vehicle Technologies office has funded NREL to focus on research that addresses three vehicle-related issues to supporting long-term integration with grid and building operations:

- Open architecture communication and control implementation needs
- Assessment of potential life impacts of auxiliary battery applications
- Holistic system value creation.

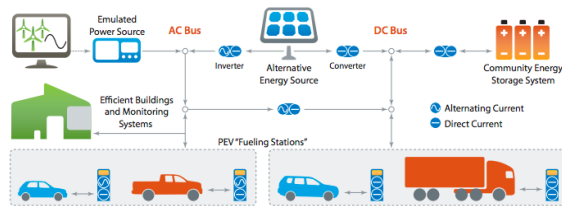


Figure VII-51: Systems diagram depicting the interaction of PEV loads with buildings and renewables

Figure VII-51 provides a depiction of the physical connections between vehicles, buildings, and renewables. Under this project connections such as these will be formed with physical infrastructure to support the characterization of individual devices, the development of open architecture communications layers, and the understanding of system level value that may be accessible.

Approach

The INTEGRATE efforts are a collaborative effort among multiple DOE program areas that include, vehicle technologies, hydrogen and fuel cells, efficient buildings, wind power, and solar power. Teams at NREL representing each of these program areas coordinate efforts and collaborate to achieve the project objective of developing responsive systems that aid in the cost effective integration of high penetration renewable generation. Figure VII-52 suggests a scenario of multiple DOE technologies interacting for a common objective.

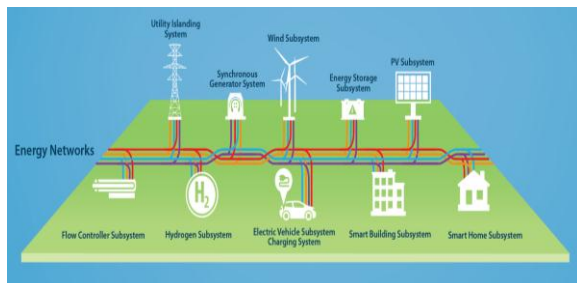


Figure VII-52: INTEGRATE networking strategy to address grid needs using systems and devices from multiple levels and technologies

To achieve the project goals, three focus areas have been developed. These include:

- Device and system characterization
- Communications and controls architectures
- Holistic system value and demonstration.

By characterizing devices, in this case, plug-in electric vehicles, and the connecting power interface hardware, data on operational ranges and performance can be developed and used for larger scale system impacts modeling.

The communications layer efforts are important for collaboration across the program areas so that all have equal opportunity to participate at the system level and potentially even coordinate among themselves to achieve an optimal system value.

Finally, the value determination of the operating system will suggest the likelihood of success of these technologies in the long-term. Integration of multiple devices to achieve an overall grid benefit is not a simple task and requires some level of early implementation thought and testing to evolve to a functional cost effective future design.

Results

The INTEGRATE efforts in support of the Vehicle Technologies program are still in the early stages of planning and execution as the project scope was finalized mid-year FY2014.

Technology surveys and research of current status has uncovered that the breadth of available vehicle technologies and systems for characterization with respect to grid functions is limited and will take sufficient time to collect for testing purposes.

Thus far, a Mini-E electric vehicle with a unique charging station has been acquired to be the first and primary unit for vehicle-to-grid bi-directional power flow testing and communications integration. This vehicle has ~35kWh of stored energy and provides ~19kW of power flow on command either to charge or discharge the vehicle battery. Interfacing with the vehicle is accomplished through an API to the owners control server.

Other devices that are expected include:

- Aerovironment frequency responsive EVSE
- GE managed charging station
- Smith EV with bi-direction power transfer
- Wireless power transfer charging infrastructure
- Vehicles with export power to a load (non-grid tied)
- Bi-directional fast charger.

For the development of communications and controls architectures, several options exist and will be explored including:

- Volttron (a PNNL developed operating system)
- Smart Energy Protocol (SEP) 2.0
- OpenADR.

A system hardware testing environment called iLab is being developed as part of INTEGRATE that will allow evaluation of the performance of the various communications and control options.

Finally, with regard to system-level values for device-level units, analysis is being done leveraging the grid modeling expertise of those at NREL. The analysis will highlight the changes and cost associated with operating a high renewables grid. An attempt will be made to demonstrate how the individual devices can collaborate to create system level value that is shared among the participants.

Conclusions

The INTEGRATE initiative has invigorated research teams across the national labs to begin tinkering about how their specific technologies and systems function in the context of the future grid. It has become clear that there are many gaps and unknowns that will need to be resolved for the research to be fruitful. The coordination between program areas both at DOE and at NREL are expected to accelerate the pathways to success.

The Vehicle Technologies program efforts supporting INTEGRATE contribute to developing device-level operational data for characterizing and future modeling, they are supporting the development of open architecture communications and control systems evolution, and will highlight near-term and long-term opportunities to create grid value that can accelerate advanced vehicle adoption.

VII.I.3. Products

Publications

1. N/A

Patents

1. N/A

Tools and Data

1. N/A

THERMAL CONTROL

VII.J. Thermal Control of Power Electronics of Electric Vehicles with Small Channel Coolant Boiling

Principal Investigator: Dileep Singh

Argonne National Laboratory
9700 S. Cass Ave.
Argonne, IL 60439
Phone: (630) 252-5009
E-mail: dsingh@anl.gov

DOE Program Manager: Lee Slezak

Phone: (202) 586-2335
E-mail: Lee.Slezak@ee.doe.gov

- Conduct experimental tests of coolant boiling heat transfer.
- Develop predictive boiling heat transfer correlations based on the experimental data.
- Refine simulation models and results of coolant boiling in cooling of vehicle power electronics.



VII.J.2. Technical Discussion

Background

The current cooling technology for the power electronics in commercial hybrid electric vehicles (HEVs) uses a liquid-cooled heat sink with fins. This technology requires a separate low-temperature radiator and pumping system, in addition to the main engine radiator and pumping system, to provide a low coolant inlet temperature. This second radiator and pumping system increases the weight and the cost of the vehicle and decreases the efficiency. This project is aimed at using subcooled or low-vapor-quality saturation flow boiling for cooling of vehicle power electronics. It is expected that this cooling technology will enhance cooling of vehicle power electronics, control junction temperatures of vehicle power electronics, and eliminate the second cooling system currently used in hybrid electric vehicles.

Introduction

Various technologies have been proposed to enhance the cooling of the power electronics in HEVs and, therefore, reduce the system weight and volume of the power electronics and increase the efficiency and the lifetime of vehicles. These cooling technologies include single- or two-phase jet impingement, two-phase spray, immersion pool boiling, and two-phase saturation boiling. However, all of these previously studied technologies require installation of significant additional hardware to cool the power electronics.

In the new system under investigation, with subcooled flow boiling in the cooling channels of power electronics in HEVs, no major additional components are required. The low-temperature radiator and pumping system can be eliminated and single existing main engine radiator and pumping system would be used. Nucleated boiling would occur only in the cooling channels of power electronics and nowhere else in the HEV cooling system. The uniqueness of this technology lies in the use of subcooled flow boiling in addition to liquid convection under controlled conditions in current power

VII.J.1. Abstract

Objectives

- Explore possibilities of using coolant boiling in cooling of power electronics in hybrid electric vehicles (HEVs).
- Eliminate the HEV low-temperature cooling system and simplify the cooling system configuration.
- Increase the heat removal capacity and enhance cooling of HEV power electronics.
- Control the junction temperature of HEV power electronics and improve the efficiency and lifetime of electronic components.
- Cool high-power-density electronics such as wideband-gap semiconductor-based power modules.

Major Accomplishments

- Developed thermal analysis models of coolant boiling in cooling of vehicle power electronics.
- Developed numerical simulation models of coolant boiling in cooling of vehicle power electronics using the commercial COMSOL Multiphysics software.
- Conducted numerical simulations investigating the effects of various parameters on the boiling cooling system:
 - Thermal conductivity of thermal interface materials
 - Coolant flow velocity
 - Fluid inlet temperature
 - Heat flux of vehicle power electronics.

Future Achievements

- Design and fabricate an experimental test system for investigating coolant boiling in cooling of vehicle power electronics.

electronic cooling channels to improve the cooling capacity without exit vapor from the channels or major additional components in HEVs. These desirable conditions are in contrast to other cooling technologies.

Approach

As illustrated in Figure VII-53, the subcooled flow boiling system proposed in the present study can be integrated into the main engine cooling system without major additional hardware installation. The conventional engine coolant, a 50/50 ethylene glycol/water (EG/W) mixture, is used for cooling of vehicle power electronics. The coolant flowing out from the radiator is pumped by the main engine coolant pump and divided into two flow paths. One follows the normal engine cooling route, and the other goes into the cooling channels of the power electronics. The coolant in the cooling channels absorbs heat from the power electronics through subcooled flow boiling. Then, the two coolant flows combine in the flow mixer to form a uniform-temperature fluid. The coolant then enters the radiator to reject the absorbed heat to air. The flow divider and mixer components are considered to be minor additions to an HEV, as they may be little more than types of piping tees.

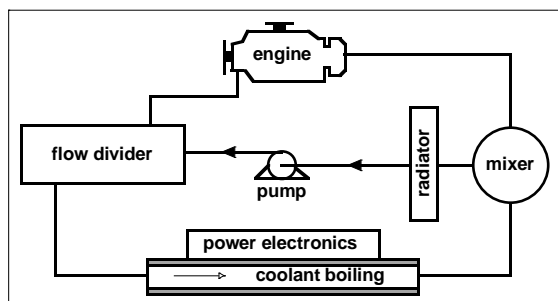


Figure VII-53: Concept of subcooled flow boiling system

Results

The subcooled flow boiling technology for vehicle power electronics cooling was studied in this project through numerical simulations conducted using the commercial COMSOL Multiphysics software. The effects on coolant subcooled flow boiling of various parameters, including the thermal conductivity of thermal interface materials (TIMs), the coolant flow velocity, the fluid inlet temperature, and the heat flux of vehicle power electronics, were studied. Furthermore, the subcooled flow boiling system was compared to the current single-phase liquid-cooled technology. Results presented show that coolant subcooled flow boiling in the cooling channels can enhance the cooling for vehicle power electronics and remove the need for a low-temperature radiator and pumping system to simplify the cooling system in HEVs.

Simulation Models and Key Considerations

The vehicle power electronic package studied in the simulations is shown in Figure VII-54. There are two semiconductors on the top, an insulated gate bipolar transistor

(IGBT), and a diode. The cooling channels on the bottom are divided by costly fins. A typical power electronics package in a HEV has about a dozen of these semiconductor pairs. This power electronics module was chosen for the simulations of this study because it is used in commercial HEVs.

Furthermore, this package allows cooling on both sides of the semiconductors. Figure VII-55 shows a side view of the configuration of Figure VII-54, identifying each layer of the power electronics and cooling channels. Table VII-17 gives the materials and dimensions of each layer. The fin structure of the cooling channels for the vehicle power electronic package of Figure VII-54 is enlarged in Figure VII-56. There are 20 channels under each pair of semiconductors.

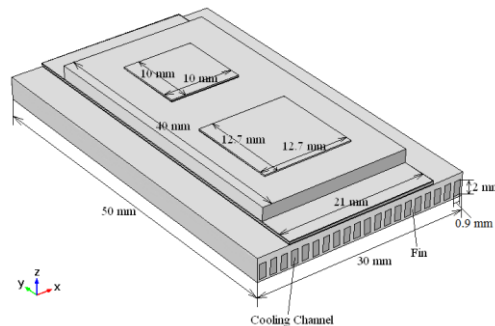


Figure VII-54: Vehicle power electronics package

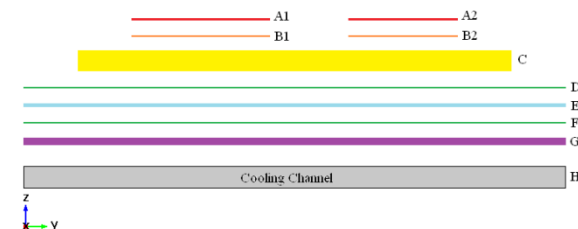


Figure VII-55: Side view of vehicle power electronics package

Table VII-17: Materials and Dimensions of Each Layer

| Index | Material | X (mm) | Y (mm) | Z (mm) |
|-------|---------------------|-----------|-----------|-----------|
| A1 | IGBT: Si | 12.7 | 12.7 | 0.145 |
| A2 | Diode: Si | 10.0 | 10.0 | 0.145 |
| B1 | Solder | 12.7 | 12.7 | 0.076 |
| B2 | Solder | 10.0 | 10.0 | 0.076 |
| C | Heat spreader: Cu | 21.0 | 40.0 | 1.85 |
| D | TIM: Thermal grease | 21.0 | 50.0 | 0.1 |
| E | Substrate: SiN | 21.0 | 50.0 | 0.3 |
| F | TIM: Thermal grease | 21.0 | 50.0 | 0.1 |
| G | Heat sink: Al | 30.0 | 50.0 | 0.6 |
| H | Cooling channel | 30.0 | 50.0 | 2.0 |

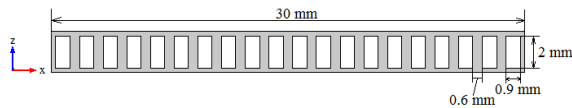


Figure VII-56: Fin structure

The mesh structure in the numerical model of the configuration of Figure VII-54 is displayed in Figure VII-57. The simulation model consists of 2,007,316 domain elements, 443,403 boundary elements, and 15,374 edge elements. Based on a mesh independence study, these mesh elements are sufficient for the 3-D numerical simulations.

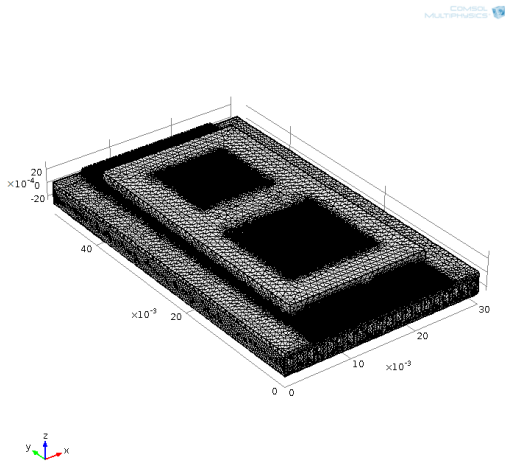


Figure VII-57: Mesh structure (all units in meters)

For the simulation boundary condition of the subcooled flow boiling heat transfer coefficients in the cooling channels, the widely used Shah correlation in the engineering literature was chosen. While the Shah correlation was not developed for subcooled flow boiling of a 50/50 EG/W mixture, the differences between the experimental data from our current project of 50/50 EG/W subcooled flow boiling for engine cooling and the simulation results based on the Shah correlation are within 10% at various coolant flow velocities. This agreement validates the applicability of the Shah correlation for the simulations.

Other key considerations include the following: (a) because the subcooled flow boiling system is integrated into the main engine cooling system, the conventional engine coolant, a 50/50 EG/W mixture, is used for cooling of power electronics; (b) the pressure in the cooling channels for power electronics in HEVs is 2 atm, and the saturation point of a 50/50 EG/W mixture is 129°C; (c) to eliminate the low-temperature radiator and the associated pumping system, the coolant inlet temperature is 105°C; (d) the coolant flow velocity is 0.16 m/s to keep the coolant outlet temperature below the saturation point and to generate desired subcooled flow boiling; (e) the coolant outlet temperature is below the saturation point with no net vapor in the rest of the system (outside the power electronics cooling channels); and (f) to achieve desired subcooled flow boiling, the cooling channel wall temperature is 10°C–30°C above the saturation point, i.e., a wall superheat of 10°C–30°C.

TIM Thermal Conductivity Effects

Figure VII-58 shows the junction temperature (the IGBT surface temperature) versus the TIM thermal conductivity for a double-sided cooling system with or without fins for a 100-W/cm² heat flux on the IGBT and diode surfaces, the current commercial heat flux level. The coolant inlet temperature is 105°C. Various TIM thermal conductivities of 1.5 W/m·K, 7.5 W/m·K, and 15 W/m·K were considered. Figure VII-58 shows that use of subcooled flow boiling in the cooling channels reduces the junction temperature compared to single-phase convective heat transfer. Single-phase cooling at this 105°C coolant inlet temperature cannot keep the junction temperature below 175°C at any TIM thermal conductivity. With a 7.5-W/m·K TIM thermal conductivity, the junction temperature is reduced to 175°C without fins in the cooling channel and to 137°C with fins by using subcooled flow boiling as shown in Figure VII-58 and Figure VII-59. At a TIM thermal conductivity of 1.5 W/m·K, the junction temperature is still maintained far below the 175°C limit using the subcooled flow boiling system with fins. TIM thermal conductivities higher than 7.5 W/m·K do not significantly reduce the junction temperature of the power electronics, as displayed in Figure VII-58. This finding indicates little benefit to TIM thermal conductivities above 7.5 W/m·K. By using a TIM thermal conductivity of 7.5 W/m·K, fins can be eliminated in the double-sided subcooled flow boiling system while maintaining a 175°C junction temperature. This feature reduces the capital cost and pumping power. Using subcooled flow boiling with fins, the junction temperature can be reduced below 155°C for all TIM thermal conductivities studied, as displayed in Figure VII-58.

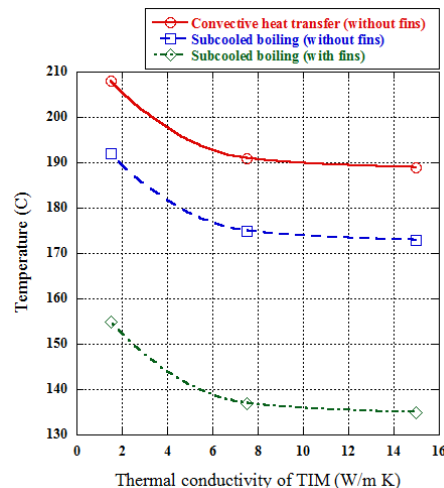


Figure VII-58: TIM Thermal Conductivity Effects

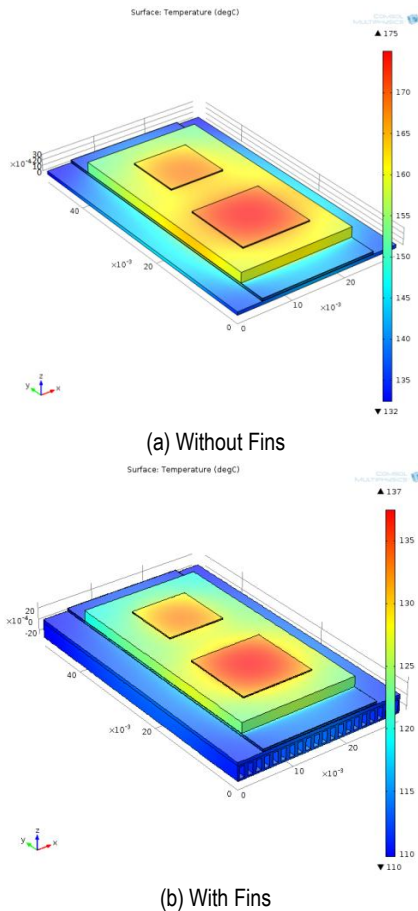


Figure VII-59: Junction Temperatures

Coolant Flow Velocity Effects

Figure VII-60 is a plot of the junction temperature versus the coolant flow velocity for a double-sided cooling system with a 7.5-W/m·K TIM thermal conductivity and a 100-W/cm² heat flux on the IGBT and diode surfaces. The coolant flow inlet temperature is 105°C. It is seen that the finned channels combined with subcooled flow boiling can reduce the junction temperature below 140°C for all coolant velocities. Without fins, the junction temperature can be controlled below 175°C when the coolant flow velocity is 0.16 m/s or higher. Figure VII-60 shows that the coolant flow velocity does not have a significant effect on the junction temperature for the subcooled flow boiling system.

Efficient cooling using subcooled flow boiling occurs at low coolant flow velocities. This condition reduces pressure drops and pumping power requirements. If fins are used in the cooling channels, the coolant flow velocity range for subcooled flow boiling is 0.06 m/s to 0.4 m/s, as shown in Figure VII-60. When the velocity is lower than the lower limit of this range, the coolant outlet temperature would be likely above the saturation point. When the velocity is higher than the higher limit of this range, the cooling channel wall temperature cannot reach 10°C above the saturation point, and therefore, subcooled flow boiling is unlikely to occur. The drop in subcooled flow boiling pressure along the cooling channel predicted based on correlations in the engineering literature is

quite small (approximately 1443 Pa), which would result in low pumping power requirements.

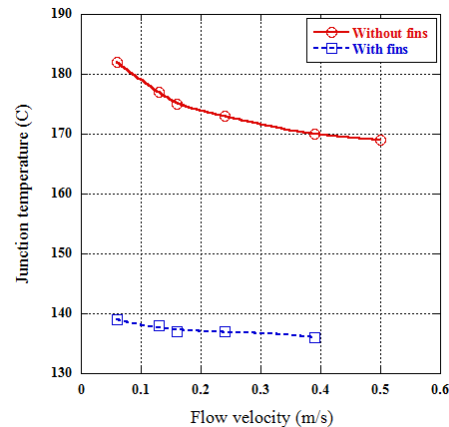


Figure VII-60: Coolant Flow Velocity Effects

Fluid Inlet Temperature Effects

A double-sided cooling system with a 7.5-W/m·K TIM thermal conductivity for a 100-W/cm² heat flux on the IGBT and diode surfaces was considered in the next simulations. Based on the results shown in Figure VII-61, the junction temperature can be controlled below 175°C without fins in the cooling channel and below 150°C with fins when subcooled flow boiling is used. Without fins, the subcooled flow boiling dominates the cooling process. High coolant inlet temperatures cause strong subcooled flow boiling due to the high heat transfer coefficients for subcooled flow boiling caused by low liquid subcooling levels. Therefore, a higher coolant temperature results in a lower junction temperature. With fins in the cooling channels, convective heat transfer is also important. Consequently, a higher coolant temperature results in a higher junction temperature. To maintain subcooled flow boiling in the cooling channels, the fluid inlet temperature cannot be below 100°C with fins, while the fluid inlet temperature cannot be below 90°C without fins, because lower fluid inlet temperatures cause the channel wall temperature to be below the subcooled flow boiling range. Furthermore, according to the simulation results displayed in Figure VII-61, the coolant inlet temperature does not have significant effects on the junction temperature, especially for the non-finned cooling channel.

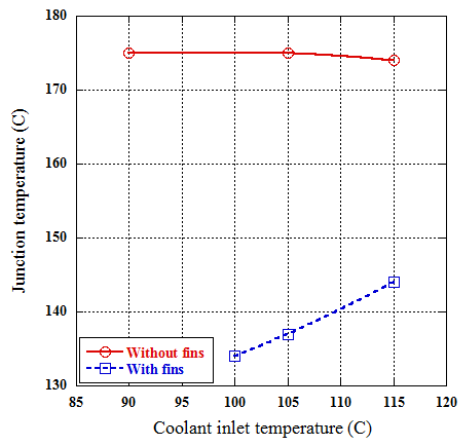


Figure VII-61: Fluid Inlet Temperature Effects

Heat Flux Effects

Figure VII-62 shows the semiconductor junction temperature versus the heat flux from the numerical simulations. The simulations were performed for a single-sided finned cooling system with a coolant inlet temperature of 105°C and a coolant flow velocity of 0.16 m/s. The 7.5-W/m•K TIM thermal conductivity was applied. When the heat flux on the IGBT and diode surfaces is small, less than 30 W/cm², a single-phase flow occurs, as indicated by the steep slope of the curve in Figure VII-62. Here, little to no subcooled flow boiling occurs. As the heat flux increases, subcooled flow boiling becomes stronger in the cooling channels, and the slope of the curve is reduced in Figure VII-62. The junction temperature increases more gradually with subcooled flow boiling because of the increased heat transfer rates compared to those of a single-phase flow. By means of subcooled flow boiling, the junction temperature can be controlled below 175°C with a heat flux on the IGBT and diode surfaces up to 125 W/cm², as shown in Figure VII-62. For a double-sided cooling system, the heat flux value would be doubled to 250 W/cm². This heat flux is a 25% increase over conventional single-phase cooling of HEV power electronics, and it is accomplished without a low-temperature radiator cooling system.

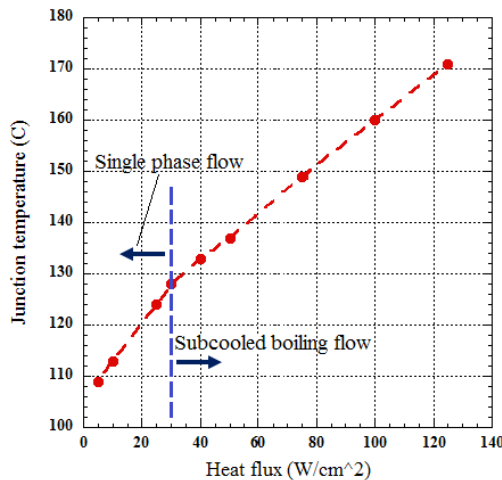
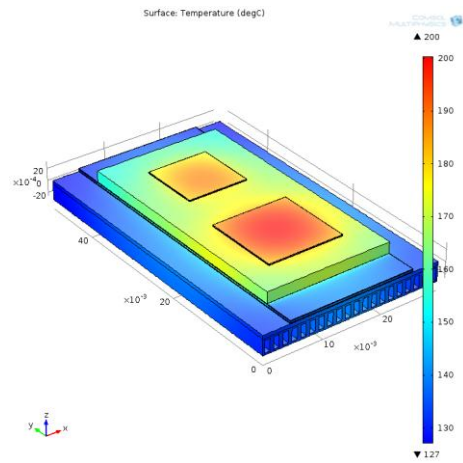
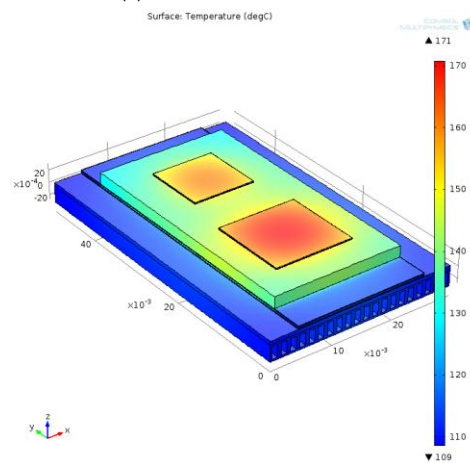


Figure VII-62: Heat Flux Effects

Figure VII-63 shows the temperature profiles through the power electronics for the high heat flux (250 W/cm²) application (such as wideband-gap semiconductors) when subcooled flow boiling and convective single-phase cooling are used. The junction temperature can be maintained below 175°C by using subcooled flow boiling combined with fins in a double-sided cooling system with a 7.5-W/m•K TIM thermal conductivity, as shown in Figure VII-63(b). Without subcooled flow boiling, the junction temperature would be 200°C, as shown in Figure VII-63(a).



(a) Convective Heat Transfer



(b) Subcooled Flow Boiling

Figure VII-63: Junction temperatures for high heat flux applications

Comparison of Convection and Subcooled Boiling

Table VII-18 presents a comparison between single-phase convection and subcooled flow boiling for cooling power electronics in HEVs, where SS and DS indicate single- and double-sided, respectively. The TIM thermal conductivity is 7.5 W/m•K in the simulations. Without fins (as indicated in Column 2, Table VII-18), double-sided subcooled flow boiling can control the junction temperature below 175 °C. With fins, subcooled flow boiling can increase the cooling rate by 25% (Column 3, Table VII-18) compared to convection cooling or reduce the junction temperature (Column 4, Table VII-18). By using subcooled flow boiling combined with fins, the double-sided subcooled flow boiling system can cool wideband-gap semiconductors with a heat flux up to 250 W/cm² (Column 5, Table VII-18). It should be pointed out that all these results apply for a coolant inlet temperature of 105°C without the second low-temperature radiator and the associated pumping system.

Table VII-18: Comparison of Convection and Subcooled Boiling

| | Subcooled flow boiling | | | | Convection | |
|--|------------------------|------|------|------|------------|------|
| | | | | | | |
| Coolant inlet temperature (°C) | 105 | 105 | 105 | 105 | 70 | 70 |
| Total heat flux on IGBT and diode surfaces (W/cm²) | 100 | 125 | 100 | 250 | 127 | 100 |
| Coolant flow velocity (m/s) | 0.16 | 0.16 | 0.16 | 0.16 | 0.24 | 0.24 |
| Fins in the channel | No | Yes | Yes | Yes | Yes | Yes |
| Cooling system | DS | SS | SS | DS | DS | SS |
| Junction temperature (°C) | 175 | 175 | 160 | 175 | 150 | 175 |

Conclusions

Use of subcooled flow boiling in the cooling channels to reduce the junction temperature of power electronics in HEVs is a novel cooling technology. Using subcooled flow boiling in the cooling channels can enhance the cooling capacity for vehicle power electronics while the coolant outlet temperature is still below the saturation point. Thus, there is no vapor in the rest of the cooling system. Based on the current numerical simulations, the subcooled flow boiling technology can (a) eliminate the second low-temperature cooling system currently used in HEVs by increasing the coolant inlet temperature to 105°C, thus reducing the weight and cost of HEVs and increasing the efficiency; (b) increase the cooling rate by 25% or reduce the junction temperature compared to convection cooling due to its improved heat transfer; (c) achieve HEV power electronics cooling and junction temperature control at low coolant flow velocities, thus reducing pressure drops and pumping power requirements; and (d) simplify the cooling system of HEV power electronics by integrating it into the main engine cooling system. The subcooled flow boiling system can also be used for cooling of high-power-density electronics with a heat flux up to 250 W/cm² and for cooling of all-electric vehicle power electronics.

Future work will focus on (a) designing and fabricating an experimental test system based on the realistic cooling channels of commercial HEV power electronics; (b) conducting subcooled flow boiling experiments and data analyses with a 50/50 EG/W mixture; (c) developing experimental-data-based predictive correlations of the subcooled flow boiling heat transfer coefficients under the application conditions of cooling vehicle power electronics; and (d) refining simulation models and results of coolant subcooled flow boiling in cooling of vehicle power electronics based on experimental heat transfer data.

VII.J.3. Products

Publications

1. Weihuan Zhao, David M. France, Wenhua Yu, Dileep Singh, "Subcooled Boiling Heat Transfer for Cooling of Power Electronics in Hybrid Electric Vehicles," submitted to the ASME Journal of Electronic Packaging, October, 2014.
2. Wenhua Yu, Weihuan Zhao, David M. France, Dileep Singh, "Coolant Boiling for Thermal Control of Hybrid Electric Vehicle Power Electronics," SAE 2014 Thermal Management Systems Symposium, September 22-24, 2014, Denver, Colorado, USA.

Patents

1. David M. France, Wenhua Yu, Dileep Singh, Weihuan Zhao, "Subcooled Boiling System for Cooling Hybrid Electric Vehicle Power Electronics," Argonne Invention Report ANL-IN-14-005, January 2014.

VII.K. Aerodynamics and Underhood Thermal Analysis of Heavy / Medium Vehicles

Principal Investigator: T. Sofu

Argonne National Laboratory
9700 S. Cass Avenue
Argonne, IL 60439
Phone: (630) 252-4500, E-mail: tsofu@anl.gov

Other Collaborators: S.N.P.Vegendla

E-mail: svegendla@anl.gov

DOE Program Manager: Lee Slezak

Phone: (202) 586-2335
E-mail: Lee.Slezak@ee.doe.gov

VII.K.1. Abstract

External aerodynamics and underhood thermal analyses of two heavy-duty vehicles (i) Cab-over engine, i.e., European style flat-front, and (ii) Conventional truck, i.e., North American class-8-style front engine, are being studied to assess their aerodynamic and underhood cooling performances. Each of these two vehicles has similar geometrical dimensions, i.e., widths, heights, and lengths.

Overall, a 2.4% aerodynamic drag increase is observed alone with a curvy-edge trailer in each of the trucks. The optimal curvature radius of the curvy-edge trailer corner is 12.5 cm and the arc length would be 19.63 cm. A significant aerodynamic drag reduction of 1.1% is observed at Yaw 6° with wheel covers installed. In contrast, 1% aerodynamic drag increased at Yaw 0° with wheel covers installed.

In conventional trucks, a lower aerodynamic drag coefficient is predicted, as compared to that of the cab-over engine design at various yaw angles ranging from 0° to 12°. At 0° yaw angle, the conventional design has 21.8%, 15.3%, and 14.7% lower aerodynamic drag coefficients than the cab-over engine design for cabin only, cabin with flatbed, and cabin with trailer (full vehicle) configurations, respectively. Furthermore, an additional 21.8% reduction in aerodynamic drag coefficient is observed with side skirts in the conventional truck with flatbed configuration. Reduction with side skirts is 14.42% in the conventional cabin with trailer configuration. Similar observations apply at 6° and 12° yaw angles.

Apart from the aerodynamic drag analysis, underhood thermal analysis is also being performed to compare the two heavy-duty vehicle configurations. Based on engine coolant temperatures, 11.75% and 10.13% thermal efficiency improvements are observed in the conventional truck in comparison to thermal efficiency of the cab-over design for the charge air cooler (CAC) and radiator, respectively.

Objectives

- **Vehicle aerodynamic drag analysis:** The aim of this project is to develop a methodology to simulate external aerodynamics of heavy- and medium-duty vehicles. The main focus of the project is to optimize the external vehicle design by modifying the external surfaces of the cabin and trailer.
- **Vehicle thermal analysis:** The aim of this project is to develop a methodology to simulate underhood thermal performance of heavy-duty vehicles. The main focus of this project is to optimize the underhood compartment by modifying heat exchanger designs, i.e., the CAC and the radiator.

Major Accomplishments

- Significant aerodynamic drag reduction is observed with optimal curvature radius of the trailer corners. The predicted curvature radius and arc length are 12.5 cm and 19.63 cm, respectively.
- Significant aerodynamic drag reduction is observed at Yaw 6° with wheel covers.
- Significant fuel savings are observed in the conventional truck compared to fuel use in the cab-over engine design.
- Aerodynamic drag results are verified with two commercially available computational fluid dynamics (CFD) softwares, StarCCM+® and PowerFlow®; results from both are in good agreement.
- Significant thermal performance improvements are observed in conventional trucks in comparison to results from the cab-over engine design.



VII.K.2. Technical Discussion

Background

Optimization of heavy- and medium-duty vehicle aerodynamic drag and thermal loads is an important design consideration with significant implications for fuel efficiency. A heavy-duty vehicle's drag-producing components include the cabin, mirrors, side extenders, cabin roof, wheels, and trailer, and also including engine and cooling devices. A component-based analysis helps to identify improvements in aerodynamic drag and cooling performance. Aerodynamic drag optimization lies mostly in redesigning the external surfaces of the above-mentioned components. On the other hand, thermal analysis is focused on the underhood compartment, which comprises the Charge Air Cooler (CAC), radiator, fan, and engine. An

efficient cooling system reduces thermal loads and maximizes the use of power because conventional underhood configurations allow conversion of only a fraction of the total fuel energy into mechanical power and the rest is lost through the exhaust system and heat rejection. An ideal temperature distribution in and around the engine allows redesign of a heavy vehicle’s underhood configuration and helps to achieve fuel efficiencies through cooling system optimization. This ongoing study is aimed at replacing costly experiments by designing feasible modeling prototypes of the heavy vehicle. Computational fluid dynamics (CFD) is the main tool in designing, simulating, and optimizing the underhood configuration and the external aerodynamics of the heavy-duty vehicle.

Technical Barriers

- Developing methodology to analyze separately for each phenomena/component and its effect on overall full-vehicle performance
- Model validation with prototypes
- Scarcity of acceptable-quality heat exchanger performance data and pressure drop

Technical Targets

- Development of physics-based models and numerical techniques
- Cross code verification with an available commercial package, and validation with test data.
- Identification and improvement of external vehicle surfaces to reduce aerodynamic drag
- Identification of optimal thermally efficient underhood configuration design

Introduction

In the automotive industry, optimized efficiency in vehicle aerodynamics and thermal management of an engine cooling system and underhood components is highly desirable for achieving durable and fuel-efficient designs that meet today’s energy demand [1-2]. CFD analysis offers an inexpensive and fast alternative to experiments. Commercially available CFD simulation software such as StarCCM+® can be used to investigate and assess the various factors that affect aerodynamic drag and underhood thermal vehicle performance [1]. Aerodynamic and thermal optimization of vehicles can reduce fuel consumption and vehicle emissions while improving vehicle durability.

Aerodynamic analysis of two optimized heavy-duty vehicle designs (cab-over engine and conventional) are performed and compared in this study. These two vehicle designs were previously optimized [1,2], using the following design and modeling sequences: (i) a comprehensive study to determine efficient design of the external body of the vehicle, (ii) development of a model of the vehicle for aerodynamic studies, (iii) locating the components of the vehicle that generate significant drag, (iv) modifying the components to improve the overall drag coefficient of the vehicle, (v) simulating the vehicle in multiple configurations, and (vi) conducting a complete set of aerodynamic drag

simulations to improve the drag coefficient with all modified components [3].

In this work, the following configurations are modeled for both cab-over engine and conventional designs and simulated separately for: cabin only, cabin+flatbed, and cabin+trailer (base case) configurations, including or excluding side skirts. In addition, wheel cover simulations are performed for the base case configuration. An aerodynamic drag sensitivity analysis of the cabin-trailer gap is also performed for the base case/full-vehicle simulations.

Approach

Aerodynamic drag simulations: 3D isothermal steady-state simulations are conducted using the segregated solver in StarCCM+. Gas-phase turbulence is modeled using k-ε with standard parameters [4]. Operating and inlet conditions are listed in Table VII-19.

Table VII-19: Heavy-duty vehicle wind-tunnel operating conditions for aerodynamic drag simulations

| Operating conditions | |
|---|---------------|
| Velocity Inlet [mph] | 55 |
| Temperature Inlet [K] | 300 |
| Yaw Angle [deg] | 0 - 12 |
| Outlet Pressure [atm] | 1 |
| Wind-Tunnel Dimensions [m ³] [Length x Width x Height] | 110x 100 x 50 |
| Number of Hexahedral Cells [millions] | ~30 |
| Side Walls | Periodic |

Underhood simulations: 3D non-isothermal steady-state simulations are carried out using the segregated solver in StarCCM+. Gas-phase turbulence is modeled using k-ε with standard parameters. For Fan, the Moving Reference Frame (MRF) is implemented. Operating and inlet conditions are shown in Table VII-20.

Table VII-20: Heavy-duty vehicle wind-tunnel operating conditions for underhood simulations

| Operating conditions | |
|---|---------------|
| Velocity Inlet [mph] | 20 |
| Temperature Inlet [K] | 300 |
| CAC Heat Rate [kW] | 48.5 |
| Radiator [kW] | 110 |
| Fan Rotation Speed [rpm] | 1400 |
| Yaw Angle (deg) | 0 |
| Outlet Pressure [atm] | 1 |
| Wind-Tunnel Dimensions [m ³] [Length x Width x Height] | 100 x 50 x 40 |
| Number of Polyhedral Cells [millions] | ~27 |

Results

As seen in Figure VII-64 and Figure VII-65, four configurations are studied to analyze each vehicle's aerodynamic drag performance.

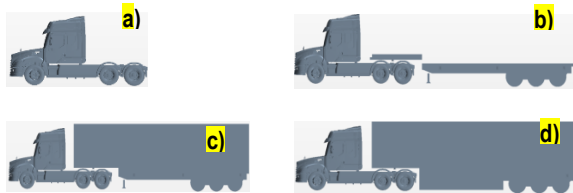


Figure VII-64: Conventional heavy-duty vehicle, a) cabin, b) cabin+flatbed, c) base case, and d) base case+side skirts.

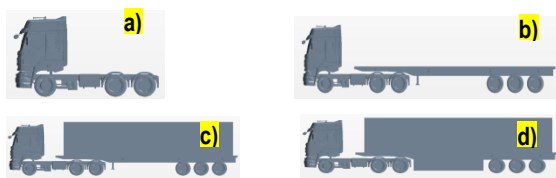


Figure VII-65: Cab-over engine heavy-duty vehicle; a) cabin, b) cabin+flatbed, c) base case, and d) base case+side skirts

Table VII-21: Conventional vehicle normalized aerodynamic drag

| | 0 deg | 6 deg | 12 deg |
|---------------------------|-------|-------|--------|
| Base case | 0.853 | 1.227 | 1.413 |
| Base case+side skirts | 0.824 | 1.063 | 1.284 |
| Cabin | 0.747 | 0.796 | 0.862 |
| Cabin+flatbed | 0.793 | 0.947 | 1.096 |
| Cabin+flatbed+side skirts | 0.728 | 0.856 | 1.001 |

Table VII-22: Cab-over engine vehicle normalized aerodynamic drag

| | 0 deg | 6 deg | 12 deg |
|---------------------------|-------|-------|--------|
| Base case | 1.0 | 1.369 | 1.879 |
| Base case+side skirts | 0.963 | 1.233 | 1.721 |
| Cabin | 0.955 | 0.996 | 1.094 |
| Cabin+flatbed | 0.936 | 1.044 | 1.263 |
| Cabin+flatbed+side skirts | 0.932 | 1.014 | 1.159 |

Table VII-21 and Table VII-22 show normalized aerodynamic drag results for both conventional and cab-over designs.

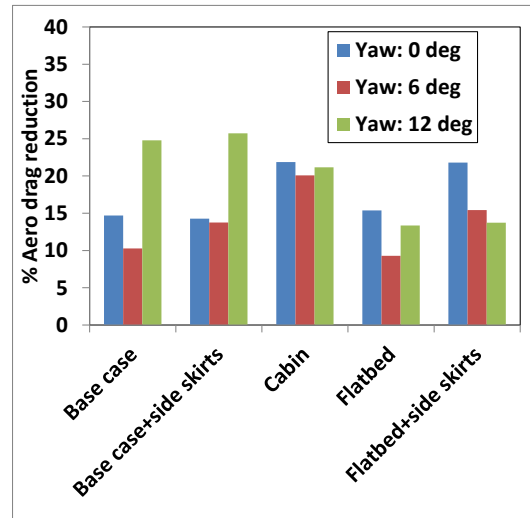


Figure VII-66: Aerodynamic drag performance of conventional design over cab-over engine design for Yaw 0, 6 and 12°.

As seen in Figure VII-66, significant aerodynamic drag reduction is observed at all yaw angles in the conventional design as compared to drag in the cab-over engine design. This is mainly due to the large vortex zone at the front of the cab-over engine design that significantly increases aerodynamic drag (not shown). [Note: aerodynamic drag results are normalized with cab-over engine base case value.]

Significance of trailer curvy edges:

As seen in Figure VII-67, a 2.4% decrease in aerodynamic drag coefficient is predicted with curvy edges at the trailer rear end as compared to the base case with 0° yaw angle. This is due to lower turbulence with curvy edges. The optimal curvature radius of the curvy-edges is 12.5 cm with an arc length of 19.63 cm. These values are also valid for all types of trailers.

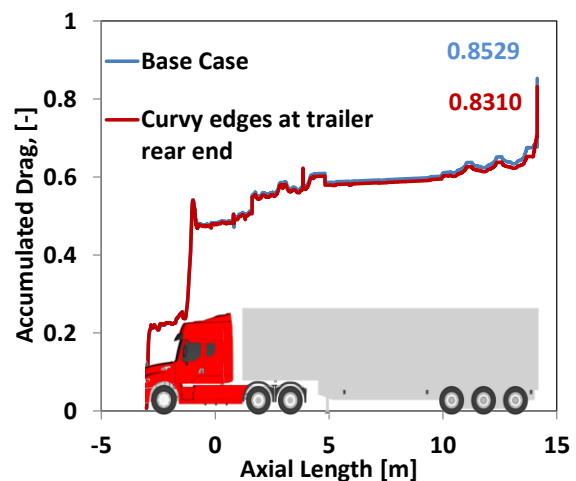


Figure VII-67: Conventional heavy-duty vehicle performance with curvy-edges at trailer rear end [Yaw 0°]

Significance of wheel covers:

A total of 1.1% reduced in aerodynamic drag coefficient is observed with wheel covers as compared to the base case configuration at 6° yaw angle. In contrast, fuel efficiency drops by 0.5% with wheel covers and with a 0° yaw angle. This is mainly due to deflected air flow from the drive-axle wheels that directly strikes the trailer rear-axle wheels. as highlighted in Figure VII-68(ii). Note that the base case does not include wheel covers.

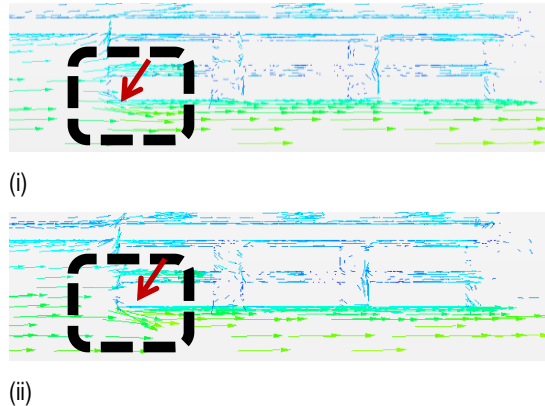


Figure VII-68: Conventional heavy-duty vehicle velocity profile at trailer wheels [Yaw 0°] (a) without wheel covers and (b) With wheel covers

Significance of cabin-trailer gap:

As seen in Figure VII-69 and Table 5, significant aerodynamic drag drops with reduced cabin-trailer gap in all yaw angles. This is mainly due to the smaller volume of the space that generates the vortex zone.

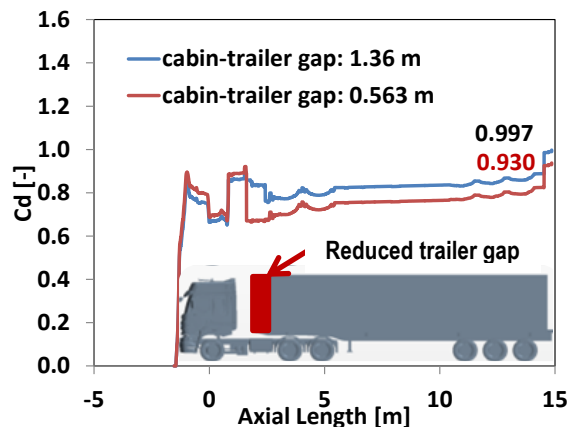


Figure VII-69: Cabin-trailer gap analysis of cab-over engine design at Yaw 0°

Table VII-23: Cabin-trailer gap sensitivity analysis of Cab-over engine at three yaw angles (normalized aerodynamic drag profiles)

| Cabin-Trailer gap | 0 deg | 6 deg | 12 deg |
|-------------------|-------|-------|--------|
| 1.360 m | 1.0 | 1.369 | 1.879 |
| 0.563 m | 0.936 | 1.214 | 1.518 |
| % drag drop | 6.3 | 11.3 | 19.24 |

Underhood thermal simulations:

As shown in Figure VII-70 and Figure VII-71, significant differences are seen in thermal performances for both conventional and cab-over engine configurations. In this work, thermal simulations are performed at the same ambient temperature of 27.3°C, inlet velocity of 20 mph, and constant heat rejection values of CAC and radiator at 48.5 kW and 110 kW, respectively. In both simulations, fan speed is considered to be constant (see Table VII-20). CAC and radiator are modeled as using a single-duty heat exchanger with constant inertial and viscous porous resistances in both conventional and cab-over engine models. In these simulations, inertial and viscous resistance values are considered to be 67 kg/m⁴ and 415 kg/m³.s, respectively.

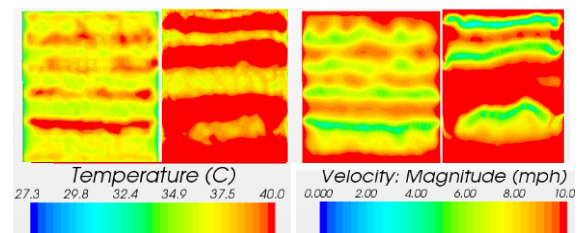


Figure VII-70: Temperature and velocity profiles of CAC (i,iii) Conventional (ii,iv) Cab-over engine

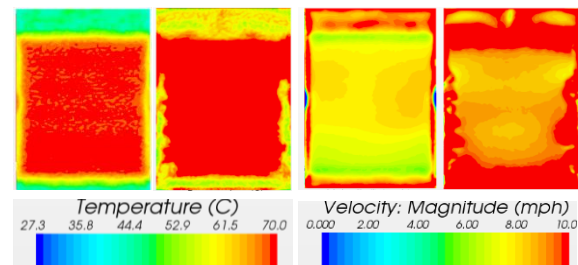


Figure VII-71: Temperature and velocity profiles of radiator (i,iii) Conventional (ii,iv) Cab-over engine

From the data below in Table VII-24, an overall 11.75% thermal efficiency is observed in the conventional truck’s CAC as compared to that of the cab-over engine design. Also, 10.13% higher efficiency is observed in the conventional-truck radiator. This is mainly due to the smooth/uniform air passage through the underhood that leads to higher mass flow rates in both CAC and radiator. Also, high mass flow rates are driven by the fan, as seen in the same table. The thermal efficiencies are calculated on the basis of average temperatures of the CAC and radiator.

Table VII-24: Conventional and Cab-Over Engine thermal Performance Data of CAC, Radiator, and Fan

| | Conventional | | Cab-over engine | |
|----------|--------------------------|-----------------------|--------------------------|-----------------------|
| | Average temperature [°C] | Mass Flow rate [kg/s] | Average temperature [°C] | Mass Flow rate [kg/s] |
| CAC | 45.08 | 1.773 | 50.38 | 1.398 |
| Radiator | 74.90 | 2.468 | 82.49 | 2.409 |
| Fan | - | 3.198 | - | 2.626 |

As seen in Figure VII-70 and Figure VII-71, the conventional-truck velocity profiles are more uniform than those in the cab-over engine configuration. This might be due to one or more of three reasons (i) cabin-grill openings are not the same in both models, (ii) off-centered fan location in cab-over engine, and (iii) air flow restriction due to engine location in the cab-over engine version. Within the CAC, low-velocity zones are mainly due to the support components of the cabin-grill, which obstruct air flow. These low velocities can lead to high temperatures, as shown in Figure VII-70 and Figure VII-71(i-ii).

Conclusions

Aerodynamic drag and underhood thermal analyses are performed for two heavy-duty vehicles, i.e., conventional and cab-over engine trucks. A significant fuel saving potential was observed for the conventional truck over that of the cab-over design at all yaw angles. The main fuel saving was observed in the cabin part alone.

In both vehicles, aerodynamic drag performance was improved with side skirts at all yaw angles due to air flow deflection away from the underbody. Significant aerodynamic drag reduction was observed with trailer curvy edges.

In wheel cover configuration, aerodynamic drag reduction was observed in Yaw 6°, but overall drag was greater in Yaw 0°. Cab-over engine cab-trailer gap sensitivity aerodynamic drag analysis indicated significant aerodynamic drag drop when the gap distance was shortened.

In underhood thermal simulations, better cooling performance was obtained for the conventional model in the CAC and radiator than in the cab-over engine model. This was mainly due to less restrictive underbody air flow in the conventional model.

Future Plan

- Thermal analysis of heavy-duty off-road vehicles, i.e., farm tractors and wheel loaders
- Analysis of cooling-package performance with suction and blower fan configuration
- Tradeoff between cooling performance and fan acoustics

- Off-road vehicles use several heat exchangers, and appropriate locations for each may increase cooling performance.
- Nonetheless, CAD import and surface cleaning to generate a quality mesh to perform the numerical analysis.

Acknowledgments

The authors gratefully acknowledge the financial support of the U.S. Department of Energy under contract number C1201001.

References

1. Sofu, T. Aerodynamics and underhood thermal analysis of heavy/medium vehicles. US DOE Annual Report for Vehicle Technology Program, DOE/EE-1023.
2. Vegendla, S.N.P., Sofu, T. ANL-Cummins CRADA: "Integrated External Aerodynamic and Underhood Thermal Analysis for Heavy Vehicles." Argonne National Laboratory, Lemont, IL, Intra-lab Memo, March 2014.
3. Driant, T., Fellouach, H., Moreau, S., Desrochers, A., Remaki, L. Numerical simulation and wind tunnel measurements on a tricycle wheel sub-system. IJESMS, 2013.5, pp: 159-167.
4. Vegendla, S.N.P., Heynderickx, G.J., Marin, G.B. Micromixing effects on series-parallel and autocatalytic reactions in a turbulent single-phase gas flow. Chemical Engineering Science. 2010. 65, pp: 4621-4629.

VII.K.3. Products

Publications

1. Vegendla, S.N.P and Sofu, T. External Aerodynamic Analysis for Optimization of Medium/Heavy Vehicles. 2013 PostDoctoral Research and Career Symposium, Oct. 10–11, 2013.
2. Vegendla, S.N.P and Sofu, T. Underhood Thermal Analysis for Optimization of Heavy Vehicles. 2013 PostDoctoral Research and Career Symposium, Oct. 10–11, '2013.
3. Sofu, T. Aerodynamics and underhood thermal analysis of heavy/medium vehicles. US DOE Annual Report for Vehicle Technology Program, DOE/EE-1023.
4. Vegendla, S.N.P and Sofu, T. ANL-Cummins CRADA: "Integrated External Aerodynamic and Underhood Thermal Analysis for Heavy Vehicles." Argonne National Laboratory, Lemont, IL, Intra-lab Memo, March 2014.

Tools and Data

1. STAR-CCM+V8®
2. Pro-Engineer, PTC®
3. Exa-PowerFLOW®

VII.L. Development of Nanofluids for Cooling Power Electronics for Hybrid Electric Vehicles

Principal Investigator: Dileep Singh

Coworkers: E. Timofeeva, W. Yu, D. France

Argonne National Laboratory

9700 S Cass Ave.

Lemont, IL 60439

Phone: (630) 252-5009

E-mail: dsingh@anl.gov

DOE Program Manager: Lee Slezak

Phone: (202) 586-2335

E-mail: Lee.Slezak@ee.doe.gov

- Target power electronics cooling in HEVs, but also address the thermal management issues related to heavy vehicles.
- Capitalize on our prior work on nanofluid development, in particular, the nanofluid engineering approach.

Major Accomplishments

- Analysis of a power electronics cooling system allowed establishment of criteria for efficient nanofluid coolant, such as thermal conductivity ratio of more than 1.5. Such enhancements are possible with graphitic nanoparticles that are commercially available at reasonable costs (20% added cost to coolant).
- Graphitic nanofluids in 50/50 mixture of ethylene glycol and water showed:
 - morphology-dependent thermal conductivity;
 - 50-130% increases in thermal conductivity at 5 wt% loading (room temperature) – indicating possibilities for dramatic improvement in liquid cooling;
 - better dispersion stability, lower viscosity, and higher thermal conductivity after nanoparticle surface treatment; and
 - enhanced performance with temperature.
- The optimized and scaled-up nanofluid was tested in a heat transfer loop (fouling and pumping power tests) to demonstrate the commercial viability of the GnP nanofluid technology.



VII.L.1. Abstract

This project studied the possibility of elimination of the lower temperature cooling system in hybrid electric vehicles (HEVs), such that all cooling is done with a single higher temperature cooling system by using nanofluid coolant with advanced heat transfer properties. We have conducted thermal analysis of the power electronics cooling module and formulated criteria for the nanofluid properties required to successfully meet the performance goals. Further, the project focused on assessment, optimization, and experimental evaluation of nanofluids with commercially available carbon nanomaterials in 50/50 ethylene glycol/water (EG/H₂O) base fluid. Using a simple, low cost, and scalable surface modification method for graphitic nanoparticles, we were able to formulate a nanofluid coolant with advanced combination of properties that allows 90+% improvement in heat transfer coefficient when used in laminar flow and 30+% enhancement in heat transfer coefficient when used in turbulent flow. The implementation of this technology in hybrid and all-electric vehicles will result in reducing the size, weight, and number of heat exchangers, further improving vehicle efficiency and fuel economy.

Objectives

- Assess use of nanofluids to cool power electronics in HEVs, namely:
 - Use heat transfer analysis to determine the requirement for nanofluid properties that would allow eliminating the low temperature cooling system in HEVs.
 - Develop nanofluid formulations with a defined set of thermophysical properties.
 - Identify and address engineering issues related to use of nanofluid(s).
 - Experimentally evaluate the heat transfer performance of the developed coolant fluids.

VII.L.2. Technical Discussion

Background

Power electronics is a critical component of hybrid electric vehicles (HEVs) and electric vehicles (EVs) since it provides control and conversion of electric power. Higher power loads result in increased heat fluxes; thus, uninterrupted operation of power electronics requires liquid cooling systems to enhance heat dissipation, improve energy efficiency, and lengthen device lifetime. In current HEVs, two cooling systems are used: a higher temperature system for cooling the gasoline engine and a lower temperature system for cooling the power electronics. A Department of Energy (DOE) goal is to eliminate the lower temperature system and to accomplish all cooling with a single higher temperature system. This would obviously reduce system complexities and weight, thereby increasing fuel economy.

Introduction

To satisfy the thermal management needs, the heat transfer efficiency of conventional fluids must be improved. In FY 2011-FY 2012 [1], a heat transfer analysis for a typical heat exchanger [2, 3] was performed to determine the magnitude of enhancement in the thermal properties of a heat transfer fluid required to improve the cooling. Calculations showed that, for the designated heat exchanger (laminar flow), an enhancement in thermal conductivity of between 50% and 100% could, without a significant increase in pumping power, allow either elimination of one radiator in HEVs or an increase of the power loading.

One of the approaches that would help improve the heat transfer rates of liquids is use of nanofluids. Nanofluids are nanotechnology-based heat transfer fluids that are engineered by stably dispersing nanometer-sized solid particles in conventional heat transfer fluids at relatively low particle volume concentrations to enhance the thermal conductivity and the heat transfer coefficient.

Previous studies of nanofluids [4] demonstrated that such a level of enhancement in thermal conductivity can be achieved with either addition of metallic or high-aspect-ratio graphitic nanoparticles. Production of metal-containing nanofluids faces some major challenges, such as stability towards agglomeration and surface oxidation, availability, cost of materials, and manufacturing issues. On the other hand, carbon nanomaterials are commercially available, and prices are dropping each year. At the same time, 20%–300% increases in thermal conductivity have been reported for nanofluids with carbon nanotubes [5-8] and graphene oxides [9, 10]. Such dramatic increases in thermal conductivity of nanofluids are most likely due to the unique nature of the anisotropic carbon nanomaterials that allows engaging multiple heat transfer mechanisms in suspensions (effective medium theory, percolation, and plasmon resonances).

The drawback of using carbonaceous nanofluids with high aspect ratio particles is very high viscosity (up to three orders of magnitude higher than the viscosity of the base fluid). Such viscosity increases result in pumping power penalties that are higher than the benefits in thermal conductivity of the suspensions. Thus, the practical heat transfer values for previously reported carbonaceous nanofluids are not sufficient for commercialization of the technology.

The selection of carbon nanomaterials for this study was based on our previous work on nanofluid engineering [11, 12], indicating that spherical or nearly spherical particles are more beneficial for heat transfer applications compared to nanomaterials with high aspect ratio. Our recent findings in nanofluid engineering indicate that enhancements significantly above the effective medium theory can be achieved by engaging alternative heat transfer mechanisms through the nanofluid and nanoparticle morphology. Concentration effects are deemed to be critical for balancing the benefits of increased thermal conductivity and penalties from increased viscosity.

Approach

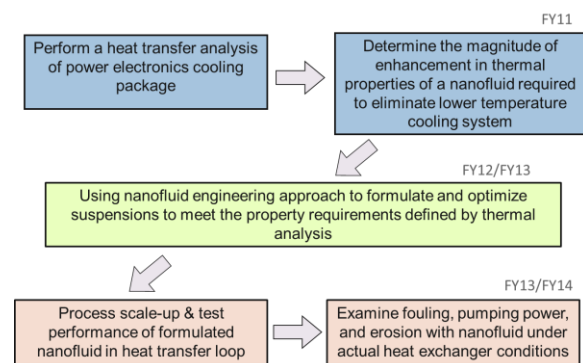


Figure VII-72: Schematics of the project approach

The general approach for this project is a multistep R&D process as depicted on Figure VII-72 and includes analysis, formulation, and testing stages. The formulation approach was to use commercially available graphitic or graphene-based nanoparticles and disperse them in base cooling fluid formulations to enhance the thermal performance. The testing approach included thermal and mechanical testing for evaluation of nanofluid performance.

Results

Heat Transfer Analyses

This program was started in FY 2011 by funding from Propulsion Systems Materials (FWP 49766) for an assessment of the viability of using nanofluids for reduction of one of the heat exchangers for double-sided cooling of power electronics in HEVs. Analyses were performed to estimate the effectiveness of the cooling that can be achieved with a 50/50 mixture of ethylene glycol and water at 105°C (base fluid) and with nanofluids specifically engineered for this application. The nanofluids consist of nanoscale solid particles suspended in the same base fluid that is currently used in hybrid vehicles. The analyses were multifaceted. First, properties of nanofluids were estimated that would be required to meet current heat flux and junction temperature conditions. Next, nanofluid properties were identified for conditions at or exceeding current parameter levels. These properties were identified for single- and double-sided cooling with and without thermal interface materials (TIMs). Finally, nanofluids were identified with potential for achieving those properties based on a research program with reasonable goals (based on the state of the art in the field).

To estimate requirements for nanofluids to meet and exceed current hybrid vehicle cooling requirements, a one-dimensional mathematical analysis of composite materials was undertaken. One boundary condition was the power semiconductor junction temperature of 150°C. The other boundary condition was convective heat transfer to the laminar flow of a coolant at 105°C, which was taken either as a nanofluid or as the base fluid. The resistance of the composite materials between the power semi-conductors and the coolant was divided into two groups. The first was the resistance of the TIM, taken as 100 mm²•K/W, and the second

was the balance of the resistance in the composite determined from results presented in reference [1] for the case of no TIM in the composite. With these boundary conditions, the heat removal rate was calculated for various coolants. Alternatively, the first boundary condition was replaced by a heat flux of 100 W/cm², and the junction temperature was calculated for various coolants.

Based on the thermal analysis, the main conclusions was that DOE’s goal of eliminating the second radiator used for cooling power electronics can be achieved if the ratio of heat transfer (equal to the ratio of thermal conductivity in laminar flow) of the nanofluid to the base fluid is about 2 without the TIM in single-sided cooling. In double-sided cooling, the second radiator can be eliminated, and the current standards of 100 W/cm² heat flux and/or 150°C junction temperature can be improved substantially with a thermal conductivity ratio of about 1.5, with or without the TIM.

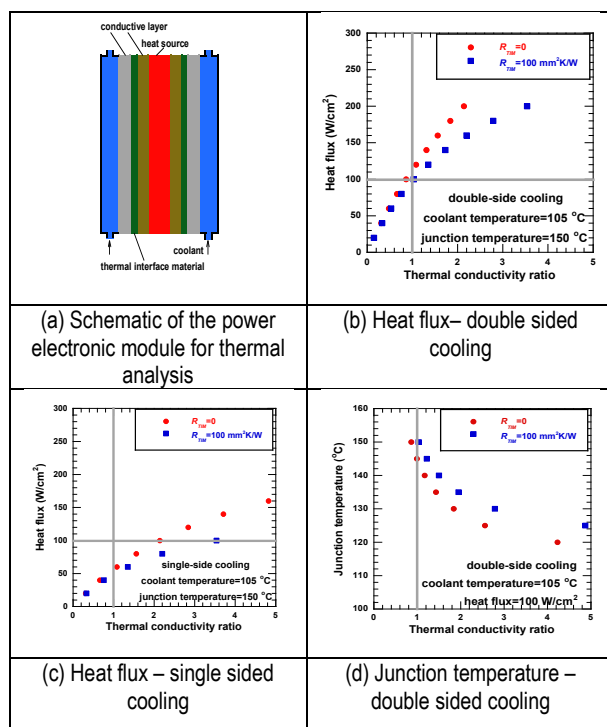


Figure VII-73: Results of the heat transfer analysis

That assessment indicated that if the ratio of the thermal conductivity of the nanofluid to that of the base fluid is ≥ 1.5 , one heat exchanger can be eliminated in the laminar flow region. The results and conclusions of the heat transfer analysis are shown on Figure VII-82. Nanofluids (dispersion of nanomaterials in liquids) have proven ability to increase thermal conductivity and heat transfer, and thus are promising for reducing the size, weight, and number of heat exchangers for power electronics cooling in HEVs per DOE’s goals. In this regard, various cooling fluids are being developed with enhanced thermal properties.

Further investigation was focused on the effects of nanoparticle morphology and surface treatment on the thermophysical properties of nanofluids with graphitic nanomaterials in EG/H₂O base fluid.

Morphology of GnP graphitic nanoparticles

Graphitic nano-platelets, also marketed as multilayered graphene nan-platelets (GnP) by XG Sciences, were selected for study due to their variety of sizes and platelet thicknesses, and also the low cost of these graphitic nanomaterials (current cost \$70/lb and projected future cost of less than \$20/lb) makes them a commercially feasible candidate as a heat transfer fluid additive as they add less than 20% to the total cost of the coolant.

Scanning electron microscopy (SEM) images of three as-received GnP powders (A, B, and C) are presented in Figure VII-74 (left). The difference in platelet thickness is not obvious from the image resolution, but the platelet diameters are clearly different. All GnP nanoparticles have irregular shape with particle diameters of 0.1–1 micron in C-750 grade, 1–10 microns in M-5 grade, and 3–25 microns in H-5 grade. As-received GnPs assemble into compact clusters on a Si wafer surface, especially C-750 grade, indicative of the hydrophobic nature of the platelets.

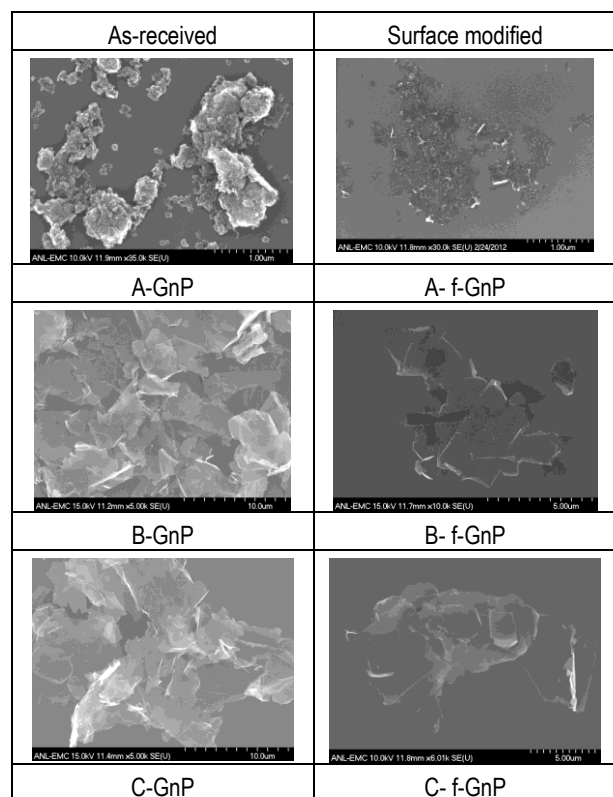


Figure VII-74: SEM images of three graphite morphologies before and after the surface modification

Dispersion of GnP nanoparticles As-received GnP graphitic nanopowders have very poor suspension ability in water, especially at low concentrations. Suspension with unmodified GnPs settles within a few hours, but an initial reading of the thermal conductivity showed enhancements slightly above those predicted by effective medium theory. Suspensions stabilized with cationic (CTAB) or anionic (SDS) surfactants show similar improvement in stability; however, the thermal conductivity of those suspensions is below the base fluid due to very low thermal conductivity of organic molecules compared to water, as segregation of surfactants at the

liquid/nanoparticle interface creates additional thermal resistance for heat flow. Thus, organic surfactants are detrimental for the thermal conductivity of water-based suspensions. Use with a non-surfactant approach to stabilizing dispersions of nanoparticles involves an additional surface functionalization step.

Surface modification of graphitic nanoparticles

The nanoparticles were surface treated to create hydrophilic surface groups for improved suspension stability. Essentially, the functionalization process is an oxidation of the GnP powder in a mixture of concentrated sulfuric and nitric acids (3:1 ratio) that converts sp² graphite layers on the surface into OH⁻, COO⁻, and CO groups. These groups create the electrostatic charge at the nano-platelet surfaces that keeps the particles separated from each other due to repulsion and prevents particle agglomeration and settling. Thus, good stability of graphitic nanofluids in a water or ethylene glycol/water base fluid can be achieved.

The functionalized f-GnP nanoparticles were studied with SEM and Raman spectroscopy, and the findings compared to unmodified GnPs of the same grade. The SEM of GnPs (Figure VII-74) shows dramatic change in morphological appearance of the nanoparticles before and after functionalization. The f-GnPs are very well distributed on the surface of the Si wafer support, with clearly seen individual nano-platelets lying flat, compared to the granular agglomeration and clustering seen with the unmodified nanoparticles. This is a clear sign of the hydrophilic nature of functionalized nanoparticles, which also helps in the stability of f-GnP suspensions.

Raman spectroscopy also confirmed the surface oxidation of the treated f-GnP platelets (Figure VII-75a). The ratio of oxide/graphite may be critical for efficient thermal conductivity enhancements, i.e., surface area and morphology of nanoplatelets need to be optimized for advanced heat transfer performance.

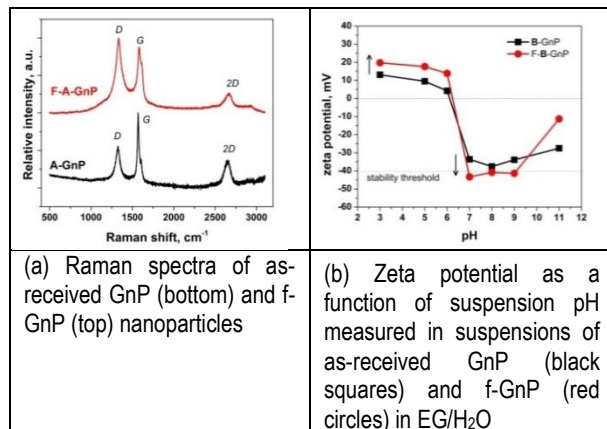


Figure VII-75: Effects of the GnP surface treatment

The zeta potential can be related to the stability of suspensions and is defined as the electric potential in the interfacial double layer at the location of the slipping plane versus a point in the bulk fluid away from the interface. The higher the value of the zeta potential, the higher is the electrostatic repulsion between nanoparticles and, therefore,

the dispersion stability. When the potential is low, attraction between particles exceeds repulsion, resulting in agglomeration and settling of nanoparticles. On the one hand, the zeta potential is an indication of nanoparticle surface chemistry; on the other hand, it changes with ionic composition of the bulk solution. For water-based systems, the solution pH could be adjusted for controlling the stability of the suspensions. We have investigated the zeta potential as a function of pH in a diluted suspension of unmodified GnP and f-GnP in EG/H₂O (Figure VII-75b). The results clearly demonstrate that f-GnP nanoparticles have 10 mV higher zeta potential than GnPs due to a higher concentration of surface groups, resulting in higher stability of f-GnP suspensions. At pH between 7 and 9, the zeta potential values for f-GnP suspension are below 40 mV, which is considered as a threshold for good stability of suspensions. High zeta potential minimizes agglomeration of nanoparticles and also results in lower viscosity of nanofluids for the same particle concentration [13]. Thus, for optimized heat transfer performance, nanofluid pH should be maintained between 7 and 9. Further comparisons of nanofluids with different particle shapes were conducted at the same pH.

Thermophysical properties of graphitic nanofluids

The effect of GnP surface functionalization on the thermophysical properties of nanofluids was compared for unmodified GnP and f-GnP at 5 wt% (~2.25 vol. %) loadings. Thermal conductivity enhancements measured in different grades of GnP and f-GnP nanofluids are presented on Figure VII-76a. One can see that the highest increases in thermal conductivity were achieved with C grade, followed by B grade, and the A-GnPs provided the smallest thermal conductivity increases.

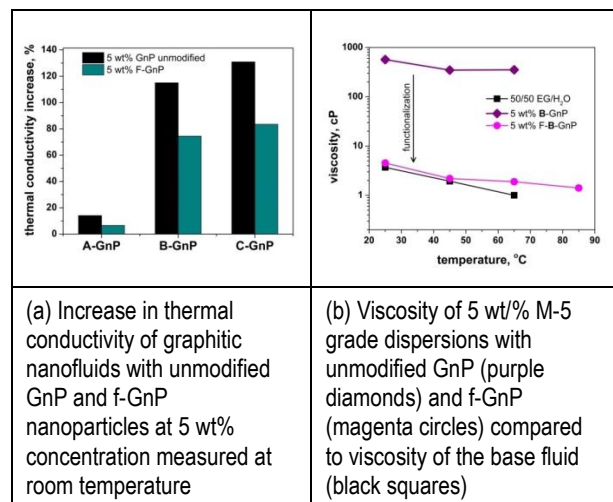


Figure VII-76: Effects of surface treatment of thermophysical properties of nanofluids

The observed enhancements are well beyond the predictions of effective medium theory. Surface functionalization of graphitic nanoparticles reduces the decreases in the thermal conductivity enhancements across all grades by 30%–50% of the analogous GnP suspensions. Nevertheless, the increases in thermal conductivity are above the effective medium prediction, reaching 75%–85% higher than the base fluid values. The effect of surface modification

on the viscosity of nanofluids is demonstrated in Figure VII-76b with unmodified GnP and f-GnP dispersed in EG/H₂O at the same concentration. The viscosity of f-GnP is nearly two orders of magnitude less than that of the similar suspension with unmodified GnP. The viscosity of nanofluid with f-GnP is ~30% higher than that of base fluid, which is very promising for heat transfer, considering the significant increase in thermal conductivity. It should be mentioned that B grade had the most dramatic drop in viscosity due to the surface modifications among all three grades.

The thermal conductivity of nanofluids with various particle morphologies was measured as a function of particle concentrations for the f-GnP series (Figure VII-77a). Particles with the smallest diameters and thicknesses (A grade) show the smallest increase in thermal conductivity, closely following the prediction of effective medium theory. This finding indicates that no percolation paths are formed in this nanofluid, or a high surface area of graphite oxide prevents effective thermal conduction through such percolation networks. Grades B and C provide much higher thermal conductivity increases at higher particle concentrations. This agrees with the proposed percolation heat transfer mechanism for anisotropic carbon nanomaterials. Interestingly, C grade shows slightly lower enhancements than B grade at lower concentrations and slightly higher enhancements at higher particle concentrations. These results can be interpreted as an effect of two particle morphologies. For the thinner B particles there is a large number of particles for the same concentration; thus, the percolation threshold can be achieved at lower concentration than in nanofluid with C grade particles. However, once the percolation threshold is achieved, the efficiency of thermal conduction is better in thicker, larger-diameter particles as compared to a network of smaller diameters and thinner B-GnP nanoparticles. Smaller particle diameter/thickness of B grade creates more interfaces and increases the interfacial thermal resistance, and thus there are less-efficient thermal pathways.

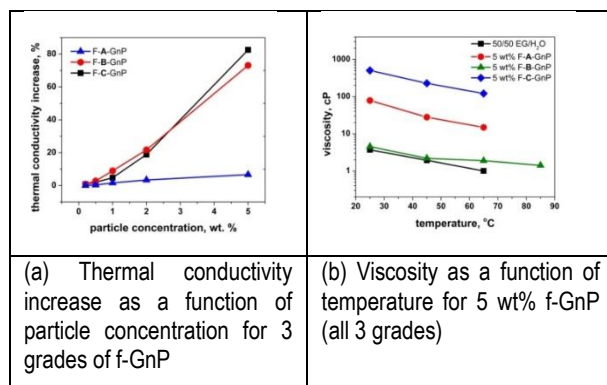


Figure VII-77: Effects of nanoparticle morphology of thermo-physical properties of nanofluids

The viscosities of f-GnPs with different morphologies are compared in Figure VII-77b for 5 wt% loadings. Despite similar functionalization treatment and pH being adjusted to 8.5±0.5, the viscosity of the f-GnP nanofluids varies significantly with the particle morphology. The lowest viscosity is observed in nanofluid of B grade, and it is only 20%–30% higher than that of the base fluid. At 65°C, the viscosity of this nanofluid

becomes close to the lower limit of viscosities that can be measured with a rotational spindle viscometer. The viscosity of C grade changed insignificantly after surface functionalization, from ~600 cP to 500 cP at 25°C. An interesting result was obtained with A grade, where f-GnP suspensions actually showed higher viscosity than the same concentration of unmodified GnPs in EG/H₂O. At the same time, the stability of the nanoparticle suspension was noticeably improved. This effect is most likely due to very poor dispersion of unmodified GnP: the granular nanoparticle structure agglomerates those powders, as seen with SEM images, while f-GnP appears as individual platelets. Broken apart A-grade GnP flakes represent significantly higher area of solid/liquid interface than granules, and thus result in increased effective volume fraction and viscosity of nanoparticles.

Heat transfer coefficient ratio for laminar and turbulent flow

Since the cooling efficiency of the heat transfer fluids is the main consideration in the current nanofluid development, the ratio of heat transfer coefficients for the suspensions and the base fluid was estimated for fully developed (hydrodynamically and thermally) laminar and turbulent flow regimes using the fluid dynamic equations [14,15]. The ratio of heat transfer coefficients is a convenient measure for comparison of two fluids flowing in the same geometry and at the same rates. In a laminar flow regime, the heat transfer coefficients are proportional to the thermal conductivity (within the acceptable range of inlet/outlet temperature difference), but in a turbulent flow regime, the heat transfer coefficients depend on a set of thermophysical properties [14].

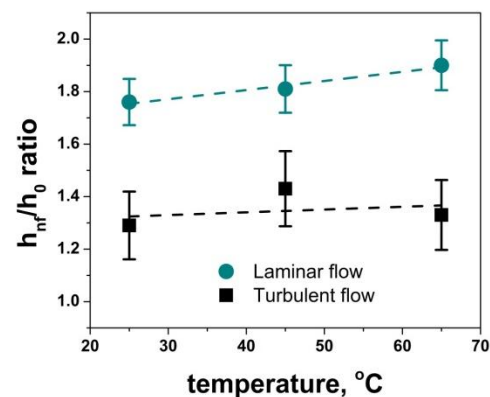


Figure VII-78: Calculated ratio of heat transfer coefficients for 5 wt% B-grade f-GnP in EG/H₂O with laminar and turbulent flow regimes

Introduction of nanoparticles to the fluids changes the density (ρ), thermal conductivity (k), viscosity (η), and specific heat (c_p) of the coolant. Experimental values for thermal conductivity and viscosity and calculated values from the rule of mixtures for density and specific heat were used for evaluation of the heat transfer benefits of nanofluid with 5 wt% of B grade f-GnPs (Figure VII-78). The ratio of heat transfer coefficients (h_{nf}/h_0) for the nanofluid and the base fluid, calculated for different temperatures, shows that the inclusion of graphitic nanoparticles in EG/H₂O coolant can provide significant (75%–90%) improvement in heat transfer rates

when used in the laminar flow regime, improving with increasing temperature. Heat transfer coefficients in the turbulent flow regime show 30%–40% improvement in heat transfer compared to the base fluid. Uncertainty in the viscosity measurement at higher temperatures doesn't allow us to reach a conclusion on the temperature dependence, but it can be established in future experimental heat transfer tests. Previously, it was observed that the heat transfer coefficient improves with temperature for nanofluids in both water-based and organic based fluids [13, 16, 17]. These results are very encouraging, since the enhancements not only meet the power electronics cooling criteria, but also will be beneficial in thermal management in other medical, transportation, and military applications.

Optimization of nanofluid preparation procedure and scale-up

Next, the project focused on optimization of the formulation procedure and the scale-up. We prepared the nanofluids using a 50/50 mixture of H₂O and EG, as well as the commercial coolant Prestone 50/50. The thermophysical properties of the suspensions are presented on Figure VII-79. Results are given before and after an additional ball-mill processing step to achieve better homogenization of the nanofluids.

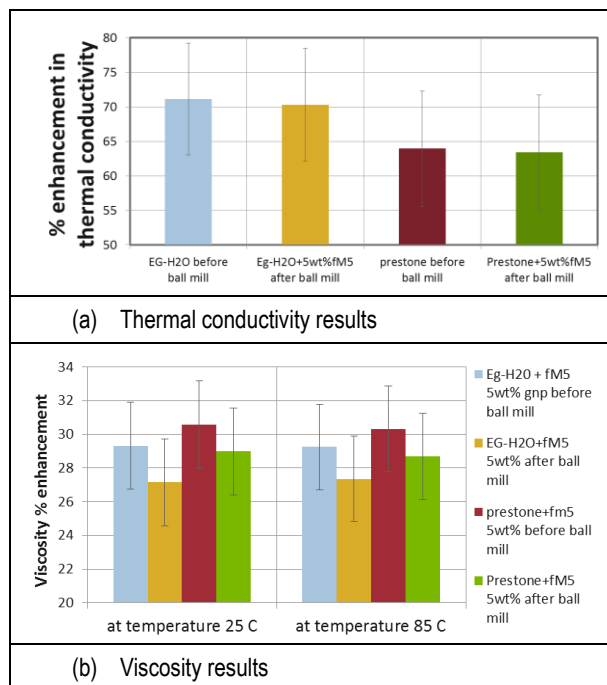


Figure VII-79: Effects of base fluid and ball-milling for the 5 wt.% B-grade f-GnP nanofluids

We concluded that additives in the Prestone coolant slightly interfere with our graphitic additives. They result in ~7% lower thermal conductivity and ~4% higher viscosity, with all other variables being the same. We also found that ball-milling decreases viscosity by ~3%, while thermal conductivity is not affected. Therefore, ball-milling is a beneficial step for improving the heat transfer of nanofluids.

Scale-up to several 0.5 L batches of f-GnP nanofluids revealed sensitivity of the nanofluid properties to the fluid parameters (concentration, pH, degree of surface

functionalization) and the necessity of quality control steps (thermogravimetric analysis, Raman spectroscopy, zeta potential measurement, etc.).

Efficiency of nanofluid at real heat exchanger conditions

Experimental evaluation of the most promising nanofluid formulation was conducted using an in-house apparatus that allows measuring the experimental heat transfer coefficient at various temperatures and flow rates.

Heat transfer coefficients were measured in the laminar flow regime for the fluid with as-projected thermal conductivity but viscosity slightly higher than that of the small batch nanofluid. Results are presented on Figure VII-79.

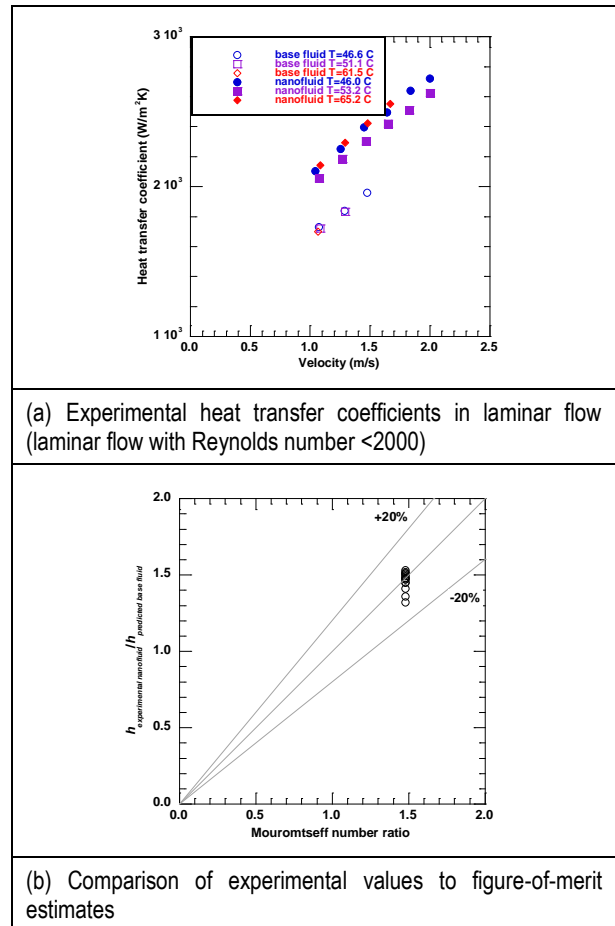


Figure VII-80: Experimental heat transfer coefficient results

As evident in Figure VII-80b, the experimental nanofluid heat transfer coefficient showed enhancement between 1.32 and 1.53 with an average of 1.46. This value is close to the figure of merit (Mouriomtseff number ratio), which (for laminar flow with Reynolds number <2000) was estimated to be 1.48.

Testing of fouling and erosion of the nanofluid coolant

The final evaluation of nanofluids was for their mechanical properties in close-to-real heat exchanger conditions. Two custom apparatus were prepared for erosion and clogging tests. Figure VII-81a shows the apparatus designed for determining the erosion of the target material at fixed angle and velocity and measuring the power required to pump nanofluids and the base fluids Figure VII-81b shows the

fouling test apparatus, which is a closed-loop system that allows for evaluation of fouling/clogging within pipes/channels at the flow rates that are maintained in a radiator cooling system. The pressure drop is measured as a function of time and temperature.

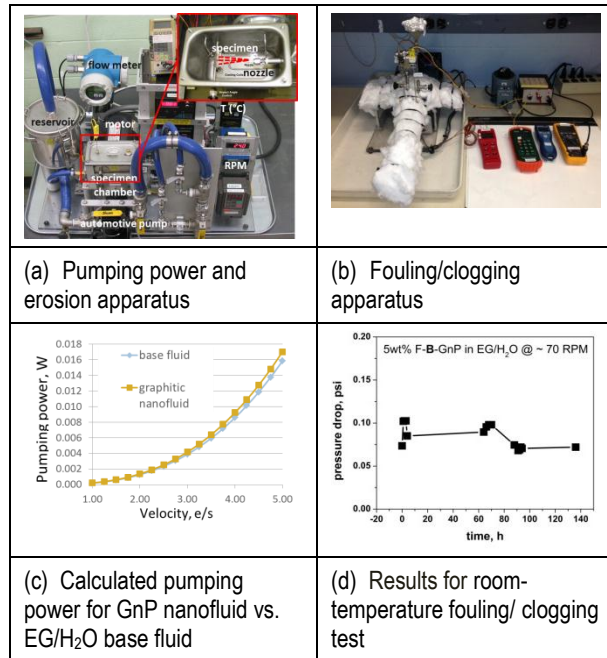


Figure VII-81: Experimental heat transfer coefficient results

Results from these tests are presented in Figure VII-81c and 10d and clearly indicate no clogging or erosion after hundreds hours of testing. The estimated pumping power penalty for nanofluid is ~7.5% vs. EG/H₂O base fluid. This value is significantly lower than the 75+% advantage offered in thermal conductivity of the new coolant; in addition, lower flow rates can be used to achieve the same heat transfer.

Conclusions

This study reports on an investigation of the effects of morphology and surface functionalization of graphitic nanoparticles on the thermophysical properties and heat transfer performance of nanofluids in EG/H₂O base fluid. Suspensions with larger diameter and thickness of nanoparticles provided the highest increase in thermal conductivity (~130%) at 5 wt% loading; however, a viscosity increase of ~100 times makes this fluid impractical for heat transfer applications. The optimization of viscosity and thermal conductivity increases in nanofluids is required for development of practical nanofluids with advanced heat transfer.

Surface functionalization of GnP nanoparticles created core/shell graphite/graphene oxide. The optimization of nanoparticle surface chemistry and selection of particle morphology allowed production of a nanofluid that meets the property criteria for efficient power electronics coolant.

Such enhancements are possible with graphitic nanoparticles that are commercially available at reasonable costs. Graphitic nanofluids in a 50/50 mixture of ethylene

glycol and water showed morphology-dependent thermal conductivity; a thermal conductivity ratio between 1.5 and 2.3 at 5 wt% (room temperature). These results imply possibilities for dramatic improvement in power electronics cooling. Further, surface chemistry/functionalization provides better dispersion stability, lower viscosity, and higher thermal conductivity, and enhanced performance with temperature with graphitic nanoparticles.

The optimized and scaled-up nanofluid(s) was tested in a heat transfer loop, and the results confirmed the projected cooling efficiency while showing no fouling or erosion effects, demonstrating the commercial viability of the nanofluid technology.

Publications

1. **Effective thermal conductivity models for carbon nanotube-based nanofluids**, W. Yu, D.M. France, E.V. Timofeeva, D. Singh, *J. Nanofluids*, 2, 69–73 (2013).
2. **Comparative review of turbulent heat transfer of nanofluids**, W. Yu, D.M. France, E.V. Timofeeva, D. Singh, J.L. Routbort, *Int. J. Heat Mass Transfer*, 55, 5380–5396 (2012).
3. **Pumping power of 50/50 mixtures of ethylene glycol/water containing SiC nanoparticles**, J.L. Routbort, D. Singh, E.V. Timofeeva, W. Yu, D.M. France, R.K. Smith, *Ceramics Engineering and Science Proceedings*, 32 (10), 147 (2011).
4. **Nanofluids for heat transfer: An engineering approach**, E.V. Timofeeva, W. Yu, D.M. France, J.L. Routbort, *Nanoscale Res. Lett.*, 6, 182 (2011).
5. **Pumping power of nanofluids in a flowing system**, J.L. Routbort, D. Singh, E.V. Timofeeva, W. Yu, D.M. France, *J. Nanopart. Res.*, 13, 931–937 (2011).
6. **Base fluid and temperature effects on the heat transfer characteristics of SiC in ethylene glycol/H₂O and H₂O nanofluids**, E.V. Timofeeva, W. Yu, D.M. France, D. Singh, J.L. Routbort, *J. Appl. Phys.*, 109, 014914 (2011).
7. **Thermophysical property-related comparison criteria for nanofluid heat transfer enhancement in turbulent flow**, W. Yu, D.M. France, E.V. Timofeeva, D. Singh, J.L. Routbort, *Appl. Phys. Lett.*, 96, 213109 (2010).
8. **Particle size and interfacial effects on thermo-physical and heat transfer characteristics of water and a-SiC nanofluids**, E.V. Timofeeva, D.S. Smith, W. Yu, D.M. France, D. Singh, J.L. Routbort, *Nanotechnology*, 21, 215703 (2010).
9. **Mechanisms and models of effective thermal conductivities of nanofluids**, W. Yu, D.M. France, D. Singh, E.V. Timofeeva, D. Smith, J. Routbort, *J. Nanoscience and Nanotechnology*, 10, 1–26 (2010).

Patents

1. US 12/828,025 US Patent Application, **Heat transfer fluids containing nanoparticles**, Inventors: Dileep

- Singh, Jules L. Routbort, Wenhua Yu, Elena Timofeeva, David Smith and David France, filed July 2, 2009. Publication US20110001081 A1.
2. US 13/627,749 US Patent Application, **Nanoparticles for heat transfer and thermal energy storage**, Inventors: Dileep Singh, Cingarapu, Sreeram; Timofeeva, Elena V.; Moravek, Michael R., filed September 30, 2011. Publication US 20140084205 A1.
 3. US 14/257775 US Patent Application, **Advanced thermal properties of a suspension with graphene nano-platelets (GNPs) and custom functionalized F-GNPs**, Inventors: Elena V. Timofeeva; Dileep Singh, filed April 21, 2013.
 13. Timofeeva, E.V., et al., *The particle size and interfacial effects on thermo-physical and heat transfer characteristics of water based a-SiC nanofluids*. Nanotechnology, 2010. **21**(21): p. 215703–13.
 14. Yu, W., et al., *Thermophysical property-related comparison criteria for nanofluid heat transfer enhancement in turbulent flow*. Applied Physics Letters, 2010. **96**: p. 213109–3.
 15. Etherington, H., ed. *Nuclear Engineering Handbook*. 1958, McGraw-Hill Book Company, Inc.: New York, USA.
 16. Timofeeva, E.V., M.R. Moravek, and D. Singh, *Improving the heat transfer efficiency of synthetic oil with silica nanoparticles*. Journal of Colloid and Interface Science, 2011. **364**(1): p. 71–79.
 17. Timofeeva, E.V., et al., *Base fluid and temperature effects on the heat transfer characteristics of SiC in EG/H₂O and H₂O nanofluids*. Journal of Applied Physics, 2011. **109**: p. 014914 (5pp).

Tools and Data

References

1. Yu, W. and D. France, *Assessment of nanofluid properties required to eliminate one heat exchanger in HEV power electronics cooling*. 2013 (unpublished results).
2. O'Keefe, M. and K. Bennion, *A comparison of hybrid electric vehicle power electronics cooling options*. IEEE Vehicle Power and Propulsion Systems Conference, 2007.
3. K., B. and K. Kelly, *Rapid modeling of power electronics thermal management technologies*. IEEE Vehicle Power and Propulsion Systems Conference, 2009.
4. Timofeeva, E.V., *Nanofluids for heat transfer: Potential and engineering strategies*, in *Two Phase Flow, Phase Change and Numerical Modeling*, A. Ahsan, Editor. 2011, InTech. p. 435–450.
5. Sastry, N.N.V., et al., *Predicting the effective thermal conductivity of carbon nanotube based nanofluids*. Nanotechnology, 2008. **19**: p. 055704.
6. Choi, S.U.S., et al., *Anomalous thermal conductivity enhancement in nanotube suspensions*. Applied Physics Letters, 2001. **79**(14): p. 2252–2254.
7. Zhang, X., H. Gu, and M. Fujii, *Effective thermal conductivity and thermal diffusivity of nanofluids containing spherical and cylindrical nanoparticles*. Journal of Applied Physics, 2006. **100**(4).
8. Hwang, Y., et al., *Stability and thermal conductivity characteristics of nanofluids*. Thermochemica Acta, 2007. **455**(1-2): p. 70–74.
9. Yu, W., H.Q. Xie, and D. Bao, *Enhanced thermal conductivities of nanofluids containing graphene oxide nanosheets*. Nanotechnology, 2010. **21**(5): p. 055705.
10. Yu, W., et al., *Significant thermal conductivity enhancement for nanofluids containing graphene nanosheets*. Physics Letters A, 2011. **375**(10): p. 1323–1328.
11. Timofeeva, E.V., J.L. Routbort, and D. Singh, *Particle shape effects on thermophysical properties of alumina nanofluids*. Journal of Applied Physics, 2009. **106**: p. 014304.
12. Timofeeva, E.V., et al., *Nanofluids for heat transfer: An engineering approach*. Nanoscale Research Letters, 2011. **6**: p. 186.

VII.M. Experimental Investigation of Coolant Boiling in a Half-Heated Circular Tube – CRADA with PACCAR

Principal Investigator: Dileep Singh

Coworker: W. Yu

Organization: Argonne National Laboratory
 Address: 9700 S. Cass Ave., Argonne, IL 60439
 Phone: (630) 252-7361
 E-mail: wyu@anl.gov

DOE Program Manager: Lee Slezak

Phone: (202) 586-2335
 E-mail: Lee.Slezak@ee.doe.gov

VII.M.1. Abstract

Objectives

- Understand and quantify subcooled boiling heat transfer of engine coolant in heavy-duty vehicles.
- Experimentally determine subcooled flow boiling heat transfer rates and limits in the cylinder head region of heavy-duty vehicle engines.
- Develop predictive mathematical models for subcooled flow boiling heat transfer.
- Provide measurements and models for development/validation of computer codes developed for heavy-duty vehicle engines.

Major Accomplishments

- Completed the concept design, the technical design, and the fabrication of the experimental test facility and support systems.
- Completed the LabVIEW-based data acquisition system and test control hardware and software.
- Completed the heat loss calibrations of the experimental test facility.
- Completed single-phase convective heat transfer experiments and data reduction with three test fluids.
- Completed experiments and data reduction for subcooled flow boiling heat transfer with three test fluids for a range of flow rates.
- Developed three experimental data-based predictive correlations for the subcooled flow boiling heat transfer coefficient.
- Modified the experimental test facility by adding a pressurizing system for subcooled flow boiling tests at higher pressure.

Future Achievements

- Perform subcooled flow boiling experiments and data analyses for three test fluids at higher pressures of heavy-duty vehicle engines.



VII.M.2. Technical Discussion

Background

Started in FY 2010 as a CRADA between Argonne National Laboratory and PACCAR Inc./DAF Trucks N.V. (PACCAR/DAF), this project aims to provide heat transfer and critical heat flux measurements and models of coolant subcooled boiling in the cylinder head region of heavy-duty vehicle engines for development and validation of computer codes.

Introduction

Currently, the engine cooling systems in heavy-duty vehicles are designed to use an approximately 50/50 ethylene glycol/water (EG/W) mixture in the liquid state. Boiling is usually a phenomenon that has been avoided in conventional engine cooling systems in heavy-duty vehicles. However, while the conventional engine cooling systems in heavy-duty vehicles are designed to eliminate coolant saturation boiling, coolant subcooled boiling in the cylinder head regions is unavoidable at high thermal loads due to high metal temperatures. Because of the order-of-magnitude higher heat transfer rates, there is interest currently in using controllable nucleate-boiling precision cooling instead of conventional single-phase forced convection cooling in vehicle cooling systems under certain conditions or in certain areas to remove ever-increasing heat loads, to eliminate potential hot spots in engines, or to further optimize the parasitic losses of the coolant pump. Theoretical, numerical, and experimental investigations have been conducted on the potential and the practical applications of nucleate boiling cooling systems in heavy-duty vehicles. Consequently, there is great interest in the flow boiling heat transfer rates and limitations under these application conditions.

One of the unique characteristics of coolant subcooled boiling in the cylinder head regions of heavy-duty vehicle engines is that boiling generally occurs only on the cooling channel side facing the flame plate, because of the one-sided heating condition. Although many investigations have been conducted on subcooled flow boiling with one-sided heating, most effort has been focused on a fusion reactor system with

water as the coolant. Despite their importance in practical applications, theoretical and experimental studies of EG/W mixture boiling under engine cooling applications are generally lacking.

PACCAR/DAF is designing engines to take advantage of coolant subcooled boiling heat transfer below the critical heat flux, but the critical heat flux and the heat transfer rate have not been determined under realistic conditions. The experiments of this program address this situation by using a design specified by DAF. The data will be used in computational fluid dynamics models and designs by PACCAR/DAF, which could result in more efficient engines for heavy-duty vehicles. The objective of this project is to measure heat transfer rates during subcooled flow boiling of engine coolants in a geometry typical of valve bridge areas in heavy-duty vehicle engines under various operating conditions.

Approach

The general approach for this project is to experimentally investigate subcooled flow boiling of water and EG/W mixtures for heavy-duty vehicle engines.

The experimental apparatus used in this study is shown in Figure VII-82. It consists of a closed-loop system with main components of a pump, two preheaters, an experimental test section, a heat exchanger (cooler), and a flowmeter. The system was designed and fabricated to study the heat transfer of subcooled flow boiling of water and EG/W mixtures with heat supplied only to the bottom half surface of the experimental test section. As shown in the schematic diagram of the experimental apparatus in Figure VII-82, the test fluid was pumped through the test loop by a turbine pump (MTH Pumps, Model T31FAB), and the system was open to the atmosphere through the fill port at the flowmeter. The turbine pump was driven by an alternating-current adjustable-frequency driver (Dayton Electric Manufacturing Company, Model 1XC95), which made it possible to fine adjust flow rates through the experimental test section. Exiting the pump, the test fluid flowed through two preheaters arranged in series, in which, for a given test, the fluid temperature was raised to the desired subcooled level and monitored through two in-stream thermocouples. Each preheater, being made of an AISI type 304 stainless steel tubing with a 9.779-mm inside diameter, a 15.875-mm outside diameter, and a 3.9624-cm resistance-heated length, was heated by passing current through its wall. A direct-current power supply (Sorensen Company, Model DCR 16-625T) was used for each preheater, the output power of which could be regulated from 0 to 10 kW with a maximum voltage drop of 16 V and a maximum current of 625 A. As a safety precaution for protecting the preheaters from overheating, each was provided with a temperature interlock. At the end of each preheater, the wall temperature was measured and then fed to a high-temperature limit switch (Omega Engineering, Inc., Model CN8500) that would terminate power to the preheater when a preset upper-temperature limit was reached. After passing through the preheaters, the fluid entered the horizontal experimental test section. The experimental test section was heated with a

Model EMHP 40-450-D-11111-0933) by passing current through a 1.6256-mm diameter AISI type 304 stainless steel heating wire attached to the bottom half of the experimental test section surface, shown schematically in Figure VII-83. The output power could be regulated from 0 to 18 kW with a maximum voltage drop of 40 V and a maximum current of 450 A. The voltage drop across the heating wire was measured directly, and the current through the heating wire was determined from a measurement of the voltage drop across a shunt resistor with known resistance of 0.00001 Ω. The heat input to the experimental test section was calculated from the product of the voltage drop and the current. Electrical isolation for eliminating ground loops was provided for the preheaters and the experimental test section by short high-pressure hoses, designated ISO in Figure VII-82. The test fluid out from the experimental test section was cooled in the compact plate-and-frame heat exchanger (Affiliated Steam Equipment Company, Model WP1-14), which used laboratory water as a heat rejection fluid. The volumetric flow rate of the test fluid was measured by an electromagnetic flowmeter (Endress+Hauser, Inc., Model 10H08-A00A1RA0B4AA). A thermocouple probe (Omega Engineering, Inc.) upstream from the flowmeter provided a means to determine the density of the fluid and, subsequently, the mass flow rate of the fluid. Flowing out of the flowmeter, the test fluid returned to the pumps to close the test loop.

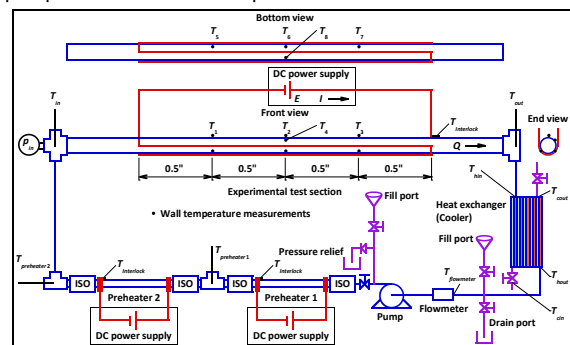


Figure VII-82: Schematic of heat transfer facility

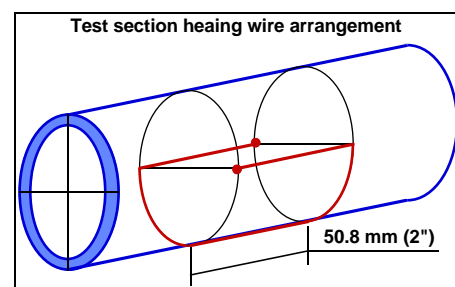


Figure VII-83: Test section heating wire arrangement

The experimental test section, shown schematically in Figure VII-82, was fabricated from an AISI type 1010 carbon steel tube with 10.9 mm inside diameter, 12.7 mm outside diameter, and a 50.8 mm heated length. The in-stream bulk fluid temperatures were measured at the inlet and the outlet of the experimental test section with type K thermocouple probes (Omega Engineering, Inc.). As shown schematically in Figure

VII-82, the wall temperatures were measured at eight locations along the experimental test section and around the test section circumference over the heated length with type K thermocouple junctions (Omega Engineering, Inc.) spot welded to the test section surface. The inlet fluid pressure was measured in all tests with a diaphragm pressure transducer (Omega Engineering, Inc., Model PX309–100A5V). These measurements were incorporated in the data reduction to calculate the average in-stream temperatures and the average wall temperatures. As a safety precaution for protecting the experimental test section from overheating, it was provided with a temperature interlock. At the end of the experimental test section, the wall temperature was measured and then fed to a high-temperature limit switch (Omega Engineering, Inc., Model CN8500) that terminates power to the experimental test section when a preset upper-temperature limit is reached.

A data acquisition system consisting of a personal computer and a multiplexor (Hewlett-Packard Company, Model HP 75000 Series B) was assembled to record outputs from all sensors. A data acquisition program, including all calibration equations and engineering-unit conversions, was written with LabVIEW graphical programming software. The data acquisition system functioned in two modes. During experimental test setup, it provided an on-screen display of analog signals from all sensors and graphs of representative temperature measurements as a function of time to facilitate determination of steady-state conditions. When the system reached a steady-state condition at desired parameters, it read all sensor-output voltages of in-stream temperatures, wall temperatures, ambient temperature, inlet pressure, volumetric flow rate, voltage drop across the heating wire, and current through the heating wire. These sensor-output voltages were read 30 times, averaged, and stored as a data set for future data reduction.

An overview of the completely fabricated heat transfer test facility is shown in Figure VII-83 before it was insulated.



Figure VII-84: Overview of heat transfer facility

Results

Heat Loss Calibration

Although the experimental test section is well insulated thermally from the atmosphere to minimize heat loss to the environment, the heat loss was not negligible during the flow

boiling heat transfer experiments because of the relatively high driving temperatures. Therefore, heat loss experiments were performed for the experimental test section walls up to the boiling heat transfer conditions, and the heat loss was subsequently incorporated into the data reduction procedures for single-phase convective and subcooled flow boiling heat transfer data. The heat loss was characterized through a special series of experiments with no fluid in the experimental test section. Power was applied to the experimental test section to bring its wall temperature to a selected level. The heat loss rate (q_{loss}), the input power required for maintaining the wall temperature at the selected value, was calculated from the product of the voltage drop across the heating wire and the current through the heating wire ($q_{loss}=EI$). This rate is related to the difference between the experimental test section wall temperature (T_w) and the ambient temperature ($T_{ambient}$). Experimental results confirmed a linear dependence on this temperature difference. Then, the heat loss rate was expressed approximately as $q_{loss}=c(T_w - T_{ambient})$, where the proportional constant c , which depends on the heat transfer coefficient and the heat transfer surface area between the experimental test section and ambient for this particular experimental apparatus, was determined from the heat loss experiments. Figure VII-85 shows the heat loss rate as a function of the driving temperature difference for the experimental test section. The test section heat loss was <3% of the applied input power to the experimental test section in all subsequent heat transfer tests.

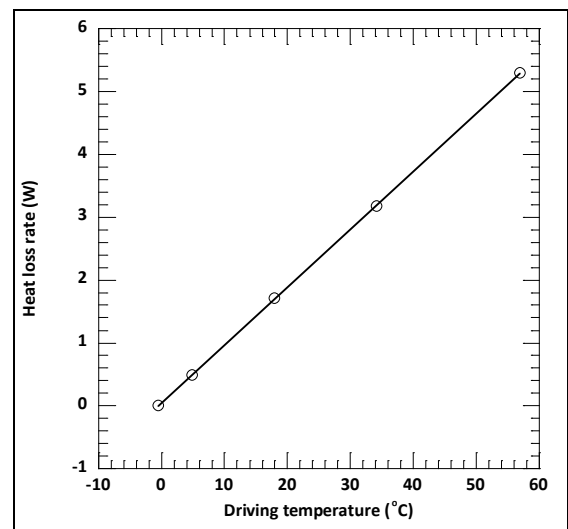


Figure VII-85: Heat loss calibration

Single-Phase Heat Transfer Experiments

Investigations of heat transfer under the condition of heat supplied only to one-half surface of an experimental test section are limited in the engineering literature, and no standard data reduction process exists. Therefore, to validate the test apparatus in this study and to establish a baseline, a series of single-phase heat transfer experiments was carried out prior to the subcooled flow boiling experiments. For the single-phase heat transfer experiments, the system pressure was kept near atmosphere pressure, similar to the subcooled flow boiling experiments. The single-phase heat transfer

experiments were performed under a turbulent flow condition mirroring the flow region of the subcooled flow boiling experiments, and the liquid heat transfer coefficients were correlated as functions of the Reynolds number (Re) and the Prandtl number (Pr) by modifying the Dittus-Boelter equation. As shown in Figure VII-86, where the heat transfer coefficients are plotted, the experimental data are in good agreement with the predicted values from the modified Dittus-Boelter equation, with a mean deviation of $<4\%$. Almost all experimental data are within $\pm 5\%$ of the predictions. The fact that modification was required to the Dittus-Boelter equation is not surprising because this equation is not based on one-sided heating conditions. The fact that different equations were needed for each fluid is also not surprising because the Dittus-Boelter equation was not developed for fluid mixtures. These equations were only used in the data reduction of this study to account for the single-phase heat transfer at the top of the experimental test section under subcooled boiling at the bottom.

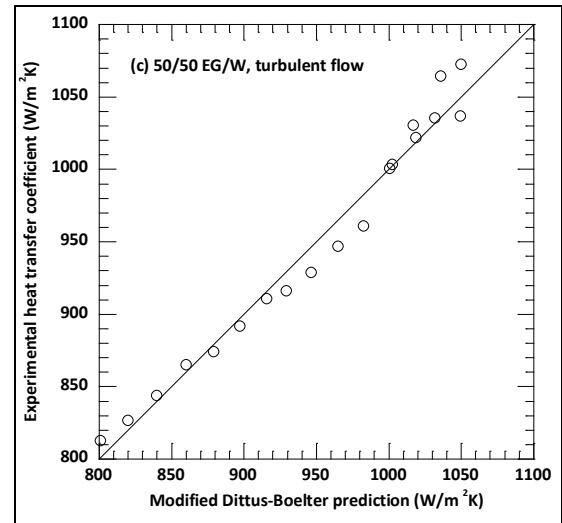
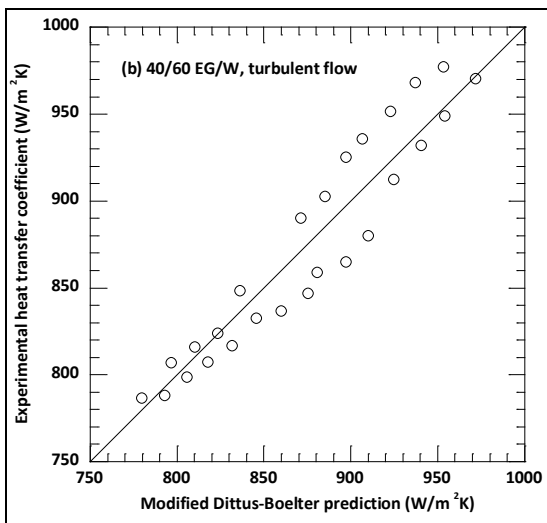
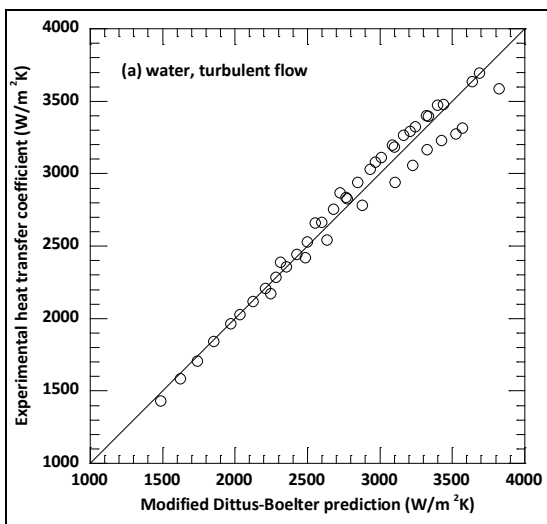


Figure VII-86: Experimental versus calculated turbulent heat transfer coefficients for (a) water, (b) 40/60 EG/W, and (c) 50/50 EG/W



In addition to the turbulent flow, single-phase heat transfer experiments were performed under the laminar flow condition with EG/W mixtures to establish a baseline for the subcooled laminar flow boiling that occurred at the lowest flow velocity with EG/W mixtures. The liquid heat transfer coefficients were correlated as a function of Re and Pr by modifying the Shah equation. As shown in Figure VII-87, where the heat transfer coefficients are plotted, the experimental data are in good agreement with the predicted values from the modified Shah equation, with a mean deviation of $<2\%$. All experimental data are within $\pm 5\%$ of the predictions.

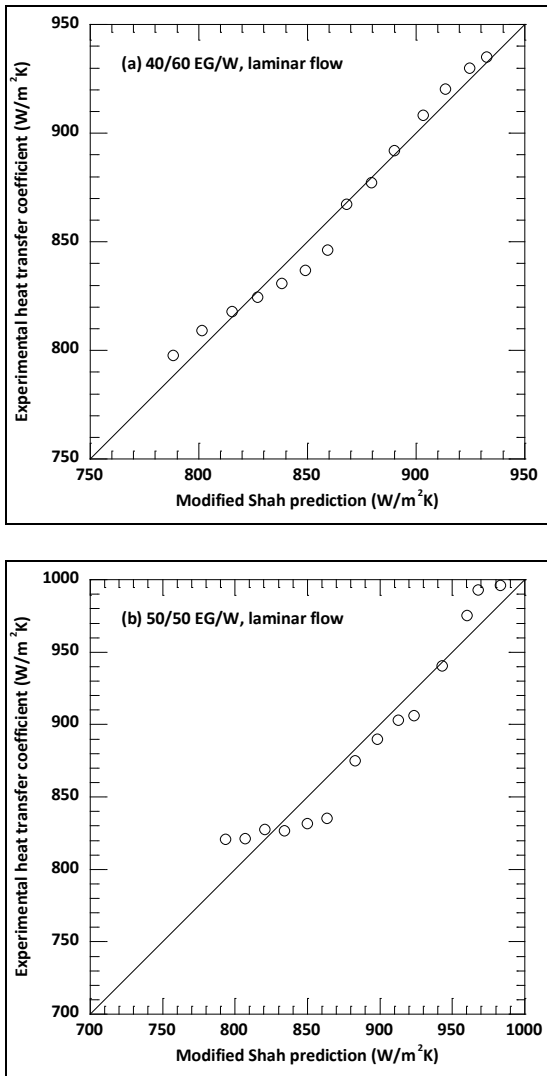


Figure VII-87: Experimental versus calculated laminar heat transfer coefficient for (a) 40/60 EG/W and (b) 50/50 EG/W

Subcooled Flow Boiling Heat Transfer

A series of subcooled flow boiling heat transfer experiments was conducted for several conditions: water under the turbulent flow condition with the Reynolds number in the range of 3500–51,000; 40/60 and 50/50 EG/W mixtures under the turbulent flow condition with the Reynolds number in the range of 2900–26,000; and 40/60 and 50/50 EG/W mixtures under the laminar flow condition with the Reynolds number in the range of 1400–2200. The inclusion of the 40/60 EG/W mixture was to account for deviations from the 50/50 EG/W mixture specification in practical cooling systems of heavy-duty vehicle engines. For each test fluid, the subcooled flow boiling heat transfer experiments were performed for parameters of five flow velocities and four fluid inlet temperatures. For each set of the subcooled flow boiling heat transfer experiments, the system pressure was kept close to atmospheric pressure through the open fill port at the flowmeter; the heating power of the preheaters was adjusted to maintain the test fluid inlet subcooling temperature at a desired level; and the heating power of the experimental test

section was increased progressively until the top wall temperature of the experimental test section reached the upper-temperature limit that was preset to avoid subcooled flow boiling on the top wall of the experimental test section. Because of this limitation, the subcooled flow boiling in this study is generally in the weak boiling range, especially for high flow velocities. For each test-section heating power increment, the test fluid changed gradually from heat transfer dominated by single-phase convection toward subcooled flow boiling. After enough time for the experimental system to reach a steady-state condition, all the test-related sensor outputs were averaged and recorded in a data set with appropriate engineering units for future data reduction, such as generating boiling curves and computing heat transfer coefficients.

According to the above experimental procedure for subcooled flow boiling, the top wall superheat was always below a certain threshold, and consequently, the top section heat transfer was single-phase convection for all test times, even when subcooled flow boiling occurred at the bottom section. Based on this assumption, the approach used for analyzing subcooled flow boiling heat transfer was to separate the overall heat transfer into two parts: top heat transfer and bottom heat transfer. The detailed results for boiling curves and boiling heat transfer coefficients are shown and discussed below.

Water Turbulent Flow Boiling Curves

A series of subcooled flow boiling heat transfer experiments was conducted for water under the turbulent flow condition at five flow velocities (0.125, 0.25, 0.5, 1, and 1.5 m/s) and four fluid inlet temperatures (75°C, 80°C, 85°C, and 90°C). The fluid inlet temperatures were chosen to obtain the inlet liquid subcooling in the range of approximately 10°C–25°C. The corresponding boiling curves are shown in Figure VII-88. The essential conclusion from Figure VII-88 is that, for the unique experimental setup of this study with heating only from the bottom of the experimental test channel, the heat transfer can generally be divided into a region dominated by single-phase convection and another region dominated by subcooled flow boiling. This condition is similar to heat transfer of fluids in channels with the all-around heating condition. Several other important characteristics related to the two regions can be seen from Figure VII-88. First, the wall superheats at which heat transfer changes from single-phase convection to subcooled flow boiling are at approximately 10°C. This transform temperature is most obvious for the lowest flow velocity and the lowest inlet liquid subcooling. Second, the boiling curves display different increase gradients for the two regions. Because of these different increase gradients, for the same heat flux increment, the wall superheat increment in the subcooled flow boiling region is smaller than that in the single-phase convection region. Third, for various inlet liquid subcooling levels, the boiling curves follow an approximately parallel pattern in the single-phase convection region but a gradually merging pattern in the subcooled flow boiling region. Moreover, due to the limitation of the wall superheat and, therefore, the experimental data for the subcooled flow boiling region in this study, the merging pattern is most evident at the lowest flow velocity, then gradually becomes less noticeable with the increase of the flow velocity, and is almost unnoticeable at the highest flow velocity. Fourth,

the boiling curves with the highest inlet temperature or the lowest inlet liquid subcooling show the sharpest trend change at the transform temperature from single-phase convection to subcooled flow boiling due to the above-mentioned gradually merging pattern. Finally, based on the gradually merging pattern in the subcooled flow boiling region, it is expected that the influence of the inlet liquid subcooling on overall heat transfer gradually becomes less significant with the increase of subcooled flow boiling.

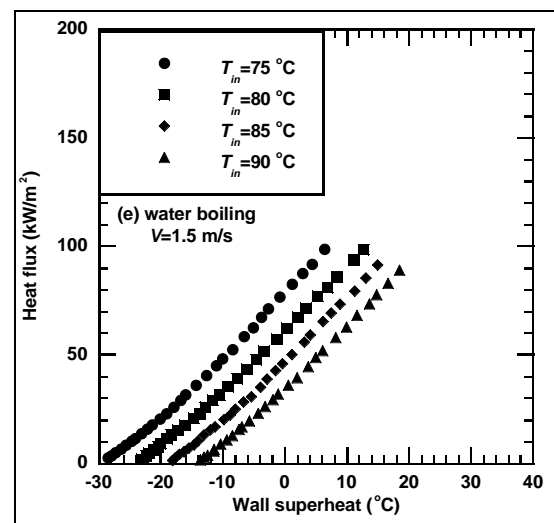
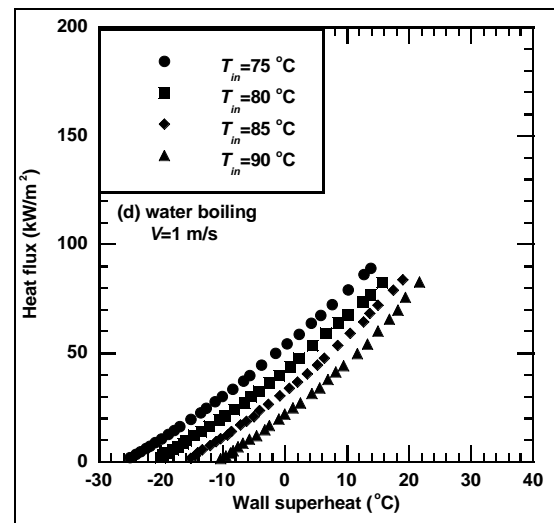
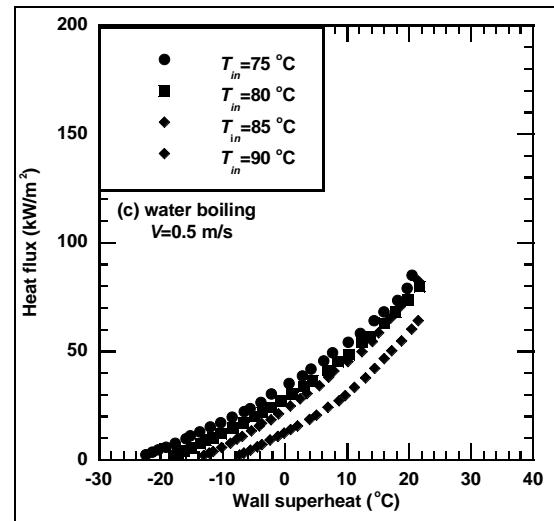
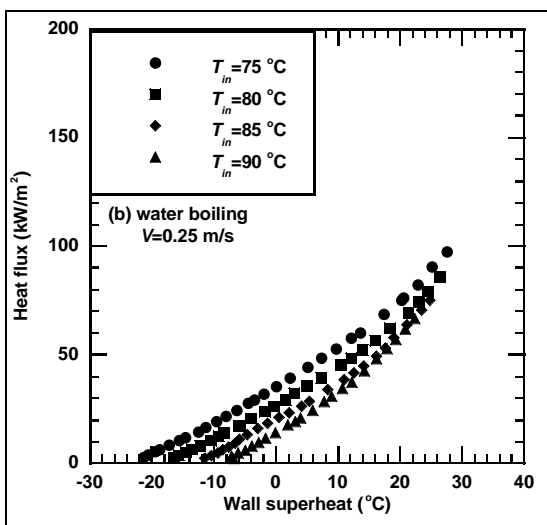
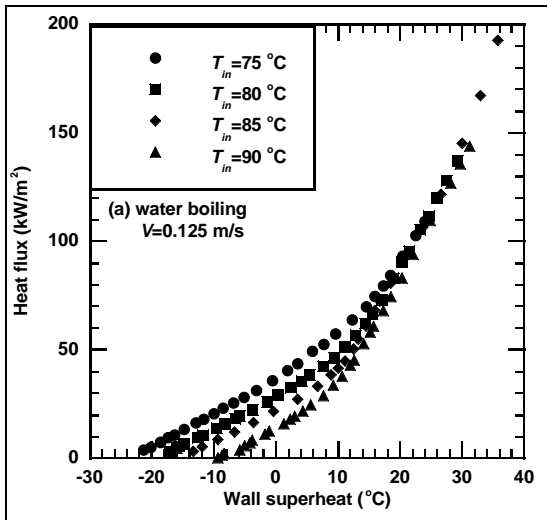


Figure VII-88: Water turbulent flow boiling curves at 75°C–90°C and (a) 0.125 m/s, (b) 0.25 m/s, (c) 0.5 m/s, (d) 1 m/s, and (e) 1.5 m/s

EG/W Mixture Turbulent Flow Boiling Curves

A series of subcooled flow boiling heat transfer experiments was conducted for 40/60 and 50/50 EG/W mixtures under the turbulent flow condition at four flow velocities (0.25, 0.5, 1, and 1.5 m/s) and four fluid inlet temperatures (80–82°C, 85–87°C, 90–92°C, and 95–97°C). The fluid inlet temperatures were chosen to obtain the same inlet liquid subcooling as that of water subcooled flow boiling in the range of approximately 10°C–25°C. The corresponding boiling curves are shown in Figure VII-89 for the 40/60 EG/W mixture and Figure VII-90 for the 50/50 EG/W mixture. Several characteristics can be seen from Figure VII-89 and Figure VII-90. First, the differences of the boiling curves between the 40/60 EG/W mixture and the 50/50 EG/W mixture are generally small. Based on this finding, it is expected that a volume concentration deviation of ethylene glycol in practical vehicle cooling systems will not change coolant subcooled flow boiling much. Second, the general trends identified above for water subcooled flow boiling are also applicable and are also more observable at lower flow velocities for the EG/W mixture with subcooled flow boiling. Finally, for the same wall superheat, the heat flux for water is higher than that for EG/W mixtures. This finding is consistent with the fact that water has a higher heat capacity than EG/W mixtures.

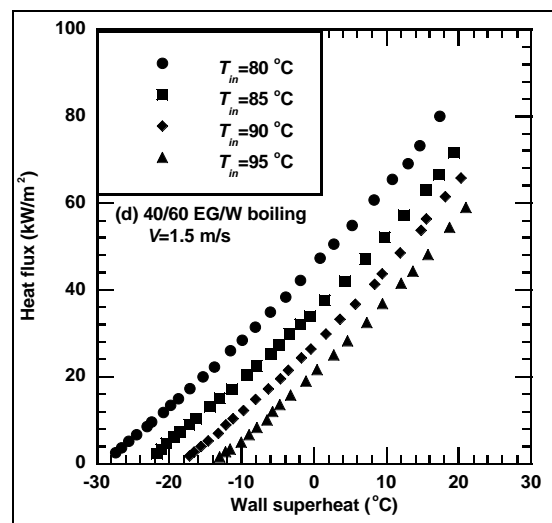
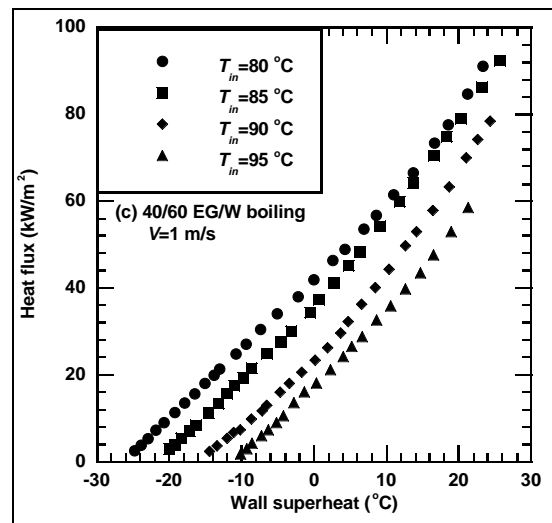
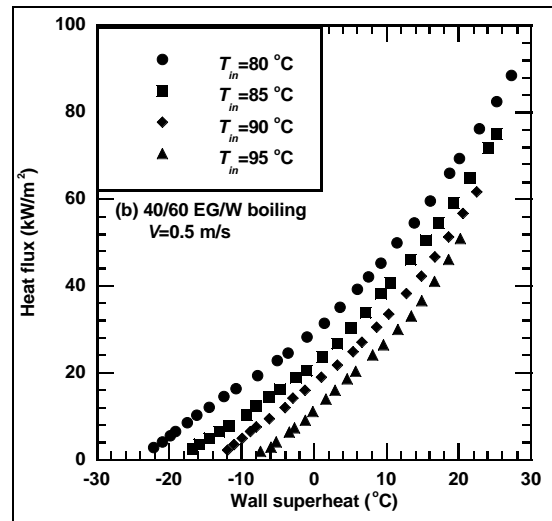
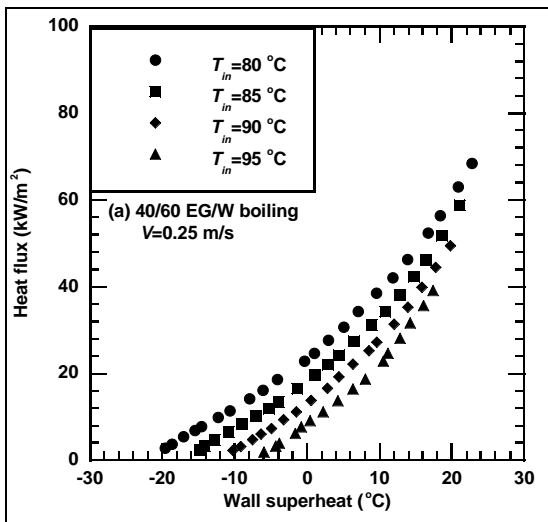


Figure VII-89: Turbulent flow boiling curves for 40/60 EG/W mixture at 80°C–95°C and (a) 0.25 m/s, (b) 0.5 m/s, (c) 1 m/s, and (d) 1.5 m/s

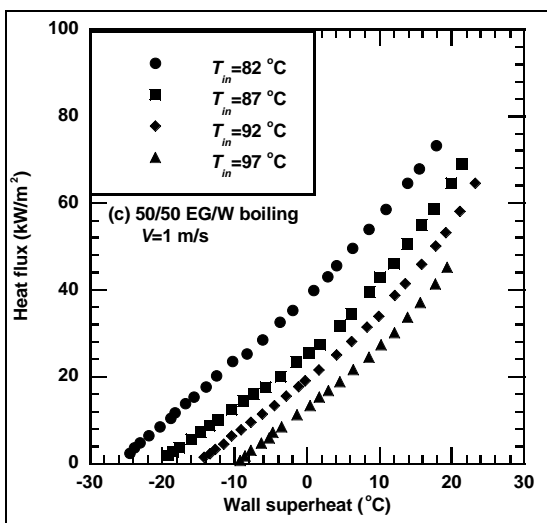
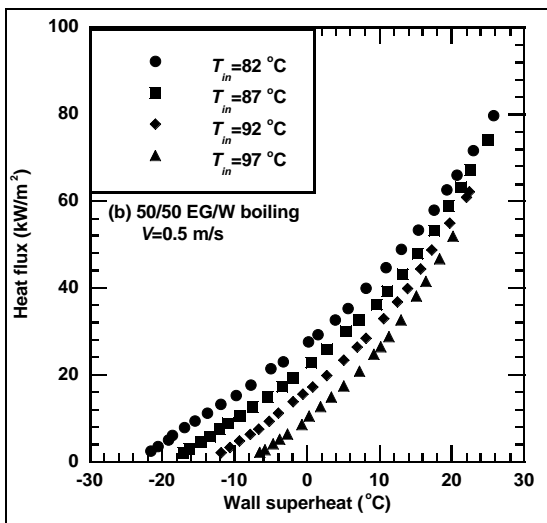
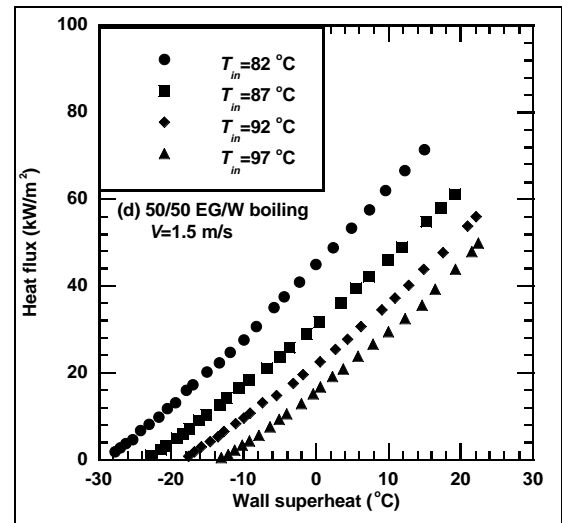
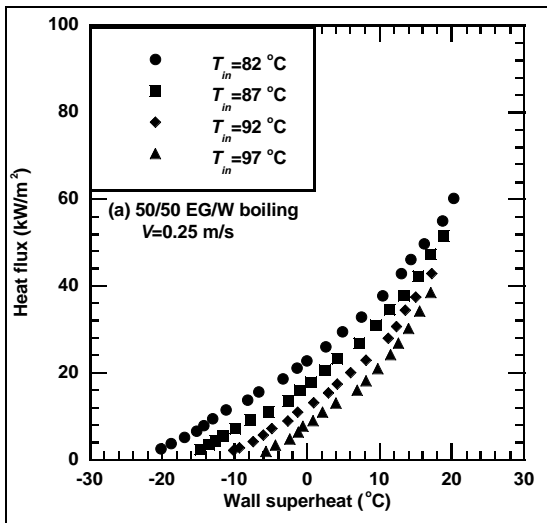


Figure VII-90: Turbulent flow boiling curves for 50/50 EG/W mixture at 82°C–97°C and (a) 0.25 m/s, (b) 0.5 m/s, (c) 1 m/s, and (d) 1.5 m/s

EG/W Mixture Laminar Flow Boiling Curves

A series of subcooled flow boiling heat transfer experiments was conducted for 40/60 and 50/50 EG/W mixtures under the laminar flow condition at a flow velocity of 0.125 m/s and four fluid inlet temperatures (80–82°C, 85–87°C, 90–92°C, and 95–97°C). The fluid inlet temperatures were chosen to obtain the same inlet liquid subcooling as that of water subcooled flow boiling in the range of approximately 10°C–25°C. The corresponding boiling covers are shown in Figure VII-91a for the 40/60 EG/W mixture and Figure VII-91b for the 50/50 EG/W mixture. Figure VII-91 shows that the boiling curves for the EG/W mixture with subcooled flow boiling in laminar flow are very similar to those for the EG/W mixture with subcooled flow boiling in turbulent flow; however, the boiling curve trends mentioned above are more observable for the EG/W mixture with subcooled flow boiling in laminar flow, due obviously to its lower flow velocity.

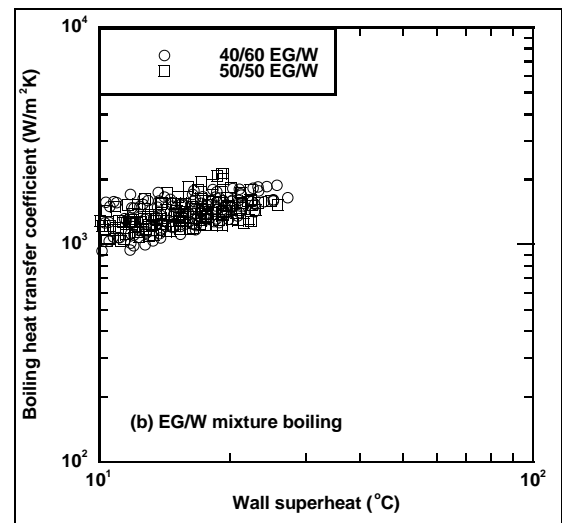
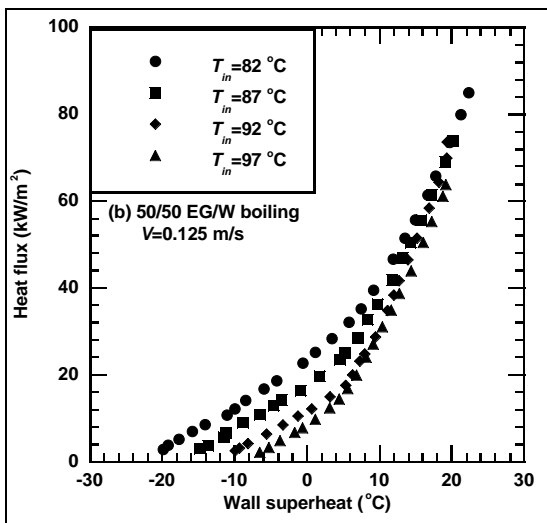
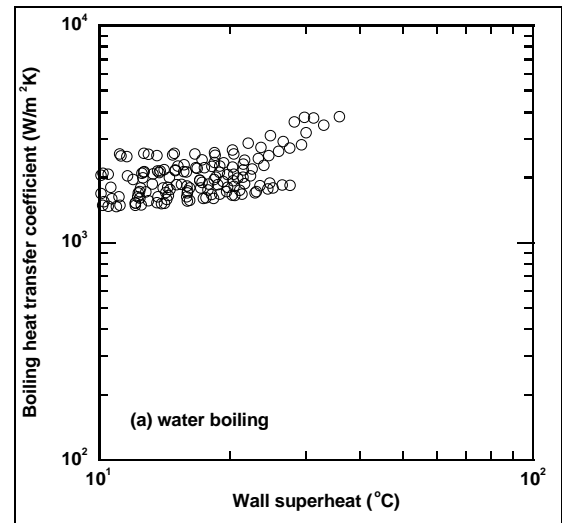
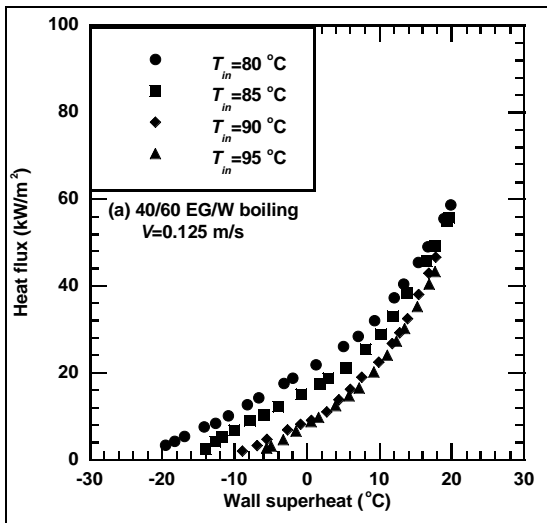


Figure VII-91: Laminar flow boiling curves for (a) 40/60 EG/W and (b) 50/50 EG/W mixtures

Figure VII-92: Boiling heat transfer coefficients for (a) water and (b) EG/W mixtures

Boiling Heat Transfer Coefficients

The subcooled flow boiling heat transfer coefficients with the wall superheat higher than the transform temperature are shown in Figure VII-92a for water and Figure VII-92b for EG/W mixtures as a function of the wall superheat. There are several features that can be seen from Figure VII-92. First, the subcooled flow boiling heat transfer coefficients increase with the wall superheat, indicating the further development of subcooled flow boiling with the increase of the channel wall temperature. Second, the differences of the subcooled flow boiling heat transfer coefficients between the 40/60 EG/W and the 50/50 EG/W are insignificant. This finding is due to the relatively small difference of their ethylene glycol concentrations and is consistent with their boiling curve characteristics. Finally, for the same wall superheat, the subcooled flow boiling heat transfer coefficients for water are larger than those for EG/W mixtures. This effect is caused by the higher heat flux for water boiling than for EG/W mixture boiling under the same wall superheat.

Many predictive correlations have been developed for the heat transfer coefficients with subcooled flow boiling. However, they were generally developed for the all-around heating condition, not for the one-side heating condition, especially not for the mixture boiling with one-side heating as in this study. While the correlations in the engineering literature may give reasonable predictions of the experimental data in this study, the prediction errors are expected to be high, as shown in our previous report. Therefore, better predictive correlations based on the experimental data in this study were developed. The details of the proposed correlations are discussed below.

Boiling Heat Transfer Coefficient Correlations

For the correlation of the experimental data in the present investigation of subcooled water and EG/W mixture flow boiling under the condition of heating supplied only from the bottom of the experimental test section, the wall superheat was correlated as functions of the boiling heat flux, the convective heat transfer coefficient predicted by the Dittus-Boelter correlation, the EG volume concentration, and a

boiling number term based on the experimental data of water, EG/W mixtures (both 40/60 and 50/50), and all three tested fluids. Figure VII-93 shows the boiling number term, $f(Bo)$, computed from the experimental wall superheats for water and EG/W mixtures. The predicted heat transfer coefficients for subcooled flow boiling based on the $f_w(Bo)$ for water and $f_m(Bo)$ for EG/W mixtures are compared with the experimental data in Figure VII-94a and Figure VII-94b, respectively. As can be seen, almost all of the experimental data are within $\pm 20\%$ of the predictions, and the mean deviations for both water subcooled flow boiling and EG/W mixture subcooled flow boiling are $<10\%$.

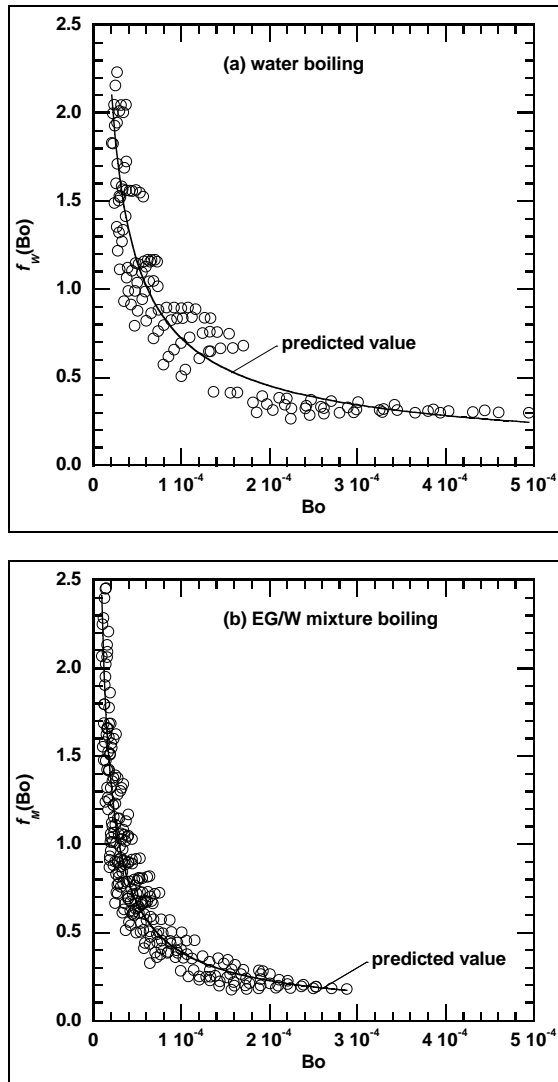


Figure VII-93: Correlation of boiling number term for (a) water and (b) EG/W mixtures

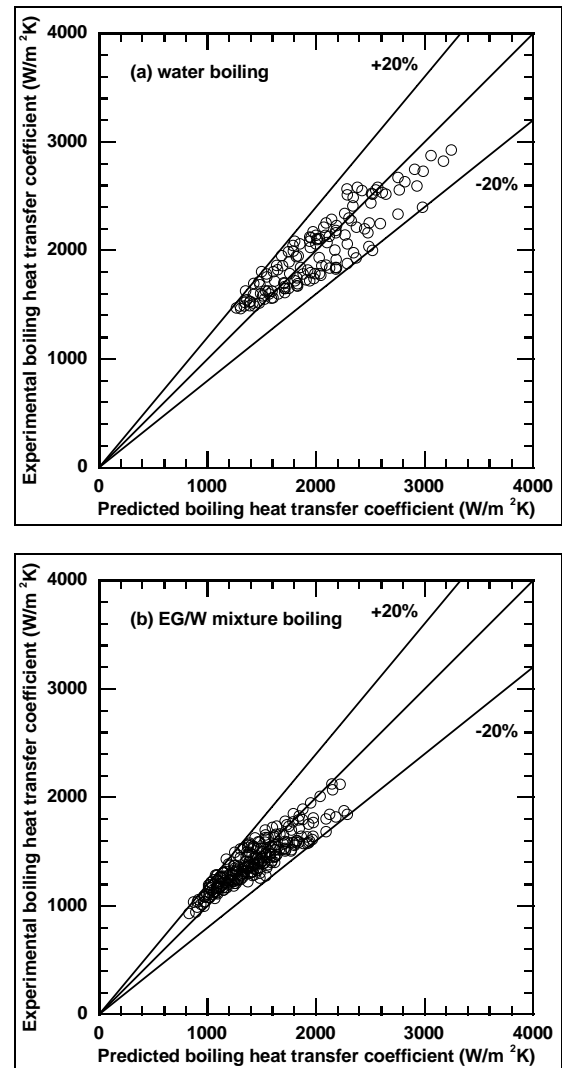


Figure VII-94: Experimental versus predicted heat transfer coefficient for (a) water and (b) EG/W mixtures

Figure VII-95 shows the $g(Bo)$ computed from the experimental wall superheats for all three tested fluids. The predicted subcooled flow boiling heat transfer coefficients based on $g(Bo)$ for all three tested fluids are compared with the experimental data in Figure VII-96. As can be seen, almost all of the experimental data are within $\pm 20\%$ of the predictions, and the mean deviations are $<10\%$.

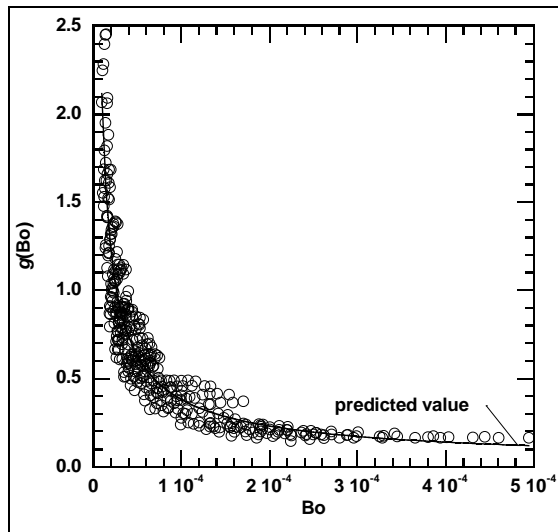


Figure VII-95: Correlation of boiling number term for all data

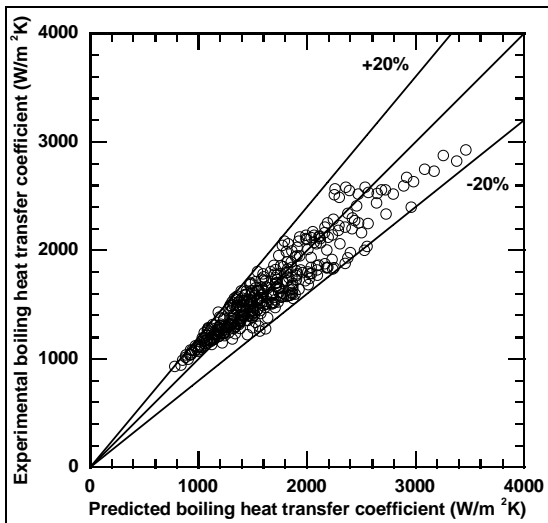


Figure VII-96: Experimental versus predicted heat transfer coefficient for all data

Wall Temperature Simulations

To further validate the proposed predictive correlations for the heat transfer coefficients with subcooled flow boiling, numerical simulations were conducted to compute wall temperatures and compare them with the experimental measurements. The numerical simulations were carried out using the COMSOL Multiphysics commercial software with the model boundary condition of the heat transfer coefficient computed by the above proposed correlations. Figure VII-97 shows the experimental and predicted wall temperatures at the location of thermocouple 6 with 50/50 EG/W mixture boiling at various flow velocities and two fluid inlet temperatures. For the simulation results of Figure VII-97, the test section heat fluxes were the same as the experimental values, and the heat transfer coefficients as the model boundary condition were computed by the predictive correlation based on $g(Bo)$ for all tested fluids. It can be seen

from Figure VII-97 that the simulation results agree with the experimental measurements very well, with differences <6%.

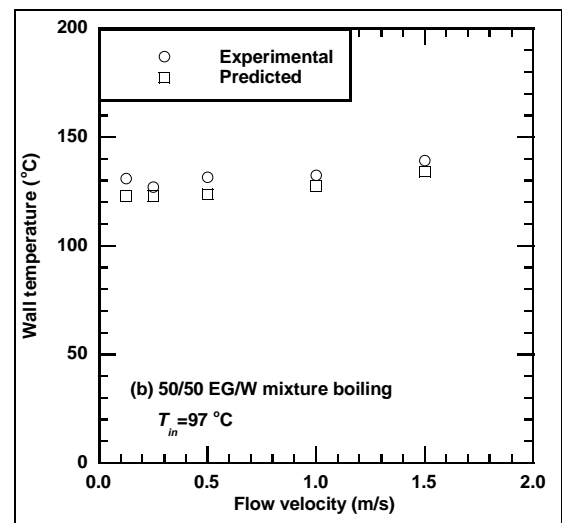
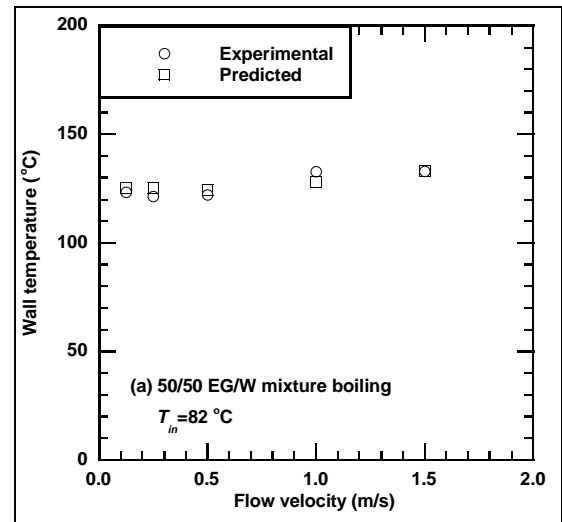


Figure VII-97: Experimental and predicted wall temperatures for 50/50 EG/W at (a) 82°C and (b) 97°C

Experimental Test Facility Modifications

To prepare for experimental tests at higher pressure for subcooled flow boiling of water and EG/W mixtures, the experimental test facility was modified by addition of a pressurizing system. As shown in Figure VII-98, a bladder-type hydraulic accumulator (Greer Hydraulics, Inc.), connected to a high-pressure nitrogen cylinder, will be used to pressurize and control the fluid pressure in the experimental test section within the experimental specifications by adjusting the pressure in the accumulator. As a safety precaution for protecting the experimental test section from overpressure, a pressure relief valve is attached to the accumulator with a preset relief pressure of 100 psi, high enough for the experimental test pressure requirements of <50 psi.



Figure VII-98: Pressurizing system

Conclusions

In summary, the design and fabrication of the PACCAR heat transfer test facility have been finished; the LabVIEW-based data acquisition system and test control hardware and software have been established; the experiments and data reduction for single-phase convective heat transfer with three test fluids have been completed; the experiments and data reduction for subcooled flow boiling with three test fluids have been completed; three predictive correlations have been developed for the subcooled flow boiling heat transfer coefficient of water and EG/W mixtures; and the experimental test facility has been modified for higher-pressure subcooled flow boiling experiments with water and EG/W mixtures. The project is on schedule. The future work will be focused on experimental tests, data reduction, and correlation developments of higher-pressure subcooled flow boiling of water and EG/W mixtures.

VII.M.3. Products

Publications

1. Wenhua Yu, David M. France, Dileep Singh, Roger K. Smith, Jason Ritter, Thomas Vijlbrief, and Yves Menger, "Subcooled Flow Boiling of Ethylene Glycol/Water Mixtures in a Bottom-Heated Tube," *International Journal of Heat and Mass Transfer* 72 (May 2014) 637–645.
2. W. Yu, D. M. France, W. Zhao, D. Singh, and R. K. Smith, "Investigation of Subcooled Flow Boiling Heat Transfer to Water and Ethylene Glycol/Water mixtures in a Bottom-Heated Tube," to be submitted to *Experimental Heat Transfer*.

VII.N. Thermal Control through Air-Side Evaporative Heat Removal

Principal Investigator: Dileep Singh

Coworker: W. Yu
Argonne National Laboratory
9700S. Cass Ave.
Argonne, IL 60439
Phone: (630) 252-5009
E-mail: dsingh@anl.gov

DOE Program Manager: Lee Slezak

Phone: (202) 586-2335
E-mail: Lee.Slezak@ee.doe.gov

VII.N.2. Technical Discussion

Background

This project is aimed at exploring the possibilities of reducing cooling system size and, therefore, aerodynamic drag on heavy-duty trucks by using evaporative cooling under extreme temperature, load, and road grade conditions that would be encountered in the United States.

Introduction

Aerodynamic drag is a major contributor to fuel consumption in heavy-duty trucks, especially at highway speeds. Aerodynamic drag, i.e., the resistance to a truck's movement through the air, consists of two main components, pressure drag and shear drag. The shear drag for trucks usually is small compared to the pressure drag, and the basic shape of a truck imposes the pressure drag on the vehicle. Typically, a high-pressure zone is created in the front of the tractor due to a stagnation effect, and a low-pressure zone is created in the rear of the truck, both resulting in pressure drag. The frontal shape of the tractor is dictated in large part by the radiator, resulting in a large stagnation area. The method for reducing aerodynamic drag on trucks proposed in this study is to modify the frontal shape of the tractor by using a hybrid radiator-cooling system, a combination of conventional air-side finned surface cooling and active evaporative water cooling.

Approach

Figure VII-99b shows a hybrid radiator along side a conventional radiator in Figure VII-99a. The example hybrid system shown in Figure VII-99b is similar to the conventional radiator, both having vertical coolant channels and fins between them on the air side. However, the channels have been extended beyond the fins on the downstream air side of the radiator. Liquid water flows downwards by gravity along the extended surfaces, providing evaporative cooling to the engine coolant. The hybrid radiator also has a liquid supply and distribution system, not shown in Figure VII-99b.

VII.N.1. Abstract

Objectives

- Explore possibilities of using evaporative cooling in air-side heat removal for radiator applications.
- Determine potential increase of air-side heat removal rate in radiator using evaporative cooling.
- Determine potential reductions in radiator size using evaporative cooling.
- Optimize designs of radiator evaporative fin.

Major Accomplishments

- Developed theoretical models for analyses of radiator air-side evaporative cooling.
- Completed detailed calculations to establish the benefits of the concept.
- Conducted numerical simulations for investigations of the air flow effect on water droplets.
- Designed and fabricated an experimental test system simulating the air flow of moving vehicles.

Future Achievements

- Investigate coating or surface treatment methods and materials to generate proper surface tension.
- Experimentally measure the droplet contact angle.
- Experimentally investigate droplet evaporation and movement under the influence of the air flow of moving vehicles.



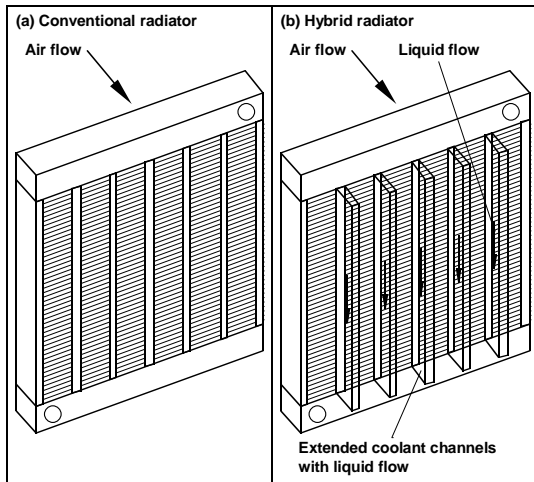


Figure VII-99: Hybrid Radiator System

Figure VII-100 shows a top view of a section of the hybrid radiator. In this schematic, the extended channel surfaces are cooled by evaporating water flowing downwards by gravity into the plane of the figure. The combination of the conventional cooling from the finned surfaces and the evaporative cooling from the extended channel surfaces equals the total heat transfer from the radiator to the atmosphere. Under the thermal design condition, both cooling mechanisms would be functioning. However, at most thermal loads below the design condition, only the conventional air-side finned surface cooling would be required. Thus, the active cooling of the water evaporation would be used only at or very near the thermal design condition.

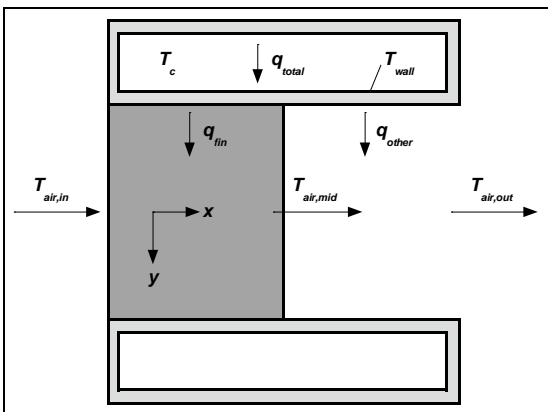


Figure VII-100: Top View of a Section of the Hybrid Radiator

This limited use of the active evaporative cooling component of the hybrid system is important because evaporative cooling requires a supply of water. Using evaporative cooling only at or very near the thermal design condition serves to optimize the parameters of reduced radiator size (or increased maximum radiator heat transfer) and minimized water use/transport.

Results

Heat Transfer Increase

Heat removal rates were calculated from the radiator of Figure VII-99 and Figure VII-100 with a 221.8-kW heat rejection rate, where the outside air temperature was fixed at 47°C. The heat removal rate as a function of water consumption rate generated using falling liquid film evaporation is shown in Figure VII-101. At water consumption rates of 76 L/h (20 gal/h) and 189 L/h (50 gal/h), the total heat removal rate is increased by 42 kW and 102 kW, respectively. These values are equivalent to a heat removal rate increase of 19% and 46%, respectively. A small part of this increase (~3 kW) is due to the increased surface area associated with the coolant channel extensions of the hybrid radiator design. The rest of the sizable increase in the heat removal rate is due to evaporative cooling. At both flow rates, the cooling water completely evaporated before reaching the bottom of the radiator.

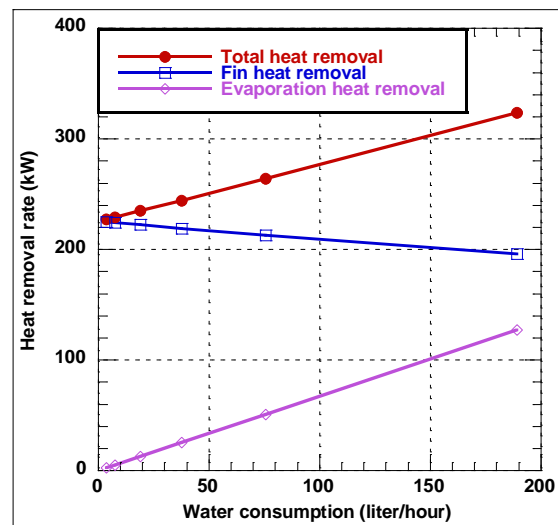


Figure VII-101: Radiator Heat Transfer

Radiator Size Reduction

Figure VII-102 shows the effect of the radiator width on the water consumption rate, calculated from a thin falling film under the conditions of an engine speed of 1700 rpm with a 221.8-kW heat rejection rate and outside air temperature of 47°C. The original width of the radiator in this study was 988 mm. As shown in Figure VII-102, at water consumption rates of 76 L/h (20 gal/h) and 189 L/h (50 gal/h), the width could be reduced to 778 mm and 478 mm, respectively. These values correspond to radiator frontal area decreases of 21% and 52%, respectively. In each case studied, the film was assumed to completely evaporate before reaching the bottom of the radiator. Using droplets instead of a film will give the same potential for area reduction as long as the droplets completely evaporate. Note that if the frontal area of the tractor were modified, to account for the reduced radiator size that can be achieved by the hybrid cooling system, aerodynamic drag would also be reduced, thereby increasing fuel efficiency.

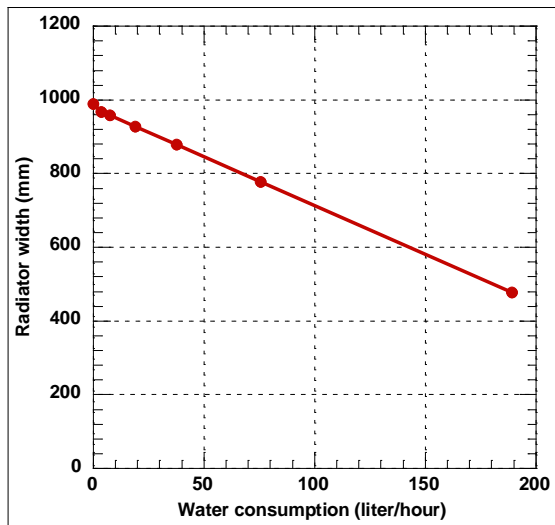


Figure VII-102: Effect of Radiator Size

Radiator Design Optimization

The design condition for truck and automobile radiators usually is the most severe condition possible: the highest air temperature and the steepest road grade. Many vehicles may never encounter conditions found at places such as Baker Grade in California or Union Pass in Arizona on a hot summer afternoon. A good potential utilization of evaporative cooling is to size the finned portion of the radiator for an alternative design condition corresponding to a steep road grade away from desert hills. Thus, water for evaporative cooling would be needed only when a vehicle travels through desert hills under extremely hot conditions. An 11 km (7-mile) stretch of land along Interstate Highway 24 near Monteagle, Tennessee, is an example of a steep road grade that could be used for the alternative design condition for the finned portion of the radiator. According to the typical meteorological year for Chattanooga, Tennessee, near Monteagle, the highest temperature can reach 37°C. If the radiator were sized for this location with the same coolant temperatures and heat transfer rates, then the radiator could be 22% smaller in width compared to that for the Baker Grade design condition. Thus, on the majority of roads in the United States, the smaller radiator would be sufficient. Under conditions of 47°C and constant full engine power for a long period of time, the water flow rate of approximately 76 L/h (20 gal/h) would be needed to remove the remainder of the heat. Since it takes less than one hour to traverse 40 km (25 miles) at Baker Grade and 48 km (30 miles) at Union Pass, the amount of water consumed would be less than 76 L (20 gal) for either condition with this design modification.

Effect of Surface Contact Angle

At a 76 L/h (20 gal/h) flow rate, the actual flow rate on each extended surface of the hybrid radiator is only 0.107 mL/s. At this low flow rate, the liquid film across the 20 mm radiator extension surface is only 0.11 mm thick and has a tendency to break up into rivulets or droplets, such as streaks. Because of this tendency, an analysis was performed with the evaporating liquid film replaced by evaporating discrete droplets falling downwards along the extended radiator

channel surfaces. Such droplets have good potential to be maintained at the required thickness. For 100% evaporation of the droplets as they reach the bottom of the radiator, the amount of additional heat transfer using the droplets is similar to that using the falling film.

The droplet evaporation results show that the thickness of the droplets from the radiator extension surfaces is the most important parameter governing both the evaporation rate of the droplets and the speed at which the droplets travel along the surfaces. As shown in Figure VII-103, the droplet moves downwards under the influence of gravity. On the basis of this model, the droplet evaporation percentage was determined as a function of the initial contact angle (a key factor for the thickness of the droplet). It can be seen in Figure VII-104 that a small droplet contact angle or equivalent small droplet thickness is necessary for complete evaporation.

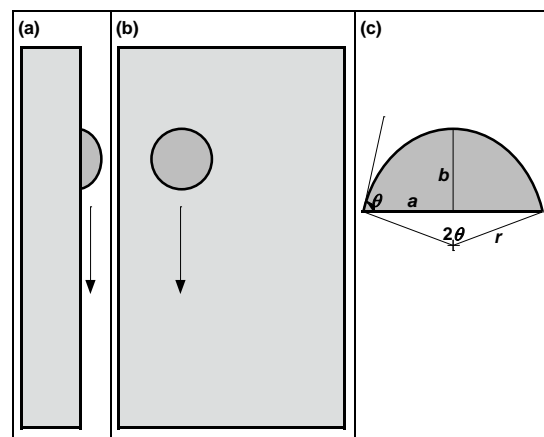


Figure VII-103: Droplet Movement

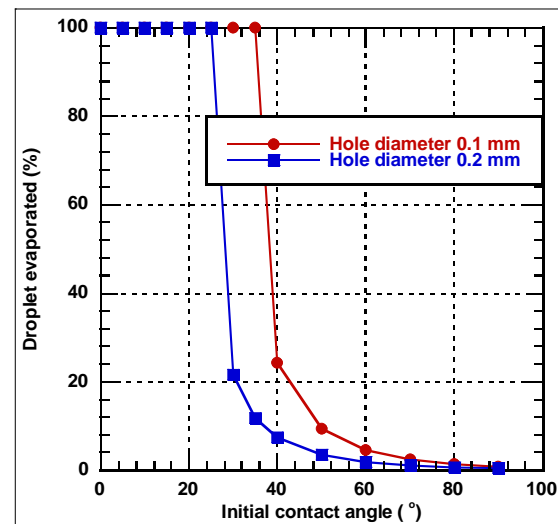


Figure VII-104: Droplet evaporation

Air Flow Effect on Droplet Movement

For a moving vehicle, the droplet in the hybrid system is under the influence of the drag force in addition to gravity. As shown in Figure VII-105, the droplet moves downwards and in the air flow direction during the evaporation process. The droplet movement is dependent on the force balance

among gravity (F_g), air drag force (F_d), and wall shear force (F_s). These forces and the velocity (u) are related by the following equations for a droplet volume of V :

$$\begin{cases} F_d - F_s \frac{\bar{u}_x}{\sqrt{\bar{u}_x^2 + \bar{u}_z^2}} = \rho_w V \frac{d\bar{u}_x}{dt} \\ F_g - F_s \frac{\bar{u}_z}{\sqrt{\bar{u}_x^2 + \bar{u}_z^2}} = \rho_w V \frac{d\bar{u}_z}{dt} \end{cases}$$

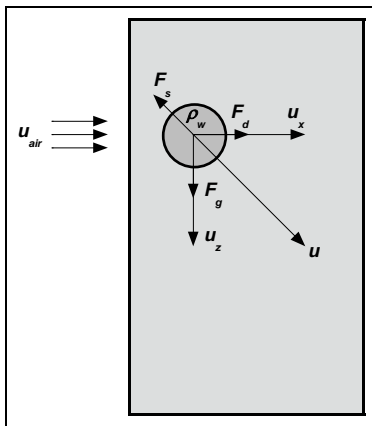


Figure VII-105: Air flow effect

To analyze the air flow effect on droplet movement, numerical simulations for various air flow speeds and droplet hole sizes were conducted with the commercial software COMSOL Multiphysics. Figure VII-106 shows the evaporation percentage of the droplet as a function of its initial contact angle for an air flow speed of $u_{air}=35$ mph at an extended surface width of 20 mm with the droplet hole sizes of 0.1 mm and 0.2 mm. As can be seen from Figure VII-106, droplets with a small initial contact angle were able to stay on the surface until they completely evaporated. Thus, the droplet generation and surface characteristics of the radiator extension surface must produce a small initial drop thickness for the most efficient operation of the hybrid radiator-cooling system. This condition requires a small droplet size and a small surface contact angle.

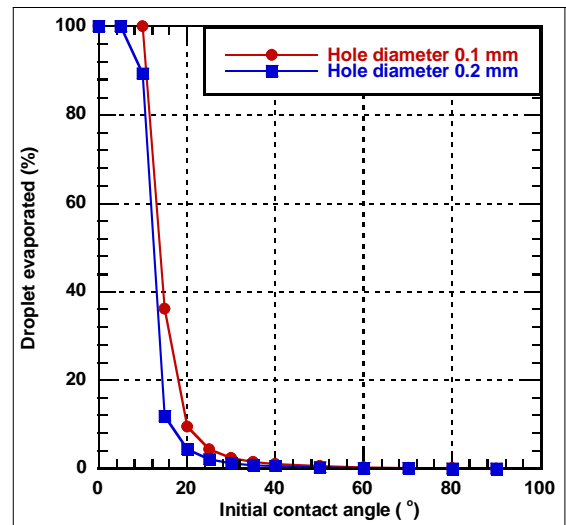


Figure VII-106: Droplet Evaporation with Air Flow Effect

There are several ways to increase the droplet evaporation percentage: (a) larger width of the extended surface, which is usually limited by the available space, (b) frontal extended surface arrangement instead of rear extended surface arrangement, which increases the effective surface width for droplet movement, and (c) smaller surface contact angle, which reduces the air drag force and enhances evaporation. Because the surface contact angle for the common radiator material 3003 aluminum alloy is about 90°, surface treatment or coating will be necessary to reduce the surface contact angle to acceptable levels. Current technologies are able to attain such levels. Therefore, the third option provides good potential for generating droplets with small thicknesses and achieving effective evaporative cooling of vehicle engines.

Experimental Test System

The experimental test system shown in Figure VII-107 was designed and fabricated to investigate the evaporation and movement of droplets under the air flow of moving vehicles. Experiments conducted using this experimental test system can study the effects of the surface contact angle, the initial droplet size, and the air flow velocity on the evaporation and movement of droplets. The experimental test system consists of mainly an enclosed experimental test system housing, a radiator, a fan, an experimental test strip, a droplet dispersing subsystem, a camera, a computer for controlling the droplet dispersing subsystem and for collecting experimental data, and a direct-current power supply (Electronic Measurements, Inc., Model EMHP 40-450-D-11111-0933, not shown in the photograph) for heating the test strip.

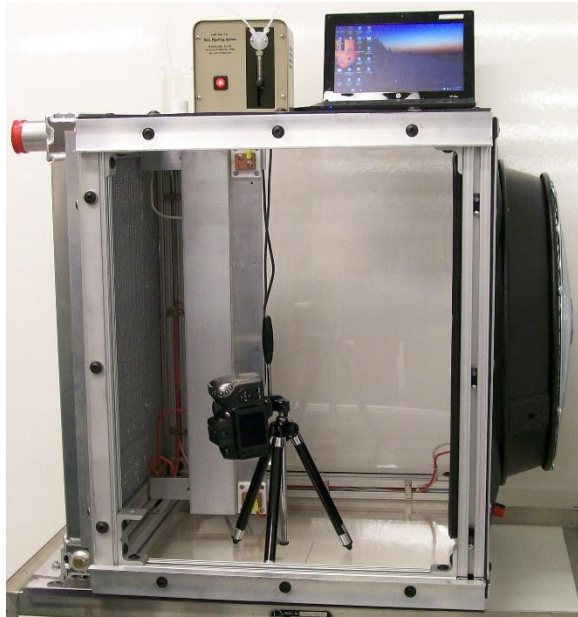


Figure VII-107: Experimental test system overview

Experimental Test System Housing

The purpose of the enclosed experimental test housing is to eliminate any air flow effects other than those from the fan. The experimental test system housing consists of two main parts: the frame and the walls. The frame is made from aluminum stock with extended slots on all four sides, which make it easy to mount the radiator, the fan, the walls, and any other necessary components. The walls are made of machinable Lexan sheets for the purpose of easily monitoring experimental tests. The Lexan sheet thickness is 1/2 in. for the base and 1/8 in. for the top and the sides.

Radiator and Fan Assembly

The radiator and fan assembly (Flex-A-Lite, 62180L) was chosen to represent the air flow of heavy-duty vehicles. The radiator and fan assembly was separated, and then the radiator and the fan were integrated individually into the experimental test system as two side walls of the experimental test system housing. A fan cover was installed for safety purposes.

Experimental Test Strip

The purpose of the experimental test strip is to simulate the extended surfaces of the hybrid radiator coolant channels. The experimental test strip, shown schematically in Figure VII-108, is made from aluminum alloy that is 24-1/8 in. long, 3 in. wide, and 1/4 in. thick. As shown graphically in Figure VII-109, a single glass serve insulated heating wire (Pelican Wire Company, P2323ADVSGS) is epoxied to the back of the experimental test strip for simulating the heat from the coolant channels. Five thermocouples are also epoxied to the back of the experimental test strip for monitoring the experimental test strip temperature during testing. The experimental test strip assembly installed inside the experimental test system housing has a two-dimensional adjustment arrangement for positioning the droplet dispersing tip at the desired location.

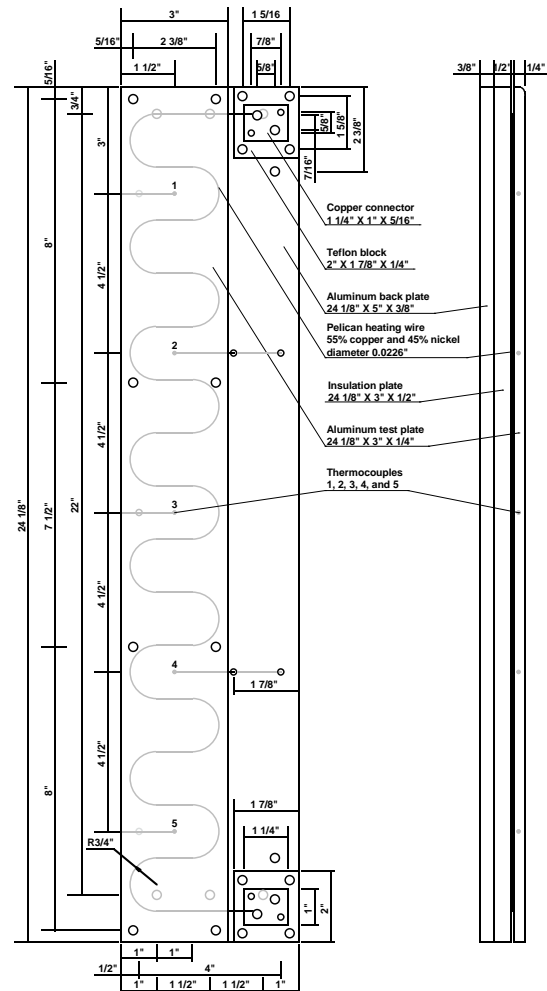


Figure VII-108: Experimental test strip assembly

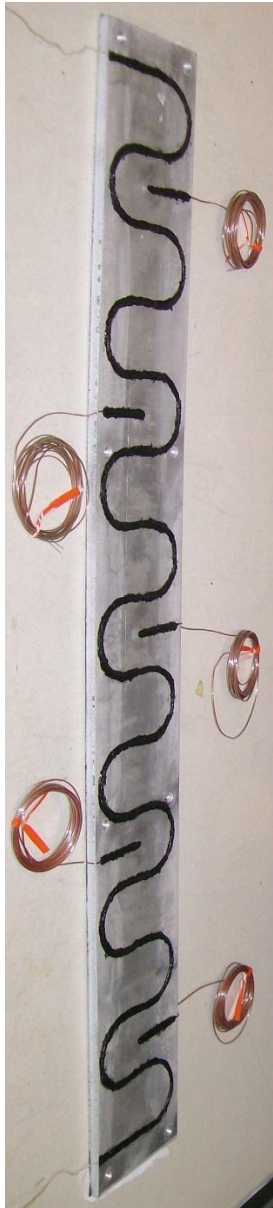


Figure VII-109: Heating Wire and Thermocouples

Droplet Dispersing Subsystem

A goniometer droplet dispensing system from Ramé-Hart is used for delivering droplets for experimental tests. This system allows for the control of the total dispensed volume and the time interval during which the volume is displaced. While there is no direct control over the droplet size, manipulating the size of the opening tip changes the droplet size. The droplet dispensing process is controlled by Ramé-Hart's Dropimage software. The droplet dispersing head assembly, shown schematically in Figure VII-110, is attached to the top wall of the experimental test system housing, and its opening tip height can be adjusted by adding or removing spacing washers.

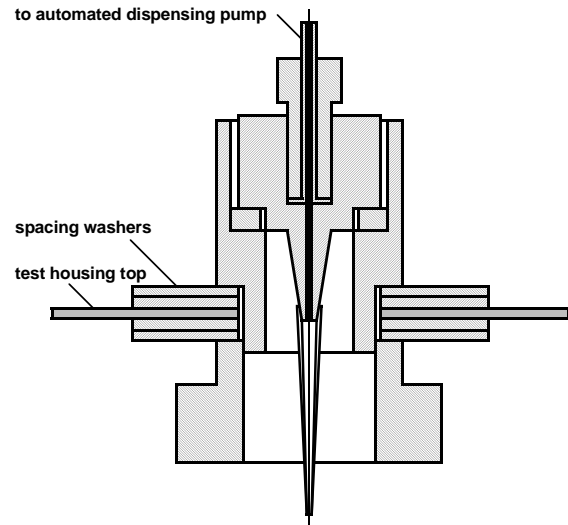


Figure VII-110: Droplet dispersing head assembly

Conclusions

Coolant radiators in trucks and automobiles were shown to be amenable to evaporative cooling. Using a hybrid radiator, 19% and 46% heat transfer increases were obtained with 76 L/h (20 gal/h) and 189 L/h (50 gal/h) water flow rates, respectively. These results were dependent on the establishment of water flow with a small thickness from the radiator surfaces. It was found that such thickness could readily be obtained by using droplet flow with contact angle management.

An alternative to the heat transfer increase from an existing radiator with the addition of evaporative cooling is a reduction in radiator size. It was shown that, at the design heat load, the 76 L/h (20 gal/h) and 189 L/h (50 gal/h) water flow rates yield radiator area reductions of 21% and 52%, respectively.

A good potential utilization of evaporative cooling in the finned portion of the radiator is to design the radiator to accommodate all driving conditions except for desert hills. In this case, water for evaporative cooling would only be needed when a vehicle travels through desert hills under extremely hot conditions. It was found that the radiator area could be reduced by 22% if only 76 L (20 gal) of water were used to traverse an extreme desert hill such as Baker Grade.

A series of numerical simulations was conducted with the commercial software COMSOL Multiphysics. It was found that the key factor for effective usage of evaporative cooling is the initial droplet thickness, which depends largely on the droplet size and the surface contact angle. Small droplets and contact angles generate small droplet thicknesses with effective evaporative cooling.

An experimental test system simulating the air flow of moving vehicles was designed and fabricated for investigating the droplet evaporation and movement under realistic application conditions of heavy-duty vehicles.

Future research will focus on experimental investigations of the effects of various surface coating and treatment methods and materials on the droplet evaporation and movement under the realistic air flow conditions of moving vehicles.

VII.N.3. Products

Publications

1. D. M. France, D. S. Smith, W. Yu, Efficient, "Active Radiator-Cooling System," SAE International Journal of Commercial Vehicles 6 (1) (May 2013) 249–256.

Patents

1. D. M. France, D. S. Smith, W. Yu, J. L. Routbort, "Hybrid Radiator Cooling System," pending US patent, US 2013/0233517 A1, September 2013.

DRAG REDUCTION

VII.O. DOE's Effort to Improve Heavy Vehicle Fuel Efficiency through Improved Aerodynamics

Principal Investigator: Kambiz Salari

Lawrence Livermore National Laboratory
7000 East Ave. L-090, Livermore, CA 94551
Phone: (925) 424-4635
E-mail: salari1@llnl.gov

DOE Program Manager: Lee Slezak

Phone: (202) 586-2335
E-mail: Lee.Slezak@ee.doe.gov

VII.O.2. Technical Discussion

Approach

Design the Next Generation of Highly Aerodynamic and Integrated Class 8 Tractor-Trialer Geometry – Generic Speed Form 1 (GSF1)

From our previous full-scale and small-scale wind tunnel studies and computational modeling, we have demonstrated that a complete aerodynamic treatment of existing on the road heavy trucks can be achieved by installation of add-on drag reduction devices (sealed tractor-trailer gap, full trailer skirts, and optimized trailer boattail) to achieve significant drag reduction and hence improved fuel economy. While further reductions in drag can be achieved with additional add-on devices, their benefit is likely to be incremental at best.

The LLNL has taken the initiative to design the next generation of an integrated tractor-trailer geometry from ground up that radically decrease aerodynamic drag and improves fuel efficiency. A 1/8th scale wind tunnel model of the new integrated design GSF1 was fabricated for testing at NASA Ames 7'x10' wind tunnel facility. For ease of construction and handling, the model is comprised of a tractor component and a trailer component. The tractor component (Figure VII-111a) is formed around a plywood structure, which is covered with modeling foam and clay, whereas the trailer component is supported by an aluminum structure that is similarly covered with foam and clay. This construction technique allows the entire model (Figure VII-111b) to be quickly reshaped during wind tunnel testing, thereby making it possible to evaluate the impact of curvature changes, corner rounding, and tapering upon the vehicle drag coefficient (Figure VII-112).

VII.O.1. Abstract

There are roughly 2.2 million combination trucks on the road today, each traveling an average of 65,000 miles/year and consuming 12,800 gallons of fuel/year for a total of 36 billion gallons of fuel/year. These trucks consume roughly 11-12% of the total United States petroleum usage. At highway speeds, a class 8 tractor-trailer uses over 50% of the usable energy produced by the vehicle engine to overcome aerodynamic drag. To improve the fuel economy of these vehicles Lawrence Livermore National Laboratory has been conducting research on enhanced aerodynamics through the use of add-on devices and new tractor-trailer shape designs.

Objectives

- Provide guidance to industry to improve the fuel economy of class 8 tractor-trailer through the use of aerodynamics.
- Develop innovative aerodynamic concepts for heavy vehicles that are operationally and economically sound.
- Demonstrate the potential of new drag-reduction concepts.
- Design the next generation of an integrated highly aerodynamic tractor-trailers and tanker-trailers.
- Establish a database of experimental, computational, and conceptual design information.

Major Accomplishments

- Design and Fabrication of a Next Generation Class 8 Heavy Vehicle Model – Generic Speed Form 1 (GSF1)
- Wind tunnel test results for the new tractor-trailer design GSF1 and modified tanker-trailer conducted at NASA Ames Research Facility operated by Army Research Development and Engineering Command



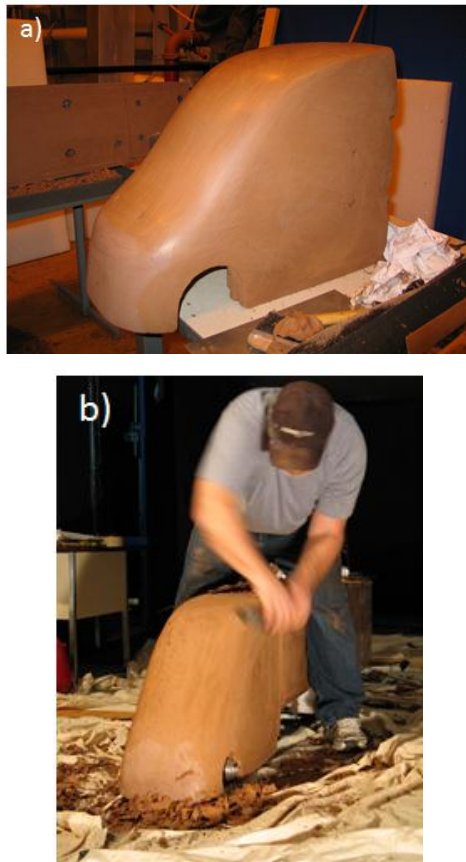


Figure VII-111: a) Clay exterior of the GSF1 tractor; b) tractor and trailer reshaping during a wind tunnel test

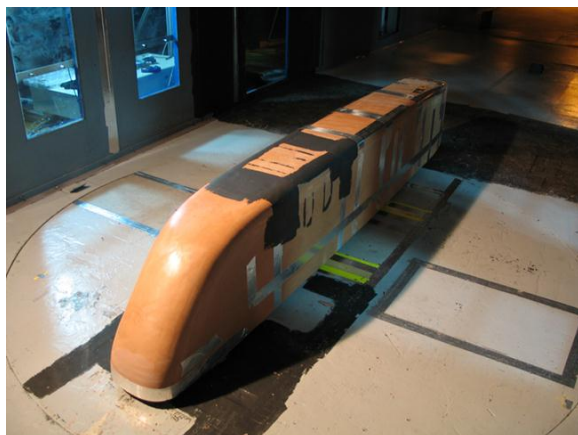


Figure VII-112: GSF1 model (1/8th scale) in the NASA Ames 7x10 wind tunnel

Wind Tunnel Test Results for GSF1 and Modified Tanker-Trailer

In collaboration with NASA Ames, Navistar, and the U.S. Army Research, Development and Engineering Command, we conducted an experimental test at the NASA Ames 7x10' wind tunnel. Over the course of six weeks, 132 wind tunnel runs were completed on a number of heavy vehicle configurations, designs, and drag reduction devices. The most noteworthy result of this test is the aerodynamic performance of our next generation heavy vehicle design called GSF1. This

configuration has a reduced vehicle ground clearance, lateral and vertical trailer tear-dropping, trailer edge rounding, an optimized boattail, and tractor-trailer integration (Figure VII-113). The measured wind-averaged drag coefficient is about 65% smaller than that of a modern aerodynamic on the road tractor-trailer.



Figure VII-113: GSF1 tractor-trailer design

The corresponding body-axis drag coefficient versus vehicle yaw angle plot (Figure VII-114) highlights the performance of this vehicle design for various crosswinds. For yaw angles beyond 9°, the drag coefficient decreases. Computational fluid dynamics (CFD) simulations of this vehicle indicate that the decrease in drag is due to a low pressure region (suction force) that develops as the flow rounds the leeward leading edge of the tractor and remains attached to the leeward side of the tractor (Figure VII-115). For even larger yaw angles (Figure VII-116), the drag coefficient becomes negative and, as noted previously by Cooper (2003), the vehicle begins to sail.

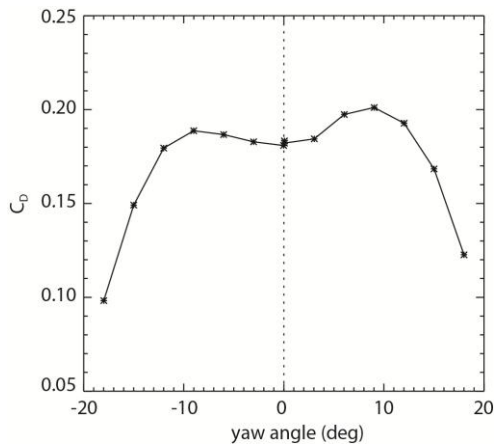


Figure VII-114: Body-axis drag coefficient as a function of vehicle yaw angle (-18° to 18°) for the GSF1 configuration shown in Figure VII-113

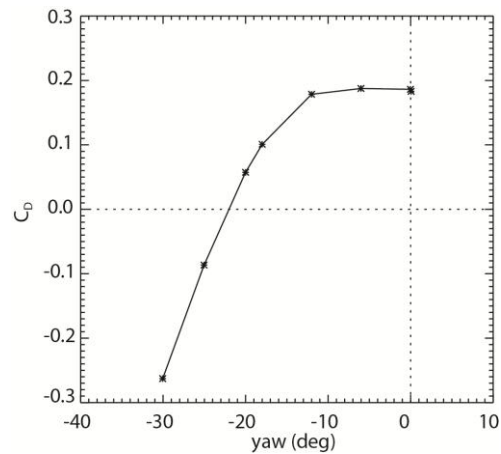


Figure VII-116: Body-axis drag coefficient as a function of vehicle yaw angle (-30° to 0°) for the configuration shown in Figure VII-113

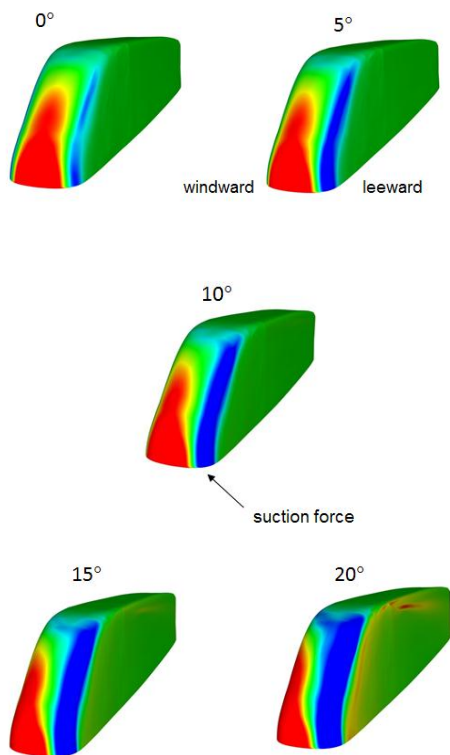


Figure VII-115: Body-axis surface force (pressure and shear stress) obtained from CFD simulations of the GSF1 configuration shown in Figure VII-113

We also investigated the aerodynamic drag reduction of tanker-trailers using add-on devices. The baseline case consisted of a Navistar Pro-Star day cab and a liquid tanker model configured with a 60" (full-scale) tractor-tanker gap (Figure VII-117a). Gap fairings of varying size were evaluated as a means of reducing the tractor-tanker gap drag (Figure VII-117b). Completely eliminating the gap with a fully extended fairing produced a 12% reduction in the wind-averaged drag coefficient, though it should be noted that the smallest fairing (42.5" gap) also resulted in a nearly 10% reduction in drag (Figure VII-118). Even larger reductions in the wind-averaged drag coefficient were achieved with tanker skirts (24%) and a tanker "drape" (36%) (Figure VII-119).

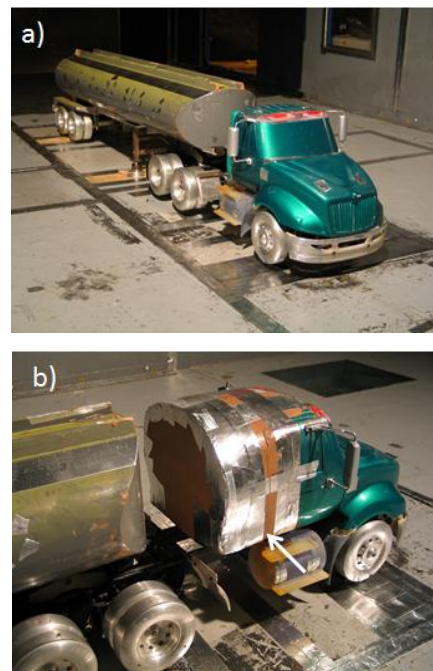


Figure VII-117: a) Baseline tanker-trailer; b) gap fairing

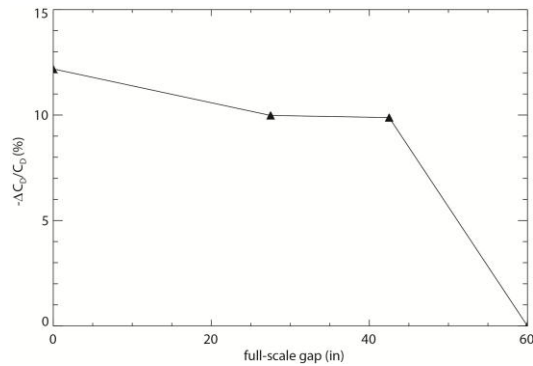


Figure VII-118: Percent reduction in the wind-averaged drag coefficient as a function of tractor-tanker gap size (Figure VII-117)

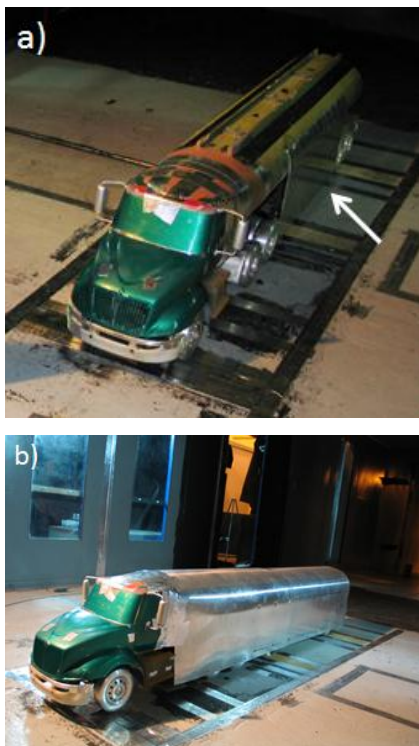


Figure VII-119: Tanker-trailer with a fully extended gap fairing and a) tanker skirts and b) a tanker “drape”

In addition to the aerodynamic drag force measurements, an extensive particle image velocimetry (PIV) data set was collected for the Pro-Star short sleeper straight-frame trailer configuration. The PIV setup consisted of two lasers and two cameras attached to vertical traverses on either side of the wind tunnel, thereby allowing all three components of the velocity field to be acquired (Figure VII-120). PIV measurements were made in nine horizontal planes in the wake of the vehicle with and without a 48" (full-scale) trailer boattail at an optimum deflection angle of 11° (Figure VII-121). The data within in each plane was recorded for 10 minutes in order to achieve statistically converged mean quantities. The results of the PIV measurements demonstrate that the boattail device reduces the aerodynamic drag by inducing a downwash that decreases the size of the trailer wake

(Figure VII-122). Additional details of the PIV measurements are provided in the Appendix.

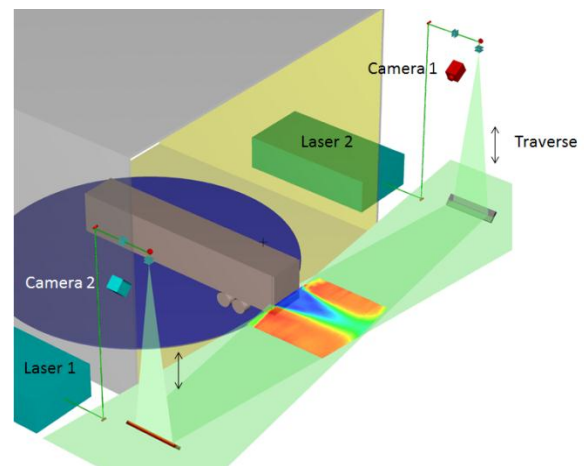


Figure VII-120: PIV setup in the NASA Ames 7x10 wind tunnel

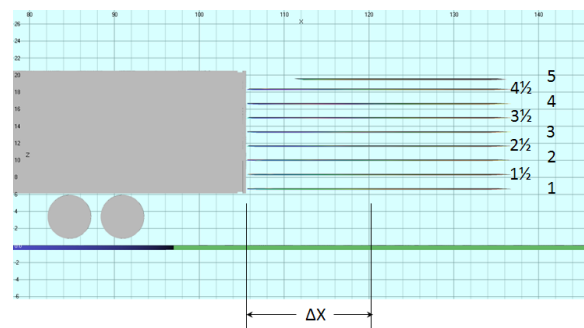


Figure VII-121: PIV measurement planes

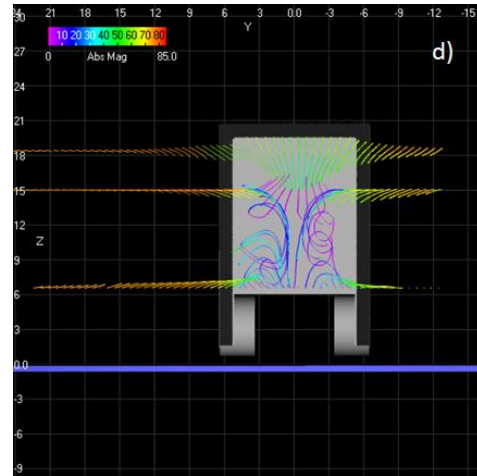
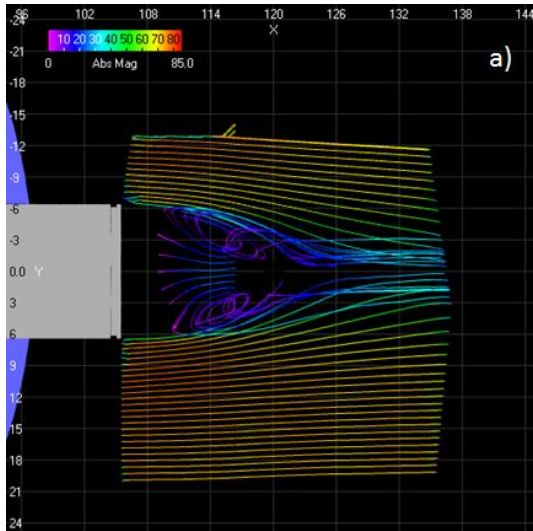
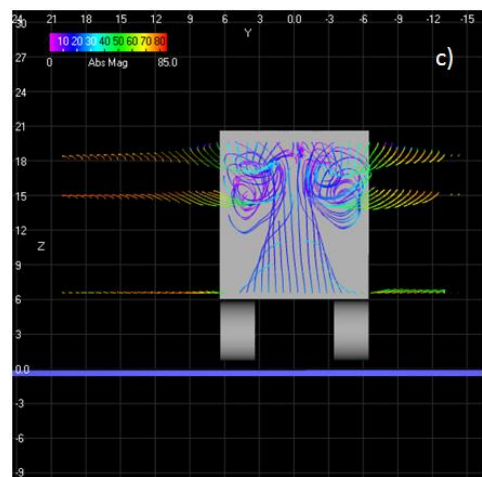
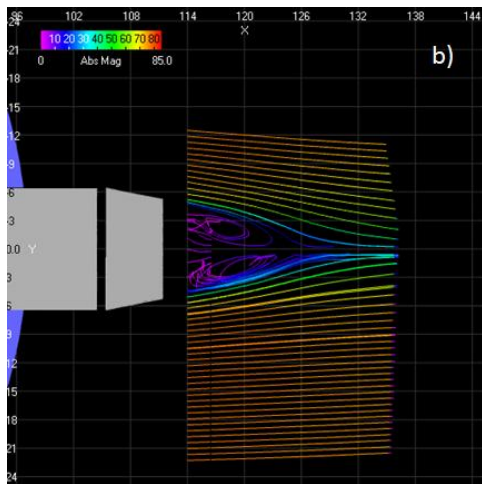


Figure VII-122: Velocity streamlines in the wake of Pro-Star tractor and straight-frame trailer at 0° yaw: a, c) baseline configuration and b,d) 48" (full-scale) trailer boattail and trailer skirts configuration



Acknowledgments

This work was performed under the auspices of the U.S. Department of Energy by University of California, Lawrence Livermore National Laboratory under Contract W-7405-Eng-48.

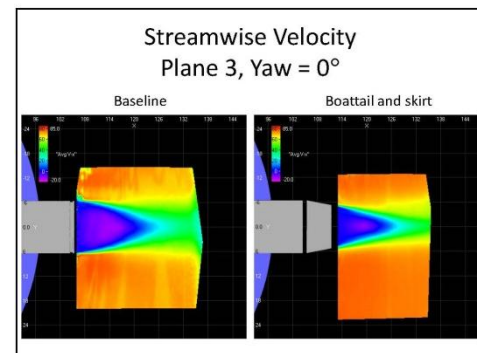
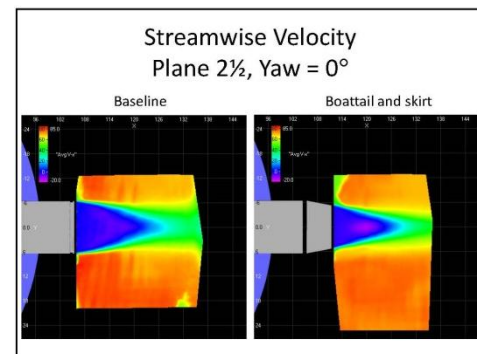
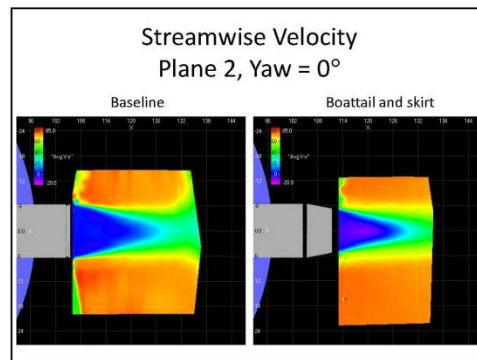
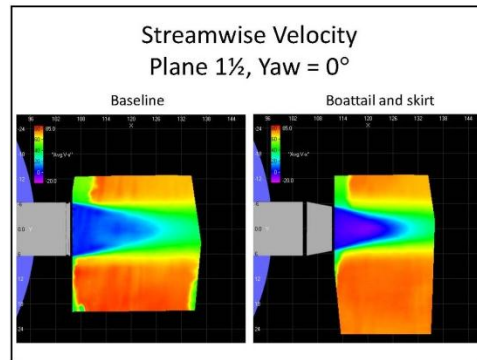
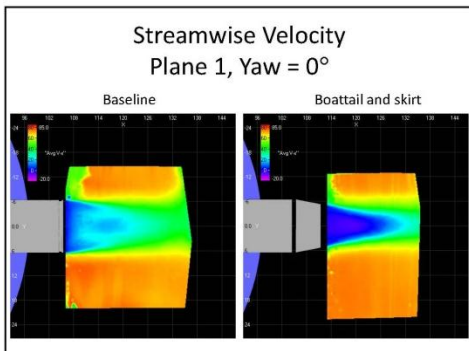
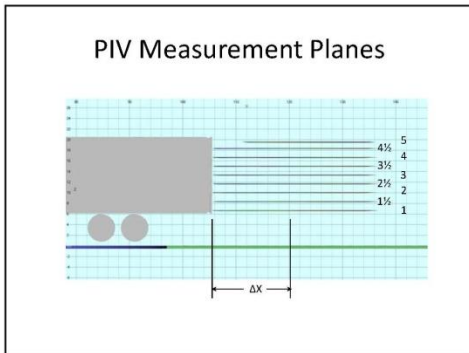
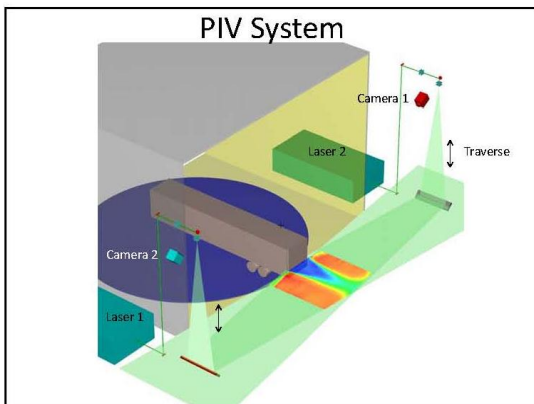
References

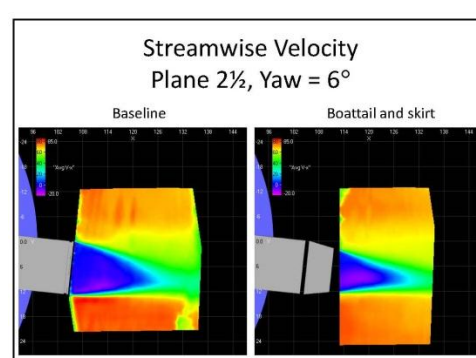
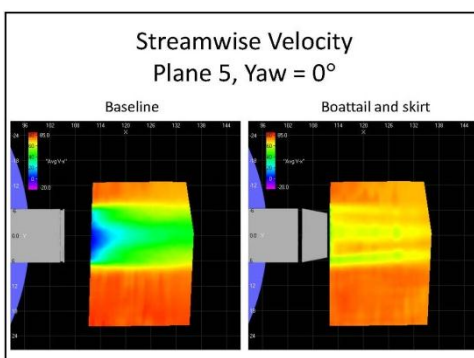
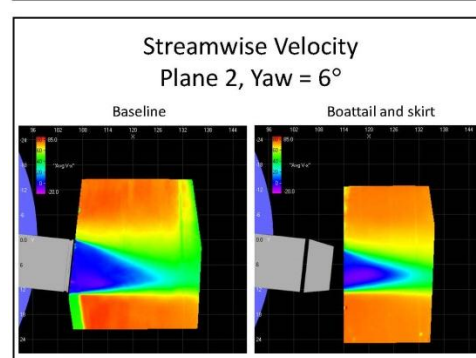
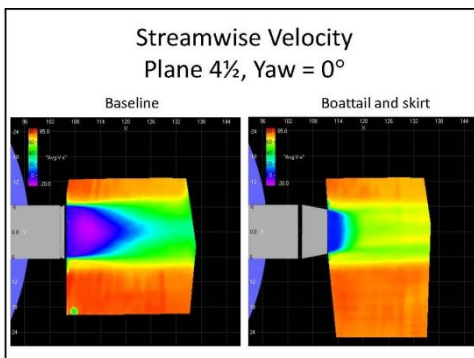
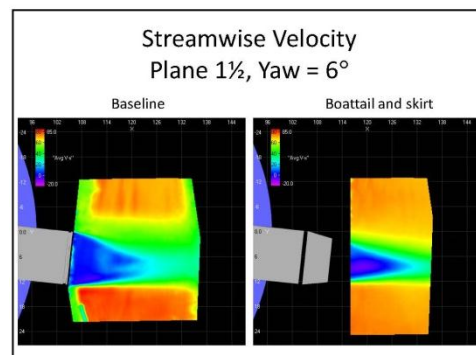
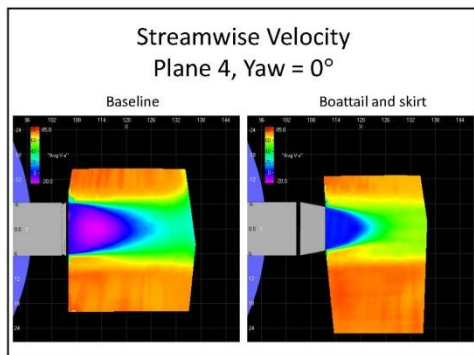
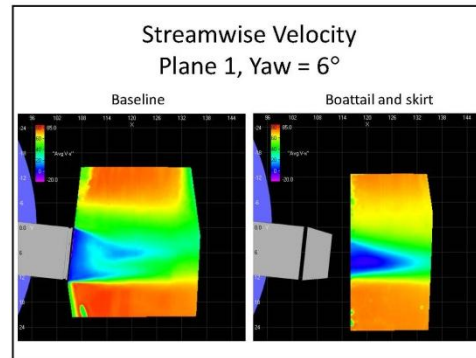
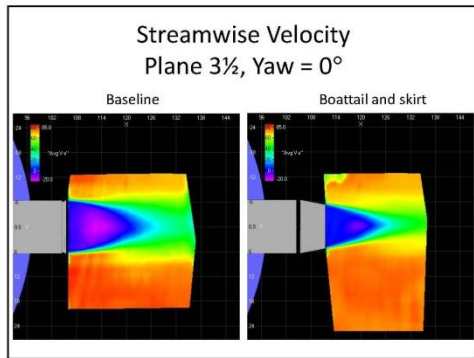
1. Cooper, K.R., 2004. Commercial vehicle aerodynamic drag reduction: historical perspective as a guide, in: McCallen, R., Browand, F., Ross, J., (Eds.), *The Aerodynamics of Heavy Vehicles: Trucks, Buses, and Trains*, Lecture Notes in Applied and Computational Mechanics 19. Springer, Heidelberg, pp. 9–28.

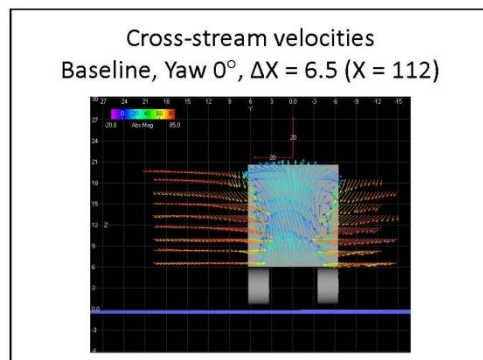
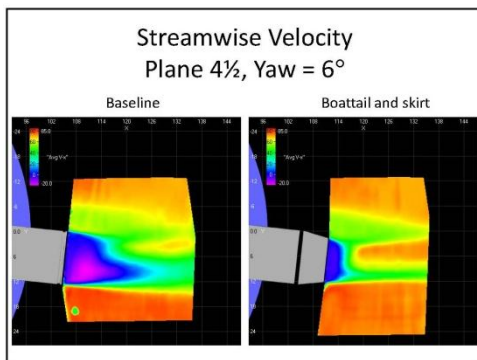
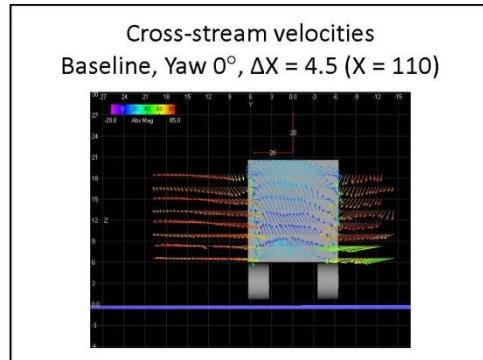
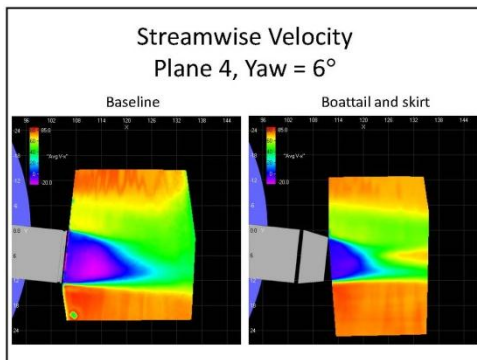
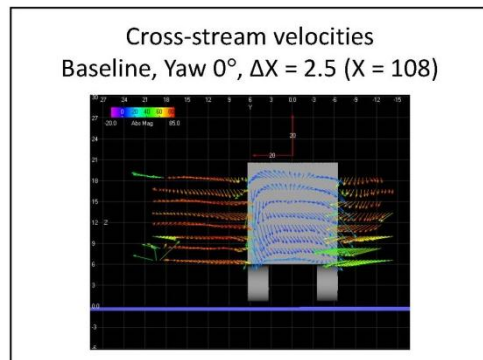
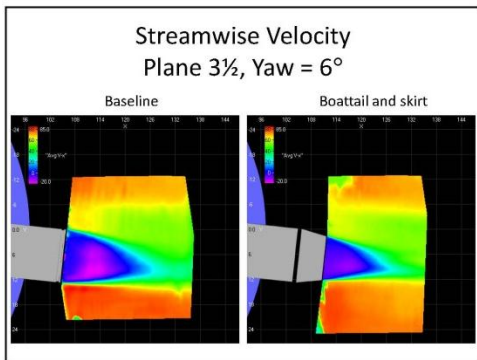
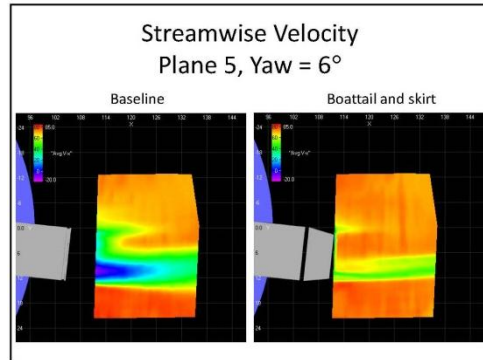
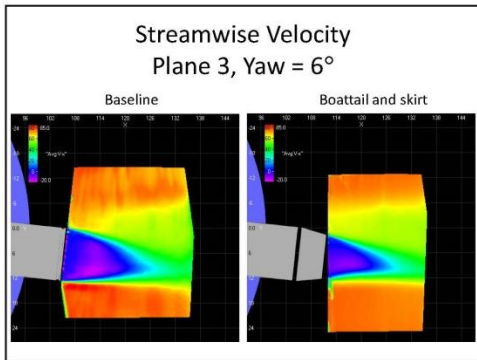
Appendix

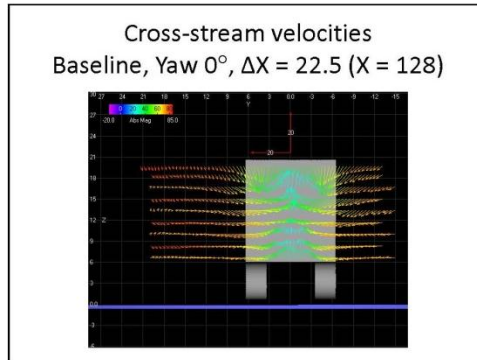
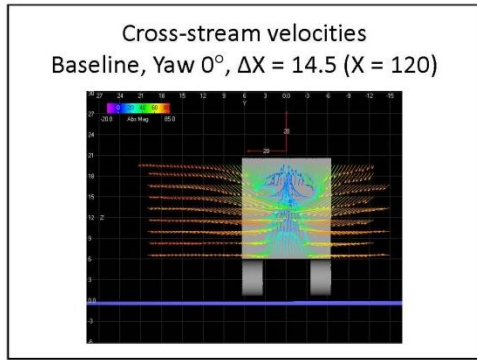
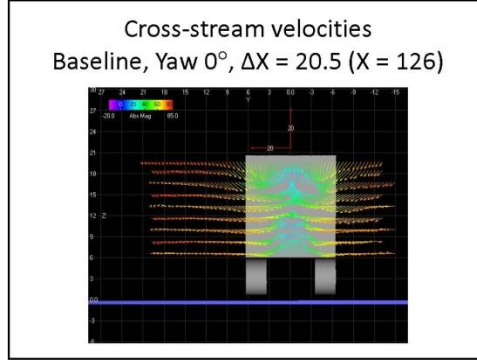
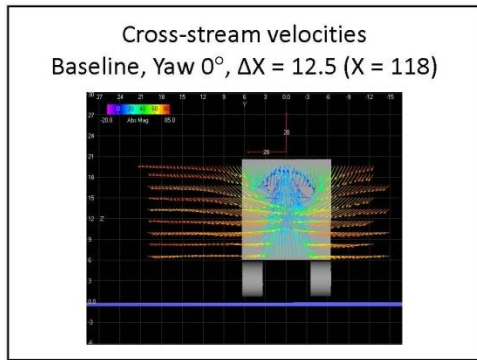
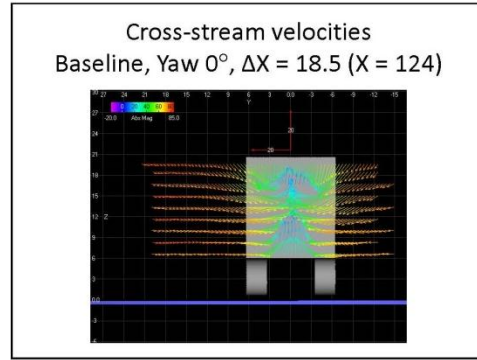
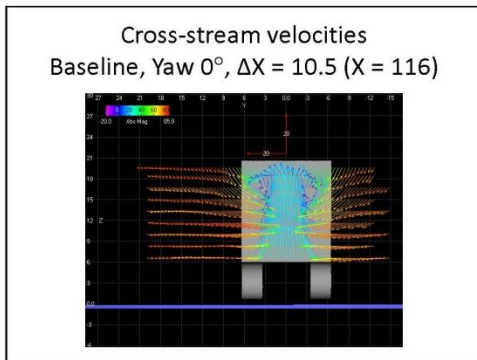
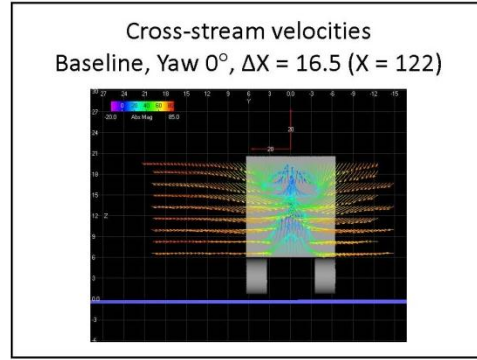
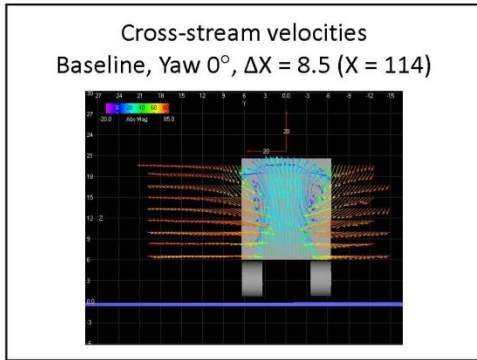
**Truck Wake Measurements by
Stereo Particle Image Velocimetry
in the 7 x 10 Ft Wind Tunnel**

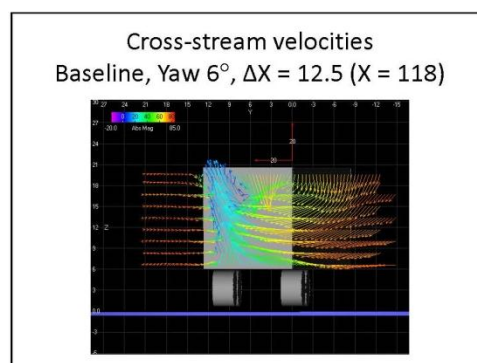
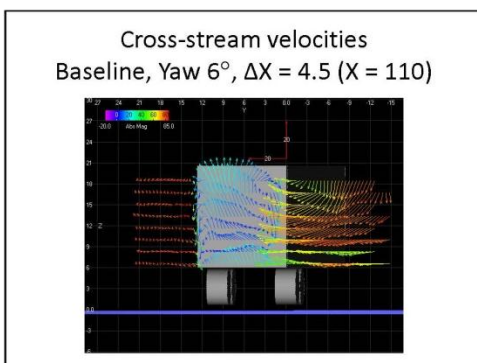
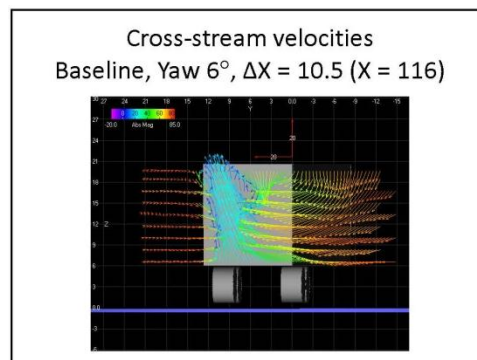
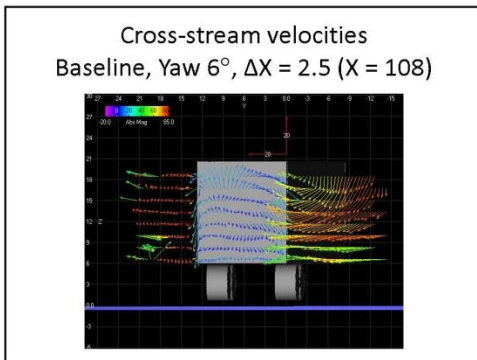
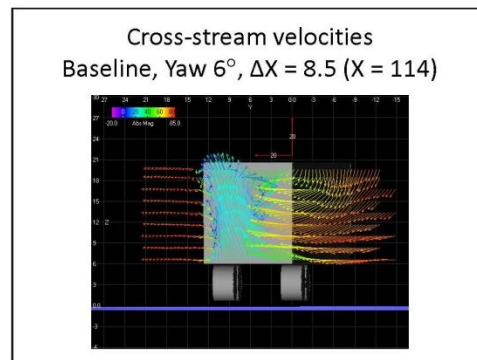
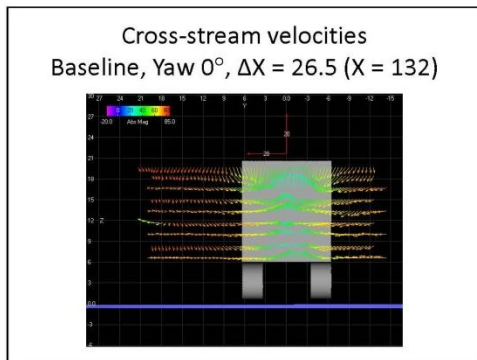
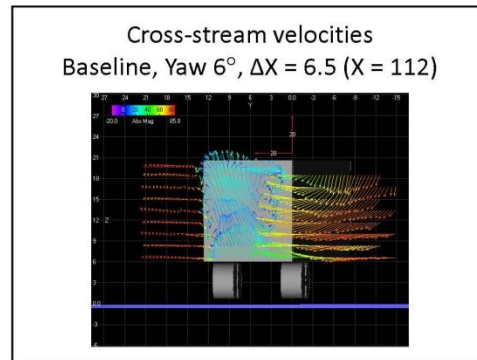
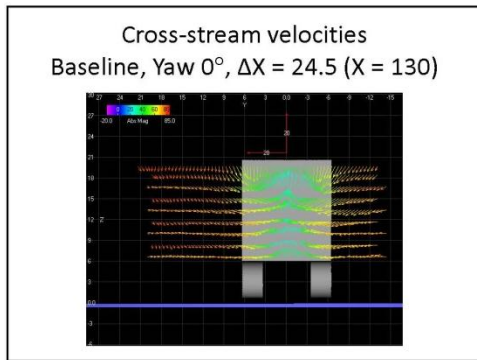
 JT Heineck and Edward Schairer
 Experimental AeroPhysics Branch (AOX)
 NASA Ames Research Center
 August 5, 2014

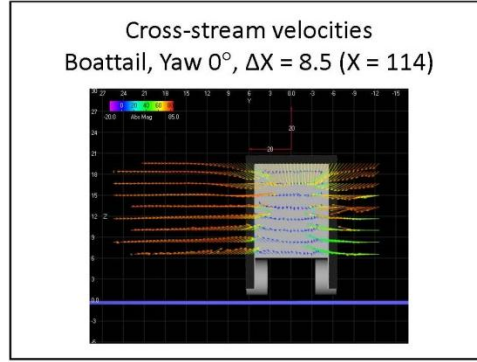
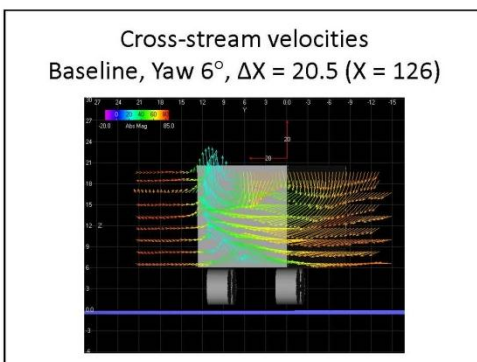
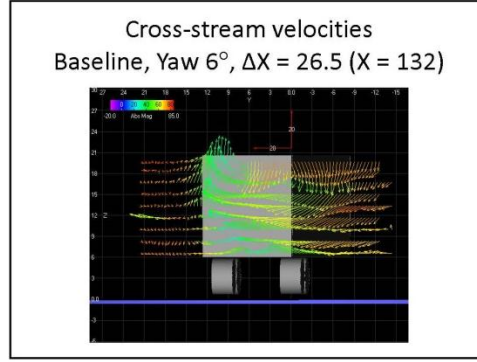
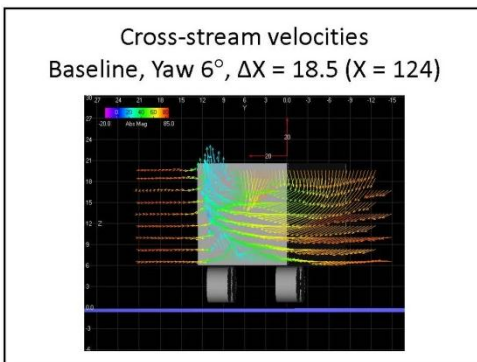
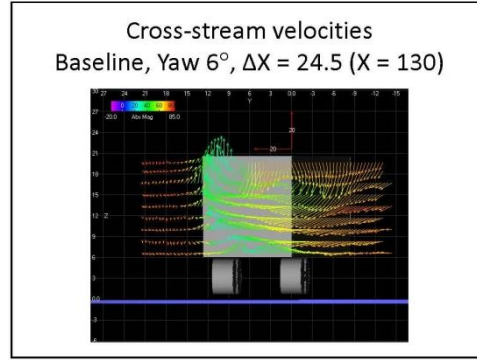
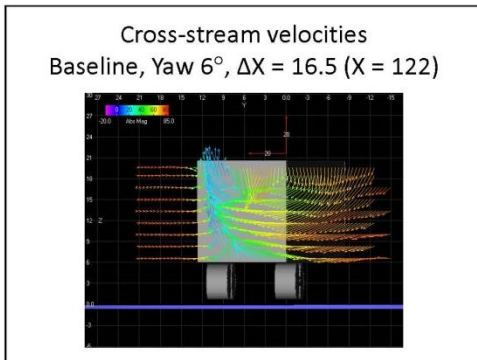
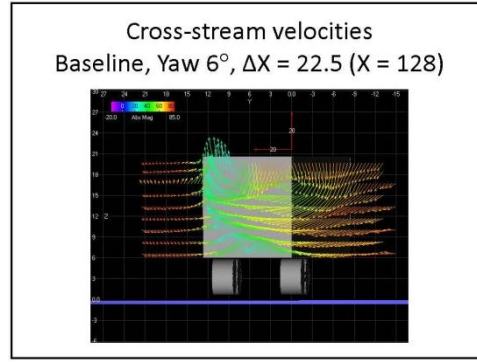
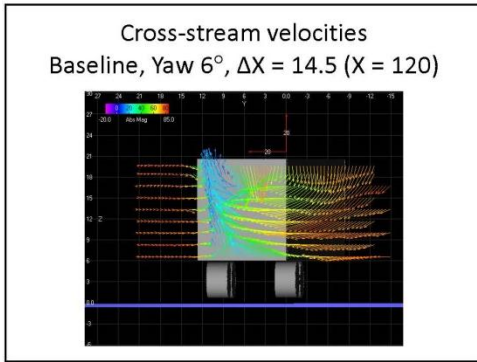


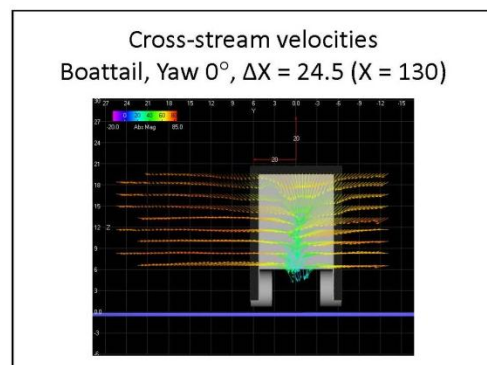
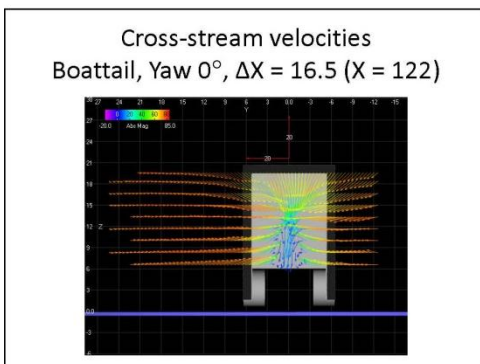
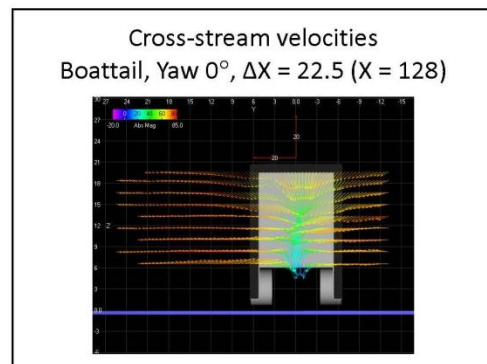
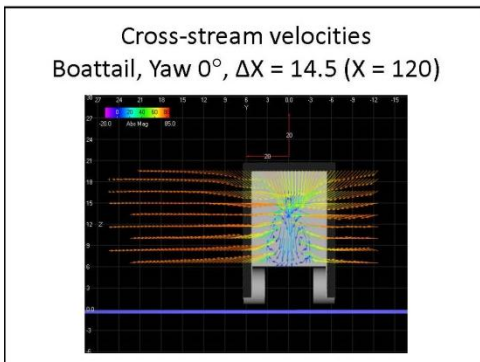
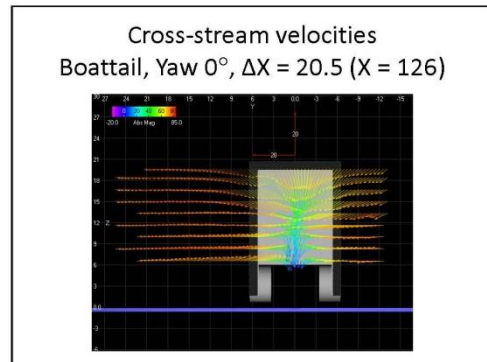
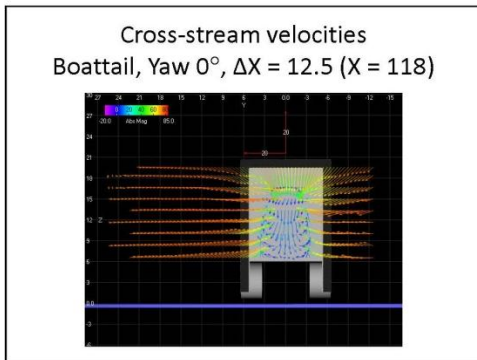
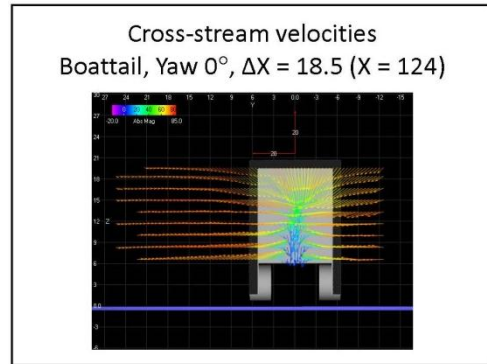
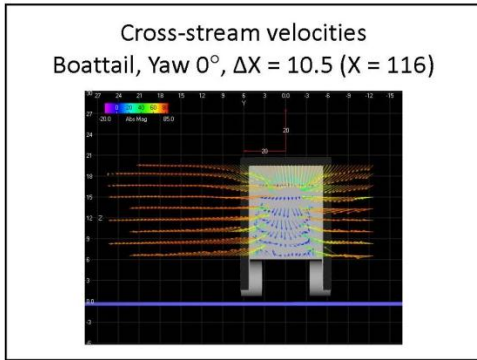


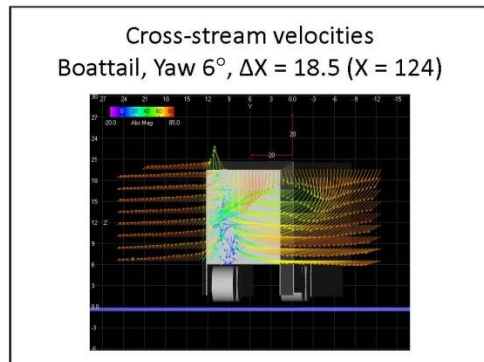
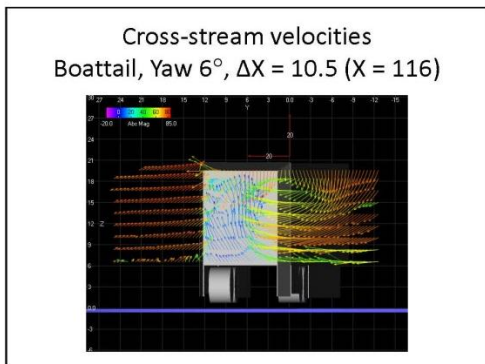
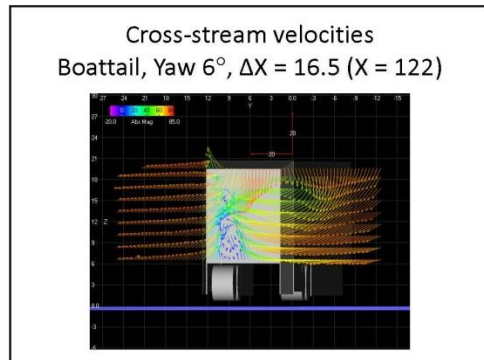
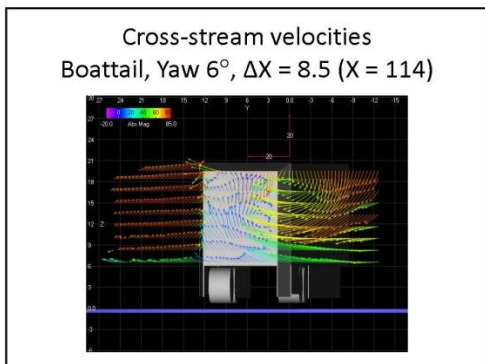
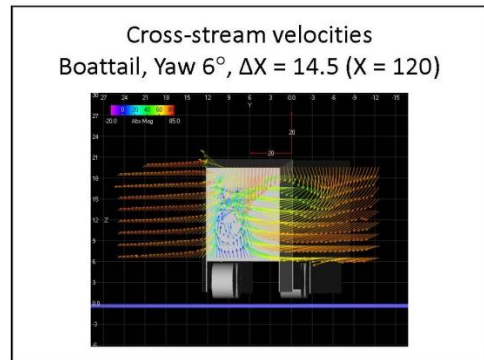
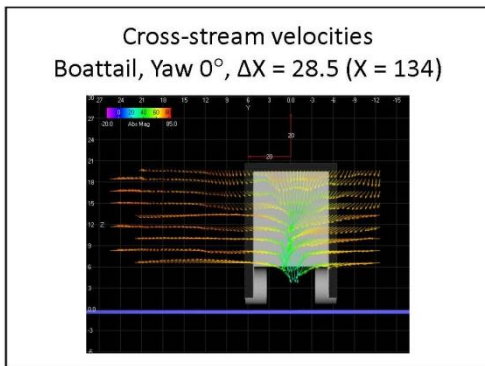
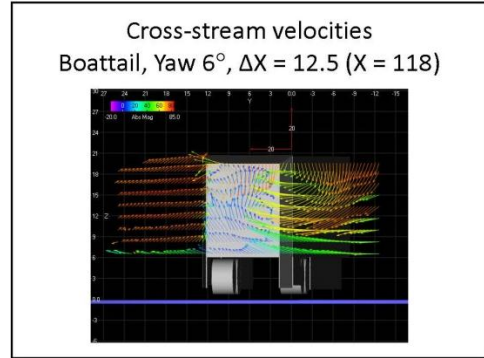
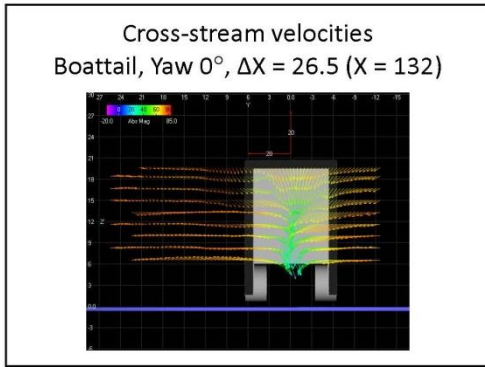


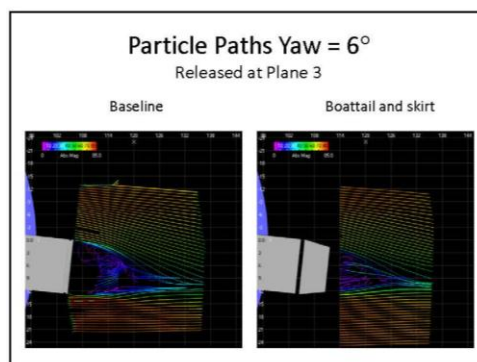
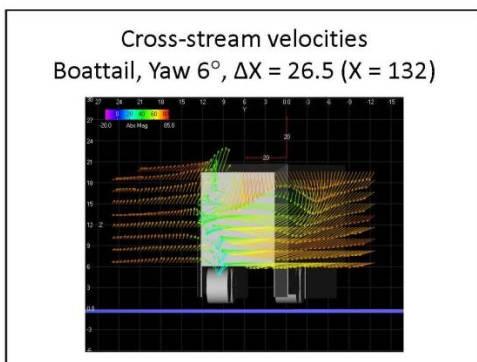
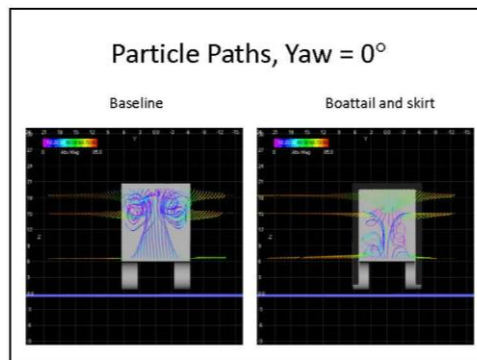
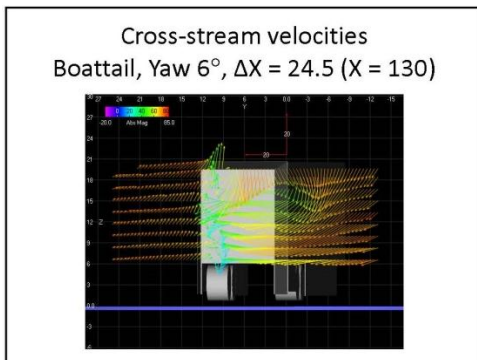
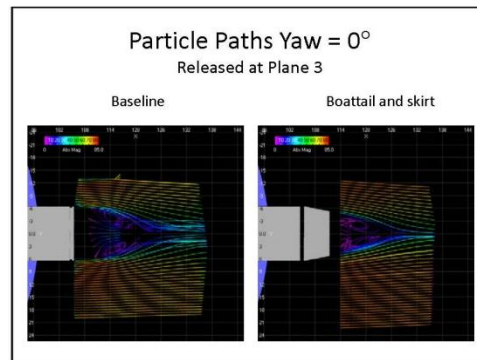
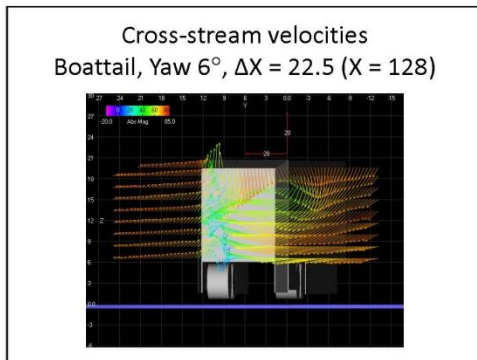
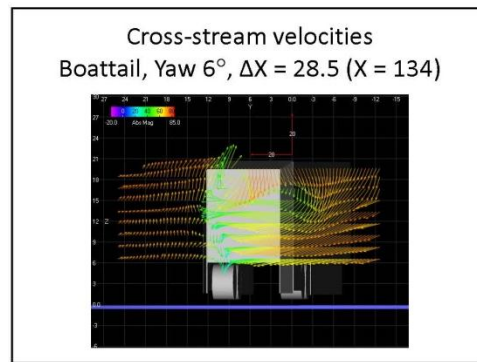
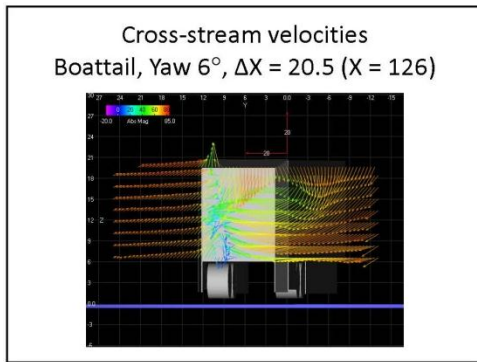


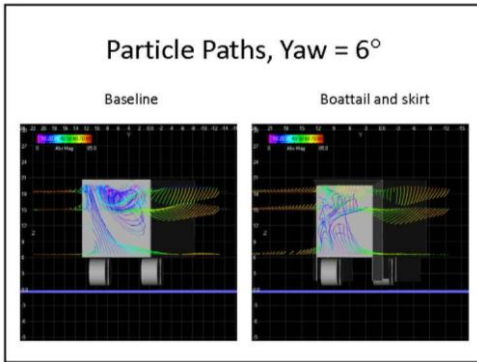


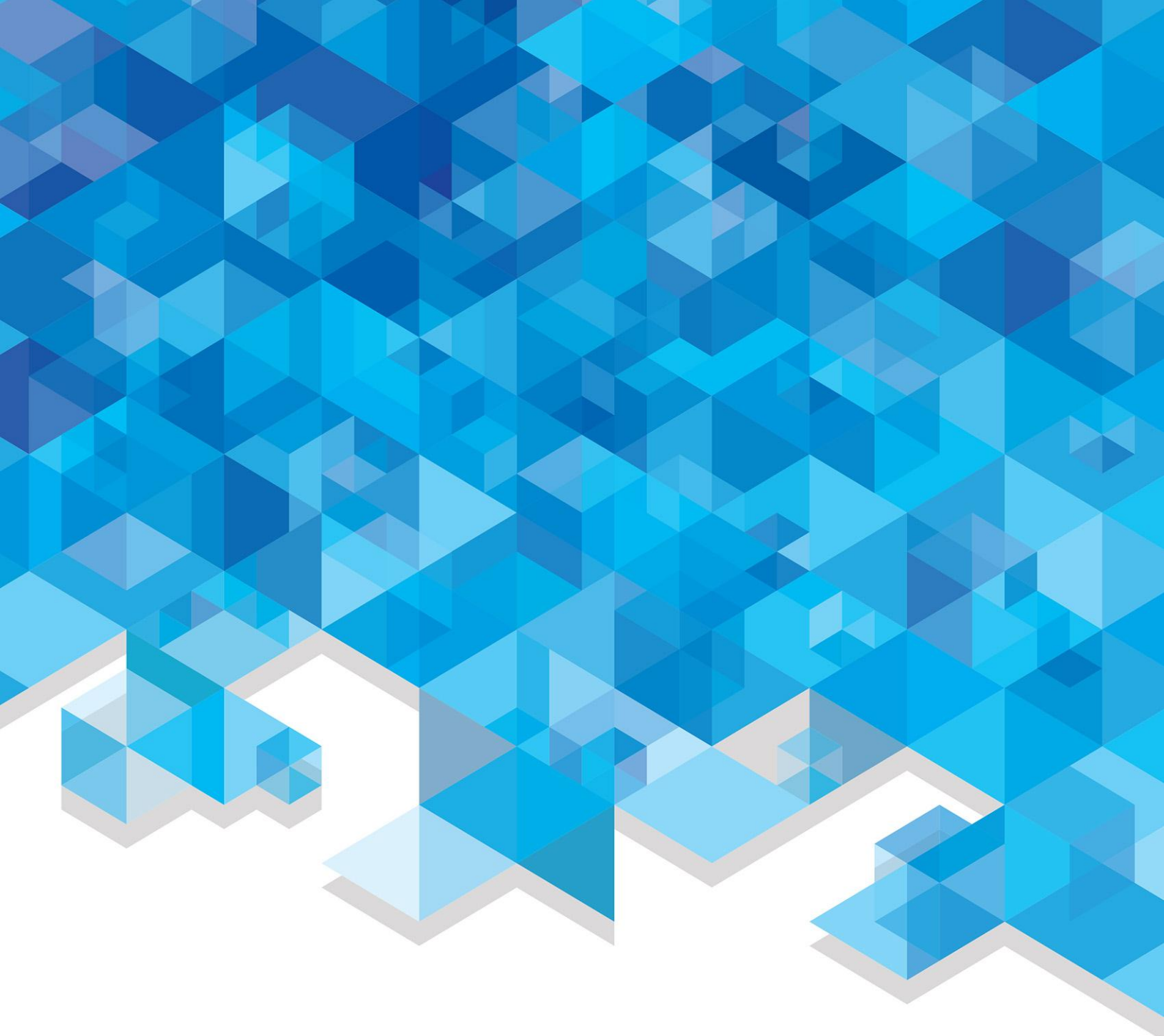












U.S. DEPARTMENT OF
ENERGY

Energy Efficiency &
Renewable Energy

For more information, visit: energy.gov/eere

DOE/EE-1165 • March 2015